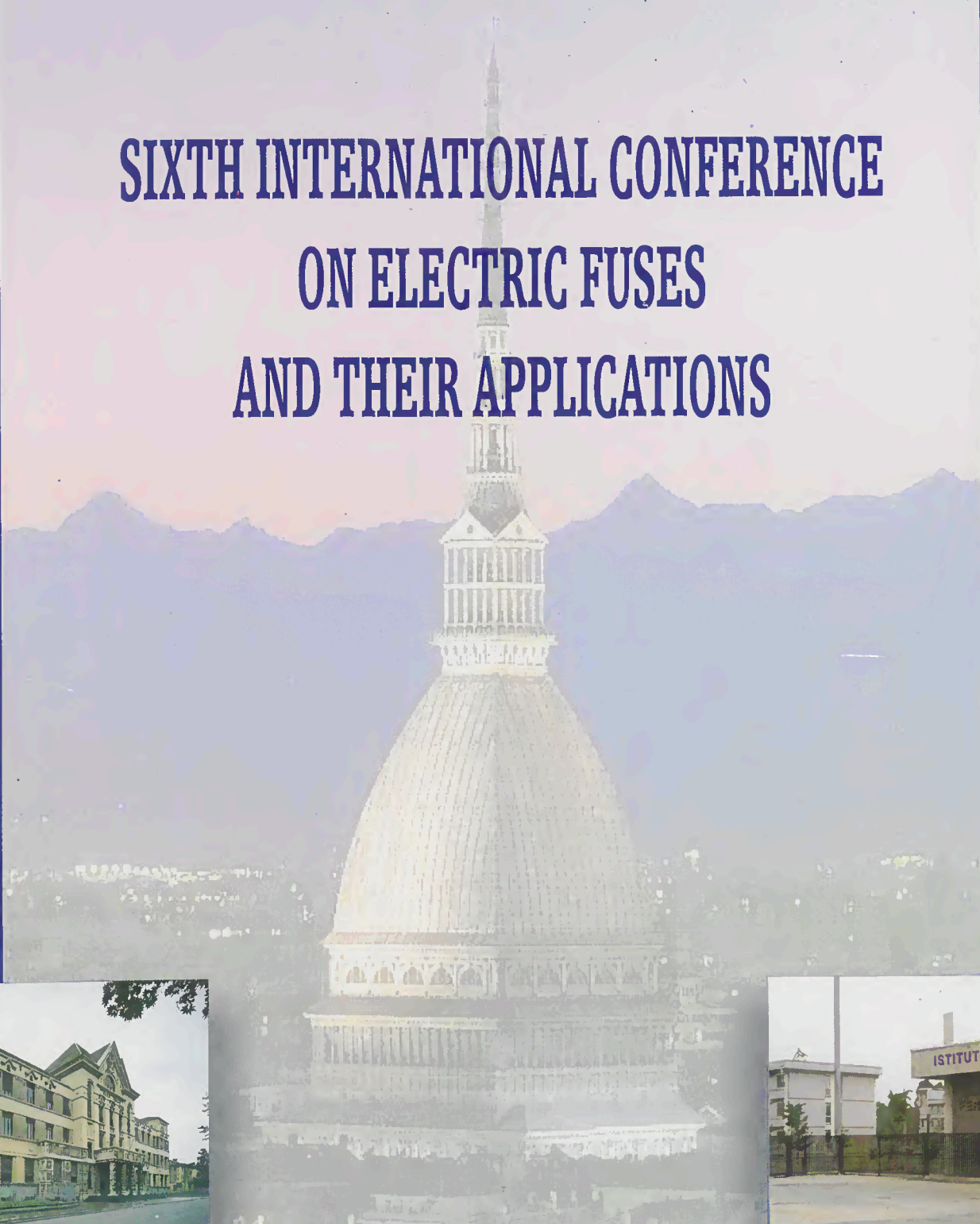




**SIXTH INTERNATIONAL CONFERENCE  
ON ELECTRIC FUSES  
AND THEIR APPLICATIONS**



**20-22 September 1999  
Istituto Elettrotecnico Nazionale  
Galileo Ferraris  
Torino, Italy**



Regione Piemonte



Provincia di Torino



Città di Torino



AZIENDA ENERGETICA METROPOLITANA TORINO S.p.A.



Pogliano dei Frat. Pogliano  
TORINO



# **SIXTH INTERNATIONAL CONFERENCE ON ELECTRIC FUSES AND THEIR APPLICATIONS**

Under the Patronage of

REGIONE PIEMONTE  
PROVINCIA DI TORINO  
COMUNE DI TORINO

Co-sponsored by:

Azienda Energetica Metropolitana - Torino  
AEM S.p.A. - Milano  
Banca CRT  
ABB  
bticino  
Pogliano dei Fratelli Pogliano  
Schneider Electric  
SIEMENS  
WEBER

**20-22 September 1999  
Istituto Elettrotecnico Nazionale  
Galileo Ferraris  
Torino, Italy**

**Istituto Elettrotecnico Nazionale Galileo Ferraris**  
Corso Massimo d'Azeglio, 42  
10125 – Torino  
Italy

**ISBN 88-900352-1-8**

*Proceedings of the Sixth International Conference  
on Electric Fuses and their Applications*

Editors:  
Gabriella Crotti, Giovanni Farina  
Electromechanics Department  
Istituto Elettrotecnico Nazionale  
Galileo Ferraris-Turin, Italy

The Editors and the International Scientific and Organising Committees of the *Sixth International Conference on Electric Fuses and their Applications* are not responsible for the opinions expressed in the papers published in these Proceedings. The contents of the papers express entirely the views of the authors.

## FOREWORD

Fuses have been used in electric circuit to protect plants and apparatus against overcurrent for more than 120 years. They are usually regarded as very simple devices containing wires or strips that melt when current values above certain levels flow through them. After a century, a complete knowledge of the phenomenon occurring in fuse operation has still not been obtained as demonstrated by the high number of research projects carried out on this subject around the world.

The effort in research and development is evident from the success obtained in the Conferences held in Liverpool, Trondheim, Eindhoven, Nottingham and Ilmenau. Now in Turin, we hope to continue the success of the previous editions.

The Istituto Elettrotecnico Nazionale "Galileo Ferraris" is pleased to host the Sixth edition of this Conference. Authors coming from 16 countries will present 59 papers concerning both theoretical and applicative aspects of fuse behaviour. The delegates from many countries around the world provide further evidence of the interest in electric fuses. A warm welcome is extended to all of them, with the hope that they will find the Conference both interesting and enjoyable.

I would like to thank the International Scientific Committee and the Organising Committee for their fruitful collaboration in organising this Conference. Thanks are also due to the Comune di Torino, Provincia di Torino, Regione Piemonte, Banca CRT, AEM-Torino, AEM-Milano and to the industries ABB, bticino, Pogliano, Groupe Schneider, Siemens and Weber for their generous sponsorship.

Professor Giovanni Cantarella

Chairman of the International Scientific Committee

PLATE 1

The first part of the text discusses the general principles of the theory, including the definition of the variables and the initial conditions. It also mentions the importance of the boundary conditions and the role of the parameters in the model.

The second part of the text describes the numerical methods used for the simulation, including the choice of the time step and the spatial discretization. It also discusses the convergence criteria and the stability of the numerical scheme.

The third part of the text presents the results of the simulation, showing the time evolution of the variables and the comparison with the analytical solutions. It also discusses the physical interpretation of the results and the implications for the theory.

The fourth part of the text concludes the study, summarizing the main findings and the limitations of the current work. It also suggests directions for future research and the potential applications of the theory.

The final part of the text contains the references and the acknowledgments, as well as the author's contact information and the date of the publication.

## INTERNATIONAL SCIENTIFIC COMMITTEE

Prof. G. Cantarella (Chairman)  
Polytechnic of Turin (Italy)

Dr. A. Alberici  
Comitato Elettrotecnico Italiano (Italy)

Prof. S. Arai \*  
Tokyo Denki University (Japan)

Dr. H. Bessei \*  
EFEN GmbH (Germany)

Dr. O. Bottauscio  
IEN Galileo Ferraris (Italy)

Mr. P. Brogl \*  
LINDNER GmbH (Germany)

Dr. L. Cheim \*  
CEPEL - ACET (Brazil)

Prof. M. Chiampi  
Polytechnic of Turin (Italy)

Dr. G. Crotti  
IEN Galileo Ferraris (Italy)

Mr. W.H. Curtis \*  
Cooper Bussman Ind. (USA)

Mr. R. Deshayes \*  
Soc. FERRAZ (France)

Dr. G. Farina  
IEN Galileo Ferraris (Italy)

Dr. A. Formica  
Groupe Schneider (Italy)

Prof. J.C. Gomez \*  
University of Rio Cuarto (Argentina)

Dr. A.F. Howe \*  
University of Nottingham (UK)

Prof. W. Jimei \*  
Xi' An Jiaotong University (China)

Prof. D. König \*  
Technical University of Darmstadt (Germany)

Dr. J.G. Leach \*  
HI-Tech Fuses Inc. (USA)

Prof. M. Lindmayer \*  
Technical University of Braunschweig (Germany)

Prof. T. Lipski \*  
Technical University of Gdansk (Poland)

Dr. K. Möllenhoff \*  
SIEMENS AG (Germany)

Mr. P.G. Newbery  
Cooper Bussman Ind. (UK)

Dr. G. Nutsch \*  
Technical University of Ilmenau (Germany)

Dr. D. Pennati  
SIEMENS S.p.a. (Italy)

Dr. G. Pogliano  
Pogliano dei Fr. Pogliano (Italy)

Dr. M. Re  
bticino (Italy)

Mr. P. Rosen \*  
Consultant (UK)

Prof. W. Rother \*  
Technical University of Ilmenau (Germany)

Prof. J.G.J. Slood \*  
Eindhoven University of Technology (NL)

Prof. A.D. Stokes \*  
University of Sidney (Australia)

Prof. M. Tartaglia  
Polytechnic of Turin, Italy

Mr. H.W. Turner \*  
Consultant (UK)

Dr. R. Wilkins \*  
Consultant (UK)

(\* ) Corresponding Member

## ORGANISING COMMITTEE

Dr. G. Farina (Chairman)

Mr. D. Arato

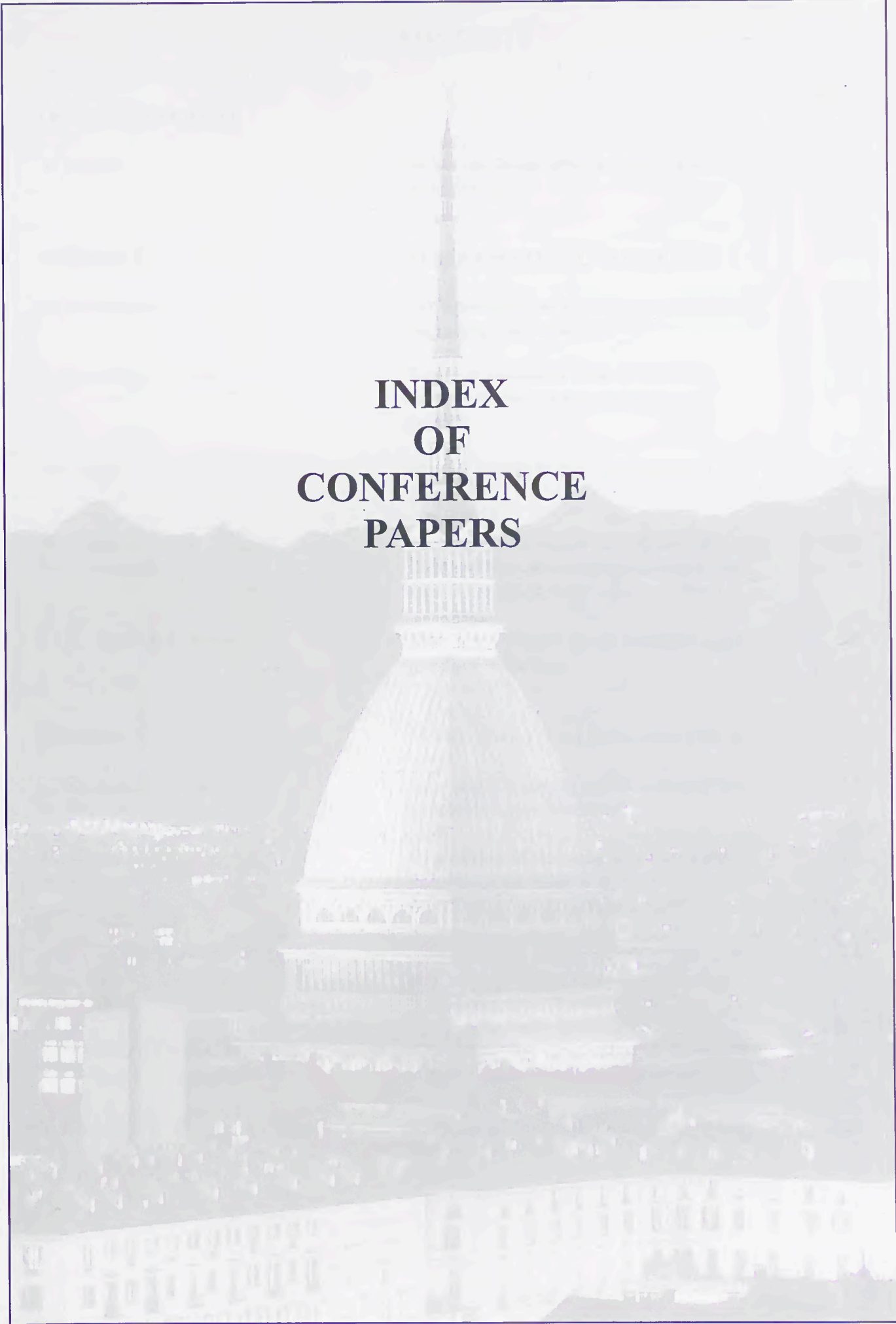
Prof. G. Cantarella

Dr. G. Crotti

Mr. A. Mistrangelo

Mrs. E. Melli (Treasurer)

Mrs. D. Nesci



**INDEX  
OF  
CONFERENCE  
PAPERS**



## CONTENTS

		<i>page</i>
<b>OPENING LECTURE</b>		
<i>A. Wolny</i>	What can fuses offer to survive the next century	1
<b>SESSION 1</b>	<b>MATHEMATICAL MODELLING I</b>	
<i>M. Lindmayer</i>	3D simulation of fusing characteristics including the "M-effect"	13
<i>C. Garrido, J. Cidras</i>	Study of fuselinks with different <i>t-i</i> curves using a mathematical model	21
<i>R. Wilkins</i>	Fitting curves to fuse time-current test data	25
<i>M. Wilniewicz, D. Crellin, P.M. McEwan</i>	Finite element analysis of thermally-induced film de-bonding in single and two-layer thick-film substrate fuses	29
<i>J.G.J. Sloot, X.Z. Meng</i>	Fuse arc voltages, from striation until gradual burn back	35
<b>SESSION 2</b>	<b>MATHEMATICAL MODELLING II</b>	
<i>E. Hnatiuc, R. Burlica, B. Hnatiuc</i>	New aspects on the multi-element fuse protection characteristic	43
<i>JL. Gelet, D. Tournier, M. Ruggiero</i>	Evaluation of thermal and electrical behaviour of fuses in case of paralleling and/or high frequencies	49
<i>Jin Lijun, Ma Zhiying, Wang Jimei</i>	The research on the stable temperature-rise of high-voltage current-limiting fuse-link	55
<i>A.Baraboi, I. Ciutea, M. Adam, C. Pancu, T. A. Baraboi</i>	Modelling and simulation of the thermal stress at the electric fuses contacts	59
<i>V. Giurgiu, Gh. Oarga, S. Purdel</i>	Analysis of thermal phenomena in high voltage fuse-links	65

	<i>page</i>
<i>C. S. Cañas Peñuelas, L. Fernández, R. Gonzàles</i>	<b>Minimum breaking current obtaining in fuses 69</b>
<b>SESSION 3</b>	<b>FUSE OPERATION I</b>
<i>J. Gärtner, E. Gockenbach, H. Borsi</i>	<b>Influences of high voltage fuses on partial discharge measurement of electrical equipment 77</b>
<i>M.A. Saqib, A.D. Stokes, P.J. Seebacher</i>	<b>Pressure inside the arc channel of a high-voltage fuse 83</b>
<i>H.G. Rex</i>	<b>The influence of the striker wire on the voltage rise after the beginning of the arcing process in HV fuse links 89</b>
<i>K. Jakubiuk</i>	<b>Secondary striation during fuse-elements disintegration 95</b>
<i>R.E. Brown, P.M. McEwan</i>	<b>Unduloid formation and causation of current interruption in current-carrying wires 101</b>
<b>SESSION 4</b>	<b>ARCING PHENOMENA</b>
<i>M.A. Saqib, A.D. Stokes, B. W. James, I. S. Falconer</i>	<b>Arc temperature measurement in a high voltage fuse 107</b>
<i>W. Bussière, P. Bezborodko, R. Pellet</i>	<b>Spectroscopic study of a cutting electrical arc in HBC fuse 113</b>
<i>S. Arai</i>	<b>Geometrical model of discharge space in the state of the high arc voltage generation of capillary arcs 119</b>
<i>V. Murin-Borel, M. Lieutier, M.J. Parizet</i>	<b>Electric field and pressure measurements in high voltage fuses 125</b>
<i>M.A. Saqib, A.D. Stokes, B. W. James, I. S. Falconer</i>	<b>Measurement of electron density in a high-voltage fuse arc 129</b>
<b>SESSION 5</b>	<b>FUSE OPERATION II</b>
<i>A. Wolny</i>	<b>Effect of fuse element confinement on the rate of rise of fuse arc ignition voltage 135</b>

<i>R. Wilkins, H.C. Cline</i>	Assessment of complex loading cycles and estimation of fuse life	141
<i>G. Nutsch, J. Blum, G. Jünemann, P. Linke, T. Reichelt</i>	Overload and rating operations of HBC low voltage fuses at reduced heat transfer	145
<i>J.C. Gómez, J.C. Amatti, C.A. Reineri, M. Principi</i>	Reliability of high breaking capacity fuse	151
<i>H.G. Rex</i>	Variable voltage rise before the beginning of the arcing process in a LV fuse link	157
<i>V.J. Saporita</i>	Using current-limiting fuses to reduce hazards due to electrical arc-flashes	163

**SESSION 6****CIRCUIT PROTECTION**

<i>T. Lipski, R. Partyka</i>	Protection of disturbance arc on bus-bars by means of LV fuses	171
<i>J.C. Gómez, D.H. Tourn, G.R. Zamanillo, J. Lepori</i>	Fuse unexpected operations in soft-starters by dissimilar current distribution	177
<i>J.C. Gómez, G.N. Campetelli, M.A. Basilico, M. Felici</i>	Overcurrent protection of cables by fuses: considering life loss and M-effect	183
<i>C. Ravetta, M. Verdi, M. Tartaglia</i>	Protection of a distribution system: a wide application of electric fuses	189
<i>J. Horiszny, K. Jakubiuk, T. Lipski, R. Partyka</i>	Electrothermal response of fuses on inrush current of distribution transformers	193
<i>H. Bessei, T. Klemme</i>	Dual-element high voltage back-up fuses for power distribution transformer protection	197

**SESSION 7****COORDINATION WITH ELECTRICAL SYSTEMS AND APPARATUS**

<i>Ma Zhiying, Jin Lijun</i>	Research on the operation characteristic of the fuse striker in the switch-fuses combinations	205
<i>W. Aftyka, K. Jakubiuk, T. Lipski</i>	An analysis of coordination of low-voltage circuit-breakers and HBC fuses	209

		<i>page</i>
<i>D. Arato, G. Cantarella</i>	<b>Results of short-circuit tests on contactors protected by fuses</b>	<b>215</b>
<i>V. Giurgiu, Gh. Oarga, S. Purdel</i>	<b>High-voltage fuse-links for motor circuits protection</b>	<b>221</b>
<i>D. Arato, G. Cantarella</i>	<b>Overload protection of contactors by fuses</b>	<b>225</b>
<b>SESSION 8</b>	<b>TESTING AND STANDARDS</b>	
<i>J. Czucha, K. Jakubiuk, T. Lipski</i>	<b>Prospective TRV for test duties 1 and 2 of d.c. traction 3 kV fuses</b>	<b>233</b>
<i>A. Avila Ramirez, E. Baqueiro Absalon, C. Cabrera Rueda</i>	<b>An experimental revision of test duties IEEE C37.41 for distribution cutouts and fuse links</b>	<b>239</b>
<i>E. Furnica, P. Leonte, T. Plesca</i>	<b>Electrical fuses testing modular source used with a new method for plotted time-current characteristic without fusing</b>	<b>245</b>
<i>N.A. Ilyina, G.G. Zhemerov, E.I. Zaika, I.G. Shklovsky</i>	<b>The real-life severity and peculiarities of interrupting test duties of semiconductor fuses</b>	<b>251</b>
<i>G. Crotti, G. Farina, R. Tommasini</i>	<b>Overvoltages produced by low rated current fuse operation in LV installations</b>	<b>257</b>
<b>SESSION 9</b>	<b>MANUFACTURING METHODS AND FUSE RECYCLING</b>	
<i>Lee Sei-hyun, Kim In-Sung, Han Sang-Ok</i>	<b>The test method to acquire the optimal parameter for CL-fuse</b>	<b>265</b>
<i>Wang Jimei, Kong Fanhong, Ma Ziecheng</i>	<b>Study on fluid sand (stone-sand) method for high voltage fuses</b>	<b>271</b>
<i>M.A. Saqib, A.D. Stokes</i>	<b>Characteristics of fuse arcing in different fillers</b>	<b>275</b>
<i>I. Ciutea, T. Plesca, P. Leonte, O. Dumbrava, N. Sufletel, C. Iacob</i>	<b>Reconditioning the HRC fuse links. A test plant</b>	<b>279</b>
<i>G. Fink</i>	<b>Environmentally compatible recycling of high performance fuse links</b>	<b>283</b>

		<i>page</i>
<b>SESSION 10</b>	<b>NEW TYPES OF FUSE AND COMPARISON WITH CIRCUIT-BREAKERS</b>	
<i>J. Sulikowski, K. Cwidak, J. Ossowicki</i>	<b>Miniature layer fuses of high breaking capacity</b>	<b>289</b>
<i>J. Czucha, T. Lipski, J. Zyborski</i>	<b>New current-limiting and interrupting device contra current-limiting fuses</b>	<b>293</b>
<i>Kong Fanhong, Wang Jimei, Ma Ziecheng</i>	<b>A new replaceable fuse-element with current limiting characteristics used on drop-out fuse</b>	<b>299</b>
<i>P. Leonte, T. Plesca, E. Furnica</i>	<b>New high breaking capacity fuses</b>	<b>303</b>
<i>C. Brazzola</i>	<b>Current limitation by circuit-breaker and polymer combination</b>	<b>307</b>
<b>SESSION 11</b>	<b>SEMICONDUCTOR PROTECTION AND TRACTION FUSES</b>	
<i>N.A. Ilyina, G.G. Zhemerov E. I. Zaika, I.G. Shklovsky</i>	<b>The basic principles to engineer high quality fuses for protection of power semiconductor converters</b>	<b>315</b>
<i>M. Adam, A. Baraboi C. Pancu, T. Plesca</i>	<b>Thermal stresses of fuses and protected semiconductor devices</b>	<b>319</b>
<i>G. A. Antonacci</i>	<b>Short-circuits in 3 kV d.c. traction system and fuses - simulation and testing</b>	<b>323</b>
<i>T. Plesca, P. Leonte, E. Furnica</i>	<b>Special ultrarapid fuses to power semiconductor converters protection</b>	<b>329</b>
<i>B. Dilecce, F. Muzio, A. Canova, M. Tartaglia</i>	<b>Behaviour of electric fuses in automotive systems under intermittent fault</b>	<b>333</b>

STATE OF NEW YORK  
IN SENATE

January 15, 1914.

REPORT OF THE COMMISSIONERS OF THE LAND OFFICE  
IN RESPONSE TO A RESOLUTION PASSED BY THE SENATE  
MAY 15, 1913.

ALBANY: JAMES BROWN PUBLISHER, 1914.

PRINTED BY THE STATE PRINTING OFFICE, ALBANY, N. Y.

RECEIVED JAN 20 1914

COMMISSIONERS OF THE LAND OFFICE

ALBANY, N. Y.

STATE OF NEW YORK

IN SENATE

January 15, 1914.

REPORT OF THE COMMISSIONERS OF THE LAND OFFICE

IN RESPONSE TO A RESOLUTION PASSED BY THE SENATE

MAY 15, 1913.

ALBANY: JAMES BROWN PUBLISHER, 1914.

PRINTED BY THE STATE PRINTING OFFICE, ALBANY, N. Y.

RECEIVED JAN 20 1914

## INDEX OF AUTHORS

Adam, M.	59, 319	Dilecce, B.	333
Aftyka, W.	209	Dumbrava, O.	279
Amatti, J.C.	151	Falconer, I.S.	107, 129
Antonacci, G. A.	323	Fanhong, Kong	271, 299
Arai, S.	119	Farina, G.	257
Arato, D.	215, 225	Felici, M.	183
Avila Ramirez, A.	239	Fernández, L	69
Baqueiro Absalon, E.	239	Fink, G.	283
Baraboi, A.	59, 319	Furnica, E.	245, 303, 329
Baraboi, T. A.	59	Garrido, C.	21
Basilico, M.A.	183	Gärtner, J.	77
Bessei, H.	197	Gelet, J.L.	49
Bezborodko, P.	113	Giurgiu, V.	65, 221
Blum, J.	145	Göckenbach, E.	77
Borsi, H.	77	Gómez, J.C.	151, 177, 183
Brazzola, C.	307	Gonzáles, R.	69
Brown, R.E.	101	Hnatiuc, B	43
Burlica, R.	43	Hnatiuc, E.	43
Bussière, W.	113	Horiszny, J.	193
Cañas Peñuelas, C.S.	69	Iacob, C.	279
Cabrera Rueda, C.	239	Ilyina, N.A.	251, 315
Campetelli, G.N.	183	In-Sung, K.	265
Canova, A.	333	Jakubiuk, K.	95, 193, 209, 233,
Cantarella, G.	215, 225	James, B.W.	107, 129
Cidras, J.	21	Jimei, Wang	55, 271, 299
Ciutea, I.	59, 279	Jünemann, G.	145
Cline, H.C.	141	Klemme, T.	197
Crellin, D.	29	Leonte, P.	245, 279, 303, 329
Crotti, G.	257	Lepori, J.	177
Cwidak, K.	289	Lieutier, M.	125
Czucha, J.	233, 293	Lijun., Jin	55, 205

Lindmayer, M.	13	Saporita, V J..	163
Linke, P.	145	Saqib, M.A.	83, 107, 129, 275
Lipski,	171, 193, 209, 233, 293	Seebacher, P.J	83
McEwan, P.M.	29, 101	Sei-hyun, Lee	265
Meng, X.Z.	35	Shklovsky, I.G.	251, 315
Murin-Borel, V.	125	Sloot, J.G.J.	35
Muzio, F.	333	Stokes, A.D.	83, 107, 129, 275
Nutsch, G.	145	Sufletel, N.	279
Ossowicki, J.	289	Sulikowski, J	289
Oarga, Gh.	65, 221	Tartaglia, M.	189, 333
Pancu, C.	59, 319	Tommasini, R.	257
Parizet, M.J.	125	Tourn, D.H.	177
Partyka, R.	171, 193	Tournier, D.	49
Pellet, R.	113	Verdi, M.	189
Plesca, T.	245, 279, 303, 319, 329	Wilkins, R.	25, 141
Principi, M.	151	Wilniewczyc, M.	29
Purdel, S.	65, 221	Wolny, A.	1, 135
Ravetta, C.	189	Zaika, E.I.	251, 315
Reichelt, T.	145	Zamanillo, G.R	177
Reineri, C.A.	151	Zhemerov, G.G.	251, 315
Rex, H.G.	89, 157	Zhiying, Ma	55, 205
Ruggiero, M.	49	Zhiecheng, Ma	271, 299
Sang-Ok, Han	265	Zyborski, J.	293



*System pro M.*  
Non smettiamo  
mai di dare  
alla luce  
nuove idee.

ABB Elettrocondutture

**ABB**

1950

Dear Mr. [Name]  
I have your letter of the 15th and am glad to hear that you are interested in the [Project Name]. I am sure that the [Project Name] will be of great benefit to you and your organization. I will be glad to discuss the details of the [Project Name] with you at your convenience. Please let me know when you would like to meet.

Very truly yours,  
[Name]  
[Title]  
[Organization]

ABB

ABB Engineering

# SIEMENS

## The most complete low voltage fuse system



- High rated breaking capacity
- Strong current limiting
- First class quality
- Minimal heat dissipation
- High ageing resistance
- Extensive range for all types of application - from 2 to 1250 A

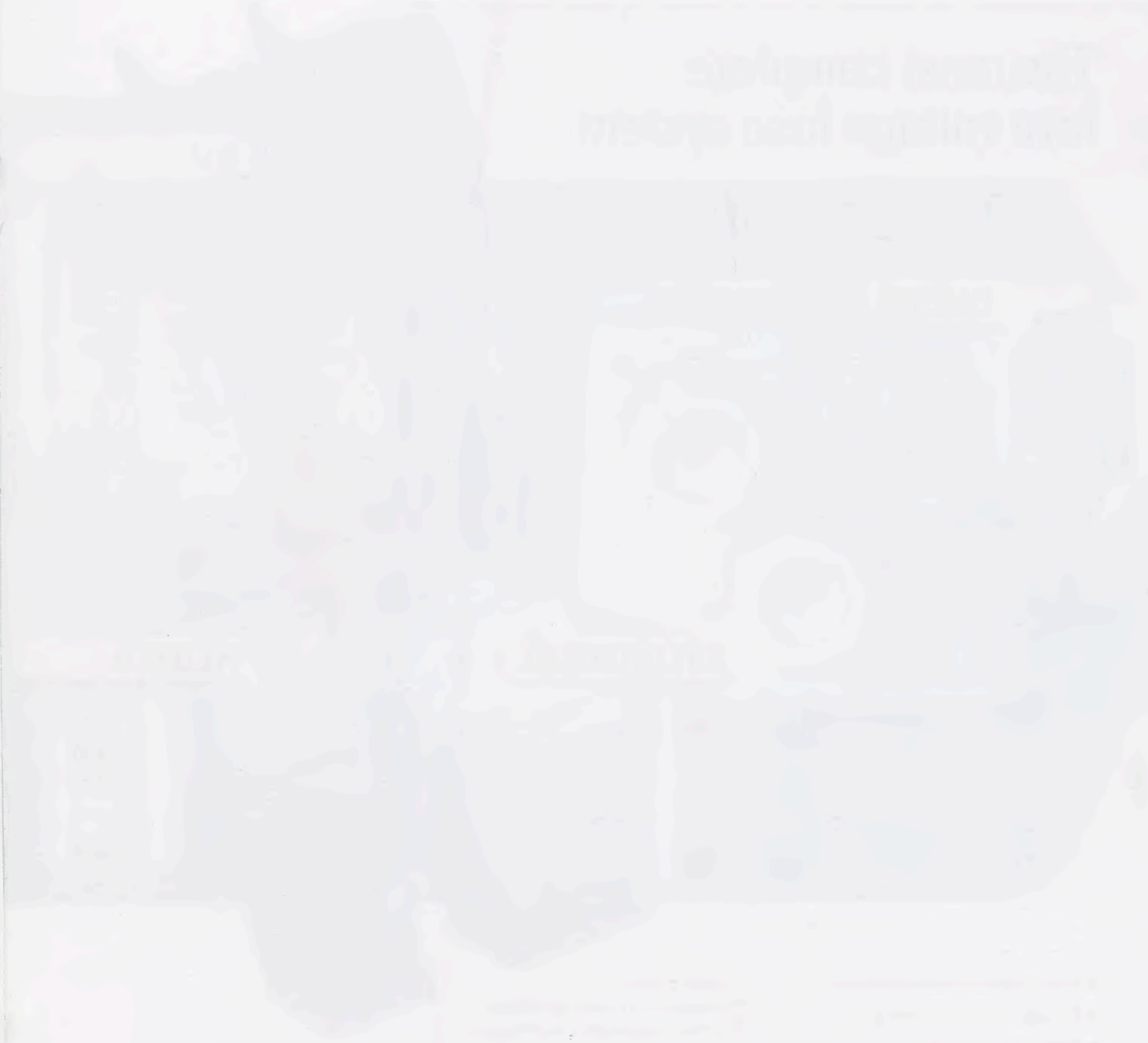
Siemens S.p.A.  
Settore Automation and Drives  
Electrical Installation Technology  
Viale Piero e Alberto Pirelli, 10  
20126 Milano  
Tel. 02.6676.2517  
Fax 02.6676.2231



**The world knows our care for your safety!**

SIEMENS

Intelligent computer  
control systems



Siemens is a leader in the development and production of intelligent computer control systems for industrial plants and power stations. These systems are designed to optimize the performance of complex processes, ensuring maximum efficiency and reliability. The systems are based on advanced computer technology and are capable of handling large amounts of data in real-time. Siemens offers a wide range of solutions, from small-scale control systems for individual machines to large-scale systems for entire industrial plants. The company's expertise in this field is backed by a long history of innovation and a commitment to excellence in engineering and technology.

Siemens AG, Munich, Germany



•Fusibili e portafusibili miniatura in vetro e steatite

•Fusibili e basi tipo Diazed e Neozed

•Fusibili e basi portafusibili cilindrici 8 x 23 - 10,3 x 38 - 14 x 51 - 22 x 58 anche con approvazione UL/CSA

•Fusibili e basi NH

•Sezionatori sottocarico con fusibili NH

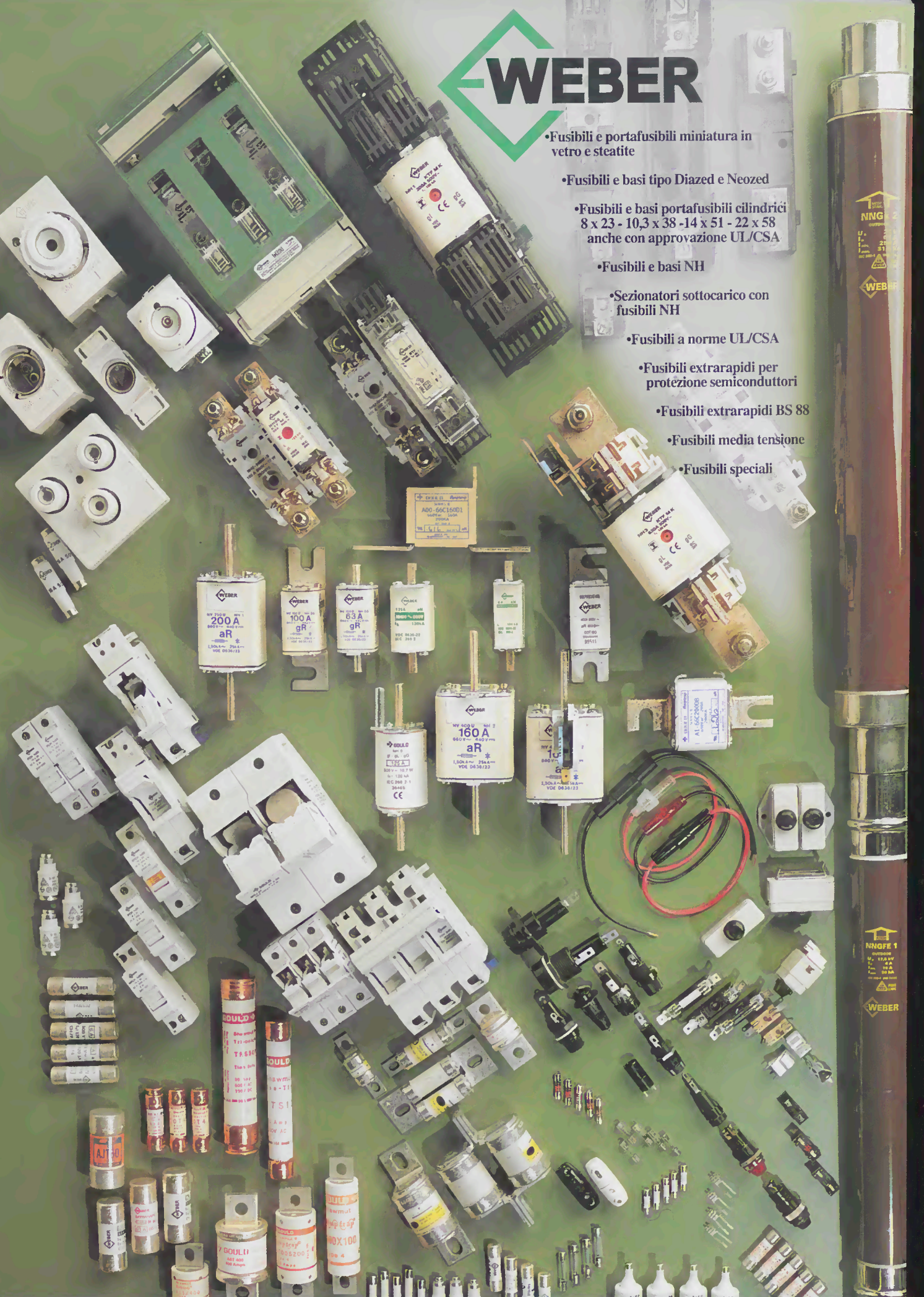
•Fusibili a norme UL/CSA

•Fusibili extrarapidi per protezione semiconduttori

•Fusibili extrarapidi BS 88

•Fusibili media tensione

•Fusibili speciali



**ITALWEBER S.p.A.**

20017 Rho (MI) - Via Risorgimento, 84 - Tel. 02 93 977.1 - Fax 02 93 90 45 64 - e-mail:itw@ibm.net





## Istituto Elettrotecnico Nazionale (IEN) Galileo Ferraris

Strada delle Cacce, 91 - 10135 - Torino, Italy

Phone: +39-011-3919.1 (switchboard)

Fax: +39-011-34 63 84

E-mail: [segr@amm.ien.it](mailto:segr@amm.ien.it)

IEN is a public research institute under the responsibility of the Italian Ministry of University and Scientific and Technological Research. Since its foundation in 1934, IEN has performed fundamental and applied research activity, paying attention to the diffusion of the results on the scientific literature, in industrial sectors, in every day life.

The current research activities can be classified within the following scientific areas (in brackets some major current programmes):

- **Metrology** (new frequency atomic standards, AC quantum Hall effect, absolute electrical experiments, precision measurement of sound velocity in a gas-filled cavity, standards and measuring techniques of high voltage, heavy current and ELF fields, participation in international comparisons, metrology for environment and chemistry);
- **Innovative materials and devices** (preparation, study and characterisation of magnetic materials, thin film technologies for metrology and sensors, production and characterisation of porous silicon, traditional and high critical temperature superconductors, CAD of electromechanical devices);
- **Methodologies for quality** (analysis of electrical apparatus and systems by numerical techniques, computer vision techniques);
- **Education and training** of students, young scientists, scientific and technical personnel.

IEN performs, in the framework of the National Calibration System (SNT) instituted by the Italian law no. 273/1991, the duties of primary metrology institute for time and frequency and for electromagnetic, photometric, radiometric and acoustical quantities, comprising studies and researches aimed at the realisation of the primary standards of the SI measurement units, their maintenance and comparison at international level, dissemination of the SI units.

IEN co-operates with universities and other research institutes devoted to similar scientific and technical objectives; participates in national, European and international research programmes; performs research activities in the framework of contracts with public and private bodies; participates in the scientific and technical activities of national, European and international bodies operating in the areas of metrology and standardisation.

IEN is involved in technical certification activities, concerning specifically:

- calibration of measurement standards and high quality measuring instruments, accreditation of laboratories as SIT calibration centres in the framework of the SNT (105 of the 121 SIT centres till now accredited are in operation; 46 of the 105 SIT centres are traceable and accredited by IEN);
- evaluation of magnetic, dielectric, photometric, radiometric and acoustical properties of materials, components and devices, electromagnetic compatibility measurements;
- short circuit and high voltage tests of components and apparatus of electrical plants, calibration of voltage and current transformers, PD calibrators and ELF meters.

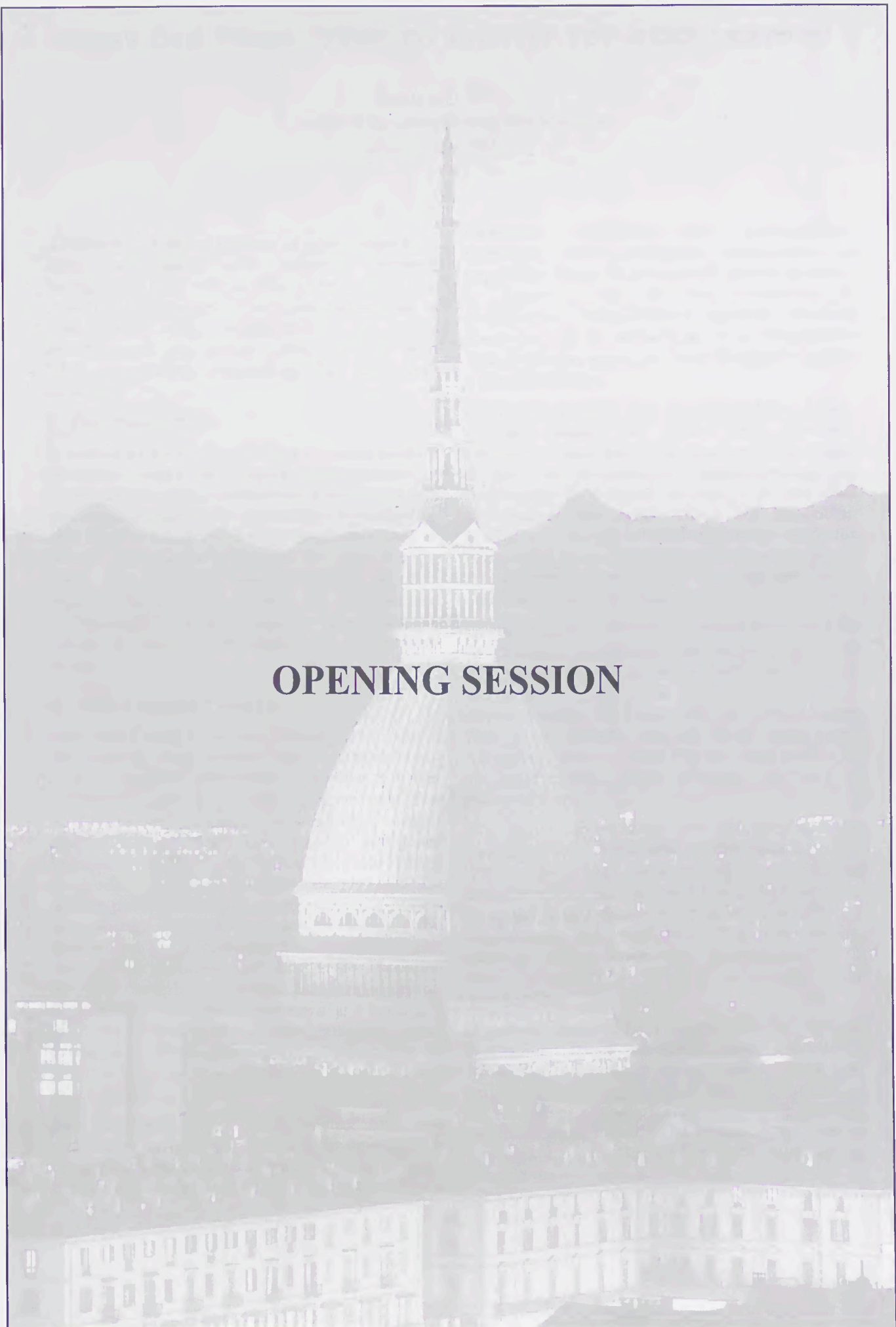
IEN, aware of its role and responsibility, devotes part of its research efforts to the affirmation and strengthening of its cultural heritage.

The activities are performed by the following Departments: Time, frequency and electromagnetic metrology, Electrical metrology, Photometry, Acoustics, Materials, Electromechanics, System engineering, Accreditation of laboratories.

Staff: 139 (60 scientists, 50 technicians, and 29 administrative staff).

THE UNIVERSITY OF CHICAGO  
LIBRARY

[The following text is extremely faint and illegible due to the quality of the scan. It appears to be a multi-column document, possibly a ledger or a list of entries, with a header section at the top and several columns of data below. The text is mirrored across the page, suggesting a bleed-through from the reverse side.]

An aerial photograph of the Illinois State Capitol building in Springfield, Illinois. The building features a prominent, ribbed dome and a tall, slender tower. The surrounding area includes other government buildings and a city street grid. The text "OPENING SESSION" is centered over the image in a bold, serif font.

**OPENING SESSION**



# WHAT CAN FUSES OFFER TO SURVIVE THE NEXT CENTURY

Andrzej Wolny  
Technical University of Gdańsk  
Gdańsk - Poland

**Abstract** A short survey of most important kinds of fuses and current limiters, accompanied by evaluation of impact of the observed trends in fault-current protection is concluded with examination of three technologies: substrate fuses, HCLID and VAF considered promising for the next century.

## I. INTRODUCTION

It seems to be the right time to raise such a question, since the rapid development of power semiconductor devices, increasing role of computerisation in protection techniques, and first of all, the change in preferences of people can cause reduction in demand for fuses. Not only for those conventional. Can some features of fuses be considered „unbeatable”? If the answer were positive efforts of researchers should be centred on them.

## II. THE PRESENT STATE

Over more than a century, fuses play a role of the fastest, most reliable and relatively low-cost current protection devices. Their unquestionable success is undoubtedly due to the idea of application of sand filler, which offered to the fuses the current limitation features, difficult to achieve with other methods over many decades. Hence, in spite of the development of many systems of arc quenching, applicable also to fuses, the sand-filled fuse remains the most popular kind, and probably will, for a few decades more, although the automation and demand for maintenance-free equipment will probably limit their importance. At DC currents, sand fuses have little competition. Hence, e.g. in electric traction the demand for them looks quite stable.

Low price and easy manufacturing make the expulsion fuses still attractive in some areas of application. For instance, the miniature fuses (MF) are manufactured for protection of

electronic circuits, and automobiles. However, the traditional application of expulsion fuses in household power systems in America, and in the protection of distribution transformers against internal short-circuits is shrinking. It is imaginable that the latter area can even disappear in not a distant future.

Some old designs like the liquid-filled fuses, or the simple air fuses with ceramic chambers have probably reached their limit, if not an unexpected break-through in technology or demand occurs. It is true that the former are well suited for mounting inside oil tanks of transformers and for protecting them, however the interest in oil transformers is reducing, for safer dry resin-cast designs are on the market.

In the era of fast development of vacuum and SF<sub>6</sub> contact arc quenching devices, the idea of application of the same methods to fuses surfaced [1-3]. However, the new constructions of fuses fail to revolutionise this area, mostly due to their high cost. Moreover, vacuum and SF<sub>6</sub> are best suited to HV application, where demand for fuses is relatively low.

The most interesting and promising idea seems to be a substrate, or thin film fuse [4-10]. It facilitates far-reaching reduction in volume of current limiting fuses, and permits to avoid utilisation of sand filler. The sand is unpleasant for manufacturers, due to its adverse effect upon the reproducibility of fuse characteristics and automation of production.

A special field of fuse application is current limitation. There are many ideas on taking advantage from melting, overheating or rupturing of a segment of current path, due to the effect of a fault current, which should be interrupted, limited or commutated into a parallel device. Some relatively new ideas emerged.

Presently, such current limiters as  $I_s$ -Limiter of Calor Emag, Ultrup Fuse of Fuji, or PPF of Mitsubishi [11-15], can be called conventional. In these cases, the melting or mechanically disrupted part of the current path is merely used to current commutation into a parallel device, and the final current interruption may be completed by an additional switch.

Effective fault-current limitation and its interruption can also be performed by means of current commutation from an operating fuse into a parallel device, such as a varistor. In such application, the role of the fuse is only to generate an arc voltage high enough to force the current through the parallel varistor.

As a new idea of fuse-like current limiters, a superconductive device can be mentioned [16], which operates by virtue of a sudden increase of its resistance, due to a heating of a fuse-element-like current path above the critical temperature. Some researchers express their expectations with respect to this kind of current limiters.

Another CLID, which cannot be strictly referred to as a fuse is a hybrid current limiting and interrupting device (HCLID), presented by Zyborski [17,18]. HCLID is related to fuse-similar current limiters since, common features with  $I_s$ -Limiters of Calor Emag or Ultrup Fuses are noticeable. In place of explosives used in  $I_s$ -Limiters for the current path interruption, in HCLID a magnetodynamic drive deforms a "one-shot contact" to make a gap facilitating current commutation into a TCB, which substitutes for a parallel HBC fuse used in the former device.

The above-presented short survey of devices, which should pretend to be called fuses, makes it clear that the classical and intuitive definition of fuse needs some modification to embrace all the mentioned kinds of current limiters.

### III. CONDITIONS OF FUSE APPLICATION

There are some new factors influencing fuse application, which are mainly connected with the new possibilities offered by broadly understood computers and power electronics, facilitating automation of protection, drastic reduction in labour-force,

and changes in peoples preferences. On the other hand, quality of transformers, machines and other equipment has increased significantly, thus internal errors occur so seldom that investment in very developed protection systems seems to be unreasonable. The opinion becomes common (not only in the field of protection) that it is more economic letting complete destruction of a device and next replacing it, than preventing (thanks to the protection) far-reaching deterioration and next fixing the faults. Such reasoning would lead to a simplification of protection: only the indispensable means should be left, those preventing disastrous economic effects of faults, and reducing danger to human life. First to remove would be some kinds of fuses owing to their inherent inability to be included in automatic protection system, and the necessity of maintenance.

There is also a different thinking. Cost of undelivered energy increases due to the rise of efficiency of manufacturing. Therefore, any fault should be localised and cleared in the shortest time possible. The break in electric power delivery, due to a fault, should be limited to as few consumers as possible. Such ideas are opposite to the presented above. They will result in application of a fast individual protection just to cut off devices and appliances being out of order. In such a case a simple and reliable "one shot" protection, such as a fuse, is perfect.

Another factor to take under consideration is connected with fault current limitation, which is very important for many devices sensitive to high currents, among others semiconductor power devices and contactors, as well as for systems with very high short-circuit currents. In such cases fuses are almost unbeatable. They are also well suited for the "last resort" protection.

Summing up, factors exist, both reducing and stimulating demand for fuses. These factors will affect, the field of fuse implementation. Undoubtedly, fuses remain attractive as current limiters and individual protection, preventing extensive cutting off in power delivery. However, in all cases when fuses can be replaced by other maintenance-free current breaking devices, or distance controlled protection, probably they will be removed.

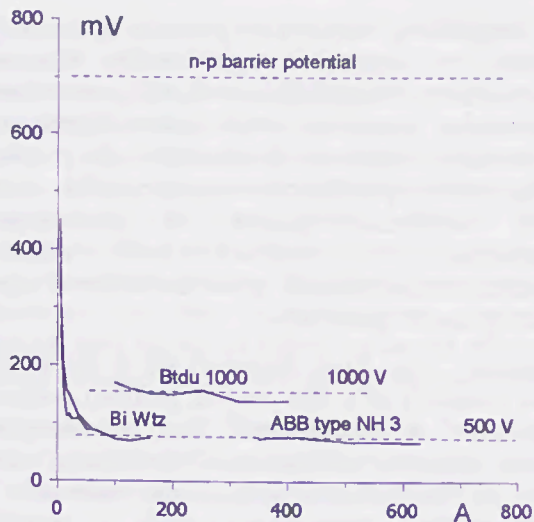


**Fig. 1.** Voltage across terminals of variety of sand filled fuses versus the rated current. Polish make fuses and ABB are compared, both power and semiconductor types.

#### IV. SOME OTHER FUSE FEATURES

Some advantageous features of fuses, such as a small volume compared with that of contact CBs, low cost, as well as low power losses (although higher than those of CBs, significantly lower than losses of semiconductor devices) affecting their demand, should also be mentioned. In Fig. 1 voltage drop across fuse terminals of a variety of Polish make and ABB fuses are compared. It is noticeable that typically, the voltage produced over fuses is lower by a factor of several than that of a n-p barrier potential. Only substrate fuses generate higher voltages across terminals [8] at rated currents. For the same sand fuses, in Fig. 2. power losses are shown, and in Fig. 3. a unit volume per ampere. Except for low rated fuses, the voltage drop across fuse terminals and the unit volume per ampere of fuses of the same rated voltage differ insignificantly each other. Consequently, the power losses are proportional to the rated current of fuse and its rated voltage.

Low volume, low cost, as well as power losses and voltage drop lower than those of semiconductor devices are other features stimulating and facilitating application of fuses [16].

#### V. PROSPECTIVE TECHNIQUES

The above presented concise discussion

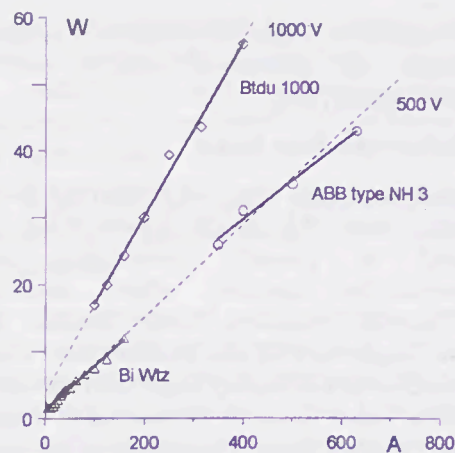


**Fig. 2.** Power losses of a variety of sand filled fuses versus the rated current. Polish make fuses and ABB are compared, both power and semiconductor types.

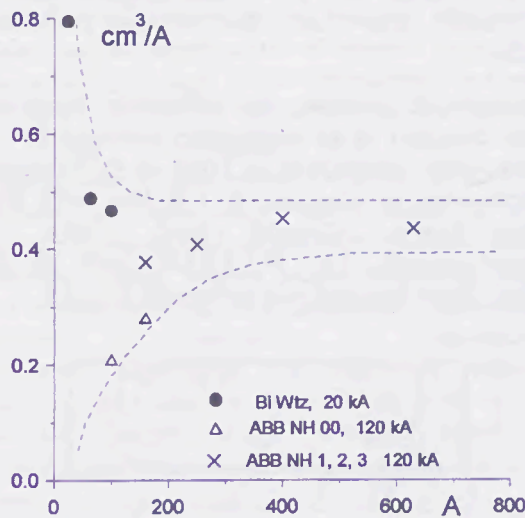


**Fig. 3.** Unit volume of a fuse link per ampere of a variety of sand filled fuses versus the rated current. Polish make fuses and ABB are compared, both power and semiconductor types.

shows that fuses in some fields of application increase their competitiveness by improvement of such appreciated features as: miniaturisation, current limitation, and technology enabling automation of manufacturing. Presently, only special current limiters such as PPF, Ultrup Fuse, or HCLID can be thought of as fuses applicable to, gaining popularity, automatic protection systems.

Examples of developing technologies and ideas are discussed below. The

superconductor current limiters extensively presented on previous ICEFA are not surveyed again [16].

### V.1 Substrate fuse links

Technology of thin film, or substrate fuses is relatively new [4]. Such fuses have been designed to protect developing power semiconductor devices, when sand-filled fuses almost reached their limits. Small thermal capacities of the thinner and thinner semiconductors of costly high current diodes, thyristors and power transistors required shorter thermal time constants of protecting devices. This implied a significant reduction in the fuse-element mass of a given rating fuse, which was only possible by significant increase in cooling conditions. The fuse should also display good current limiting characteristic, and its Joule integral should be readily less than that of the protected device.

Although, at present, the substrate fuses are often thought of as miniature semiconductor fuses, they exemplify a kind of technology, which may be applied to full-size and full-range fuses. Already, such fuses are manufactured, e.g. FULLRAN, and in the future their ratings will probably extend.

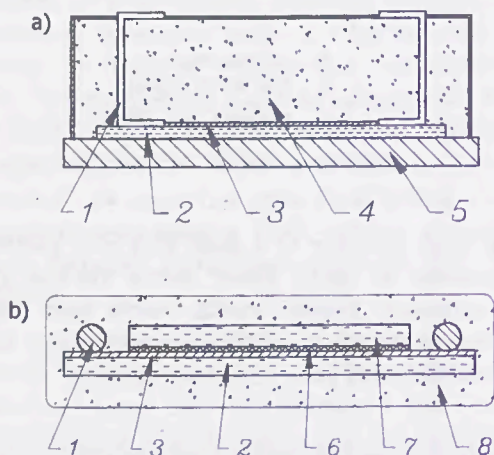


**Fig. 4.** Substrate fuses: a) substrate, sand filled fuse with copper base [8]; b) substrate fuse with cover plate (MLF) [10]: 1-connection, 2 - substrate, 3 - fuse element, 4 - sand, 5 - copper plate, 6 - glaze, 7 - cover plate, 8 - resin

Competitive efforts to substitute a different grain filler for quartz sand [18-22], and this way to improve cooling conditions failed to bring expected results. However, this cannot

be surprising, since any porous material is unable to improve significantly thermal conductivity. Hence, the idea of fuse element deposition upon a well heat conducting substrate, seems presently the most attractive. Typically this substrate is made from alumina, quartz or pyroceram. Sometimes, to improve heat transfer conditions the ceramic plate is soldered upon a thick metal base [8].

Typically, the fuse element of a substrate fuse consists of a few layers, printed, vapour deposited or galvanised. The intermediate layers improve adhesion of the main silver layer to the ceramic plate. Good adhesion is particularly important at sudden overcurrents due to, e.g. motor starting, when the temperature can change in a short time, say by 200 °C. Features of the layers influence  $t-I$  characteristic of a fuse, and can be considered a tool in its formation.

Thickness of the fuse element is very important. The thinner the fuse element, the better its cooling, however, the steeper its  $t-I$  characteristic. Presently, layers of a fuse element are approximately of 1  $\mu\text{m}$  in the thickness, and investigations are in progress on creation of even thinner ones. The problem consists in homogeneity and uniformity of the fuse element. Known methods produce thin layers slightly porous, so their resistivity is readily higher than that of a typical wire or strip.

Formation of fuse elements of substrate fuses is performed by means of similar methods to those used in the technology of integrated circuits. Hence, precision of their shapes is high, and the reproducibility of fuse features depends basically on the thickness and homogeneity of layers. In substrate fuses rated current density acquires unbelievable values. It can exceed 6 kA/mm<sup>2</sup> [8]. Application of laser technology in fuse element formation is also attractive [23,24].

It is interesting, that the technology of manufacturing of fuses tends to resemble that of integrated circuits, and not long ago the success of vacuum arc quenching devices was based on the zone refining method also developed for semiconductors.

In some substrate fuses [4-8], the fuse body, with the ceramic plate inside, on which the fuse element is deposited, is filled with quartz sand. The filler helps to quench the

arc and to recover the post-arc withstand in the same way as that in conventional sand-filled fuses. The basic difference consists in the significantly lower quantity of metal vapours in substrate fuses. Application of a sand filler is inconvenient, since the homogeneity of the filling affects fuse characteristics, and it is not easy to ensure perfect reproducibility of filling parameters. Moreover, in the manufacturing process special care must be taken to avoid adverse effects of sand grains on operating machines.

Therefore, a next important step has been done by substituting another ceramic plate for the sand [9,10]. In such a case the fuse element is placed in a very narrow slot, causing the arc pressure increase and the arc voltage rise. Unlike in sand filled fuses, metal vapours of the decomposed fuse element have no chance to escape rapidly from the arc zone. So, they must be absorbed and bound chemically with the ceramic plates, to ensure sufficient recovery withstand. Thus, the plates material must be carefully selected. It should be chemically active, binding metal vapours of the fuse element, and creating non-conductive compounds. The conventional metal-oxide ceramic fails to meet such requirements. Ossowicki and Sulikowski [9,10] applied for their MLF (miniature layer fuse) plates from a special kind of glass covered with a material reacting endothermically with metals.

In substrate fuses, due to the very high current density, the volume of metal vapours is small compared to the conventional fuses, which facilitates reduction in the fuse volume. Therefore, the fuse sealing becomes easy, and a possible application of additional gas filling, improving current-interruption features of fuses, looks simple.

In conventional sand filled fuses the fuse-element length is due to conditions of overcurrent breaking. Fuse elements of substrate fuses are at least by an order of magnitude shorter than those of sand fuses. This fact positively affects dimensions of MLF.

On the other hand, the voltage drop across the fuse and power losses at rated current may increase, due to the very small cross-section area of the fuse element. Hence, it would be beneficial undertaking efforts to reduce these values.

Substrate fuses display some advantageous features, due to their technology, improving their reliability and reproducibility of characteristics, compared to conventional fuses. First of all:

- the state of the fuse element notch is practically independent of assembly conditions,
- the possibility of mechanical damage, while repeated overloads, e.g. by motor starting, (stress due to dynamic forces and dilatation) to notches of the fuse element is notably limited, which prevents changes in the  $t-I$  characteristic.
- automation of manufacturing is simpler than in the case of sand filled fuses.

Summing up, the conclusion can be formulated that thin film technology may be a similar milestone in the history of electric fuses, as the application of quartz sand filler was a century ago. This technology not only enables a dramatic reduction in the volume of fuses increasing this way their predominance compared to other protection devices, but also improves stability of their characteristics, and facilitates automation of manufacturing, which helps reducing prices and strengthening their economic advantage, despite of complexity of production processes. Moreover, the degree to which a fault current can be limited, as well as the low let-through Joule integral allow for considering them as the best semiconductor fuses.

Presently MLF are exclusively used to protect semiconductors. At 250 V, typically, a single notch is applied. Hence, high voltage designs with several notches in series are expected in the future.

## V.2 Current limiting devices (CLD)

Fuses are considered the most effective and economic current limiting devices (CLD), especially in the case, when high short-circuit currents appear in LV circuits of high rating currents, or at moderately high voltage and relatively low rated currents. In the former case, exploding current limiters, and PPF are applicable, and in the latter one, typically, sand fuses are used.

However, new possibilities emerge. E.g. at low voltages HCLID [17,18], akin to the exploding CLD, can be used, and at high voltages, current commutation to a parallel

varistor, in a varistor assisted fuse (VAF) assembly [25,26] can be beneficial.

### V.2.1 HCLID assembly

The hybrid current limiting and interrupting device (HCLID) was developed by Zyborski [17], based upon the concept of DHR circuit breaker presented by Collard and Pellichero in 1989 [28]. In both devices, there are contacts and a thyristor circuit breaker (TCB) connected in parallel. This way, significant power losses due to a high voltage drop across the TCB are avoided. Also the thyristors can be selected smaller.

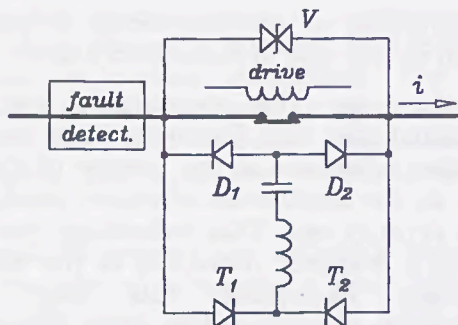


Fig. 5. Simplified diagram of HCLID [17]

On opening contacts, the current is commutated into the parallel TCB and interrupted as soon as possible. The interruption energy is absorbed by a varistor, Fig. 5. If the commutation takes place shortly after a fault has occurred, the fault current will be limited. Thus, the span of time between the fault initiation and contacts opening is crucial for current limitation. Therefore, in place of a heavy mechanical switch used in HDR, Zyborski applied a special contact system with reduced mass and inertia, driven by an electromagnetic drive, operating in less than 100  $\mu$ s. To speed up the operation, the contacts are simply bent by the force of the drive at a moment selected by a fault detection system (SDS), Fig. 5.

The adequate control of magnetodynamic drive and TCB thyristors is the basic problem. The state off should be reached after the gap between open contacts gains full recovery withstand. The current commutation proceeds thanks to the rising voltage across the contacts. To limit fault current effectively, the latter should be triggered as soon as possible, however never

before the electrical withstand of contacts gap is enough to withstand the transient voltage. Zyborski used the delay of 220  $\mu$ s. In Fig.6. the oscillogram of Czucha, Pikon and Zyborski [18] is reproduced, showing traces of the current and the voltage across contacts of their HCLID. In this model IGBT was used in place of TCB.

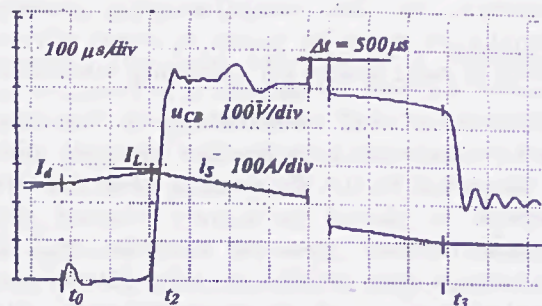


Fig. 6. HCLID: traces of contacts current and voltage.  $u_{CB}$  the voltage across contacts,  $t_0$  the moment of fault discrimination,  $t_2$  the moment of TCB triggering,  $t_3$  the fault current off.

The current limitation and reduction of the let-through Joule integral achieved are comparable in a broad range with those of semiconductor fuses. Presently, the investigations have been carried on substitution of IGBT for the TCB. More detailed information concerning HCLID is provided in the paper of Zyborski in this proceedings.

The point of this short examination of HCLID is a demonstration that methods based upon current commutation used in conventional CLDs like PPF, Ultrap Fuse, or Is-Limiter are still actual, however new elements are also being involved, e.g. such as semiconductor devices, and that their presence must be taken into consideration in the future current limiters designs.

### V.2.2 Varistor assisted fuse (VAF)

Varistor assisted fuse (VAF) was presented a few years ago by Wolny, Stokes and Kacprzak [25]. Its idea was born on comparison of operation costs and features of a sand filled fuse and that of expulsion type. A question surfaced: must current limitation cost so much, if current interruption by an expulsion fuse needs only a fraction of this amount? Moreover, unlike HV sand-filled fuses, expulsion fuses have typically full range

features. The problem consists in the current interruption energy. Just after the arc ignition, in expulsion fuses the gas evolving confinement walls are still relatively cold, and time is needed to increase the pressure, causing gas stream flow efficiently cooling the fuse arc. Therefore, typically, expulsion fuse fail to limit fault currents. However, if the current is commutated into a parallel varistor during the fuse-arc ignition period, the varistor will limit the current, forcing it to zero. The energy deposited in the fuse reduces by an order of magnitude or more [25]. Typically, the energy deposited in a current commutating fuse during the process of commutation is approximately the same as that in the period of arc ignition [27]. This facilitates simplification of the fuse design, and lowers its cost. In Fig.7. typical assemblies of VAF are presented, in which the diagram b) shows that in some cases, typically for HV application, or when  $u-I$  characteristic of the varistor is far from rectangular, an additional switch can be welcome to avoid through-varistor currents after the fault clearing.

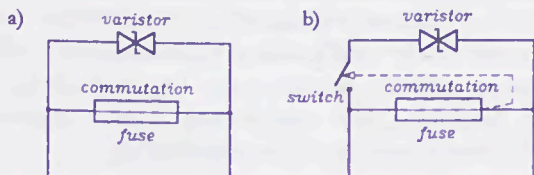


Fig. 7. VAF: a)  $U_v / E \gg 1$ ; b)  $U_v / E \geq 1$

A bulk of the current interruption energy is deposited in the varistor. Dimensioning of the latter depends on the relationship between the varistor threshold voltage  $U_v$  and the system voltage  $E$  (peak value). The higher the varistor voltage the lower the energy deposited in the varistor. This energy  $W_v$  equals to the energy stored in the magnetic field at the moment of current commutation  $W_{mag}$ , and that additional taken from the system  $W_s$  [25].

$$W_v = W_{mag} \cdot \frac{U_v / E}{(U_v / E) - (I_f / \omega)} \quad (1)$$

where  $I_f$  is the normalised rate of fault current rise at the cut-off point, and  $\omega$  is the frequency.

The magnetic field energy  $W_{mag}$  depends on cut-off current and the reactance of the fault circuit, which in turn is related to the prospective fault current. The maximum energy  $W_{mag, max}$  calculated for the peak value of the prospective current is inversely proportional to the inductance of fault circuit:

$$W_{mag, max} = \frac{E^2}{2\omega^2 \cdot L} \quad (2)$$

This implies that the component  $W_{mag}$  of the energy  $W_v$  under the worst conditions reduces as the prospective current rises.

It is evident that the maximum energy  $W_{v, max}$  is deposited in the varistor when current commutation occurs at the peak of current wave. In such a case  $W_{v, max}$  is given by the formula [25]:

$$W_{v, max} = 0.05E \cdot \frac{U_v / E}{U_v / E - 0.72} \sqrt{S_f} \quad (3)$$

where  $S_f$  is the cross-section area of the fuse element. This equation demonstrates that the maximum energy deposited in the varistor is independent of the prospective current. However,  $W_{v, max}$  rises as the system voltage and the square root of the cross-section area of fuse element, which shows that on application of fuses with reduced cross-section area of the fuse element, e.g. a substrate fuse, a reduction in varistor dimensions should be achieved.

Having in mind the fact that the increase in prospective current is due to reduction in the inductance of fault circuit, it can be demonstrated that the energy deposited in the varistor decreases inversely as the prospective current, Fig. 8., [25].

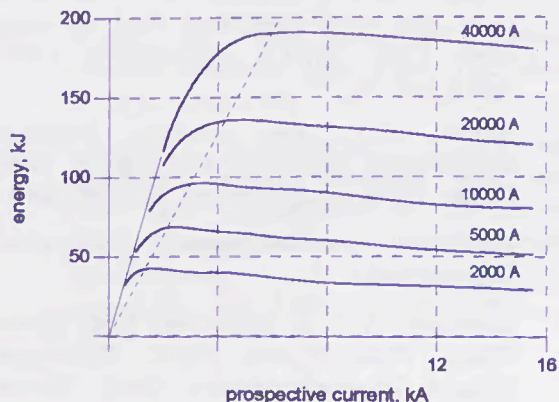
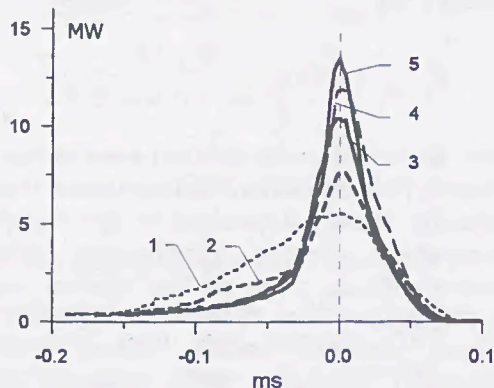


Fig. 8. Energy deposited in the varistor of VAF at  $U_v = 18$  kV,  $E = 11$  kV

Equation (3) also yields another important conclusion, indicating the importance of a proper selection of the varistor voltage  $U_v$ . If the ratio  $U_v/E$  is high enough, the varistor only absorbs the energy stored in the magnetic field, and this energy can be significantly reduced by selecting a commutating fuse with small  $S_f$ , e.g. a substrate fuse.

The analysis given in [27] shows that the energy deposited in the fuse, during current commutation process, is approximately equal to the energy of the fuse element disintegration, Fig. 9., which is almost independent of fault conditions. However, it is proportional to  $S_f$ . This implies that a decrease in  $S_f$  facilitates reduction in both the fuse and the varistor dimensions, without adverse effects on breaking capacity.



**Fig. 9.** Power deposited in the current commutating fuse at various prospective currents: 1 - 1 kA, 2 - 2.2 kA, 3 - 4.4 kA, 4 - 8 kA, 5 - 12 kA; for copper fuse element  $\varnothing$  0.36 mm;  $U_v = 6$  kV

## REFERENCES

- [1] Wang Jimei: Research on horse-shoe core type axial magnetic field vacuum fuse. Proc. ICEFA Nottingham (UK), 1991, pp. 33-36
- [2] Akers, D.J.: SF<sub>6</sub> designs improve distribution switching and fusing, 1989 Power Technology Intern., pp. 267-268.
- [3] Yorkshire Switchgear: Dyscon Interrupter
- [4] Marriage, A.J., B. McIntosh: High speed Thick Film Fuses. Proc. European Hybrid Microelectronics Conf. Stresa (Italy), 1985, pp. 282-287.
- [5] Harrison, R.D., I. Harrison, A.F. Howe: Ageing of film fuses on substrates. Proc. ICEFA, Nottingham (UK), 1991, pp. 85-91.
- [6] Takahashi, H., K. Hirose: A semiconductor fuse-link on a ceramic substrate. Proc. ICEFA, Nottingham (UK), 1991, pp. 92-95.
- [7] Lindmayer, M., M. Luther: Fusing and short-circuit interruption behaviour of metal film fuses. Proc. ICEFA, Nottingham (UK), 1991, pp. 107-113.
- [8] Harrison, R.D., I. Harrison, A.F. Howe: Thin film fuse link. Proc. ICEFA, Ilmenau (Germany), 1995, pp. 169-175.

The above discussion demonstrates that:

- any VAF has almost unlimited current breaking capacity,
- reduction in the cross-section area of a VAF is very beneficial,
- application of substrate fuses in VAF assemblies would be advantageous.

## VI. CONCLUSIONS

Further development of automatic, computerised protection systems, rising importance of automatic manufacturing, increasing reliability of transformers, machines and other devices, and changes in peoples preferences affect the demand for conventional fuses.

Since most kinds of fuses are considered very effective current limiters at LV and medium HV, their application is often associated with the limiting features. However, at LV in some areas they compete with semiconductor CBs.

Special kinds of current commutating fuses can improve current limitation technique at both LV and medium HV.

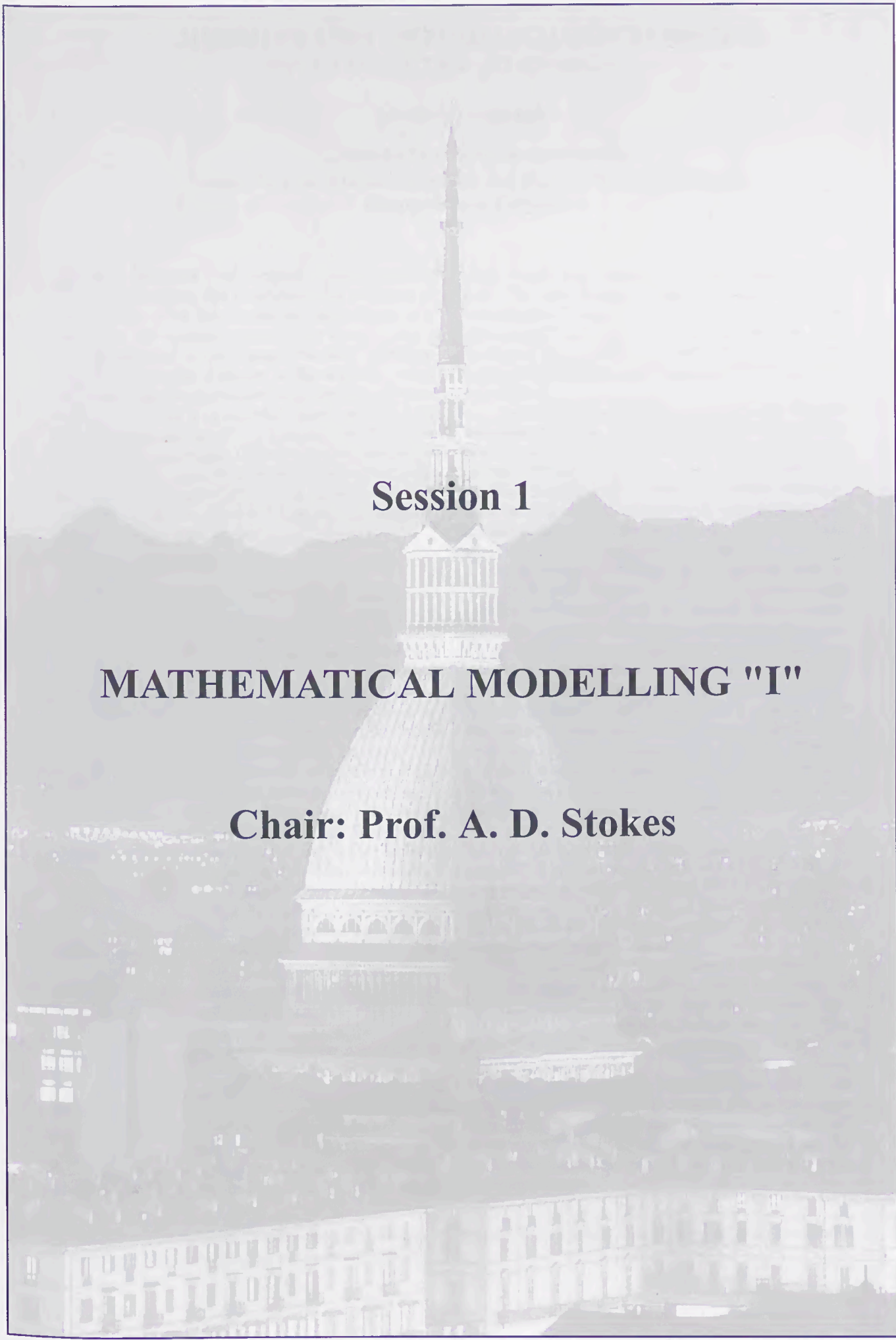
Possible extension of parameters of substrate fuses to higher voltages and currents can increase their application. Combination with ablation effects should not be excluded. It may happen that substrate fuses replace sand filled fuses in some applications.

Thin films technology, ablation effects, and new current commutation techniques seem to be interesting areas of the future development.

- [9] Ossowicki, J., J. Sulikowski: Bezpieczniki warstwowe na podłożu szklano-krystalicznym. Zeszyty Naukowe Wydz. Elektr. Politechniki Gdanskiej, No. 9, 1996, pp. 95-99.
- [10] Ossowicki, J., J. Sulikowski: Postępy w rozwoju bezpieczników topikowych o charakterystyce ultraszybkich. Zeszyty Naukowe Politechniki Poznańskiej, No. 44, 1997, pp. 201-208.
- [11] Itoh T., Miyamoto T., Wada Y., Mori T., Sasao H.: Design considerations on the P.P.F. for a control center. IEEE Trans., vol. PAS-92, No.4, pp.1292-1297, 1973.
- [12] Wada Y., Takagi Y., Mori T., Hamano S., Miyamoto T., Itoh T.: Usefulness of permanent power fuse in control centers with molded case circuit breakers. IEEE Trans., vol. IA-16, No.1, pp.30-39, 1980.
- [13] Nakayama H., Fukazu T., Wada Y., Shinozaki Y., Ibuki K.: Development of high voltage, self-healing current limiting element and verification of its operating parameters as a CLD for distribution substations. IEEE Trans., vol. PD-4, No.1, pp. 342-348, 1989.
- [14] Brückner, P.: Ein neuartiges Schaltgerät mit äußerst kurzen Schaltzeiten. 1958, ETZ-A. vol. 78, pp. 33-40.
- [15] Böttger, C.: The application of I<sub>s</sub>-Limiters in three phase systems. Calor-Emag Elektrizitäts - Aktiengesellschaft D-403 Ratingen (Germany)
- [16] Lindmayer, M., M. Schubert: Current limitation by high temperature superconductors and conducting polymers. Proc. ICEFA, Ilmenau (Germany), 1995, pp. 1-14.
- [17] Zyborski, J., T. Lipski, S. Hassan, J. Wittstock: A new hybrid AC current limiting interrupting device for semiconductor converter protection. Proc. European Conf. on Power Electronics and Application EPE'95, Vol. 3, 1995, Seville (Spain), pp. 3.117-3.120.
- [18] Czucha, J., M. Pikon, J. Zyborski: Ultra rapid IGBT-contact current limiting interrupting device of very high breaking capacity. Inter. Symposium on Short-Circuit Currents in Power Systems. Brussels (Belgium) 1998, pp. 219-222.
- [19] U.S. Patent, Jan. 9, 1990, No. 4,893,106 (solidified sand)
- [20] Eliade, R., E. Budescu: Contributions concerning new extinction media in ultra-fast fuses up to 2000 V a.c. Proc. ICEFA, Nottingham (UK), 1991, pp. 81-84.
- [21] Lipski, T.: Behaviour of stone-sand fuses in short-circuit conditions. Int. Conf. on Gas Discharges and Their Appl., Swansea, (UK), 1992, pp. 204-207.
- [22] Lipski, T., J. Ossowicki: Some aspects of application of stone-sand arc-quenching medium in H.B.C. fuses. Int. Symp. on Switching Arc Phenomena, Łódź (Poland), 1993, pp. 231-235.
- [23] Pawlak R.: Optimization of conditions of laser alloying of silver surface layer. Proc. SPIE: Laser Technology IV, vol. 2202, Bellingham, 1994.
- [24] Pawlak R., Raczyński T.: Selected properties of surface layers of metals alloyed with pulsed laser. Materials Science and Engineering 1993, A168, pp. 67-70.
- [25] Wolny, A., A.D. Stokes, B. Kacprzak: High voltage fuse behaviour with varistor commutation. Proc. IEE, Gen., Transm., Distrib., vol. 141, No. 1, pp. 33-37, 1994.
- [26] Wolny, A., A.D. Stokes: Varistor assisted fuse current breaking. Int. Symp. on Switching Arc Phenomena, Łódź, s. 245-248, 1993.
- [27] Wolny, A.: New protection means: varistor assisted fuse. Proc. ICECAAA, X'ian (China) 1997, pp. 524-528.
- [28] Collard, P., S. Pellichero: A new high speed DC circuit breaker: the DHR. Proc. IEE, Colloquium on Electronic-aided Current-limiting Circuit Breaker Developments and Applications, IEE Digest No. 137, 1989, London (UK).

*[Faint, illegible text, likely bleed-through from the reverse side of the page.]*

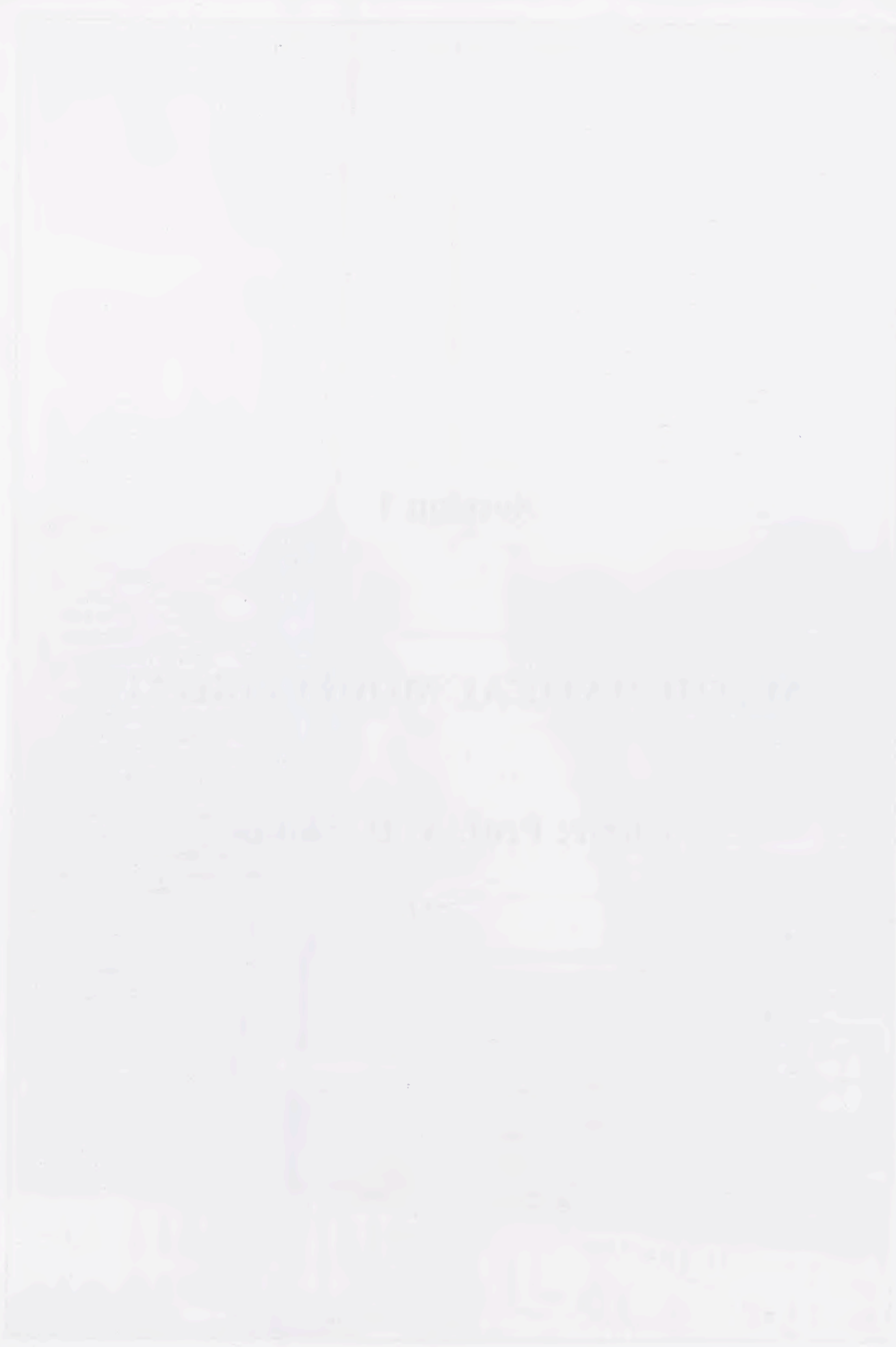
*[Faint, illegible text, likely bleed-through from the reverse side of the page.]*



**Session 1**

**MATHEMATICAL MODELLING "I"**

**Chair: Prof. A. D. Stokes**



# 3D SIMULATION OF FUSING CHARACTERISTICS INCLUDING THE „M-EFFECT“

Manfred Lindmayer <sup>1</sup>

Technische Universität Braunschweig  
Institut für Hochspannungstechnik und Elektrische Energieanlagen  
Braunschweig, Germany

**Abstract:** To predict the melting characteristics of fuses by simulation, the combined field problems of current flow in the fuse conductor, and of heat conduction in the complete fuselink are solved using a three-dimensional Finite Volume Method. Additionally, the dissolution of copper in liquid solder, which serves to adjust the characteristics in the low overload region („M-Effect“), is modeled, based on data from furnace measurements of this process. The simulation method allows to predict the local temperature evolution in the fuse, from the adiabatic short-circuit range to the overload region with fusing times in the hour range. Examples are given and compared to measurements. The agreement is good.

## 1 INTRODUCTION

The time-current characteristic of high-power fuselinks is mainly determined by the geometry of the fuse conductor, the insulating enclosure and the sand filler volume, as well as by their thermal and electrical data (thermal conductivity and capacity, electrical resistivity). Two methods are widely used to adjust the fusing characteristics. Periodic notches in the conductor (current constrictions) determine the near-adiabatic range at high short-circuit currents. The melting- $i^2t$  in this range is directly proportional to the minimum cross-section of the fuse conductor. In time-lag fuses the so-called „M-Effect“ is utilized in the range of low overload current and long fusing times (minute to hour), respectively. A soft solder deposit, generally of tin or tin alloy, in the vicinity of some of the constrictions becomes liquid when a certain overload current is exceeded. It gradually dissolves the fuse conductor of Cu or Ag by diffusion and reduces its cross-section, which in turn leads to further heating until finally melting occurs. This effect shifts the current limit between fusing and non-fusing to lower currents. Related to the same nominal current, M-Effect fuses yield a longer time delay in the overload and short-circuit range, compared to fuses of the same basic design, but without solder.

The adjustment of the fusing characteristic caused by the M-Effect in the overload area depends on many parameters, such as conductor-solder combination, solder volume, conductor thickness and geometry, position of the solder relative to the constrictions, heating intensity in the solder vicinity, and all

other factors that influence the heat balance in the fuse. The new-design of fuses or changes in their characteristics have therefore been a laborious and time-consuming iterative experimental process. Software tools able to model all processes influencing the fusing characteristics could considerably decrease this expenditure.

A realistic simulation has to model the coupled processes of current flow, which determines the local heating power, and of the thermal power balance (= heat diffusion equation), both in a complicated structure consisting of a variety of different materials. Both are described by second order partial differential equations that must be solved by either analytical approximations or numerical methods.

Approaches to simulate these processes have already been made in earlier work. In [1,2,3,4] the temperature distribution, and the thermal and electrical resistances of basic elements of the fuses are described by exact or semi-empirical analytical equations, and combined with iterative solution procedures. In [5] the fuselink is represented by an equivalent R-C network, in [6,7] a similar approach leads to a „transmission line model“. Other simulations discretize the fuselink including its conductor according to Finite Element (FEM) or Finite Difference (FDM) schemes. Because of the typical geometry of fuses a three-dimensional discretization is generally necessary, at least for the heat diffusion problem. In [8,9] a commercial FEM package has been used to model heating of relatively simple fuse geometries without notches and with one single notch, respectively. Other FEM work has been reported in [10,11]. In [12] a 3-dimensional FDM Method, which is similar in principle, was chosen to simulate pre-arcing characteristics.

The dissolution process behind the „M-Effect“ has either not been taken into account in some work, it has been simplified by an „effective melting temperature“ [1], or modeled by a temperature-dependent dissolution speed derived from measurements [8,9]. In [5,13] the basic 2nd order partial differential equation for the local and temporal concentration of Ag in Sn (Fick's second law) has been used. The problem was transferred to an equivalent electric network and solved by a network simulation package. For this the solder and conductor must be finely meshed around the solder spots.

<sup>1</sup> The author is indebted to Messrs. Brogl, Rückling, and Zenkel from Lindner GmbH, Eggolsheim for valuable discussions and for providing measured fuse data.

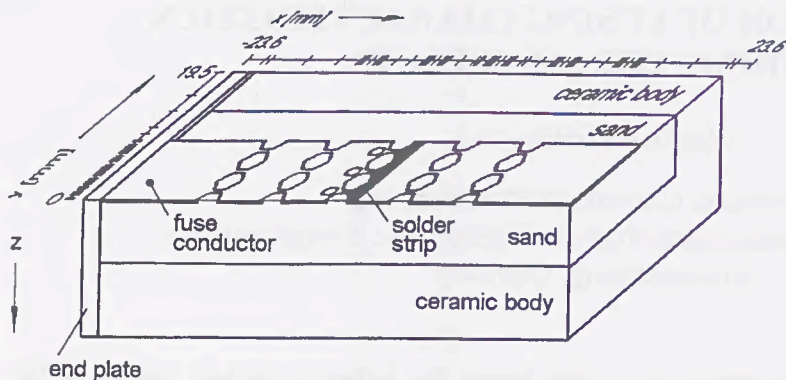


Fig. 1: 3D model of a fuse 100 A, NH 00. (Right end plate removed)

While former work, due to limited computer capabilities, often had to concentrate on partial problems or on parts of the fuse geometry only, the progress in computer technology enables the modeling of more and more complex structures in less time. It has therefore been the aim of this work to develop a Windows-based program code for modeling complete fuses, including the M-Effect, on PCs.

## 2 FDM SIMULATION METHOD

### 2.1 Heat Balance (Heat Diffusion)

The starting point is the power balance equation for each volume element  $dV$  in the integral formulation

$$\iiint \frac{j^2}{\sigma} dV = \iiint \rho c_p \frac{\partial T}{\partial t} dV - \iiint \text{div}(\lambda \cdot \text{grad } T) dV \quad (1)$$

elec. gener.    heat storage    thermal conduction

The left term of equ. 1 (it exists only in the fuse conductor elements) denotes the heating power from the current flow. It is in balance with the heat stored by temporal change of temperature, and the power removed from the element by thermal conduction. For steady state temperature calculations the heat storage term is zero. By using Gauss' integral law, the last term is replaced by

$$- \oint (\lambda \cdot \text{grad } T) d\vec{n}, \quad (2)$$

which expresses that the heat conduction term is equivalent to the power that traverses the surface of the volume element.

### 2.2 Potential Equation and Current Density Distribution

The equation for the electric potential (Laplace equation) is of the same type as equ. 1, but only consists of the conduction term:

$$\iiint \text{div}(\sigma \cdot \text{grad } U) dV = 0 \quad (3a)$$

and

$$\oint (\sigma \cdot \text{grad } U) d\vec{n} = 0, \quad (3b)$$

respectively. When the potential is known from solving equ. 3, the current density  $j$  necessary in equ. 1 follows from

$$j_x = \sigma \cdot \partial U / \partial x, \quad j_y = \sigma \cdot \partial U / \partial y, \quad j_z = \dots \quad (4)$$

$$j = \sqrt{j_x^2 + j_y^2 + j_z^2}$$

The calculation of equ. 3 can be restricted to the region of the fuse conductor. If this is a flat strip it could further be simplified two-dimensionally. To allow for more complicated geometries, the 3D representation was kept throughout. In this case it has proved satisfactory to model the complete thickness of the conductor (in Fig. 1 in  $z$ -direction) by only one element.

### 2.3 Discretization

Fig. 1 gives an example of a fuselink with indications of the discretization. The scheme is in principle identical for both field problems. It is also referred to as Finite Volume Method. The complete three-dimensional simulation volume is divided in  $x$ -,  $y$ -, and  $z$ -direction by a rectangular, not necessarily equidistant grid. The grid points are indexed  $i$  in  $x$ -,  $k$  in  $y$ - and  $l$  in  $z$ -direction. Each brick-shaped domain between 8 adjacent grid points has thermal and electrical properties, which are constant within each domain, but dependent on its average temperature, which changes with time. The domains are indexed according to their left, frontal, upper edge point. The temperature equation (equ. 1, 2) and the potential equation (equ. 3), respectively, are set up as difference equations and solved for all grid points. For this the balance over the control volume around each point  $i, k, l$  consists of the contributions of the 8 neighbor regions, namely:

$i, k, l$  and  $i+1, k, l$  and  $i, k+1, l$  and  $i, k, l+1$  and  $i+1, k+1, l$  and  $i+1, k, l+1$  and  $i, k+1, l+1$  and  $i+1, k+1, l+1$ .

The principle can best be seen for the two-dimensional case, Fig. 2, where only the indices  $i$  and  $k$  are used in  $x$ - and  $y$ -direction, and where each point  $i, k$  shares only 4 neighbor regions. The balance is set up for the area within the dashed lines, which divide each grid distance in two. Further details about the two-dimensional discretization can be seen in [14,15,16]. The three-dimensional procedure is equivalent and yields for each grid point  $i, k, l$  a linear equation of the form

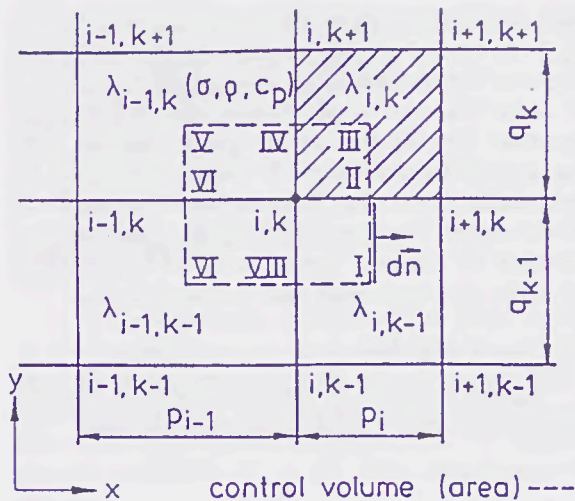


Fig. 2: Discretization (2D).

$$\begin{aligned}
 & -N_{i,k,l} \cdot T_{i,k+1,l} - W_{i,k,l} \cdot T_{i-1,k,l} \\
 & -S_{i,k,l} \cdot T_{i,k-1,l} - E_{i,k,l} \cdot T_{i+1,k,l} \\
 & -G_{i,k,l} \cdot T_{i,k,l+1} - H_{i,k,l} \cdot T_{i,k,l-1} \\
 & + M_{i,k,l} \cdot T_{i,k,l} = D_{i,k,l}
 \end{aligned} \quad (5)$$

This equation links the temperature of point  $i, k, l$  ( $M$  stands for *Middle* coefficient) to its 6 neighbor points in the directions *North, West, South, East, Ground, and Heaven* via the appropriate coefficients. Because of symmetry of the problem, e.g.  $W_{i,k,l} = E_{i-1,k,l}$ , only three sorts of coefficients ( $N, E, G$ ) are needed for each point. They contain the grid distances and the temperature-dependent properties of the partial volumes. The right-hand side  $D_{i,k,l}$  contains the known temperature of point  $i, k, l$  at the old time step, the links to neighboring boundary points (if existing), and, if the volume is a conductor element, the heating power  $j^2/\sigma$  integrated over the control volume. The latter results from the current distribution simulation in the conductor.

Equ. 5 for all points constitutes a system of linear equations of the form

$$\underline{A} \cdot \underline{x} + \underline{b} = \underline{0}, \quad (6)$$

where  $\underline{A}$  is a square matrix containing the  $M, N, E, G$  links to the neighbors,  $\underline{x}$  the vector of the unknown temperatures in the grid points at the new time step, and  $\underline{b}$  the vector of known values that result from the boundary points and the temperatures at the last time step as well. As the coefficients of  $\underline{A}$  depend on the temperatures, equ. 6, which is an implicit scheme for the unknown temperatures, must be set up and solved for every time step. (It has proved that the temperature values from the latest time step are accurate enough for this, so iterations of these coefficients within each time step are not necessary.)

#### 2.4 Boundary Conditions

In the potential calculation the Dirichlet condition  $U=0$  is taken for the left end plate and  $U=1$  V for the right one, while the other boundaries are iso-

lated ( $\partial/\partial n = 0$ ). After integrating the resulting current densities across one of the end plates the voltage drop is corrected linearly to the actual current. The current may be kept constant or vary with time, e.g. sinusoidally. For the work reported here D.C. current was used, yielding directly the virtual melting time.

For the temperature boundaries the outer coordinates of the end plates were assumed to have constant temperature (Dirichlet). To account for the heating by the contact resistance and the current leads [1], temperatures higher than room temperature, e.g. 80 °C, were taken. The outer areas of the ceramic body were treated as heat transmission to the surroundings with  $1.2 \cdot 10^6$  Watts per square millimeter and Kelvin of super-temperature. It was found, however, that this has little effect, and that these areas could be regarded as thermally isolating.

Symmetries were taken into account by appropriate symmetry conditions. The example of Fig. 1 represents the complete fuse length in  $x$  direction, but it is symmetrical with respect to  $y=0$  and  $z=0$ . (Though the solder layer is applied only one-sided in  $z$  direction, the method described in section 3.2, Fig. 5b allows to use symmetry conditions.)

#### 2.5 Computation Procedure

To solve the large equation system (equ. 6) - the thermal model of Fig. 1 consists of approx. 35 000 nodes - a fast iterative solution method with preconditioning [17] was chosen. For simulations of the stationary state the potential/current density simulation and the stationary temperature simulation were carried out alternately with actualized material data at every step, until the results converged. For the simulation of temporal temperature evolution the potential/current density calculation should normally be followed by the next time step of the dynamic temperature calculation, and so on. It was found out that it is sufficient for the usual fuse conductor geometries to compute the current distribution only once at the beginning, despite of the considerably changing temperature and hence electrical conductivity distribution. The current has to flow through the constrictions anyhow, so the current density distribution, especially in the notches where most of the heat is generated, does not vary much.

The dynamic calculation is finished when the melting point in the hottest spot of the conductor is reached.

### 3 MODEL OF FUSE CONDUCTOR DISSOLUTION IN SOLDER

#### 3.1 Diffusion Data

The dissolution of silver or copper in solder, which becomes appreciable when the liquidus temperature of the solder is exceeded, is a rather complex process, and it has to be more or less simplified. Following Cu and Sn stand also for other combinations of solid metal and solder. Diffusion may be described by Fick's second law [13] for the concentration  $C$  (in this

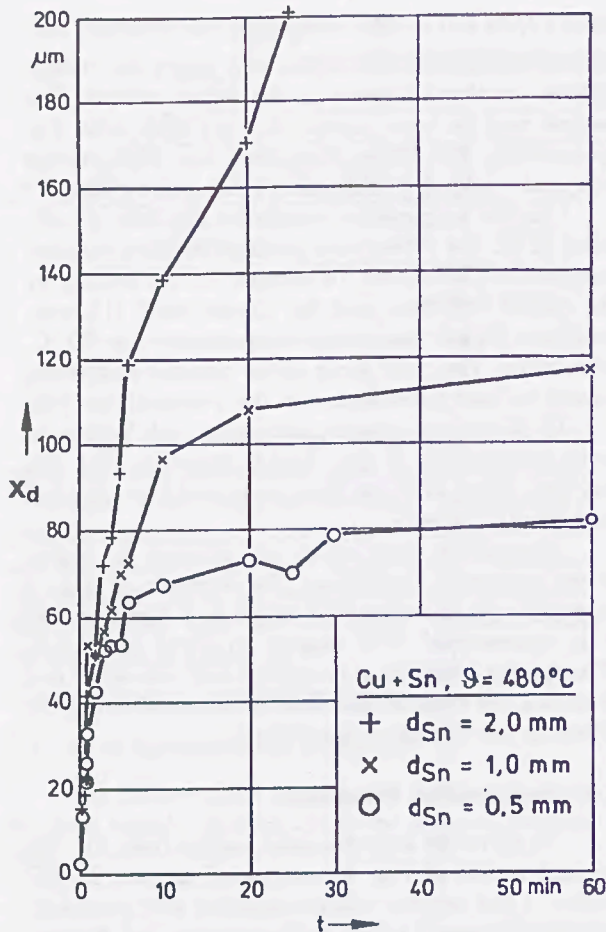


Fig. 3: Mean dissolution depth of Cu in Sn for different solder thickness  $d_s$ ,  $d_{Cu} = 200 \mu\text{m}$ ,  $\theta = 480^\circ\text{C}$ .

case the concentration of copper in liquid tin or tin alloy).

$$\frac{\partial C}{\partial t} = D \frac{\partial^2 C}{\partial x^2} \quad (7)$$

The diffusion constant  $D$  is temperature-dependent and follows the Arrhenius law.

$$D = D_0 \cdot \exp[-Q / (kT)], \quad (8)$$

where  $Q$  is an activation energy.

Equ. 7 also describes the diffusion of liquid Sn into solid Cu, however this process is negligible in comparison [18]. The solution of equ. 7 yields a quadratic increase of dissolution depth with time, which has been observed by some authors [13,19]. Equ. 7, which describes any diffusion process in principle, applied to the diffusion of a solid metal (concentration  $C=100\%$ ) into a liquid metal (solder) would yield an ever increasing concentration and cannot account for the fact that there is clearly a temperature-dependent saturation. Also the exact local gradient of concentration within the solder would play an outstanding role. It has been shown clearly in furnace experiments [8] that the depth of Cu (and Ag, respectively) consumption („dissolution depth“) by liquid Sn or Sn alloy approaches a temperature-dependent saturation value,

which is roughly proportional to the solder thickness, Fig. 3. A detailed consideration in [8] proves that this correlates with the maximum amount of Cu soluble in the liquid Sn, and which follows the temperature-dependent liquidus line of the phase diagram [20], plus an additional amount of copper consumed by intermetallic layers that form between the solid Cu and the solder. The dissolution depth  $x_d$  and the concentration by volume  $C$ , respectively, of Fig. 3 follow a  $[1 - \exp(-t/\tau)]$  curve rather than a square root law:

$$x_d(t) = x_{\text{sat}} \cdot [1 - \exp(-t/\tau)] \quad (9)$$

$x_{\text{sat}}$  and  $\tau$  depend on the temperature  $\theta$ . The differentiation of equ. 9 yields the dissolution speed:

$$v_d = v_0 \cdot \exp(-t/\tau) \quad (10)$$

This means that the dissolution speed starts with an initial value  $v_0$  and decreases to zero as the final concentration  $C_{\text{sat}}(\theta)$  is approached. The simplest and physically sound way to account for this is to assume that the volume concentration of conductor metal in the liquid solder is constant across the molten pool, and that the dissolution speed depends on the concentration ratio

$$v_d(C, \theta) = v_0(\theta) \cdot [1 - C/C_{\text{sat}}(\theta)] \quad (11)$$

The momentary concentration by volume  $C$  is related to the dissolution depth  $x_d$  by

$$C = x_d / (d_s + x_d) \quad (12)$$

Fig. 4 shows results of  $C_{\text{sat}}(T)$  derived from the liquidus line [20] and of  $v_0(T)$  measured by [8] in an

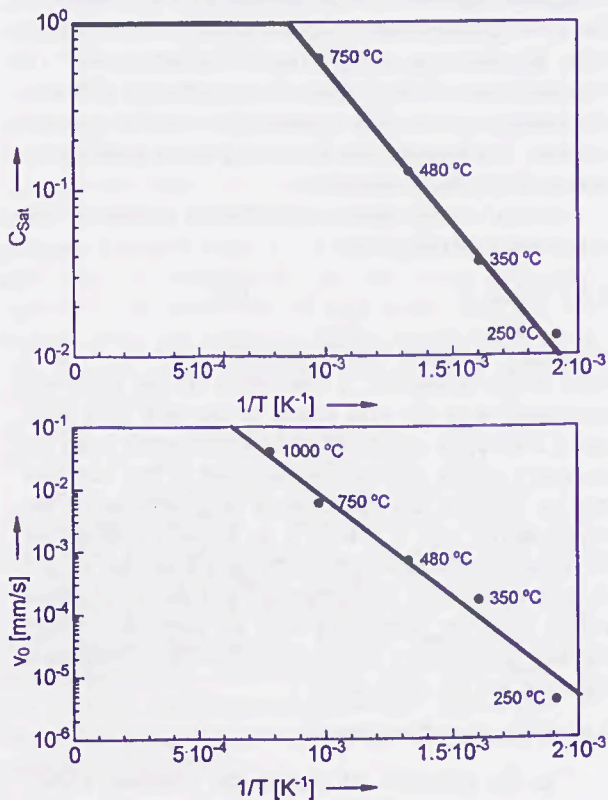


Fig. 4: Saturation concentration  $C_{\text{sat}}$  and initial dissolution speed  $v_0$  of Cu in liquid Sn.

Arrhenius plot. They can be approximated by

$$C_{Sat} = \max \left\{ \frac{32.8 \cdot \exp\left(\frac{-4150 \text{ K}}{T}\right)}{1} \right\} \quad (13)$$

$$\frac{v_0}{\text{mm/s}} = 155 \cdot \exp\left(\frac{-7640 \text{ K}}{T}\right) \quad (14)$$

In the subsequent simulations the factor in equ. 13 was doubled, i.e. 65.6 instead of 32.8, because this gave the best correlation with measurements. This is physically justified because the additional consumption of Cu by intermetallic layers (at lower temperatures up to 100% [8]) is not taken into account by equ. 13.

### 3.2 Implementation into FDM Model

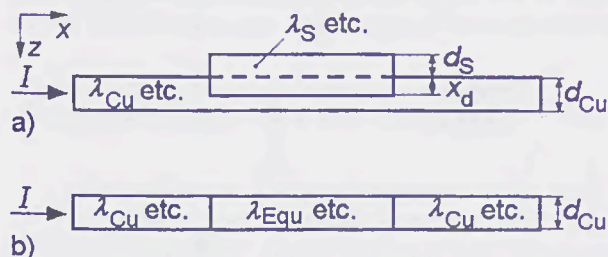


Fig. 5: Replacement of conductor/solder sandwich by an equivalent conductor.

a) original sandwich b) equivalent

The assumption of a concentration  $C$  independent of the local position within the solder pool enables the simplification in  $z$  direction illustrated in Fig. 5. Instead of a complete discretization across the conductor/solder sandwich, this cross-section is replaced by an equivalent conductor of the original thickness  $d_{Cu}$ , but with equivalent data for the electrical and thermal conductivity, such as

$$\lambda_{Equ} = \frac{\lambda_{Cu}(d_{Cu} - x_d) + \lambda_S(d_S + x_d)}{d_{Cu}}, \quad (15)$$

i.e. both parts are switched parallel and concentrated into one equivalent conductor. This is justified because the current flows mainly perpendicular to the  $z$  direction and the temperature difference across the sandwich thickness is only small. The data of  $\lambda$ ,  $\sigma$  for the solder vary with the solder composition and are not known. It was found out by comparison be-

tween simulations and measurements, however, that the best approximation is to assume them to be negligibly low. Then the electrical and thermal transport is only determined by the remaining copper thickness. This seems justified, too, because the conductivities of liquid solder and of intermetallic Cu-Sn compounds are known to show low values compared with the base metal. The heat capacity of the solder is treated accordingly, but not neglected.

The dissolution depth  $x_d$  at each time step and each solder location is calculated by adding  $\Delta t \cdot v_d$  to the  $x_d$  values accumulated during the previous time steps.  $v_d$  follows from equ. 11.

## 4 SIMULATION EXAMPLES AND COMPARISON WITH MEASUREMENTS

### 4.1 Fuse Models

As an example Fig. 6 shows a section of the 100 A fuse conductor of Fig. 1. Due to symmetry only one half of the six parallel rows of constrictions is modeled in  $y$  direction. If the effect of the sand and the ceramic part lying outside the conductor geometry in  $y$  direction could be neglected, it would have been sufficient to model only a small disc-shaped portion (1/12) of the complete fuse between  $y = 0$  and the dashed line. The trapezoidal notches (neck width 0.5 mm, length 1 mm) plus the additional round heating holes are replaced by step-shaped contours. The hatched area covered by solder extends over a multitude of elements, thus enabling the local resolution of the Cu dissolution process.

In order to model the adiabatic range at high currents correctly, the heat capacity of the  $z$  layer adjacent to the conductor layer (whose thickness is half of the conductor thickness of  $\approx 0.15$  mm) should not add much to the resulting heat capacity of the relevant nodes. This means that the thickness of the first sand layer has to be small [21], e.g.  $< 0.1$  mm. The thickness of the following layers is increased gradually.

There are in principle many ways to fit the simulation data to measurements, especially the data of solder dissolution. For the electrical resistivity, heat conductivity and heat capacity of the Cu conductor and the ceramic body standard data from the literature were taken, with a first order dependence on temperature. The data for sand are based on measurements in [8]. Depending on the sand quality the heat conductivity ranged between 0.27 and 0.4 W/(m·K), with a temperature coefficient between  $1.26 \cdot 10^{-3}$  and  $1.37 \cdot 10^{-3} \text{ K}^{-1}$ . Due to the best agreement the lower

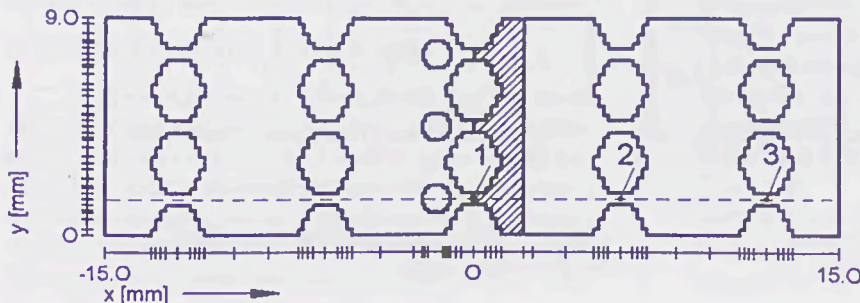


Fig. 6: Section of the fuse conductor of Fig. 1. Dashed Line: Temperature path for Fig. 8

values were taken. The specific heat was taken as  $0.6 \text{ Ws/(g}\cdot\text{K)}$ , with a temperature coefficient of  $1.7 \cdot 10^{-3} \text{ K}^{-1}$  [8]. The solder diffusion was modeled with the data from section 3.1.

#### 4.2 Simulation Results

The simulation yields the temporal evolution of electric potential, current density, and temperature at any point. The following typical results were gained for the fuse of Fig. 1, Fig. 6 with a deposit of solder 0.6 mm thick.

Fig. 7 depicts the simulated evolution of the temperatures as well as the solder dissolution depth with three currents that are typical for different regimes. In Fig. 8 the temperature profiles when the hottest spot just reaches melting temperature are shown for these cases.

At  $1.6 \cdot I_n$  the solder dissolution is the governing mechanism. The solder dissolution starts slowly when the solder melting point is exceeded. The temperatures

after an initial rise to nearly stationary conditions increase only slowly due to the decreasing Cu thickness. (Without solder the hottest point, position 1, would reach a stationary temperature of around  $350 \text{ }^\circ\text{C}$ .) Finally, when most of the copper thickness has been consumed, the situation tilts. The temperature approaches quickly the melting point in the central constrictions with the solder deposit, the complete Cu thickness is being diffused through in these spots. Except for the sharp peak resulting from the final heating, the temperature profile (Fig. 8) shows a continuous drop from the center to the end plates

At  $25 \cdot I_n$  on the other hand, the heating process is nearly adiabatic. All constrictions - except for the central ones (position 1), whose heat capacity is higher due to the solder - show an identical progressive temperature rise until they melt after a few milliseconds. The profile clearly shows that the heat generated in the necks has not diffused outward yet. The solder dissolution in this short time is practically zero.

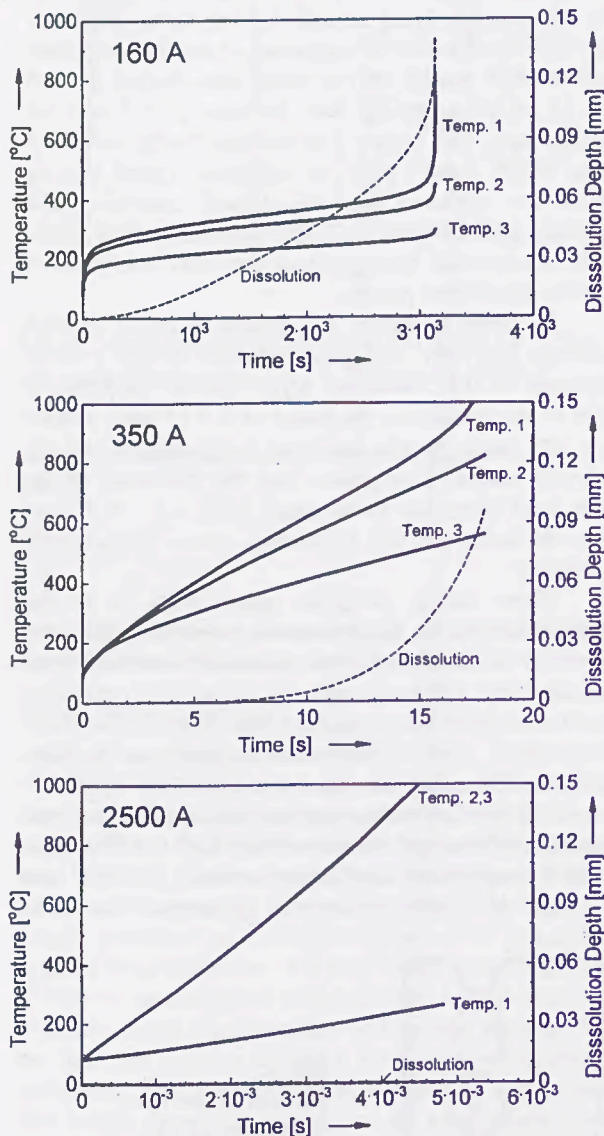


Fig. 7: Temporal evolution of temperature at different points and dissolution depth at point 1 for different currents.

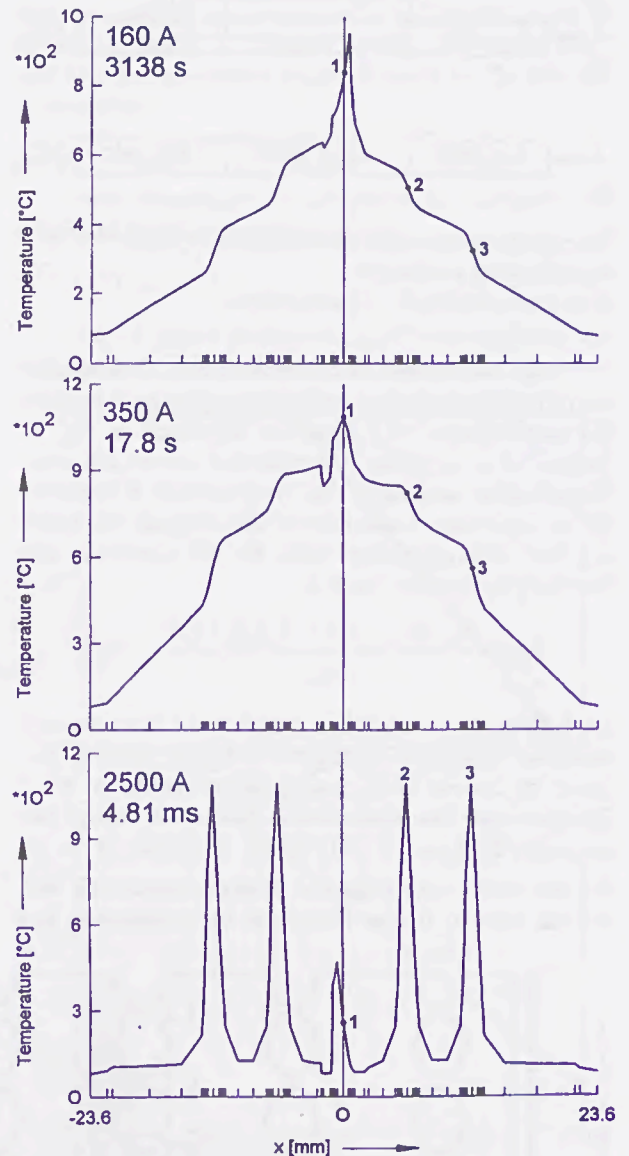


Fig. 8: Temperature profiles on melting for different currents.

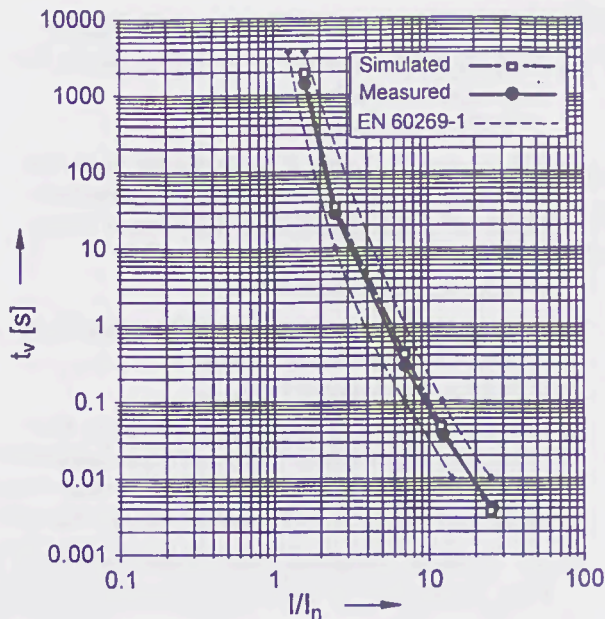


Fig. 9: Comparison of simulated and measured fusing characteristics. 50 A Fuse NH 00, gG.

The current  $3.5 \cdot I_n$  with a fusing time of the order of 20 seconds is an intermediate condition where the solder dissolution just begins to play a role. The time scale is long enough for the heat to diffuse out of the constrictions, but still far from near-stationary. The dissolution depth at the moment of melting has reached about  $2/3$  of the total conductor thickness, the reduced copper cross-section has already contributed to some additional heating. The peak in the temperature profile in the center is also an indication of this. A comparison with Fig. 10 shows that in this current range the time-current characteristic begins to deviate from that of an identical fuse without solder.

Fig. 9 compares time-current characteristics of simulations and measurements of a 50 A fuse. It has three parallel rows of necks with similar main dimensions as those of Fig. 1/ Fig. 6. The dashed lines mark the region determined by EN 60269-1 / IEC 269-1. The good agreement, which was also found for fuses with other rated currents, confirms the usefulness of the simulation method as a tool for fuse design.

To demonstrate the influence of the „M-Effect“ on the fusing characteristic, Fig. 10 shows a comparison with an additional simulation, where the solder has been removed. The fusing characteristics are identical for  $I/I_n \geq 4$ . Below this threshold the dissolution process becomes effective and shifts the characteristic towards lower currents and times, respectively.

## 5 SUMMARY AND CONCLUSION

A three-dimensional FDM model for the simulation of fuses has been presented, including a model of the dissolution of the fuse conductor in liquid solder („M-Effect“). It simplifies the diffusion process by a dissolution speed, which depends on the temperature and the concentration of conductor metal in the solder. Examples of typical simulation results have been

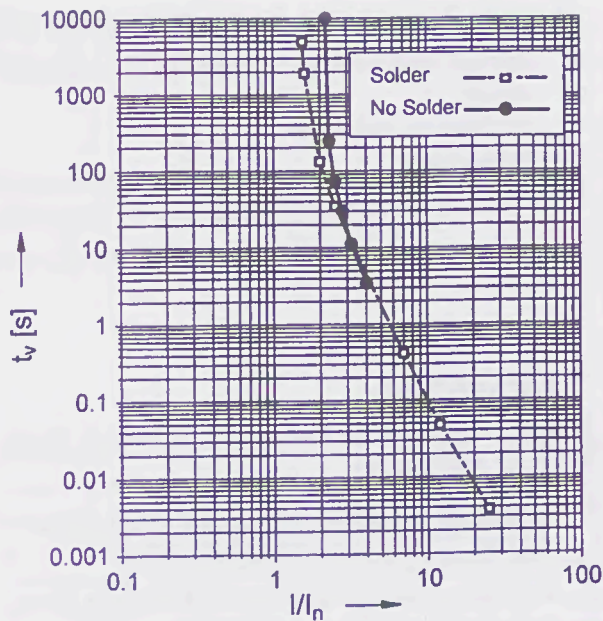


Fig. 10: Simulated pre-arcing times without solder and with solder.

presented and discussed. The good agreement between simulated and measured time-current characteristics confirms the usefulness of the simulation method as a design tool.

## 6 LIST OF SYMBOLS

$A$	coefficient matrix
$b$	vector of known quantities
$C$	concentration (by volume)
$C_{\text{Sat}}$	saturation concentration
$c_p$	specific heat
$D, D_0$	diffusion constant
$d_{\text{Cu}}$	thickness of (Cu) conductor
$d_s$	thickness of solder layer
$d\vec{n}$	element of surface area
$dV$	volume element
$I$	current
$I_n$	rated current
$i, k, l$	indices
$k$	Boltzmann constant
$j$	current density
$t$	time
$Q$	activation energy
$T$	absolute temperature
$t_v$	virtual melting time
$U$	voltage, electric potential
$v_d$	dissolution speed
$v_0$	initial dissolution speed
$x, y, z$	Cartesian coordinates, directions
$x_d$	dissolution depth
$x_{\text{Sat}}$	saturation dissolution depth
$\underline{x}$	vector of unknown temperatures (potentials)
$D, E, G, H, M, S, W$	coefficients of difference equation
$\Delta t$	time increment
$\lambda$	thermal conductivity

- $\lambda_{Cu}$  thermal conductivity of (Cu) conductor  
 $\lambda_s$  thermal conductivity of solder  
 $\rho$  density  
 $\sigma$  electrical conductivity  
 $\vartheta$  temperature  
 $\tau$  time constant

## 7 REFERENCES

ICEFA = International Conference on Electric Fuses and their Applications.

- 1 R. Wilkins: Simulation of Fuselink Temperature-Rise Tests. 2<sup>nd</sup> ICEFA, Trondheim 1984.
- 2 R. Wilkins: Steady-State Current Sharing in Fuses with Assymmetrical Arrangements. 4<sup>th</sup> ICEFA, Nottingham 1991.
- 3 M. Laurent, P. Schaditzki: Fuse-Element - Ageing and Modeling. 3<sup>rd</sup> ICEFA, Eindhoven 1987.
- 4 J.G.J. Sloot: Analog Simulations of the Heat Flow in a High Voltage Fuse. 3<sup>rd</sup> ICEFA, Eindhoven 1987.
- 5 D.A. Beaujean, P.G. Newbery, M.G. Jayne: Modelling Fuse Elements using a C.A.D. Software Package. 5<sup>th</sup> ICEFA, Ilmenau 1995.
- 6 D. de Cogan, M. Henini: TLM Modelling of Thin Film Fuses on Silica and Alumina. 3<sup>rd</sup> ICEFA, Eindhoven 1987.
- 7 L.A.V. Chepel, A.F. Howe: Calculation of Pre-Arcing Times by Transmission-Line Modelling (TLM). 4<sup>th</sup> ICEFA, Nottingham 1991.
- 8 M. Hofmann: Experimentelle und rechnerische Untersuchung von Ansprechennlinien und Alterungsvorgängen bei Sicherungsschmelzleitern. Thesis TU Braunschweig 1987.
- 9 M. Hofmann, M. Lindmayer: Precalculation of Time/Current Characteristics of „M“-Effect Fuse Elements. 3<sup>rd</sup> ICEFA, Eindhoven 1987.
- 10 M. Xian-Zhong, W. Ji-Mei: The Simulation of Prearcing Characteristics of Fuse Elements in the Finite Element Method. 3<sup>rd</sup> ICEFA, Eindhoven 1987.
- 11 J.C. Gomez, D. Tourn, P.M. McEwan: Investigation of the Pre-Arcing Behaviour of Dissimilar Uniform Double-Elemented Filled Fuses, Using CAD Techniques. 4<sup>th</sup> ICEFA, Nottingham 1991.
- 12 C. Garrido, J. Cidras: Analysis of Prearcing Time-Current Characteristic of Fuselinks. 4<sup>th</sup> ICEFA, Nottingham 1991.
- 13 D.A. Beaujean, M.G. Jayne, P.G. Newbery: Determination of M-Effect Diffusion Parameters in High Breaking Capacity Fuses. IEE Proc.-Sci. Meas. Technol., Vol. 142, March 1995, p. 162
- 14 S.V. Patankar: Numerical Heat Transfer and Fluid Flow. Hemisphere Publishing Corporation 1980.
- 15 H. Eckhardt: Numerische Verfahren in der Energietechnik. Teubner Studienskripten, Stuttgart 1978.
- 16 M. Lindmayer: Simulation of Stationary Current-Voltage Characteristics and of Back-Commutation in Rectangular Arc Channels. 17<sup>th</sup> Int. Conf. on Electrical Contacts, Nagoya 1994.
- 17 D.S. Kershaw: The Incomplete Cholesky-Conjugate Gradient Method for the Iterative Solution of Systems of Linear Equations. Journal of Computational Physics, 26, 1978, pp.43-65.
- 18 H. Fidos, H. Schreiner: Feuerverzinnung von Kupferschaltdrähten, Teil1. Zeitschrift für Metallkunde 61 (1960), pp.225-228.
- 19 S. Øvland, J. Kulsetås, H. Förster, W. Rondeel: Metallurgical Deterioration of Copper Fuse Elements in High Voltage Fuses. 2<sup>nd</sup> ICEFA, Trondheim 1984.
- 20 M. Hansen: Constitution of Binary Alloys. McGraw-Hill 1958.
- 21 M. Luther: Flinke Hochleistungs-Metallschicht-sicherungen - Experimente und Simulationen. Thesis TU Braunschweig 1993.

# STUDY OF FUSELINKS WITH DIFFERENT t-I CURVES USING A MATHEMATICAL MODEL.

Carlos Garrido and José Cidrás

University of Vigo, Lagoas, Marcosende 9, 36280-VIGO (SPAIN).

e-mail: garrido@le.uvigo.es

**Abstract:** Taking into account that in some applications one requires fusibles with different characteristic curves from those available commercially, we have applied a model to the study of fuse behaviour using different geometric forms with the purpose of verifying and obtaining different t-I characteristic curves. In this study we have seen that the opening time (prearcing time) of the fuselink depends on the geometric form of the fuse element, the possibility of varying the t-I curve through modification in the dimensions of the variable sections of a fuse allows fuses to be obtained for specific customised applications.

## I. INTRODUCTION

Fuses have as a goal to act as protection devices for equipment, systems, installations, etc. in the case of anomalous situations or behaviors. The designer of such equipment, installations, etc. studies the limits within which the fuse must act in each case, so that the protected element does not suffer deterioration. Depending on the type of element to protect, a wide range of fuses is needed to suit the various needs. Therefore, one of the objectives of fuse design is to obtain fuses with different t-I performance curves, so that for each specific application the most suitable protection fuse can be obtained. To carry out versatile studies in this field without having to resort to real tests through prototypes, it is desirable to have mathematical models that adequately simulate their real behaviour. Nowadays, to obtain a better characteristic curve, the fuselink has been an evolution towards more complicated geometric shapes, presenting restrictions at regular intervals along their length (Fig. 1). Due to this complicated geometry and to the fact that, as a rule, parameters such as electrical resistivity, thermal conductivity and specific heat vary with temperature, it is not possible to undertake the study using simple analytical techniques and it is necessary to resort to numerical calculations to obtain a theoretically valid model of

fuselink behaviour. Several authors [1-8] have developed models for estimating prearcing time for fuselinks. However, these models have some deficiencies, and so, in our work on fuselinks [9], we have developed a mathematical model to obtain t-I fuselink curves taking into account that the electric resistivity of the fuse element varies with temperature and that this is also true for the thermal conductivity and specific heat of the fuse element, the filler and the ceramic body. The heat losses to the filler and ceramic body are also taken into account in our model.

In this work, our model is used to study the t-I curves that can be obtained by modifying some of the dimensions that characterize the fusible element. At the same time, it demonstrates the validity of the developed model as a test tool for designers, since the t-I curve for the most adequate fuse for our needs can be calculated without the need for a prototype.

## II. DESCRIPTION OF THE MODEL

The model has been described in detail in [9]. The model is based on the solution of the electric potential  $V$  (2), current density (1) ( $J_x$  and  $J_y$ ) and heat diffusion (3) equations using the approximation of the partial derivatives by central finite differences. In this model the variation of the different parameters with temperature is taken into account in the equations. Briefly, As the fuselink used for the experimental contrasting of the theoretical model presents the shape shown in figure 1, due to the symmetry, figure 2 shows the element of fuselink that has been used for the solution of equations. To calculate prearcing time it is necessary to solve the heat equation in the fuselink using as the energy source the heat produced by Ohmic losses (4) computed using the current density:

$$\text{div} \mathbf{J} = -\text{div}(\text{grad } V/\rho) = 0, \Rightarrow J_x = -\frac{1}{\rho} \frac{\partial V}{\partial x}, J_y = \frac{1}{\rho} \frac{\partial V}{\partial y} \quad (1)$$

$$\frac{1}{\rho} \nabla^2 V + (\nabla \cdot \frac{1}{\rho}) (\nabla V) = 0 \Rightarrow \frac{1}{\rho} \left[ \frac{\partial^2 V}{\partial x^2} + \frac{\partial^2 V}{\partial y^2} \right] + \frac{\partial(1/\rho)}{\partial T} \left[ \frac{\partial V}{\partial x} \frac{\partial T}{\partial x} + \frac{\partial V}{\partial y} \frac{\partial T}{\partial y} \right] = 0 \quad (2)$$

$$dC_p \frac{\partial T}{\partial t} = K \left[ \frac{\partial^2 T}{\partial x^2} + \frac{\partial^2 T}{\partial y^2} + \frac{\partial^2 T}{\partial z^2} \right] + \frac{\partial K}{\partial T} \left[ \left( \frac{\partial T}{\partial x} \right)^2 + \left( \frac{\partial T}{\partial y} \right)^2 + \left( \frac{\partial T}{\partial z} \right)^2 \right] + Q_v \quad (3)$$

$$Q_v = \rho \left[ J_x(i,j)^2 + J_y(i,j)^2 \right] \quad (4)$$

where  $\rho$ ,  $d$ ,  $C_p$ ,  $K$  and  $T$  are, respectively, the resistivity, density specific heat, thermal conductivity and temperature.  $Q_v$  represents the energy generated in the material per unit of volume and per unit of time.

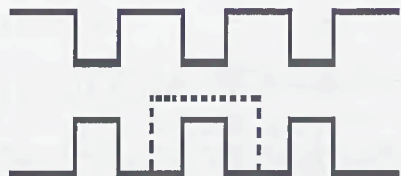


Fig.1: Typical fuselink element

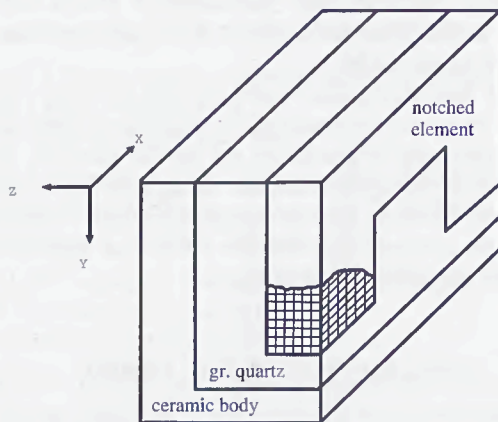


Fig.2: Symmetrical part of an element used in our model and finite-difference mesh.

By using a discretization in the fuselink as shown in figure 2, the approximation of partial derivatives by central finite differences [10] allows us to obtain the electric potential and the components of the current density at each discrete point  $(i,j)$ .

Taking into account thermal conductivity variation with temperature, the discretization of (3) around central points allows the new temperature  $T'(i,j,k)$  at discrete coordinates points  $(i, j, k)$  after a discrete time interval  $\Delta t$  to be computed by means of:

$$dC_p \frac{T'(i,j,k) - T(i,j,k)}{\Delta t} = K \left[ \frac{T'(i+1,j,k) - 2T'(i,j,k) + T'(i-1,j,k)}{\Delta x^2} + \frac{T'(i,j,k+1) - 2T'(i,j,k) + T'(i,j,k-1)}{\Delta y^2} + \frac{T'(i,j,k) - T(i,j,k)}{\Delta z^2} \right] + Q_v$$

$$+ \frac{\partial K}{\partial T} \left[ \left( \frac{T(i+1,j,k) - T(i-1,j,k)}{2\Delta x} \right)^2 + \left( \frac{T(i,j,k+1) - T(i,j,k-1)}{2\Delta y} \right)^2 + \left( \frac{T(i,j,k) - T(i,j,k-1)}{2\Delta z} \right)^2 \right] + \rho \left[ J_x(i,j)^2 + J_y(i,j)^2 \right] \quad (5)$$

Taking into account that equation (5) is non-linear, in order to be able to use the implicit method [10] in the calculation of the partial derivatives by finite differences, the non-linear terms are estimated at the previous discrete time where the temperatures are known. This has allowed us to obtain a set of linear equations whose unknown quantities are the temperatures at all discrete points  $(i,j,k)$  at the moment of discrete time  $n+1$ , (the heat generation and temperatures at the previous discrete moment  $n$  being known), relating the temperature at a discrete point  $(i,j,k)$  with the temperature at the adjacent discrete points. The solution of the set of equations for every discrete time has been obtained using the Gauss-Seidel relaxation method. First, the potential distribution with the temperature existing at the beginning of every discrete time step or iteration is obtained, then, the current density is obtained and is used in equation (5) to obtain the new temperature at every discrete point at the end of the discrete time step. The new temperatures substitute the first ones repeating the process in the following iterations. The process ends when melting temperature is reached in the copper fuse element, thereby determining prearcing time.

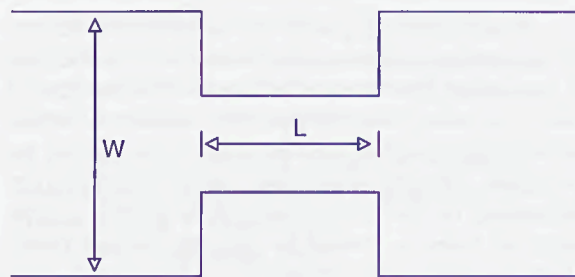


Fig.3: L and W: dimensions of the fuse element modified to study their influence on the t-I curve.

### III. RESULTS

The developed model has been contrasted through the results comparison with a real fuse [9]. The objective of this work is to check the versatility of the model to be used in fuse design. Since the real fuse has given dimensions, it is interesting to check how the t-I characteristic curve of the fusible varies when modifying specific dimensions of the same. In this case, the fusible element presents the form in fig.1. For this work, only the length  $L$  of the restriction and the width  $W$  of the fusible element were modified (fig.3), that is, the width and the thickness of the restriction have been preserved

as well as the length and the thickness of the broad part of the fusible.

With the purpose of studying how the increase or decrease of the restriction length  $L$  can affect the  $t$ - $I$  characteristic curve of the fusible, the prearcing time of the fusible was calculated using different length  $L$  measurements, while keeping the remaining dimensions constant. Figure 4 shows the prearcing time as a function of the r.m.s. current obtained for three different values of the length  $L$  of the restriction: 0.5, 2 and 10 mm.

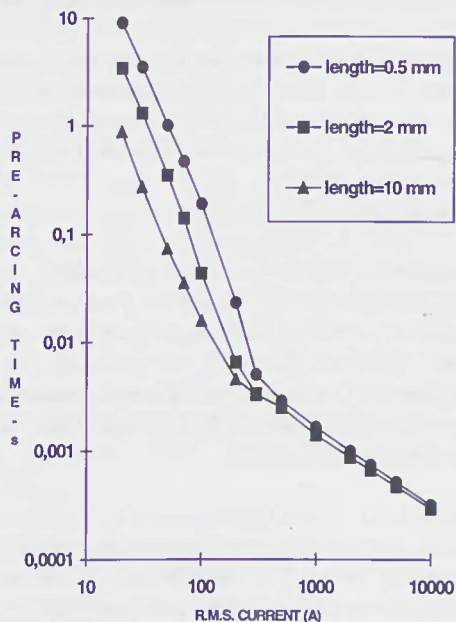


Fig.4: influence on  $t$ - $I$  curve of the restriction length.

In this case the real fuse used for the calculations has a thickness of 0.1 mm, a restriction width of 0.5 mm and a restriction length ( $L$ ) of 2 mm. In this case, resistive short-circuit has been assumed, that is, the current is totally symmetrical. Such as we have already demonstrated in [9], the theoretical values of prearcing time obtained with our model coincide totally with those obtained experimentally. If (theoretically) the length of the restriction is reduced (in our case to 0.5 mm) the prearcing times are increased notably (three times longer), and values that practically coincide with those for the real fuse are obtained solely r.m.s currents over 300 A.

Clearly, the reduction of the restriction to so small a length gives rise to an important part of the heat generated in the restriction being lost through conduction toward the broad part of the fusible, even in spite of the fact that the short circuit r.m.s. current will be increased. If we increase the length of the restriction (10 mm), the opening time is reduced by a

factor of 4 with respect to the times obtained for the length of 2 mm, at least for r.m.s. currents with typical overcharge values. As the short-circuit current increases, both  $t$ - $I$  curves approach each other, practically coinciding for currents over 300 A. It is clear that the increase in the length of the restriction causes the losses of heat toward the broad part of the fusible to be quite a lot less than for the other cases, therefore affecting to a great extent the prearcing time in the area for overcharge and weak short-circuit currents. For high short-circuit current values the process is practically adiabatic, therefore the prearcing times are not affected by the restriction length.

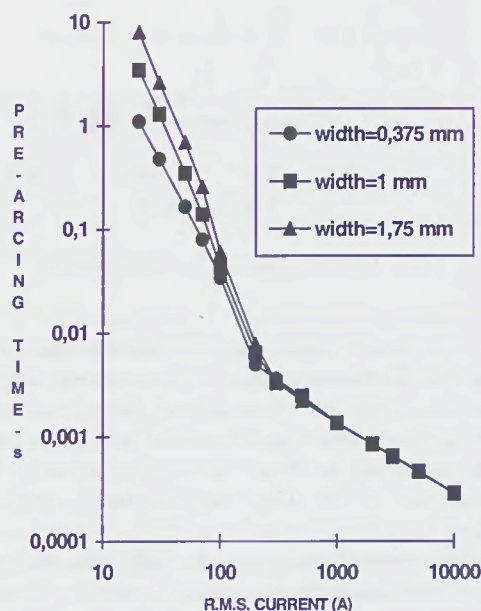


Fig.5: influence on  $t$ - $I$  curve of the broad part width.

Figure 5 shows the prearcing time as a function of the short-circuit current for three width values  $W$  of the broad part of the fusible. The restriction length measures 2 mm for the three cases. Likewise, the remaining parameters are identical. As can be observed, the  $t$ - $I$  characteristic of the fusible depends on the width  $W$ , although the effect is greater for typical overcharge currents. This influence is reduced as the short circuit currents is increased. For currents over 300 A, identical prearcing times are obtained for the three widths tested.

The reduction of the broad area of the fusible (with high thermal conductivity) causes the thermal losses to be smaller (low thermal conductivity of the material - sand - in contact with the copper), so the time needed to reach the melting point is reduced. At r.m.s. currents, the melting process is quasi-adiabatic, therefore the reduction in the broad part of the fusible does not affect the time needed to reach melting point. It is clear that, by

varying both the reduction of the restriction length and the width of the broad part, quite different t-I characteristics can be obtained.

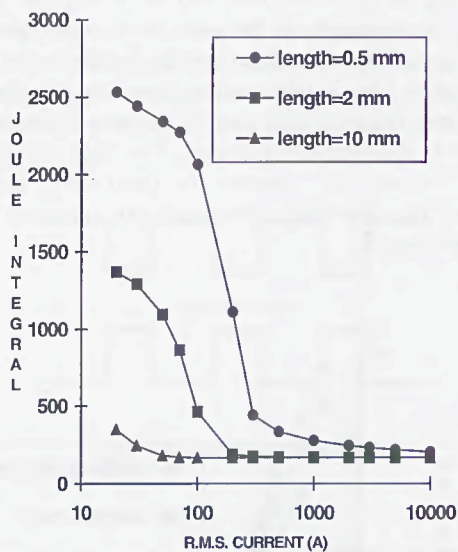


Fig.6:  $I^2t$  as a function of the r.m.s. current.

Figure 6 shows the  $I^2t$  characteristic of the fusible for the prearcing time values corresponding to Figure 4. As can be observed, the energy needed to reach melting point is a function of the restriction length, according to Figure 4. Energy decreases with the increase of the short circuit current reaching a constant value for currents over 200 A for the case of 2 and 10 mm of restriction lengths. For the given current, the fuse starts to limit the short-circuit current (prearcing time  $<0.05$  s). For the 0.5 mm case, a constant energy value is reached only for current values over 10 kA.

#### IV. CONCLUSIONS

The studies carried out have permitted us to show that the use of mathematical models in fuse design is a necessary tool that will avoid loss of time and material in prototypes and trials in order to obtain a fuse that is better adapted to the characteristics required by the client. The use of such models will reduce costs, since tests will only be carried out on prototypes once the mathematical model has obtained the sought-after t-I curve.

#### REFERENCES

[1] Wilkins R. And McEwan P.M., "A.C. short-circuit

performance of notched fuse elements", Proceeding IEE, 1975, 122 (3), pp.289-292.

- [2] Wilkins R., Wilkinson A. and Cline C., "Endurance of semiconductor fuses under cyclic loading", Proceeding of IV International Conference on Electric Fuses and their Applications (ICEFA), 23-25 Sep. 1991, Nottingham (U.K.), pag.43-48.
- [3] Meng X.Z. and Wang J.M., "The simulation of prearcing characteristics of fuse elements in the Finite-Element Method" Proceeding of III International Conference on Electric Fuses and their Applications (ICEFA), 1987, Eindhoven (Nederland), pag.24-19.
- [4] Kürschner H., Ehrhardt A., Nutsch G., Harrison I., Boerner A. and Mickley T., "Calculation of prearcing times using the Finite Element Method"; Proceeding of V International Conference on Electric Fuses and their Applications (ICEFA), 25-27 Sep. 1995, Ilmenau (Germany), pag.156-161.
- [5] Fernández L., Cañas C., Llobell J., Curiel J., Aspas J., Ruz F. and Cavallé F., "Model for Prearcing behaviour simulation of H.V. full-range fuse-links using the Finite Element Method"; Proceeding of V International Conference on Electric Fuses and their Applications (ICEFA), 25-27 Sep. 1995, Ilmenau (Germany), pag.162-168.
- [6] Bottauscio O., Crotti G. and Farina G., "Non-adiabatic process in fuse elements with heavy current faults", Proceeding of IV International Conference on Electric Fuses and their Applications (ICEFA), 23-25 Sep. 1991, Nottingham (U.K.), pag.151-155.
- [7] Sasu M. and Oarga C., "Mathematical modelling of the heat transfer phenomena in variable section fusible elements", Proceeding of IV International Conference on Electric Fuses and their Applications (ICEFA), 23-25 Sep. 1991, Nottingham (U.K.), pag.156-161.
- [8] Cheim L.A.V. and Howe A.F., "Calculating fuse prearcing times by transmission-line modelling (TLM)", Proceeding of IV International Conference on Electric Fuses and their Applications (ICEFA), 23-25 Sep. 1991, Nottingham (U.K.), pag.162-167.
- [9] C. Garrido y J. Cidrás, "A method for predicting time-current characteristics of fuselinks"; Electric Machines and Power Systems Vol.26, N° 7, 1998, pag.685-698.
- [10] Euvrard D., "Résolution numérique des équations aux dérivées partielles", Paris: Ed. Masson, 1988.

# FITTING CURVES TO FUSE TIME-CURRENT TEST DATA

R Wilkins  
Consultant, Heswall, UK

**Abstract:** The general problem of finding a least-squares best-fit curve to noisy test data is discussed and the advantages of singular-value decomposition are described. This method is applied to typical fuse time-current test data using (a) polynomial functions and (b) a special TCC template function.

## I. INTRODUCTION

The time-current characteristic (TCC) of a fuse is its best-known and most widely published characteristic. However, generation of a set of time-current characteristics for a series of fuse products is not a simple matter, requiring considerable testing and analysis of the data. The shape of the TCC depends upon the construction of the fuse, and contains bends which are associated with the thermal response times of the fuse elements, filler, tube, cables, and other components.

A published TCC usually has a tolerance of  $\pm 10\%$  on the current axis, which can give a very much larger variation in melting time, since the curve is very steep. Factors such as manufacturing tolerances and the loading effect of the fuse on a low-voltage test circuit give rise to scatter in measured test data.

For melting times less than 0.1s test data is usually obtained from high-power short-circuit tests. In this region of time the waveshape of the test current becomes important, and the degree of asymmetry in the test wave has a profound effect upon the melting time. The scatter due to this cause can be minimised, but not eliminated, if virtual r.m.s. current is chosen for the presentation of the data. The best solution to this is to stop the TCC at 0.1s and publish  $I^2t$  data only for shorter times [1]. However there remains a requirement for TCCs to be published for times down to 0.01s or lower.

This means that when fitting curves to fuse time-current data the time variable may vary extend over 8 decades. There may be relatively few data points covering this wide domain. In this paper the fitting of curves to TCC test data is illustrated with a set of data obtained from tests on a 100A fuse.

## II. GENERAL LEAST-SQUARES [2]

Given  $M$  sets of data points  $(x_i, y_i)$  the problem is to evaluate the coefficients  $(a_1, a_2 \dots a_N)$  in the relationship

$$y = a_1 \phi_1(x) + a_2 \phi_2(x) + \dots + a_N \phi_N(x) \quad (1)$$

which gives a least-squares "best-fit" to the data, where  $M \geq N$ .  $N$  is referred to here as the order of the fit. The functions  $\phi(x_i)$  must be chosen according to the type of problem. They are usually non-linear functions of  $x$ , but the method results in a *linear* set of equations which need to be solved for  $(a_1, a_2 \dots a_N)$ .

If  $M=N$  the equation (i) passes exactly through all the data points, but for noisy data this solution is of no use. In practice there should be more sets of data than there are unknown coefficients, in which case the solution is the one which minimises the sum of the squares of the errors (SSE) between the values of  $y$  predicted by (1) and the data.

However, even if  $M > N$  the solution can contain very large errors if the linear set of equations is ill-conditioned (contains singularities or near-singularities). This is a very common situation, and is produced when dependencies, or near-dependencies exist between data sets. The problem can be resolved by using the method of singular value decomposition (SVD) to solve the linear equations. In this method singularities are automatically filtered (edited out) during the solution process. If an attempt is made to fit a model whose order  $N$  is higher than is justified by the data, SVD will automatically reduce the order of the model to the correct level. SVD is the recommended method for solving for the unknown coefficients [2].

## III. POLYNOMIAL FUNCTIONS

For general purposes, the most popular choice for the approximating functions is  $\phi_1 = 1, \phi_2 = x, \phi_3 = x^2 \dots$  which makes (1) a polynomial function of  $x$ . With a time-current curve, time must be chosen as the independent variable for curve-fitting, since the

resulting current is a continuous function of  $T$ . (If current were taken as the independent variable, the curve shows a discontinuity at the minimum fusing current).

The raw  $(T, I)$  data should not be used because the values vary over such a wide range. Minimising the SSE would then give a good fit for that part of the curve where the currents are large, and a poor fit over the rest of the curve. A good fit over the whole of the curve can be obtained by using the logarithms of time and current as data, by transforming the test data as follows :

$$x_i = \log_{10} T_i \quad \text{and} \quad y_i = \log_{10} I_i$$

Figs.1 to 3 show the results of fitting a polynomial function to a set of 15  $(T, I)$  data pairs obtained from tests on a 100A fuse. (For the short-time test data the virtual r.m.s. current is plotted). The data shown is of good quality but several of the data sets are closely grouped - the results of tests on a set of samples at the same test current.

For a 2nd-order fit (Fig.1) the fitted curve is a straight line ( $y = a_1 + a_2 x$ ) and is not a good model of the data. Increasing  $N$  to 3 gives a parabola and when  $N=4$  (Fig.2) the resulting cubic curve gives a much better fit to the data.

However, increasing  $N$  to 5 (Fig.3) gives a quartic curve which bends unrealistically at both the short-time and long-time ends of the curve. This is typical of fitting time-current data with polynomials. Although there are 15 sets of data in 6 distinct groups, a cubic is the highest-order polynomial which gives a realistic fit to the data.

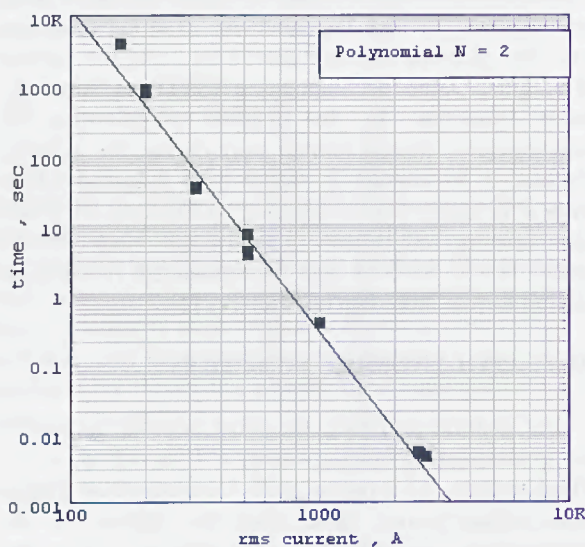


Fig.1 2nd-order polynomial fit

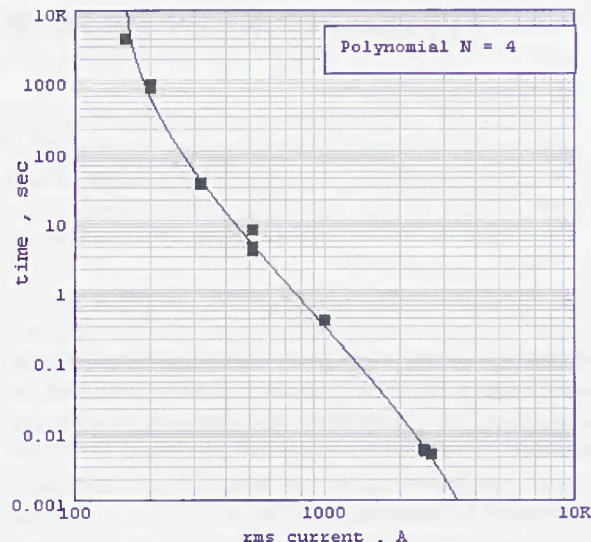


Fig.2 4th-order polynomial fit

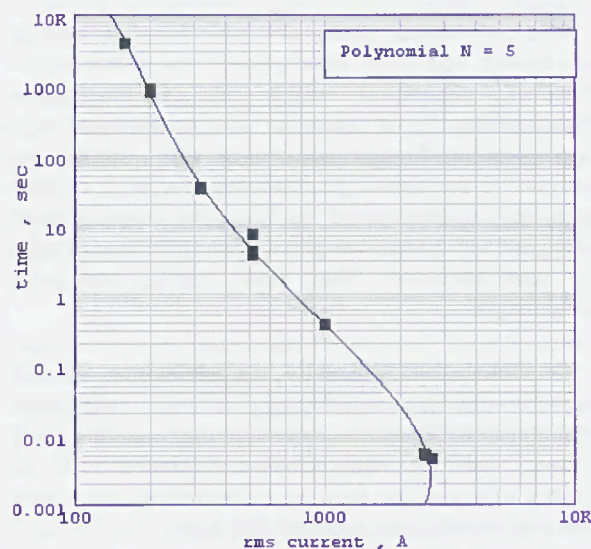


Fig.3 5th-order polynomial fit

#### IV. TCC TEMPLATE FUNCTIONS

In the previous section the behaviour of the polynomial function for short-times was described as "unrealistic". This is because we know that real fuses do not behave like this. For long times, the melt current tends towards a constant vertical asymptote, the minimum fusing current ( $I_m$ ). For very short times the  $I^2T$  product becomes constant. It is therefore useful to search for functions which have this asymptotic behaviour, for use as alternatives to the polynomial. These functions will be called "TCC templates", and when used, the fitted curve will show a realistic behaviour near to and outside the short- and long-time ends of the data.

Equation (2) gives a function which at first sight is attractive. Each term on the r.h.s. has the correct

asymptotic behaviour and corresponds to a time-current curve with a bend near to a characteristic time  $T_k$ .

$$\frac{I}{I^2} = \sum_I^N a_k (1 - e^{-T/T_k}) \quad (2)$$

However to obtain accuracy of fit over the whole curve we need to transform the data using e.g.  $y = \log_{10}(1/I^2)$  and  $x = \log_{10}(T)$ , and this gives functions which cannot be expressed as linear combinations of the  $a_k$ .

In this paper a template function based on the relationship between  $I^2T$  and time is used. The general form of this relationship is shown in Fig.4, where  $T_0$  is an arbitrarily-chosen reference time in the adiabatic region. Fig.4 illustrates the shape that the function needs to have to represent the behaviour of a fuse.

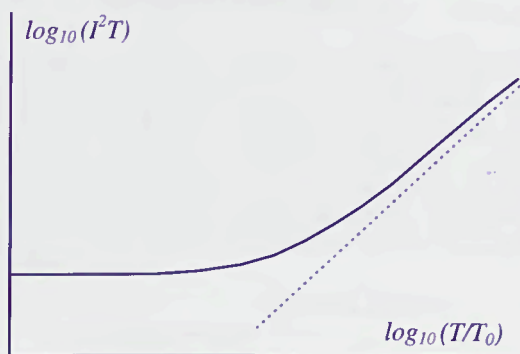


Fig.4 Basic TCC template function

We need a function such that :

(a) as  $T \rightarrow T_0$   $I^2T \rightarrow \text{constant}$

(b) as  $T \rightarrow \infty$   $I \rightarrow I_m$  so that

$$\log_{10}(I^2T) \rightarrow \log_{10}(I_m^2T) \rightarrow \log_{10} I_m^2 + \log_{10} T$$

$$\log_{10}(I^2T) \rightarrow K + x$$

i.e. a function which has a slope of zero as  $x \rightarrow 0$  and a slope of 1 as  $x \rightarrow \infty$ . A function with a suitable shape is  $\sqrt{(u^2 + x^2)}$  where  $u$  is a constant. The curve can then be fitted using

$$\log_{10}(I^2T) = a_1 \sqrt{u_1^2 + x^2} + \dots + a_k \sqrt{u_k^2 + x^2} + \dots \quad (3)$$

where the  $u_k$  are parameters which determine the time regions where bends occur in the TCC. If there are  $R$

terms on the r.h.s. of (3) only  $R-1$  of them are independent because of the requirement that the slope of the function must be unity as  $x \rightarrow \infty$ . This means that

$$a_1 + a_2 + \dots + a_N + a_R = 1$$

where  $N = R-1$ . Substituting for  $a_R$  in (3) and rearranging then gives

$$\log_{10}(I^2T) - \sqrt{u_R^2 + x^2} =$$

$$a_1 \left\{ \sqrt{u_1^2 + x^2} - \sqrt{u_R^2 + x^2} \right\} + \dots$$

$$+ \dots + a_N \left\{ \sqrt{u_N^2 + x^2} - \sqrt{u_R^2 + x^2} \right\}$$

This is of the form of equation (1), with the data transformed as follows :

$$y_i = \log_{10} I_i^2 T_i - \sqrt{u_R^2 + x^2}$$

$$x_i = \log_{10}(T_i / T_0) \quad \text{and}$$

$$\phi_k(x) = \sqrt{u_k^2 + x^2} - \sqrt{u_R^2 + x^2} \quad (k=1 \dots N)$$

$T_0$  and  $U_R$  were chosen to be 0.001s and 7.0 respectively. The number of  $u_k$  parameters is equal to the order of the fit, and these were chosen to be uniformly distributed across the range of  $x$  from 2 to 6 (corresponding to times of 0.1s and 1000s). This is illustrated in Fig.5

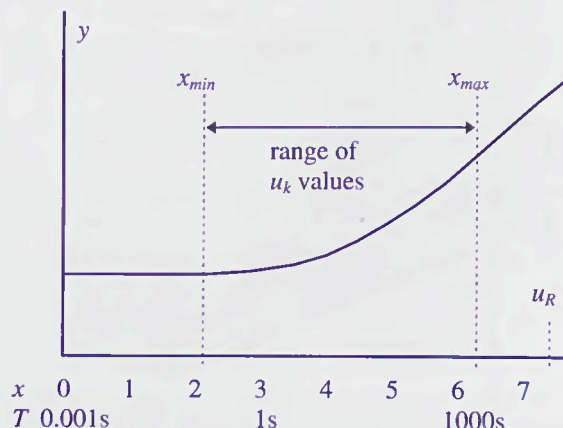


Fig.5 Choice of parameters for template functions

Figs 6-8 show the curves fitted to the 100A fuse data using these template functions.

The 2nd-order fit (Fig.6) produces a curve which is a poor fit to the data. Increasing  $N$  to 4 (Fig.7) gives a much better fit, and  $N=5$  gives a further slight improvement. Attempts to use higher-order fits than this are defeated by the SVD algorithm, which detects singularities and removes them, so  $N=5$  is the highest value which can be used with the template function.

Within the range of the data values there is little to choose between the best polynomial fit and the best fit using the TCC template function. However the template function has the advantage that in all cases the "free" ends of the fitted curves behave in a manner which is consistent with the physical behaviour of real fuses.

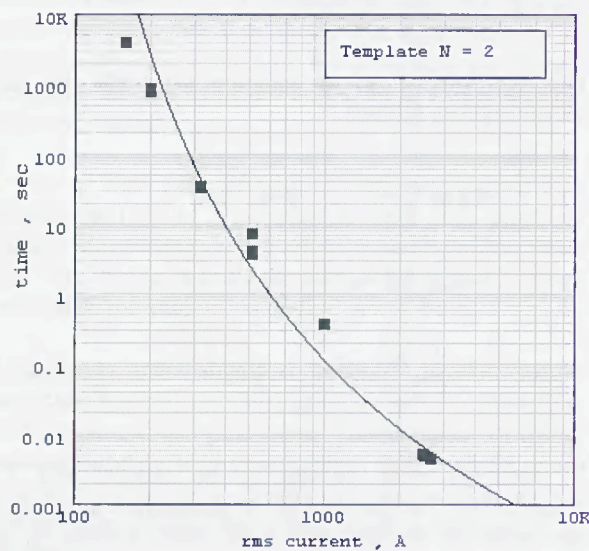


Fig.6 2nd-order template fit

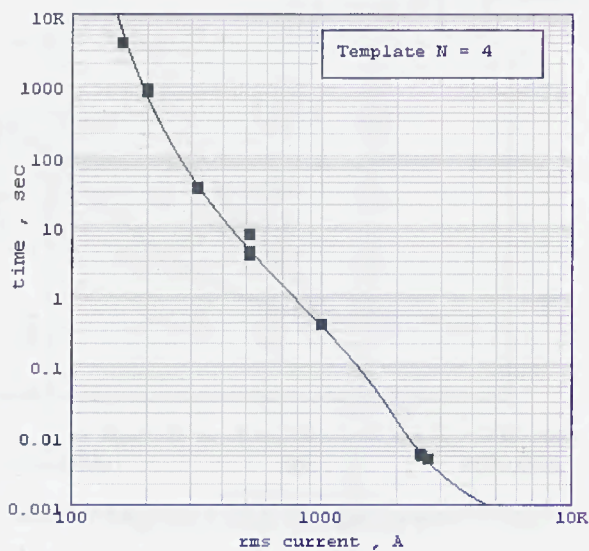


Fig.7 4th-order template fit

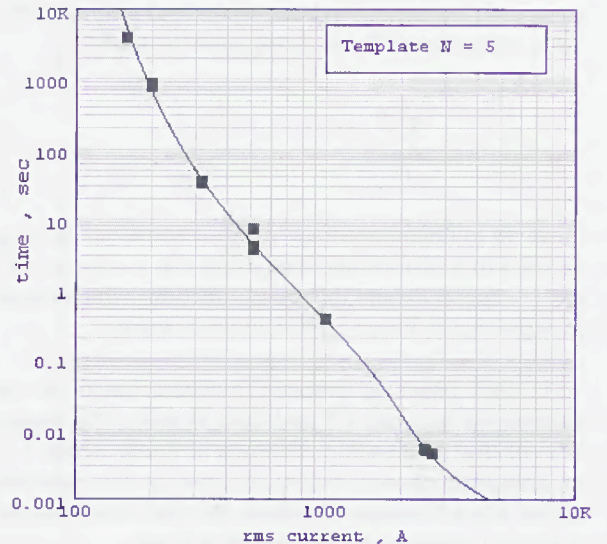


Fig.8 5th-order template fit

The disadvantage of the template function is that its basic shape (Fig.4) has an upwards curvature, and it does not perform so well when the TCC contains sharp bends, containing adjacent concave and convex sections. Such curves are commonly encountered with "time-delay" fuses, for which a change in the operating mechanism occurs in the middle of the TCC.

## V. CONCLUSION

Curves can be fitted to time-current test data using polynomial approximating functions but problems arise because these functions do not behave sensibly at the long-time and short-time ends of the fitted curve. This problem can be solved by the use of "TCC template" functions as the approximating functions. One example of a template function has been given, which gives a good fit to a typical data set.

However the template function described is not as "flexible" as the polynomial, and the search must continue for a better template function, (or combination of functions) which is both flexible (can bend both ways) and has the required asymptotic behaviour.

In all cases the use of SVD is essential for reliability in parameter estimation.

## VI. REFERENCES

- [1] J.G.J. Sloot and X.Z. Meng, "Choices for the presentation of fuse melting curves", Fourth International Conference on Electric Fuses and their Applications, Nottingham 1991, pp 206-209.
- [2] W.H. Press, B.R. Flannery, S.A. Teukolsky and W.T. Vetterling, "Numerical Recipes", Cambridge University Press, 1989.

# FINITE-ELEMENT ANALYSIS OF THERMALLY-INDUCED FILM DE-BONDING IN SINGLE AND TWO-LAYER THICK-FILM SUBSTRATE FUSES

M. Wilniewicz, P.M. McEwan  
Sheffield Hallam University  
Sheffield, UK

D. Crellin  
GE Power Controls  
Liverpool, UK

**Abstract:** The paper presents a linear elastic finite element (FE) design tool which has been developed for evaluating the electro-thermally-induced stresses that occur in current-carrying thick-film substrate fuses and to quantify their effect on de-bonding of single conductive film from the substrate. The methodology necessitates semi-concurrent solution of the electric current distribution, temperature distribution, stress-strain distribution and displacement distribution fields throughout the substrate fuse [5, 6, 7]. Analyses of film de-bonding are given and some practical fuse design options are also examined using the tool. How the tool can be exploited to analyse the film-substrate interfacial stresses is also discussed as is a two-layer substrate fuse design for reducing the magnitude of the critical stress components.

## I. INTRODUCTION

Thick-film substrate fuses are becoming more commonly used for fuse protection of power semiconductor devices [3, 4]. This type of fuse typically comprises a multi-notch metal film electro-deposited on to a non-conductive substrate. Compared to conventional fuses, film fuse designs are capable of achieving faster operation and better control of the let-through energy and the arcing voltage. However, intermittent currents found frequently in power electronic circuits, produce cyclic temperature differentials that, due to the unmatched mechanical properties of the metal film and the substrate, create high thermal stresses within the conductive film and at the film-substrate interface. De-bonding of the film from the substrate therefore occurs where the interfacial shear stresses exceed the adhesive strength of the film-substrate bond.

The FE models were constructed using PATRAN [1] and the FE solver used was ABAQUS [2]. All analyses were performed on a SunUltra 10 workstation.

## II. INVESTIGATED SUBSTRATE FUSE

The electro-mechanical behaviour of a single-notch and a three-notch single layer substrate fuse was modelled.

The fuse embodies an alumina substrate with a thin silver film laid on to it. Conventional quartz sand filler completely surrounded the fuse element and substrate. The geometry and dimensions of the fuse element and substrate are shown in Figure 1.

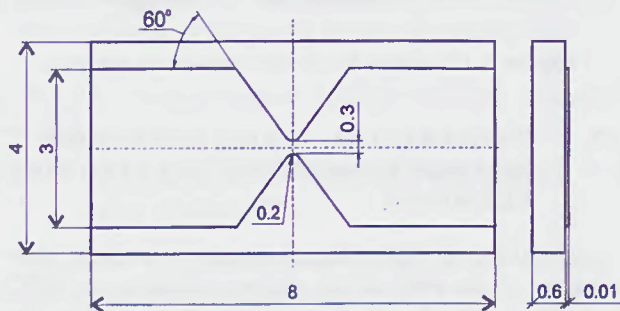


Figure 1. Geometry of the substrate fuse.

3D FE modelling was used and axi-symmetry was exploited, i.e. only one quarter of the fuse was modelled.

### II.1 FE model for the thermal-electrical analysis.

The FE model for the thermal-electrical analysis comprised 31,157 finite elements. The model is shown in Figure 2 in which the film and substrate mesh are just distinguishable through the filler mesh.

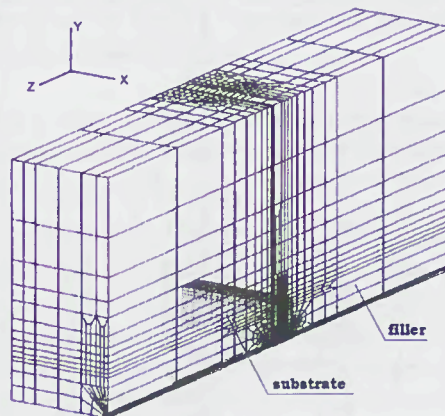


Figure 2. Finite element model for the thermal-electrical analysis.

## II.2 FE model for the thermal stress analysis.

The FE model for the thermal stress analysis comprised 13,365 finite elements, of which 7,290 were used for the metal film, Figure 3. The filler mesh was omitted from this model.

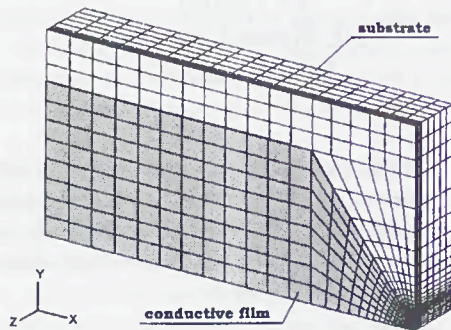


Figure 3. FE model for the thermal stress analysis.

## III. TEMPERATURE, STRESS AND STRAIN DISTRIBUTIONS IN SINGLE-LAYER FUSE ELEMENTS

All nodes on the external boundary surfaces were assumed to be fixed at the ambient temperature (20°C) and the electrical and thermal properties of the fuse materials were allowed to vary with temperature [8, 9]. Both electrical and thermal fields were solved concurrently using the \*Coupled thermal-electrical procedure of the FE solver [2]. The current was selected to produce a maximum element temperature of 200°C under steady-state conditions for all substrate fuse designs.

The critical temperature occurs at the film-substrate interface along the 'Z' symmetry axis of the model. The temperature profile of the element and filler-substrate composite along this axis is shown in Figure 4.

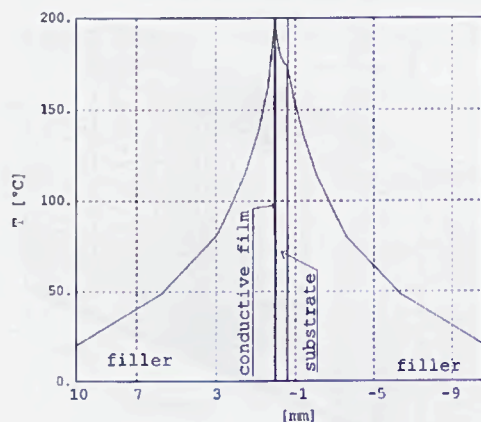


Figure 4. Temperature profile along the 'Z' symmetry axis of model.

Given that the thermal expansion coefficient of silver is approximately three times that of alumina, large shear stresses develop at the film-substrate interface.

The distribution of the shear stress  $\sigma_{zy}$  at the film substrate interface is illustrated and given in tabular form in Figure 5. The conductive film and filler are omitted from the illustration for clarity.

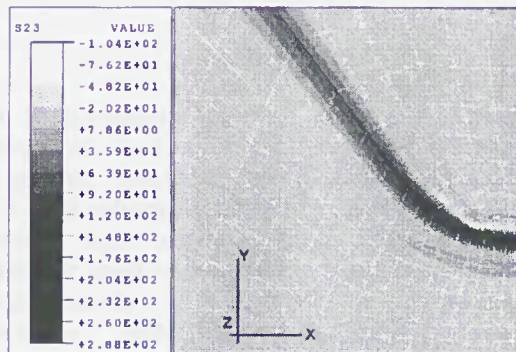


Figure 5. Shear stress  $\sigma_{zy}$  distribution at the film/substrate interface.

From Figure 5 it can be seen that the shear stresses are largest along the interfacial film-substrate notch edge. Hence, given that the criterion for film de-bonding is where the magnitude of the maximum shear stress exceeds the film adhesion strength, de-bonding, if it were to occur, would theoretically be initiated at the point of the maximum shear stress along this leading edge. In fact the model shows that the maximum shear stress occurs at the point along the film-substrate leading edge coincident with the minimum cross-section of the notch.

Compressive stresses are also produced within the film-substrate geometry due to the temperature increase. The compressive stresses in the conductive film produce deformation (buckling) of the film-substrate and the longer the fuse element the more pronounced it becomes. The deformation of a three-notch substrate fuse, magnified 150 times for clarity, is shown in Figure 6.

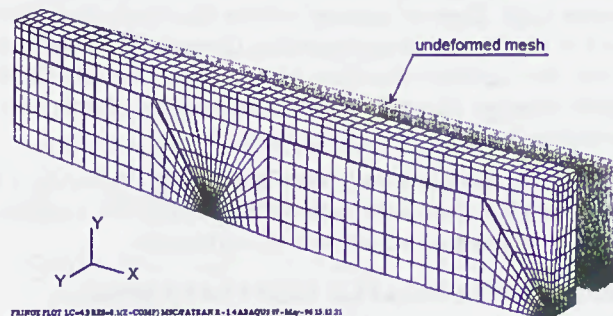


Figure 6. Film-substrate deformation in a three-notch substrate fuse (deformation magnified 150 times).

### III.1 Effect of varying the film thickness on the magnitude of the stresses and deformation

The tool is a useful design aid for evaluating the effects of changing the properties, dimensions and shapes of elements on the critical stresses and, hence, on the precipitation of film de-bonding. As an example, the FE tool was used to examine the fuse design shown in Figure 1 where only the film thickness was varied. The variation of the critical orthogonal shear stress components and the corresponding displacement are shown, graphically, for three film thicknesses, in Figure 7.

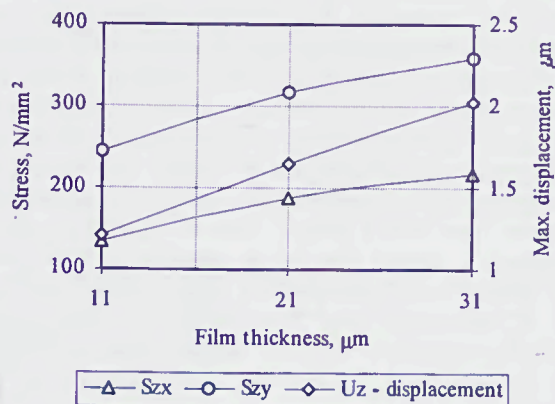


Figure 7. The effect of varying the film thickness on the magnitude of the critical stresses & displacement.

From Figure 7 it is observed that increasing the film thickness produces greater trapped stress in the film and increased deformation since the trapped stress produces greater interfacial shear stresses. Thin conductive films are, therefore, superior to thick films in this respect, i.e. thinner films produce smaller deformation and also all significant stress components are smaller in thinner film fuse elements.

### III.2 Effect of varying the substrate thickness on the magnitude of the stresses and deformation

The same substrate fuse design was examined for three cases where only the substrate thickness was allowed to vary. The magnitudes of the interfacial shear stresses and the deformation for the three samples are given in Figure 8.

It is clear from Figure 8 that the substrate thickness has a significant effect on the magnitude of the deformation since as the substrate thickness is decreased the magnitude of the deformation increases markedly. This is, of course, because thinner substrates are more flexible than thick substrates. The substrate thickness, however, has no significant effect on the magnitude of the interfacial shear stresses, which increased only slightly as the substrate thickness was increased, due, mainly, to a smaller portion

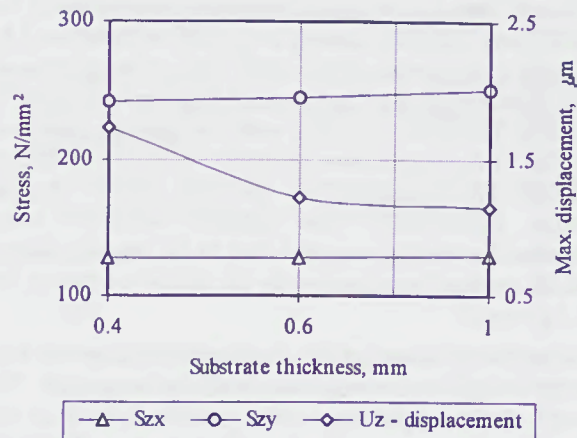


Figure 8. The effect of varying the substrate thickness on the magnitude of the critical stresses & displacement.

of the stress being released through observed substrate buckling.

## IV. STRESS MAGNITUDES IN TWO-LAYER FUSE ELEMENTS

Two-layer FE film-substrate designs using different metals for the substrate bonded film (SBF) were evaluated using the tool in an attempt to reduce the interfacial stresses. The results obtained were compared with the corresponding results for a single-layer silver film of the same thickness ( $10.5\mu\text{m}$ ). The thickness of the SBF was  $0.5\mu\text{m}$ . The thickness of the main conductive silver layer, termed the metal bonded film (MBF), was  $10\mu\text{m}$  and that of the substrate was  $6\text{mm}$ , as in the previous example. The stresses can be calculated in several ways [7] depending on whether the absolute value of the stress is critical (MISES) or whether the maximum shear stress (TRESCA) is critical. The resultant stresses were determined for eight two-layer film cases, the results for which are given in Table 1, together with the orthogonal shear stress components  $S_{zx}$  and  $S_{zy}$ .

Table 1 - Stress magnitudes in two-layer samples compared with the single-layer silver film sample.

SBF	MISES N/mm <sup>2</sup>	TRESCA N/mm <sup>2</sup>	$S_{zx}$ N/mm <sup>2</sup>	$S_{zy}$ N/mm <sup>2</sup>
Au	434	485	125	230
Al	519	560	128	236
Mg	432	484	124	225
Ti	413	461	125	230
Cu	550	584	131	243
Mo	436	494	129	239
W	518	597	131	244
Ag	478	524	127	234

From Table 1 it is observed that the magnitudes of the MISES and TRESCA stresses are significantly affected by the elastic properties of the SBF. The greatest increase was observed for the Cu-Ag metal combination (MISES: +15.1%, TRESCA: +11.4%) with the greatest reduction for the Ti-Ag combination (MISES: -13.6%, TRESCA: -12.0%). The magnitudes of the shear stresses did not change significantly, the greatest reduction being observed for the  $S_{zy}$  stress (-3.8%) in the Mg-Ag sample and the greatest increase for the  $S_{zy}$  stress (+4.3%) in the W-Ag sample.

The effect of varying the elastic properties of the SBF on the overall stress magnitude was also examined. The overall stress magnitude, in this case, is defined as the normalised scalar sum of the critical stresses TRESCA, MISES,  $S_{zx}$ , and  $S_{zy}$ . In the examples considered, no relationship was found between either the magnitude of the overall stress and the thermal expansion coefficient or between the magnitude of the overall stress and Young's modulus. However, the overall stress is a function of the product of the thermal expansion coefficient and Young's modulus, which shows a reasonable linear relationship between the corresponding normalised stress and SBF elastic properties, Figure 9.

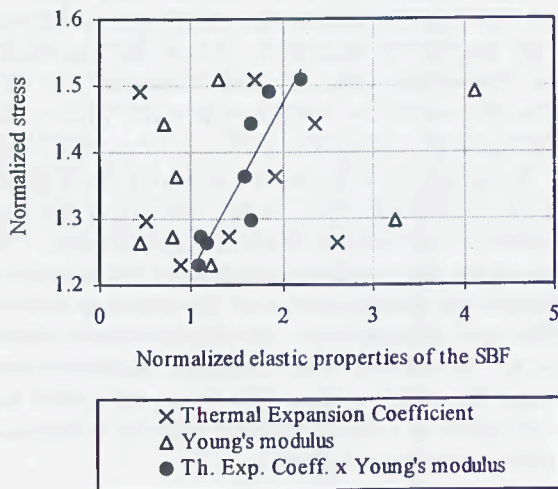


Figure 9. The effect of varying the elastic properties of the SBF on the overall magnitude of the stress.

The linear behaviour of the normalised product of Young's modulus and thermal expansion coefficient for varying elastic properties can be explained as follows:

- The larger the thermal expansion coefficient the larger is the elastic strain (defined as the difference between the total strain and thermal strain) and, consequently, the larger is the stress;

- Coincidentally, the larger the Young's modulus the larger is the magnitude of the stress for a given magnitude of strain. However, it should be noted that the strain is primarily affected by the elastic properties of the substrate and the MBF.

## V. EXPERIMENTAL VERIFICATION OF CONDUCTIVE FILM DE-BONDING FROM THE SUBSTRATE

The stresses presented in previous sections were considered to be too small to produce film de-bonding from the substrate under steady-state current-carrying conditions. Increasing the current incrementally was considered impracticable in this case as it would result in the film material melting and fuse operation before de-bonding would occur. However, it was envisaged that under pulsed-current loading conditions the cyclic stresses could produce de-bonding due to fatigue. This hypothesis was investigated experimentally using a manufactured substrate fuse (MSF) design, rated at 20A/300V, which comprised a copper film on an alumina substrate. The MSF samples were subjected to a square pulsed current of 40A of mark:space ratio 50% for an ON time of 18s. Following operation, the MSF samples were dismantled and, as envisaged, de-bonding was observed in the constrictions, Figure 10.

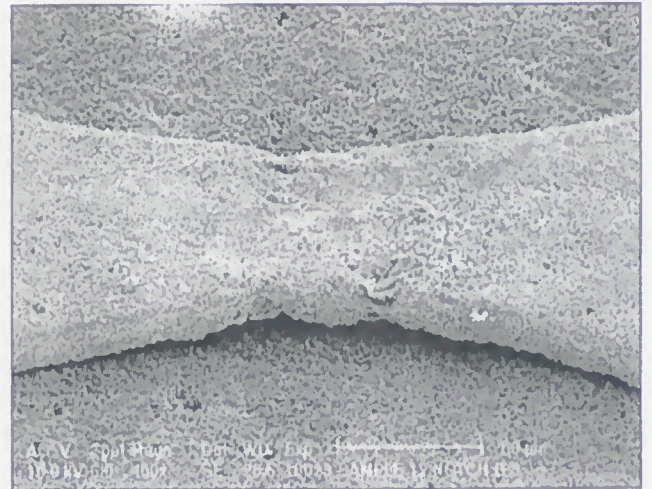


Figure 10. Film de-bonding from the substrate.

## VI. CONCLUSIONS

The paper demonstrates how a FE tool can be developed and used to design thick-film substrate fuses and to prevent the on-set of the conductive film de-bonding from the substrate. Examples of varying the dimensions of films and substrates and the film material properties have been given which, further, demonstrate the scope and generality of the design tool. In this latter

respect the tool was shown to be useful for evaluating single and two-layer substrate fuses and, in the latter case, to be capable of evaluating different combinations of metal films using normalised characterisation.

Film-substrate de-bonding was taken as an example of the generality of the tool's application, since film de-bonding impairs the film-substrate thermal path and, hence, affects its electro-thermal characteristics. If not allowed for, the impairment, of course, will precipitate fuse operation and reduce the withstand capacity of this class of fuse.

The presented design evaluations indicate that large interfacial shear stresses develop in thin-film substrate fuses at the film-substrate interface due to mismatches in the elastic properties of the substrate and conductive film materials. It has been shown that the magnitude of these stresses and corresponding deformation can be computed using the FE tool for any current loading, in order to determine, for example, the criticality of the film de-bonding stresses.

The reported design evaluations were not intended to be exhaustive, however, some general principles were indicated by the presented results. For example, it is clear that (i) the stresses and deformation increase as the film thickness is increased, (ii) varying the substrate thickness has only a limited effect on the magnitude of the stresses and (iii), as a consequence of (ii), thinner, more flexible, substrates are prone to increased deformation. It was also predicted using the tool, that for the particular substrate fuse geometry examined, the deformation and stresses would not cause film de-bonding.

Finally, it was envisaged, and established by experiment and by use of the FE tool, that de-bonding of the conductive film from the substrate would occur for excessive pulsed-current loading.

## VII. REFERENCES

- [1] PATRAN ver.1.4 User's Manuals, The MacNeal-Schwendler Corporation, Los Angeles, May 1995.
- [2] ABAQUS ver.5.5/5.6 User's Manuals, Hibbit Karlsson & Sorensen Inc., 1995.
- [3] Ossowicki, J. & Sulikowski J.: 'Bezpieczniki Warstwowe na Podłożu Szklano-Krystalicznym', Prospects of Development of Current Breaking Techniques, Electrical Engineering Faculty, Technical University of Gdańsk, Poland 1996.
- [4] Harrison, Robert: 'Development and Characterisation of Thin Film Electric Fuselinks', Ph.D. Thesis, University of Nottingham, May 1994.
- [5] Gomez, J.C. & McEwan, P.M.: 'Investigation of the Pre-Arcing Behaviour of Dissimilar Uniform Double-Elemented Filled Fuses Using FE CAD

Techniques', Proc. ICEFA, Nottingham, Sept.1991, pp.65-67.

- [6] Bruno A. Boley et al.: 'Theory of Thermal Stresses', Robert E. Krieger Publishing Company, Malabar, Florida 1985.
- [7] Kobayashi, Albert S.: 'Manual of Engineering Stress Analysis', Prentice-Hall, New Jersey, 1982.
- [8] Samsonov, G.V.: 'Handbook of the Physicochemical Properties of the Elements', Oldbourne, London 1968.
- [9] Morrell, R. 'Handbook of Properties of Technical & Engineering Ceramics', Part 2: High Alumina Ceramics, HMSO publication, London 1987.
- [10] Elshabini, Aicha: 'Thin Film Technology Handbook', McGraw-Hill Companies, New York 1998.

## VII. ACKNOWLEDGEMENTS

The Authors thank GE Power Controls Ltd., Liverpool UK, for their support of the fuse research undertaken at Sheffield Hallam University.

THE  
FIRST  
PART  
OF  
THE  
HISTORY  
OF  
THE  
REIGN  
OF  
HENRY  
THE  
SEVENTH  
BY  
JAMES  
HARRISON

IN  
FOUR  
VOLUMES  
THE  
FIRST  
VOLUME

THE  
FIRST  
PART  
OF  
THE  
HISTORY  
OF  
THE  
REIGN  
OF  
HENRY  
THE  
SEVENTH

BY  
JAMES  
HARRISON

THE  
FIRST  
PART  
OF  
THE  
HISTORY  
OF  
THE  
REIGN  
OF  
HENRY  
THE  
SEVENTH

BY  
JAMES  
HARRISON

THE  
FIRST  
PART  
OF  
THE  
HISTORY  
OF  
THE  
REIGN  
OF  
HENRY  
THE  
SEVENTH

BY  
JAMES  
HARRISON

# FUSE ARC VOLTAGES, FROM STRIATION UNTIL GRADUAL BURNBACK

J.G.J. Sloot  
Eindhoven University of Technology  
Eindhoven, Netherlands

X.Z. Meng  
Gould Shawmut  
Newburyport, USA

*Abstract: For fuses the character of of the arc voltage generation can be distinguished in the ultrafast voltage peaks as observed for uniform wires and the more continuous arc voltage generation during gradual burnback. This article intends to present one general model which combines both arcing descriptions into one general model, based on many experimental observations. The work is mainly to extend Daalder's model for sand filled fuses to substrate fuses. It proved to be able to describe measured performances of test samples and commercial high voltage fuses.*

## I. Introduction

Fuses, especially with sand filling, have been widely used as protective devices in electric power networks. In case of a fault, fuses operate to interrupt the circuit, by introducing a circuit element with a voltage fall above the source. However, for a critical range of currents the heat dissipation inside fuses may cause fracture of the fuse body. To establish certain criteria for developing fuses, it is therefore of importance to understand the arcing behavior of fuses. During the past 30 years, several empirical or semi-empirical models have been proposed for the arcing process, concerning arc initiation, burnback and column expansion, and the related voltage rise. For system studies, where it may be required to model several fuses simultaneously in 3-phase systems, preferably a simplified model like Wilkins' model [1] seems most appropriate. For fuse designers however, a more complicated model, describing real physical processes, might be preferred. The objective of this work is to contribute to the physical arc modelling: the choice has been made for Daalder's model [2] extended to substrate type fuses, including experimental results with test samples as well as commercial fuses.

## II. Combined modeling

### II.1 General description of arcing mechanisms

In principle three situations can be distinguished, dependent upon the fuse configuration and the level of the current:

1. For uniform wires or strips, as used in miniature fuses, a number of small arcs with fixed distances are initiated across the whole length of the conductor. Within an extremely short time these arcs merge to one arc, if there is sufficient energy available. This arcing process is known as striation[6].
- 2a. For fuse strips with notches, in the high current range, initial arcing takes place in the notches similar to the uniform wire behavior. Afterwards the wider strips gradually burn back. During this period the arc elongation has a positive effect on the voltage increase, while the expansion of arc column has a negative effect. Probably also the pressure rise in the arc causes a voltage increase, while the pushing away of molten sand surroundings enable a pressure relief with on its turn a fall of voltage. The solid strip part is heated during this whole process, which can accelerate the burnback. However if the melting energy is reached an exponentially rise of the burnback rate occurs, again with similarity to the striation process [7].
- 2b. Many fuse designs have abilities to stimulate fast arc initiation in over load range, for instance, fuse strips with M spots. In the overload current range the arcing of these fuses is initiated at the M spots. Afterwards a gradual burnback takes place. The voltage rises because of arc lengthening, which is more or less compensated by arc broadening. Alternative concepts use isolated low temperature melting conductors in series.

### II.2 Expression for the arc voltage

In general, arc voltage consists of the electrode voltage fall and column voltage. After fuse wires or strips are melted, one or more arcs are initiated. Each resulting arc voltage  $U$  is described with a general equation

$$U = U_{ac} + \int_0^{l_{arc}} E dl$$

where  $E$  is electric field, which can vary along the arc

column.  $U_{ac}$  is the anode - cathode voltage, and  $l_{arc}$  is arc length. In case of more arcs in series, the total arc voltage can be obtained by considering individual contributions.

### II.3 Initial arc voltage

In the case of striation, which is supposed to be relevant for short arcs in notches and sometimes for the wider cross sections, a sudden peak arcing voltage is reached within a very short time. The peak value of the arc voltage for the individual arcs, as well as the total voltage can be described by the equations as presented by Hibner [3]. At the arc initiation, striation takes place, the peak arcing voltage can be assumed to be contributed by several short arcs. The initial peak arcing voltage for a large range of initial current values  $i_0$  and cross sections  $S$  has been found to be

$$U_o = \rho_o l \sqrt{\frac{i_o}{S}}$$

where  $l$  is the initial arc length and Hibner constant  $\rho_o = 0.5 \text{ V A}^{-0.5}$ .

### II.4 The electrode voltage fall

The electrode voltage fall  $U_{ac}$  is sometimes described by the equation of Dolegowski [4], although the actual existence of the electrode voltage fall for fuses is under discussion. For current density  $j < 8 \text{ kA.mm}^{-2}$ , the electrode voltage fall  $U_{ac}$  of anode and cathode is presented as:

$$U_{ac} = 20 \pm 5 + k i^{0.39}, \text{ with } k = 1.5.$$

### II.5 Electric field E

Assuming the thickness  $D$  of the arc channel is much smaller than its width  $b$ , the energy balance equation is solved by polynomial approximations analogous to a method used by Wheeler [5]. The result of electric field  $E$  is

$$E = q(Z \ln \Lambda)^{0.4} \frac{I^{0.4}}{b^{0.4} D}$$

where  $Z$  is the average charge,  $\Lambda$  is the Coulomb cut off and  $\ln \Lambda$  varies slowly with  $Z$ ,  $T$  and the electron density  $n_e$ ,  $q$  is a constant (0.034). For copper fuse elements ( $5 \times 0.2 \text{ mm}^2$ ),  $Z \ln \Lambda = 11.5$  was found.

### II.6 Cross sectional area of arc column

If an arc column is assumed with the thickness  $D$  of the arc channel much smaller than its width  $b$ , the channel expansion can be described by

$$\frac{dD}{dt} = \gamma \left(1 - \frac{\rho_s}{\rho_l}\right) \frac{E i}{2 b H}$$

with enthalpy increase  $H$ , degree of molten silica  $\gamma$  and  $\rho_s$  or  $\rho_l$  specific density in solid or liquid state. Introducing the relation between  $E$  and  $I$ , the thickness can be found as

$$D = \sqrt{D_0'^2 + B t}$$

where  $D_0'$  is the initial thickness of the arc channel. The initial channel thickness  $D_0'$  was assumed to consist of the element thickness  $D_0$  and the contribution  $d_e$  due to sand grains, it is written as

$$D_0' = D_0 + 2 d_e$$

The increase for one side due to sand grains is

$$d_e = \left(1 - \frac{\pi}{3\sqrt{3}}\right) R$$

In principle, determination of initial thickness  $D_0'$  should be made on the basis of measurements of fulgurite expansion. In our opinion,  $D_0'$  should include element thickness, air space among sand grains and the increase due to arc pressure. Therefore, the value of initial thickness  $D_0'$  will be larger than that given by Daalder's formula here. Especially, this may effect the arc channel expansion for very thin elements.

The slope  $B$  for time  $t$  is defined as

$$B = q(Z \ln \Lambda)^{0.4} \frac{I^{1.4}}{b^{1.4}} \frac{\gamma}{H} \left(1 - \frac{\rho_s}{\rho_l}\right)$$

with  $\rho_s/\rho_l = 0.68$  and  $H/\gamma = 3.9 \times 10^9 \text{ J.m}^{-3}$ .

Again concerning the arc channel expansion,  $\gamma$  indicates the degree of the flow of molten silica. To maintain the arc, sand melts and silica vapor contributes to arc pressure, thus  $\gamma$  will be influenced by grain size of sand, the viscosity of molten silica and the pressure of arc. In case of  $\gamma = 1$ , no flow of molten silica occurs, the channel expansion is purely due to fusion of sand. For  $\gamma > 1$ , of course, the flow of molten silica takes place. Because the increase in pressure can accelerate the flow of molten silica, the effect of pressure on  $\gamma$  should be considered for further studies of arc channel expansion.

This value consists of the element thickness  $D_0$  and the contribution due to sand grains. In our opinion, it gives actually the lower limit, because the space among grains still can be taken by arc in spite of the arc pressure. If the thickness increase due to the initial arc pressure is assumed to be  $k \cdot R$ , then the minimum and the maximum initial thickness can be expressed as

$$D_0' = D_0 + d_e ,$$

$$D_0'' = D_0 + d_e + k \cdot R$$

Similar to the description of the initial arc thickness  $D_0'$ , the initial arc width  $b_0'$  in its minimum and maximum can be expressed respectively as

$$b_0' = b_0 + 2 \cdot k \cdot R ,$$

$$b_0'' = b_0 + 4 \cdot k \cdot R$$

From a wide range of experiments,  $k$  can be found to be about 2. This means that if sand is properly compressed, an extra increase in order of grain size may be expected. During arcing process, the initial width keeps more or less the same as compared with the thickness increase. For fuses with compact sand, the initial arc width is the same, while the initial thickness should include the contribution of the other side.

In relation with the arc column expansion, the constant  $B$  can be defined in accordance with different width of the elements. For substrate fuses, the expression  $B$  can be rederived as

$$B = 2.27 \cdot 10^{-12} \frac{I^{1.4}}{b^{1.4}}$$

## II.7 Burn back velocity $V$

The single side burnback rate is determined by the element erosion which is mainly due to local electrode effects, it is expressed [2] as

$$V_{th} = \frac{U_{con} \cdot j}{H}$$

where  $j$  is the current density in the strip,  $U_{con}$  is the heat loss per Ampere from the arc to the strip, and  $H$  is the enthalpy increase for arc interface before a strip part is removed due to arc.

The enthalpy increase per unit volume  $H$  is defined as

$$H = C_s \cdot \rho_s \cdot (T_m - T_b) + L \cdot \rho_s + C_l \cdot \rho_s \cdot (T_d - T_m)$$

with melting temperature  $T_m$ , initial temperature  $T_b$ ,  $C_s$  or  $C_l$  for specific heat in solid or liquid state and  $L$  heat of fusion, while  $T_d = 1700$  chosen for silver elements.

For small  $J^2 t$  value during the arcing ( $J < 8 \text{ kA} \cdot \text{mm}^{-2}$ ),  $V = C \cdot j$  is established with  $C = 1.06$  copper elements and  $C = 1.03$  silver elements. For substrate fuses with silver elements plated on the glass, the constant  $C$  was found to be 0.66. This can be realized by a lower value of  $U_{con}$  or a higher value of  $H$ , however, the exact situation in the process is not clear. For high current densities ( $> 8 \text{ kA} \cdot \text{mm}^{-2}$ ), or long enough time periods, experiments show that  $V$  increases exponentially with  $J$ . The consideration of  $H$  should be interpreted numerically with small timesteps [7].

## III. Modeling results and experimental verification

In this section, not published experimental results (with DC currents) of the Eindhoven laboratory will be compared with the values found from the complete arc modeling computer program. Substrate fuses were used in experiments as test objects. First two sets of test objects were used. The silver element was positioned on the quartz glass and surrounded by sand fillers with grain size of about 0.2 mm. The element thickness of the strip part is 10  $\mu\text{m}$ . For the first set, the width of the band was  $b_b = 2 \text{ mm}$ , while the notch had a width  $b_n = 0.3 \text{ mm}$  and length 0.8 mm. For the second set, the width of the band was  $b_b = 4 \text{ mm}$ , while the notch had a width  $b_n = 0.3 \text{ mm}$  or 1 mm, both with length 20 mm.

Figure 1 shows a typical picture of the fulgerite after arcing. Clearly the one side arc expansion is observed.



Figure 1. Fulgerite of an arc channel on substrate base.

Table 1 compares experimentally found values and calculated results for the initial arc voltage  $V_0$ , peak arc voltage  $V_{top}$  and arc voltage at the end of current pulse  $V_e$ . In Table 2 the calculated values for the cross sectional area  $A_{ecal}$  and end voltage  $V_{ecal}$  at the end of the current pulse are compared with experimental results.

**Table 1** Arc voltage comparisons of measurements with calculations ( $I_n = 0.8$  mm)

$I_p$	$V_e$	$V_e$ (T)	$V_0$	$V_0$ (T)	$V_{top}$	$V_{top}$ (T)
A	V	V	V	V	V	V
32	140		45		75	
31	117	91	39	42	-	60
31	96		39		71	
61	291		78		84	
60	366		45		81	
59	392	227	53	50	81	72
90	389		55		76	
91	431	376	58	55	85	82
92	474		70		78	
120	616	530	60	65	85	89
152	818	692	79	63	116	96
152	638		60		90	
185	-		110	65	140	101

**Table 2** Comparisons of measured and calculated cross section area and end voltage

$b_n$ [mm]	$I$ [A]	$t_b$ [ms]	$A$ [mm <sup>2</sup> ]	$A_{cal}$ [mm <sup>2</sup> ]	$V_e$ [V]	$V_{ecal}$ [V]
0.29	40	1.90	0.29±0.05	0.205	536	674
0.29	40	1.28	0.22±0.07	0.192	614	694
0.29	60	1.01	0.31±0.05	0.203	605	804
0.29	60	0.92	0.21±0.02	0.200	790	804
0.29	80	0.75	0.30±0.04	0.207	711	896
0.29	80	0.28	0.23±0.01	0.180	922	950
1	120	0.81	0.45±0.08	0.338	737	859
1	120	3.36	0.51±0.13	0.497	-	640
1	140	0.46	0.41±0.07	0.319	790	933
1	140	2.36	0.53±0.11	0.471	-	780

Finally, simulations of actual breaking tests for commercially 40A 12 kV high voltage fuses were performed: Figure 2 shows an example for prospective AC current of 41kA («+» and «o» indicates current and voltage measurements). Obviously a good agreement has been achieved.

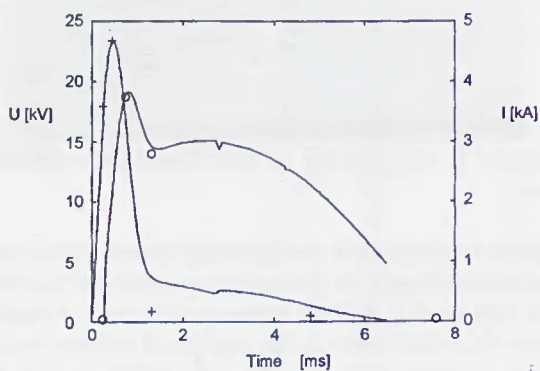


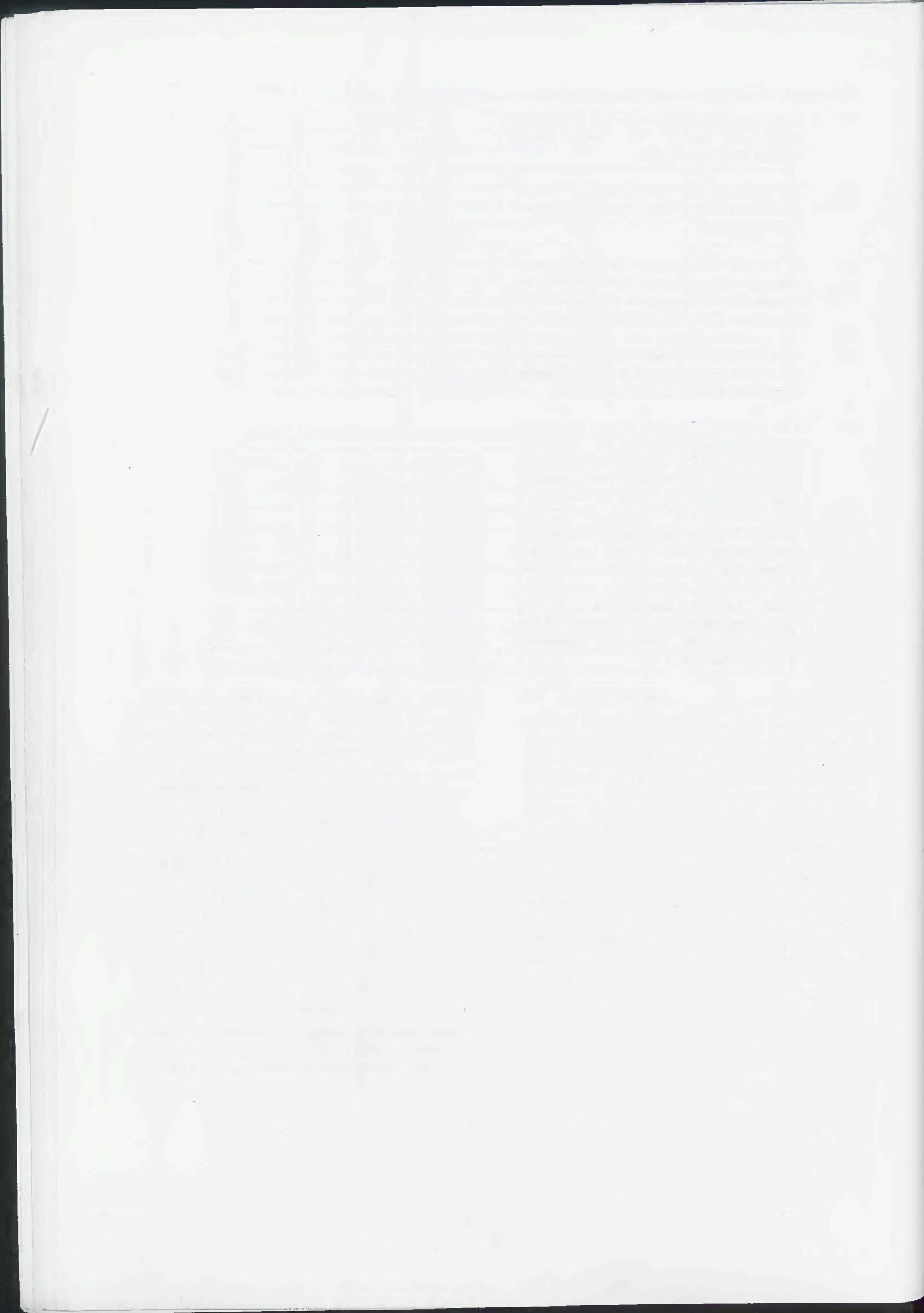
**Figure 2** Comparison of simulation and experimental results of breaking tests for 40 A 12 kV h.v. fuses,  $I_{eff} = 41$  kA,  $U_{eff} = 10400$ ,  $\psi = 45^\circ$  and p.f. = 0.2.

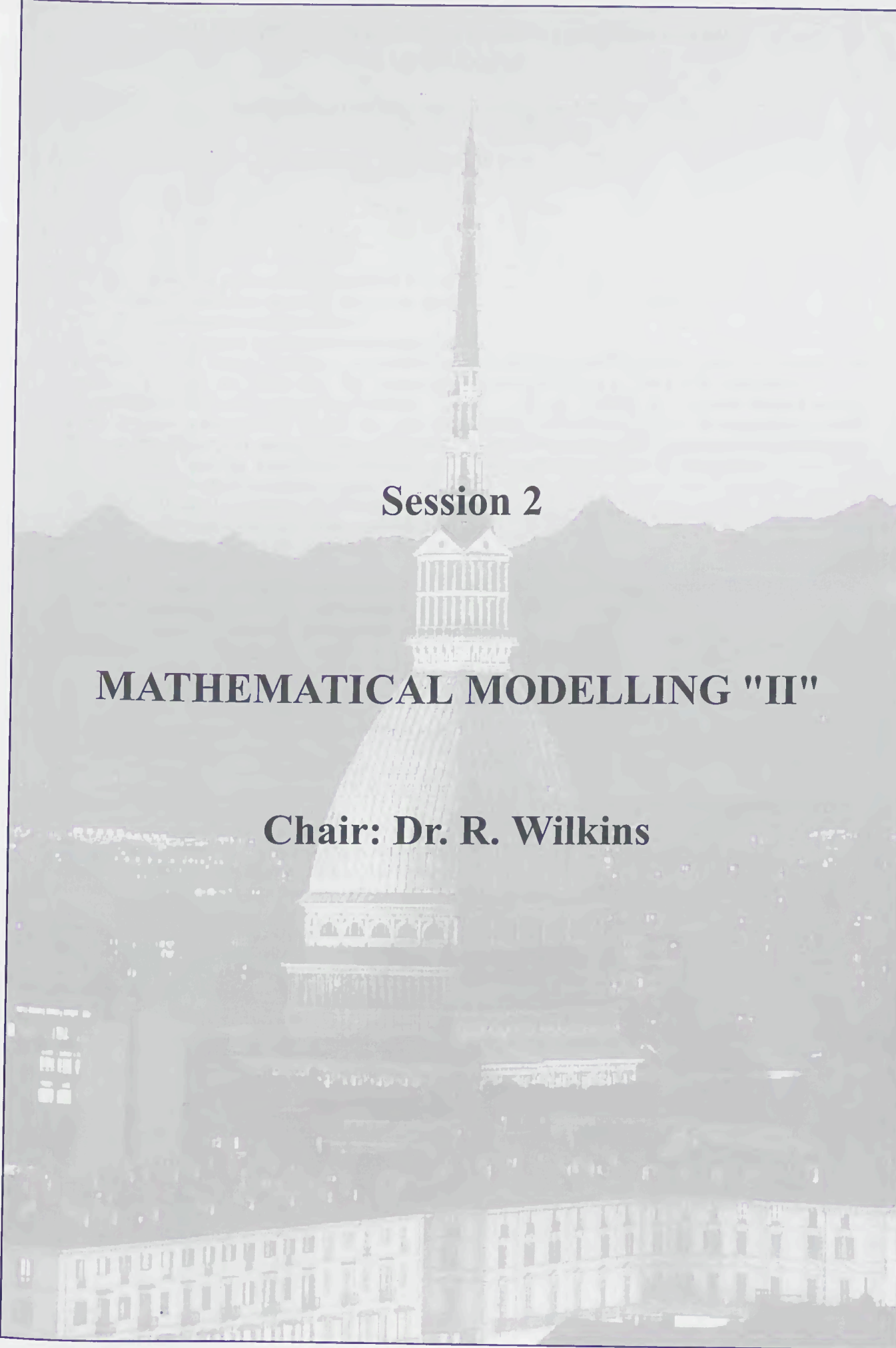
#### IV. Conclusions

For both fuses with compact sand and substrate fuses, an advanced method for simulating arcing process is proposed, which is based on Daalder's model [2]. Improvements are made on the determination of initial dimensions of arcing column and the influence of multiple fuse elements on the electric field. Agreements have been shown between measured fulgurite dimensions and calculated arc column length and cross sections. For substrate 12 kV 40 A high voltage full range fuses, simulations of arcing voltage and current are performed for breaking tests from an independent test station at different prospective currents. Theoretical results are found in good agreement with the experiment observations.

## References

- [1] R. Wilkins : Standard fuse model for system short-circuit studies. Proc. SAP, Lodz, Poland, 1997, pp.163-166.
- [2] J.E. Daalder and E.F. Schreurs: Arcing phenomena in high voltage fuses. EUT report 83-E-137, 1983.
- [3] J. Hibner: Calculation of the arc ignition voltage on single disruption of uniform fuse element by its independent disintegration in h.b.c. fuses. Proc. SAP, 1985, pp. 368-369.
- [4] M. Dolegowski: Calculation of the course of the current and voltage of a current limiting fuses. Proc. ICEFA 1976, pp. 218-232.
- [5] J.B. Wheeler: The high power constricted plasma discharge column (I. theoretical analysis). J. Phys. D: App. Phys., 3, 1970, pp. 1374-1380. (II. Experimental investigation).J. Phys. D: App. Phys., 4, 1970, pp. 400-406.
- [6] Lipski, T.: On the theory of the striated wire disintegration. IEEE Trans. on Plasma science, Vol. PS-10, no 4, 1982, pp. 339-344.
- [7] Sloot, J.G.J., Kalasek, V.I.: A two dimensional model for the burnback of fuse strips. Proc. 9th. Conf. Gas Discharges, Venice, 1988, pp.115-117.





**Session 2**

**MATHEMATICAL MODELLING "II"**

**Chair: Dr. R. Wilkins**



# NEW ASPECTS ON THE MULTI-ELEMENT FUSE PROTECTION CHARACTERISTIC

Eugen Hnatiuc, Radu Burlica, Bogdan Hnatiuc  
Technical University " Gh. Asachi"  
Iasi, Romania

**Abstract:** The fuses protection characteristics can be improved also by replacing the single way current fuse with two or more parallel connected fuses.

In our paper we proposed a mathematical model for an ensemble of two fusible elements, connected in parallel, in order to determine the protection characteristic of the ensemble for a specific load.

Based on this mathematical model, we will be analyzed the case of two symmetric and asymmetric fuse ensemble, also the possibility to control the current distribution on each fusible element.

The mathematical and experimental results lead to some new information about the multi-element fuse protection characteristic with arguments for the asymmetric fuse construction.

The results obtained permit to make some technical and economical evaluation for the multi-element fuses construction and functioning in electrical circuit protection.

## I. INTRODUCTION

The improvement performances of the fuses is an up-to-date preoccupation which provides solutions concerning their conception and structure, the materials used or the geometry of the fusible element.

This paper proposes an approach focused on the functioning of the multielement fuses during the pre-arch stage for the situation where the fusible elements are identical and different, respectively.

On may come to interesting conclusions regarding the protection characteristic of the multielement fuses and also regarding the influence of the asymmetry degree on their functioning during the pre-arch stage for  $(2-4) I_n$ .

### I. THE SYMMETRICAL MULTI-ELEMENT FUSE BEHAVIOR DURING THE PRE-ARCH STAGE

The fusible element diameter for a fuse with nominal current  $I_n$ , can be determinate using the relation:

$$\lambda \cdot I_n = k d^{\frac{3}{2}}, \quad (1)$$

the fusible diameter being:

$$d_0 = \sqrt[3]{\frac{\lambda^2 I_n^2}{k^2}}, \quad [\text{mm}], \quad (2)$$

where, if the fusible element material is copper, the constants are :  $\lambda = 1.6$  and  $k = 60$ , respectively .

If we consider the overload currents in the domain of  $(2-4) I_n$ , it can be accepted, as a first approximation, that the over-temperature evolution in time takes place conform to the expression:

$$\vartheta(t) = \vartheta_{\max} (1 - e^{-\frac{t}{T_0}}), \quad (3)$$

practically definite by the maximum overtemperature  $\vartheta_{\max}$  and the thermal time constant  $T_0$ ,

$$\vartheta_{\max} = \frac{4\rho I_n^2}{k_1 \pi^2 d_0^3}, \quad T_0 = \frac{\gamma d_0}{4k_1}, \quad (4)$$

where, in the relation (3) and (4),  $\rho$  [ $\Omega\text{m}$ ] represents the material resistivity of fusible element,  $\gamma$  [ $\text{Kg}/\text{m}^3$ ] is the density of the fusible material,  $c$  [ $\text{J}/\text{kg}^\circ\text{C}$ ] is the specific heat, and  $k_1$  [ $\text{w}/\text{m}^2 \text{ }^\circ\text{C}$ ] is the global heat transfer coefficient .

For an over-current passing through the fuse equal with  $\lambda I_n$ , the over-temperature of the element, see (4), becomes:

$$\vartheta_{\max} = \frac{4\rho \lambda^2 I_n^2}{k_1 \pi^2 d_0^3} = \vartheta_{\text{top}}, \quad (5)$$

and the melting time for the fusible element is considered to be:

$$t_0 = 4T_0, \quad (6)$$

If we consider the over current to be  $m\lambda I_n$ , the relation (4) become:

$$\vartheta_{\max} = \frac{4\rho \lambda^2 m^2 I_n^2}{k_1 \pi^2 d_0^3} = m^2 \vartheta_{\text{top}}, \quad m > 1, \quad (7)$$

and the melting time for the fusible element,  $t_{0m}$  is determined by the solution of the equation:

$$\vartheta_m(t_{0m}) = \vartheta_{\max} (1 - e^{-\frac{t_{0m}}{\tau_0}}) = \vartheta_{top} \quad (8)$$

Solving the equation (8) the melting time will be:

$$t_{0m} = T_0 \ln \frac{m^2}{m^2 - 1} \quad (9)$$

When instead of a single fusible element we use two identical elements connected in parallel, their diameter will be:

$$d_1 = \sqrt[3]{\frac{\lambda^2 I_n^2}{4k^2}} = d_0 \sqrt[3]{\frac{1}{4}} \quad (10)$$

Taking into account the relation (4<sub>2</sub>), the thermal time constant in this case become:

$$T_1 = \frac{\gamma d_1}{4k_1} = T_0 \frac{1}{\sqrt[3]{4}} \quad (11)$$

Considering the over-current going through these two symmetrical fusible elements equal with  $\lambda I_n$ , the biggest value of the over-temperature is:

$$\vartheta_{\max 1}^* = \frac{4\rho\lambda^2 \left(\frac{I_n}{2}\right)^2}{k_1 \pi^2 d_0^3 \frac{1}{4}} = \vartheta_{top} = \vartheta_{\max}^* \quad (12)$$

thus, the melting time of the first fusible element (practically of both elements in symmetrical construction) is considered to be:

$$t_1 = 4T_1 = 4T_0 \frac{1}{\sqrt[3]{4}} \leq t_0 \quad (13)$$

value that is smaller with 33.79% than the value of  $t_0$  according to the case of the fuse with a single fusible element, see (6).

In this case for the over-current value  $m\lambda I_n$ , the expression (4<sub>1</sub>) become:

$$\vartheta_{\max m,1} = \frac{4\rho\lambda^2 m^2 \left(\frac{I_n}{2}\right)^2}{k_1 \pi^2 d_0^3 \frac{1}{4}} = m^2 \vartheta_{top} \quad (14)$$

thus, the time when the first element melts and practically the circuit breaking occur,  $t_{m1}$ , is the solution of an equation like (8), resulting:

$$t_{1m} = T_1 \ln \frac{m^2}{m^2 - 1} \quad (15)$$

it's value being smaller than the value of  $t_{0m}$  with about 33.8 %.

Therefore, we can affirm that the protection characteristic for a fuse with two identical fusible elements in parallel is situated under the protection characteristic according to a fuse with a single fusible element for the overcurrents range between  $(2-4)I_n$ , even if the hypothesis imposed for the analytical approach of the proposed model (the current considered is constant, the neglecting the distribution of the temperature along the fusible element and the variation of material parameters with the temperature) are not fit for the real functioning conditions of the fuses.

## II. THE ASYMMETRICAL MULTI-ELEMENT FUSE BEHAVIOR DURING THE PRE-ARCH STAGE

The construction of the asymmetric multi-element fuses requires, the substitution of the fusible element with diameter  $d_0$  corresponding to the nominal current  $I_n$ , by two fusible elements, with different diameters, corresponding to the nominal current  $I_{n1}$ , respectively  $I_{n2}$ .

One may write the following expressions:

$$\begin{aligned} I_n &= I_{n1} + I_{n2}, \quad I_{n1} = \alpha I_n, \quad \alpha < 1/2 \\ I_{n2} &= (1-\alpha)I_n, \quad I_{n1} < I_{n2}. \end{aligned} \quad (16)$$

The two fusible element diameters will be:

$$d_1' = d_0 \alpha^{\frac{2}{3}}, \quad d_2' = d_0 (1-\alpha)^{\frac{2}{3}}, \quad (17)$$

and the expressions of thermal time constants became:

$$T_2' = (1-\alpha)^{\frac{2}{3}} T_0, \quad T_1' = \alpha^{\frac{2}{3}} T_0 \quad (18)$$

If the multi-element fuse is passing by the over-current  $\lambda I_n$  the relation (5) is:

$$\begin{aligned} \vartheta_{\max}^{(1)} &= \frac{4\rho\lambda^2 I_n^2 \alpha^2}{k_1 \pi^2 (d_0 \alpha^{\frac{2}{3}})^3} = \vartheta_{top} \\ \vartheta_{\max}^{(2)} &= \frac{4\rho\lambda^2 I_n^2 (1-\alpha)^2}{k_1 \pi^2 (d_0 (1-\alpha)^{\frac{2}{3}})^3} = \vartheta_{top}. \end{aligned} \quad (19)$$

The temperature evolution of the fusible elements takes place in according to an expression like (3), but because  $T_1' < T_2'$  the smaller diameter element will melt first after a time  $\tau_1$  that can be evaluated with the expression:

$$\tau_1 = 4T_1' = 4T_0\alpha^{\frac{2}{3}}, \quad (20)$$

at this moment the other fusible element will have the following over-temperature:

$$\begin{aligned} \vartheta_2'(\tau_1) &= \vartheta_{top} (1 - e^{-\frac{\tau_1}{T_2}}) = \\ &= \vartheta_{top} (1 - e^{-4(\frac{\alpha}{1-\alpha})^{\frac{2}{3}}}) \end{aligned} \quad (21)$$

From this moment the entire current  $\lambda I_n$  will pass only through the fusible element with diameter  $d_2$ , so that, from that moment the overtemperature evolution in time will be determined by the relation:

$$\begin{aligned} \vartheta_2'(t) &= \vartheta_2'(\tau_1) + \\ &+ [\vartheta_{max2}' - \vartheta_2'(\tau_1)](1 - e^{-\frac{t}{T_2}}), \end{aligned} \quad (22)$$

where:

$$\vartheta_{max2}' = \frac{1}{(1-\alpha)^2} \vartheta_{top} > \vartheta_{top} \quad (23)$$

The other fusible element will melt (and the circuit breaking) will appear after the time  $\tau_2$  which can be recalculated from the equation:

$$\vartheta_2'(\tau_2) = \vartheta_{top}, \quad (24)$$

thus we obtained:

$$\tau_2 = T_2' \ln \frac{\frac{1}{(1-\alpha)^2} - 1 + e^{-4(\frac{\alpha}{1-\alpha})^{\frac{2}{3}}}}{\frac{1}{(1-\alpha)^2} - 1}. \quad (25)$$

The functioning time of the asymmetric multi-element fuse will be:

$$\begin{aligned} t_2 = \tau_1 + \tau_2 &= T_0 [4\alpha^{\frac{2}{3}} + \\ &+ (1-\alpha)^{\frac{2}{3}} \ln \frac{\frac{1}{(1-\alpha)^2} - 1 + e^{-4(\frac{\alpha}{1-\alpha})^{\frac{2}{3}}}}{\frac{1}{(1-\alpha)^2} - 1}] \end{aligned} \quad (26)$$

depending on the asymmetry degree  $\alpha$ .

In order to emphasize the influence of the asymmetry degree on the breaking time of the multi-element fuse for an over-current  $\lambda I_n$ , we will consider the function:

$$\begin{aligned} f(x) &= 4x^{\frac{2}{3}} + \\ &+ (1-x)^{\frac{2}{3}} \ln \frac{\frac{1}{(1-x)^2} - 1 + e^{-4(\frac{x}{1-x})^{\frac{2}{3}}}}{\frac{1}{(1-x)^2} - 1}, \end{aligned} \quad (27)$$

with  $0 < x < 1/2$

its evolution being represented in Fig. 1.

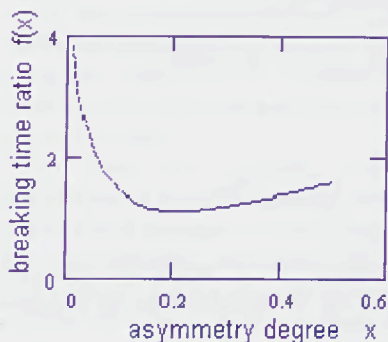


Figure 1. The influence of the asymmetry degree on the breaking time ratio.

Fig. 1 emphasizes a point of minimum for the function  $f(x)$  for a value of asymmetry degree, that indicates a decreasing of the fuse's pre-arch time in the overload currents domain. Also, the maximum value of the function  $f(x)$  is:

$$f(x) < 4 \quad (28)$$

The minimum fuse breaking time is:

$$t_{2min} = 1.126T_0, \text{ for the asymmetry degree } x = 0.215$$

Comparing this with the single element fuse, the asymmetric multi-element fuse provides a relative decreasing of the pre-arch time with about 71.8 %.

When the multi-element asymmetric fuse function at the current  $m\lambda I_n$ , with  $m > 1$ , the maximum values of the fusible element over-temperatures will be:

$$\vartheta_{max1m}' = \vartheta_{max2m}' = m^2 \vartheta_{top}, \quad m > 1 \quad (29)$$

The melting time for the thinner element  $\tau_1$  is obtained from the equation:

$$\vartheta_{1m}'(\tau) = m^2 \vartheta_{top} (1 - e^{-\frac{\tau}{T_2}}) = \vartheta_{top}, \quad (30)$$

resulting:

$$\tau_1 = T_1' \ln \frac{m^2}{m^2 - 1} = \alpha^{\frac{3}{2}} T_0 \ln \frac{m^2}{m^2 - 1}, \quad (31)$$

The value of the other element over-temperature (with diameter  $d_2$ ) at the moment  $\tau_1$  is:

$$\begin{aligned} \vartheta_{2m}'(\tau_1) &= m^2 \vartheta_{top}' (1 - e^{-\frac{\tau_1}{T_2}}) = \\ &= m^2 \vartheta_{top}' (1 - e^{-\frac{(\frac{\alpha}{1-\alpha})^{\frac{2}{3}} \ln \frac{m^2}{m^2-1}}{m^2-1}}) < \vartheta_{top}' \end{aligned} \quad (32)$$

The over-temperature evolution of the second element passing through by the current  $m\lambda I_n$  is:

$$\begin{aligned} \vartheta_{2m}^*(t) &= \vartheta_{2m}'(\tau_1) + \\ &+ [\vartheta_{max\ 2m}^* - \vartheta_{2m}'(\tau_1)] (1 - e^{-\frac{t}{T_2}}) \end{aligned} \quad (33)$$

obtaining:

$$\vartheta_{max\ 2m}^* = \frac{m^2}{(1-\alpha)^2} \vartheta_{top}' \quad (34)$$

The time  $\tau_2$ , when the second fusible element melts can be obtained from the equation:

$$\vartheta_{2m}^*(\tau_2) = \vartheta_{top}' \quad (35)$$

the time  $\tau_2$  will be:

$$\tau_2 = T_2 \ln \frac{\frac{1}{(1-\alpha)^2} - 1 + e^{-\frac{(\frac{\alpha}{1-\alpha})^2}{m^2}}}{\frac{1}{(1-\alpha)^2} - \frac{1}{m^2}} \quad (36)$$

The total function time for the asymmetric multi-element fuse is:

$$\begin{aligned} t_{2m} &= T_0 \left[ \alpha^{\frac{2}{3}} \ln \frac{m^2}{m^2-1} + \right. \\ &\left. (1-\alpha)^{\frac{2}{3}} \ln \frac{\frac{1}{(1-\alpha)^2} - 1 + e^{-\frac{(\frac{\alpha}{1-\alpha})^{\frac{2}{3}} \ln \frac{m^2}{m^2-1}}}{m^2-1}}{\frac{1}{(1-\alpha)^2} - \frac{1}{m^2}} \right] \end{aligned} \quad (37)$$

Taking into consideration the function  $g(x,m)$  described by the relation:

$$\begin{aligned} g(x,m) &= x^{\frac{2}{3}} \ln \frac{m^2}{m^2-1} + \\ &+ (1-x)^{\frac{2}{3}} \ln \frac{\frac{1}{(1-x)^2} - 1 + e^{-\frac{(\frac{x}{1-x})^{\frac{2}{3}} \ln \frac{m^2}{m^2-1}}}{m^2-1}}{\frac{1}{(1-x)^2} - \frac{1}{m^2}} \end{aligned} \quad (38)$$

it's evolution can be represented in Fig.2.

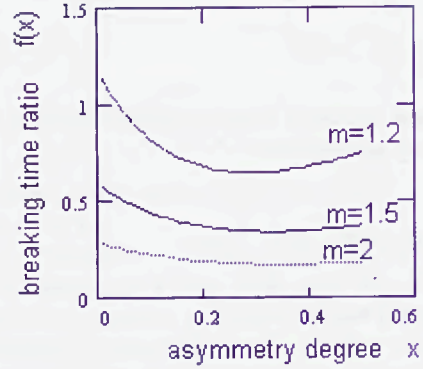


Figure 2. The influence of the asymmetry degree on the breaking time ratio for different values of factor  $m$ .

Figure 2 emphasize a minimum for the fuse breaking time ratio curves depending by the factor  $m$ , minimum that is more accentuated then the value of factor  $m \rightarrow 1$ , which correspond to an optimal design for multi-element asymmetric fuses from the point of view of the asymmetry degree. The minimum for the breaking time ratio correspond to  $x = 0.29 \div 0.35$ .

For example, for  $m = 1.2$  and  $I = m\lambda I_n$ , the multi-element fuse breaking time decrease with 45.85 %, comparing with a single fusible element fuse.

### III. EXPERIMENTAL RESULTS

The validation of the analytic results has been obtained by means of the device as the one presented in Fig.3 which permits the fixation of the number of fusible elements, identical or different, their connection in parallel and the supply assembly from an adjusting power supply.

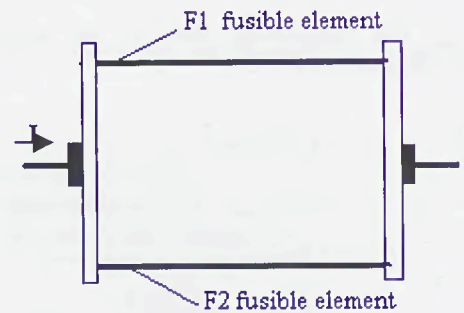


Figure 3. Multi-element fuse

The nominal current is  $I_n = 15$  A, so that the melting current is  $\lambda I_n = 25$  A. We have been made tests for over-currents up to 100 A. The conductors

diameters of the multi-element fuse are presented in Table 1.

Table 1- Fusible element diameters

$d_0$ [mm]	$d_1$ [mm]	$d_2$ [mm]	$d_3$ [mm]
0.56	0.35	0.3	0.4

In the case of the multi-element fuse we take into account different lengths in order to keep the currents distribution on the two ramifications.

The installation scheme is shown by Fig. 4 and the results of the experimental tests are given in Fig.5.

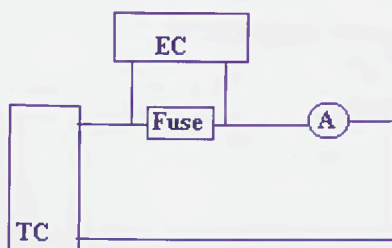


Figure 4. Experimental installation scheme

TC – current power supply  
EC – electronic chronometer  
A – ampermetre

If we compare the curve corresponding to a single fusible element with the one obtained for the symmetrical bi-element construction, we will notice that the reducing of the functioning time, in the domain of pre-arch, is about 30%, fact which confirm the analytic results.

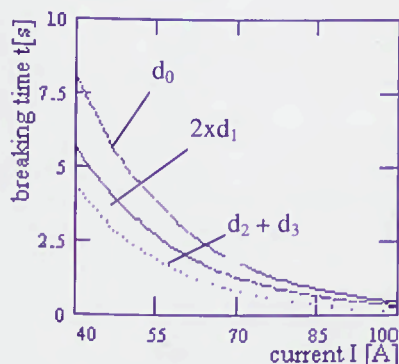


Figure 5. Experimental diagram

If we take as reference the curve corresponding to a single fusible element and we compare it to the one resulted for the asymmetrical

bi-element fuse having the asymmetry degree  $x = 0.4$ , we will observe a marked reducing of the functioning time in the pre-arch domain with about 70%, in concordance with the analytic results.

#### IV. CONCLUSIONS

The paper proposes a model for the functioning analysis of the multi-element fuses in the over-current regime taking as reference a construction with a single fusible element which is compared with symmetrical and asymmetrical fuses variants.

In the case of symmetrical bi-element fuses the experimental results concerning the functioning time reducing (about 30%), confirm the analytical ones which indicate for the breaking time a reducing ratio about 33.8%.

We may also notice a reducing of the functioning time of the asymmetrical bi-element fuse, a reducing which depends on the asymmetry degree. For the asymmetrical bi-element fuse having the asymmetry degree  $x = 0.4$ , we will observe a reducing of the functioning time in the pre-arch domain with about 71.8%, in concordance with the experimental results which indicate a reducing with about 70%.

It is to be mentioned the concordance of the experimental results with the analytical ones, though the hypothesis considered in the elaboration of the model may be meliorated.

An important observation regarding the functioning of the asymmetrical multi-element fuses relies on the dependence of the melting time on the asymmetry degree. Has been obtained minimum values for the breaking time which emphasize an optimal domain for the asymmetry degree  $\alpha$  ( $\alpha = 0.2 \div 0.35$ ), values which are different from the ones that are indicated in the literature [1].

#### REFERENCES

- [1] K. K. Namitokov, N. A. Ilina, I. G. Scholovski, "Apparati dlia zaschiti poluprovodnikovik ustroiv", Energoatom izdat, Moscow, 1988.
- [2] E. Hnatiuc, Em. Furnica, P. Leonte, "Possibilities for the extension of use of electrical fuse in fault current limiter devices", Proc. of the Fifth International Conference on electrical Fuses and their Applications, Ilmenau, Germany, 1995.
- [3] I. Barbu, "Sigurante electrice de joasa tensiune", Ed. Tehnica, Bucharest, 1983.

100

...

...

...

...

...

...

...

...

...

...

...

...

# EVALUATION OF THERMAL AND ELECTRICAL BEHAVIOUR OF FUSES IN CASE OF PARALLELING AND/OR HIGH FREQUENCIES

JL. GELET\*, D. TOURNIER\*, M. RUGGIERO\*\*

\*FERRAZ

Rue Vaucanson - 69720 SAINT-BONNET-DE-MURE- France

Tel (33) (0)4 72 22 66 11

Fax (33) (0)4 72 22 66 12

E-Mail : Ferraz\_rdf@compuserve.com

\*\*GLE

14 Connell Court TORONTO-Canada M8ZIE7

Tel 1-416-252-4531

Fax 1-416-252-4533

**Abstract :** The calculation of the right fuse for a power semiconductor equipment is requiring more and more sophisticated calculations and simulations. Due to new semiconductors like IGBT/IGCT, fuses are undergoing high current duty cycles, high frequencies and are required by end users for longer life durations and lower  $I^2t$ .

In order to face these new requests and to understand how the fuses behave, we have developed a method which allows to evaluate thermal and electrical parameters.

This method consists in a coupling between two simple models for fuses and their surroundings.

First is a thermal model, including thermal resistances, capacitances and generators. This model takes into account fuse itself with its connections, and also heat generated by semiconductor and surrounding. The parameters for the thermal characteristics of the fuse have been expressed in a very simple way.

Second is a simulation of the circuit, using HOER and LOWE's formula [1] in order to evaluate electrical resistance, self and mutual inductances for each component of the circuit. A so-called InCa software [2] is used in this way.

Finally both models are coupled in a solver-software which gives temperature of each component and current in each conductor. The results are used for the choice of the fuse, in addition with consideration of  $I^2t$  for protection and duty-cycles for life-duration.

An example of modelisation is presented. A specific customer application solved by this modelisation is also presented.

**1. Introduction :** The choice of a fuse depends on its thermal and electrical surrounding, and on electrical protection ( $I^2t$ , cut-off voltage...).

The multiplication of high frequency static converters leads to take care to high frequency effects on fuses. Numerical methods exist to solve electromagnetism- and thermal-equations. But such models are difficult to use because they require a lot of parameters such as thermal conductivity or emissivity values. The goal of our study is to have simple tools which permit to describe both thermal and electrical behaviors of the fuse. The model we need must :

- be very simple to use,
- allow to solve a lot of systems.

The build-up of those models answers to the necessity of help for fuses-design and research of solutions for customers specific applications.

Firstly, we will describe the thermal model, its structure with an example. Secondly, the electrical modeling will be presented. And then an example of actual application will be shown.

## 2. Thermal modelisation:

The general method needs parameters in order to take into account the temperature effects on the fuse derating [3]. Nowadays, numerical models based on the finite-differences resolution method [4] have been developed. But those models require data such as thermal conductivity, thermal constants values which are never well known or at least difficult to get.

The presented thermal model allows the calculation of the temperature for each element of the fuse : the copper terminals, the ceramic body and the fuse element, with the thermal and electrical characteristics of the fuse (see figure n°1). Instead of using a numerical method, we use a « global view » of the fuse, by describing thermal exchanges between its elements.

The following figures explain this global view.

**Keywords :** thermal design, device modelisation, high frequency power converters, diagnostics.

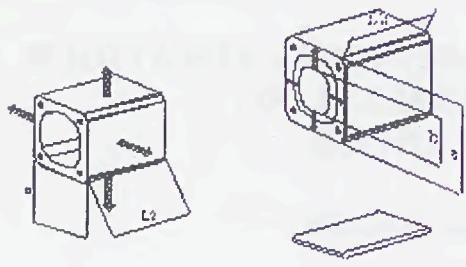


figure 1-a

figure 1-b

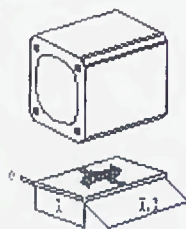


figure 1-c

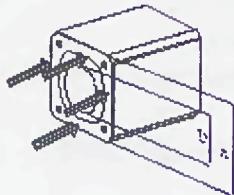


figure 1-d

figure n°1

We can see the different exchange paths of the heat, and so the associated equivalent components. This method permits to reduce the number of parameters of the model, and to have very simple equations. In order to calculate the temperature we used the well known electro-thermal analogy. The model involves resistors, capacitors and current generator. Each components value is linked with very simple parameterized equations to the fuse geometry and to the material used (ceramic, silver, copper...). A statistic analysis based on tests-data allows to calculate the parameters of the model.

The integration of this model in an electrical solver (Simplorer [5], or Spice) permits to investigate several kinds of simulation, depending on the criteria to be optimized or on the effect to be underlined. By using this model, we can obtain several characteristics for a given fuse and its surrounding such as :

- $I_{max} = f(\text{surrounding...})$ ,
- Link size =  $f(I_{max}, \text{surrounding...})$ ,
- Cooling =  $f(I_{max}, \text{geometry})$ .

An illustration of a characteristic calculated with this model is shown on the figure n°3. This graph shows the evolution of the losses in a fuse, versus the evolution of the electrical current. The resolution was made for different normalized conditions (of surrounding temperature, links size). The values were normalized in relation to the nominal electrical current of the fuse. The following figure describes the geometrical disposition of the fuse in the case C2 of simulation.

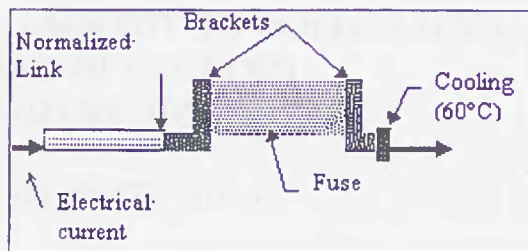


figure n°2.

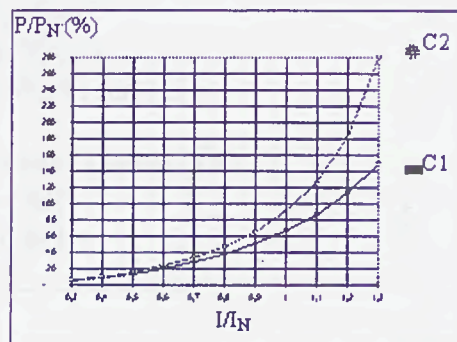


figure n°3 : example of curve performed with th thermal model.

Conditions of resolution of the lasts characteristics :

- ambient temperature = 30°C

	left terminal	right terminal
C1	Temp= 60°C	Temp= 60°C
C2	Temp= 60°C	normalized link (figure n°2)

figure n°4.

The easiness to calculate the model parameter and the use of an electrical solver permit to get those characteristics very quickly. This can be made without building a new model for each application, thanks to the solver composed of two coupled solvers : an electrical solver (based on Spice), and a state graph solver (based on the « Réseaux de Pétri » [6]). The coupling of those solvers, permits to adapt the model to any electrical application including fuse. So, it allows to predict the fuse-derating, when fuses are subjected to specific surrounding and cooling conditions.

The robustness of this model comes from the method of calculation of its parameters. More precise models could be done but our purpose is not to know the volumic distribution of temperature. The aim is to have an easy tool in order to estimate the global thermal behavior of fuses. This tool must be as simple as possible in order to be use with the electrical model for frequency-effects.

Keywords : thermal design, device modelisation, high frequency power converters, diagnostics.

### 3. Electrical circuit simulation:

As it was explained in the preceding paragraph, the choice of a fuse depends on its thermal surrounding, but not only. The evolution of power semiconductors leads to fast operations in electrical circuits, with high current variations (and induced overvoltages) and high frequency values. It is difficult to estimate the current distribution in an electrical circuit. Measurements are also difficult to carry out. Building of a model able to solve electromagnetism equations is possible on a simple structure, but difficult on a complex one. The goal is to have simple and adaptive models. We decided to use a software which solves electromagnetism equation and gives the equivalent electrical circuit of a structure.

On a first point of view, the electrical circuit simulation considers the fuse as an « equivalent inductor » added to an existing application: the overvoltage caused by high current commutation must be limited. So the fuse inductance value must be as low as possible. As fuse works under high frequencies, the interaction between fuses and their surrounding must be taken into account. Two electromagnetic effects are involved: skin and proximity effects.

The first one depends on the frequency and can be expressed as:

$$\delta = \sqrt{\frac{2}{\omega \cdot \sigma \cdot \mu}} \quad (1)$$

- where:
- $\delta$  is the skin depth
  - $\omega$  is the pulsation  $\omega = 2 \cdot \pi \cdot f$
  - $\mu$  is the magnetic permeability
  - $\sigma$  is the electrical conductivity of the metal

and leads to unequal current distribution in a conductor (see figure n°5). The second effect (proximity effect) is caused by induced current between conductors by mutual effect (due to eddy current [1]).

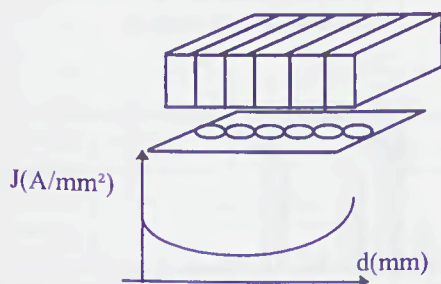


figure n°5.

The result of those interactions is an unsharing between parallel conductors (for example).

The following figure presents the effect of frequency on the current sharing between three parallel conductors. The total current is 450A. At frequencies higher than 40Hz, the unbalanced is important.

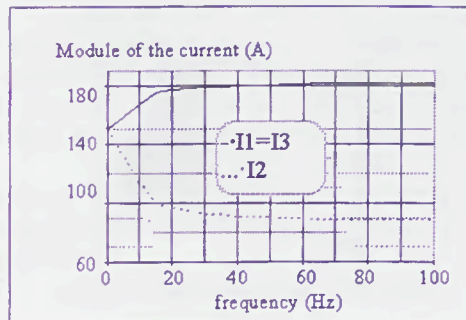


figure n°6 : Distribution of the current as a function of frequency [7]

The principle of the resolution used is based on the PEC<sup>1</sup> method [2]. From a geometrical description of a structure, a dedicated software calculates an electrical equivalent circuit, involving resistors, self inductors and mutual inductors.

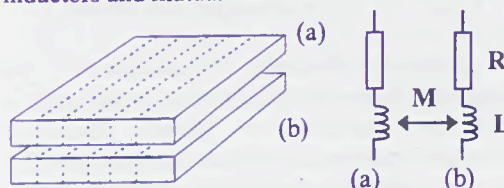


figure n°7.

After calculation, we get, a matrix equation, describing the circuit, with the impedance matrix Z:

$$[\vec{V}] = [\vec{Z}] \cdot [\vec{I}] = \begin{bmatrix} R_1 + jL_1\omega & M_{12} \\ M_{21} & R_2 + jL_2\omega \end{bmatrix} \begin{bmatrix} \vec{I}_1 \\ \vec{I}_2 \end{bmatrix} \quad (2)$$

Because we use an electrical software, with the equivalent net-list file of the geometry, we can calculate the current distribution in the entire structure, and the interaction between the different elements.

The example of a coupled resolution (electro / thermal) is presented in the following section. It shows the advantage of using coupled simulation of electrical and thermal models. The study of the electrical behavior permits to know the exact value of the electrical current flowing across the fuse, and then to predict the global thermal behavior of the fuse.

**4. An example of a coupled resolution:** We received a claim from a customer because fuses were subjected to a quick ageing and failure. Abnormal ageings were noticed in a power factor corrector device by a customer, specifically on the same electrical line wire. The aim of this study was to find the reason why fuses were ageing rapidly, and to find a replacement solution. One possible origin of this trouble may be a high value inductance of a coil, close to the two parallel fuses.

<sup>1</sup> PEC : Partial Equivalent Circuit.

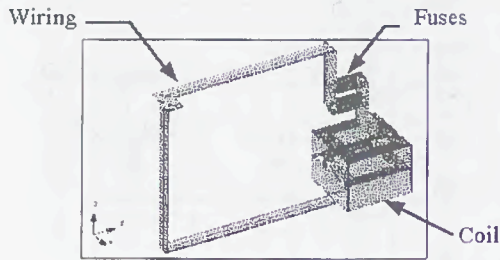


figure n°8 : InCa modelised structure

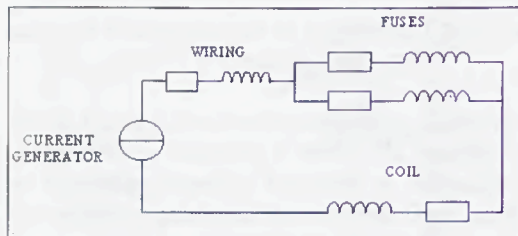


figure n°9 :Equivalent electrical circuit

The electrical simulation demonstrated the influence of this coil on the fuses, and how it derated the characteristics of the fuses. A geometrical modelisation of the wiring (figure n°8), using the software called InCa coupled with an electrical software gives the global electrical equivalent circuit on the structure (figure n°9). Several resolutions for different frequencies show the evolution of interactions between the different elements. For frequencies from 50 Hz to 10kHz, the changes of impedances (self- and mutual-inductances are very low). The following calculations were made for a frequency of 1kHz. The first result of this resolution is an unequal current sharing into fuses elements.

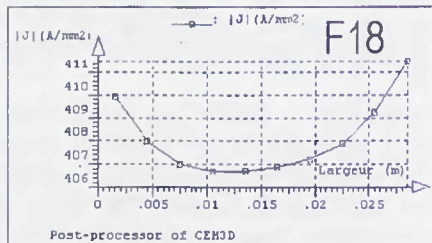


figure n°10 : Current density sharing on the width for different fuses elements.

Using the equivalent electrical circuit with an electrical software (such as Spice), with the actual current waveforms, we get the current sharing into the two fuses.

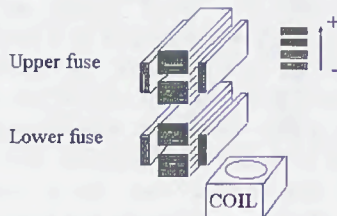


figure n°11 : synthesis of the results.

The total current across the fuses is unequally shared into each fuse-element. For a total current equal to 100A, the upper fuse supports 45A as the lower supports 55A (figure n°12).

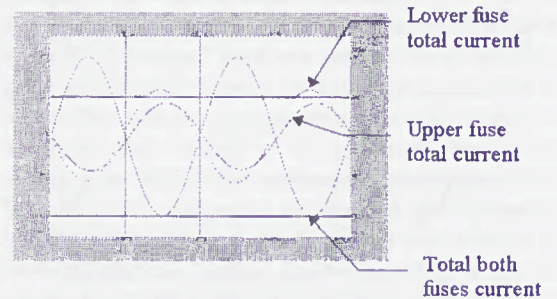


figure n°12.

And, inside a fuse (made of 8 elements), one can support 10A while another one is only flown by 1A as shown in figure n°12. The effect of the coil on the fuse is then well demonstrated.

The next step was the study of different fuses orientations, in order to find the right fuse with the best disposition. The following figures present some modelised structures.

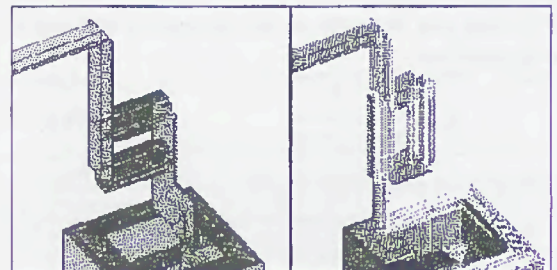


figure n°13.

figure n°14.

More precise results of the current sharing between fuses and into a fuse are presented on figure n°15 for the geometrical disposition n°2 (figure n°14).

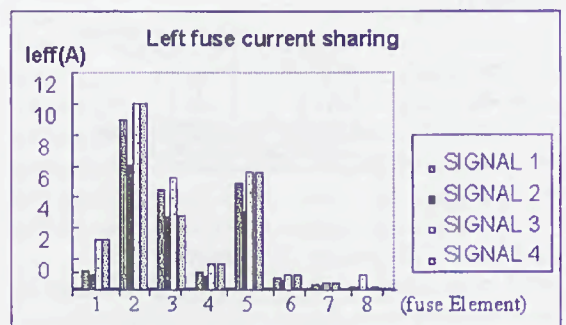


figure n°15.

Those results were performed for different electrical current waveforms (depending of the working operation of the device). The damage of characteristics due to the coil for the parallel fuses is then well precise. All the combined currents lead to an unequal current sharing between

Keywords : thermal design, device modelisation, high frequency power converters, diagnostics.

fuses, and also inner fuse elements, leading to a thermal unequal heating of the different fuse elements. The result of this is mechanical stresses, whose on/off cycling leads to metallurgical-fatigue phenomenon and then to the derating of the fuse [8]. The final result can be an abnormal fuse blowing.

*Research of the best solution* : Changing the two paralleled fuses by a bigger one allows to minimize the proximity effect on the coil. An appropriated disposition of the fuse was determined. The following figure n°16 shows the replacement solution proposed to our customer.

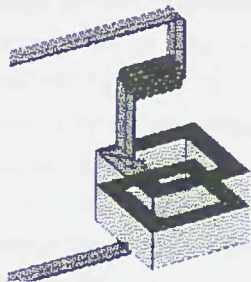


figure n° 16.

### 5. Conclusion

The use of coupled models allows to give quick and precise answers to specific problems, in the choice of a fuse and in its geometrical location in an electrical circuit. The global view of our thermal model permits to adapt it easily to a lot of structures. The electro/thermal resolution permits to study interactions between a fuse and its surrounding.

The principle of the solving method is explained by the following figure .

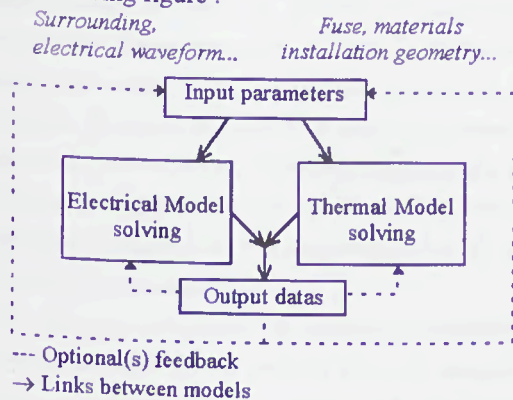


figure n°17.

Each parameter can be fixed or calculated; feedback between input(s) and output(s) can be made in order to optimize parameters (for example the cooling, the links size). Single or mixed resolution(s) can also be performed.

We have now simple tools to work on the Electro-Thermal and Electromagnetism Compatibility of fuse. We have also the possibility to simulate structures in order to optimize the choice of the fuses and eventually their design.

Thanks to those models, the global behavior of fuses is precise, and the interactions of both electrical and thermal surroundings are easily understood.

### 6. References :

- [1] G.FOURNET, Electromagnétisme à partir des équations locales. Ed. Masson, 1985.
- [2] « Vers un outil de conception de câblage, le logiciel InCa », E.Clavel Thèse de Doctorat de l'INPG, Grenoble, Nov 1996.
- [3]. *Doc technique détermination calibre de fusible en fonction de la température.*
- [4]. A.B de Vriendt, La transmission de la chaleur, Vol. 1, Tome 2. Ed. Gaëtan Morin, 1982.
- [5]. Applications notes Simplorer. Analysis of complex systems.
- [6]. Les réseaux de Pétri, <http://www.laas.fr/surf/what-fr.html>
- [7]. « Distribution of high-frequency currents through the elements of a fuse », S. Duong, C. Schaeffer (LEG-Grenoble), R.Deshayes, J.L. Gelet (FERRAZ) / ICEFA 95
- [8]. *Doc technique détermination calibre de fusible en fonction des cycles de marches/arrêts.*
- [9]. « Etude de l'intégration d'une protection par fusible dans les convertisseurs à IGBT » S.Duong, Thèse INPG, Grenoble, Juillet 1997.
- [10]. « Simulation de circuits électriques à hautes fréquences » J.L Gelet (FERRAZ), D.Tournier (CEGELY-INSA), Proceeding of Journée SEE, Lyon 18/03/99.

*Keywords* : thermal design, device modelisation, high frequency power converters, diagnostics.

卷之四

四

四

四

四

四

四

卷之四

四

四

四

四

四

四

# THE RESEARCH ON THE STABLE TEMPERATURE-RISE OF HIGH-VOLTAGE CURRENT-LIMITING FUSE-LINK

Jin Lijun Ma Zhiying Wang Jimei  
Division of Electric Apparatus  
School of Electrical Engineering  
Xi'an Jiaotong University  
Xi'an, 710049,  
People's Republic of China

**Abstract:** Through the theoretical analysis of nature heat convection between the air and the surface of high-voltage current-limiting fuses in normal service, a mathematical model for the temperature-rise distributing of the surface of the fuse-link is put forward. The results of study show that the temperature-rise has a great difference between the up and down contact of fuse when the fuse-link is fixed vertically, it is proved by the experiment research. The mathematical model and the analysis method could apply to other similar structural appliances.

## 1. INTRODUCE

Electric appliances will be heated when it in service, especially for fuses. Fuse is a device that by fusing its proportioned components, opens the circuit in which it is inserted by breaking the current when this exceeds a given value for a sufficient time. It is very important to find a simulation calculation method for the temperature-rise of fuse. On account of complicated structure, the temperature-rise of fuse is difficult to calculate. For example, the electric power loss and heat of fuse-link, the heat conduction of many layers amount the fuse-link, sand stone and insulation bushing, the heat convection between the air and the fuses, The effect of the different mounting on the temperature-rise of fuse-link (vertical or horizontal).

In this paper. Through the analysis of nature heat convection between the air and the fuse, the simulative calculation method of temperature-rise of fuse is obtained, and it is proved by the experiment.

## 2. THE COEFFICIENT OF CONVECTIVE HEAT TRANSFER

When the fuse is in normal service, The heat

exchange is done by the heat convection, here, the dimensionless equation is used to solve the coefficient of convective heat transfer, The Nusselt number equation of nature heat convection defined as<sup>[1]</sup>:

$$Nu = f(G_r, P_r) \quad (1)$$

$$\text{and: } G_r = g\beta ql^4 / \lambda\gamma^2 \quad (2)$$

where  $Nu$ —Nusselt number, dependent dimensionless number;

$G_r$ —Grashof number;

$l$ —Characteristic dimension (m);

$q$ —Specific rate of heat flow( $Wm^{-2}$ );

$g$ —gravitational acceleration( $ms^{-2}$ );

$\beta$ —volumetric thermal expansion coefficient ( $K^{-1}$ );

$\gamma$ —diffusion momentum( $m^2s^{-1}$ ), ;

$\lambda$ —thermal conductivity( $Wm^{-1}K^{-1}$ );

$P_r$ —Prandtl number, which has a strong effect on heat convection.

In the dimensionless equation, some coefficient can be obtained by reference [2], for example, if the reference temperature  $t=70^\circ C$ , we can know from the index of reference [2] that:  $\lambda=0.0296Wm^{-1}C^{-1}$ ,  $\gamma=20.02 \times 10^{-6}m^2s^{-1}$ ,  $Pr=0.694$ .

The coefficient of convective heat transfer ( $\alpha$ ) is included in Nusselt number, so the  $Nu$  is a dependent dimensionless number  $\alpha$  can be known from  $Nu$ . When the independent dimensionless numbers that includes in the  $Nu$  number has be defined. There are different laws to suit  $Nu$ . Laminar flow and turbulent flow are described by different experiment relationships under different condition[3].

Laminar flow:  $10^5 < Gr \cdot Pr < 10^{11}$

Dimensionless number:

$$Nu_x = 0.6(Gr \cdot Pr)^{1/5} \quad (3)$$

Laminar flow:  $10^{13} < Gr \cdot Pr < 10^{16}$

Dimensionless number:

$$Nu_x = 0.568(Gr \cdot Pr)^{1/4} \quad (4)$$

$$\text{with: } Nu_x = \frac{\alpha_x x}{\lambda} \quad (5)$$

where  $Nu_x$ —Nusselt number;

$\alpha_x$ —Partial coefficient of convective heat transfer ( $Wm^{-2}K^{-1}$ );

$x$ —coordinate of boundary layer of tube wall.

Coefficients of convective heat transfer are different under vertical and horizontal mount. When the fuse is mounted vertical, the characteristic dimension is the length ( $L$ ) of fuse. Great change of heat convection has taken place from bottom to top of fuse. The coefficient of convective heat transfer must be described by partial  $\alpha_x$ .

$$\alpha_x = \frac{Nu_x \lambda}{x} \quad (6)$$

When fuse is mounted horizontal, The characteristic dimension is the diameter ( $D$ ), for the diameter is small relatively. Taking the coefficient of convective heat transfer as a constant under horizontal mount, so that an area-averaged value can be defined as:

$$\bar{\alpha} = \frac{5}{4} \alpha_x = \frac{5Nu\lambda}{4D} \quad (7)$$

The  $\alpha$  varies around the length of the fuse while the fuse vertical mount. From eqn.(3).(6). The relationship between the  $\alpha_x$  and the length  $x$  can be calculated the results are shown as fig. 1. the  $\alpha_x$  decreases as the length  $x$  increases. The conditions heat dissipation are very different between the up and the

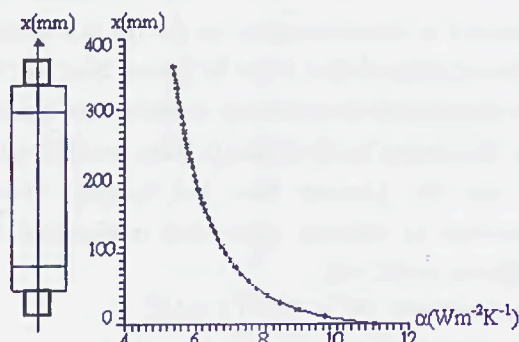


Fig.1 The particular coefficient of convective heat transfer along the wall of fuse-link fixed vertically

down for fuse when it is vertical mount.

### 3. CALCULATION FOR THE TEMPERATURE-RISE DISTRIBUTION OF FUSE-LINK

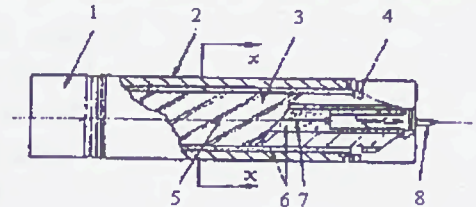


Fig.2 The structure of fuse

1-fuse-link contact cap; 2-insulation bush; 3-star shaped support; 4-airtight; 5-fuse-element; 6- sand stone; 7-striler coil; 8-striker

The structure of H-V current-limiting fuse-link is present in fig.2. The fuse-elements are twisted helicoidal around a star shaped ceramic support, fuse shell is insulation tube, it is often made up of ceramic. Between support and bush, sand stone are filled up.

The fuse-link can be simplified as a bar in order to calculation T, shown on fig.3. The fuse-link is symmetry on the center.  $L_2$ . the section between  $L_1$  to  $L_0$  is fuse's metal contact cap of fuse, the section from  $L_0$  to  $L_2$  is ceramic bush. The temperature-rise distribution of fuse-link can be divided into two part to calculate.  $Q$  the internal source,  $dx$  the calculus element;  $S$  the section area.  $P$  the circumference.  $\lambda$  thermal conductivity,  $T$

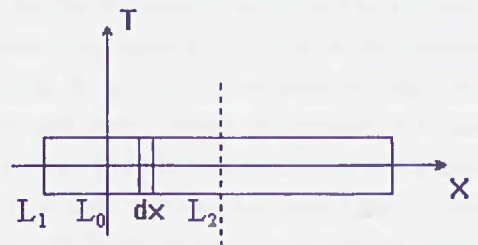


Fig.3 The coordinate of the axial temperature-rise distribution of fuse-link

temperature-rise.

$$\frac{d^2 T}{dx^2} - \frac{\alpha P}{\lambda S} T + \frac{Q}{\lambda} = 0 \quad (8)$$

The solution of eqn.(8) as follows :

$$T = T_w + C_1 e^{mx} + C_2 e^{-mx} \quad (9)$$

Where coefficient  $C_1, C_2$  can be obtained from the

boundary condition. For the part of conductor,  $S_1$  the section area;  $P_1$  the circumference.  $\lambda_1$  thermal conductivity,  $T_1$  temperature-rise.  $\theta_1$  the stable temperature-rise of conductor far from fuse, boundary condition is presented follow:

$$\begin{cases} T|_{x=-\infty} = \theta_1 \\ \left. \frac{dT_1}{dx} \right|_{x=-\infty} = 0 \end{cases} \quad (10)$$

For the part of ceramic bush,  $S_2$  the section area;  $P_2$  the circumference.  $\lambda_2$  thermal conductivity,  $T_2$  temperature-rise.  $\theta_{max}$  the highest temperature-rise of fuse, the boundary condition is given:

$$\begin{cases} T|_{x=L_2} = \theta_{max} \\ \left. \frac{dT_2}{dx} \right|_{x=L_2} = 0 \end{cases} \quad (11)$$

At  $L_0$  the temperature-rise of fuse is assumed as  $\theta_0$ , the boundary condition is given:

$$\begin{cases} T_1 = T_2 = \theta_0 \\ \left. \frac{dT_1}{dx} \right|_{x=L_0} = \left. \frac{dT_2}{dx} \right|_{x=L_0} \end{cases} \quad (12)$$

Through deduced and solved, the different sections of temperature-rise distribution are given

$$T_1 = \theta_1 + (\theta_0 - \theta_1)e^{m_1x}$$

$$(L_1 \leq x \leq L_0) \quad (13)$$

$$T_2 = \theta_2 + \frac{\theta_{max} - \theta_2}{2} \left( \frac{e^{m_2x} + e^{m_2L_2}}{e^{m_2L_2}} + \frac{e^{m_2x}}{e^{m_2x}} \right)$$

$$(L_0 < x < L_2) \quad (14)$$

where,  $m_1$ 、 $m_2$ 、 $\theta_0$ 、 $\theta_1$ 、 $\theta_2$  ( $\theta_2$  the stable temperature-rise far from the  $\theta_{max}$ ) are known terms, they are given

$$m_1 = \sqrt{\frac{\alpha_1 P_1}{\lambda_1 S_1}}; \quad m_2 = \sqrt{\frac{\alpha_2 P_2}{\lambda_2 S_2}};$$

$$\theta_0 = \frac{m_1 \theta_1 (e^{-m_2 L_2} + e^{m_2 L_2}) - m_2 \theta_2 (e^{-m_2 L_2} - e^{m_2 L_2})}{m_1 (e^{-m_2 L_2} + e^{m_2 L_2}) - m_2 (e^{-m_2 L_2} - e^{m_2 L_2})}$$

$$\theta_1 = \frac{Q_1 S_1}{\alpha_1 P_1}; \quad \theta_2 = \frac{Q_2 S_2}{\alpha_2 P_2};$$

$$\theta_{max} = \theta_2 + \frac{2(\theta_0 - \theta_2)}{e^{-m_2 L_2} + e^{m_2 L_2}}.$$

According to the symmetry principle, the temperature-rise of the other part of fuse-link can be

known, The inter heat sources  $Q(Wm^{-3})$  can be obtained follow:

$$Q = I^2 R / V \quad (15)$$

where:  $I(A)$  the current,  $R(\Omega)$  the resistance of fuse,  $V(m^3)$  the volume of conductor that produces heat.

#### 4. CALCULATION AND TEST

To validate the mathematical model, some comparisons between experiments and calculation results have been made. Rated current of the fuse is 100A; The resistance is  $5 \times 10^{-3} \Omega$ . The diameter is 76.2mm, the length is 360mm. The temperature-rise is measured by thermocouple method. Two different mountings (horizontal and vertical) are tested under 100A current for fuse-link sample. The comparisons between experiments and calculations have been performed with the results presented fig.4, fig.5. According to the mathematical model, the calculation results are shown as the curve 2 in fig.4 and fig.5. A good agreement observed on fig 4, fig.5 between experiment and calculation. The No.3 in the two fig is the symbolization of fuse-link. The length of fuse-link is signified by axis x. The temperature-rise of fuse-link surface is signified by axis Y.

In the fig.4, the fuse-link mounting horizontal, the stable temperature-rise distributes symmetry center, the center temperature-rise is the highest, the calculation is 112K, the value of measurement is 119K, the error of calculation is 5.8%. The temperature-rise of two contact caps is the same as 41K.

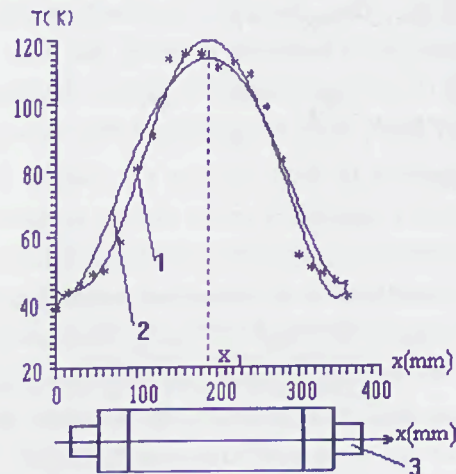


Fig.4 The temperature-rise distribution of fuse-link fixed horizontal

1—experiment; 2—calculation 3—fuse-link

In fig.5 when the fuse-link mounted vertical in

serves. The highest temperature-rise is above the center, the T of up contact is greater than the down. The distribution of stable T is unsymmetrical. At the  $X_2=220\text{mm}$ , It has the highest temperature, the value of calculation is 107K, the value of experiment is 114K, the error of calculation is 5.7%. The temperature-rise of up contact cap is 62K, and the down contact cap is 34K. It is above one times of temperature-rise between the up and down contact cap.

It is different that the stable temperature-rise distribution of fuse under horizontal and vertical

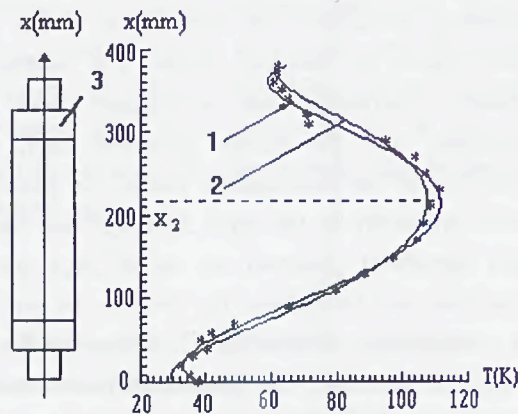


Fig.5 The temperature-rise distribution of fuse-link fixed vertically

1—measurement; 2—calculation; 3—fuse-link

mounting. When fuses are withstanding the same current,

This case can be explained by the heat convection condition. The characteristic dimension is fuse's diameter (D), in horizontal mounting. The (CD) is fuse's length (L) in vertical mounting. Because the diameter (D) is very small, the  $\alpha$  of horizontal fuse is determined by the diameter D. From equation (7), taking  $\alpha$  for  $\alpha$ , which is a constant. It means that the condition of the heat convection is the same for two tops of fuse.

When fuse is in vertical orientation, the  $\alpha$  varies the inverse of the length l, from fig.1 we known that the  $\alpha$  of two tops are different. The  $\alpha$  of up contact cap is smaller than the  $\alpha$  of down. So the closer to the up contact cap is, the smaller the heat exchanges. The T of up of fuse is higher than down. The T distribution is unsymmetry.

## 5. CONCLUSIONS

A mathematical model for temperature-rise distribution of the fuse-link is put forward by theoretical analysis. Different a equation has be presented to suit different mounting of fuse-link.

The T distribution of fuse-link is symmetry under horisontical mounting. When the fuse-link is installed vertical, T-r distribution is unsymmetry, it is because that the  $\alpha$  varies from bottom to top. The calculation has been validated by test.

## REFERENCES

- [1] Frank P. Incropera & David P. DeWitt John Wiley and Sons, " Fundamentals of Heat Transfer ", Published Simultaneously in Canada. 1981.
- [2] Yang shiming, "Heat Transfer", Higher Education Publishing Company. 1989
- [3] Frank M White . "Heat Transfer". Addison-Wesley Publishing Company . 1984

Jin Lijun was born in Zhejiang China in 1964. He received B.Sc., M.Sc. degrees in Xi'an Jiaotong University in 1987,1997 respectively. Now he is studying in Xi'an Jiaotong University as a doctor candidate and engaging in the study of "Self-Adapting Intelligent Control Device of High Voltage Circuit Breakers "

Ma Zhiying was born in Zhejiang China in 1937. He graduated from the department of Electric Engineering of Xi'an Jiaotong University in 1958, and he completed his graduate school work In 1963. He is presently a professor in Xi'an Jiaotong University, and he has been engaged in the investigation of arc phenomena and R & D of high voltage switchgears. He is a senior member of CES, of CSEE and of IEEE.

Wang Jimei was born in Zhejiang China in 1922. He graduated from the department of Electric Engineering of Shanghai Datong University in 1946, He is presently a professor in Xi'an Jiaotong University, and he has been engaged in the properties of fuse and vacuum arcs. He has published 8 books and more than 230 papers.

# MODELING AND SIMULATION OF THE THERMAL STRESS AT THE ELECTRIC FUSES CONTACTS

A. Baraboi\*, I. Ciutea\*\*, M. Adam\*, C. Pancu\*, T. A. Baraboi\*\*\*  
 «Gh. Asachi» Technical University\*,  
 National Company of Electricity\*\*, Artinfo Co.\*\*\*  
 Iasi-Romania

**Abstract:** An electrical RC or R model of the thermal process, with numerical EMTP treatment and results concerning the thermal stress at the electric fuses contacts are presented.

## 0 INTRODUCTION

Electric fuses are protection apparatus with the role to limit current and power in electrical circuit when is crossed by an overcurrent or a short-circuit current.

Also, at the first sight the electric fuse manufacture and its working principle don't seem a hardly gain insight into matters, in fact, this device working is complex [1], [7], [8].

Its working must be considered like a logical succession, from cause to effect, by many different kind processes (electrical, thermal, sometime mechanical processes, etc) which unfold in different ways. These processes can be investigated like transient condition (states), in certain period of times or, interesting for their space localization, at a given moment.

Proceeding from working principle, fuse elements must have minimum thermal stability in the protected circuit, so that, under overcurrents or short-circuit currents action, the circuit switching off must be done inside electric fuse during a limited time.

Working fuse means melting fuse element during a limited time, which takes place at a fixed temperature. The heating conduction, giving off by Joule-Lenz effect into fuse element, leads to temperature increasing in different manufactured parts, closes or farther by fuse link.

During on working fuse, the conduction heating transmission thermal flux reaches component parts closes or farther by thermal source-fuse link, depending on current intensity which brings about fuse working.

At short-circuit currents, the thermal processes are adiabatically and, so, the temperature increasing is located on fuse link, where specific losses through electrical-thermal effect are maximum.

In the case of normal condition or overload currents, when working period of times are bigger, the temperature increasings because of fuse link heating reach peripheral manufactured parts such as, for instance, the electric fuse contacts.

The electric fuse contacts heating depends on current and fuse features, so, working time. On the other hand, the electric contacts are thermal sources themselves. The contacts technical condition influences their temperature and fuse link temperature, so, fuse working characteristics.

Making evident these aspects is possible to use an adequate model to fuse working and a software to allow numerical simulation of a thermal transmission complex model, not depending on transient or permanent conditions.

## 1 ELECTRICAL MODEL OF THE THERMAL PROCESS

### II.1 Theory on the RC modeling

The electrical modeling of thermal processes makes possible thermal transmission analyse both in transient and permanent conditions.

Table I – Thermal conduction equation

Coordinate system	Equation
Cartesian	$p = \gamma c \frac{\partial \theta}{\partial t} - \lambda_x \frac{\partial^2 \theta}{\partial x^2} - \lambda_y \frac{\partial^2 \theta}{\partial y^2} - \lambda_z \frac{\partial^2 \theta}{\partial z^2}$
Cylindrical	$p = \gamma c \frac{\partial \theta}{\partial t} - \lambda \left( \frac{\partial^2 \theta}{\partial r^2} + \frac{1}{r} \frac{\partial \theta}{\partial r} + \frac{1}{r^2} \frac{\partial^2 \theta}{\partial \varphi^2} + \frac{\partial^2 \theta}{\partial z^2} \right)$
Spherical	$p = \gamma c \frac{\partial \theta}{\partial t} - \lambda \left( \frac{\partial^2 \theta}{\partial r^2} + \frac{2}{r} \frac{\partial \theta}{\partial r} + \frac{1}{r^2 \sin \vartheta} \frac{\partial^2 \theta}{\partial \varphi^2} + \frac{1}{r^2 \sin \vartheta} \frac{\partial \theta}{\partial \vartheta} + \frac{1}{r^2} \frac{\partial^2 \theta}{\partial \vartheta^2} \right)$

The giving of heating by Joule-Lenz effect into volume of conduction material crossed by current is continuously transported from warmer temperature zones to smaller value temperature zones.

The heating transfer in the solid materials takes place by conduction.

This phenomenon is ruled by Fourier law which allow to establish the general equation of thermal conduction in transient conditions.

In accordance to coordinate system to use, this equation can have one of shown formula from Table I, [4], [5].

The notations mean:  $p$ -specific losses from Joule-Lenz effect;  $\theta$ -temperature;  $\gamma$ -density,  $c$ -specific heating;  $\lambda$ -thermal conductivity;  $x, y, z$ -cartesian coordinates;  $r, \varphi, z$ -cylindrical coordinates;  $r, \varphi, \theta$ -spherical coordinates.

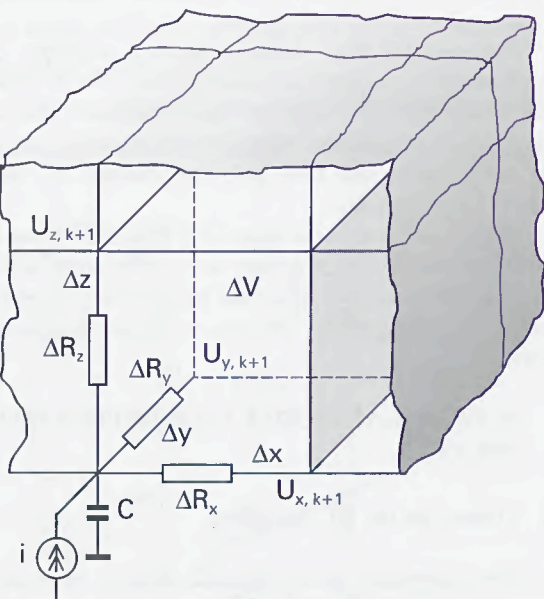


Fig.1 Electrical RC model of the thermal transmission into elementary volume

If thermal conduction refers to an elementary volume  $\Delta V$  (Fig.1), using finite differences method, first equation from Table I, it gets:

$$p = \gamma c \frac{d\theta}{dt} \Big|_k - \lambda_x \frac{\theta_{x,k-1} - 2\theta_k + \theta_{x,k+1}}{(\Delta x)^2} - \lambda_y \frac{\theta_{y,k-1} - 2\theta_k + \theta_{y,k+1}}{(\Delta y)^2} - \lambda_z \frac{\theta_{z,k-1} - 2\theta_k + \theta_{z,k+1}}{(\Delta z)^2} \quad (1)$$

where:  $\theta_{k,k-1}, \theta_k, \theta_{k,k+1}$  are recorded temperatures in three successive points to  $x, y, z$  directions.

Equation (1) may be written under next form:

$$\frac{\Delta P}{2} = \frac{\Delta m}{2} c \frac{d\theta}{dt} \Big|_k + \frac{\theta_k - \theta_{x,k-1}}{\Delta R_{tx}} + \frac{\theta_k - \theta_{x,k+1}}{\Delta R_{tx}} + \frac{\theta_k - \theta_{y,k-1}}{\Delta R_{ty}} + \frac{\theta_k - \theta_{y,k+1}}{\Delta R_{ty}} + \frac{\theta_k - \theta_{z,k-1}}{\Delta R_{tz}} + \frac{\theta_k - \theta_{z,k+1}}{\Delta R_{tz}}, \quad (2)$$

where it was noted:

$$\Delta V = \Delta x \Delta y \Delta z, \Delta P = p \Delta V, \Delta R_{tx} = \frac{2\Delta x}{\lambda_x \Delta y \Delta z}, \quad (3)$$

$$\Delta R_{ty} = \frac{2\Delta y}{\lambda_y \Delta x \Delta z}, \Delta R_{tz} = \frac{2\Delta z}{\lambda_z \Delta x \Delta y},$$

Starting from correspondence relationships:

$$\frac{\Delta P}{2} \Leftrightarrow i, \frac{\Delta m}{c} \Leftrightarrow C, \Delta R_t \Leftrightarrow \Delta R, \theta \Leftrightarrow u \quad (4)$$

it can simulate the thermal conduction into volume  $\Delta V$  using electrical equivalent network RC with the electrical circuit, [6], shown in Fig.1.

The Joule-Lenz effect losses into considered volume are modeled using current source  $i$ . If the volume  $\Delta V$  not represent an electrical-thermal conversion headquarters, then this current source is missing from equivalent circuit.

Referring to physical reasons it is necessary that at heating transmission describing to add initial and limit thermal conditions at considered model.

Regarding to initial conditions could be considered under next form:

$$\theta(x, y, z, 0) = \theta_0(x, y, z) \Leftrightarrow u_k(0) = u_{k0}. \quad (5)$$

About limit conditions if environment temperature has constant and known values it supposes that thermal changing are ruled by Newton law.

The thermal resistance  $\Delta R_{ts}$  of changing surface is modeled by an adequate resistance  $\Delta R_s$  connected to equivalent electrical circuit of reference conductor, meaning environment temperature:

$$\Delta R_{ts} = \frac{1}{\alpha_t \Delta S} \Leftrightarrow \Delta R_s = \frac{1}{\alpha_t \Delta S}. \quad (6)$$

In the relation (6),  $\Delta S$  means thermal changing surface and  $\alpha_t$ -global coefficient of heating transfer.

The electric contact presence on analysed conductor is considered by its supplementary power contribution:

$$\Delta P_c = R_c (\Delta i)^2, \quad (7)$$

where  $R_c$  is contact resistance, [2] and  $\Delta i$  means current fraction which crossed conductor.

## II.2 EMTP simulation program

Thermal stresses simulation of electrical equipment using EMTP logical programming has the advantage to solve electrical circuits into transient conditions.

In this way it is possible to make the connection from cause to effect in the case of Joule effect electrical-thermal conversion of energy.

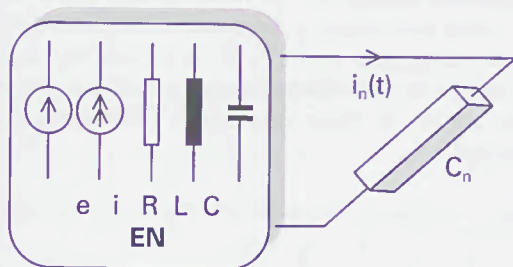


Fig. 2 Electrical network with thermal processes

In Fig.2 is shown the simulation object materialized through conducting section  $C_n$  crossed by current  $i_n(t)$ , which belongs to electrical network EN.

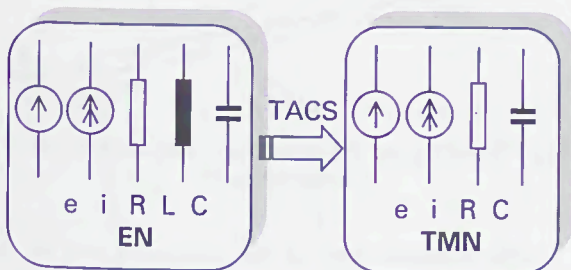


Fig.3 EMTP connection of the TMN thermal model to EN electric network

With the possibility to make analogue models using TASC, EMTP allow to cause-effect sense connection of TMN network, which means electrical model of thermal processes, to proper electrical network, EN (Fig. 3). So, it is possible the simulation of thermal processes inside conductor because of Joule effect under current actions to any electrical conductions.

This kind of model in a practical using entails to go over following stages:

- to make a scale drawing of studied reference point;
- to make partitions into modeled reference point volume, so that will be divided in elementary volumes by  $\Delta x, \Delta y, \Delta z$  sizes;
- to any elementary volume  $i$  attaches a knot  $n$  where converge thermal resistance from those three directions and thermal capacity. It gets electrical model of thermal processes like a RC network which it solves using EMT Program in the transient conditions.

As it can notice, the stages b) and c) request a very laborious hardworking so, from this reason, it searched for a better solution to solve automatically these stages and, implicitly, to generate the simulation EMTP software.

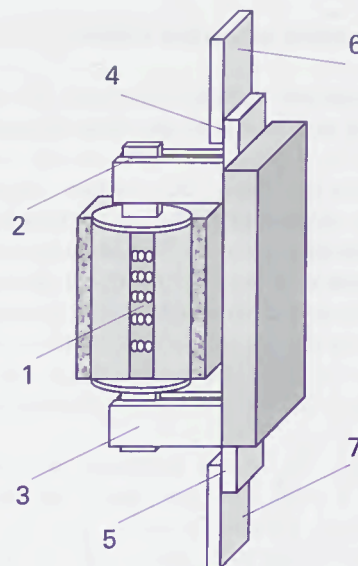


Fig.4 Modeled rapid fuse

The automation drawing up of EMTP simulation software can make using an one's own software named «RC Network» by authors. This software is achieved using Turbo Pascal language to IBM PS compatible computers. The software structure is a conversational type, input data are introduced into windows which contain enough information about processes.

After compiling, «RC Network» software achieves a file with a name given by user. This file means just EMTP solve program of EN-TMN networks which supplies voltages in different knots of analyse reference point like output data.

## 2 NUMERICAL TREATMENT. RESULTS

### III.1 Construction of modeled electric fuse

There have been modeled the thermal states of a fast low-voltage electric fuse type like in Fig. 4. The fuse element 1 is an unique band of copper. On the fuse conducting path were considered contacts 2 and 3 of the replacing element and 4 and 5 of the socket. At these ones, are linked the conductors 6, 7, each one with a length of 1m.

Using «RCNetwork» program, were generated EMTP files of more than 1800 lines, for the numerical simulation of both steady (resistive circuits) and transient (RC circuits) thermal states.

The resistivity of the metals on the conducting path traversed by current in fuse working, was considered linear variable with the temperature.

We preferred to use at it's maximum the TACS capability for electric modeling of thermal processes, in order to prove the contacts thermal stress.

That's why the heating current was considered with it's effective values, independent of the simulated thermal state.

### III.2 Steady states numerical results

We simulated the thermal stress for the steady working state of a fuse with the value of the current of 125 A.

The thermal state of electric contacts was simulated by the heat from the contact resistance. This, and the values of the current traversing the electric fuse and its contacts were parameterized. For the comparison was considered the ideal case, with a null contact resistance.

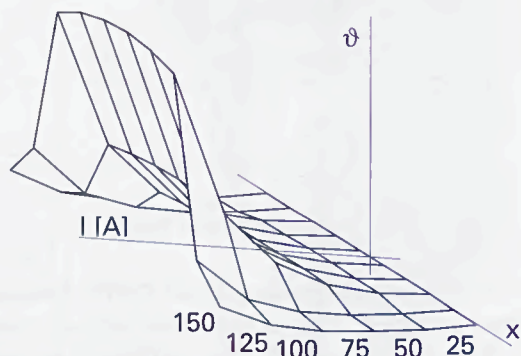


Fig.5 Over-temperatures in thermal steady state

Fig.5 presents the repartition of the over-temperatures in steady state, computed on the conducting path, for different values of the current. The contacts are considered ideal, with null contact resistance.

The influence of the contacts over the thermal state of the fusible element is illustrated in Fig.6, where is presented the repartition of the steady state temperature, computed for an 125 A current and for different given values of the contact resistance  $R_c$ .

The values of the contact resistance are influencing the thermal state of both the fusible element and the contact.

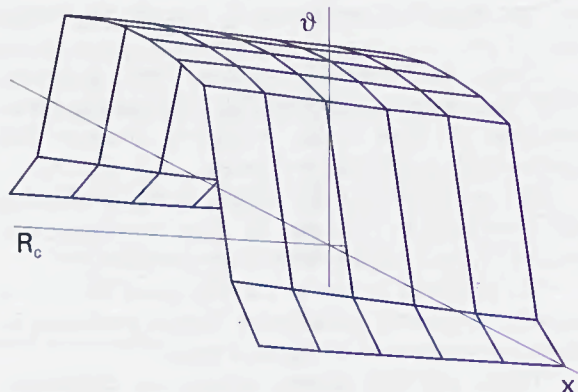


Fig.6 Influence of the contact resistance

That's why for 20 mV voltage falls over the fuse's contacts, that are normal for its working state, their temperature reaches 75 °C. If the voltage fall is of 100 mV, when the contact is damaged, the over-temperature for the steady state is of 117 °C. If we take into account the influence of temperature on mechanical properties of the metal, [3], those temperature fluctuations can be corrected.

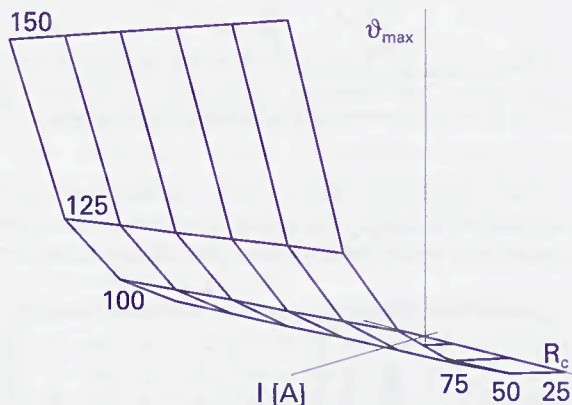


Fig.7 Steady state maximal over-temperature of the fusible element

The technical state of the contacts, given by the value of the contact resistance is influencing the thermal state of the fusible element. In Fig.7 are showed curves obtained from the computing of the maximal over-temperature in steady state from the central part of the fusible element, function with the values of the contact resistance, for different values of the current. If in the steady nominal state ( $I=125$  A), for 20 mV voltage falls on contacts, the maximal computed over-temperature of the fusible element is of 212 °C, after the contacts technical state alteration, considering for the same current voltage falls of 100 mV, arises a rise of the maximal over-temperature of the fuse at 253 °C. The supplementary contacts heating due to their technical state, are influencing through the maximal temperature of the fusible element, the melting time and the fuse's time-current characteristic.

### III.3 Numerical results concerning the transient states

The electrical model of the thermal process that takes place at the transient state fuse working is an RC network with more than 1700 branches, with their nodes.

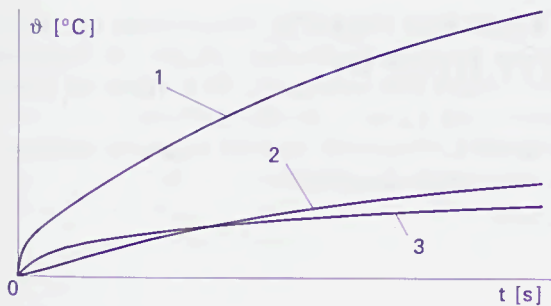


Fig.8 Over-temperatures in transient state

This allows the monitoring of the transient thermal response for an random shape of the current traversing the fuse. In this case this was considered step.

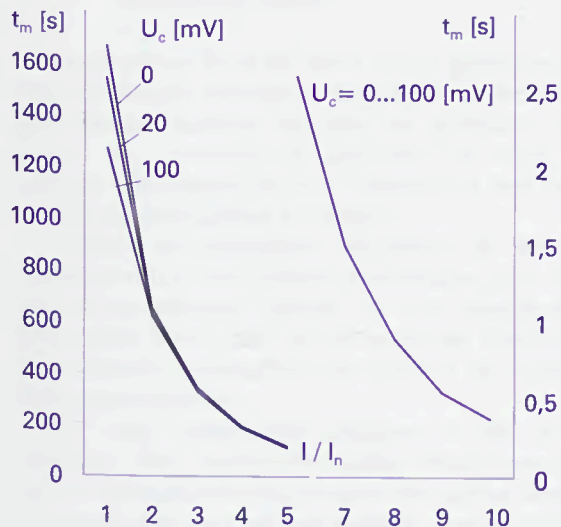


Fig.9 Influence of the electric contacts state on the melting time-current characteristic

In Fig.8 is presented the transient state of the over-temperature, in the case of nominal working current (125 A), localized in the area of the fusible element (curve 1) with the biggest temperature on the contacts of the replacing element (curve 2) and of the socket of the fuse (curve 3). The contact resistance values are for a normal technical state characterized by 20 mV voltage falls.

The excessive heating of the contacts is transmitted to the fusible element and causes the lowering of it's melting time. This fact is illustrated in Fig.9, that contains the time-current characteristics computed with our model.

We observe that at the rise of the contact resistance, big influences over the melting durations appear only at low overcurrents. As the current rises, the heat propagation becomes more restricted, because the thermal processes are more and more adiabatic ones.

### 3 CONCLUSIONS

The RC electric circuits modeling of the conductance thermal transmission allows the using of EMTP for the numerical simulation of the thermal transient states.

We propose a software that allows the automatization of the EMTP files replacement, and makes possible a fast way of building complex models with thousands of branches and nodes. There are electrically modeled the thermal phenomena that appear in a fast low voltage fuse, and there are analysed the reciproc influences between the fusible element and the contacts.

There are presented results of the numerical simulation of the steady state, and there is emphasized the rise of the maximal fusible element over-temperature as the contacts thermal state becomes worse.

These results are orienting the analysis of the transient states towards the problem of the influence of the contacts technical state over the time-current fuse characteristic.

There is emphasized the lowering of the fusion time due to the overheating of the conductor in the contact zones, fact that introduces errors in the fuse's time-current characteristic.

The model allows the analysis of any transient or permanent processes, directly or indirectly influenced by the thermal states of the fusible element and of the contacts.

### REFERENCES

- [1] Baraboi A., Adam M., Leonte P., «Modelling of circuit breaking at the fuses working». Proc. of the Fifth International Conference on Electric Fuses and their Applications, pp.143, Ilmenau, Germany, 1995.
- [2] Johannet P., «Le problème des contacts électriques à courant fort: caractérisation, implémentation, échauffement et vieillissement». EDF, Bulletin de la direction des études et recherches, France, 1995.
- [3] Baraboi A., «L'influence de la variation par rapport à la température du taux de plasticité du matériel de contact sur la sollicitation thermique au court-circuit des contacts électriques», Bul. Inst. Polit. Iași, XXXV(XXXIX), 3-4, s. III, pp. 45, 1989.
- [4] Adam M., Baraboi A., Leonte P., «Modelling of the thermal stress and the monitoring of circuit breakers», Proc. of the 5th International Conference on Optimization of Electric and Electronic Equipments «OPTIM'96», vol. III, pp. 641, Braşov, Romania, 1996.
- [5] Baraboi A., Adam M., Leonte P., T. A. Baraboi, «Simulation des contraintes thermiques de l'appareillage électrique», Proc. of the International Conference on Applied and Theoretical Electrotechnics "ICATE'96", vol. II, pp. 11, Craiova, Romania, 1996.

[6] Beaujean D. A., Newbery P. G., Jayne M. G., «Modelling fuse elements using a CAD software package», Proc. of Fifth International Conference on Electric Fuses and their Applications, pp. 133, Ilmenau, Germany, 1995.

[7] Kojovic Lj., Hassler S., «Application of current limiting fuses in distribution systems for improved power quality and protection», IEEE Trans. on Power Delivery, vol. 12, no. 2, pp. 791, 1997.

[8] Barbu I.: «Siguranje electrice de joas@ tensiune», Ed. Tehnic@, Bucure}ti 1983.

# ANALYSIS OF THERMAL PHENOMENA IN HIGH-VOLTAGE FUSE-LINKS

V. Giurgiu, Gh. Oarga, S. Purdel  
Research Institute for Electrical Engineering – ICPE  
Bucharest, Romania

*Abstract:* There are presented the main results obtained by numerical simulation of temperature distribution in fuse-links, considering adiabatic and non adiabatic process for heat flow in fuse-elements and in fuse-link, respectively. Results were used for development of a new series of fuse-links for motor starting circuits of 7.2 kV, 25... 250 A.

## I. INTRODUCTION

High-voltage fuses for motor circuit protection have been continually developed, in general on the basis of experimental methods. Because the processes which govern the operation of fuse-link are many and complex, its analysis is very complicated and several simplifying assumptions are required.

Analysis of temperature distribution in the fuse-elements with a non-uniform cross-section area, in the case of an adiabatic process, is very important for determining some parts of the prearcing time-current characteristics, especially in the region of the extremely short prearcing times.

The very complicated situation is that of the prearcing times longer than those which correspond with an adiabatic process, because the current densities in the fuse-elements are not constant over their cross-section or along their lengths due to the presence of the restrictions. In addition, resistivity increases as the fuse-element temperature rises, and the effects of various component parts, like fine-grain filler, outer body, end caps, connecting cables must be considered in temperature distribution.

Numerical methods are very useful to determine the temperature distribution for adiabatic and non adiabatic process, and were applied with success in our works in developing a new series of high-voltage fuse-links for motor circuits protection, [1].

## II. ANALYSIS OF TRANSIENT AND STEADY-STATE TEMPERATURE DISTRIBUTION

The processes which govern the heat movement in a fuse-link are very complex, except the case of the very short prearcing times, when there is an adiabatic process.

An overall model, which allows to compute the temperature distribution in the fuse-link from the extremely short prearcing times to long prearcing times must consider the heat generated within the fuse-elements by Joulean heating, which is lost axially by conduction to the end caps and radially by conduction through the filler and fuse-link body and then by radiation and convection from the body and end caps.

Application of numerical methods for such a simulation conducts to a number of simplifying assumptions, [2]. The finite-difference method, using the Crank-Nicholson approximation and successive overrelaxation, [3], [4] was used for the transient and steady-state temperature distribution, [5], [6].

The temperature distribution in fuse-elements, in the case of an adiabatic process, is governed by the equation:

$$\frac{\rho(\theta)j^2}{\lambda} = -\left[\frac{\partial^2\theta(x,y)}{\partial x^2} + \frac{\partial^2\theta(x,y)}{\partial y^2}\right] + \frac{c\gamma}{\lambda} \frac{\partial\theta(x,y)}{\partial t} \quad (1)$$

where:

- $\theta$  temperature of element [ $^{\circ}\text{C}$ ]
- $\rho(\theta)$  resistivity [ $\Omega\text{m}$ ]
- $c$  specific heat [ $\text{Ws/kg}^{\circ}\text{C}$ ]
- $\lambda$  thermal conductivity [ $\text{W/m}^{\circ}\text{C}$ ]
- $\gamma$  density of material [ $\text{kg/m}^3$ ]
- $j$  current density [ $\text{A/m}^2$ ]

The left term corresponds to the heat generated in the fuse-elements and the right term represents the sum of the heat lost by conduction within the fuse elements and the heat stored in the elements. If the prearcing times are very short, the term corresponding to the heat lost by conduction is practically zero and entire energy generated in elements is used for rise the temperature of the elements. Fig. 1 represents the scheme used for numerical simulation of temperature distribution, in the case of an adiabatic process, which refers only to the fuse-elements, with a certain form of restriction. The shape of restriction is very different from a firm to another, depending on the imagination of engineers, but all fuse-elements must satisfy the conditions imposed for motor type fuse-links, to have a "fast-slow" prearcing time-current characteristics, that is the operation should be as rapid as possible on heavy faults and to resist indefinitely under repeated starting conditions of motors.

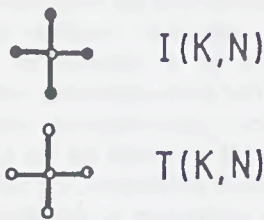
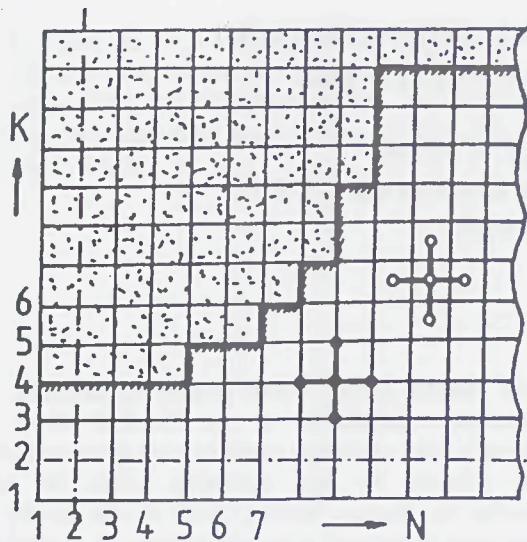


Fig. 1 Finite-difference mesh for an adiabatic process analysis

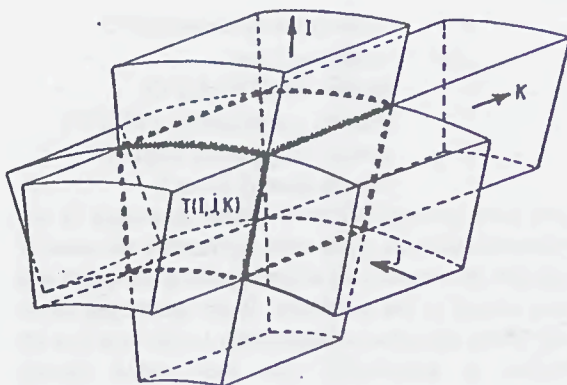


Fig. 2 Spatial subvolumes used in the case of a non adiabatic process analysis

It can be seen that there are two grids, one for current distribution, and another one for temperature distribution. Using the Crank-Nicholson approximation and extrapolated Liebmann method of successive overrelaxation, the temperature of a subvolume  $(k,n)$  at  $(w+1)$ th iteration, after determination of the current density by numerical differentiation, can be computed with following equation:

$$T^{w+1}(n,k) = (1-\alpha) \cdot T^w(k,n) + \alpha \cdot T5 \quad (2)$$

where:

- $w$  – order of iteration
- $\alpha$  – accelerating factor of convergence; the value of  $\alpha$  lies between 1 and 2;
- $T5$  – a general term, depending on temperatures of the subvolumes adjacent to the subvolume  $(k,n)$  and the flow of energy generated within the subvolume  $(k,n)$ .

In the case of a non adiabatic process analysis, used for a 3D simulation of temperature distribution in all parts of the fuse-link, the scheme is that of Fig. 2 and the terms corresponding to the heat lost from the body of fuse-link by convection and by radiation must be added to equation (1). For calculation it was utilised only a part of fuse-link, like that in Fig. 3, with two axis of symmetry, one in fuse-element and another at the middle distance between two fuse-elements

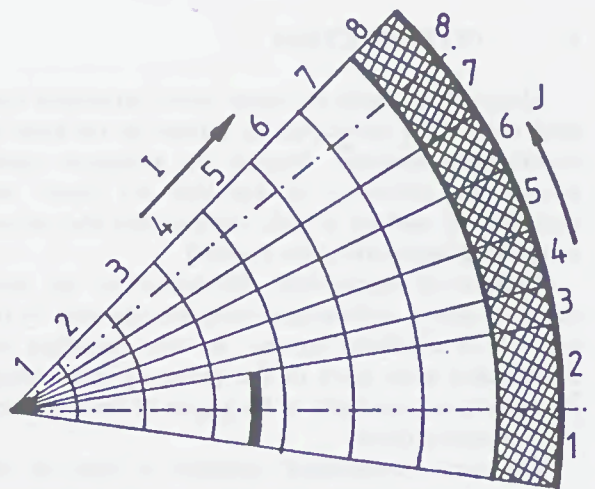


Fig. 3 A cross-section in a part of fuse-link, with two axis of symmetry

At each time step  $\Delta t$ , a specified number of iterations were executed, to determine the steady-state temperature distribution inside the fuse-link, taking into account that the heat is transmitted only in radial direction in the filler, because of relatively high length/diameter ratio. The values obtained were used as initial conditions for the next time step. For the heat transmission from the external surface of the body of fuse-link having temperature  $T(i,j,k)$ , to the ambient air having temperature  $T_{amb}$  must be considered the transmission by radiation and by convection.

Heat transmitted by radiation  $Q_r$  is obtained using:

$$Q_r = 5.77 S c_r (T_1^4 - T_a^4) \Delta t \quad (3)$$

where:

- $S$  – external surface of fuse-link
- $c_r$  – coefficient of radiation
- $T_1 = [T(i,j,k) + 273] / 100$
- $T_a = [T_{amb} + 273] / 100$

Heat transmitted by convection  $Q_c$  is obtained using:

$$Q_c = \lambda_a S [T(i, j, k) - T_{amb}] \Delta t \quad (4)$$

where:

$\lambda_a = 33 d^{-0.625}$  coefficient of transmission by convection, for laminar flow of air  
 $d$  - characteristic dimension of fuse-link (diameter)

The values for coefficients  $c_r$  and  $\lambda_a$  were established on the basis of a great number of test in laboratory, for determining temperature-rise limits of fuse-links.

### III. COMPUTATIONAL RESULTS AND COMPARISON WITH TEST RESULTS

Fig.4 shows a temperature distribution obtained by finite-difference method, in the region of a restriction of the fuse-element used for fuse-link of 7.2 kV, 250 A.

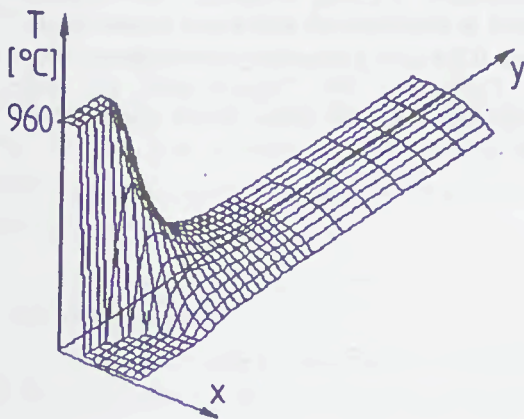


Fig. 4 Temperature distribution calculated in fuse-element (adiabatic process)

It can be seen the strong difference between the temperature of restriction area in comparison with the rest part of fuse-element. The difference between the calculated time necessary to obtain the melting temperature of the fuse-element and the measured time obtained in high breaking capacity is about 10%, which is an acceptable value.

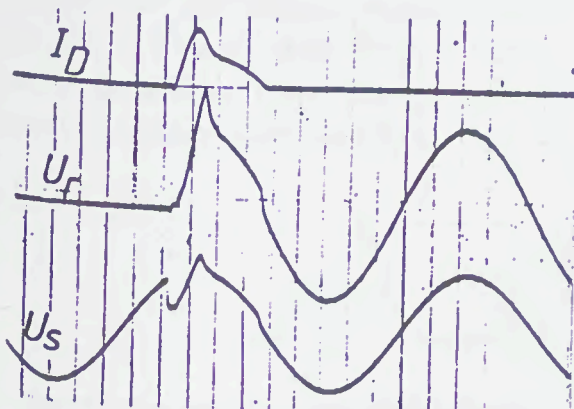


Fig.5 Oscillogram obtained at test duty 1 for a fuse-link 7.2 kV, 100 A

Fig.5 represents an oscillogram obtained in high power laboratory, test duty 1 with a prospective current testing of 31.5 kA<sub>ef</sub> for a fuse-link of 7.2 kV- 100 A. It must be pointed out the small value of transient recovery voltage, due to the adequate number of restrictions, with a shape wich allows the cooling of the electric arc.

Table 1 shows the measured ( $t_m$ ) and calculated ( $t_c$ ) values of time necessary to attain the temperature-rise  $\Delta\theta$ , in a test for determining the temperature-rise limit (steady-state regime) at a rating current of 250 A. The differences between these values are in the range of  $\pm 10\%$ .

Table 1 Measured and calculated time for attain certain value of temperature-rise, at test with rated current of 250 A

$t_m$ [s]	3000	7500	12000	15600	16200	21600
$\Delta\theta_1$ [°C]	42	56	57	58	58.5	60
$t_{c1}$ [s]	3100	6700	11990	15100	15800	21550
$\Delta\theta_2$ [°C]	26	58	64	66	66.5	68
$t_{c2}$ [s]	2650	7600	12900	15950	16560	23600

$\Delta\theta_1$  = temperature-rise at end cap

$\Delta\theta_2$  = temperature-rise at the middle of fuse-link

In Table 2 are shown measured and calculated values of the energy disipated by convection  $Q_c$  and by radiation  $Q_r$ , for a medium temperature-rise  $\Delta\theta$  of the external surface of the fuse-link, in the case of testing with rating currents and the currents corresponding to the withstand tests, [7]. The difference between these values can be accepted in practice and this calculation eliminates a great number of long and expensive tests in laboratory.

The determination of factor K require a great number of expensive tests, to sequence no.1 (100 cycles of 1 h) and sequence no.2 (2000 cycles of 10 min.). The difficulty for fuse-elements consists not in withstanding the value of the current but in providing corresponding flexibility to take up thermal cycling associated with the starting requirements of motors.

Table 2 Measured and calculated values for energy disipated from external surface of fuse-link

Testing type	Rating current testing		Withstand testing	
	$I_n$ [A]		$I_n$ [A]	
	100	250	100	250
$\Delta\theta$ [°C]	32	68	18	32
$Q_c$ [W]	23	59	11.4	23.4
$Q_r$ [W]	23	57	9.9	20.4
$Q_{tc}$ [W]	46	116	21.3	43.8
$Q_m$ [W]	44	112	20.8	43.52

$Q_{tc} = Q_c + Q_r$  (calculated)

$Q_m$  (measured)

For example, the same fuse-element, used for a fuse-link of 125 A rating current, subjected to 115 cycles of sequence no.1 failed after 720 cycles of sequence no.2, for a factor  $K=0.65$  but resisted to 110 cycles of sequence no.1 and 2500 cycles of sequence no.2, for  $K=0.6$ .

This type of thermal stress is very important and must be taken into account in determination of final constructive solution for fuse-element.

#### IV CONCLUSIONS

The calculation of the temperature distribution in fuse-element and in fuse-link has been confirmed the validity of the method, in comparison with experimental investigations, and has been used for development of a new series of fuse-links for motor circuit applications,  $U_n=7.2\text{kV}$ ,  $I_n=25\text{...}250\text{ A}$ .

The differences between the measured and calculated values of temperature-rise, time to attain a certain value of them or between energy dissipated by fuse-links are normally, because of the assumptions made in calculation.

#### REFERENCES

- [1] FS-377 "High-voltage fuse-links 7.2 kV, 100...400A for motors". ICPE Firm Standard, 1996.
- [2] J.G.Leach, P.G.Newbery, A.Wright, "Analysis of high-rupturing-capacity fuselink prearcing phenomena by a finite-difference method", Proc.IEE, vol.120, no.9, pp 987-993, 1973.
- [3] J.T.Storey, M.J.Billings, "General digital-computer program for the determination of 3-dimensional electrostatic axially symmetric fields", Proc.IEE, vol.114, no.10, pp.1551-1555, 1967.
- [4] D.Greenspan, "Discrete Numerical Methods in Physics and Engineering", Academic Press,Inc., New York-San Francisco - London, 1974.
- [5] R.Wilkins, P.M.McEvans, "A.C. short-circuit performance of notched fuse elements", Proc.IEE, vol.122, no.3, pp.289-292, 1975.
- [6] O.Bottauscio, G.Crotti, G.Farina, "Non adiabatic process in fuse elements with heavy current faults", Fourth ICEFA'91, University of Nottingham, UK.
- [7] IEC Publication 644, "Specification for high-voltage fuse-links for motor circuit applications", 1976.

## MINIMUM BREAKING CURRENT OBTAINING IN FUSES

César S. Cañas Peñuelas (E-mail [cscanas@die.upv.es](mailto:cscanas@die.upv.es))

GEEDDEE. Departamento de Ingeniería Eléctrica. Universidad Politécnica de Valencia.

Lorenzo Fernández (E-mail [lorenzo.fernandez@iberdrola.es](mailto:lorenzo.fernandez@iberdrola.es))

Iberdrola S.A.

Rafael González. (E-mail [iberapa@iberapa.es](mailto:iberapa@iberapa.es))

Ibérica de Aparellajes S.L.

### Summary:

In this report it has been developed a method for the time-current characteristics obtaining referring to all kinds of fuses, using for that techniques of finite elements analysis. We reach to obtain the necessary model for each rated current without the previously needing of know the melting time value. The methodology used allows to know in each instant the temperature along all the fuse element points, having the possibility to prospect which will be the minimum breaking current value ( $I_3$ ).

### 1. Adiabatic model.

When the fuse is submitted to currents with values equal or near to the breaking capacity, the melting time values don't use to be above half millisecond. During this time and taking into account the big difference of the thermal conductivity between the fuse element ( $.400 \text{ W/m}^\circ\text{C}$ ) and the sand ( $0.4 \text{ W/m}^\circ\text{C}$ ), there is no heat transmission from the fuse element to the sand, and the melting process is considered as adiabatic. Making these considerations, only is modeled the fuse element, which in several cases uses to have the shape shown in figure 1. (Due to the existing symmetries, we only will simulate the quarter of the fuse strip.)

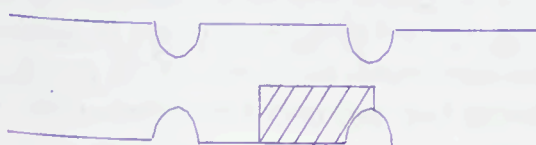


Figure 1. Fuse strip. Lined area (simulated zone).

Model characteristics:

- Three-dimensional simulation.
- The model has real dimensions.
- Adiabatic behaviour.
- Using of only  $\frac{1}{4}$  strip.
- Temporal evolution of the current.
- Prospective error at the simulation 6.25%.

During the simulation has to be considered the temporal evolution of the current. The obtained results for a prospective current with value 20.000 A, with power factor 0.1 and making angle of  $60^\circ$  is the one shown in figure 2 .



```
NOV 25, 97
13:27:19
NODAL SOLUTION
STEP=14
SUB =2
TIME=0.260E-03
TEMP
IEPC=26.933
SMN =79.217
SMX =1093
79.217
191.885
304.554
417.222
529.89
642.558
755.226
867.894
980.562
1093
```

Initial temperature 20°C

Figure 2. Model and simulation at current  $I_1$

On figure 2 it can be observed that it has been reached the melting at the neck, while the wide zone only has suffered a thermal step of about  $60^\circ\text{C}$ , due mainly to its

own heating and not to the heat transmission from the narrow zone to the wide zone.

While the current diminishes, the melting time increases and the established model for  $I_1$  leaves to be reliable. It has to be needed to begin to consider the sand influence, but because the melting time values are still small, the sand thickness which takes place is also very small and besides it can be assumed that the heat transmission is done in radial direction. Even now, exist the difficulty to know or to sense the melting time to have the possibility to choose the correspondent model.

## 2. Definitive models.

In front of this fact we decided, taking the base of the adiabatic model, to increase progressively the sand thickness which takes part as the current is diminishing.

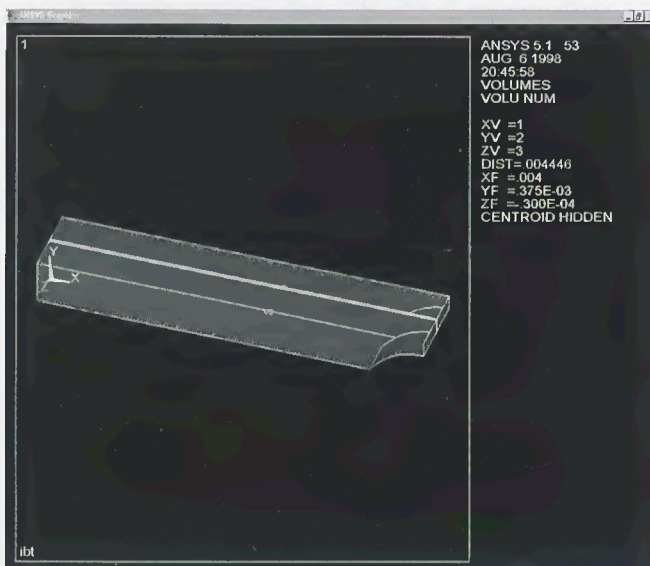


Figure 3 Fuse strip with surrounded sand.

On figure 3 the silver strip is placed on the central zone (blue) and the sand volumes (red and violet) will be increasing, as the current will be diminishing.

The volumes which are placed at the front and at the rear of the strip (fuse element) have the mission to transmit the generated heat into the fuse strip (pre-arcing) towards the external part, and to absorb the generated energy in the arcing phase.

The sand thickness has to have its dimensions in accordance so that the last sand layer will not surpass the temperature of  $20^\circ\text{C}$ , which is the initial temperature of the simulation process.

In case of melting times above five milliseconds, the used models have to count with the sand layer. In all the simulations made inside the high currents range (from  $I_1$  to 20 times the rated current), is the neck that one which generates the enough heat to cause the fuse melting. As the current diminish, it can be proved how the entire fuse element goes reaching the same temperature (wide zone and narrow zone). This fact indicates that it's been reaching the current value  $I_3$  (corresponding to the minimum breaking current assured by the manufacturer, and which comes imposed by that one). (figure 4.).



Figure 4 Simulation at  $4I_n$ .

The generated heat is transmitted in axial direction along the strip and in radial direction towards the external. Being proved how the fuse strip (placed at the centre of the model) has a temperature distribution quite homogeneous (thermal gradient of  $100^\circ\text{C}$ ), due to the great difference of thermal conductivity values between the sand and the silver.

Model characteristics:

Three-dimensional simulation.

- Using of ¼ strip.
- Using of the current prospective value.
- No utilisation of the convection phenomena.
- Simulation estimated error 6.25%.

The obtained melting time is 2.925 sec.

Using these models, the time-current characteristics are obtained, which range is between the breaking capacity to four times the rated current. The results are shown on the <sup>1</sup>table 1

J (A/mm <sup>2</sup> ) <sub>wide zone</sub>	Sand thickness (mm)	T <sub>melting</sub> (ms)
22222.22(20000 A)	0	0.14
4055.55(365 A)	0.25	3.8
2222.22(200 A)	0.4	6
1666.66 (150 A)	0.4	12
1555.55 (140 A)	0.5	20
1111.11(100 A)	0.7	70
1000(90 A)	0.8	100
888.88(80 A)	0.9	140
777.77 (70 A)	1	220
555.55(50 A)	1.5	820
444.44 (40 A)	3.5	3000
252(252 A)	5	4500

Table 1. Melting time for some current density values.

The method explained before has been applied one time more to a new geometry, where have been maintained the same materials used before. Now we vary the fuse strip length, keeping constant the thickness and the rest of the neck dimensions.

The obtained results are the following ones:

<sup>1</sup> Strip geometry is not included due to be considered as manufacturer privacy.

J (A/mm <sup>2</sup> ) <sub>wide zone</sub>	Sand thickness (mm)	T <sub>melting</sub> (ms)
22222.22(20000 A)	0	0.14
4055.55(365 A)	0.25	3.8
2222.22(200 A)	0.4	6
1666.66 (150 A)	0.4	12
1555.55 (140 A)	0.5	20
1111.11(100 A)	0.7	70
1000(90 A)	0.8	100
888.88(80 A)	0.9	140
777.77 (70 A)	1	220
555.55(50 A)	1.5	700
444.44(40 A)	3.5	2475

Table 2. Melting times for some current density values.

On tables 1 and 2 is used the current density value which allows to make independent current that circulates along the fuse from the number of fuse elements and its dimensions. We have calculated two current density values, but we choose the one obtained from the wide zone of the fuse element because it has much more length and has a bigger contact surface with the refrigerating element (sand). It has been observed that exist a direct relation between the current density mentioned before and the necessary thickness to make the simulation (figure 5). Using the relation found and knowing the strip geometry, the current density (expressed in A/mm<sup>2</sup>) is calculated. It's introduced the datum into figure 5, obtaining the sand thickness necessary for the simulation. In this way is avoided the needing, exposed in all the bibliography, of to know previously the melting time to can choose the appropriate model.

The explained method has been applied to a fuse composed by four strips with different dimensions than the previous ones. Table 3.

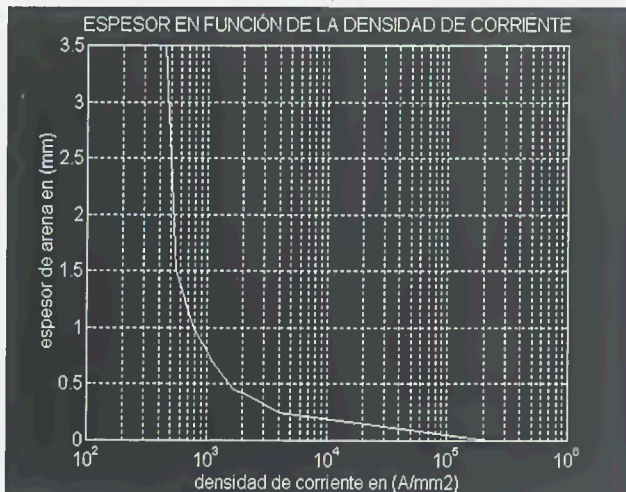


Figure 5. Thickness in function to the current density.

Prospective current (A)	Current density (A/mm <sup>2</sup> )	Needed sand thickness (mm)	Melting time obtained in simulation (s)	Experimental time (s)
1000	1400	0.5	0.018	0.015
800	1111	0.7	0.03	0.025
600	833	0.9	0.152	0.14
500	700	1.1	0.31	0.25
400	555	1.5	1	0.9
300	416	5	3.5	3.3

Table 3. Melting times obtained with the described model.

When very high melting times are reached, at very low currents (near to three times the rated current), the three-dimensional model begins to bring process times very long (rounding the 24 hours). The heat has time enough to reach the porcelain, transmitting itself to the external environment fundamentally by convection and the fuse element reaches a

uniform temperature. In these conditions the previous model is not valid. Due to that we will adopt a model with axial symmetry (figure 6 with two dimensions) where the fuse element is considered with uniformly section and wound in spiral round the star core. Its dimensions (high and width) are exactly the same than the ones belonging to the fuse strip and has an electrical resistance equivalent to one helix

step of the original strip. The obtained results can be shown on the simulation of figure 7.

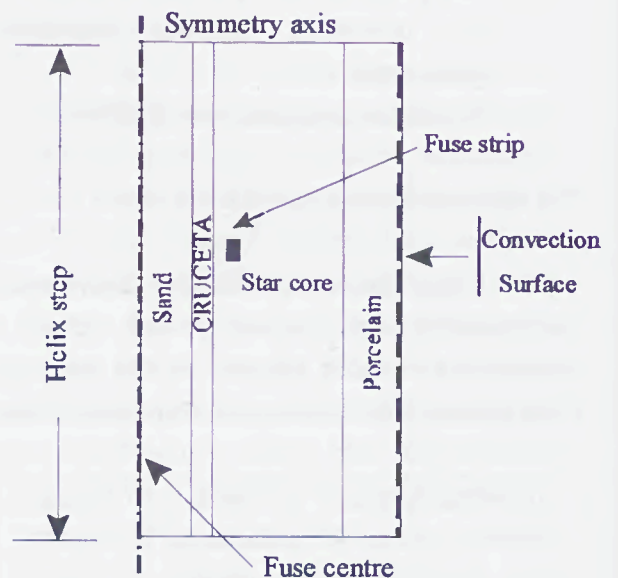


Figure 6. Two dimensions model.

It can be checked that the hottest zone is the internal zone (left part of the figure) and the heat flows towards the external part (right part of the figure) where exist a convection surface.

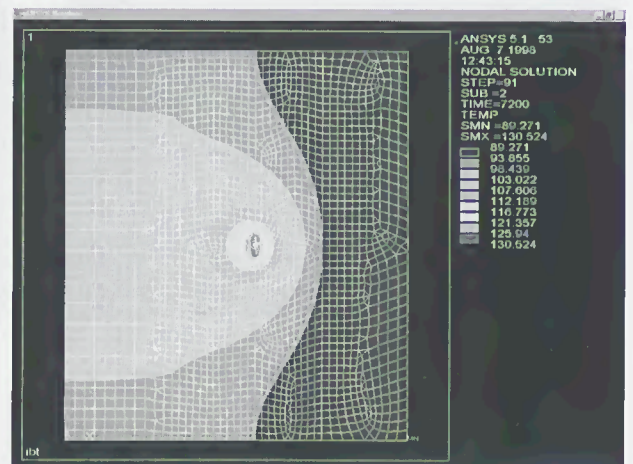


Figure 7. Simulation at rated current

At figure 7, the simulation devises the situation of the fuse behaviour at the rated current.

The exhibited method allows to obtain the melting times for every current

with a maximal error of 6.25% (in calculation), using only two models:

1. Three-dimensional model
    - Adiabatic for currents with values near to the breaking capacity.
    - Sand contribution for currents until four times the rated current.
  2. Two-dimensional model
    - Currents from three times the rated current to the rated current.
3. Minimal breaking current determination.

In the exhibited methods it can be observed that there is a limit current between the three-dimensional model and the two-dimensional one. The lowest current that causes a secure breaking can be obtained from the melting phase analysis.

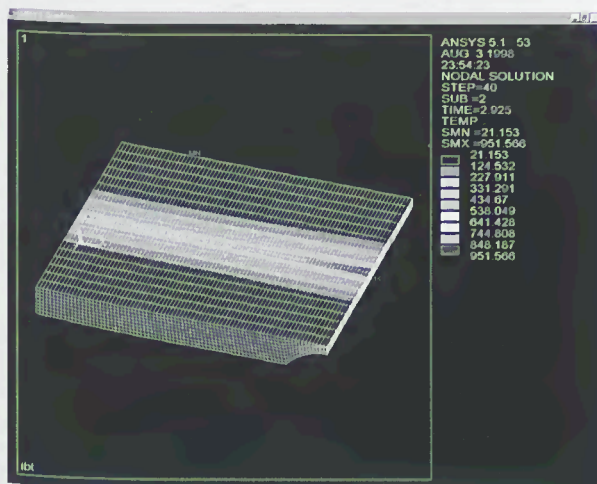


Figure 8. Simulation at four times the rated current. High rated current fuse.

The temperature distribution belonging to the simulation exhibited on figure 8 shows that it has been reached the melting point at the neck and also that at the wide part of the fuse strip exist a temperature near to the melting point (round 800 °C). This fact indicates that the arc will appear in a simultaneous way at all the necks, giving place to a secure functioning. The current that won't cause this fact will give place to a random appearance of

arcs in position and in time, for which it can't be assured the correct fuse functioning.

#### 4. Summary.

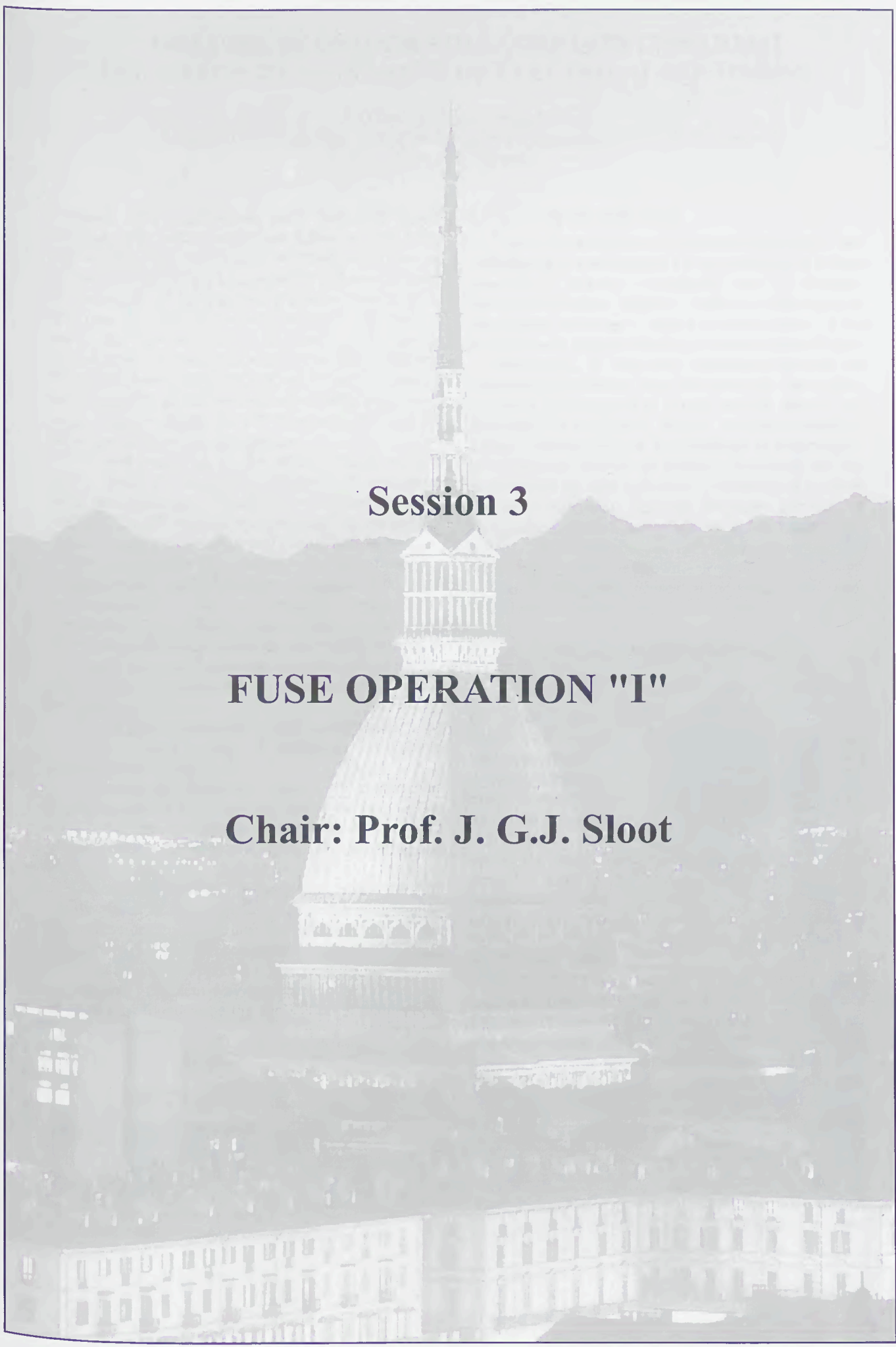
As more important conclusions for the time-current characteristics determination we can conclude:

1. Using of only two kinds of models.
2. Elimination of the previous needing to know the melting time corresponding to the simulated current.
3. Real temperatures obtaining at any place of the fuse, allowing to know perfectly which are the conditions of the surrounding sand at the place where will appear the electric arc (neck).
4. Minimum breaking current determination without needing of tests.

#### Bibliography

- [1] Leach, J. G.; Newbery, P.G.; Wright, A.: *Analysis of high-rupturing-capacity fuse links prearcing phenomena by a finite-difference method*. Proc. IEE 120 (1973) n° 9, pp. 987-993.
- [2] Wilkins, R.; Mc Ewan, P.M.: *AC short-circuit performance of notched fuse element*. Proc. IEE 122 (1975) n° 3, pp. 289-292.
- [3] Mc Ewan, P.M.; Warren, L.; *Survey of numerical methods for solving time-varying fuse equation*. Int. Conference Electric Fuses an Their Applications, Liverpool/GB (1976), Proc. pp. 21-22.
- [4] Mc. Ewan, P.M.; Wilkins, R.; *A decoupled method for predicting time-current characteristics of H.R.C. fuses*. Int. Conference Electric Fuses an Their Applications, Liverpool/GB (1976), Proc. pp. 33-41.
- [5] Wright A & Newbery PG: *Electric Fuses*, London, Peter Peregrinus LTD, 1984.
- [6] Xian-zhong, Meng; Ji-mei, Wang; *The simulation of prearcing characteristics of fuse elements in the finite element method*. Int. Conference Electric Fuses an Their Applications(1987), Proc. pp. 24-29.
- [7] J. Trott. *The influence of gaseous an solid static arc extinguishing media on the*

- dielectric strength of arc gaps pre-stressed by small overload current. Fifth International Symposium on high voltage engineering. 24-28 Agosto 1987.
- [8] Sasu, M. ; *Computing algorithm of the variable section fusible elements heating equation*. Int. 90 Cetinje AMSE- Conf. Signals & Systems, Cetinje, Montenegro/YU 1990, Proc.1, pp.213-221.
- [9] M. Sasu; G. Oarga; *Simulation of the heat transfer phenomena in variables section fusible elements in non-adiabatic regime*. Springer-Verlag 1992.
- [10] C. Garrido , J. Cidrás., *Cálculo de tiempos de prearco*.1993.
- [11] Beaujean, D.A.; Jayne. M.G.; Newbery, P.G.; *Long-time operation of high breaking capacity fuses*. IEE Proceedings-A, Vol.140, No 4, Julio de 1993
- [12] Hofman M., Lindemayer M.; *Pre-calculation of time-current characteristics of M effect fuse elements*. Institut für Elektrische Energieanlagen Technische Universität Braunschweig D-3300 Braunschweig, Germany.
- [13] C. Cañas, F. Ruz, J. Curiel, F. Cavallé. *Modelización con acoplamiento termoeléctrico por elementos finitos de un fusible de media tensión*. Jornadas Hispano-Lusas, Oporto 1995.
- [14] H.Kürschner, A.Ehrhardt, G. Nutsh, I. Harrison, A.Boerner, T. Mickley; *Calculation of prearcing times using the Finite Element Method*.Int. Conference Electric Fuses an Their Applications, Ilmenau/Germany (1995), Proc. pp. 156-161.
- [15] Fernández, L.;Cañas, C.; Llobell, J.; Curiel, J.; Aspás, J.; Ruz, F.; Cavallé, F.; *A model for pre-arcing behaviour simulation of H.V. full-range fuse-links using the finite element method*. Int. Conference Electric Fuses an Their Applications, Ilmenau/Germany (1995), Proc. pp. 162-167.
- [16] D.A. Beaujeau; P.G. Newbery and M.G. Jayne; *Modelling fuse elements using a C.A.D. software package*. Int. Conference Electric Fuses an Their Applications, Ilmenau/Germany (1995), Proc. pp. 133-142.
- [17] Beaujean, D.A.; Jayne. M.G.; Newbery, P.G.;*Determination of M-effect diffusion parameters in high breaking capacity fuses*. IEE Proc. Science Measurement and Technology., Vol.142 n°2 (1995).
- [18] C, Garrido. J, Cidrás. *Study of different materials as fuse element*.Int. Conference Electric Fuses an Their Applications, Ilmenau/Germany (1995), Proc. pp. 201-206.
- [19] Zhang Juan. Ma Zhiying. *Mathematic model of two dimensional temperature field and its application in high-voltage current-limiting fuse-link*. Power System Technology. Vol.19. No. 12. Dec 1995.
- [20] M. Sasu; *Simulation of the heat-transfer phenomena in Electrical Fuses by means of the digital computer*. E.T.E.P. Vol. 5, N° 3, Mayo/Junio de 1995 .
- [21] C. Cañas, L. Fernández, J. Aspás. *Proceso de determinación de  $I_1$ ,  $I_2$ ,  $I_3$  en fusibles limitadores de corriente*. Jornadas de Grupos de Investigación en Ingeniería Eléctrica. Cádiz 1998.



**Session 3**

**FUSE OPERATION "I"**

**Chair: Prof. J. G.J. Sloot**



# INFLUENCES OF HIGH VOLTAGE FUSES ON PARTIAL DISCHARGE MEASUREMENT OF ELECTRICAL EQUIPMENT

J. Gärtner, E. Gockenbach, H. Borsi

Schering-Institute of High Voltage Technique and Engineering, University of Hannover  
Hannover - Germany

**Abstract:** This contribution deals with the partial discharge (PD) behaviour of sand filled current limiting high voltage fuses (HV-fuses). HV-fuses are often used in combination with switchgear and transformer stations for protection of the equipment against over-currents. HV-fuses are part of those installations and have to meet the corresponding standards and quality requirements. If fuses are exposed to high electrical stress, they may produce PD. When PD measurement is used for quality assessments and monitoring purposes of the switchgear station, the HV-fuse may affect the PD behaviour of the whole installation.

PD are generated in the arc-quenching medium (quartz sand) by the melting elements. The shape of these elements leads to high electrical stress and PD activity. The PD activity was recorded by the help of digital storage oscilloscopes and PD analysis systems.

The source of the PD generation and the influence of parameters like applied voltage, temperature, pressure, and moisture of the arc-quenching medium was investigated on different fuses and on a model reproducing the inhomogeneous field configuration. It was found that ozone generation is one result of the PD activity and an important factor describing the PD behaviour.

PD may also damage the melting elements of the fuse by electrical erosion. A long-time investigation revealed such effects.

To show the important impact of construction parameters on the electrical field inside the fuse and on the PD activity, a computer model based on the finite element method (FEM) was used for optimising the geometry.

Concepts preventing PD generation inside the fuse are discussed in detail. Field grading and modification of the fuse design can reduce the field strength and the PD activity. Special conductive layers for stress relieving may also support the reduction of PD.

The most efficient way to decrease the PD activity of fuses was found to be the application of additives to the arc-quenching medium.

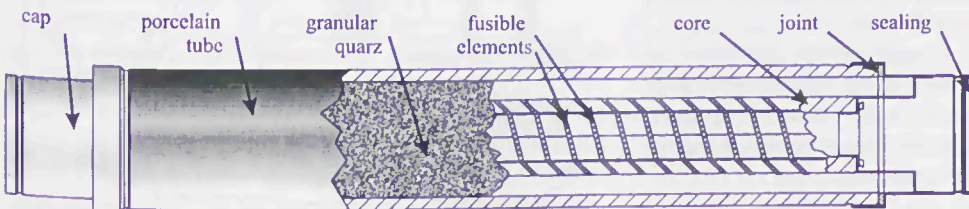


Fig. 1: Schematic view of a HV-fuse (6/12 kV - 40 A)

## I. INTRODUCTION

Due to decreasing size of electrical equipments, like switchgears or transformers, PD generation of HV-fuses becomes a problem: Decreasing size of electrical equipment implies reduced distances between the components resulting in higher electrical stress. If the stress exceeds a certain level, PD generation may occur.

Monitoring of electrical equipment becomes an increasingly important issue for achieving high quality in power delivery and to extend the life time of the equipment. If the current state of an electric device is known, maintenance can be scheduled in larger cycles or on demand. Among the multiple parameters that can be evaluated for state estimation, PD behaviour is one of the most important. Because HV-fuses are part of electrical equipment, and often the whole assembly is tested, the influence of the HV-fuses on PD measurements must be known.

This investigation focuses on the widely used sand-filled type of current limiting HV-fuse (Fig. 1).

### I.1 Mechanisms of PD generation

The main reason for PD generation inside fuses is the inhomogeneous electrode arrangement formed by the thin fusible elements and surrounding components on earth or high-voltage potential. Because melting elements are shaped mat-

ching the fuses' purpose [1, 2] they form a sharp electrode: Commonly used silver bands only have a thickness of some dozens of micrometers. To resist the recovery voltage, they are often notched, leading to extreme electrical stress. For arc-quenching purpose, the melting elements are embedded in sand. Sand forms a porous dielectric filled with air, which is a weak dielectric in terms of high-voltage engineering. If this

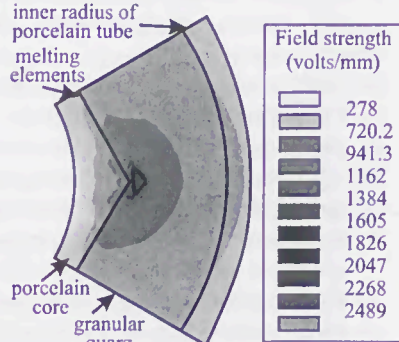


Fig. 2: El. field in HV-fuses (cross section in radial direction)

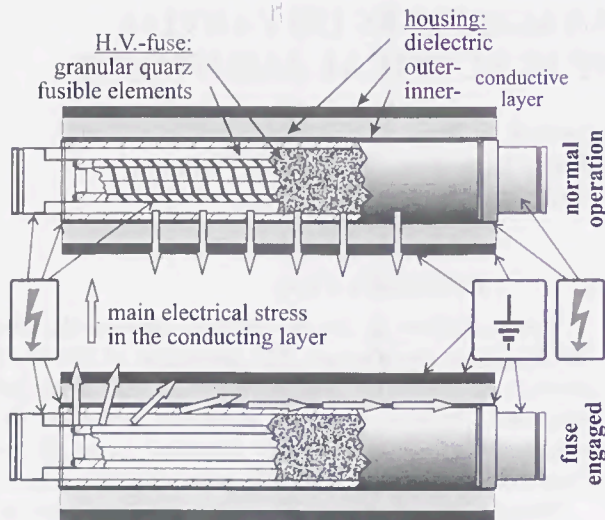


Fig. 3: Fuse housing with field grading

dielectric is exposed to high electrical stress, electrical breakdown in the air gaps between the sand grains occurs. The breakdown begins near the fusible elements, because the electrical stress is more than 50 times higher than in the rest of the fuse (Fig. 2).

If the electrical stress is high enough, discharge channels can propagate until the inner border of the porcelain tube. The role of the sand grains is ambivalent in this case, because they can stop the propagation of the discharge channel mechanically, or sustain it by surface effects.

### I.2 Concepts preventing PD generation

PD activity of H.V.-fuses can be decreased in several ways:

1. Field grading, such that critical el. field strength for PD generation is not exceeded.
2. Insertion of metallic shields (shielding).
3. El. filtering, to prevent that generated PD impulses propagate into the switchgear installation.
4. Modification of material properties, to reduce the electrical stress in the sand.
5. Constructional changes in the design of the fuses.

Field grading can be implemented by fuse housings with conductive layers (Fig. 3). The layer must be capable to feed the capacitance of the dielectric during normal operation but must prevent current flow after the fuse has opened. This can be accomplished with materials having a voltage dependent non-linear conductivity [3, 4, 5, 6].

Insertion of metallic shields is disadvantageous because the fuses operation is inhibited.

Filtering implies additional components added in the current path and is not cost-efficient.

Modification of the arc-quenching medium can affect the switching behaviour. If the supplement to the sand is gas evolving, care must be taken not to overstress the fuses' enclosing tube. Gas evolving additives tend to support the arc interruption [7].

Constructional changes can be performed on nearly all parts of the fuse, with respect to existing standards.

Impacts on the electrical stress can be obtained by changing the melting elements' shape, enlarging the clearances of the inhomogeneous "electrode setup" etc. Often these changes are disadvantageous with respect to the fuses' switching behaviour or costs.

## II. INVESTIGATIONS, TEST SET-UP, AND SAMPLES

Preliminary measurements showed that the highest electrical field occurs in fuses employed under oil. Here the distance between melting elements and grounded environment (for example the transformer tank) is very small. In gas-insulated switchgears clearances are larger and therefore electrical stress is less critical. The lowest electrical stress can be found in air-insulated switchgear stations, because clearances are even larger.

### II.1 Switching behaviour

The switching behaviour of the fuses was tested according to IEC 282-1. To determine the post-arcing behaviour, a shunt was

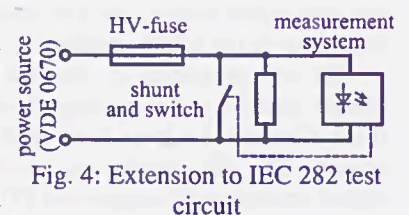


Fig. 4: Extension to IEC 282 test circuit

connected in series to the fuse (Fig. 4). The shunt was shortened by a switch that was opened after arcing to allow sensitive current measurement.

### II.2 PD measurements

For long-time observations, the fuses were equipped with an earth electrode located in the middle of the porcelain tube and were connected to earth via an automatic PD-measurement system (Fig. 5). The fuses were supplied with 20 kV AC voltage. The electrode was glued directly on the surface of the porcelain tube and graded with semi-conducting material. The test set-up contained 10 fuses in parallel. The PD activity was

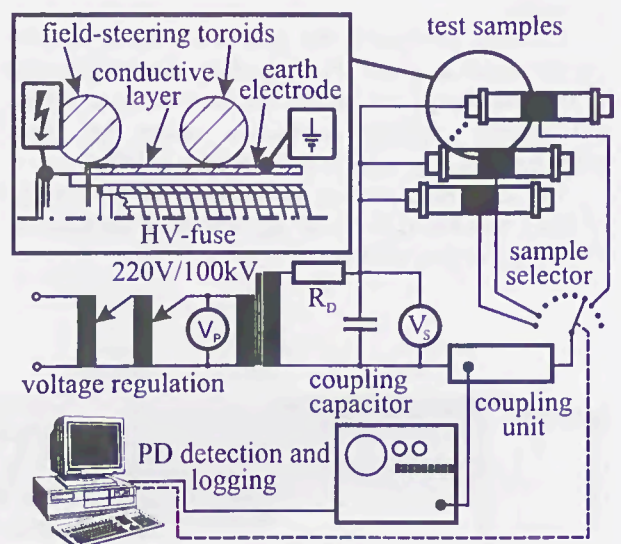


Fig. 5: Test set-up for long-time investigations

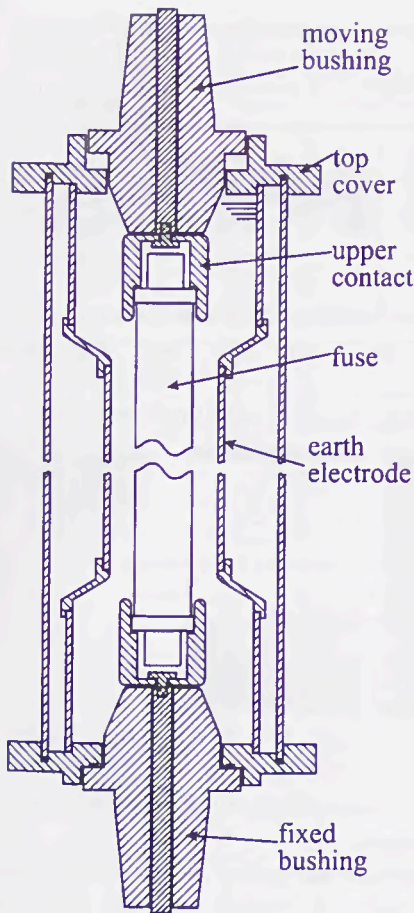


Fig. 6: PD measurement tank

recorded for 1000 hours. The samples were cyclically selected for a measurement time of one minute.

Fig. 6 shows the PD measurement tank used to test the short-time PD behaviour of HV-fuses. It consists of an outer cylindrical oil-filled tank, embedding the fuse to prevent from PD generated on the fuses' surface. At a distance of 10 mm around the porcelain tube of the fuse, a cylindrical earth electrode was placed and connected to the PD detector.

### II.3 FEM model

For the field-computation, a three dimensional model was used and calculated by means of FEM. The calculation was run on a workstation cluster in the university's calculation centre.

### III. RESULTS

The PD behaviour of HV-fuses over the voltage is shown in Fig. 7. The values of the apparent charge rise fast up to levels inhibiting sensitive PD measurement of other components in the switchgear assembly.

The influence of the melting elements' shapes is negligible. The PD inception voltage varies within 2.0 kV between individual fuses of the same series. Fuses can even change their PD behaviour between distinct measurements if they are physically moved. This is related to the displacement of sand grains inside

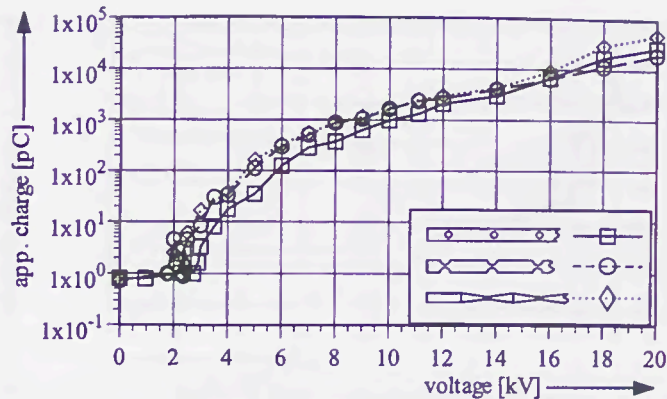


Fig. 7: PD behaviour over voltage with different elements' shapes

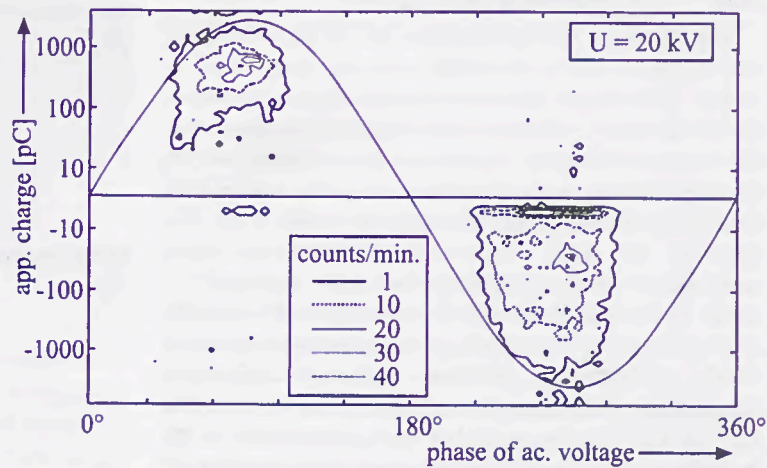


Fig. 8: PD fingerprint (PD number vs. phase and apparent charge)

of the fuse, resulting in differently shaped air gouges in the sand. Therefore PD conditions may change unpredictable. At high voltages, the apparent charge remains constant, because further propagation of the PD arcs is inhibited by the porcelain tube. The position of PD impulses relative to the phase of the supplying voltage is similar to corona impulses in air [8, 9]. The number of PD impulses rises very fast from individual impulses near inception voltage to more than thousand pulses per second at 10 kV.

In Fig. 8 a "fingerprint" of a 12/20 kV fuse at 20 kV is shown. The number of PD impulses with a specific level is mapped over the phase of the supplying voltage and the corresponding PD charge. Darker shading indicates a higher amount of counts. As can be seen, PD arise most frequently in the interval between the zero-crossings and the maximum of the half-waves. At lower voltages, the impulses occur in the negative half-wave only. With increasing voltage the impulses rise and affect also the positive phase. At high voltages, strong pulses in the negative phase combined with a high impulse rate in the positive phase are dominant.

The characteristic feature of the fuses' PD behaviour is the occurrence of impulse clusters instead of single impulses. This can be explained with the inhomogeneous configuration of the melting elements. The PD are generated along longer parts of the wire, not only at discrete sites.

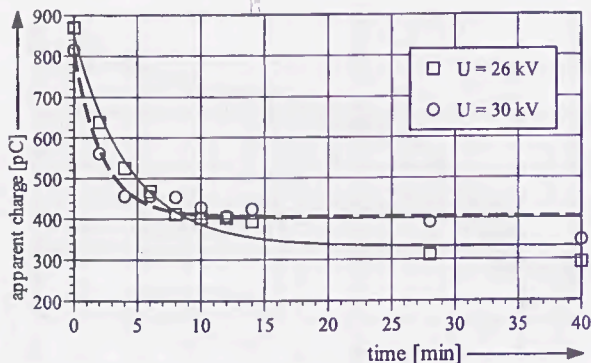


Fig. 9: PD behaviour of 6/12 kV fuse

### III.1 PD behaviour over the time

Fig. 9 shows the development of PD over the time. The apparent charge decreases with the stress time as well as the impulse rate (not shown). This is related to the development of ozone in the high-field region, near the fusible elements [10, 11]. The results of an investigation on a needle-plane electrode set-up [10] correspond to the ones obtained on fuses (Fig. 10), although the fuses were only measured at room temperature. When temperature increases above 60 °C, ozone is not generated and no decrease of PD activity can be observed. This is related to ozone disintegration, which depends on different parameters: pressure, temperature, field-strength, and chemical reactions [10, 12, 13, 14]. The ensemble of parameters leads to an equilibrium in ozone generation and disintegration. If ozone generation is stopped, disintegration continues by chemical reactions. Therefore, after 24 hours without electrical stress, the PD activity of HV-fuses rises to initial values.

When voltage is applied for longer time (1000 hours), apparent charge and impulse rate still decrease (Fig. 11). This can be explained by electrical erosion [15]: After the ageing process the fusible elements show erosion effects (Fig. 12). The excavated material moves to the enclosing sand. If the material excavated from the fusible elements is deposited around the sharp edges of the wires, electrical stress and PD

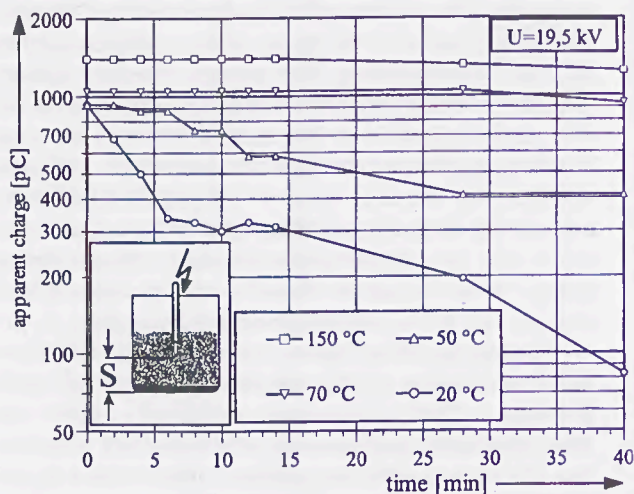


Fig. 10: PD behaviour of needle-plane set-up in sand

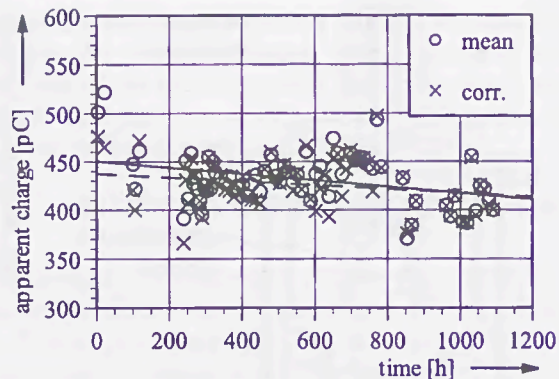


Fig. 11: App. charge in long-time observation

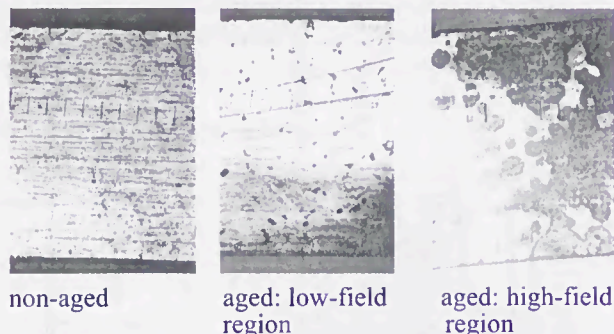


Fig. 12: Erosion effect on melting elements

generation decrease.

Other fuses from the ageing test have been tested to show the impact of erosion on the current-time characteristic (Fig. 13). The influence is negligible. This may also be related to the material excavated by electrical erosion, because it "glues" the sand to the melting elements, resulting in better heat transfer to the sand and by filling the air gaps to a higher thermal capacitance.

### III.2 Results from field-computation

Figures 2 and 14 show results obtained from field-computations. Because FEM cannot calculate the exact results at the edges of the fusible elements, the mean of 5 % from the most charged finite elements was used as "maximum" electrical field-strength. Starting from a set of global constraints, only one single parameter was

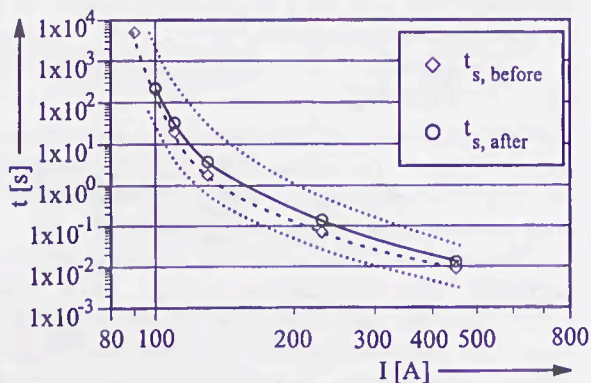


Fig. 13: Current-time characteristic of 6/10 kV fuses before and after ageing, band of tolerance

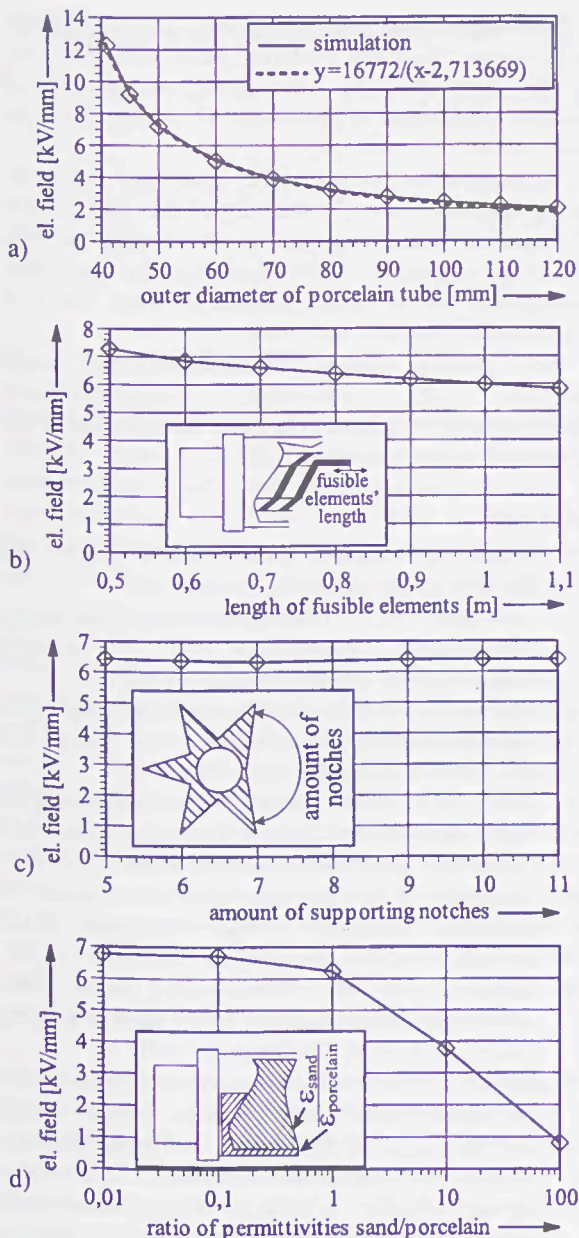


Fig. 14: Results from field-computation

varied on each calculation as described below.

As proof of reliability for the calculations the variation of the porcelain tubes' diameter can be interpreted (Fig. 14a): It follows the  $1/r$ -ratio known from cylindrical electrode set-ups. The diameter has the strongest impact on the maximum electrical field, but enlargement leads to higher weight and costs of the fuse.

The enlargement of the fusible elements' length (Fig. 14b) yields to better field behaviour, because the windings of fusible elements are approaching. The total length of the fuse was held constant. Longer fusible elements reduce the maximum electrical field. However, a minimal distance between distinct windings must be respected, because of switching behaviour.

The variation of the number of supporting notches (Fig. 14c) does not affect the field strength at all,

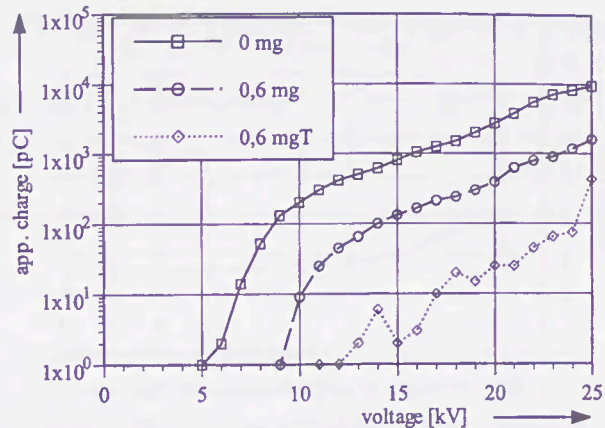


Fig. 15: Influence of adding water to the filler (12/20 kV fuse)

although with growing amount of notches the support becomes rounder. The non-homogeneity of the field depends on the thickness of the fusible elements compared to the grain size of the sand. This corresponds to Fig. 7 where differently shaped melting elements show comparable PD behaviour.

Variation of the permittivity ratio (sand to porcelain, Fig 14d) can be used to boost the field strength in the porcelain and therefore reducing it in the sand. Increasing of sand's permittivity is possible by adding additives based on elements like titanium to the sand, but it is unknown how this may affect the switching behaviour of the fuse. At least the fuse becomes more expensive, because large amounts of additives have to be added to the sand to achieve relevant changes in the permittivity ratio.

If the electro-conductive analogy is taken into consideration, the results of Fig. 14d can be interpreted in a second way: A high ratio of conductivity (sand to porcelain) also leads to lower electrical stress in the sand. As porcelain is a very good insulator, only a small amount of additives in the sand needs to be employed.

### III.3 Reduction of PD activity

The effect of increasing the conductivity of the sand is shown in Fig. 15: If a small amount of water is added to the fuses' sand, the PD inception voltage rises and the increase of PD over voltage becomes smaller. If the fuse

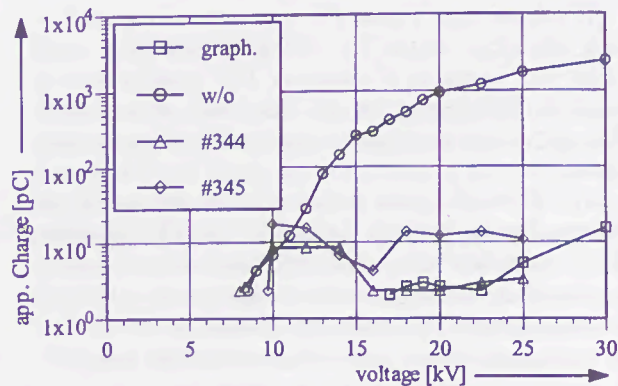


Fig. 16: PD behaviour of fuses with field grading layer

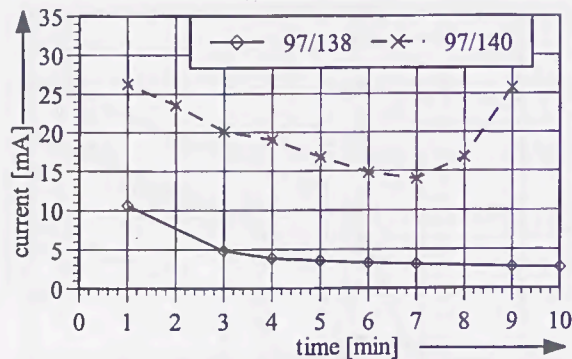


Fig. 17: Post-arcing behaviour of fuses

is tempered after applying water, the PD activity decreases even more (Fig. 15: "0,6 mgT").

Another attempt to reduce PD generation of the fuses is field grading. Based on coatings elaborated in [6], test fuses were made and tested for switching behaviour. The SiC based coating was applied to the surface of the porcelain tube and a 10 kV fuse inlet was mounted. Fig. 16 shows the results of PD measurement. Contrary to a fuse without coating (Fig. 16: "w/o"), PD activity shows a significant decrease for all samples. Samples 344 and 345 were graded using a ceramic overglaze. Most fuses successfully fulfilled the switching test. Fuses with graphitized surface show the best PD behaviour (Fig. 16: "graph") but are unable to switch.

To explore the post-arcing behaviour of the conducting layers, the recovery voltage was applied for 10 minutes. The remaining current in this period is shown in Fig. 17. Nearly all samples manifest decreasing currents.

The high initial current ( $t = 1$  min. in Fig. 17) results from the conductivity of the fuses' fulgurite. After cool-down of the fulgurite, the remaining current is dominated by the conductive layer. In case of 97/140, the conductivity was chosen too high, leading to self-heating of the layer and finally destruction of the fuse due to over-heat. The turn-around point at seven minutes results from the heat produced during the arcing phase, which propagates slowly from the inner of the fuse (arcing channel) to the surface.

#### IV. CONCLUSION

HV-fuses may create PD impulses, if exposed to high electrical stress. The PD generated may reach levels not tolerable if sensitive PD measurement is required. The impact on the fuse itself is negligible, although electrical erosion of the fusible elements takes place.

The PD mechanisms are complicated, because of the inhomogeneous sand-air dielectric. The PD behaviour of HV-fuses depends on different parameters:

- the electrical field the fuse is exposed to,
- temperature, pressure inside the fuse,
- moisture and properties of sand inside the fuse,
- ozone generation and electrical erosion.

Shielding of the fuses is difficult, because metallic shields impair the fuses' switching behaviour. However, shielded fuses may be used during on-site tests of electrical equipment to eliminate PD coming from the fuse.

The easiest way to reduce PD generation inside the fuse is to enhance the conductivity of the filler. In this investigation water was used. Its impact on the switching behaviour of the fuse has not yet been investigated, but the small amount of water that was added does not seem to be critical.

Field grading reduces PD generation. SiC based materials with non-linear voltage-resistance characteristics can be used. However the selection of the appropriate resistances is difficult.

#### References

- [1] Wright A., Newbery P.G.: "Electric fuses", 2nd Ed., IEE power series 20, London 1995
- [2] Dreischke W.: "Hochspannungs-Hochleistungs-Sicherungen", Publication E1T1, Wickmann-Werke GmbH, Witten (Germany) 1994
- [3] Wesner F.: "Elektrische Eigenschaften von spannungsabhängigen Widerständen auf Basis von SiC", PhD-thesis, Stuttgart 1971
- [4] Weedy B.M. et al.: "Resistive stress relieving for XLPE cable joints", 2nd Int. Conference on Power Cables and Accessories, London 1986
- [5] Auckland D.W. et al.: "Nonlinear fillers in electrical insulation", IEE Proc.-Sci. Meas. Technol., Vol. 144, No. 3, May 1997
- [6] Gärtner J. et al.: "Field-grading with Semiconducting Materials Based on Silicon Carbide (SiC)", ISEI 1998, Washington, 1998
- [7] Shea, J.J.: "Gas evolving materials for improved low current interruption in high voltage current limiting fuses", IEEE Trans. on Power Delivery, Vol. 10, No. 1, pp. 258-265, 1995
- [8] Kreuger, F. H.: "Partial discharge detection in high-voltage equipment", Butterworths, London 1989
- [9] Beyer M., Boeck W., Möller K., Zaengl W.: "Hochspannungstechnik", Springer Verlag, Berlin 1986
- [10] Gärtner J. et al.: "The Partial Discharge Behaviour of Gas-filled Granular Porous Material", 10th ISH, Montreal 1997
- [11] Nettelblad B.: "Dielectric properties of liquid-impregnated porous material", PhD-thesis, Göteborg 1996
- [12] Heuser C.: "Zur Ozonbildung in elektrischen Gasentladungen", PhD-thesis, Aachen 1985
- [13] Labrenz M.: "Elektrische Gasentladungen zur Ozonerzeugung", PhD-thesis, Brunswick 1983
- [14] Hollemann-Wiberg A.F.: "Lehrbuch der Chemie", 91th Ed., de Gruyter, Berlin 1985
- [15] Spur G.: "Handbuch der Fertigungstechnik", Vol. 4, pp. 61-152, Carl Hanser Verlag, Munich 1987

# PRESSURE INSIDE THE ARC CHANNEL OF A HIGH-VOLTAGE FUSE

M.A. Saqib, A.D. Stokes and P.J. Seebacher  
School of Electrical & Information Engineering  
The University of Sydney  
NSW 2006 Australia

## I. INTRODUCTION

Pressure is one of the key arcing parameters of high-voltage, high breaking capacity fuse. An accurate mathematical model will require exact estimates of pressure values inside the arc. Most of the models assume constant pressure that is not realistic in the fuse arc. Therefore, these models fall short in predicting the exact behaviour of these arcs.

The phenomena of generation and propagation of pressure when a fuse wire is exploded in air have been studied for a long time [1]. It is generally accepted that when a wire is exploded the instantaneous release of energy causes a cylindrical shock wave [2-4]. The generation of pressure associated with the HBC fuses was first addressed in the 1970's [5]. There have been several reports of pressure estimates inside the fuse arcs [6-8]. However, all these studies are restricted to the determination of the pressure values at the cartridge wall of the fuse. Empirical relations correlate these pressure values to the pressure inside the channel.

Our studies are related to the experimental determination of the pressure evolution inside the arc channel of a sand-filled high-voltage fuse. We have successfully measured the pressure inside the arc channel with the help of a piezoelectric pressure transducer that has a frequency response of 100 kHz.

## III. EXPERIMENTAL SETUP

We have constructed an experimental model of a high-voltage, high breaking capacity fuse. It consists of a cylindrical ceramic fuse holder with length of 240 mm and diameter of 43.70 mm. Both ends of the fuse holder are fitted with metal end-caps and a uniform silver wire of 0.55 mm diameter is used as the fuse element. Pressure near the fuse element, after it had exploded, was transmitted to a transducer located outside the cartridge.

The fuse is energised using the synthetic test circuit as shown in Figure 1. A short-circuit prospective current was varied from 1 kA to 4 kA, in steps of 1 kA, by using different combinations of parallel inductors and

capacitors. The capacitors were charged at 6 kV and the frequency of the waveforms of current through and voltage across the fuse was 50 Hz.

## III. EXPERIMENTAL RESULTS

The voltage across the fuse was measured as a function of time by a resistive voltage divider: a Tektronix P6015, 1000:1, 20 kV, 100 M $\Omega$  voltage probe (rise time of 5 ns). Current was measured using a 190.8 A/V coaxial current shunt (rise time approximately 60 ns). The pressure developed inside the arc was measured using a piezoelectric pressure transducer. The pressure wave generates an electrical pulse in the transducer which, is calibrated in terms of pressure. The pressure signal in Figures 2-5 before the start of the arcing actually represents atmospheric pressure. Thus a correction was applied to values for pressure after the arcing. The pressure transducer was linked to the arc space through a high-temperature ceramic tube that was filled with glycerine. The function of glycerine is two-fold; first to transmit the pressure generated and second to protect the transducer from the high-temperature arc. When the arc burns in the fuse, the generated gas exerts pressure on one end of the tube that is transmitted through the filled glycerine to the transducer.

Voltage, current and pressure signals associated with the test fuse are recorded using a Nicolet Pro 42C digital oscilloscope. The measured pressures are from the radial forces. From the curves of the voltage across and current through the fuse, the energy and instantaneous power in the arc was calculated. These curves are shown in Figures 2-5.

## VI. DISCUSSION

Disintegration of fuse element is associated with sudden release of energy that causes an arc to be generated. As a result, arc behaviour is determined by the development of pressure inside the HBC fuse. Lipski [7, 9, and 10] found out that there are two components to the pressure wave when the fuse interrupts a heavy current. One component is fast rising and due to the initial explosion. The other is slow rising and due to burn-back. The second component is

more important when the fuse element contains constrictions. The wire melts first at the constrictions and then burns back. When the fuse wire is uniform, as in the present case, the second component is insignificant. The whole length of the fuse wire is subjected to erode simultaneously in this case and the pressure wave is dominated by the first component. Table 1 shows the results of our study. The peak pressure in column 2 corresponds to an explosion of the fuse element whereas pressure afterwards decreases very sharply and stays almost constant towards the arc

extinction. This corresponds to the second component of pressure as discussed by Lipski. It is the pressure shown in column 8. It is evident that both values of pressures are proportional to the arc's prospective current and energy. Peak values of pressure are proportional to maximum values of instantaneous arc power. Maximum values of pressure lags almost between 0.2 ms to 0.3 ms behind the peak instantaneous power. This delay underlines the importance of thermal storage in the molten phase [6].

Table 1: Summary of results for pressures, arc energy and speed of pressure shock waves at different prospective currents.

Prosp. Current (kA)	Peak pressure (bar)	Time between arcing and press. signal (ms)	Max. inst. power (MW)	Time lag between (2) - (4) in ms	Arc energy (kJ)	Initial slope of (6) (kJ/ms)	Press. at zero (bar)	Speed of the press. wave (m/s)
(1)	(2)	(3)	(4)	(5)	(6)	(7)	(8)	(9)
1	16.54	0.200	4.10	0.240	2.123	3.395	1.32	425
2	25.58	0.120	7.35	0.222	6.690	5.242	1.48	708
3	45.63	0.110	10.90	0.275	13.080	8.850	1.72	773
4	55.64	0.108	12.46	0.199	17.870	9.235	2.35	787

Column 3 of Table 1 shows the time between the arc initiation and the rising of the pressure wave. In each of the tests, the length of the ceramic tube used was 85 mm. Thus we can calculate the speed of the pressure shock wave detected by the pressure transducer. These values shown in column 9 of Table 1 are dependent upon the arc energy (and prospective current); the higher the arc energy the larger the speed of the spherical shock wave generated. These values are to be compared with 700 m/s, a value calculated by Yukimura et al [11]. These authors used a copper wire exploded in air with a test energy that was very low as compared to that used in our study. According to Barbu [12], the pressure is less dependent on the electric arc energy than on the shape and dimension of the interruption arc itself. Our study reveals that the pressure is strongly dependent upon arc energy when physical parameters of the fuse i.e., size and shape of the wire, fuse cartridge and filler are not changed.

Our measurements show that the peak of the pressure wave follows almost immediately the arc initiation and the magnitude of the peak depends upon the energy to be dissipated in the arc. We have recorded the pressure peak above 50 bars when the fuse was energised at 6 kV, 50 Hz, for 4 kA prospective current.

## REFERENCES

- [1]. W.G. Chace and H.K. Moore, "Exploding Wires", Plenum Press, New York, Vol. 1, 1959.
- [2]. F.D. Bennet, "Cylindrical shock waves from exploding wires", *Phys. Fluids*, 1, 1958, pp. 347-352.
- [3]. A. Sakurai, T. Takao and T. Taira, "Effect of applied magnetic field on the exploding wire phenomena - II", *Exploding Wires*, Vol. 4, Plenum Press, New York, 1968, pp. 63-69.
- [4]. M. Motoki and K. Yukimura, "Formation and behaviours of compression waves produced by underwater exploding wires", *The Sci. and Engg. Rev. of Doshisha Univ.*, 17, 1977, pp. 192-201.
- [5]. A. Gul and T. Lipski, "Pressure shock-wave investigations during the wire-element explosion in a H.B.C. fuse", *Switching Arc Phenomena*, Lodz, 1985.
- [6]. M.R. Barrault, "Pressure in enclosed fuses", *Proceedings of the first ICEFA*, 1976.
- [7]. T. Lipski, "Generation and propagation of the pressure due to the fuse-element disintegration in H.B.C. fuse", *Gas Discharges and their Applications*, Oxford, 1985.
- [8]. K.K. Namitokov and Z.M. Frenkel, "Pressure in the electric arc channel of a fusible link", *Soviet Electrical Engineering (USA)*, Vol. 60, No. 12, 1989, pp. 102-109 [English Translation of *Elektrotehnika*, Vol. 60, No. 12, 1989, pp. 63-68.
- [9]. T. Lipski, "Review lecture: What next with the H.B.C. fuses?", *Proceedings of the third ICEFA*, Trondheim, Norway, 1984, pp. 1-11.
- [10]. J. Hibner, K. Jakubiuk and T. Lipski, "Evaluation of pressure explosive component of high rupturing capacity

fuse", International Conference On Gas Discharges and their Applications, Venice, Italy, September, 1988.

- [11]. K. Yukimura and J. Urabe, "Spherical shock waves produced by explosive partial disintegration of a copper wire in air", Switching Arc Phenomena, Lodz, 1985.
- [12]. I. Barbu, "Correlation of the arc energy with electrical and dimensional parameters of fuses", Switching Arc Phenomena, Lodz, 1985.

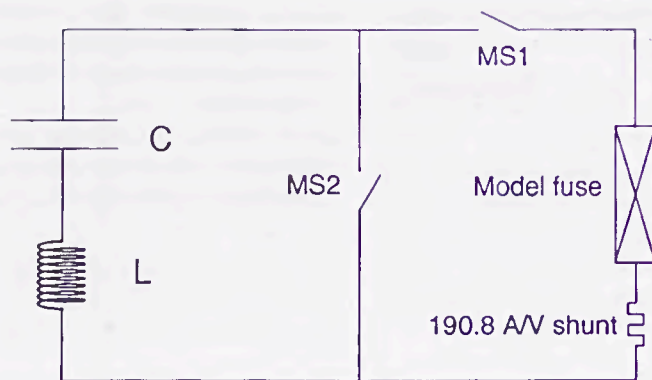


Figure 1: Electrical circuit to energise the test fuse.

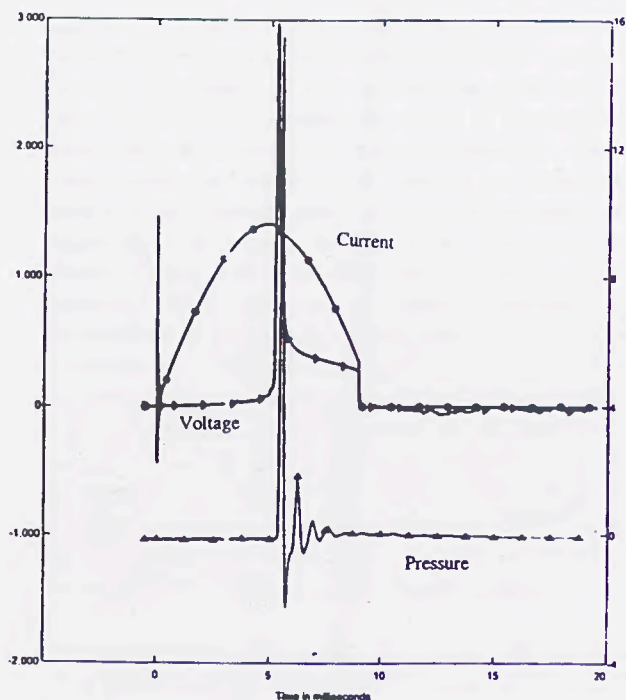


Figure 2A: Plots for current and voltage (on left side) and pressure (on right side) for 1kA prospective current.

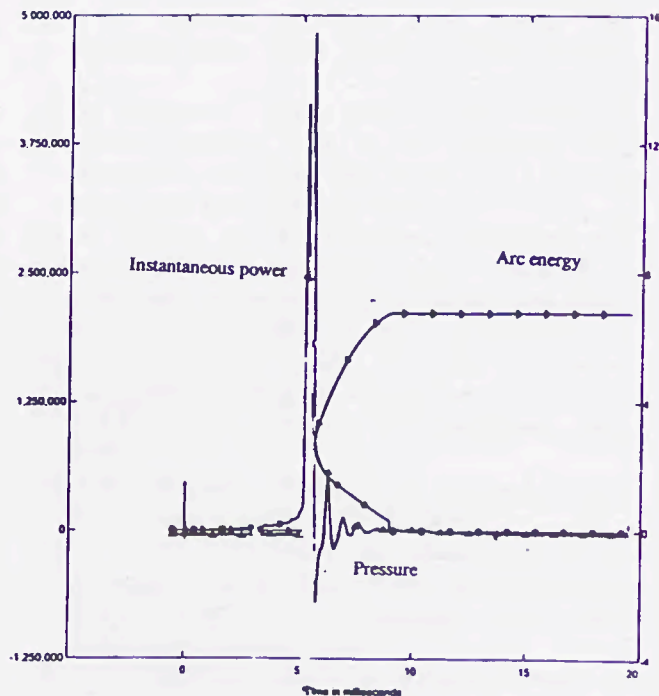


Figure 2B: Variation of pressure (right side) with instantaneous arc power and arc energy for 1 kA prospective current.

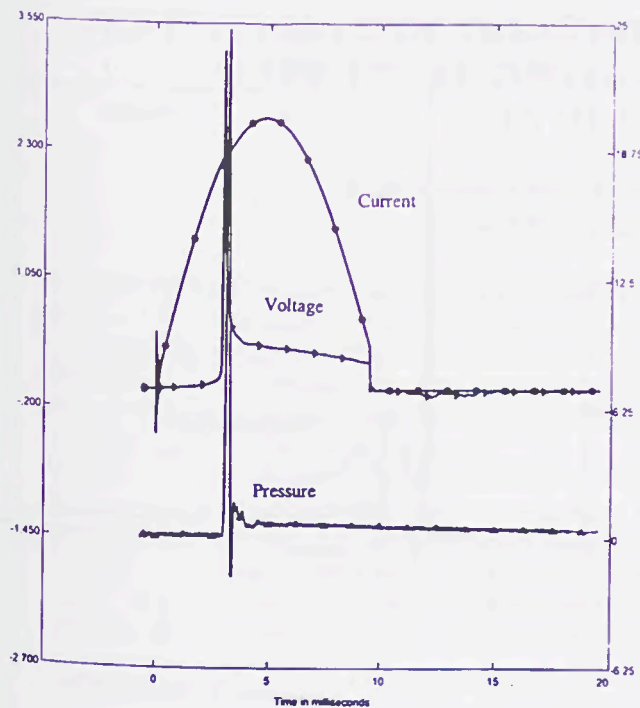


Figure 3A: Plots for current and voltage (on left side) and pressure (on right side) for 2kA prospective current.

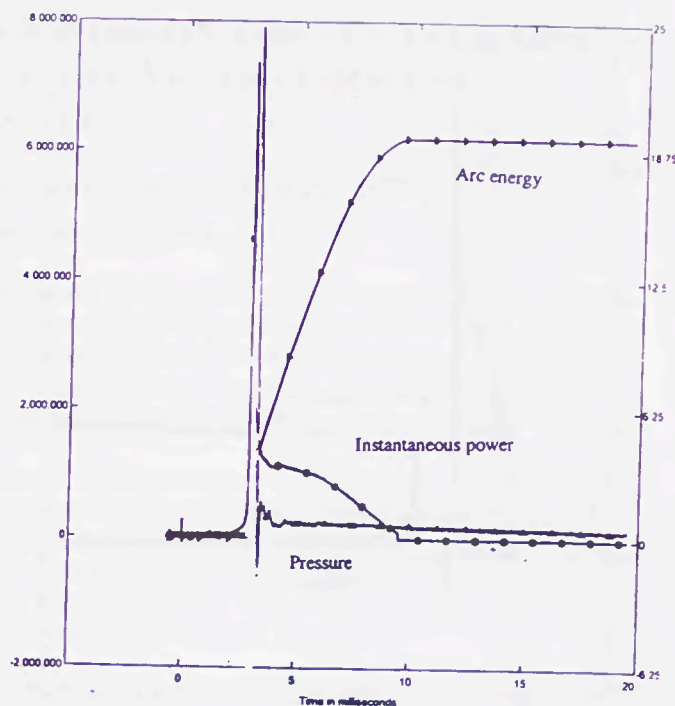


Figure 3B: Variation of pressure (right side) with instantaneous arc power and arc energy for 2 kA prospective current.

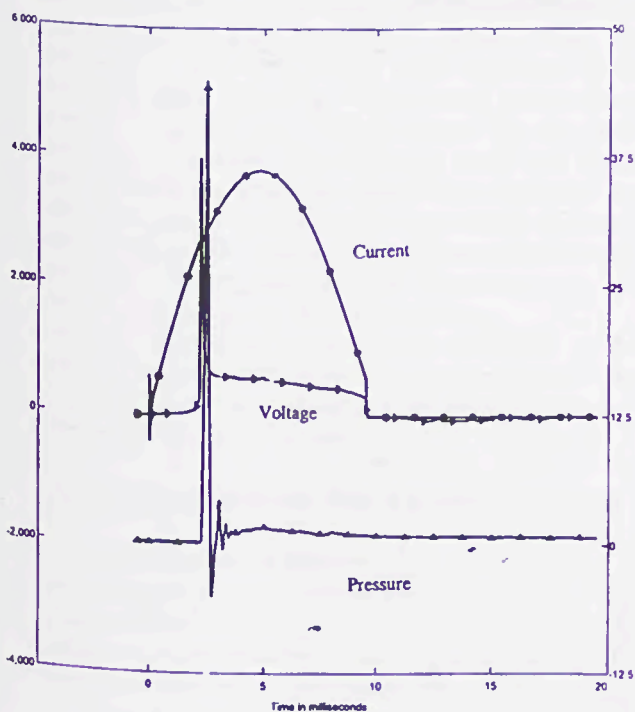


Figure 4A: Plots for current and voltage (on left side) and pressure (on right side) for 3 kA prospective current.

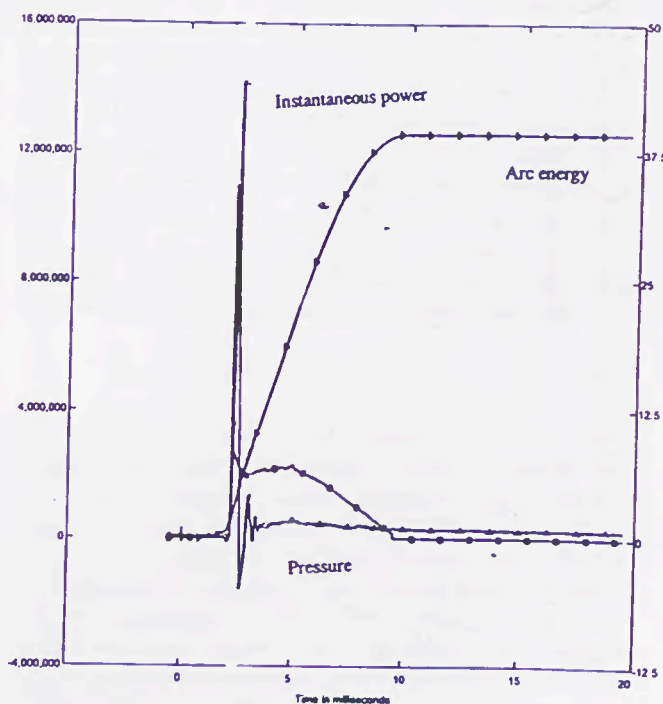


Figure 4B: Variation of pressure (right side) with instantaneous arc power and arc energy for 3 kA prospective current.

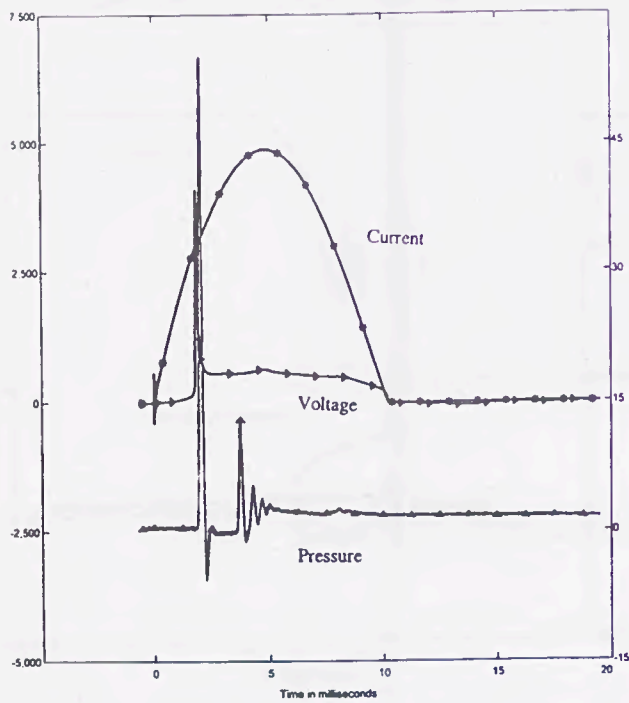


Figure 5A: Plots for current and voltage (on left side) and pressure (on right side) for 4 kA prospective current.

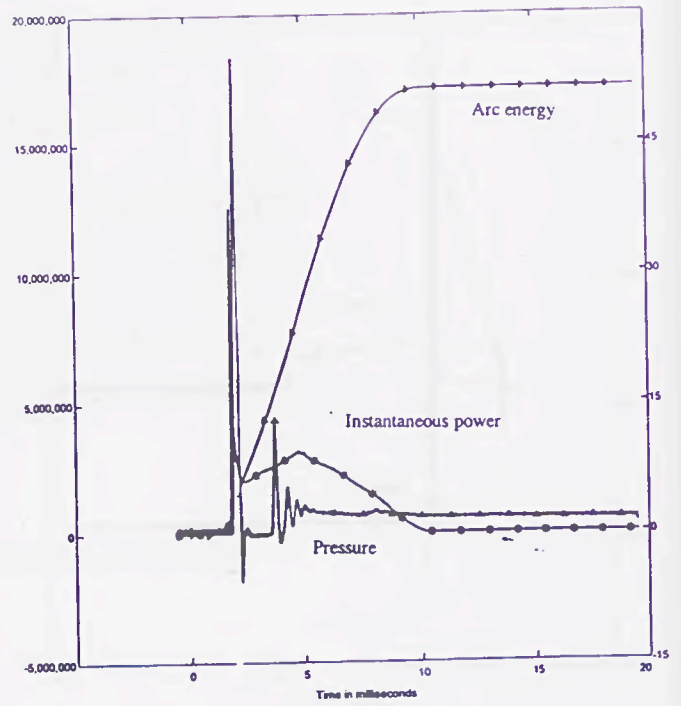


Figure 5B: Variation of pressure (right side) with instantaneous arc power and arc energy for 4 kA prospective current.

# THE INFLUENCE OF THE STRIKER WIRE ON THE VOLTAGE RISE AFTER THE BEGINNING OF THE ARCING PROCESS IN HV FUSE LINKS

Hans-Günter Rex, Consultant Quality Assurance  
D-69207 Sandhausen, Germany

**Abstract:** When  $N$  rows of constrictions of a melting element are cut by a short circuit current, the arcing voltage starts with the value  $u_{ME} = N \cdot U_E$ . In this moment a well defined amount of the current is directed across the striker wire. Breaking tests with HV fuse links show that the arcing voltage along the melting element is limited to the voltage drop along the striker wire. The arcing process of the melting element is delayed, until the shunted current has built up the melting integral of the striker wire. For small rated currents the striker wire causes a pause up to 0.4 ms in the arcing process of the melting element.

Wenn ein Kurzschlußstrom  $N$  Engstellenreihen eines Schmelzleiters unterbrochen hat, beginnt die Lichtbogenspannung mit dem Wert  $u_{ME} = N \cdot U_E$ . In diesem Augenblick weicht ein festgelegter Teil des Stromes auf den Kennmelderdraht aus. Schaltversuche mit HH-Sicherungen zeigen, daß die Lichtbogenspannung über den Schmelzleiter begrenzt wird durch den Spannungsfall längs des Kennmelderdrahtes. Der Lichtbogenvorgang beim Schmelzleiter wird verzögert, bis der parallele Strom das Schmelzintegral für den Kennmelderdraht erreicht hat. Für kleine Nennströme verzögert der Kennmelderdraht den Lichtbogenvorgang beim Schmelzleiter bis zu 0.4 ms.

## 1 INTRODUCTION

When the arcing process in a fuse link is analysed there must be no striker wire in parallel to the melting element in order not to disturb the analysing. The result therefore cannot be transferred to a fuse with a melting element and a parallel striker wire inside. We look at a short circuit current  $I_2$  in a RL-circuit that contains a fuse. The resistance of the striker wire is higher than that of the melting element. When the voltage creates the necessary current, the striker wire will be heated up and interrupted. For big rated currents only a small part of the current will flow along the striker wire and influence little the arcing process in the melting element. For small rated currents the influence lasts remarkably longer. When the voltage along the fuse begins to rise, the current along the striker wire is still small.

For fuses with small rated currents the pause in the voltage rise may reach several 100 microseconds. The diagram 1 shows the beginning of the arcing process in a HH-fuse with a rated current of 20 A..

## 2 THE BEGINNING OF THE ARCING PROCESS

A lot of evaluations of breaking tests with fuses lead to the expression of an electrode effect voltage  $U_E$ . The moment arcing starts in quartz sand as a arc quenching medium, in each interrupted constriction of the melting element the electrode effect voltage  $U_E = 55$  V is created [2]. When a short circuit current interrupts  $N$  rows of constrictions of a melting element, the arcing voltage along the melting element starts with the value

$$u_{ME} = N \cdot U_E \quad (1)$$

The voltage  $u_{ME}$  along the melting element acts against the test voltage. The melting current  $i_M$  creates a voltage drop along the circuit resistance  $R$  and reduces the active test voltage. When the current decreases, the voltage  $u_L$  across the inductivity  $L$  rises in order to have the current unchanged.. At the melting element you measure the voltage  $u_{ME} = u_B - R \cdot i_M - L \cdot di/dt$ . The voltage  $u_{ME}$  creates a current  $i_{SW}$  in the parallel striker wire. This current is missed for the build up of the arc resistance in the interruptions of the melting element. A breaking test with a fuse link as described in the annex delivered a melting current  $i_M = 1000$  A and a melting integral  $i^2t = 869$  A<sup>2</sup>s. The rated current of that fuse is below 20 A.

The current along the melting element is  $i_{ME} = i_M - i_{SW}$ . We assume the current  $i_{SW}$  along the striker wire to be constant. The resistance  $R_X$  of the melting element in the moment the constrictions disrupt, can be calculated.

$$R_X = N \cdot U_E / (i_M - i_{SW}) \quad (2)$$

The current  $i_{ME}$  vaporizes the material next to the interruptions and creates additionally an arc resistance  $R_{LB}$  across each interruption.. The resistance  $R_{ME}$  along the melting element grows according to  $R_{ME} = R_X + R_{LB}$ . The current along the melting element must be big enough in order to build up the isolating distance needed for the maximum arc voltage. We assume to have a fuse with small rated current. When the striker wire is heated up, we assume the resistance of the melting element to be constant. The arc voltage along the melting element rises slowly. The interruptions in the melting element also grow slowly. The danger of reignition rises too. Only when the striker wire disrupts, the arc voltage can rise remarkably.

### 3 THE STRIKER WIRE

The striker wire has a higher resistance than the melting element. A short circuit current heats up the striker wire only when the necessary voltage is present and when the necessary current flows. For heating up times of less than 1 ms we calculate the heating up as an adiabatic process. The currents along the melting element and the parallel striker wire are in inverse proportion to their resistances. The voltage  $u_{ME}$  and the resistance of the striker wire define the current  $i_{SW}$ . With  $R_{SW}$  as cold value resistance of the striker wire, in the first moment after the arcing process created the arc voltage  $u_{ME} = N \cdot U_E$ , the current  $i_{SW}$  is flowing along the striker wire.

$$i_{SW} = N \cdot U_E / R_{SW} \quad (3)$$

The current  $i_{SW}$  heats up the wire. The resistance  $R_{SW}$  of the wire rises with rising temperature, the current  $i_{SW}$  decreases. The length and the cross section  $Q_{SW}$  of the striker wire deliver the resistance and the ratio of the currents along the striker wire and along the melting element. The melting time of the wire and therefore the duration of the pause in the voltage rise can be determined by the current and the melting integral  $(i^2t)_{SW}$  of the homogenous wire. The melting integral is

$$(i^2t)_{SW} = K_{SW} \cdot (Q_{SW})^2 \quad (4)$$

The melting value  $K_{SW}$  for adiabatic heating is easy to determine. For silver material e.g. the melting value for adiabatic heating is  $K_{Ag} = 73\,000 \text{ A}^2\text{s/mm}^4$  [1]. The striker wire changes into liquid before the wire is constricted. The resistance rises until the wire disrupts. We assume the resistance of the wire to be constant from low temperatures up to the melting temperature. Additionally we assume 85% of the melting integral to be reached when the wire has reached the melting temperature.

### 4 THE PAUSE IN THE VOLTAGE RISE

When we know how the resistance of the striker wire depends on the temperature, we can calculate the momentaneous values  $i_{SW}$  of the current and the  $(i^2t)_{SW}$ -value for the same moment. If we agree to have a good approximation, we assume the resistance  $R_{SW}$  of the striker wire to be constant up to the melting temperature. Then the current along the striker wire is constant too. Formulas (3) and (4) allow to calculate the time  $t_{SW}$  to reach 85% of the melting integral of the striker wire.

$$\begin{aligned} t_{SW} &= 0.85 \cdot K_{SW} \cdot (Q_{SW})^2 / (i_{SW})^2 \\ &= 0.85 \cdot K_{SW} \cdot (Q_{SW})^2 \cdot (R_{SW})^2 / (N \cdot U_E)^2 \end{aligned} \quad (5)$$

We replace the resistance  $R_{SW}$  of the striker wire by its length  $L_{SW}$ , its cross section  $Q_{SW}$  and its resistivity  $\rho$  and receive the expression  $R_{SW} = \rho \cdot L_{SW} / Q_{SW}$ . We insert this

in (5) and get the pause time  $t_{SW}$  in the voltage rise.

$$t_{SW} = 0.85 \cdot K_{SW} \cdot \rho^2 \cdot (L_{SW})^2 / (N \cdot U_E)^2 \quad (6)$$

$K_{SW}$  and  $\rho$  are material values. A big resistivity  $\rho$  means a small melting value  $K_{SW}$ . A long striker wire results in a large pause, a short striker wire in a short pause in the rise of the arcing voltage across the melting element. Because the ohmic resistance of the striker wire rises with rising heating time, the current along the wire will decrease. Therefore the time to reach the melting temperature of the wire will rise too. Formula (5) delivers a value  $t_{SW}$  something smaller than the experiment.

### 5 THE DISRUPTION OF THE STRIKER WIRE

The striker wire disrupts at the beginning of the arcing process in the melting element. When striker wire has changed into liquid and the current has built up the melting integral of the wire, the wire disrupts. When there is only the wire in a RL-circuit, the inductivity  $L$  delivers the energy to disrupt the wire. The current density in the wire and the cross section of the wire define the number  $N_{SW}$  of the interruptions in the wire. The arcing voltage along the melting element defines the voltage along the striker wire. When there should be any current flowing along the striker wire, a voltage value of  $N_{SW} \cdot U_E$  must exist.

The disruption of homogenous wires and strips have already been described in the literature. Jan Nasilowski reports the average distance between two disruptions caused by a heavy short circuit current in the wire. The formula has been found experimentally [3].

$$A = 2.08 \cdot D + 0.555 \quad (7)$$

Distance  $A$  and diameter are measured in mm. The distance  $A$  is a characteristic of the single wire. When we have several parallel wires, the cross section increases. If the test current density remains constant, the distance will remain constant too. With the length  $L_D$  of the wire and the average distance  $A$  of the disruptions, we find the number  $N_D = L_D / A$  of the created arcs. Is there sufficient current flowing across the arcs in the melting element, the melting element creates the voltage  $N \cdot U_E$ . When the heating up of the striker wire takes over all the current, the arcing process in the melting element ends. The voltage  $N \cdot U_E$  disappears. The resistance of the disruptions in the melting element rises, the dielectric strength  $u_{IS}$  rises only minimal.

Formula (7) delivers also the number  $N_{ME}$  of the disruptions of the striker wire. When the wire disrupts, it creates a voltage until a current begins to flow along the melting element.

(1) defines the maximum voltage  $u_{SW} = N_{SW} \cdot U_E$ , that arises, when the striker wire disrupts. With the melting element parallel to the striker wire, the voltage along the striker wire rises up to the value  $u_{ME}$ . In the moment the

current along the melting element creates arcing, the voltage decreases to the value  $N_{ME} \cdot U_E$ . At the same time the current along the striker wire decreases.

## 6 EXPERIMENTAL RESULTS

The fuse voltage and current were measured all 30  $\mu$ s. The resistance was calculated for each measurement. All values were plotted in the diagrams 1 to 6. In the pause time the resistance is almost constant.

### 6.1 TEST HH98461

Before the constriction disrupts, the resistance of the constriction has grown so much that the current creates a voltage drop equal to the voltage  $U_E = 55$  V. According to (1) a row of 78 single arcs in line deliver the voltage value  $u_{ME} = 78 \cdot U_E = 4290$  V. The test confirms the calculated value. This voltage is big enough to create a current along the striker wire. The known values of the melting element and the striker wire of Konstantan lead to both the resistance values and the melting integrals. The resistance of the four parallel melting elements is  $R_X \approx 45$  m $\Omega$  cold value, the resistance of the striker wire is  $R_{SW} \approx 9.3$   $\Omega$  cold value. We did not measure the values before the test. When the constrictions disrupt, we measure the current  $i_M = 1088$  A. The arcs in the melting element and the parallel striker wire result in a resistance  $R_M = 4290/1088 \Omega = 3.94 \Omega$  (diagram 3).

The striker wire takes over a part of the measured current. When the resistance of the striker wire is 9.3  $\Omega$ , the resistance  $R_{ME}$  of the interrupted melting element must have the value 6.8  $\Omega$ . Along the wire the current is  $1088 \cdot 6.8/16 A = 460$  A, along the melting element the current is  $1088 \cdot 9.3/16 A = 630$  A. In this breaking test the striker wire takes over 42% of the total current  $i_M$ . This means a remarkable influence of the striker wire on the arcing process of the melting element. In Diagram 2 we see, that the current rises for another 400  $\mu$ s. Hence the current along the wire and along the melting element rise too. When we assume the resistance along the melting element and the striker wire to be constant, the voltage along the fuse link rises.

With the melting constant  $K_{SW} = 16400$  A<sup>2</sup>s/mm<sup>4</sup> for Konstantan formula (4) delivers the melting integral of the wire  $(i^2t)_{SW} = K_{SW} \cdot (Q_{SW})^2 = 39.5$  A<sup>2</sup>s. According to formula (6) the influence of the striker wire to the pause in the voltage rise is  $t_{SW} = 1.6 \cdot 10^{-4}$  s = 160  $\mu$ s. The oscillogram delivers the value 200  $\mu$ s.

### 6.2 TEST HH98668

A wire melting element with 5 short constrictions creates the voltage  $u_{ME} = 5 \cdot U_E = 275$  V at the beginning of the arcing process. If each constriction is a homogenous wire, we had to consider formula (7). The wire diameter

$D \approx 0.18$  mm delivers the average distance  $A \approx 0.93$  mm between the disruptions. The length  $s \approx 18$  mm of the constriction yield the number  $N_S = s/A = 18/0.93 = 19$  disruptions. Five of these constrictions in line deliver  $N_{ME} = 5 \cdot 19 = 95$  single arcs in line and the arcing voltage  $u_{ME} = 95 \cdot U_E = 5225$  V. The test confirms the calculated value (diagram 4). The resistance of the 3 parallel wires of the melting element is calculated to be  $R_{ME} \approx 80$  m $\Omega$  cold value, the resistance of the striker wire is  $R_{SW} \approx 7$   $\Omega$  cold value. We did not measure the values before the test. The arcing voltage  $u_{ME}$  and the measured melting current  $i_M = 700$  A deliver the resistance value  $R_M = 5225V / 700A = 7.5 \Omega$ . The current along the striker wire is  $i_{SW} = 5225 V / 7.5 \Omega = 700$  A. Thus the striker wire needs the whole current in the fuse. There is no current left to keep the arcs burning. The arcs cool down, their resistance rise. The dielectric strength of the interruptions is only minimal above the value  $N_{ME} \cdot U_E$ .

Again formula (6) delivers the pause time  $t_{SW}$  in the voltage rise:  $t_{SW} = 0.85 \cdot 16400 \cdot (0.5)^2 \cdot (0.6)^2 / (95 \cdot 55)^2$  s =  $4.6 \cdot 10^{-5}$  s = 46  $\mu$ s. The test delivers about 50  $\mu$ s (diagram 4, before the first maximum).

After the melting integral of the striker wire has been reached, the wire disrupts. The voltage rises fastly. The dielectric strength of the interruptions in the melting element does not withstand the voltage. The interruptions break. The current shifts from the striker wire to the melting element. The arcing process with its electrode effect voltage  $u_{ME} = N_{ME} \cdot U_E = 95 \cdot 55$  V = 5225 V starts once more.

## 7 CONCLUSIONS

In melting elements for small rated currents a remarkable part of the melting current is shifted to the parallel striker wire. This creates a pause in the arcing process along the melting element. A short striker wire takes over the whole current and interrupts the arcing process along the melting element. In order not to disturb the arcing process, the minimum length of the striker wire must create a voltage drop equal to the arc voltage  $u_{ME}$ . Formula (6) shows, that we have a short pause in the voltage rise. When we calculate the arc voltage along a fuse element after disruption of the constrictions, we must regard the resistance of the parallel striker wire.

## 8 REFERENCES

- [1] H.G.Rex: Calculations of adiabatic processes, ICEFA papers 1984, Trondheim, N
- [2] H.G.Rex: The arcing process in LV-HRC-fuse links as a combination of two simple processes, SAP papers 1997, Lodz, P
- [3] J.Nasilowski: Chain of arcs as determining factor in electrical explosion of wires, ICEFA papers 1976, Liverpool, UK

HH98461

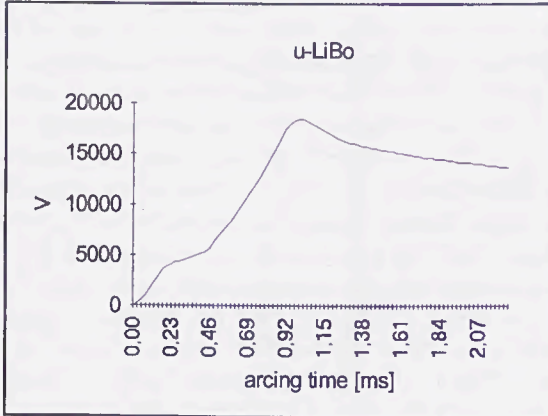


diagram 1: fuse voltage

HH98461

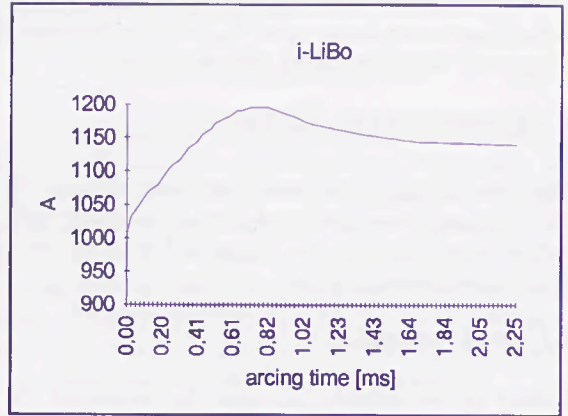


diagram 2: fuse current

HH98461

melting element: Ag ; 4 strips parallel  
 1.8 mm width ; 0.03 mm thick ; 550 mm long  
 constrictions: round holes ; 1.0 mm diameter  
 distances : 7.0 mm ; 78 rows of constrictions per strip  
 cross sections:  $Q_E = 0.096 \text{ mm}^2$  ;  $Q_B = 0.216 \text{ mm}^2$

striker wire: Konstantan  
 0.25 mm diameter; 930 mm long  
 $Q_{SW} = 0.049 \text{ mm}^2$  ;  $R_{SW} = 9.5 \Omega$

Test:  
 50 Hz/ 10.5 KV/ 1020 A/  $\cos \varphi = 0.07$  /  $\psi = 10^\circ$   
 melting time: 3.4 ms ; melting integral: 869 A<sup>2</sup>s  
 melting current: 1000 A

HH98461

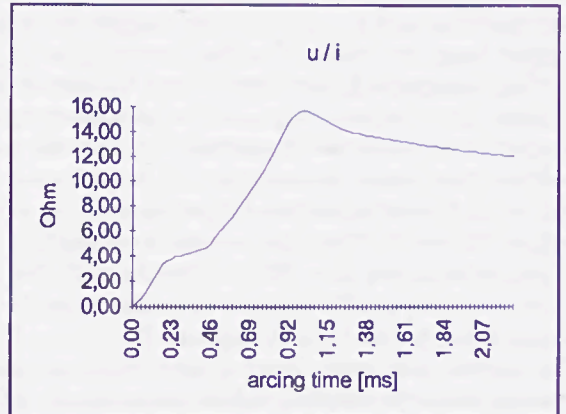


diagram 3: fuse link calculated as a resistance

HH98668

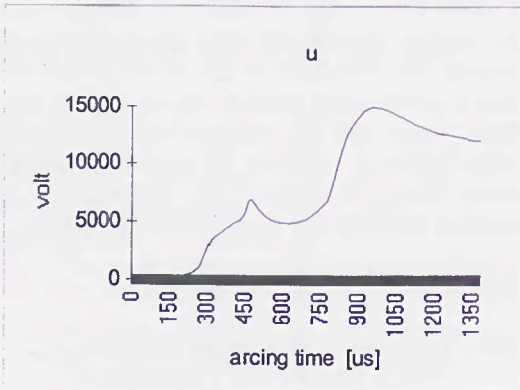


diagram 4: fuse voltage

HH98668

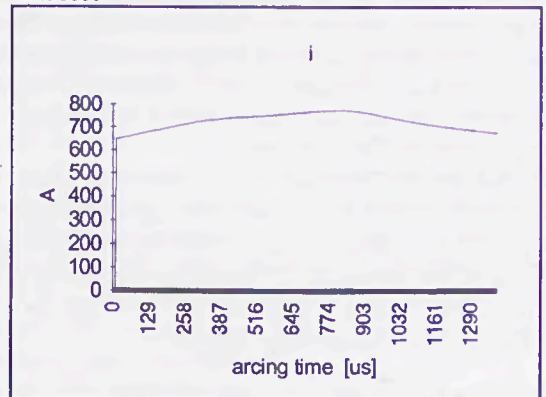


diagram 5: fuse current

### HH98668

wire melting element:

Ag ; 3 wires parallel, with constrictions

wire: 0.33 mm diameter; 330 mm long

constrictions: wire 0.18 mm diameter

18 mm long; distances : 65 mm;

5 rows of constrictions per wire

cross sections:  $Q_E \approx 0.078 \text{ mm}^2$  ;  $Q_D \approx 0.256 \text{ mm}^2$

$R_{ME} \approx 80 \text{ m}\Omega$  cold

striker wire: Konstantan

0.25 mm diameter; 600 mm long

$Q_{SW} = 0.049 \text{ mm}^2$  ;  $R_{SW} \approx 7 \Omega$  cold

Test: 50 Hz/ 6.3 KV/ 694 A/  $\cos \varphi = 0.07$

melting time: 3.9 ms ; melting integral: 466 A<sup>2</sup>s

melting current: 700 A

### HH98668

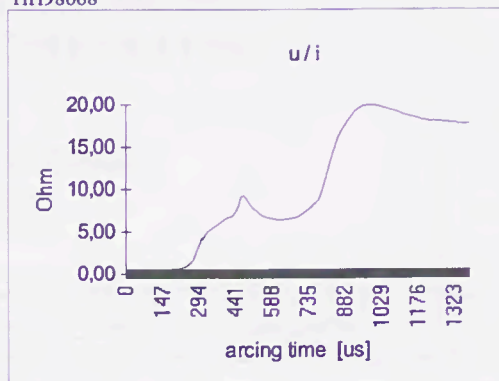
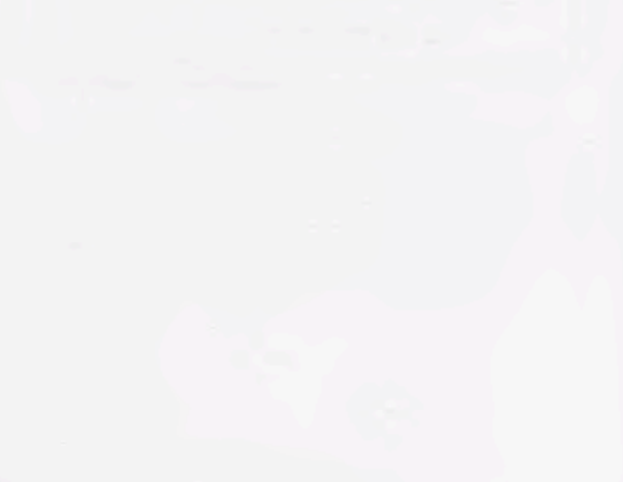
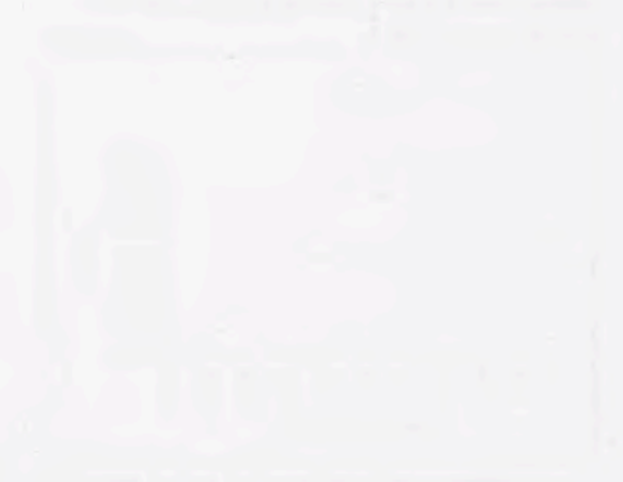
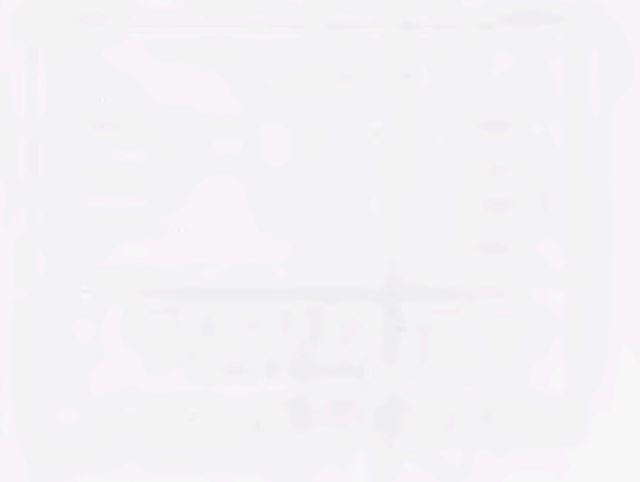


diagram 6: fuse link calculated as a resistance



# SECONDARY STRIATION DURING FUSE-ELEMENTS DISINTEGRATION

Jakubiuk K.  
Technical University of Gdansk  
Gdansk – Poland

**Abstract:** Fuse –element overloaded by currents giving the current density from 5 up to ab 100 kA/mm<sup>2</sup> demonstrate two-stage striated disintegration: primary and secondary. Primary striation is due to magneto-hydrodynamic (MHD) vibration. In course of the primary striation can arise the secondary one. The paper pushes forward two possible mechanisms of the secondary striation: one is “plasma-metal-plasma” model and second “plasma-metal-bridge”. For both models an analysis has been given. The conclusion is that “plasma-metal-bridge” model is more realistic one.

fulgurite streaks after finishing of the fuse operation, i.e. they are not related to the changeable number of streaks in course of their formation. The experiments of Arai [1,2] and others stated a dependence of mentioned module during the disintegration process. This observation gave an impulse to introduce [6,7] the term “two stage striated disintegration: primary and secondary”. The primary, within small disintegration modulus, is a result of instability of the MHD vibrations of a conductor being in the liquid state. A very complicated MHD model can not be described by some simple formulae on the module, however, it is possible these module to determine using directions given in [6]. One of the conclusion of just quoted paper speaks that the striation can arise in the wires of diameter up to 1 mm and by the current density  $j_m \approx 5 \div 1000$  kA/mm<sup>2</sup>.

## I. INTRODUCTION

Striated disintegration of conductors overload by a current has take place if the maximum current density, in the instant of disintegration, is  $j_m \approx 5 \div 1000$  kA/mm<sup>2</sup>. An analysis of the disintegration, given in [7] based upon experiments [1,2,3,4,9,10,11,12] showed that the fuse-element striation depends on the cross-sectional shape of the conductor, i.e. wire or strip. Hitherto investigation of the striated disintegration, that lasted already many decades, despite many achievements, still generates several controversial views on the physics of phenomena associated and on the value of the disintegration modulus. The modulus given as the simple experimental relations in [4,9,10] are related to the wire or strip dimensions and do not take into account the current density  $j_m$ . Meanwhile the paper [7] demonstrate that mentioned module are correct for defined current densities only. Moreover the relations in question are based on observation of the number of

Nevertheless, after some time from arising of a primary disintegration can appear the secondary striation that demonstrate a considerably longer modulus. After suggestions given in [5], the secondary disintegration is a result of joining together in one of the several neighbouring streaks. This phenomenon has take place at relatively small current densities, viz.  $j_m \approx 5 \div 100$  kA/mm<sup>2</sup>. The upper limit of this zone is approximate only. The reason of it is a minimum time needed to develop the secondary striation. Above mentioned current density there is lack of time to join together the neighbouring streaks. They transform quickly direct into a plasma. Table 1 shows the conditions to get disintegrations and the module of primary and secondary striation.

Table 1 Juxtaposition of experimental and analytical results

Material	Wire diameter [mm]	$j_m$ [kA/mm <sup>2</sup> ]	Primary modulus of experiments [mm]	Kind of striations	Source	Calculation modulus of primary striation [mm]	Modulus calculated after the formula [7] [mm]
Ag	0.3	8.2	0.31	primary ,secondary	[2]	0.27	1.18
Ag	0.5	6.0	0.36	primary, secondary	[2]	0.38	1.60
Ag	0.5	12.0	0.24	primary, secondary	[1]	0.28	1.60
Cu	0.625	170.0	0.23	primary	[3]	0.22	1.85
Cu	0.625	260.0	0.20	primary	[3]	0.19	1.85

Moreover visible is a good agreement of experiment and calculation.

Up to now there is no attempt to clarify the physics of the secondary disintegration appearance.

The paper gives such an attempt, based on X-ray photography (Fig.1) of a wire striation that shows both primary and secondary striation. There are suggested two possible models why arising the secondary striation.

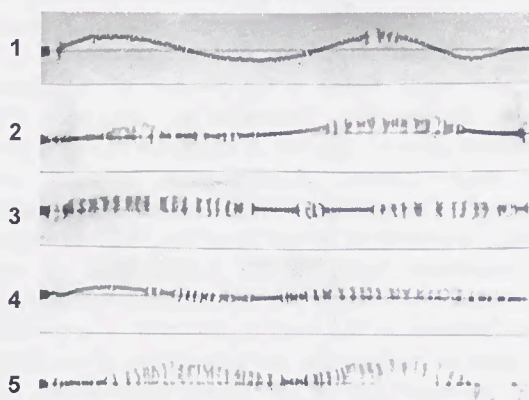


Fig.1 X-ray photography of consecutive phases of striation disintegration, Ag-wire  $d=0.4$  mm,  $l=50$  mm in sand,  $j_m=11$  kA/mm<sup>2</sup> [1,2]. Pictures shots are taken 1 ms later than disintegration peak voltage. Time distances from that peak are: 1 - 7  $\mu$ s, 2 - 17  $\mu$ s, 3 - 21  $\mu$ s, 4 - 24  $\mu$ s, 5 - 28  $\mu$ s

First suggestion pertains to a dynamics of an action on metal primary streak of bothsided plasma layers. This model be called "plasma-metal-plasma model". Second, called "plasma-metal-bridge model" refers to a not simultaneous arising of the wire necks during the primary striation. A most constricted neck will explode at first causing the arc ignition in it. A dynamics of this squash the is due to neighbouring necks behaviour.

## II. PRIMARY STRIATION

It was already mentioned that the primary disintegration is due to instability of the MHD vibrations [6,7]. An analysis of such vibrations assumes that in some instant the outer surface of a wire gets the perturbations according to the relations [7]

$$r_p(z, t_0) = R + \sum_{n=1}^{\infty} \delta R_n(t_0) \cos(k_n z + \psi_n) \quad (1)$$

in which:  $R$  - radii of wire,  $t_0$  - instant of the complete wire liquefaction,  $r_p(z, t_0)$  - equation describing of the conductor side surface in instant  $t_0$ ,  $\delta R_n(t_0)$  - disturbance amplitude of wave number  $k_n$  in instant  $t_0$ ,  $\psi_n$  - phase of angle of wave number  $k_n$ .

Initial perturbations are of small amplitude, of order 1%  $R$ . On the evolution of vibrations affect:

- electrodynamics compression of the liquid conductor;
- inertia forces;
- viscosity of metal;
- non-uniform heating, that is larger in the constrictions, causing diminishing of the electric conductivity and enhancing of the metal viscosity.

As a result the speed of evolutions of the perturbations within different wave numbers  $k_n$  (1) is different. Highest speed demonstrates a perturbation within number  $k_{kr}$  corresponding to the striated disintegration [7]. At the end of evolution, in most overheated parts of metal, it gets lose the thermodynamic stability and hence appears a sudden disintegration. Details of the process are given in [6,7]. X-ray photography (Fig.1) witnesses the non simultaneous wire disintegration.

## III. SECONDARY STRIATION

### III.1 Plasma - metal - plasma model

Assumed sequence of the events in „plasma-metal-plasma” model is:

- As a result of the current flow arises the primary striation (Fig. 1).
- Individual streaks come to existence not simultaneously. In an early streaks ignites the arc, whereas in neighbouring striates the arcs ignite with some delay (range of  $\mu$ s), however, also not simultaneously.
- After initiation of the arcs there is alternate metal layers divided by plasma ones.
- Dynamic action of the plasma layers (particularly the one which started as first) on the metal layers can make a sudden displacement of the metal and squash of the nearest next plasma layer. As a result the neighbouring metal layers can join together. In this manner can arise the secondary striation (disintegration) modulus of much longer dimension.

In some instant of lasting of the primary striation starts formation of the secondary one. Fig. 2 shows the magnified fragment 3 (Fig. 1) that gets form of the secondary striation.

Process are going extremely fast. In conditions related to Fig. 1 the secondary striation forms within ab  $1-10\mu$ s. In this model it is assumed that this disintegration is due to dynamic action of the plasma being on both sides of liquid metal fragment.



Fig. 2 Magnified fragment 3 of X-ray photography (Fig. 1)

In the model it was assumed that the metal layer  $k$  (Fig. 3) is able to move under influence of the pressure difference ( $p_1 - p_2$ ) of plasma placed on both sides of layer  $k$ .

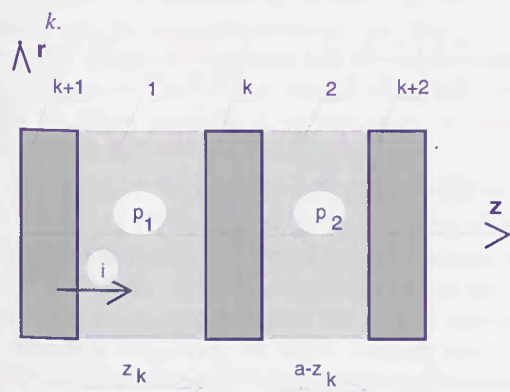


Fig. 3 Sketch of fuse-element fragment assumed in model  
1,2 – volume of plasma filling space with  $z_k$  and  $a - z_k$  and corresponding pressures  $p_1$  i  $p_2$ , cross-section  $A_k$

The equation describing displacement of the metal is

$$\frac{m_k}{A_k} \ddot{z}_k = p_1 - p_2 \quad (2)$$

in with:  $A_k$  – the cross section of metal.

It is assumed the constant metal mass  $m_k$ , despite the fact that each layer vaporises during the disintegration. The assumption justify a very short time of the striated disintegration [6]. Assuming moreover the plasma in volumes 1 and 2 as an ideal gas, its "static" pressure is described by

$$p_l = n_l k T_l \quad (3)$$

where:  $l=1,2$ ;  $n_l$  – density of the particles of their total number  $N_l$  in the volume  $V_l$ ;  $k$  – Boltzmann constant,  $T_l$  – plasma temperature.

But in reality there is an explosive pressure, not static one [5]. The explosive pressure that arises at very beginning of the explosion, according to [7] can initiate the secondary disintegration by creating some initial

speed of the metal layer. This speed can be taken into account by a member of form  $\dot{z}_k(t = t_0)$ .

The plasma temperature has been determined from a simplified energy equation on the adiabating heating plasma

$$\frac{3}{2} n_l k \frac{dT_l}{dt} = \frac{j_l^2}{\sigma_l} \quad (4)$$

where:  $j_l$  – current density in the plasma,  $\sigma_l$  – electrical conductivity of the plasma according to relation

$$\sigma_l = \sigma_{ol} \left( \frac{T_l}{T_{ol}} \right)^{\frac{3}{2}} \quad (5)$$

$\sigma_{ol}$  – initial plasma conductivity,  $T_{ol}$  – plasma temperature in instant  $t_{ol}$ .

Integrating the relation (4) including (5), the final relation on the temperature is

$$T_l = T_{ol} \left( 1 + \frac{5}{3\sigma_{ol} k n_l T_{ol}} \int_{t_{ol}}^t j^2 dt \right)^{\frac{2}{5}} \quad (6)$$

During the fast secondary striation the current and its density is nearly constant. For such assumption and remembering (6) and (3) the relation (2) gets the form

$$\ddot{z}_k = \frac{k A_k}{m_k} \left[ \frac{N_1 T_{ol}}{A_1 z_k} \left( 1 + \frac{5 i^2 A_1 z_k (t - t_{ol})}{3 k \sigma_{o1} N_1 T_{ol}} \right)^{\frac{2}{5}} + \right. \\ \left. - \frac{N_2 T_{o2}}{A_2 z_k} \left( 1 + \frac{5 i^2 A_2 z_k (t - t_{ol})}{3 k \sigma_{o2} N_2 T_{ol}} \right)^{\frac{2}{5}} \right] = f_1(z_k) \quad (7)$$

A qualitative profile of the function  $f_1(z_k)$  is given in Fig. 4.

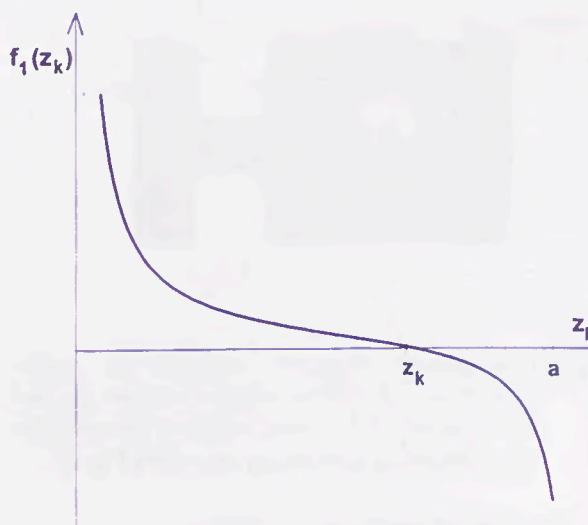


Fig. 4 Qualitative profile of the function  $f_1(z_k)$  (7)

From the profile (Fig. 4) outcomes that course of metal layer displacement from one its side arises a decompression of plasma layer and from opposite side, a compression of plasma. In this way arises braking of the metal layer and then a move in opposite direction. It generates a classical vibration system.

Not described in this paper investigations of (7) reveal that the metal layer can vibrate around some equilibrium position.

The probability that the model described has take place is rather small. Author expresses this opinion because the model does not include a very important factor, i.e. an explosive radial ejection of the plasma out of wire cross-section.

### III.2 Plasma – metal – bridge model

Assumed sequence of the events in „plasma-metal-bridge” model is nearly this same in “plasma-metal-plasma” model, but there is a substantial difference too. Namely, an arc ignites in one streak so early that in a neighbouring one the current flows through an overheated metal bridge. The plasma pressure (explosive and static [5]) is so high, that before bridge explosion a metal layer gets some move causing absorption of that bridge. In this manner the neighbouring layers are joining together giving a secondary striation within modulus much longer that the primary one.

Fig. 5 illustrates assumed nature of the secondary disintegration according to the model in question. Situation shown lasts a very short time: from an arc ignition in the space 1 up to moment of the bridge 2 disappearance, i.e. up to joining in one of the layers  $k$  and  $k+1$  and possibly of be the next nearest metal layers.

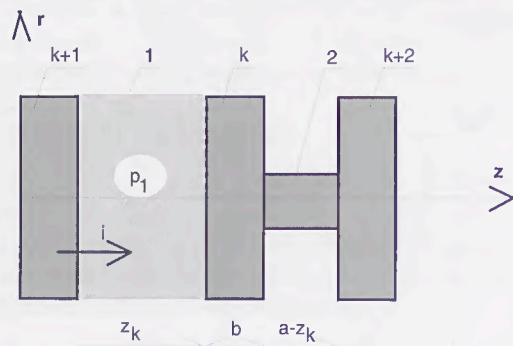


Fig. 5 Fuse-element fragment assumed in model 1- volume of plasma within pressure  $p_1$  and cross-section  $A_1$ , 2 – metal bridge of cross-section  $A_b$  (outstanding denotations according Fig. 3)

The equation describing this event is

$$\frac{m_k}{A_k} \ddot{z}_k = p_1 - p_e - p_h \quad (8)$$

in which:  $p_1$  - plasma pressure (3),  $p_e$  - explosive pressure [5,13];  $p_h$  - pressure as a result of hydrodynamic resistance, i.e. caused by layer and bridge deformation.

Hydrodynamic pressure can be define by an approximate relation [6]

$$p_h \approx \frac{2 v b \dot{z}_k}{d^2} \quad (9)$$

where:  $v$  - kinematic viscosity;  $d = \sqrt{\frac{4A_b}{\pi}}$  - bridge diameter;  $\dot{z}_k$  - velocity of layer displacement.

Introducing (3), (6) and (9) into (8), bearing in mind the assumption identical with taken for (7), one can get

$$\ddot{z}_k = \frac{A_k}{m_k} \left[ \frac{k N_1 T_{01}}{A_1 z_k} \left( 1 + \frac{5i^2 A_1 z_k (t - t_{01})}{3 k \sigma_{01} N_1 T_{01}} \right)^{\frac{2}{5}} - p_e - \frac{2 v b \dot{z}_k}{d^2} \right] = f_2(z_k) \quad (10)$$

Of course, the time of layer moving according (10) up to the bridge disappearance (Fig. 5) shall not lasts longer then that to the bridge explosion. A substantial role in the process plays the explosive pressure. Its value is considerably higher than the static one [5,7]. Since explosive pressure lasts a very short time, it can be omitted in (8). This pressure, however, shall be taken into consideration in form of an initial velocity  $\dot{z}_k(t = t_{01})$ .

A qualitative profile of the function  $f_2(z_k)$  is given in Fig. 6.

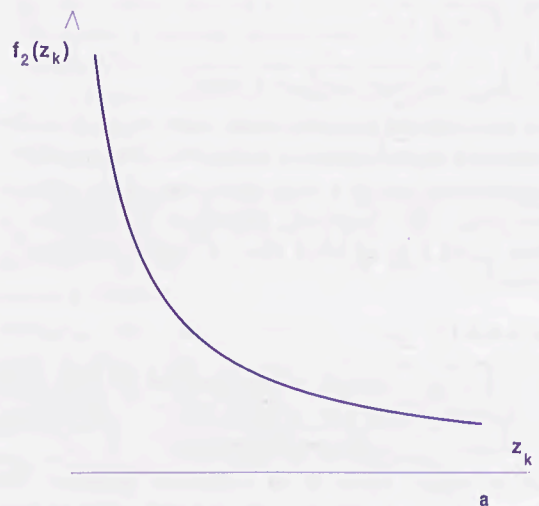


Fig. 6 Qualitative profile of the function  $f_2(z_k)$  (10)

From profile (Fig. 6) it is evident that the metal layer that displaces due to plasma pressure and is braked only by a pressure appearing as a result of shape changes of the layer (process of absorption of the bridge by the metal layer). By decompression of the plasma layer it gets smaller, however, a resultant pressure does not change its direction. Qualitative profile of the function  $f_2(z_k)$ , given in Fig. 6, shows that the plasma-metal-bridge model is possible.

#### IV CONCLUSION

Described analysis is of qualitative character. Qualitative analysis of the given equations is a very complicated matter, mainly due to difficulties in determination of the initial conditions and physical parameters. The solutions to the problem considerably depend on the relation between the time in which particular streaks are forming and the relation between the time of the necks and bridges explosion, etc. To reach a proper solution it is necessary to carry out further time consuming investigation.

The positive conclusion from given considerations is that formation of the secondary disintegration, it seems, more probable is the plasma-metal-bridge.

#### ACKNOWLEDGEMENT

Author have a pleasure to acknowledge that described investigations were carried out in the frame of project no 8 T10A 034 11 sponsored by the Polish Committee of Scientific Research.

#### REFERENCES

- [1] Arai S.: Deformation and disruption of silver wires. Private communication, 1977.
- [2] Arai S.: Deformation and disruption of silver wires. Int. Conf. on Electric Fuses and Their Appl., Liverpool (UK), p. 50, April, 1984.
- [3] Fansler K.S., Shear D.D.: Correlated X-ray and optical streak photographs of exploding wires. *Exploding Wires*. vol.4. p. 185, New York: Plenum Press 1968.
- [4] Hibner J.: The number of arcs initiated during striated disintegration of the uniform strip h.b.c. fuse-elements at a A.C. short-circuit current interruption. Int. Conf. on Electric Fuses and Their Appl., p. 60, Trondheim (Norway), 1984.
- [5] Hibner J., Jakubiuk K., Lipski T.: Evaluation of pressure explosive component of high rupturing capacity fuses. Proc. IX Int. Conference on Gas Discharges and their Applications, p. 583, Venezia (Italy), 1988.
- [6] Jakubiuk K.: Striated disintegration of exploding wires (in Polish). *Zeszyty Naukowe Politechniki Gdanskiej, Elektryka nr 75*, Gdansk 1994.
- [7] Jakubiuk K.: Two-stage mechanism of striated disintegration of fuse-wire. Int. Conf. on Electric Fuses and Their Appl. Ilmenau (Germany), p. 273, Sept., 1995.
- [8] Krall N. K., Trivelpiece A. W. : Principles of Plasma Physics. McGraw-Hill Book Company, New York 1973.
- [9] Nasłowski J.: Uduloids and striated desintegration of wires. *Exploding Wires*. vol 3, p. 295, New York: Plenum Press 1964.
- [10] Nasłowski J.: Fuse-wire disintegrations by short-circuit (in Polish). *Przegl. Elektrot.*, vol. 36, p.382, 1960.
- [11] Lipski T.: On the theory of the striated fuse-wire disintegration Trans. IEEE, vol. PS-10, nr. 4, p. 339, 1982.
- [12] Lipski T.: Application of the arc-pinch-forces-interaction theory to the calculation of striation modulus of strip h.b.c. fuses. Int. Conf. on Electric Fuses and Their Appl., p. 52, Trondheim (Norway), 1984.
- [13] Vermij L.: Electrical behaviour of fuse elements. Doct. Thesis. Tech. Univ. of Eindhoven (Netherlands), 1969.

Faint, illegible text in the top left column.

Faint, illegible text in the middle left column.

Faint, illegible text in the lower middle left column.

Faint, illegible text in the bottom left column.

Faint, illegible text in the top right column.

Faint, illegible text in the middle right column.

Faint, illegible text in the lower middle right column.

Faint, illegible text in the bottom right column.

# UNDULOID FORMATION AND CAUSATION OF CURRENT INTERRUPTION IN CURRENT-CARRYING WIRES

R.E. Brown,  
Sheffield Hallam University, U.K.

P.M. McEwan  
Sheffield Hallam University, U.K.

## I. ABSTRACT

Unduloids are a metallurgical phenomenon created by a series of molten swellings which form along the length of wires when wires carry moderate short-circuit currents in air. It is considered that melting of the reduced sections between the swellings precipitates a chain of short arcs to produce a fast rising arc voltage across the wire terminals which limits the current carried by the wire. It is, therefore, widely accepted that the formation of unduloids along current-carrying wires is the principal cause of current interruption of moderate short-circuit currents in wire fuses.

The behaviour of unduloids and the initiation of arcs along wires were investigated using medium- and high-speed video cameras. The video images show that the initial wire disintegration is caused by thermo-elastic vibrations which cause a single break to occur, predominantly, close to one of the ends of the wire and that the break occurs before unduloids form.

Correlation of the video images confirms that classical multiple arcing, in the spaces between all swellings, does not occur, which corresponds with the, relatively, poor current-interruption capacity of this class of wire fuse.

## II. INTRODUCTION

The first known experimental investigations into melting of current carrying wires was undertaken by Nairne[1,2], who reported on how wires on 'passing electrical fire', 'melted into red hot balls'. This, hence, was the first reported observation of unduloid-related disruption of current in wires.

Much later observations of unduloid type formation in wires focused on the causation of unduloids and on the current disruption process. Unduloids were considered early on to be caused by surface tension forces acting on the molten wire[3] and, subsequently, it was proposed [4] that unduloid formation was caused by a combination of surface tension and electromagnetic pinch forces. Unduloid formation was later shown to be dependant on wire surface melting - this being a consequence of temperature variation across the wire section due to electromagnetic pinch forces[5]. Magneto-thermo viscous elastic vibrations, produced by the current flow

in wires, were also proposed as the cause of unduloid formation[6].

Later observers of disintegration in wires indicated that the occurrence of unduloid formation was inconsistent. Consequently current density [5][7], wire diameter[7], metallurgical conditioning[8][9][10] and wire material properties[11], were all proposed as contributory influences on unduloid formation.

Currently, it is accepted that unduloid formation is associated with moderate current densities, typical of high overloads or low short circuit fault currents in the range 3~5In, corresponding to pre-arcing times in the range 30~300ms. The profile of the temperature distribution along medium and long wires, for these conditions, is virtually constant and wire surroundings and terminal cooling are thought to have insignificant influence on the cooling of wires and hence, on the current disruption process. Unduloids are considered, therefore, to form when the wire's surface is molten but the wire is not fully molten at its centre. Consequently, surface tension, allied with electromagnetic pinch force effects or wave motion, is accepted to be the primary phenomena causing the transition in wires from an unstable liquefied cylinder state to that of a chain of stable spheroids.

Investigations have also been undertaken into the voltage waveforms developed between the wire terminals as a result of the unduloid formation phenomena[4][12][13]. These studies indicated that as unduloids form, melting occurs at points between the spheroids at which short arcs subsequently ignite to create a series chain of arcs. It is considered that an arc voltage, equal to the sum of the individual arc voltage falls, appears across the wire terminals to aid current limiting[14]. Hence, it is commonly thought by many that unduloid formation is a significant current interruption mechanism.

## III. EXPERIMENTAL TECHNIQUE

Investigations into conductor disintegration were carried out on silver wires of different orientations in air. The wires were 60mm long by 0.2032mm diameter. The test currents were supplied from a 50 Hz, 200 volt, 14.5 amp rated alternator. The test circuit comprised a thyristor 'crow-bar' switch across the test wire sample terminals. The test arrangement was capable of being accurately switched to enable fault

current to flow in the test samples for precise time periods to enable observations of the formation of unduloids, wire disintegration and the initiation of arc ignitions along wires.

Visual observations of disintegrating wires were recorded using standard video (25 frames/s) and fast video (2000 frames/s) cameras. Visual images were stored and viewed using standard magnetic tape and 625 line, 50 field video monitor methods.

Static time-sequence images were acquired from video tape recordings using commercially available video-PC interface hardware and software image capture packages.

#### IV. VISUAL OBSERVATIONS

##### IV.1 Wire End/Terminal Effects

The precise control of the joulean energy released in the wire samples enabled visual image capture of the development of unduloids and the instances at which arcs ignite. Figure IV.1a shows the captured image of unduloid wire melting and the effects of cooling of the wire close to the wire terminal. The image also shows that the axial deformation of the wire in the vicinity of the wire terminal is minimal and that no unduloids occur in the cooled part of the wire.

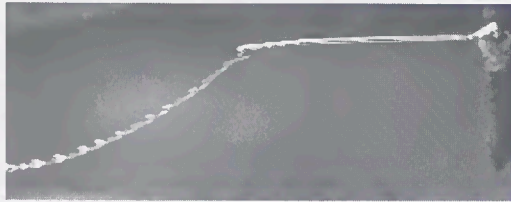


Figure IV.1a Observed Cooling Terminal End Effects

##### IV.2 Unduloid Formation

The unduloids observed along most of the wire length were, in general, evenly spaced and of uniform size, figs. IV.2a, IV.2b. The average separation distance between unduloids ( $\lambda$ ), was found, in all cases, to comply closely with Nasilowski's [13] empirical relation (eq. 1).

$$\lambda_{\text{unduloid}} = \frac{16}{3}d \quad (\text{eq. 1})$$

The observations indicated that unduloids are numerous and take on the appearance of a string of pearls. Furthermore, if the current is diverted away from the wire just following the formation of unduloids, the main part of the wire comprising fully-formed unduloids becomes catenary in form.

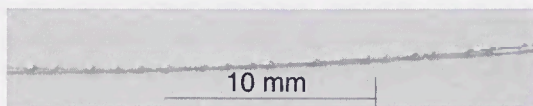


Figure IV.2a Enlarged Image of Unduloid Formation in Wire



Figure IV.2b Catenary Shape of Wire Section comprising Unduloids,

##### IV.3 Wave Motion.

Observation of video sequences of the entire period of current melting and disruption showed that rapid expansion of the wire occurred due to thermal expansion. The video recordings also showed that the wires vibrated vigorously, figures IV.3a,b,c. and that during disintegration the wire remnants were seen to be expelled also vigorously from the points along wires where arc ignition occurred, fig. IV.3d.

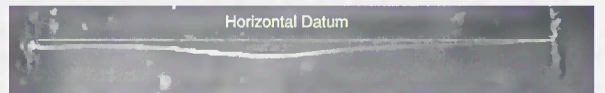


Figure IV.3a Current-Carrying Catenary 80ms after Current Injection



Figure IV.3b Current Carrying Catenary Showing Thermo-elastic Vibrations, 120 ms after Current Injection.



Figure IV.3c Catenary following Current 'Crow-Barring'.



Figure IV.3d Expulsion Wire Remnants at the Instant of Arc Initiation

#### V. DISCUSSIONS

Surface tension forces acting on the partially-melted surface of sections of wire conductors is not disputed as the primary cause of the occurrence of unduloids in current-carrying conductors. It is reasonable to conclude from the observed vibrations,

fig. IV.3b., however, that thermo-elastic vibrations also have a role in the initial unduloid formation process.

The observed uniform formation of unduloids along most of the wire length and the, subsequent, catenary form wires take, fig. IV.2b, supports the notion that the catenary part of the wire is mostly molten and that the temperature of the catenary portion of the wire is, virtually, constant. The deformation in the wire at its ends and the existence of only partially formed unduloids, fig. IV.1a, indicate that a large temperature gradient exists in the regions in the vicinity of the ends of the catenary and that these regions must be more solid in state. It is reasonable to conclude, therefore, that the ends of the catenary, i.e. the points where the wire starts to bend, must also be molten-solid interfaces.

The accepted notion that arc initiation occurs in a gap between unduloids is disputed. Firstly, it can be seen, figures Vb,d, that arc ignitions occur prior to the formation of unduloids. Consequentially, it is reasonable to conclude that the mechanical shear stress, due to rapid thermo-elastic vibrations, is greatest at the solid-molten interface and, hence, wire breakage will, and does, occur at this point first.



**Figure V.a** Video Sequence Image of Current Carrying Catenary 90ms after Current Injection

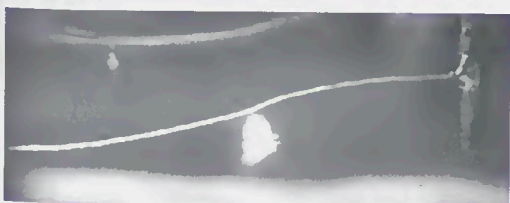


**Figure V.b** Current Carrying Catenary 130ms after Current Injection Showing a Single Arc Ignition before Unduloid Formation



**Figure V.c** Non-Current Carrying Catenary - 40ms after Arc Ignition



**Figure V.d** Current Carrying Catenary 130ms after Current Injection Showing Arc Ignitions before Unduloid Formation



**Figure V.e** Non-Current Carrying Catenary - 40ms after Arc Ignition again Showing Minimal Unduloid Formation



**Figure V.f** Non-Current Carrying Catenary - 80ms after Arc Ignition Showing the Initial Formation of Unduloids

The images that show arc ignitions can occur prior to unduloid formation, figs V.b,d, reinforce the notion that wire breakage, due to thermo-elastic vibrations, is the cause of wire disintegration and, therefore, current-interruption in wires.

The video sequence images show a whip-like action occurs following breakage of the wire which rapidly parts the wire from a fixed end. The rapid whip-like parting basically breaks the circuit and prevents further arc ignitions along the wire. The circuit current has ceased, therefore, prior to unduloids becoming fully formed and, hence, the assumed classical multiple arc formation is not possible. The images confirm that only between 1-3 arcs ignite during current interruption.

The presented observations also eliminate the influence of electromagnetic pinch forces as a significant influence on unduloid formation, since from figures Vc,e,f unduloids continue to form after current interruption occurs.

## VI. CONCLUSIONS

From the video-captured images and observations presented in this paper, it is proposed that current interruption, in the presence or non-presence of unduloids in wires, is caused by thermo-elastic induced wave motion acting at a molten-solid discontinuity or fulcrum point, close to one of the ends of wires. Current-interruption is, therefore, caused, fundamentally, by end cooling of current-carrying wires and the whipping action of the wire due to rapid thermo-elastic induced vibrations and unduloid formation is, at most, only a secondary influence on current interruption in wire fuses.

The presented observations show why the establishment of so-called multiple arcs, induced by unduloid formation, is not possible.

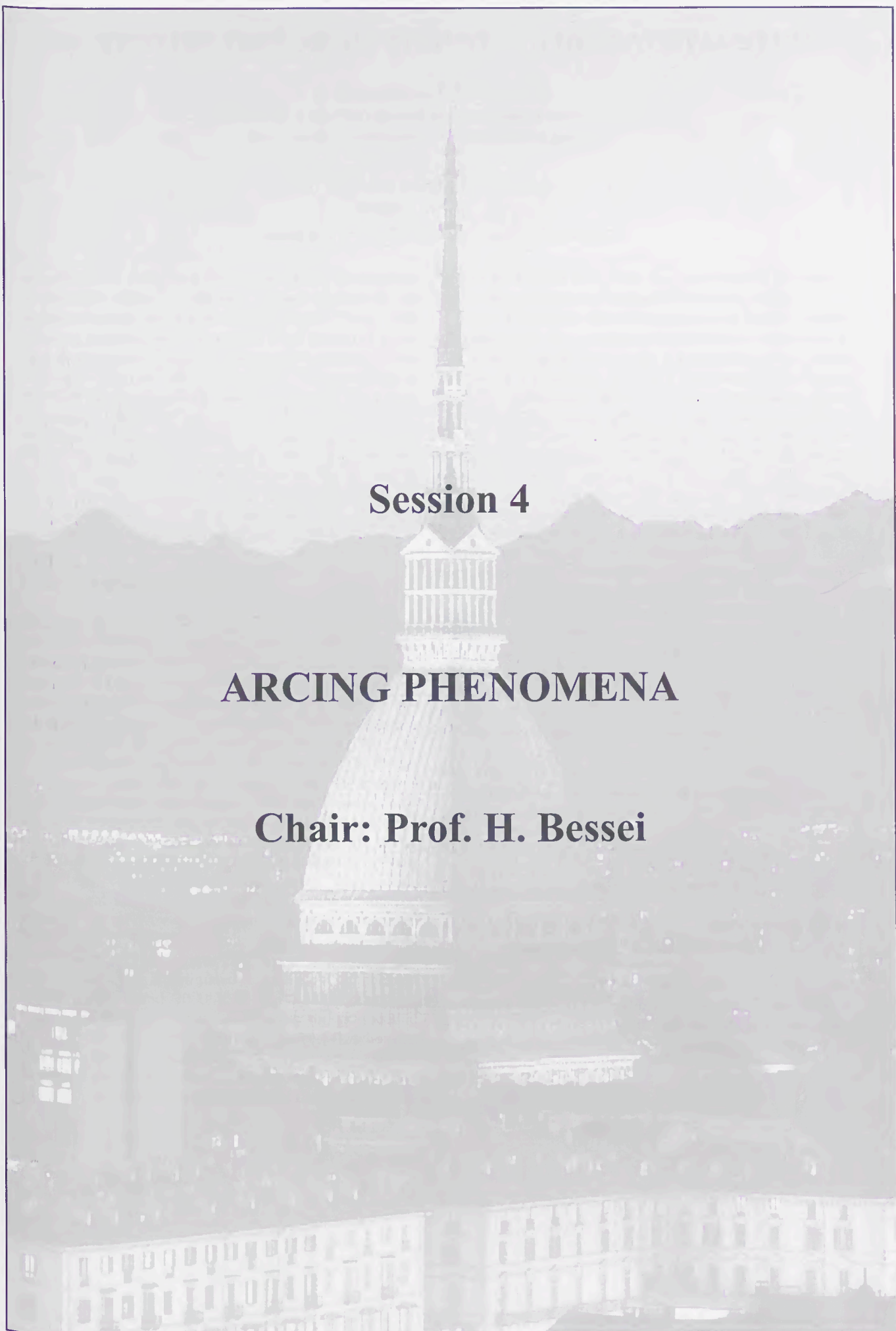
Finally, the occurrence of unduloids following current disruption, rules out electro-magnetic forces as a significant influence on the production of unduloids.

## VII. REFERENCES

- [1] Nairne E., Electrical Experiments by Mr. Edward Nairne., Phil. Transactions, Royal Society (London) 1774.
- [2] McEwan P.M., Mr. Edward Nairne FRS - Discoverer of the Electric Fuse ?, Perspektywy Rozwoju Technik Przerwywania Pradu, ISSN 1225-5766, Gdansk, 1996.
- [3] Kleen W., Uber den Durchgang der Elektrizitat durch metallisch Haardrahte. Ann.Phys., Band 11, 1931, vol 5, p579 - 605.
- [4] Baxter H.W., Electric Fuses, Pub: Edward Arnold, London, 1950,
- [5] Carne E.B., A Mechanism for the Fuse Pre Arcing Period., A.I.E.E. Transactions, Vol. 72, August 1953, p593-599.
- [6] Zimny P., On the Magneto Thermo Viscous Elastic Mechanism of Unduloids Formation on Wires., Proceedings, 2nd Int Symp on Switching Arc Phenomena, Lodz, Poland, Sept. 1973, p 241-246.
- [7] Nasilowski J., Unduloids and Striated Disintegration of Wires, Exploding Wires Vol 3, Planum Press, New York U.S.A., 1964, p 295-313.
- [8] Lipski T. Furdal A., New Observations on the Formation of Unduloids on Wires., Proc. I.E.E. Vol. 117, No. 12 Dec. 1970.
- [9] Lipski T., Why Unduloids Do Not Always Appear., Proceedings, 3rd Int. Symp on Switching Arc Phenomena, Lodz, Poland. 1977. p 305-309.
- [10] Meyer E. Linderer L., Use of Capillary and Pinch Instability for Dendritic Crystal Growing, Journal of Crystal Growth, Vol.28, 1975, p199-208.
- [11] Bisaria A.K., Appearance of Unduloids in Exploding Wire Phenomenon., Indian Journal of Pure and Applied Physics, Vol. 11, September 1973.
- [12] Vermij L., The Voltage Across a Fuse During the Current Interruption Process, I.E.E.E. Trans on Plasma Science, Vol. PS-8, NO.4, Dec. 1980, p460-468
- [13] Nasilowski J., Chain of Arcs as Determining Factor in Electrical Explosion of Wires, Proc., Int. Conf. on Electrical Fuses and their Applications, Liverpool, U.K., 1976, p122-132.
- [14] Wright A., Newbery P.G., Electric Fuses, IEE Power Engineering Series 2, Pub: Peregrinus Ltd., London 1984.

## VIII. ACKNOWLEDGMENTS

The authors thank GE Power Controls Ltd., Liverpool, UK for the loan of the high speed video camera. Additionally, appreciation is extended to Nick Allen and Dave Crellin of GE Power Controls Ltd., for their support of the studies.



**Session 4**

**ARCING PHENOMENA**

**Chair: Prof. H. Bessei**



# ARC TEMPERATURE MEASUREMENT IN A HIGH-VOLTAGE FUSE

M.A. Saqib and A.D. Stokes  
School of Electrical and Information Engineering  
University of Sydney, NSW 2006 Australia

B.W. James and I.S. Falconer  
School of Physics  
University of Sydney, NSW 2006 Australia

**Abstract:** We report measurements of the temperature at different times during the arcing period of an experimental model of a sand-filled, high-voltage, high breaking capacity fuse. An optical fibre is used to carry light from the fuse arc to a spectrograph which is used to isolate spectral lines of interest. The spectrum is recorded by an intensified photodiode array. By gating the image intensifier in front of the diode array a complete spectrum is recorded in several microseconds. By varying the timing of the gate pulse the arc spectrum can be obtained at any desired time during the arcing period. The arc temperature is determined from the relative intensities of Si II spectral lines. The arc temperature was found to be around 20,000 K.

## I. INTRODUCTION

Accurate modelling of high-voltage, high breaking capacity (HBC) fuses requires better knowledge of the arc parameters of which the electron temperature of the plasma is a key parameter. Spectroscopic determination of the electron temperature and electron density has several advantages over other methods, such as the use of probes, as it does not disturb the plasma [1]. The use of spectroscopy to investigate the properties of a fuse arc was reported first by Chikata *et al* [2]. Using a transparent Pyrex glass tube as the fuse holder, they recorded a spectrum and from the relative intensity of two Si II lines estimated the arc temperature to be about 23,000 K. To obtain a more reliable picture of the arc plasma in a sand-filled non-transparent fuse-holder, Barrow and Howe [3] inserted optical fibres into the plasma to convey light to a rapidly scanning spectrometer. They observed three pairs of Si II doublets around 505.1 nm, 597.2 nm and 635.5 nm wavelengths. Their estimated temperature of the arc varied from around 3000 K to 7000 K. The applied voltage of the circuit was 255 V with the prospective fault current of 525 A. Cheim and Howe [4], who also inserted optical fibres into a fuse arc, deduced temperatures of about 20,000 K (throughout the arcing period) from the relative intensities of the Si II 413 nm

and Si III 457 nm lines. The fuse was tested at 250 V(AC) and with a prospective symmetrical current of 600 A(rms). The result was inconsistent with that of Barrow and Howe [3], but comparable with those of Chikata *et al* [2] who tested the fuse with a prospective short circuit current of 1 kA (peak) at 1.3 kV. Although the technique used by Cheim and Howe [4] gave temperature values throughout the arcing period, it had inherent problems owing to the use of interference filters to isolate the spectral lines of interest. Saqib and Stokes [5] studied the fuse arc using optical fibre as light carrier and photographic film to record the spectrum. They found Si II lines to be most suitable for temperature estimates as they were detected throughout the lifetime of the arc plasma. They could however not estimate arc temperature due to the complexity of calibration of the photographic film for intensity measurements. Bezbordko and Fauconneau [6] used two Cu lines to measure arc temperature obtaining a result around 12000 K. The drawback of this technique was that Cu lines could not be used to measure temperature of the hot core, due to ionic migration. The high levels of continuum light background signal in studies [5] and [6] show the weakness of using interference filters to isolate spectral lines.

We report here an extension of this technique to the investigation of fuse plasma for higher applied voltage and prospective current, conditions more typical of those likely to be encountered in a commercial sand-filled fuse. Several Si II lines were used to estimate the temperatures, rather than just the two used by other researchers, in order to increase the reliability of the temperature measurement.

## II. THEORY OF SPECTROSCOPIC TEMPERATURE MEASUREMENT

Emission spectroscopy involves the analysis of light that is emitted when an excited atom undergoes a transition to a lower energy level [7]. The intensity of the emitted light can be represented by the following relationship [8]:

$$I = \frac{PgA}{\lambda} e^{-E/kT} \quad (1)$$

where  $I$  is the intensity of emitted light,  $\lambda$  is the wavelength of light,  $E$  is the energy of the excited level,  $g$  is its statistical weight,  $k$  is the Boltzmann constant,  $A$  is the transition probability for the transition,  $T$  is the electron temperature of the plasma, and  $P$  is a constant for lines from the same ionisation state. Equation (1) can be written as

$$\log \left( \frac{I\lambda}{gA} \right) = - \frac{E \log e}{kT} - \log P \quad (2)$$

When  $E$  is in electron volts and  $T$  in kelvin, the equation reduces to:

$$\log \left( \frac{I\lambda}{gA} \right) = - \frac{5040}{T} + \text{const} \quad (3)$$

Thus a plot of  $\log \{I\lambda/(gA)\}$  versus  $E$ , for several lines belonging to the same ionisation level, should be a straight line, from the slope of which the arc temperature is readily obtained. Values of the parameters  $g$ ,  $A$  and  $E$  are available in references [9-14].

### III. EXPERIMENTAL SET-UP

A simple experimental model of a high-voltage HBC fuse in which the current was forced to zero was used to study the fuse arc. Commercially available fuses are designed differently to ensure that the current goes to zero well before reaching its maximum value and that the reignition does not occur. The cylindrical holder for the experimental model HBC, of length 112.2 mm and internal diameter 59.6 mm, was filled with SiO<sub>2</sub> sand. The fuse was energised from a parallel-current-injection synthetic test circuit, as shown in Figure 1. The prospective current was 1.4 kA (peak), 50 Hz, at 6 kV. The fuse element was a 0.55 mm diameter uniform silver wire. In order to convey light to the spectrograph a multimode silica optical fibre with a core diameter of 62.5  $\mu\text{m}$  was inserted through the wall of the fuse holder to touch the fuse element [3, 4, 5]. The other end of the fibre was mounted in the middle of the 25  $\mu\text{m}$  entrance slit of a Jarrell-Ash MonoSpec 27 Monochromator [15]. The spectrum was recorded using a Princeton Applied Research model 1460 Optical Multichannel Analyser (OMA) with a 1024 element intensified photodiode array detector [16].

### IV. RECORDING OF THE SPECTRUM

The OMA is operated in its gated mode in order to synchronise it with the fuse energising circuit. The initiation pulse, provided by the OMA, closes the

mechanical make switch MS1 of the test circuit (Figure 1) which takes about 65 ms to close. A delay circuit enables the image intensifier to be triggered in order to record a spectrum at any chosen time during the arcing process. The exposure time, determined by the duration of the gating pulse, is several microseconds. A Nicolet Pro digital oscilloscope [17] is used to record the voltage across the fuse, the current flowing through the fuse and the time at which the spectrum is recorded. Figure 3 shows an example of these three traces. The voltage across the fuse is measured by Tektronix P6015, 1000:1, 20 kV, 100 M $\Omega$  resistive divider voltage probe (rise time 5 ns). Current is measured using a 190.8 A/V coaxial current shunt (rise time approximately 60 ns). A block diagram of the timing circuit is shown in Figure 2.

### V. EXPERIMENTAL RESULTS

A low-pressure mercury lamp was used to calibrate the spectrometer wavelength scale. Relative calibration of sensitivity as a function of wavelength was accomplished using a calibrated tungsten ribbon lamp. The light from the tungsten lamp traversed the same optical path, including the optical fibre, as the light from fuse arc. Thus:

$$I_{\text{lamp}} \propto S_{\text{lamp}}$$

and

$$I_{\text{arc}} \propto S_{\text{arc}}$$

where  $I_{\text{lamp}}$  and  $I_{\text{arc}}$  are the intensities of the radiation from the tungsten lamp and fuse arc respectively,  $S_{\text{lamp}}$  and  $S_{\text{arc}}$  are the corresponding signals recorded by the OMA. Since the proportionality factor is same function of wavelength in both cases the relative intensity of the fuse arc spectrum is given by:

$$I_{\text{arc}} = (S_{\text{arc}} * I_{\text{lamp}}) / S_{\text{lamp}} \quad (4)$$

Four pairs of Si II lines were identified in the arc spectrum. They were around 413 nm (412.8 and 413.1), 505 nm (504.1 and 505.6), 597 nm (595.8 and 597.9) and 636 nm (634.7 and 637.1). Because of partial overlap of the recorded line profiles the four doublets were treated as single lines with the signal value determined by calculating the area under the combined profile after subtraction of the background level. Average wavelength values were used for plotting  $I\lambda/gA$ , and  $gA$  was replaced by  $g_1A_1 + g_2A_2$  where subscripts 1 and 2 represent the first and second lines of each doublet. Figure 4 shows the spectrum of the tungsten lamp; Figures 5 and 6 show arc spectra taken at different times during the arcing period. A typical plot for determining the electron temperature is shown in Figure 7.

Table 1: Summary of measurements of arc temperature at different times during the arcing period.

Arc time (ms)	Temp. (K)	$I_{arc}$ (Amps)	$V_{arc}$ (volts)	Inst. $MW_{arc}$
0.090	21,600	1365	2768	3.7783
0.833	19,775	1183	1456	1.7224
0.925	19,205	1170	1200	1.4040
1.965	18,725	876	856	0.7499
2.263	17,555	768	848	0.6513
2.302	18,745	770	728	0.5606
2.979	17,417	566	466	0.2638
3.650	16,840	255	440	0.1122
4.102	15,000	114.5	320	0.0366
4.400	18,585	10.7	424	0.0045
4.446	19,946	55	352	0.0194

A summary of temperature measurements as a function of time are shown in Table 1 which also gives the instantaneous arc current, instantaneous arc voltage, and instantaneous arc power. The arc time was obtained by subtracting the pre-arcing time for each shot (the average value around 5.3 ms) from the time at which the spectrum was recorded. Arc temperature as a function of time is also given in Figure 8.

## VI. DISCUSSION

During the measurements care was taken to ensure that each sample fuse was identical and was energised under identical conditions so that a variation of temperature with time could be measured on a shot-to-shot basis. The spectrograph enabled us to record spectra from 300 nm to 800 nm. Since intensity calibration using the tungsten lamp was reliable above 420 nm only, we were forced to ignore the 412.8 and 413.1 Si II lines. As shown in Table 1 temperature varies in the range 15,000 K to 22,000 K. However it is clear from Figure 8 that the temperature falls slowly during the arcing period from a approximately 22,000 K at the start to around 18,000 K towards the end of the measurements. This contrasts with the findings of Chikata *et al* [2] and Cheim and Howe [4] who concluded that temperature remained constant around 20,000 K during the fuse arcing.

The fuse arc plasma was assumed to be in local thermodynamic equilibrium: this was confirmed by finding that plots of  $\log \{I\lambda/(gA)\}$  versus  $E$  did not deviate significantly from a line of best fit. According to Lochte-Holtgreven [18] there is no self-absorption in plasmas above 10,000 K, so the fuse arc plasma is

optically thin. This has also been established experimentally by Bezborodko and Fauconneau [6].

As shown in Table 1, the arc temperature falls during the arcing period at a significantly slower rate than does the instantaneous power dissipation in the arc suggesting that other factors such as arc volume and arc density may be important.

Our investigation of arc temperature during fuse arcing gives arc temperatures significantly higher than those recorded by Barrow and Howe [3]. This is not inconsistent with the significantly higher power dissipated in the arc in our experiments. The values of temperature obtained by Bezborodko and Fauconneau [6] do not correspond to the hot region of the plasma and cannot therefore be compared with the results of the present study. Cheim and Howe [4] measured temperatures comparable with those reported here, even though they used interference filters which cannot be corrected for the presence of neighbouring lines and high background levels.

### Acknowledgments:

The authors wish to thank Greg Toland for his assistance in running the laboratory during the course of this study.

### REFERENCES

- [1] R.H. Tourin, "Spectroscopic Gas Temperature Measurement", Elsevier Publishing Company, Amsterdam, (1966).
- [2] T. Chikata, Y. Ueda, Y. Murai and T. Miyamoto, "Spectroscopic Observation of

- Arcs in Current-Limiting Fuse through Sand", Proc. ICEFA, Liverpool, England, (1976).
- [3] D.R. Barrow and A.F. Howe, "The Use of Optical Spectroscopy in the Analysis of Electric Fuse Arcing", Proc. ICEFA, Univ. of Nottingham, UK, (1991).
- [4] L. Cheim and A.F. Howe, "Spectroscopic Measurement of Fuse Arc Temperature", Proc. ICEFA, Technical Univ. of Ilmenau, Berlin, (1995).
- [5] M.A. Saqib and A.D. Stokes, "Time resolved spectrum of the fuse arc plasma", to be published in Thin Solid Films, reference: TSF 12312, Elsevier Science, Ireland, (1999).
- [6] P. Bezborodko and J. Fauconneau, "Spectroscopic measurements in plasmas with silica ablated walls", Proceedings XXIII International Conference on Phenomena in Ionised Gases, CNRS, Univ. Paul Sabatier of Toulouse, France, (17-22 July 1997).
- [7] Ed Metcalfe, "Atomic Absorption and Emission Spectroscopy", John Wiley & Sons, Chichester, p185, (1987).
- [8] W.J. Pearce, in "Optical Spectrometric Measurements of High Temperatures", P.J. Dickerman, editor, University of Chicago Press, Chicago, p125, (1961).
- [9] W.L. Wiese, M.W. Smith and B.M. Miles, "Atomic transition probabilities, a critical data compilation", Vol. I and II, National Bureau of Standards, NBS 22, USA, (1965).
- [10] C. Moore, "Atomic Energy Levels", National Bureau of Standards, NBS 467, USA, (1949).
- [11] H. Drawin and P. Felenbok, "Data for Plasma in Local Thermodynamic Equilibrium (LTE)", Gauthier Villars, Paris, (1965).
- [12] W.L. Wiese and A.W. Weiss, Phys. Rev., **175**, 50, (1968).
- [13] M.W. Smith and W.L. Wiese, Astrophys. J. Suppl. Ser., **23**, No. 196, 103, (1971).
- [14] G.A. Martin and W.L. Wiese, J. Phys. Chem. Ref. Data, **5**, 537, (1976).
- [15] Jarrell-Ash MonoSpec 27 Monochromator/Spectrograph, Models 82-497, 82-498, 82-499, Operator's Manual, Allied Analytical Systems, Waltham, MA 02254, (1985).
- [16] Optical Multichannel Analyser, Model 1460, Preliminary Operating Manual, Revision D, Princeton Applied Research Corp., (1986).
- [17] Nicolet Pro Digital Oscilloscopes, Operation Manual, Nicolet Instrument Corporation, Madison, USA, (1991).
- [18] W. Lochte-Holtgreven, "Production and Measurement of High Temperatures" Reports on Progress in Physics, **21**, 312, (1958).

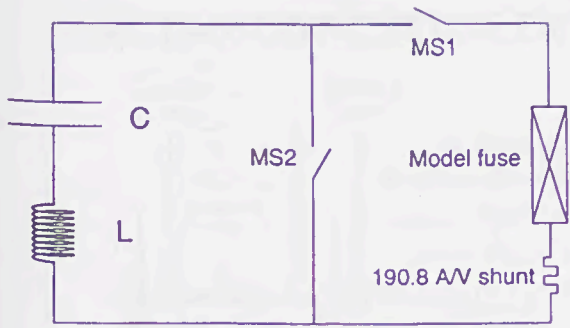


Figure 1: Electrical circuit to energise the test fuse.

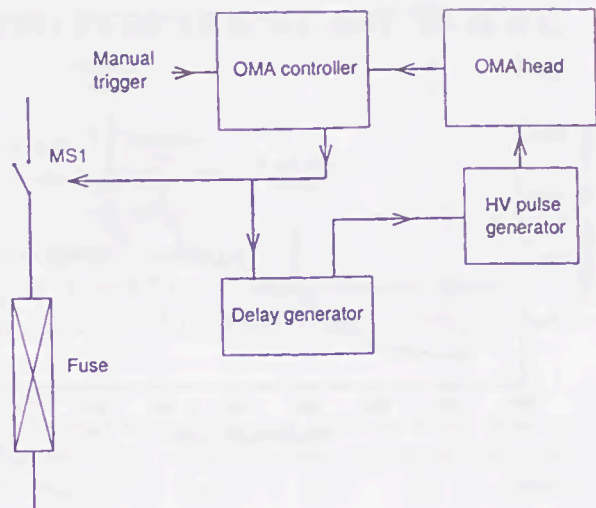


Figure 2: A simplified block diagram to synchronise OMA with the test fuse.

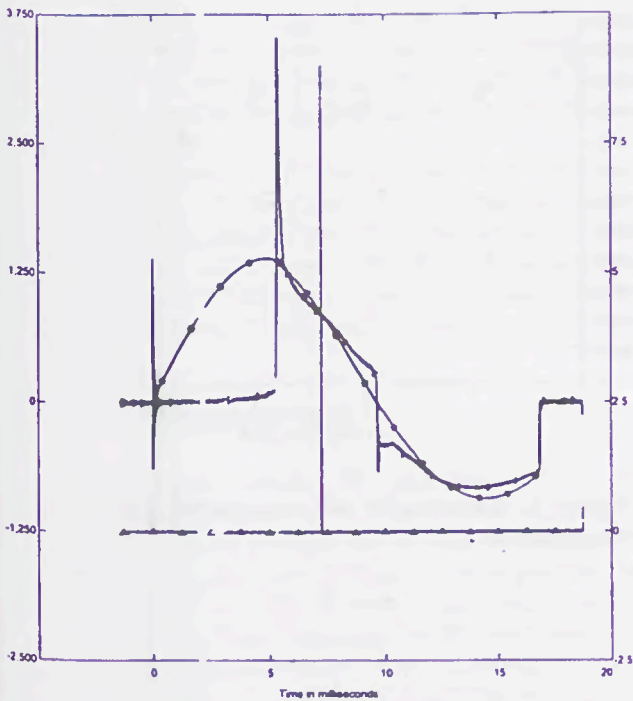


Figure 3: Plots for voltage across and current through the fuse. OMA head is opened at 7.265 ms to record the spectrum.

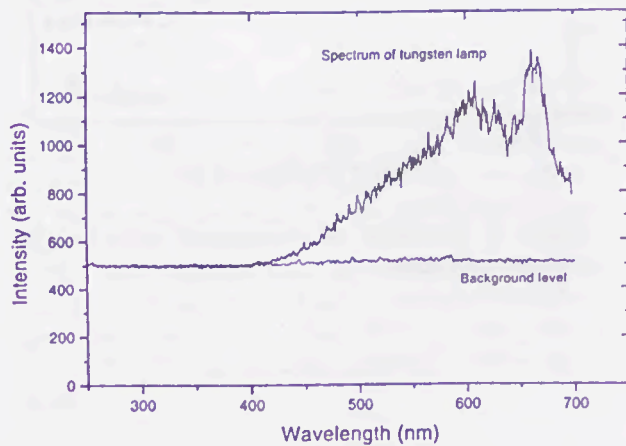


Figure 4: A spectrum of the tungsten lamp; background level is also shown.

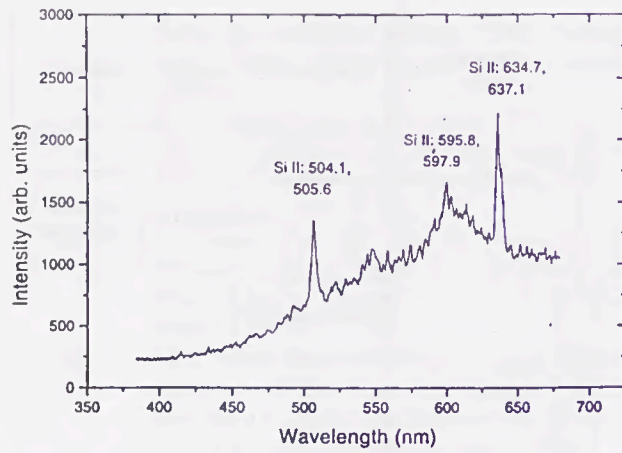


Figure 5: Fuse spectrum at 9.402 ms, ie, arc time of 4.102 ms.

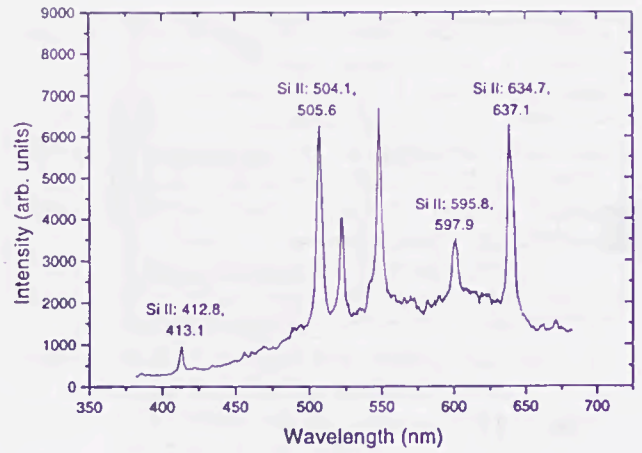


Figure 6: Fuse spectrum at 7.602 ms, ie, arc time of 2.302 ms.

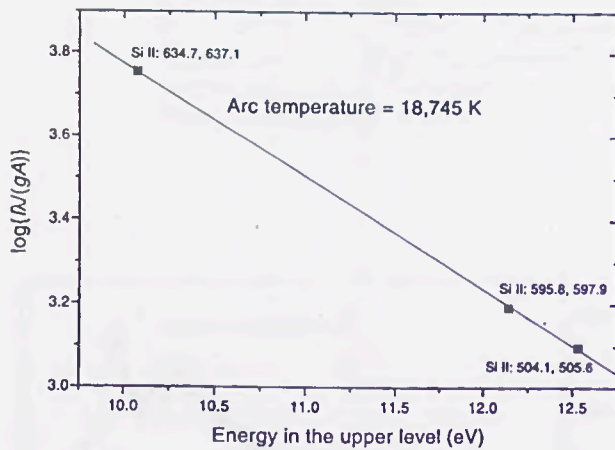


Figure 7: Deduction of temperature using relative intensity technique.

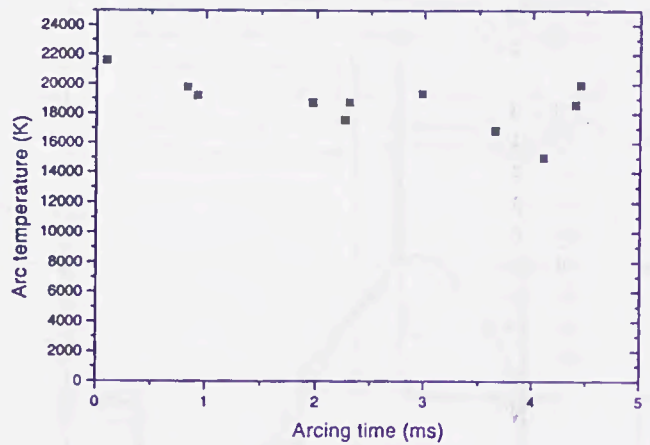


Figure 8: Variation of arc temperature during the arcing period.

# SPECTROSCOPIC STUDY OF A CUTTING ELECTRICAL ARC IN H.B.C FUSE

W.Bussière, P. Bezborodko, R. Pellet  
William.BUSSIÈRE@laept.univ-bpclermont.fr  
pierre.bezborodko@laept.univ-bpclermont.fr  
Rene.PELLETT@laept.univ-bpclermont.fr

Laboratoire Arc Electrique et Plasmas Thermiques (LAEPT) - Université Blaise-Pascal  
CNRS UPES-A 6069 - 24, Avenue des Landais - F 63177 AUBIERE Cedex - France

**Abstract:** This paper describes an experimental set up used to investigate the physic parameters of the arc, in fact the temperature and the electron density. Improvements have been made from the last set up [1]. Fuses studied here are High Breaking Capacity fuses (HBC). In this study, the arc dissipates 1,200 J, the peak of current is about 2,000 A and the duration of the arc is 3 ms. The whole of the visible spectrum has been registered, from 360 nm to 800 nm, in the exploding part of the arc. The spectrum consists of continuous light together with spectral lines which appears mostly when the electric current decreases. The behaviour of the spectra shows that there is a big gradient of species concentrations in the arc, together with a high gradient of temperature.

The temperature is measured from Si II lines and metallic spectral transitions. The calculations show a decrease from about 17,000 K at the beginning of the phenomenon, until about 7,000 K at 4 ms after the beginning of the electric current. The measured values of the electron density vary between  $10^{17}\text{cm}^{-3}$  and  $10^{19}\text{cm}^{-3}$ .

## I. INTRODUCTION

We briefly recall the specifications of the experimental fuse we use. We know that there exist very close interactions between the arc and the surrounding sand : so it is necessary to keep, as far as possible, the similar properties of the arc and its sand coating as in an industrial fuse. In an industrial fuse, it is not possible to collect suitable light because of the scattering of light by the sand grains. To completely avoid the scattering of light, one side of the experimental fuse consists of a 4-mm wide glass wall ; the fuse element in silver or in copper is directly put on it. On the other side, the fuse is filled with silica grains with a mean diameter of 0.4 mm. We distinguish two different experimental fuses, depending on the position of the fuse element on the glass wall (Figure I). In the experimental fuse (b) (in opposition to the experimental fuse (a)), the section of the fuse element is directly put on the glass wall : the area of the fuse element in contact with the glass wall is thus less important, and interactions between this two elements are weaker. Fulgurites obtained with the

experimental fuses (a) do not have the same shape as industrial ones, whereas those obtained with the experimental fuses (b) are nearly identical.

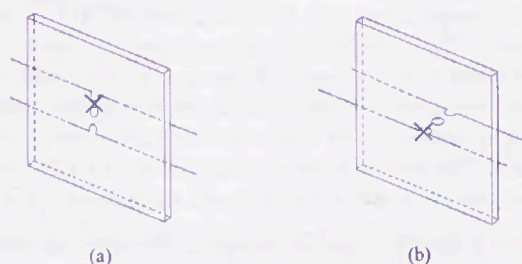


Figure I - Experimental fuses (a) and (b); the cross symbolizes the observation point.

It has been verified previously that the compactness of sand is an essential factor to obtain a good electrical cut off. In the same way, the spectra obtained later closely depend on the apparent density of sand, which is the reason why the mass of sand is checked for each fuse box.

Our fuse elements have an effective length of 36 mm, are 0.105 mm thick, 5 mm wide, and are 99.99 % pure silver (or copper). They have a single row of notches (0.5 mm in diameter) punched in the centre of the strip.

## II. EXPERIMENTAL SET UP: SPECTROSCOPIC ACQUISITIONS USING KINETIC MODE

### II.1 Light collection

The light coming from the glass wall is accurately collected via an optic fibre connected to the input of a spectroscope. The exact location of viewing is determined by way of a small laser beam. The

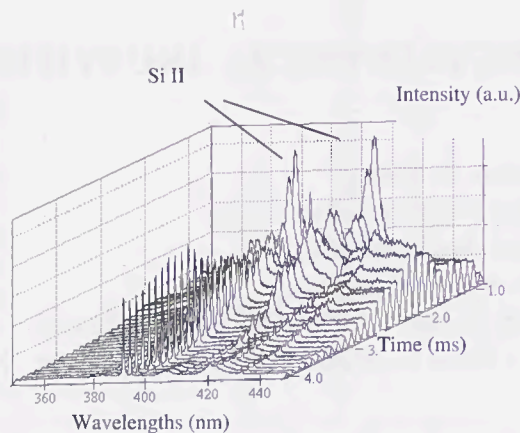


Figure II - Visible spectra obtained within [360-440] nm. The pre-arcing value is 0.87 ms.

spectroscope used is a Chromex 500 IS (0.5-m focal length). Three diffraction gratings can be used: 600; 1,200 and 1,800-gr/mm. As the aim of this work is to obtain the global visible spectra, the 600-gr/mm grating has been used in most cases. So, the bandwidth is about 90 nm. The output light is collected by a CCD matrix whose size is  $1,242 \times 1,152$  pixels. Each pixel is a  $22.5\text{-}\mu\text{m}$  side square. The 1,800-gr/mm diffraction grating is used for the evaluation of the electron density : it provides a 25-nm bandwidth.

## II.2 Use of matrix in a kinetic mode

The matrix is 1,152 lines high. It is divided in 39 tracks, 29 lines each. An area of 21 lines, on the bottom of the matrix, is never used. The spot light is aimed on the first track located at the bottom (pixels 1,131 to 1,102). Shortly before the phenomenon the mechanical shutter is open. At the beginning ( $t = 0$  ms), one imposes to the matrix  $15\ \mu\text{s}$  of time exposure. Then the shifting up of the content of lines is commanded, line after line, and this, 29 times. Shifting of one line requiring  $3\ \mu\text{s}$ , then,  $87\ \mu\text{s}$  after, the totality of the track is in the upper track (1,102-1,073). Now,  $t = 87 + 15 = 102\ \mu\text{s}$ . A time exposure of  $15\ \mu\text{s}$  is imposed again and so on until the totality of the matrix is full, at  $t = 39 \times 102\ \mu\text{s} = 3.98$  ms. The mechanical shutter is then closed, with a non reproducible long time lag.

The first and the last tracks are randomly exposed because of the inaccuracy of the mechanical shutter. For this reason these spectra are not shown later in this paper.

An electronic circuit drives simultaneously the start of the power supply and the shifting of the matrix. For each shooting, the start of the power supply, the current flowing across the fuse and the voltage drop are stored by means of two oscilloscopes.

## III. EXPERIMENTAL RESULTS AND DISCUSSION

### III.1 Evolution of radiation versus time

The whole of the visible spectrum has been registered from 360 to 800 nm [2]; each spectrum has an approximate 90-nm bandwidth, the total spectrum is a juxtaposition of 6 spectra. To avoid possible problems of reproductibility, three discharges are done for each wavelength.

Figure II reveals a typical evolution of spectra obtained for a single discharge.

We easily distinguish three different stages in the global spectrum :

- Spectral transitions which are superimposed on an intense continuous light : it corresponds to the meantime 0.8 to 1.4 ms after the beginning of the current.
- Increase of the continuous light which dominates the whole spectrum from 1.4 to 2.5 ms. Continuous light is most important in the I.R. than in the U.V. region because of the increase of the free-free transitions. Some atomic transitions are still emitted : the latters correspond to ionised species.
- The continuous light decreases fastly and atomic transitions emerge from 2.5 ms until the end of the phenomenon.

This evolution is observed in the two models of experimental fuses.

To determine the temperatures from spectral lines, we need to know precisely the origin of light. In particular we need to know whether there is a continuous light at the foot of lines or whether some specific lines are sufficiently isolated in the spectrum. For these reasons our first measurements are devoted to identify all the species which emit light in arc fuses. The totality of the visible spectrum was first studied within 3 ms after the beginning of the arc, because the narrowness of lines permits a very good estimation of wavelengths. An accurate gauging of the spectrometer had been realised with spectral lamps, it had showed that the wavelength of a line was given with an absolute accuracy of 0.07 nm.

The recognition of emitting species has required several sources. Several spectral tables have been used [3][4][5], as well as data referring to N.I.S.T. [6]. Nevertheless, this information is often insufficient because for a given wavelength there are a lot of corresponding elements. So, one has to study each atomic transition in detail.

Three groups of spectral lines have been identified (Table I) :

- The impurities : they are present in the sand and especially in the glass wall ; they consist of oxide such as CaO,  $\text{Na}_2\text{O}$ ,  $\text{K}_2\text{O}$ . All the impurity species singled out emit resonance lines (atomic transitions to the ground state).
- The metallic transitions (Ag and Cu) : we only observed neutral atomic transitions.
- The silicon transitions : observed in the neutral state and ionised once.

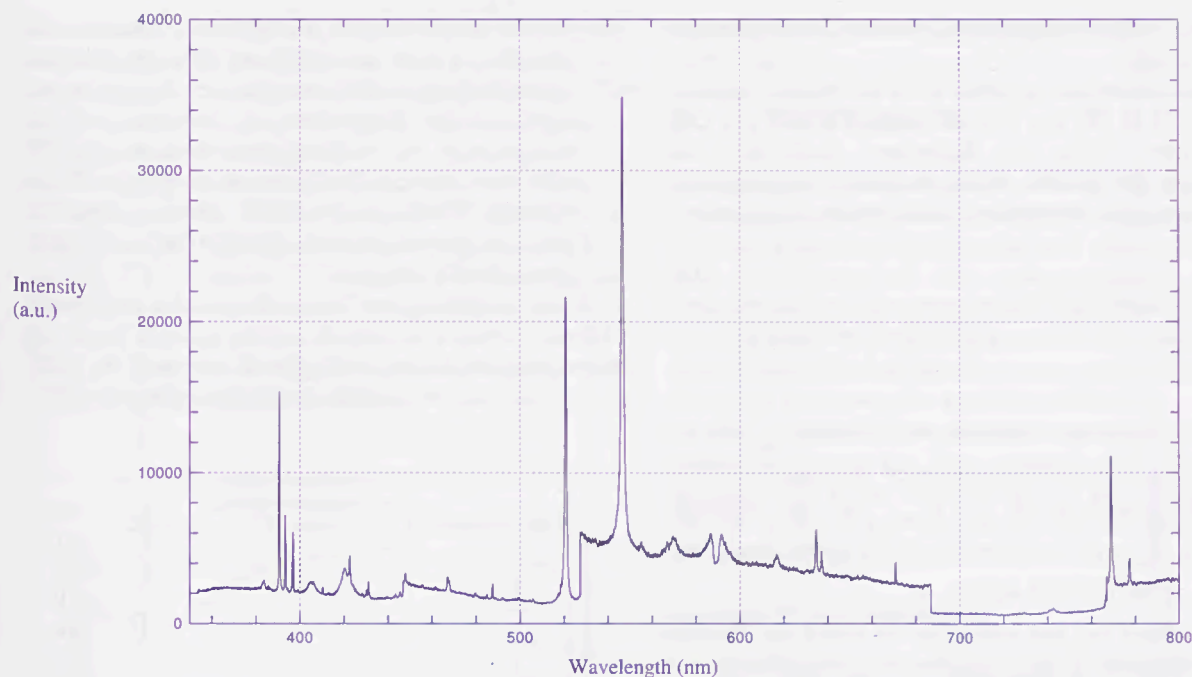


Figure III – Visible spectrum obtained 3.0 ms after the beginning of the arc.

Element	Ionization stage	$\lambda_{\text{THEORETICAL}}$ (nm)
Si	II	385.60
Si	II	386.26
Si	I	390.55
Ca (R)	II	393.37
Ca (R)	II	396.85
Si	II	412.81
Ca (R)	I	422.67
Ag	I	431.11
Ag	I	447.61
Ag	I	466.85
Ag	I	487.42
Ag (R)	I	520.91
Ag (R)	I	546.55
Na (R)	I	588.99
Na (R)	I	589.59
Si	II	634.71
Si	II	637.14
Li (R)	I	670.78
Li (R)	I	670.79
K (R)	I	766.49
K (R)	I	769.90
Ag	I	768.78
O	I	777.19
O	I	777.42
O	I	777.54

Table I – Identified transitions in fuse tests within the spectral band [360-800] nanometers. Tests done with copper fuse element revealed the  $\lambda = 510, 515, 521$  nm lines.

Within 3 ms, twenty five lines are identified with certainty (Figure III).

### III.2 Plasma temperature evaluation using the ionised silicon multiplets (1) and (3)

Among the atomic transitions identified, we have used the groups of the metallic transitions and the silicon transitions ionised once to evaluate the temperature.

As first approximation, we compare the arc in a fuse with a wall stabilised arc, the arc being closed within molten silica. In such case, it is known that metallic particules spread to the walls and the electrodes. As a consequence, we can expect to obtain different temperature values from the two groups of atomic transitions. In fact, to make calculation from lines, we have to use lines from elements which are first present in the centre of the arc and second which emitted some light at high temperature because at the beginning of

the arc's growth, temperatures in the arc are supposed to be very high.

Calculations are achieved from the relative intensity ratio of Si II 386 nm (2D-2P°) and Si II 413 nm (2D-2F°) lines. Using the Boltzmann distribution and assuming the plasma being in local thermodynamic equilibrium, the temperature at the instant  $t$  is given by :

$$T(t) = \frac{E_{m1} - E_{m2}}{k} \times \frac{1}{\log \left( \frac{g_{m1} A_{mn1} \lambda_{mn2} J(\lambda_{mn2}, t)}{g_{m2} A_{mn2} \lambda_{mn1} J(\lambda_{mn1}, t)} \right)} \quad (1)$$

where  $A_{mn1,2}$  are the transition probabilities,  $\lambda_{mn1,2}$  are the differences in wavelength between the upper levels  $m$  and the deeper levels  $n$ ,  $g_{m1,2}$  are the statistical weights,  $E_{m1,2}$  are the energies of the upper levels, and  $J(\lambda_{mn1,2}, t)$  are the lines areas.

This method has the advantage to avoid an absolute light calibration of the experimental set up. Moreover, it is not necessary to know the species concentrations. The experimental uncertainties come from spectroscopic data (especially the transition probabilities) and from the difficulty to estimate the line area, which overlaps a not-to-well defined shape of continuum. As the influence of pressure on radiation is not well known, we decided to use maximal intensities, rather than lines areas.

Calculations (Figure IV) have been made using spectra obtained from the two models of the experimental fuse.

We can summarize the results in three points :

- We observe a logical decrease of temperature in the meantime 0.9-3.0 ms ; fuse is in fact a device used to dissipate energy.
- In spite of this logical evolution, we notice a weak variation during the studied meantime. Values are still high at the end of the phenomenon.
- The discrepancies between the two types of results are justified as follows : in the case of the experimental fuse (a), the fuse element is directly put on the glass wall ; it involves the shifting of the plasma on the glass wall. On the contrary, in the case of the experimental fuse (b), the energy is closely concentrated in an ionised channel whose expansion is limited by the surrounding compact silica sand ; fulgurites obtained have a shape as good as in industrial fuses.

Evaluations have also been made using the Cu I  $\lambda = 510, 515$  and  $521$  nm lines at the end of the phenomenon in the case of the experimental fuse (b). We were motivated by two goals :

- We wanted to evaluate discrepancies between the temperature obtained from the maximal intensities ratio of ionised silicon lines and from metallic transitions.

- As the profil shapes are easier to observe, we compared values deduced from (1) using maximal intensities ratios and areas ratios. As continuous light is less important at the end of the phenomenon, we worked in the meantime 3.0-4.0 ms : from the maximal intensities we got values between 7,500K and 6,000K, whereas from the areas we got values between 12,500K and 9,500K (gaussian line shapes).

Thus we notice that the scales of size are clearly different between the silicon and the metallic lines, and that numerical values are higher if one uses the areas ratio rather than the maximal intensities ratio.

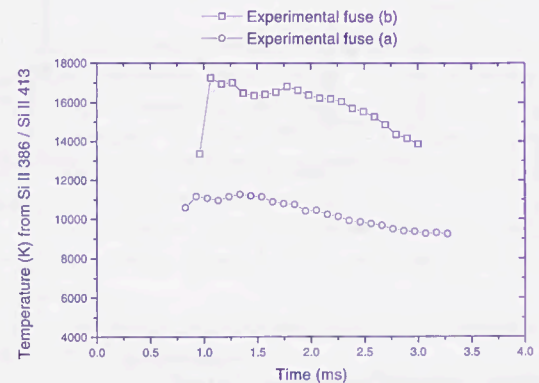


Figure IV - Temperatures obtained from the Si II  $\lambda = 386$  nm and  $413$  nm lines. Results are given for the two models of experimental fuses.

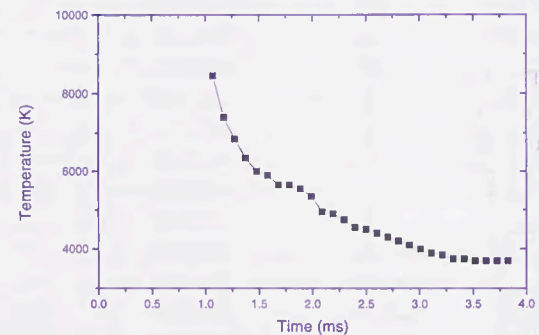


Figure V - Low threshold temperature deduced from the Planck's law within [360-800] nm for the experimental fuse (a).

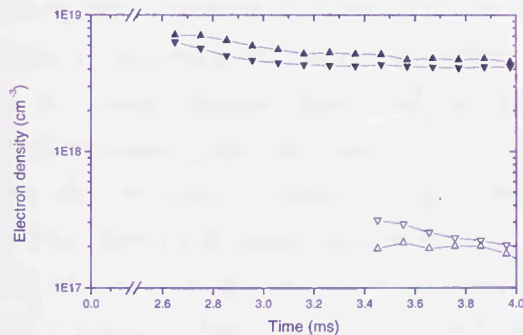
### III.3 Black body approximation

In order to improve our knowledge of the physical parameters of the plasma, we tried to characterize the plasma radiation during the meantime 1.4-2.5 ms. As there is no spectral line observed in some spectral intervals such as in [670-760] nm, we tried to evaluate the temperature by making the comparison between a

black body curve at given temperature and our spectra, within [360-800] nm. We have used the Planck's law assuming an emission coefficient equal to unity. This implies to obtain a low threshold of the temperature. Results are shown in Figure V.

The temperature obtained decreases roughly from 8,000K to 3,000K. This evolution is still logical, but the values are not available because one ignores the layer on which the radiation is integrated ; and an emission coefficient below unity should involve higher values.

#### III.4 Electron density deduced from the ionised silicon multiplet (2) Stark shifts



Fi

Figure VI - Electron densities for the two models of experimental fuses for  $T = 15,000$  K : -▼- Si II  $\lambda = 634$  nm, experimental fuse (b) ; -▲- Si II  $\lambda = 637$  nm, experimental fuse (b) ; -▽- Si II  $\lambda = 634$  nm, experimental fuse (a) ; -△- Si II  $\lambda = 637$  nm, experimental fuse (a).

To obtain an evaluation of the electron density, we did not use the line shape and thus the broadening parameters because of the difficulties we had for fitting line shapes. Thus we deduced the electron density from the shift between theoretical and experimental wavelengths.

This method is applied to the ionised silicon multiplet (2). We suppose that the observed shifts of the  $\lambda = 634.7$  and  $637.1$  nm lines are due to the Stark effect. From the theoretical values of shifts given by Griem [7] as a function of temperature and at a given density, and according to the fact that Stark effect is a linear function of the electron density and a non linear function of the temperature, we deduce the values of the electron density versus time by observing the experimental shifts. Because of the weak change of the shifts with the temperature, calculations are carried out with a temperature equal to  $15,000$  K.

Results are given in the Figure VI for the two models of experimental fuses. The results obtained with the experimental fuse (b) are rather in good agreement with Chikata's one [8] : between  $4 \times 10^{18} \text{cm}^{-3}$  and  $8 \times 10^{18} \text{cm}^{-3}$  ; whereas the results issued from the

experimental fuse (a) are rather in the range  $2-4 \times 10^{17} \text{cm}^{-3}$ .

#### IV. CONCLUSIONS

From the experimental fuse devised, we are able to conduct reproducible tests in order to evaluate the two physical parameters temperature and electron density. The first stage of the work consisted in the determination of the atomic species (together with their spectral parameters) that are present in the plasma. The following stage was to select those spectral lines we could use to evaluate the physical parameters.

The influence of the pressure broadening has to be quantified shortly for two reasons : first, it causes discrepancies in the determination of the temperature ; second, it would provide another way to evaluate the electron density.

#### ACKNOWLEDGEMENTS

We thank, both for their financial support and for their help for many discussions : Mr Barrault M R of Schneider Electric, Mr Rambaud M R of Ferraz SA, Mr V\'erit\'e J C of Electricit\'e de France, Mr Melquiond S and Mr Dides R of ALSTOM.

#### REFERENCES

- [1] Bezborodko P, Fauconneau J 1997 *Proc. Of XXIII Int. Conf. on Phenom. in Ion. Gas.* IV 69-9, Toulouse, July 17-22, 1997
- [2] Bussiere W, Bezborodko P, *Measurements of the time-resolved spectra of fuse arcs using a new experimental arrangement*, to be published in *J. Phys. D : Appl. Phys. (UK)*, Ref Number D/100661/PAP.(1999)
- [3] Massachusetts Institute of Technology 1969 *Wavelength Tables with Intensities in Arcs, Spark, or Discharge Tube* (Massachusetts M.I.T. Press)
- [4] Striganov A R, Sventitskii N S 1968 *Tables of Spectral Lines of Neutral and Ionised Atoms* (New York Washington IFI/Plenum)
- [5] Zaidel A N, Prokof'ev V K, Raiskii S M, Slavnyi V A, and Schreider E Y 1970 *Tables of Spectral Lines* (New York London IFI/Plenum)
- [6] NIST 1995 *Database for Atomic Spectroscopy version 1.0* (Gaithersburg National Institute of Standards and Technology)
- [7] Griem H R 1974 *Spectral Line Broadening by Plasmas* (New York and London : Academic Press)
- [8] Chikata T, Ueda Y, Murai Y, Miyamoto T, *Spectroscopic observations of arcs in current limiting fuse through sand* (ICEFA n°1 Liverpool April 1976 Proc. pp 114-121)

The first part of the document discusses the importance of maintaining accurate records of all transactions. It emphasizes that every entry should be supported by a valid receipt or invoice. The text also mentions the need for regular audits to ensure the integrity of the financial data.

In the second section, the author details the various methods used for data collection and analysis. This includes both manual and automated processes. The importance of data security is also highlighted, with specific recommendations for protecting sensitive information.

The third part of the document focuses on the implementation of new software systems. It describes the challenges faced during the transition and the steps taken to ensure a smooth rollout. The author also discusses the training provided to staff to ensure they are proficient in using the new tools.

Finally, the document concludes with a summary of the key findings and recommendations. It stresses the need for continuous improvement and the importance of staying up-to-date with the latest industry trends and technologies.

The second part of the document discusses the importance of maintaining accurate records of all transactions. It emphasizes that every entry should be supported by a valid receipt or invoice. The text also mentions the need for regular audits to ensure the integrity of the financial data.



The third part of the document focuses on the implementation of new software systems. It describes the challenges faced during the transition and the steps taken to ensure a smooth rollout. The author also discusses the training provided to staff to ensure they are proficient in using the new tools.

Finally, the document concludes with a summary of the key findings and recommendations. It stresses the need for continuous improvement and the importance of staying up-to-date with the latest industry trends and technologies.

# Geometrical Model of Discharge Space in the State of the High Arc Voltage Generation of Capillary Arcs

S. Arai

Tokyo Denki University

Tokyo Japan

**Abstract:** The paper describes the discharge space in consideration of the capillary arc behavior depending on the arc current density and the diameter of a capillary tube. According to increasing the arc current density or decreasing the diameter of capillary tube, the arc voltage becomes higher and the radiation intensities emitted from the capillary tube changes from the line spectral radiation to the continuous spectral radiation with spectral absorption.

The pressure in the high pressure vessel during arcing time is extremely lower than the estimated pressure due to the completely vaporized element at arc temperature. Therefore droplets and bulks of liquefied element substance remain in the capillary space.

The continuous spectral radiation suggests that the arc column is surrounded by the optical dense vapor layer including droplets, absorbing the radiation from arc column and emitting continuous spectral.

It is supposed that the layer plays an important role in high arc voltage generation by effectively carrying off the energy from the arc column.

## 1 INTRODUCTION

The study of the capillary arc behavior has been experimentally made to understand the physical mechanism governing the high arc voltage generation during the heavy current operation of current limiting fuses.[1]

The experiment was made to investigate the relation between the arc voltage and the arc temperature, the pressure of arc discharge space and the diameter of a

capillary tube in a high pressure vessel. The temperature is measured by the spectroscopic measurement systems.

From experimental results, the arc voltage becomes higher and spectral radiation profile emitted from the capillary tube changes from line spectra to continuous profile with resonant absorption as increasing the arc current density or decreasing the diameter of capillary tube. The temperature in continuous spectral radiation intensity is estimated from fact that the radiation can be coincident with the simulation of the blackbody radiation combined with resonant absorption of sodium.[2]

It is experimentally confirmed that the pressure in the high pressure vessel during arcing time is extremely lower than the estimated pressure due to the completely vaporized element at the arc temperature. These observed results suggest that a quite large proportion of liquefied element substance remain in the capillary tube as droplets and bulks of liquefied element substance. As the cause of the observation of continuous spectral radiation, it is supposed that the optical dense layer mixing vapor and droplets surrounds the arc column and absorbs the radiation from the arc column and radiates the continuous spectral radiation intensity.

It is believed that the layer plays an important role in high arc voltage generation by effectively carrying off the energy from the arc column.

## 2 EXPERIMENTAL SYSTEM

### 2.1 Experimental apparatus

The high pressure vessel mainly consists of an insulation cylinder, upper and lower stainless steel circular disk covers and flanges. The pressure measuring unit is installed on the lower cover. The opening is made through at the middle side of the insulation cylinder. A test sample set together a cylindrical spacer is inserted along the axis of the insulation cylinder.[1]

### 2.2 Pressure measuring unit

The pressure in the high pressure vessel is measured by the pressure measuring unit including the pressure transducer. The piston is pressed down by the pressure in the high pressure vessel, the pressure is transferred to the transducer through the piston-cylinder containing silicon oil.

### 2.3 Spectroscopic measurement systems

The opening to take out the radiation from the inside of high pressure vessel is holed through at the middle side and perpendicular to the axis of the insulation cylinder. The optical fiber is inserted into the opening to lead the radiation away from arc discharging space.

The two monochromatic spectroscopic system and multi channel spectroscopic analyzer system are used in this study in order to estimate the temperature of the arc discharge space by the spectral intensity measurement method. [1]~[7] The arc column temperature is estimated by the calculation from the 2 line spectral intensities obtained by the 2 monochromatic spectroscopic system under the assumption of local thermal equilibrium.

### 2.4 Experimental circuit

The arc energy is easily adjusted by the test circuit which consists of the loop circuit including a capacitor bank and a reactor and the loop circuit including the reactor and a test sample. Closing the loop circuit of the capacitor bank and the reactor, charged energy in the capacitor bank is transferred to the reactor. And then the capacitor bank is broken at the moment of completely discharging, so energy in the reactor flows

into the test sample.

### 2.5 Test samples

The 2 kinds of dimension of copper wire element are 0.18 mm, 0.20 mm in diameter and 50 mm in length. The 6 kinds of dimension of Pyrex capillary tube are 3.5 ~ 1.0 mm every 0.5 mm in inner diameter and 50 mm in length.

## 3 EXPERIMENTAL RESULTS AND CONSIDERATION

### 3.1 Arc voltage and spectral radiation intensity characteristics

The arc voltage, current, spectral radiation and pressure were measured according to the current and the diameter of capillary tube. Fig.1 shows the typical relation between the arc voltage, current and the spectral radiation intensity characteristics, for the test sample of the capillary tube of 1.5 mm in inner diameter and the copper wire element of 0.18 mm in diameter. A series of Fig.1 (b) were measured by the multichannel spectroscopic analyzer system at the same time of measurement of the arc voltage and current shown in Fig.1 (a). The sets of sign I and number indicated on the figure indicate the wavelength in nano meter unit of line spectral intensity of copper atom.

As shown in Fig.1 (a), the arc initiating currents are 160 A, 280 A and 350 A. For the arc initiating current of 160 A, the arcing time of 0.63 msec and arc energy of 30J, the arc voltage decreases like the exponential function of time. For the 280A, the arcing time of 0.77 msec and the arc energy of 82 J and 350 A, the arcing time of 0.85 msec and the arc energy of 120 J, the shoulder of arc voltage is observed during the middle of the arcing time.

The voltage of the shoulder increases with the increase of the arc initiating current, apparent arc current density that is calculated by dividing the arc current by the inner cross section of the capillary tube and the arc energy.

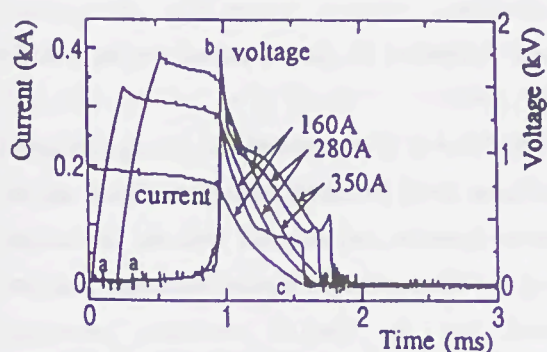


Fig.1 (a) the arc voltages and the currents

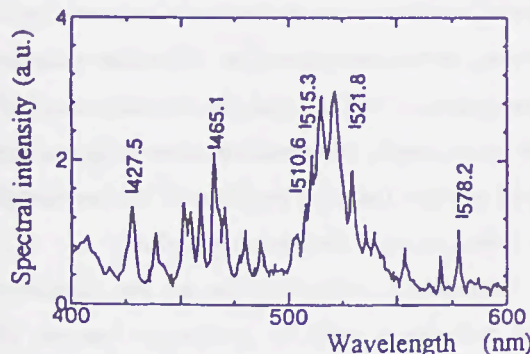


Fig.1 (b - 1) the spectral radiation characteristics for arc initiating current 160A

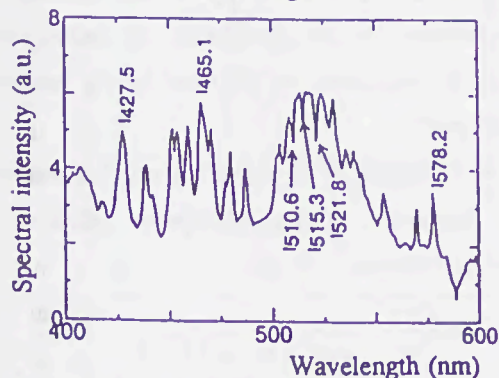


Fig.1 (b - 2) the spectral radiation characteristics for arc initiating current 280A

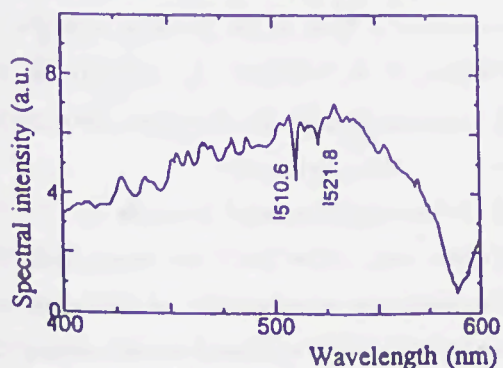


Fig.1 (b - 3) the spectral radiation characteristics for arc initiating current 350A

the capillary tube is 1.5 mm in inner diameter and 50 mm in length

Fig.1 Relation between arc voltage and spectral radiation characteristics depending on current

As shown in Fig.1 (b - 1) that is correspondent with the arc initiating instant of 160A in figure 1(a), the line spectra from copper atom are clearly recognized.

As shown in Fig.1(b - 2) corresponding with the arc initiating instant of 280A, the line spectra of 427.5nm, 465.1nm, 578.2nm in the wavelength for copper atom are clearly recognized, on the other hand spectral absorption is observed at the 510.6 nm, 515.3 nm, 521.8 nm in wavelength.

Showing in Fig.1(b - 3) that is correspondent with the arc initiating instant of 350A, the spectral radiation profile like continuous spectral radiation and spectral absorption occurs at 510.6 nm, 521.8 nm in central wavelength. And furthermore, it is observed that the significant spectral absorption occurs at 587 nm of central wavelength.

### 3.2 Partial vaporization of element

The arc process during arcing time can be divided into 3 steps for heavy current operation. The first step is the process that multi arcs ignite and each burns back along element to join together a single arc. The second step is the single arc burning process, and the last is small current conduction and recovery of dielectric strength in post arc space around current zero.

Depending on the diameter of element and the rate of flowing energy into the element, the state of the element at the instant of arc initiation may be liquid state heated up a little above melting temperature in the range of heavy current. It is observed that the arcs initiate successively along the wire element, and immediately after multi arcs are constituted, each burns back along the element to join together a single arc in a short time.[8] The input energy into the high pressure vessel during the first step mainly concentrates on the regions of arc dynamic action because of each high arc voltage, so that the consuming energy by enclosing

surroundings and the segment of element is comparatively small.

Showing in Fig.1(a), the energy flowing into the high pressure vessel during arcing time is 120J for the arc initiating current of 350 A, on the other hand, the energy of about 27J is necessary for the whole copper element to vaporize completely from liquid state of melting temperature. However part of the input energy into the high pressure vessel is spent to heat up the liquefied element substance, but the energy shared out to heat the liquefied element may not be enough to vaporize whole element at any instant during arcing time.

The reason is as follows, for the sample of the copper element of 0.18mm in diameter and 50mm in length, and the capillary tube of 3.0mm in diameter and 50 mm in length, and pressure of 1.0 MPa, temperature of 9000 K in the discharge space, the rate of number of copper atom to produce the pressure in the capillary tube to number of atom including the original wire element is about 0.3 %.

Therefore it is supposed that a large amount of liquefied element substance exist as droplets and lumps of liquid in the capillary tube during arcing time.

#### 4 ARC DISCHARGE SPACE MODEL IN HIGH CURRENT DENSITY

Under the experimental condition of the low apparent arc current density under about  $90 \times 10^6 \text{A/m}^2$  in the vicinity of the arc initiation and the Pyrex capillary tube inner diameter of 3.5~1.5 mm, the arc voltage is exponentially monotonous decreasing. And the temperature of arc column of about 7000~10000K during arcing time is estimated by the relative line spectral intensity method.[1][2]

For the heavy arc current over the apparent arc current density of about  $260 \times 10^8 \text{A/m}^2$  in the vicinity of the arc initiation and the capillary tube inner diameter of 1 mm, the arc voltage is high rectangle as shown in

Fig.2(a), the spectral radiation profile is continuous as the blackbody radiation except the distinguished resonant absorption of spectra caused by the sodium vapor.

As stated above, it is supposed that the optical dense copper vapor layer including droplets surrounds the arc column and absorbs the radiation from the arc column and radiates the continuous spectral radiation. And it is supposed that the spectral absorbing membrane including sodium is outside the layer and on the inner surface of capillary tube, because of the possibility of vaporizing the sodium vapor from Pyrex tube including the component of sodium and the coincidence of the central wavelength of resonant absorption on the observed spectral radiation profile with the wavelength of the strong resonant absorption of sodium.

The temperature estimation due to the continuous spectral radiation is made by comparison between the measured radiation intensity characteristics and the theoretical blackbody radiation. At the same time, the some parameters for the distribution of sodium and copper in the membrane are obtained by the resonant absorption profile.

These are estimated by the following set of equations. Spectral brightness of the blackbody radiation is expressed as follows

$$B_\nu = \frac{2h\nu^3}{c^2} \frac{1}{\exp(h\nu/\kappa T) - 1} \quad (1)$$

where  $h$  is Planck's constant,  $\nu$  is frequency of radiation,  $c$  is speed of light,  $\kappa$  is Boltzmann's constant. The monochromatic beam of the radiation impinges on the membrane of  $l_{Na}$  thickness. An intensity of the beam of  $I_\nu$  passing through the membrane is expressed as follows

$$I_\nu = B_\nu \exp[-(\alpha_{\nu Na1} + \alpha_{\nu Na2})l_{Na}] \quad (2)$$

where  $\alpha_{\nu Na1}$  and  $\alpha_{\nu Na2}$  are the monochromatic absorption coefficient of wavelength of 589.0 nm and 589.6 nm of sodium. The monochromatic absorption coefficient  $\alpha_{\nu Na}$  is expressed as follows

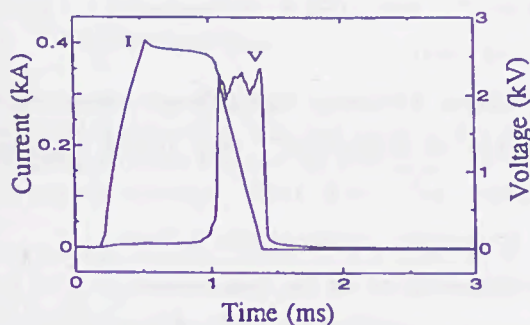
$$\alpha_{\nu Na} = \frac{\pi e^2}{mc} \quad (3)$$

where  $e$  is the electron charge,  $m$  is mass of electron,  $N$  is atom density,  $f_{Na}$  is absorptive oscillator strength of sodium,  $f_{Na1}=0.655$  at the wavelength of 589.0 nm and  $f_{Na2}=0.327$  at the wavelength of 589.6 nm,[9]  $p_{\nu}$  is normalized profile of radiation. Under assuming Lorentz's type expression,  $p_{\nu}$  is given as follows

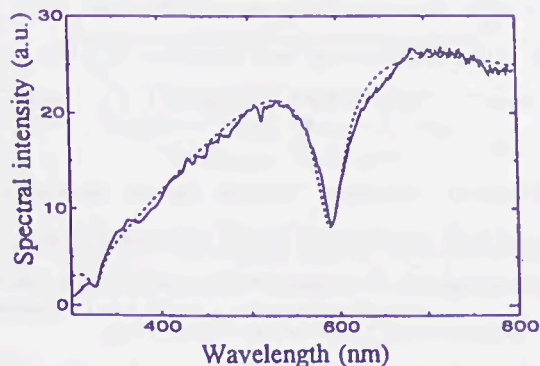
$$p_{\nu} = \frac{1}{\pi} \frac{\gamma/2}{(\nu - \nu_0)^2 + (\gamma/2)^2} \quad (4)$$

where  $\gamma$  is the width of curve at the half depth of central wavelength of absorption curve given by Margenau and Watson,[10]  $\nu_0$  is the central wavelength of resonant absorption curve.  $\gamma$  is given as follows

$$\gamma = \frac{e^2 f_{Na} N}{2 \pi m \nu_0} \quad (5)$$



(a) arc voltage and current



(b) the observed and calculated spectral radiation

Fig.2 the observed arc voltage and current, the observed and calculated spectral radiation profiles for the capillary tube is 1mm in inner diameter, the element is 0.20 mm in diameter

The dotted line curve on Fig.2 shows the spectral radiation profile calculated by using the set of equations from (1) to (5). Physical parameter of the membrane is given by the calculation.

The calculated blackbody radiation curve particularly depends on the temperature of the layer. In the resonant absorption, the depth of resonant absorption curve at the central wavelength of 590 nm depends on both sodium vapor density and optical length of the membrane. And the width of curve at half depth of resonant absorption curve depends on the sodium atom density in the membrane. For the capillary tube diameter of 1.0 mm, the calculated temperature is 4300K according to the coincidence with the theoretical blackbody radiation. The optical length of the membrane of sodium is  $2.7 \times 10^{-8}$  m and of copper is  $1.4 \times 10^{-8}$  m. The particle density of sodium in the membrane is  $8 \times 10^{26} \text{ m}^{-3}$  and of copper is  $420 \times 10^{26} \text{ m}^{-3}$ .

Fig.3 shows the proposed qualitative model of arc space in heavy current by the above considerations.

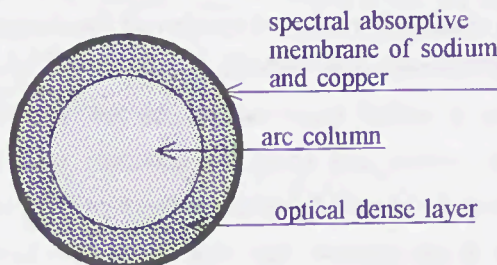


Fig.3 The basic model of the arc discharge space in the capillary tube for high current density

The model is the constitution of coaxial configuration. The arc column occupies the central section. The layer surrounding arc column contains copper vapor and droplets of liquefied element substance and is optical dense, so the layer absorbs the radiation from the arc column and emits continuous radiation. The membrane on the inner surface of the capillary tube absorbs resonantly spectra emitted by the layer.

## 5 CONCLUSION

Decreasing diameter of capillary tube or increasing

the arc current density, the shoulder of voltage grows, and the rectangular attains at last. On the other hand, the spectral radiation changes from line to continuous profile.

For capillary tube diameter of 3.5 ~ 1.5 mm, temperature of arc column of 7000 ~ 10000K is clearly estimated by the relative spectral line intensity method. And for the capillary tube diameter of 1.0 mm and the apparent arc current density over about  $2.6 \times 10^8 \text{ A/m}^2$  in the vicinity of the arc initiation, the temperatures of 4000~5000K is estimated by comparing the measured continuous spectral radiation characteristics with the theoretical blackbody radiation.

Flowing energy into the element is not enough to vaporize the element completely, the lump of liquids and droplets of element substance remain in the arc discharge space. It is supposed that the multi arcs develops into a single arc of coaxial construction in the capillary tube in the first step, the arc column burns in the center along the axis of capillary tube, and the layer of mixture of vapor and droplets of the element substance surrounds arc column in the second step. The layer is optical dense and absorbs the radiation from arc column and emits the continuous spectral radiation as the blackbody radiation. The membrane on the wall of the capillary tube and outside the layer includes the sodium vaporized from the capillary tube.

From the experimental results, it is believed that the high arc voltage generation is the cause of the high current density, the layer containing the vapor and droplets of element substance between arc column and the capillary wall and the membrane on the wall of capillary tube. It is considered that the layer and the membrane carries effectively off the energy from arc column. The distance between arc column and wall of capillary tube becomes shorter by decreasing the capillary tube diameter, cooling the arc column by the above construction between arc column and the wall is more effective.

## REFERENCES

- [1] S.Arai, S.Hamada, "Experimental investigation of capillary arc phenomena", Proc. ICEFA Ilmenau Germany pp236~242 1995
- [2] S.Arai, S.Hamada, "Temperature Estimation of Arc in Glass Capillary by Spectroscopic Measurement", Proc. SAP & ETEP-97 Lodz Poland pp 253~257 1997
- [3] M.R.Barrault, "Pressure in Enclosed Fuses", Proc. ICEFA Liverpool U.K. pp110 ~ 113 1976
- [4] L.J.Cao, A.D.Stokes, "Spectrum Analysis of an Ablation-Stabilised Arc in Ice", Proc. ICEFA Nottingham U.K. pp27~32 1991
- [5] D.R.Barrow, A.F.Howe, "The Use of Optical Spectroscopy in the Analysis of Electric Fuse Arcing", Proc. ICEFA Nottingham U.K. pp221 ~225 1991
- [6] L. Cheim, A.F.Howe, "Spectroscopic measurement of fuse arc temperature", Proc. ICEFA Ilmenau Germany pp251~258 1995
- [7] P. Bezborodko, J.Fraconneau, R.Pellet, "Experimental set up for spectroscopic measurements of plasma arcs in fuses", Proc. ICEFA Ilmenau Germany pp259~264 1995
- [8] S. Arai, "Deformation and disruption of silver wires", Proc. ICEFA Liverpool U.K. pp50~58 1976
- [9] Daidouji, Nakahara, "Atomic Spectra Measurement and their Applications", book (Japanese) 1989 .
- [10] H.Margenau, W.Watson, " Pressure Effects on Spectral Lines", Rev.Mod., Vol.8, 1936

# ELECTRIC FIELD AND PRESSURE MEASUREMENTS IN HIGH VOLTAGE FUSES

V. Murin-Borel, M. Lieutier, M. J. Parizet  
 Laboratoire Arc Electrique et Plasmas Thermiques  
 Université Blaise Pascal  
 24 avenue des Landais  
 63177 Aubière Cedex FRANCE

**Abstract :** The aim of this work is to know better the mechanisms which exist in high voltage fuses. In this way, we have chosen to study two physical parameters which are electric field and pressure.

## I. INTRODUCTION

In order to model the circuit interruption, we need to determine the electric field and the pressure which exists inside the cartridge fuse. Electric field is measured in six points along the arc column and pressure on the cartridge wall in two perpendicular directions.

## II. EXPERIMENTAL SET-UP

### II.1 Experimental fuse

To obtain repeated fuse operations, a prototype fuse has been elaborated. The fuse element is a simple silver strip stretched between the end caps, and placed in a Celoron® cartridge.

The fuse element, figure 1, is a pure (99.95 %) silver strip. Its cross-section is  $7.5 \times 0.105 \text{ mm}^2$ . It has three reduced sections of  $0.5 \times 0.105 \text{ mm}^2$ .



Figure 1 : Fuse element  
 length = 70 mm, width = 7.5 mm,  
 thickness = 0.105 mm

The filler is a silica sand with a  $350 \mu\text{m}$  average granulometry. It contains less than 0.2 % impurities and is compacted at 1.68 by a standard technique.

In order to have similar results as these observed in industrial fuses, from thermal strength  $Pt$  point of view, we use a capacitor bank providing a 3 500 J energy to the fuse. It delivers a 12 ms, 1 800 A pulse. The obtained fulgurite is of about 31 mm long. The experimental set-up is presented on figure 2.

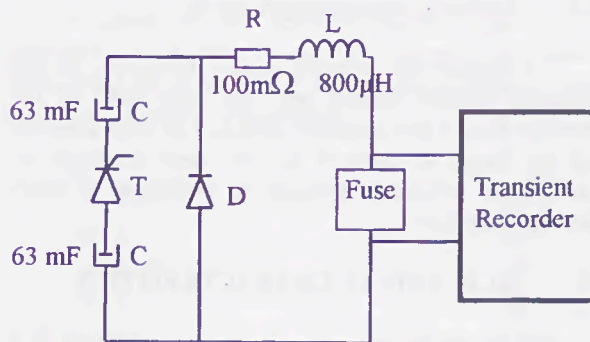


Figure 2 : Experimental set-up.

Current, voltages and pressures are measured by a transient recorder which is compound of two racks 6810 LeCroy (8 channels,  $f_{\text{max}} = 1 \text{ MS/s}$ ) and/or of a National Instruments card AT-MIO-16E2 (8 channels,  $f_{\text{max}} = 62.5 \text{ kS/s}$ ). Electrical characteristics are presented on figure 3.

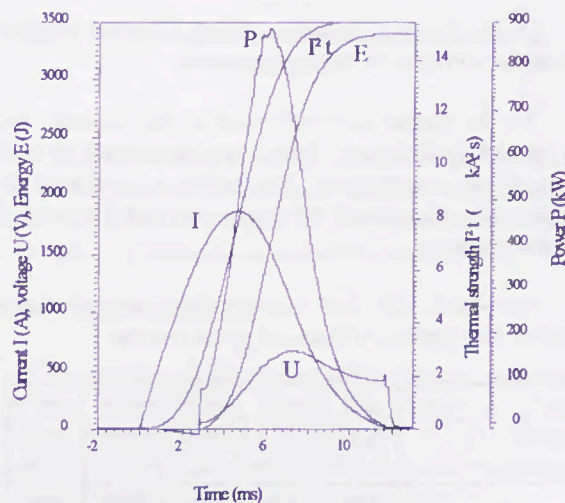


Figure 3 : Electrical characteristics versus time.

## II.2 Electric field measurement set-up

To measure the electric field in six points of the arc, the probes are 90  $\mu\text{m}$  diameter tungsten wires. All the probes are referenced to the cathode of the fuse. They are placed on both sides of the notches. We do not observe any difference between fuses with or without probes in the point of view of electrical characteristics  $U(t)$ ,  $I(t)$  and in non electrical parameters such as fulgurite dimensions and masses.

## II.3 Pressure measurement set-up

To measure the pressure in two directions, we use miniature sensors placed into the inner wall of the cartridge fuse. Their sensitive area is 5.55 mm diameter and the range is from 0 to 250 bars relatively to atmospheric pressure. Pressure is measured at sand-cartridge interface.

## III. ELECTRICAL CHARACTERISTICS

For all the 89 tests, the prearcing is of about  $(2.9 \pm 0.1)$  ms. At the end of the prearc, the energy reaches to 3 J and the  $I^2t$  to 2 000  $\text{A}^2\text{s}$ . Then, arc is established. It starts by a very short explosion phenomena which lasts about 50  $\mu\text{s}$ ; this value is in agreement with this of Chikata et al. [1]. They observed that at arc ignition, the plasma consists of ionised silver vapours during about 10  $\mu\text{s}$ , and then the arc burns in silica vapours. Then, the arcing period continues 9 ms. At the end, the energy reaches up to 3 375 J and the total  $I^2t$  to 15 400  $\text{A}^2\text{s}$ .

## IV. ARC COLUMN ELECTRIC FIELD

On the figure 4, the total voltage  $U$  across the fuse and probe voltages  $V_i$  are presented.

All the probes are referenced to the cathode and are spaced 3 mm apart. They are positioned at both sides of the constriction. The probe 1 is placed on cathode side, the probe 4 on the notches and the probe 7 on anode side.

Burn-back rate and electric field are calculated between two probes. Values are given in table 1.

	v21	v32	v35	v56	v67
v (m/s)	3.40	2.95	2.96	3.09	3.41
$u_v$ (m/s)	0.29	0.38	0.31	0.32	0.21
	E21	E32	E35	E56	E67
E (kV/m)	44	38	29	36	45
$u_E$ (kV/m)	4	3	2	3	4

Table 1 : Burn-back rate  $v$  and electric field  $E$  calculated between two probes.

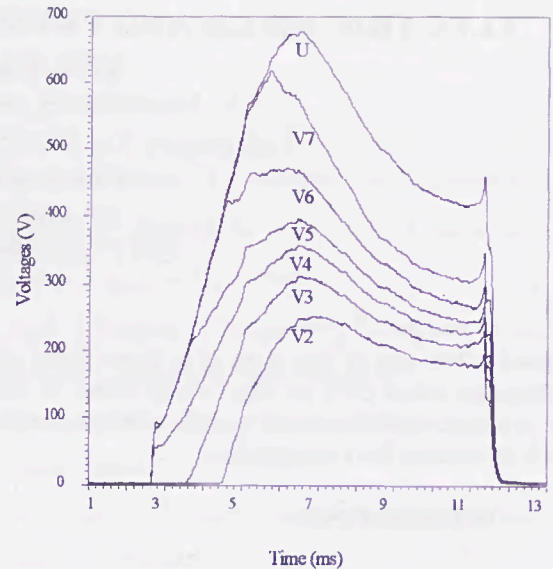


Figure 4 : Voltage  $U$  across the fuse and probe voltages  $V_2$  to  $V_7$  versus time.

For the first 6 mm, here and there of the constriction, the arc seems to go slower than after. This is due to the explosive arc ignition during which the arc spreads out in 3 directions (longitudinal, transversal and vertical ones). Next, during the burn-back phase, arc propagation is essentially a longitudinal one and the rate reaches up to 3.4 m/s.

At the same time, electric field evolution is observed. At 3 mm from the notch zone, electric field is about 29 kV/m, then it regularly increases up to 45 kV/m, 6 mm farther. To know if fuse arc can be considered as a wall-stabilised arc, arc channel width and thickness are measured. Their values are given in table 2.

	p1	p2	p3,p5	p6	p7
width (mm)	8	9.5	12	9.5	8
thickness (mm)	2.5	3	4	3	2.5

Table 2 : Arc channel width and thickness.

The product of electric field by arc channel width is constant, and this of electric field by arc channel thickness also. So, fuse arc can be treated as a wall-stabilised arc. These observations are in agreement with Ranjan & Barrault [2] and Daalder & Schreurs [3].

## V. PRESSURE MEASUREMENTS

Pressure measurements are performed on the inner wall of cartridge with two quartz pressure sensors (KISTLER 601A). Sand thickness between vertical and transversal sensors and fuse element are 10 mm and 6.25 mm respectively (figure 5).

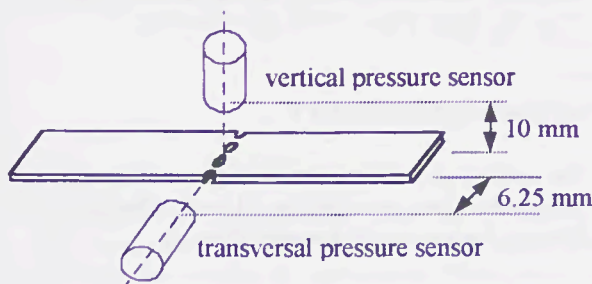


Figure 5 : Location of vertical and transversal pressure sensors.

A typical example of experimental results is given on figure 6.

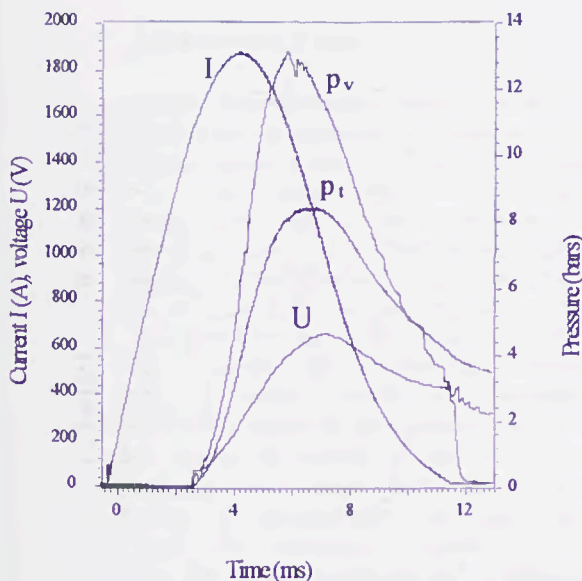


Figure 6 : Vertical  $p_v$  and transversal  $p_t$  pressures observed, at sand-cartridge interface, for a 1 800 A maximum current pulse.

Vertical pressure maximum is reached about 3.3 ms after arc ignition, its value is  $(1.5 \pm 0.2)$  MPa. We have observed that vertical pressure maximum and power maximum are simultaneous. Transversal pressure maximum comes 600  $\mu$ s later and reaches  $(0.8 \pm 0.1)$  MPa.

Pressure propagation into the sand cannot be obtained from these experimental results because two factors have to be taken in account : the sand thickness

is not the same in the two directions and the arc channel has a thickness of about 4 mm in front of transversal sensor while it has 12 mm width in front of the vertical one.

Nevertheless, we can note that the ratio of the vertical pressure to 10 mm (distance between sensor and fuse element) is equal to the ratio of the transversal pressure to 6.25 mm, during the increase.

After arc extinction, a residual pressure of about 0.2 – 0.4 MPa, exists.

A zoom on the pressure during prearcing is presented on figure 7. As we observe the same phenomena on vertical and transversal pressures, only transversal pressure is presented.

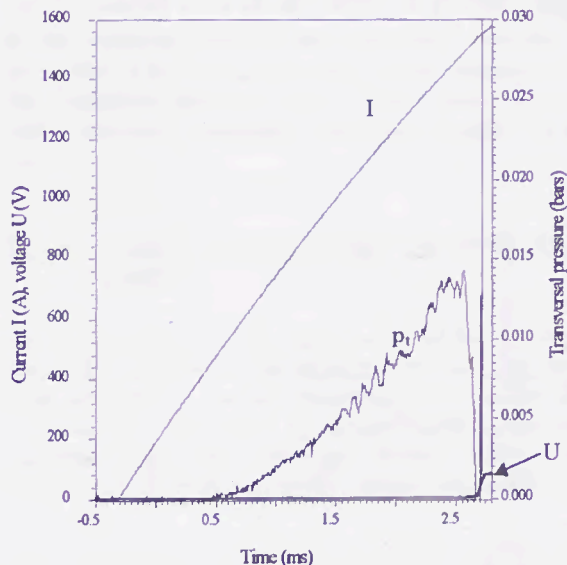


Figure 7 : Transversal pressure versus time, during prearcing.

First, we observe a regular increase of the pressure due to the heating of the fuse element constrictions. Then, 200  $\mu$ s before arc ignition, the pressure falls. This fall results of a local rearrangement of sand grains.

## VI. CONCLUSION

The electric field and pressure values obtained with this experimental set-up are similar to these obtained by other authors [2], [3] and [4], [5]. These values result from validating tests of the experimental set-up and will be used to model interruption circuit.

Especially, the measurement of low pressure existing during prearcing has been done (figure 7) and the meaning of this pressure evolution is given. With this set-up, we will be able to observe phenomena which happen when a critical current  $I_2$  is applied to the fuse.

## REFERENCES

- [1] CHIKATA T., UEDA Y., MURAI Y., MIYAMOTO T., 'Spectroscopic Observations of Arcs in Current Limiting Fuse Through Sand', 1976, International Conference on Electrical Fuses and their Applications (1 : 1976 : Liverpool, Great Britain), 1976, 114-121
- [2] RANJAN R., BARRAULT M. R., 'Axial Electric-Field Measurements of D.C. Arcs in Current-Limiting Fuses', Proc. IEE, 1980, 127 ; 3, 199-202
- [3] DAALDER J. E., SCHREURS E. F., 'Arcing Phenomena in High Voltage Fuses', 1983, Eindhoven, EUT Report 83-E-137, ISBN 90-6144-137-4
- [4] LIPSKI T., 'Generation and Propagation of the Pressure Due to the Fuse-Element Disintegration in H.B.C. Fuses', Gas Discharges and their Applications (8 : 1985 : Oxford, United Kingdom), 1985, 87-90
- [5] JAKUBIUK K., LIPSKI T., 'Dynamics of Fulgurite Formation During Arcing in HRC Fuses', J. Phys. D : Appl. Phys., 1993, 26, 424-430

## ACKNOWLEDGEMENT

The authors gratefully acknowledge the financial and technical support provided by Alstom, Electricité de France, Ferraz and Schneider Electric.

# MEASUREMENT OF ELECTRON DENSITY IN A HIGH-VOLTAGE FUSE ARC

M.A. Saqib and A.D. Stokes  
School of Electrical and Information Engineering  
University of Sydney, NSW 2006 Australia

B.W. James and I.S. Falconer  
School of Physics  
University of Sydney, NSW 2006 Australia

**Abstract:** Stark broadening of the Si II doublet at 504.1 nm and 505.6 nm has been used to estimate the electron density in two model silica-sand-filled high-voltage, high breaking capacity fuses. For a 240 mm long fuse which successfully interrupted a test circuit set up to deliver a 4 kA prospective current, the electron density fell from  $\sim 2 \times 10^{18} \text{ cm}^{-3}$  shortly after arc initiation to  $\sim 1 \times 10^{18} \text{ cm}^{-3}$  just before current zero; for a 112 mm long fuse and a prospective current of 1.4 kA the electron density was  $\leq 1 \times 10^{17} \text{ cm}^{-3}$  for the duration of the arc.

## I. INTRODUCTION

High-voltage, high breaking capacity (HBC) fuses are an important component in modern electrical energy distribution systems. They are considered superior to the equivalent circuit-breaker for interrupting short-circuit currents because of their short operating time, cost-effectiveness, and self-fault-sensing characteristics [1,2]. The pre-arcing behaviour of these fuses is now well-understood, but a lack of information as to the characteristics of the fuse arc plasma has prevented researchers developing a model which will quantify the behaviour of this phase of the operation of the fuses. Although empirical models of the arc have been developed [3] and have been used for some calculations, it is necessary to know the arc temperature and electrical conductivity, which depend on the electron density and temperature of the arc plasma, to model the arc [4]. The lack of knowledge of arc plasma parameters such as electron density and temperature is particularly acute in the case of HBC fuses which are packed with sand - usually silica sand - to absorb the arc energy.

Although there have been a number of studies to determine plasma temperatures during fuse arcing, there have been few measurements of electron density in the arc plasma. Chikata *et al.* [5] replaced an opaque fuse holder with a Pyrex glass tube in order to observe the visible radiation from the sand-filled fuse arc, and from Stark broadening of silicon

lines obtained electron densities of the order of  $10^{18} \text{ cm}^{-3}$ . Cao [6] used an arc in ice to provide access to the radiation emitted, and measured densities of the order of  $10^{18} \text{ cm}^{-3}$  from the Stark broadening of the hydrogen Balmer lines. These measurements were, however, integrated over the duration of the arc.

## II. STARK BROADENING OF SPECTRAL LINES

As a consequence of the long range of the Coulomb force the collisional broadening of spectral lines from moderately ionised plasmas such as the fuse arc plasma is dominated by the collisions of charged particles with the emitting atoms. This *Stark broadening* is given for singly ionised atoms by [7,8]

$$\Delta\lambda = 0.2 \left[ 1 + 1.75 \times 10^{-4} n_e^{1/4} \alpha \left( 1 - 0.11 n_e^{1/6} T^{-1/2} \right) \right] 10^{-16} w n_e \quad (1)$$

where  $\Delta\lambda$  = half width of the Stark broadened line in nm

$n_e$  = electron density in  $\text{cm}^{-3}$

$T$  = plasma temperature in kelvin.

The constants  $\alpha$  and  $w$  are characteristic of the transition of interest, and depend weakly on the plasma temperature. They are tabulated in Griem [9].

## III. THE EXPERIMENT

The experimental set-up for these measurements was identical to that used for the fuse arc electron temperature measurements discussed elsewhere at this conference [10]: indeed the data from which the electron density was deduced were obtained from the spectra which had been taken primarily for these electron temperature measurements. Two experimental versions of a silica-sand-filled fuse, cylindrical in shape with a 0.55 mm diameter uniform silver wire stretched along its axis, were constructed for these measurements. One was 240 mm long with an inside diameter of 43.7 mm (the

long fuse); the other 112 mm long with an inside diameter of 59.5 mm (the short fuse). (Commercial fuses use a somewhat different design to ensure the current goes to zero well before reaching its maximum value and that reignition does not occur.) A 6 kV, 50 Hz waveform was applied to the fuse by closing the pneumatically-driven mechanical make switch MS1 in the synthetic test circuit shown in Fig 1; the values of L and C in this circuit were set to give a prospective current of 1.4 kA for the short fuse, and 4 kA for the long fuse. The make switch MS2 in this circuit is switched to crowbar the fuse in the test circuit at current zero in case the fuse malfunctions. The voltage across the fuse was measured with a Tektronix P6015, 20 kV, 1,000 $\times$ attenuation high voltage probe; the current with a 190.8 A/V shunt. A Nicolet Pro 42C digital oscilloscope [11] was used to record these signals, as well as a reference pulse to indicate the time at which the arc spectra were recorded.

The arc spectra were recorded with a Princeton Applied Research Model 1460 Optical Multichannel Analyser (OMA), a spectroscopic system in which the spectrum is recorded by a linear photodiode detector array which is coupled to the exit plane of the monochromator by an image intensifier which can be gated "on" by a high voltage pulse. An optical fibre, inserted in the fuse body to touch the fuse element, was used to transfer light from the arc plasma to the OMA [12]. A 62.5  $\mu$ m core diameter multimode silica fibre was used as this material should have negligible effect on the arc characteristics. The other end of the fibre was located at the centre of the 25  $\mu$ m entrance slit of a Jarrell-Ash MonoSpec 27 Monochromator [13], which spectrally dispersed the arc radiation.

The OMA was run in the gated mode, synchronised to the triggering of the fuse test circuit. The experiment is initiated by a pulse provided by the OMA, which triggers the closing of the pneumatically operated make switch MS1 (Fig 1). This pulse is delayed to trigger the high-voltage pulser which gates "on" the image intensifier for a few  $\mu$ s at an appropriate time during the arc. This procedure is necessary to synchronise the "read" cycle of the OMA with the operation of the test circuit. The timing circuitry for this experiment is shown in Fig 2. (The switch MS1 closes around 65 ms after activation, and there is a further delay of 1-6 ms before the arc is initiated, depending on the fuse used and the prospective current.)

#### IV. AN ESTIMATE OF THE ELECTRON DENSITY

The width of the spectral lines recorded in the course of the electron temperature measurements which we are reporting at this conference [10] is such that we should be able to estimate an upper limit to the contribution of Stark broadening to the line width. This should, in turn permit the estimation of an upper

limit to the electron density in the plasma. Observation of the width of the individual spectral lines acquired at earlier times during the arcing of the long fuse, which were significantly broader than those observed for the short fuse, confirm that the line width is, at least in some cases, broader than the instrumental resolution of the monochromator used. The Doppler broadening corresponding to the electron temperatures we have measured from the relative intensity of Si II spectral lines [10] is  $< 0.01$  nm, and will not contribute significantly to the line width. Thus a deconvolution of the instrumental width of the monochromator used from the measured line width should enable the contribution of Stark broadening to be determined and an estimate made of the electron density.

Figure 3 shows the arc spectrum recorded 1.2 ms after arc initiation for the long fuse, and Fig 4 an expanded view of the region of the spectrum around the Si II doublet at 504.1 nm and 505.6 nm for which the line width measurements were made. (This doublet was chosen for the line width measurements as its components had the minimum separation of the Si II doublets in the spectrum shown in Fig 3.) Note the intense continuum emission in Fig 3, which is presumably due to thermal emission from the heated fulgarite surrounding the fuse arc. Calculating the contribution of the Stark broadening to the measured line width is complicated as we observe not a single line, but two Si lines separated by 1.5 nm which were not resolved. The following procedure was adopted to estimate the Stark broadening: the sum of the instrumental half width and the separation of the lines was subtracted from the measured width of the Si II doublet. The instrumental profile of the OMA was determined from the spectrum of a low-pressure Hg discharge lamp. This conservative approach is valid when deconvolving lines which exhibit a Lorentzian line profile [14], which is a good approximation for Stark broadening [7]. The noisy signals, the strong continuum emission and the broad effective instrumental profile for these measurements justify this simple approximation.

Table I - Estimated electron density at various times for the long fuse at 4 kA prospective current

Arcing time (ms)	0.83	0.99	1.20	1.44
Half width (nm)	6.7	5.7	5.0	5.3
Corrected half width (nm)	2.8	1.8	1.1	1.4
Electron density ( $\times 10^{18}$ cm $^{-3}$ )	2.0	1.3	0.7	0.9

## V. RESULTS AND CONCLUSION

Electron densities estimated using the above procedure on our data for the long fuse at 4 kA prospective current are shown in Table 1. These results demonstrate that, shortly after arc ignition the density is greater than  $10^{18} \text{ cm}^{-3}$ , and decreases during the arc, to  $\sim 10^{18} \text{ cm}^{-3}$ . The density was so low for the short fuse at 1.4 kA prospective current that it was possible only to show that the electron density was  $\leq 10^{17} \text{ cm}^{-3}$ .

These results confirm that it should be possible to make reliable measurements of the electron density of the arc plasma in a silica-filled HBC fuse from the Stark broadening of Si II spectral lines provided a grating of higher resolution is installed in the monochromator for the line width measurements.

### Acknowledgments

We are grateful for Greg Toland's assistance in maintaining and running the Electrical Engineering Department's High Voltage Lab.

### References

- [1] E. Jacks, "High Rupturing Capacity Fuses", E. & F.N. Spon Ltd., London, 1975.
- [2] V.K. Mehta, "Principles of Power System", S. Chand & Company (Pte.) Ltd., New Delhi, 1987.
- [3] K.K. Namitokov and Z.M. Frenkel, "Influence of the constructional features of the fusible element on arc processes in fuses", *Elektrotehnika*, vol. 55, no. 9, 1984, pp 59-61.
- [4] Z.M. Frenkel, "The calculation of the parameter of the plasma of the arc in a fuse", Proc. of the fourth ICEFA, Nottingham, UK, 1991, pp. 235-240.
- [5] T. Chikata, Y. Ueda, Y. Murai and T. Miyamoto, "Spectroscopic observation of arcs in current-limiting fuse through sand", Proc. ICEFA, Liverpool, England, 1976
- [6] L. Cao, "The ablation-stabilised arc, the free-burning arc and their radiation behaviour", PhD thesis, The University of Sydney, 1991.
- [7] R. H. Huddleston and S.L. Leonard, "Plasma Diagnostic Techniques", Academic Press, New York, London, 1965.
- [8] G. Traving, "Über die Theorie der Druckverbreiterung von Spektrallinien", G. Braun, Karlsruhe, 1960.
- [9] H.R. Griem, "Plasma Spectroscopy", McGraw-Hill Book Company, 1964.
- [10] M.A. Saqib, A.D. Stokes, B.W. James and I.S. Falconer, "Arc temperature measurement in a high-voltage fuse", Proc. of the sixth ICEFA, Turin, Italy, September 1999.
- [11] Nicolet Pro Digital Oscilloscopes, Operation Manual, Nicolet Instrument Corporation, Madison, USA, 1991.
- [12] Optical Multichannel Analyser, Model 1460, Preliminary Operating Manual, Revision D, Princeton Applied Research Corp., 1986.
- [13] Jarrell-Ash MonoSpec 27 Monochromator/Spectrograph, Models 82-497, 82-498, 82-499, Operator's Manual, Allied Analytical Systems, Waltham, MA 02254, 1985.
- [14] A.P. Thorne "Spectrophysics", Chapman & Hall, London, 1974.

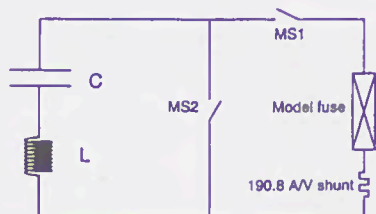


Fig. 1. Synthetic test circuit.

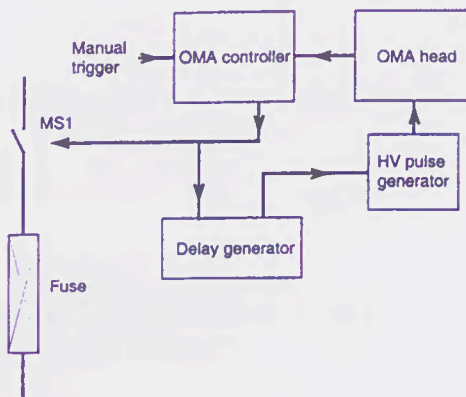
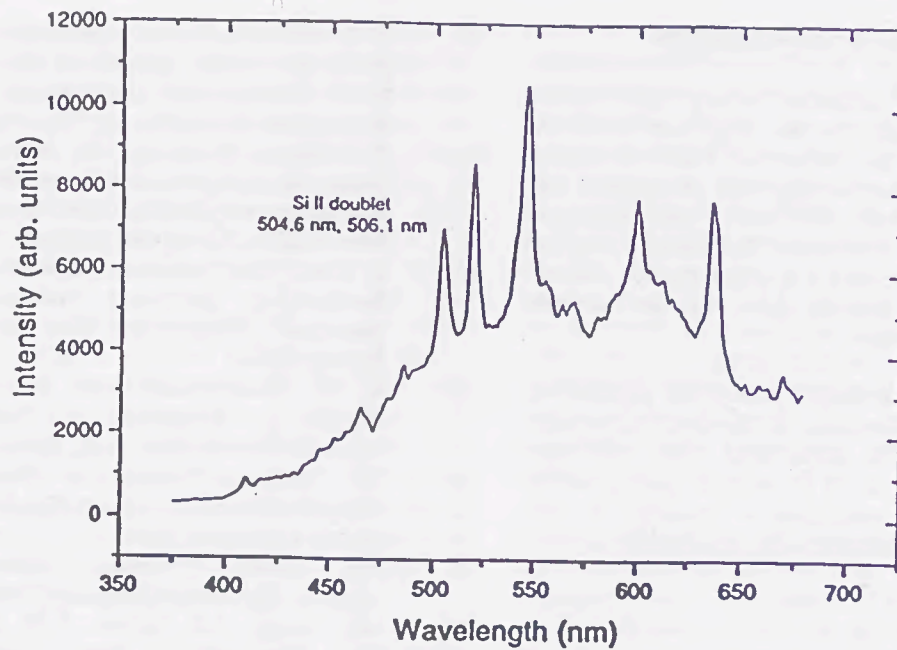
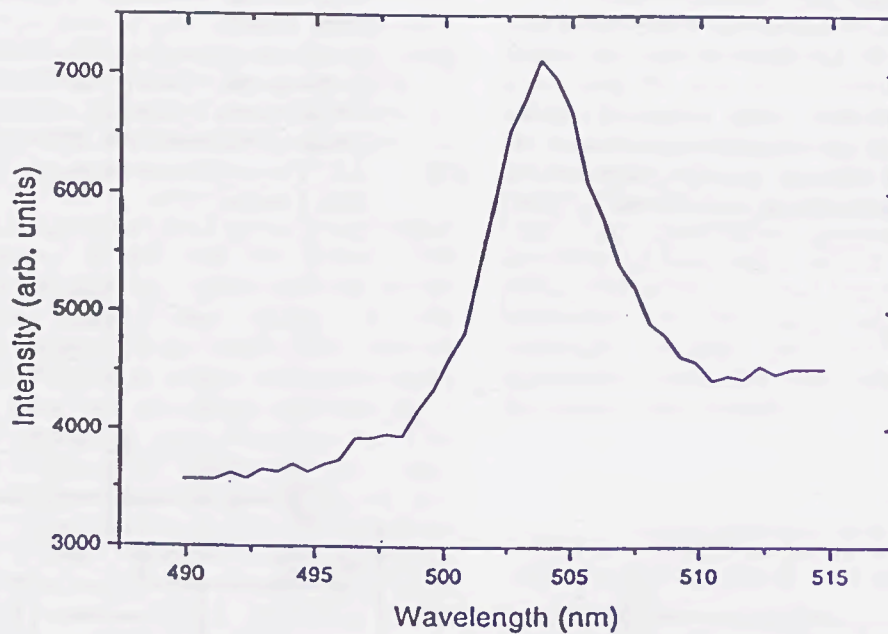


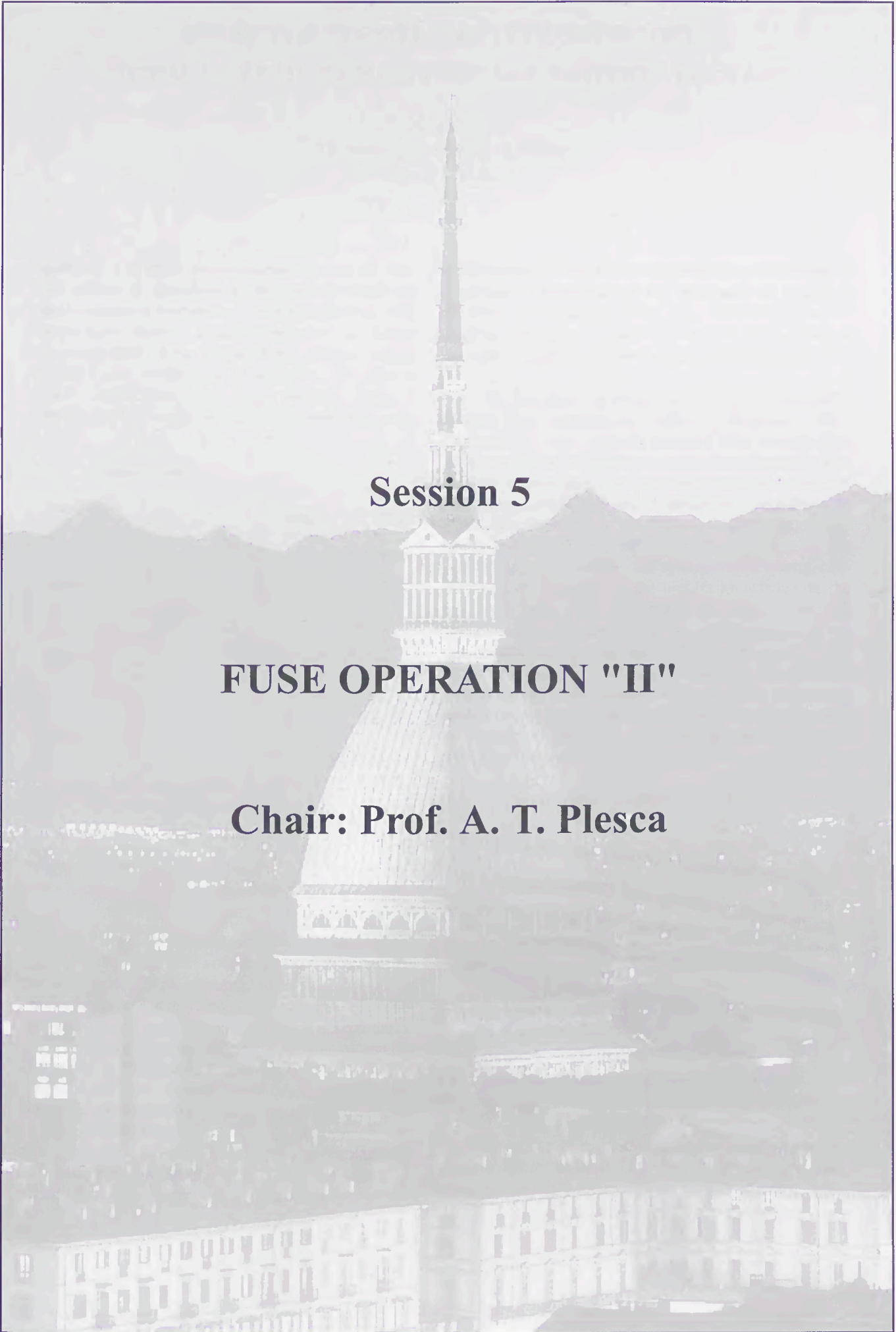
Fig. 2. Triggering circuit for time-resolved spectroscopy.



**Fig. 3.** Spectrum of the arc of a silica-sand-filled HBC fuse 1.2 ms after arc initiation



**Fig. 4.** Expanded view of the region of the spectrum shown in Fig. 3 around the Si II doublet at 504.6 and 506.1 nm.



**Session 5**

**FUSE OPERATION "II"**

**Chair: Prof. A. T. Plesca**



# EFFECT OF FUSE ELEMENT CONFINEMENT ON THE RATE OF RISE OF FUSE ARC IGNITION VOLTAGE

A. Wolny  
Technical University of Gdańsk  
Gdańsk - Poland

**Abstract** The effect of confinement on fuse arc ignition voltage is discussed. It has been demonstrated that consecutive disruptions in the fuse element differ due to the increase in metal temperature. Two factors are responsible for the course of arc ignition voltage: pressure and deformation of segments. Disrupts in nylon confinement with long modulus point to insufficient knowledge on the fuse element rupturing.

## I. Introduction

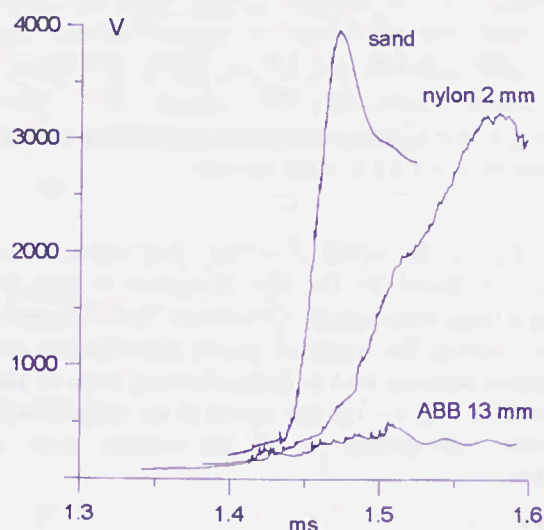


Fig. 1 Fuse arc ignition voltage  $I_p = 2.2$  kA, copper fuse element  $0.36$  mm  $\varnothing$  in various confinements.

Discussion on mechanisms of fuse element rupturing and arc ignition voltage generation cannot be yet concluded, for all presented ideas still show many imperfections. There is no doubt that fuse elements rupture at sufficiently high currents in accordance with a certain modulus defined experimentally many years ago by Nasilowski [1]. However, even the latest theories [2] are unable to prove rationally the dynamics of rupturing, initial geometry of breaks, the energy involved in the proces, or the arc development in disruptions. In spite of difficulties in explanation of differences in the rate of rise of the fuse arc ignition voltage under various conditions, when the

consideration of effect of the fuse element surroundings is neglected, a temptation of the application of a slightly modified old Baxters theory [3], describing the arc ignition voltage as a simple product of the number of disruptions and the arc root voltage, is still alive [4].

The fact that fuse arc ignition voltages measured for similar fuse elements in different enclosures differ substantially, Fig. 1, can be matched with the only possible conclusion: the voltage per gap must depend on fuse element confinement. However, the maximum number of created ruptures should not be questioned. It is difficult to relate this number to anything else than the energy comprised in the fuse element, thus influence of the surroundings is doubtful. In spite of such strong confirmation of the belief in the present knowledge on the fuse arc ignition rupturing, anxiety should be expressed, based on some experiments of the author presented below, demonstrating that the observations used for the recognised theories could be incomplete. In fact, the foundations of actual theories are static. Even the last report of Gomez [4] only provides static X-ray photographs of fulgurites. But are the disrupts always created randomly or maybe in a special order?

## II. Current commutation fuses

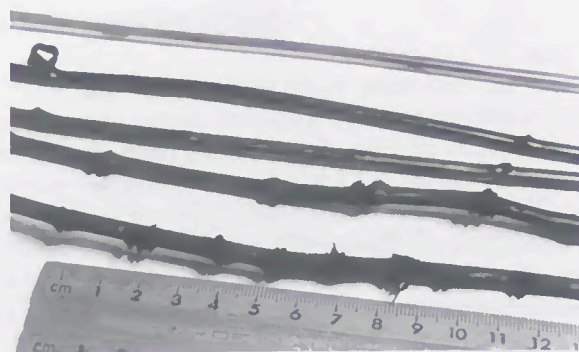


Fig. 2 Double nylon tube confinement of copper fuse elements  $0.36$  mm  $\varnothing$  after current commutation  $I_p = 2.2$  kA.

Above, in Fig. 2, photographs of nylon tubes applied as confinements of thin copper fuse elements of a current commutating fuse, after the fuse operation, and current

take-over by the parallel varistor, are presented. Clearly visible regular breaks in the tubes can be noticed. The modulus of rupturing is of approximately 17 mm. The fuse elements were 0.36 mm in diameter, and the prospective current was of 2.2 kA giving the cut-off current density approximately of 12 kA/mm<sup>2</sup>. The presented confinement consisted in two layers: the outer tube, 5 mm in the external diameter, which contained well fitted inside another nylon tube, 2 mm in the internal diameter. The confinement length varied from 0.15 m to about 1 m.

The modulus of confinement rupturing is completely different from that defined for the fuse element striation, which for the diameter of the applied wire, followed Nasilowski [1], should be as short as about 1.3 mm. Even if creation of unduloids was supposed, when the modulus of rupturing was longer, the pictures could not match. Hence a question should be raised: does the observed pattern of confinement rupturing reflect that of the fuse element breaking by the moment of current commutation, ie, all the breaks created before commutation? If so, why these disrupts are created followed special pitch of 17 mm and not in aleatory points? Moreover, current commutation occurred at the voltage exceeding half of the arc ignition peak voltage. This means that the average distance between breaks should be shorter than double modulus of Nasilowski [1].

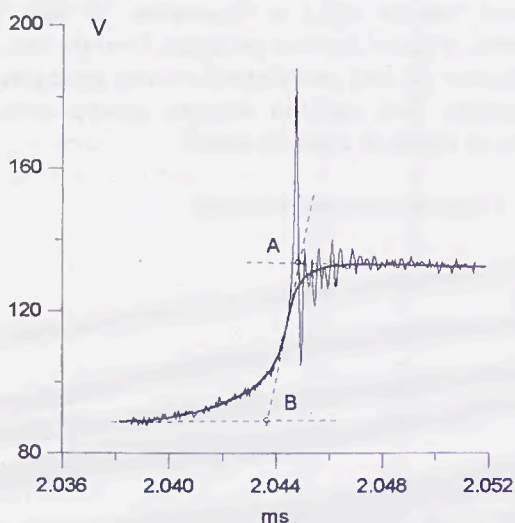


Fig. 3. Arc voltage of the first disruption in copper fuse element 0.36-mm  $\varnothing$ ,  $I_p = 1.5$  kA, ABB carrier

Other observations are also difficult to explain: damages in the breaks shown in Fig. 2 are very similar, suggesting that their "age" is comparable. Moreover, intermediate points in the enclosure, "ready" to disrupt in course of the rupturing process are missing. However, for lower currents a smaller number of disruptions is noticed.

At present it is difficult to answer these questions. They have been raised just to show that the knowledge on fuse arc ignition and the role of enclosure during that process are still unsatisfactory. Perhaps, such a state is due to the concentration of research on sand-filled fuses and exploding wires.

### III. Characteristic of typical disruptions

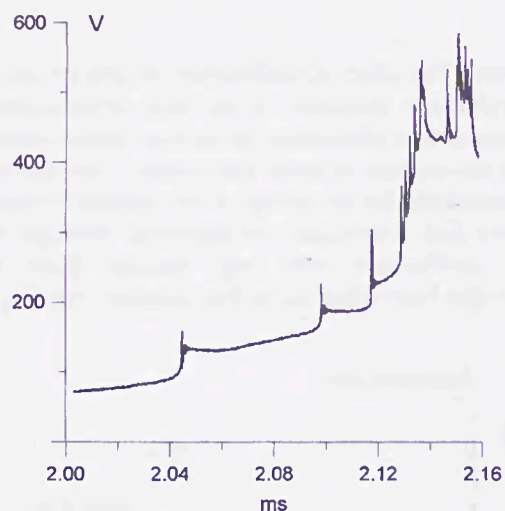


Fig. 4. Arc ignition voltage for copper fuse element 0.36-mm  $\varnothing$ ,  $I_p = 1.5$  kA, ABB carrier

In Fig. 3, the record of voltage drop between fuse terminals is shown, for the first disruption of fuse element in a large confinement. Continuous line of approximation, filtering the ripple of record digitalisation and the ignition peak, as well as broken lines of rates of rise are added. In Fig. 4, - the full record of arc ignition with consecutive disruptions up to the voltage peak is presented.

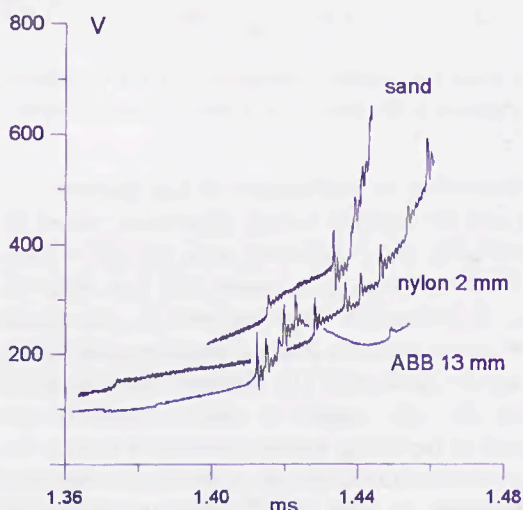


Fig. 5. Beginning of voltage traces presented in Fig. 1,  $I_p = 2.2$  kA, copper fuse element 0.36-mm  $\varnothing$

The first disruption can be considered typical for practically all confinements, since the first step on the voltage trace after zooming looks similarly for all confinements presented in Fig. 5. The time of the break creation, measured between points A and B is only 1  $\mu$ s, and quasi stabilisation of disruption voltage take approximately less than 2  $\mu$ s. Hence, assumed the process of stabilisation follows exponential curve, the time constant of this process is only about 0.5  $\mu$ s.

It is worth noticing that the voltage across the gap rises monotonously, after a very narrow voltage impulse, Fig. 3. This impulse does not play any practical role in the arc ignition voltage build-up. Its width is dependent on the effect of compensation of plasma heating in the gap by the increase of plasma pressure or gap extension.

It is interesting that such a picture is observed in the beginning of rupturing process, when the temperature of the liquefied fuse element is relatively low. The voltage traces of following disruptions show larger and larger ignition impulses, Fig. 5. Assumed, the voltage impulse is due to a low electrical conductivity of plasma in the new-born gap, the width of the impulse reflects the energy needed for heating up the gap plasma.

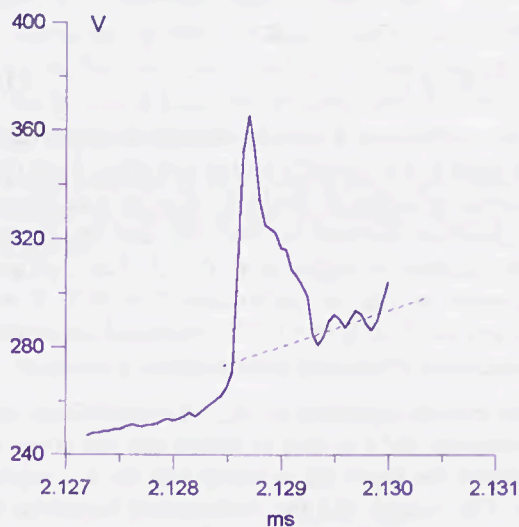


Fig. 6. Arc voltage of the fourth disruption in copper fuse element 0.36-mm  $\varnothing$ ,  $I_p = 1.5$  kA, ABB carrier

This energy rises as temperature or volume. The plasma volume in gap is defined by the gap itself, and the initial dimensions of gaps created in the process of rupturing is practically unknown. Most photographs, like those famous of Arai [5] deal with the fuse element frozen at a stage of fuse arc ignition process, which implies that a time has to pass from the instant of gap creation by the moment of

recording. The value of approximately 0.1–0.2 mm, reported many years ago by Kul'gavchuk and Novoskoltseva [6], observed in exploding wires, can be understood as very rough. There is no proof that gaps of consecutive rupturings are equal in the moment of their creation.

A reliable information on plasma temperature in the moment of gap creation is missing. However, it would be difficult to assume that this temperature should significantly differ between consecutive rupturings. Therefore, a possible explanation of the temporal widening of voltage impulses related to rupturing of fuse element, can be founded upon the fact, that in time, the temperature of liquefied fuse element rises, and viscosity of a hotter metal reduces, which can lead to enhanced deformation of necks in the process of rupturing, i.e., more fuse element material can be transformed into plasma.

The voltage step between points A and B in Fig. 3 is of 44.7 V, which is higher than the arc root voltage, and higher than that suggested by Gomez [4] for sand fuses. The rate of voltage rise between points A and B is 41.4 V/ $\mu$ s, and for the voltage impuls 254 V/ $\mu$ s.

The frequency of rupturing is not constant, at least in the beginning of the process, Fig. 4. For modest current densities two quite distinct time steps can be noticed, Fig. 6. In the beginning of the process the time between consecutive rupturings is reducing in each act of disruption, and finally stabilises at a value several times shorter than the initial one. This fact can be due to variation as time of the viscosity of liquid metal, or even presence of a thin hard core at the very beginning of rupturing process. It is true that the latter possibility was strongly criticised a time ago, nevertheless the sudden change of pace in the rupturing process requires a change of conditions, and only state of material can influence significantly properties of the fuse element.

#### IV. Large confinement

A large confinement plays practically the role of fuse element carrier. In such a case one can assume that the arc is ignited just in the air, and the plasma in gap between segments of the ruptured fuse element is marginally affected by confinement walls. The position of fuse element segments in the confinement is determined by the balance of forces due to the plasma pressure and inertia, since no support of the surroundings can be expected.

ABB expulsion fuse carriers with the internal diameter of about 13 mm were used. The fuse elements were made from a copper wire, 0.36 mm in the diameter, and from 50 mm to 200 mm in the length. Prospective currents were taken from the range of 1.2 kA to 12 kA, which ensured moderate current densities of several kA/mm<sup>2</sup>.

The pressure of plasma in gaps pushes the segments of liquefied fuse element axially. This causes deformation of segments and their dislocation. In very fast processes, such as those in exploding wires inertia prevents movement of segments, but when the current density is moderate the rupturing slows down, and dislocation of segments cannot be excluded, especially in the case of large confinements. Extensive deformation of the segmented fuse element in large confinements, affecting the arc ignition voltage can be expected. Probably, irregularities of the voltage curve in Fig. 4 are due to such mechanism.

Therefore, only deformation of fuse element segments may be considered the basic factor affecting arc ignition voltage in large confinements.

In sand fuses and in close confinements the position of fuse element segments is better controlled. Thus, the voltage traces are more regular, Fig. 2.

### V. Close confinement

In Fig. 7 traces of arc voltage referring to 2-mm  $\varnothing$  nylon confinement and 1-mm  $\varnothing$  PTFE enclosure rise at different rates and acquire different maxima, but the time to maximum is similar. Since the number of voltage steps is approximately conform to the modulus of rupturing of the fuse element, only plasma electrical conductivity in breaks can be responsible for the difference in shapes of voltage curves.

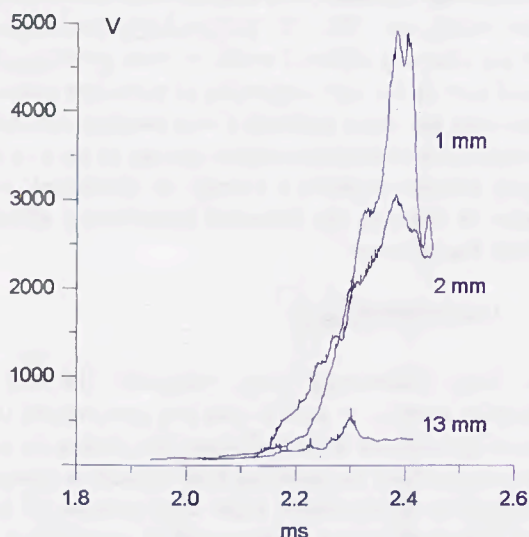


Fig. 7. Arc ignition voltage in close enclosures: PTFE 1-mm  $\varnothing$ , nylon 2-mm  $\varnothing$  compared to ABB carrier, copper fuse element 0.36-mm  $\varnothing$ ,  $I_p = 1.2$  kA.

In first instances the temperature of new-created plasma in gaps is connected with the boiling point of fuse element material, so only pressure can be considered the basic factor affecting electrical conductivity. Pressure in fuses is controlled by the confinement

diameter. Thus its effect can be evaluated in a simple way.

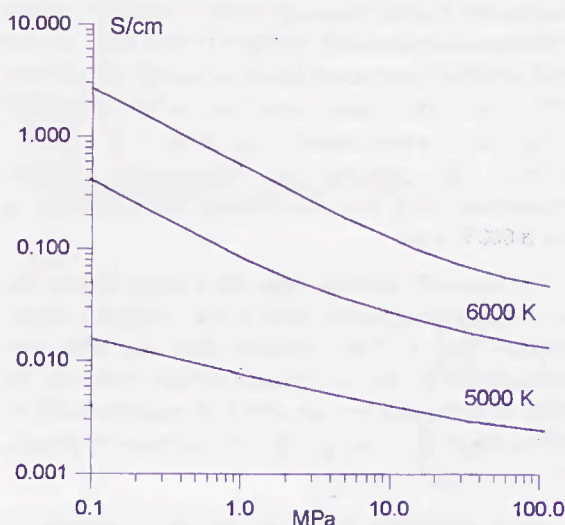


Fig. 8. Electrical conductivity of copper plasma at low temperature and high pressure

Rough characteristics of electrical conductivity  $\sigma$  of copper plasma for relatively low temperature, calculated after Kovitya [7], presented in Fig. 8 indicate very moderate reduction of  $\sigma$  by increase of pressure  $p$ . The function  $\sigma = f(p)$  may be approximated by a simple formula:

$$\sigma = k \cdot p^{-m} \quad (1)$$

The coefficients  $k$  and  $m$  depend on temperature. E.g. for 5000 K  $k = 0.00079$ , and  $m = 0.2705$ . With these coefficients, reduction of conductivity  $\sigma$  by half due to a tenfold pressure increase is observed, and the pressure  $100p$  brings about reduction of  $\sigma$  by 3.5. The coefficient  $k$  and power  $m$  rise as temperature. For 6000 K  $m = 0.4877$ , and for 7000 K  $m = 0.582$ . Increased temperature the conductivity  $\sigma$  becomes more sensitive to pressure.

The records presented in Fig. 7 roughly comply with this evaluation, for it is easy to notice that the larger the confinement the lower the pressure and the arc ignition voltage. The voltage and the confinement variations approximately follow formula (1). However it should be underlined that the larger the confinement, the stronger the effect of deformation of fuse element segments, and the voltage curve becomes more and more rugged. Hence the voltage can reduce faster than function (1). Prediction of arc ignition voltage on basis of calculation of pressure in flexible confinements is extremely difficult.

It was shown [8] that ablation of confinement is negligible in the arc ignition process.

One can conclude that mainly pressure is responsible for the arc ignition voltage in close confinements. The effect of deformation of segments is limited.

## VI. Sand fuses

In sand fuses the fuse element is practically immobilised, which facilitates prediction of its behaviour in the arc ignition process, but on the other hand, the complicated structure of filler makes difficult evaluation of pressure variation in disruptions. A virtual confinement may be introduced. However its diameter need not be constant. Influence of sand dilatation and condensation of metal vapour should be expected.

The effect of sand filler on fuse arc ignition voltage may be estimated by comparison of the voltage trace with a similar one recorded for a given regular capillary, Fig. 1. Applied of relation (1), and plasma temperature 5000 K, the virtual diameter of sand "confinement" would be comparable with the fuse element diameter, if no enlargement of diameter of the nylon confinement were considered.

## VII. Conclusions

- Initial course of fuse element rupturing process in all examined confinements is similar.
- Consecutive voltage steps due to fuse element rupturing differ one another probably because of rising temperature of liquid metal.
- The nature of effect of fuse element confinement on the fuse arc ignition voltage - time characteristics is related to plasma pressure and deformation of fuse element segments.
- Large modulus of rupturing of nylon confinement reveals deficiency of our knowledge on fuse arc ignition.

## Acknowledgement

In part the work has been done in frames of research project No 8T 10A 03411 financed by the Committee of Scientific Research in Poland.

## References

- [1] Nasilowski J.: Unduloids and striated disintegration of wires. Exploding wires. vol. 3. (ed. W.G. Chase and H.K. Moore) New York (USA): Plenum Press 1964, p. 295.
- [2] Jakubiuk K.: Two - stage mechanism of striated disintegration of fuse - wire. 5th Int. Conf. on Electric Fuses and Their Appl. Ilmenau (FRG), Sep. 1995, p. 273.
- [3] Baxter H.W.: Electric fuses. London (UK): Arnold 1950.
- [4] Gomez J.C. and P.M. McEwan: Experimental investigation of wall-stabilised arc mechanism of wires in fuse filler. 5th Int. Conf. on Electric Fuses and Their Appl. Ilmenau (FRG), Sep. 1995, p. 243.
- [5] Arai S.: Deformation and striation of silver wires. Int Conf. on Electric Fuses and Their Appl., Liverpool (UK), April 1984, p. 50.
- [6] Kul'gavchuk V.M and Novoskol'seva G.A.: X-ray study of kinetics of heating and evaporation of exploding wires. Sov. Phys., Techn. Phys. 1966 vol. 11, No. 3, p. 406.
- [7] Kovitya P.: Thermodynamics and transport properties of ablated vapours of PTFE, alumina perspex, and PVC in the temperature range 5000-30000 K. IEEE Trans. 1984, vol. PS-12, No. 1, p. 38.
- [8] Wolny A, and Stokes A.D.: Ignition of an electrical arc in a capillary: arc parameters in the initial period. Proc. IEE 1994

The first part of the document discusses the importance of maintaining accurate records of all transactions. It emphasizes that every entry should be supported by a valid receipt or invoice. The text also mentions the need for regular audits to ensure the integrity of the financial data.

In the second section, the author outlines the various methods used for data collection and analysis. This includes both primary and secondary data sources. The primary data is collected through direct observation and interviews, while secondary data is obtained from existing reports and databases.

The third section focuses on the statistical analysis of the collected data. It describes the use of descriptive statistics to summarize the data and inferential statistics to draw conclusions. The text also mentions the use of regression analysis to identify relationships between variables.

Finally, the document concludes with a summary of the findings and recommendations. It suggests that the current data indicates a positive trend in the market, but also highlights some areas of concern. The author recommends that further research be conducted to address these concerns and to explore new opportunities.

The second part of the document provides a detailed overview of the company's financial performance over the past year. It includes a breakdown of revenue, expenses, and profit. The text also discusses the company's financial ratios and compares them to industry benchmarks.

The third part of the document discusses the company's capital structure and its financing strategy. It mentions the company's debt-to-equity ratio and its plans for future financing. The text also discusses the company's risk management strategy and its efforts to diversify its investment portfolio.

The fourth part of the document discusses the company's human resources and its talent management strategy. It mentions the company's employee turnover rate and its efforts to attract and retain top talent. The text also discusses the company's training and development programs and its focus on employee well-being.

Finally, the document concludes with a summary of the company's overall performance and its outlook for the future. It suggests that the company is well-positioned to continue its growth and success in the coming years, provided it continues to focus on innovation and operational excellence.

# ASSESSMENT OF COMPLEX LOADING CYCLES AND ESTIMATION OF FUSE LIFE

R Wilkins  
Consultant  
Heswall, UK

H C Cline  
Gould Shawmut  
Newburyport, USA

**Abstract :** A new method of estimating the thermal response of fuses to complex loading cycles is described. The method is based on the use of the fuse transient thermal impedance, which can be estimated simply from its time-current characteristic. A procedure for estimating the rate of deterioration and hence the life is described, based upon the number and magnitude of straining events within a given cycle.

## I. INTRODUCTION

The long-term effects of thermal fatigue must be taken into account when selecting fuses for applications which have repetitive cyclic loads. This is particularly important with semiconductor fuses [1,2] which have small and fragile notches in their fuse elements.

Test data is normally obtained with a simple ON/OFF loading cycle such as that shown in Fig.1.

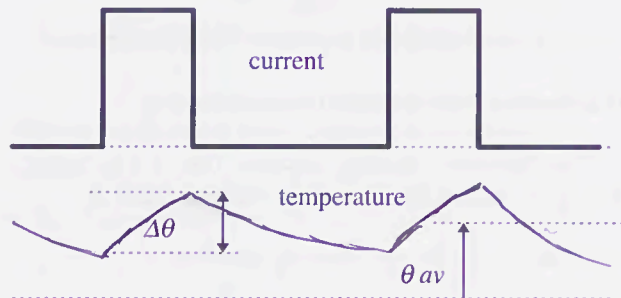


Fig.1 Fuse response to simple repetitive cycle.

For this cycle the best way to assess its severity is to compute the peak-to-peak temperature excursion  $\Delta\theta$  and the average temperature  $\theta_{av}$  of the hottest notch using a finite-difference or finite-element model to compute the fuse response. The number of cycles to failure can then be estimated using eq.(1), which is derived directly [2] from the Manson-Coffin law of mechanical fatigue.

$$N = \frac{K_{\theta}}{\Delta\theta^P \theta_{av}^Q} \quad (1)$$

The life is strongly affected by  $\Delta\theta$ , which produces a proportional thermal strain in the fuse element, but is only weakly dependent on  $\theta_{av}$ . The constant  $K_{\theta}$  depends on the mechanical construction of the fuse.  $P$ ,  $Q$  and  $K_{\theta}$  must be determined from test data by regression analysis.

Finite-difference or finite-element modelling programs are useful for special projects or investigations. However they require the full physical construction of each fuse to be supplied as data and the computations are too time-consuming to be incorporated into routine fuse selection programs, even using the fastest modern computers.

Routine selection of fuses for cyclic duty is often based upon the fuse time-current characteristic. For example, with a simple ON/OFF cycle, it may be required that the ON current does not exceed a certain fraction of the current which produces melting in a time equal to the ON time [3].

However, real applications very rarely use a simple ON/OFF cycle. Repetitive industrial processes have cycles consisting of several blocks of current at various levels and with durations from seconds to hours. Traction applications have even more complex loading profiles, which cannot be represented by an equivalent ON/OFF cycle. The cycle shown in Fig.1 contains only one **straining event** (strain reversal) within it, whereas a complex cycle may contain several such events, of different magnitudes, each of which contributes to the degradation of the fuse. The first step in assessing these cycles is to calculate the fuse thermal response, and a simple method for doing this, based upon the time-current characteristic, is given below.

## II. TRANSIENT THERMAL IMPEDANCE

The temperature response of diodes and thyristors to complex loading cycles has been calculated for many years using the transient thermal impedance curve, which is published for each device. This curve relates the device hotspot temperature to the power input, as follows :

$$\theta(t) = Z(t)P \quad (2)$$

$Z(t)$  is a function which increases from zero at  $t=0$  to a steady-state final value  $Z_{ss}$ . Using the same concept for a fuse, for a one-shot melting test from room temperature,

$$\theta_m = Z(t_m)R_m I_m^2 \quad (3)$$

where

$\theta_m$  = temperature rise up to melting point

$t_m$  = melting time

$I_m$  = current which produces melting in a time  $t_m$

$R_m$  = average fuse resistance during the melting period

Use of the average value  $R_m$  is an approximation, since the fuse power actually increases with temperature due to the positive temperature coefficient of the element metal. The average resistance over the melting period will vary with the waveshape of the temperature-time transient, but will typically be about 2.4 times the value at 20C.

The transient thermal impedance is then given by :

$$Z(t_m) = \frac{\theta_m}{R_m I_m^2} \quad (4)$$

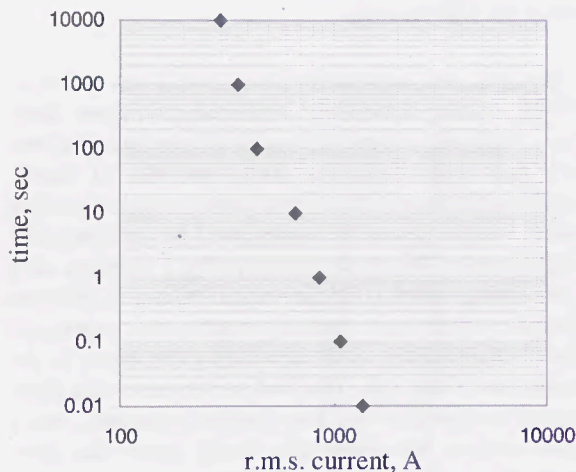


Fig. 2 Typical time-current characteristic

## II.1 Normalization

Assume that the 10000s point on the time-current curve represents a steady-state thermal condition and take the current at this point ( $I_{\infty}$ ) as a reference (base) value. This then gives

$$Z_{ss} = \frac{\theta_m}{R_m I_{\infty}^2} \quad (5)$$

Dividing (4) by (5) gives the normalised transient thermal impedance  $f(t)$  as

$$f(t) = \frac{Z(t_m)}{Z_{ss}} = \left[ \frac{I_{\infty}}{I_m} \right]^2 \quad (6)$$

$f(t)$  increases from 0 to 1 as time increases from zero to infinity, and the curve can be derived very simply from the fuse time-current characteristic. Fig.2 shows a typical time-current characteristic for a fast-acting fuse and Fig.3 shows the derived normalised transient thermal impedance curve. For each time value on Fig.2 the corresponding melt current  $I_m$  is known, and then the corresponding value of  $f(t)$  is calculated using (6).

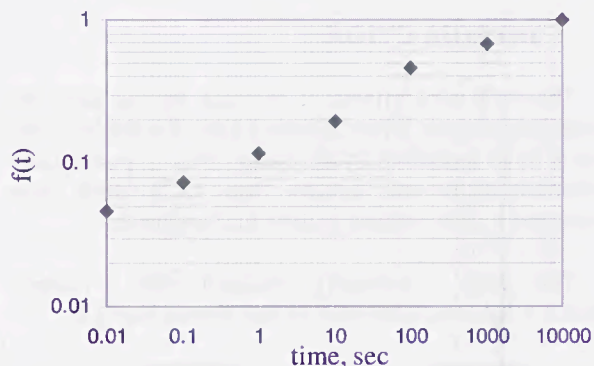


Fig.3. Transient thermal impedance derived from Fig.2

## II.2 Heating from an initial temperature $\theta_0$

The previous heating history (for  $t < 0$ ) gives  $\theta_0 = Z_{ss}P_0$  and so, for an average fuse resistance  $R$ ,

$$\theta(t) = \theta_0 + (P - P_0)Z(t)$$

$$\theta(t) = \theta_0 + (I^2 R - \frac{\theta_0}{Z_{ss}})Z(t)$$

$$\theta(t) = \theta_0 [1 - f(t)] + I^2 R Z_{ss} f(t)$$

This can be normalised by dividing by  $\theta_m (= R_m Z_{ss} I_{\infty}^2)$  to give the per-unit temperature rise as

$$\bar{\theta}(t) = [1 - f(t)]\bar{\theta}_0 + \alpha \bar{I}^2 f(t) \quad (7)$$

where the bar indicates a normalised (p.u.) value. Temperature is expressed as a fraction of the temperature rise to melting while current is a multiple of the 10000s current  $I_{\infty}$ .  $\alpha = R/R_m$  and is the ratio of

the average fuse resistance during the heating period to the average resistance from room temperature to melting.

### II.3 Response to a multipart cycle

Consider a cycle with  $N$  blocks of current as shown in Fig.4. During each block the r.m.s. current is constant.

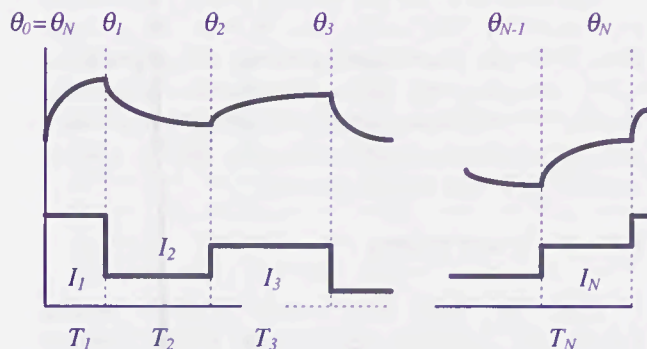


Fig.4 Fuse response to a complex loading cycle

Writing  $f(T_i) = f_i$  and applying (7) to each of the blocks in turn gives

$$\bar{\theta}_1 = (1-f_1)\bar{\theta}_N + \alpha f_1 \bar{I}_1^2$$

$$\bar{\theta}_2 = (1-f_2)\bar{\theta}_1 + \alpha f_2 \bar{I}_2^2$$

$$\bar{\theta}_k = (1-f_k)\bar{\theta}_{k-1} + \alpha f_k \bar{I}_k^2$$

...

This can be rewritten as the cyclic matrix equation

$1$	$0$	$\dots$	$0$	$-(1-f_1)$	$\bar{\theta}_1$	$= \alpha$	$f_1 \bar{I}_1^2$
$-(1-f_2)$	$1$	$\dots$	$0$	$0$	$\bar{\theta}_2$		$f_2 \bar{I}_2^2$
$0$	$-(1-f_3)$	$\dots$	$0$	$0$	$\bar{\theta}_3$		$f_3 \bar{I}_3^2$
$0$	$0$	$\dots$	$1$	$0$	$\bar{\theta}_N$		$f_N \bar{I}_N^2$
$0$	$0$	$\dots$	$-(1-f_{N-1})$	$1$	$\bar{\theta}_N$		$f_N \bar{I}_N^2$

which can be solved for the temperatures at the ends of each of the time blocks ( $\bar{\theta}_1 \dots$ ). The square coefficient matrix is very well conditioned.

The ratio of average fuse resistance within each time block to the average resistance during a melting test for this time actually varies from block to block, but in this simplified analysis an average value of  $\alpha$  has been used, assumed to apply over the whole cycle.  $\alpha$  then appears in the equations as a simple scaling factor. The temperatures can be initially calculated with  $\alpha=1$  and then scaled down as desired.

The resulting system of equations is linear. If very high currents are input the resulting per-unit temperatures can exceed 1, which corresponds to a value higher than the melting point. This is not allowable and can be dealt with by testing the results after the solution.

After the values of  $\bar{\theta}$  have been found, the actual shapes of the temperature waves within a current block can be calculated if desired using (7). However the waveshapes within a block are not needed in practice, just the temperatures at the start and finish of the block.

### II.4 Counting the number of straining events

If a **straining event** is defined by a transition from a PEAK to a TROUGH on the temperature-time wave, examination of many different cyclic temperature waves has shown that within any cycle with  $N$  blocks there is a minimum of 1 and a maximum of  $N/2$  straining events. An example is shown in Fig 5 below.

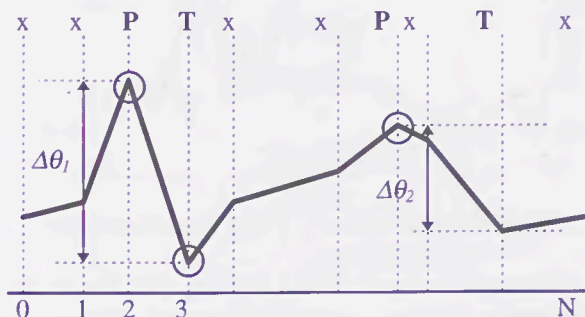


Fig.5 Temperature response with peaks and troughs

The response shown in Fig.5 contains 2 straining events with magnitudes  $\Delta\theta_1$  and  $\Delta\theta_2$ . In general the number and magnitude can be found by the following algorithm :

- a) scan all transition points and mark peaks with a 'P' and troughs with a 'T'. Otherwise mark with an 'x'. The number of straining events is equal to the number of peaks (or troughs).
- b) scan a second time and calculate the peak-to-peak temperature differences between each peak and the next trough ( $\Delta\theta_1, \Delta\theta_2 \dots$ ).

There is an ambiguity here, depending upon whether  $\Delta\theta$  is defined at the difference between a peak and a subsequent trough or vice-versa. i.e. 2 straining events within a cycle can be defined in 2 different ways. In this paper the start of an event is defined as the first peak or trough encountered within a cycle.

## II.5 Typical results

Fig. 6 shows the per-unit temperature (lower graph) response calculated using the normalised transient impedance curve of a 350A fuse used in a traction application. The current loading (upper curve in Fig.6) in this case was taken directly from measurements on a railway locomotive at 5 minute intervals over a 24-hour period, giving a duty cycle with 288 blocks of current.

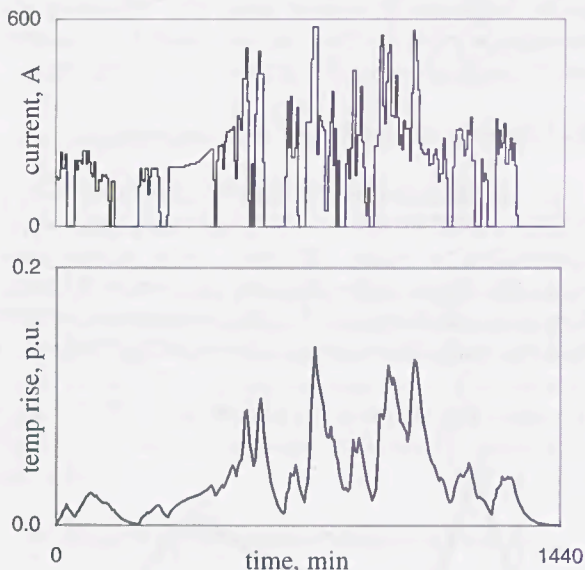


Fig.6 Thermal response of fuse to traction cycle

Although the cycle shown contains 288 blocks, the temperature response curve contains only 29 straining events.

## III. ESTIMATION OF FUSE LIFE

The average temperature rise of the fuse is assumed to depend on the r.m.s. current loading (as a fraction of the rated current), according to a power law. With this assumption eq.(1) becomes

$$N = \frac{K'}{\Delta\bar{\theta}^P \bar{I}_{rms}^Y} \quad (8)$$

For a simple ON/OFF cycle the **rate of deterioration** can be defined as the reciprocal of the number of cycles to failure. The rate of deterioration is therefore

$$r = \frac{I}{K'} \bar{I}_{rms}^Y \Delta\bar{\theta}^P$$

For a multipart cycle each straining event contributes to an increase in the rate of deterioration, according to its magnitude, and so the total rate is

$$r = \frac{I}{K'} \bar{I}_{rms}^Y [\Delta\bar{\theta}_1^P + \Delta\bar{\theta}_2^P + \dots]$$

and the number of cycles to failure becomes

$$N = \frac{K'}{[\Delta\bar{\theta}_1^P + \Delta\bar{\theta}_2^P + \dots] \bar{I}_{rms}^Y} \quad (9)$$

The value of  $K'$  for use with (9) must be determined experimentally. This can be done by tests with a simple ON/OFF cycle. The values of  $\Delta\theta$  are calculated using  $\alpha=1$ , absorbing the unknown value of  $\alpha$  into the constant  $K'$ . Alternatively, if finite-difference or finite-element methods are used to calculate the  $\Delta\theta$ s, these values can be used directly with (9).

## IV. CONCLUSION

Fuses are tested with simple ON/OFF loading cycles, but practical applications usually involve complex loading cycles. An approximate method has been described for evaluating the thermal response of a fuse using a normalised transient thermal impedance curve, derived from the fuse's known time-current characteristic. After the thermal response has been computed, the resulting life can be estimated, based upon the number of straining events produced by the cycle, and their magnitude. The method allows the severity of different loading cycles to be compared.

The main approximation in this method is that the fuse resistance is represented by an average value over the operating temperature range. For adequate life under cycling the peak-to-peak temperature excursions need to be kept relatively low, so this approximation is acceptable. For more accurate analysis full numerical modelling which takes the temperature-dependence of the element metal properly into account, must be used.

## V. REFERENCES

- [1] X.Z. Meng, "Lifetime predictions of miniature fuses and semiconductor protection fuses", Ph.D dissertation, Eindhoven University of Technology, 1995.
- [2] R. Wilkins, A. Wilkinson and H.C. Cline, "Endurance of semiconductor fuses under cyclic loading" Fourth International Conference on Electric Fuses and their Applications, Nottingham, 1991, pp 43-48.
- [3] G. Stevenson, "Cyclic loading of fuses for the protection of semiconductors", First International Conference on Electric Fuses and their Applications, Liverpool, 1976, pp 276-283.

# OVERLOAD AND RATING OPERATIONS OF HBC LOW VOLTAGE FUSES AT REDUCED HEAT TRANSFER

G. Nutsch, J. Blum, G. Jünemann, P. Linke, T. Reichelt  
 Technische Universität Ilmenau  
 Fachgebiet Plasma- und Oberflächentechnik  
 D - 98684 Ilmenau

**Abstract:** The compact mounting of fuse-links in more and more space-saving HBC fuse-rails and -switches leads to reduced heat transfer conditions for the fuse-links. While the time-current characteristic is not influenced, the rating operation is influenced due to the forced interdiffusion of solder and melting element materials. Especially, the temperature of the melting elements made of copper should not exceed 160°C in order to guarantee a life time higher than 48 hours in narrow boxes and at rating currents. Moreover, i) tests made with industrial fuses from different producers have shown that the usual 8-hour-test is not able to reflect completely the melting element behaviour, and that ii) the temperature of the upper blade contact can be used as a criterion for operating conditions of fuse-links within any chamber.

## I. INTRODUCTION

Low voltage HBC fuses operated in the past in open fuse bases, as well as in single-pole and as in three pole design. Due to the open construction, the temperature of the ambient air near the fuse-link is kept low by free convection. In accordance with these fuse-link operation conditions the time-current characteristic is related to an ambient temperature of 20°C ± 5°C according with DIN VDE 0636.

More recently, fuses are mounted in breaking fuse bases, fuse-rails or switch-disconnectors, and possibly in cable distribution cabinets, with reduced convection because of their slimline constructions. Therefore, the ambient temperature is increasing when the fuse-links are built in chambers with restricted convection.

In accordance with the statement in EN 60269-1 or IEC 269-1 the fuse should carry its rated current up to an ambient temperature of 55°C. However, there is no measurement procedure for this temperature. Moreover, the voltage drop over the entire fuse-link is not sensitive enough to reflect the changed conditions at the soldering points. It was the aim of this investigations to find out a measurement parameter which i) reflects sufficiently the thermal limit for diffusion processes of solders on the melting elements, and ii) is measurable very easily.

## II. TIME-CURRENT CHARACTERISTIC

This characteristic can be calculated with a simplified 2D-model using the Finite Element Method (FEM) and the ANSYS - Code. The results for a NH1-160 A fuse is shown in Figure 1. As is seen, the convection heat transfer has to be taken into account only for current intensities of  $1.25 \times I_{rating}$  and smaller.

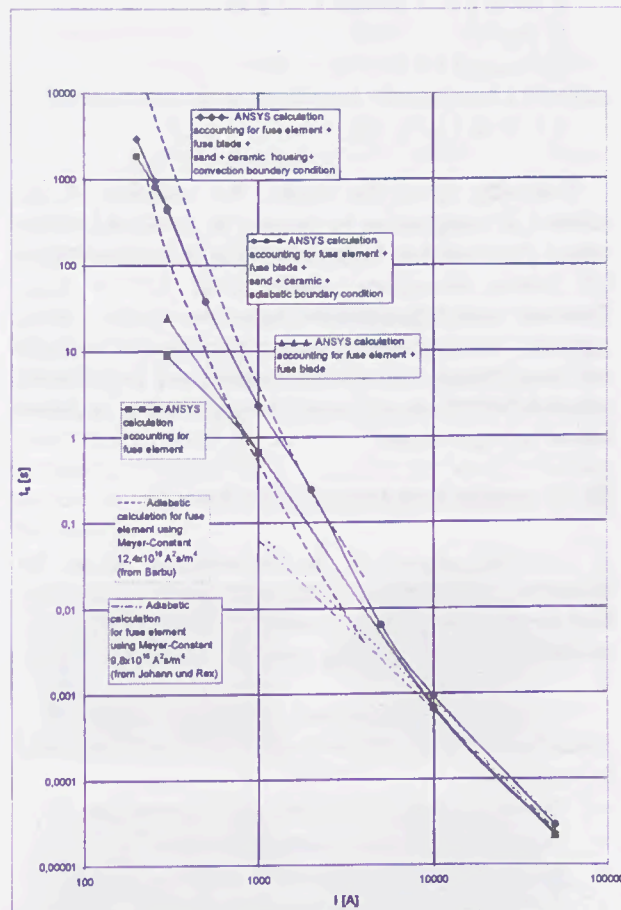


Fig. 1: Time-Current-Characteristic of NH1-160A-Fuse with time-current zones (dashed lines) acc. with IEC 269-1-2

The characteristics are calculated by assuming the following material properties inside the temperature region of  $0 \leq T \leq 1084 \text{ }^\circ\text{C}$  :

- copper melting elements [MOR]
  - $\lambda$  [W/m·K] =  $401 - 0.0675 \cdot T$  (linear fit [CRC])
  - $\rho$  [kg/m<sup>3</sup>] =  $8890 / (1 + 16.5 \times 10^{-6} \cdot T + 4 \times 10^{-9} \cdot T^2)$
  - $c$  [Ws/kg·K] =  $380 (1 + 3.55 \times 10^{-3} \cdot T + 3 \times 10^{-8} \cdot T^2)$
  - $\rho$  [Ω·m] =  $1.59 \times 10^{-8} (1 + 4.3 \times 10^{-3} \cdot T + 5 \times 10^{-7} \cdot T^2)$
- brass blades [WIE]
  - $\lambda$  [W/m·K] = 123
  - $\rho$  [kg/m<sup>3</sup>] = 8440
  - $c$  [Ws/kg·K] = 376
  - $\rho$  [Ω·m] =  $6.17 \cdot 10^{-8}$
- sand [FRE]
  - $\lambda$  [W/m·K] = 0,44
  - $\rho$  [kg/m<sup>3</sup>] = 1757
  - $c$  [Ws/kg·K] = 810
- ceramic body (cordierite)
  - $\lambda$  [W/m·K] =  $0,0125 \cdot T + 1.25$
  - $\rho$  [kg/m<sup>3</sup>] = 2100
  - $c$  [Ws/kg·K] =  $5.0 \cdot T + 700$

and with a heat transfer coefficient to the surrounding  $\alpha = 10 \text{ W/m}^2 \text{ K}$  [BEJ].

Following from the results, the variation of the ambient air temperature by heating up fuse-links within closed chambers has to be taken into the consideration for current intensities smaller than  $1,25 \times I_{\text{rating}}$ . However, for continuous operations with rating currents, the temperature increase influences strongly the interdiffusion between the solder and the element material (M-Effect) and cannot be neglected as is shown below by experiments.

### III. EXPERIMENTAL SET-UP

The scheme of the experimental set-up for measuring temperatures at different points of the fuse-link under reduced heat transfer in an enclosing box made of thermally isolating material is shown in Figure 2.

Using this arrangement, the temperatures at 5 special points under different operating conditions could be measured:

- the temperature of the upper cable connection
- the temperature of the upper fuse blade
- the temperature of the ceramic body
- the temperature of the lower fuse blade
- the temperature of the lower cable connection

The temperature of the soldering point is optionally measured with especially mounted fuse-links. The temperatures are measured by thermocouples made of NiCr-Ni or Pt-100 measuring resistances. The values are stored via the data recording system ALMEMO 8990-6 to the PC. Furthermore, the voltage drops across the fuse links and the current intensities through the fuse-links were registered. The voltage is measured by an

AC-to-true-RMS-transformer, the current is measured by a 600A/5A or a 5A/20mA transformer, respectively.

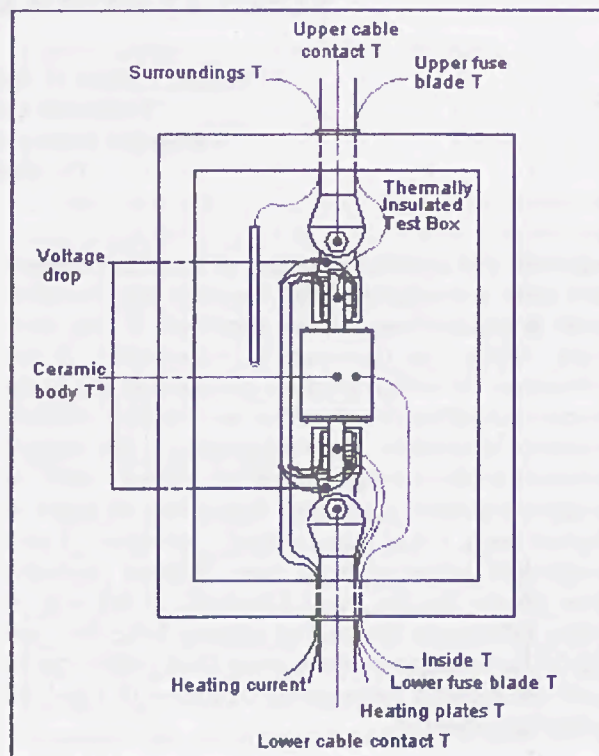


Fig. 2: Experimental set-up for temperature measurements

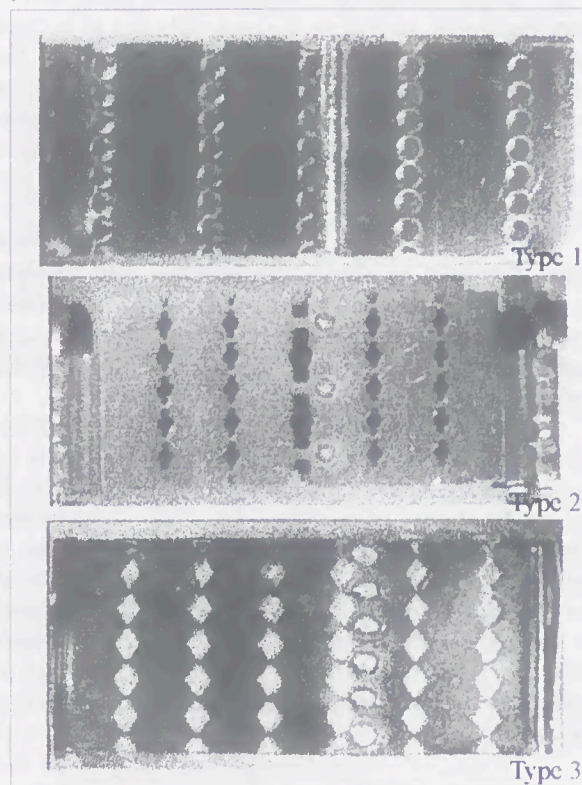


Fig.3: Types of melting elements investigated

The measurements are carried out for the NH3-315A-fuses with three different types of melting element design (Figure 3).

Moreover, to estimate the temperature limits for the upper fuse blade, both, the upper and the lower blade are heated by means of ceramic coated micro-heaters made of platinum which are fastened on each side of the blades. By means of this arrangement the temperatures at the blades can be controlled exactly.

The tests are carried out in the test field at the TU Ilmenau. The test current intensity is controlled by a motor-driven transformer in series with a high-current transformer. The current fluctuation is about 3%.

#### IV. CHARACTERISATION OF FUSE-LINK CONDITIONS

##### IV.1 The upper fuse blade temperature

At standard ambient temperatures of  $T_A = 20^\circ\text{C}$  the temperature of the upper blade is about  $65^\circ\text{C}$  as shown in the Figure 4. This temperature increases up to  $85^\circ\text{C}$  when the ambient temperature rises to  $55^\circ\text{C}$ , and up to  $140^\circ\text{C}$  at an ambient temperature of  $130^\circ\text{C}$ , as measured at the points given in Fig.2.

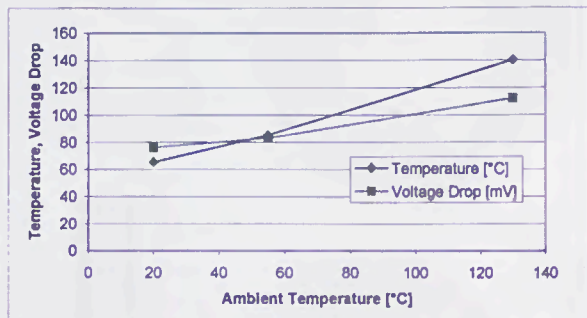


Fig.4: Temperature of the upper blade versus the ambient temperature at rated current for NH3-315A

Only the two lowest values of the ambient temperature, 20 and  $55^\circ\text{C}$ , are allowed according with the standards.

In contrast to temperature of the upper blade, the voltage drop is not so sensitive to varying ambient conditions: A temperature rise of 1 K leads only to an increasing in the voltage drop of about 0,3 mV. Thus, for voltage measurements voltage meters with a high accuracy are required.

Therefore, the temperature of the upper blade will be used in the following as the governing parameter for the operating behaviour of fuse-links or melting elements, respectively.

##### IV.2 The interdiffusion process

The interdiffusion between the solder and the fuse element material is a solid state process, and therefore it occurs already at room temperature. However, in accordance with the Arrhenius relation

$$k = A \exp(-B/T), \quad (1)$$

where  $k$  - coefficient of the reaction velocity  
A,B - process parameters

the diffusion process will be accelerated when the temperature increases. Assuming parabolic dependence for diffusion depth

$$x^2 = k \cdot t \quad (2)$$

where  $x$  - diffusion depth,  
 $t$  - time,

the  $k$  - values for the frequently used solder materials and copper as the element material are obtained by optical microscope measurements of the diffusion zones at different temperatures and times. The resulting rates are as follows:

- Sn/Cd 80/20  
 $k [\text{cm}^2/\text{s}] = 0,066 \exp(-12.190/T) \quad (3)$

- Sn/Ag 95/5  
 $k [\text{cm}^2/\text{s}] = 0,0702 \exp(-11.698/T) \quad (4)$

- Sn/Cu 97/3  
 $k [\text{cm}^2/\text{s}] = 0,0001 \exp(-8.317/T) \quad (5)$

At low temperatures the diffusion proceeds slowly. However, fuse element temperatures of about  $180^\circ\text{C}$  lead no more to stationary conditions. The reduction of the current carrying cross section due to the interdiffusion leads to the temperature rise due to the increasing current density which in turn leads to further increase of diffusion, and finally to the breaking-off of the circuit.

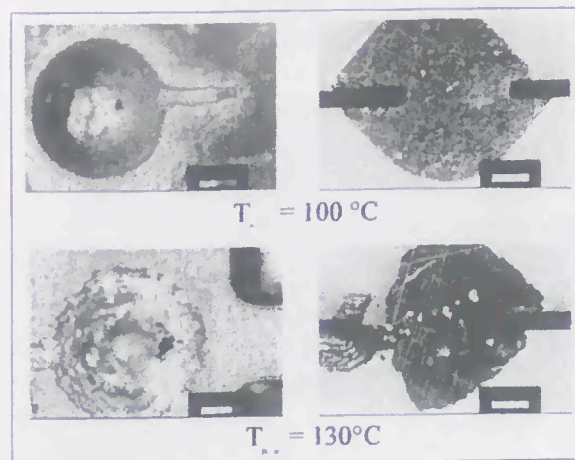


Fig.5: Top views and cross sections of solder points at two temperatures of the upper blade

Moreover, the 8-hour-test does not reflect the real solder conditions. According to the time consuming diffusion process a test time of 24 hours is chosen. During this time the solder can react with the element material and with the surrounding sand as is shown in Figure 5.

There are two possibilities for characterising the solder conditions. The top view shows if sand grains are bonded to the solder surface. Only, if the solder is sufficiently heated up, the sand grains can be pressed into the solder material. The polished cross sections show if the solder already reacted with the element material.

## V. EXPERIMENTAL RESULTS

### V.1 Ambient temperature of $T_A = 130^\circ\text{C}$

The ambient air inside the test chamber is heated up to about  $130^\circ\text{C}$  with controlled micro-heaters.

As is shown in Figure 4, the temperature of the upper blade  $T_{B,u}$  reaches about  $140^\circ\text{C}$  at this temperature of the ambient air. From former investigations it is known, that the overtemperature  $\Delta T_{ME}$  in the middle of a LV HBC melting element is about 60 K.

The consequence is that, the temperature  $T_{ME}$  could reach  $200^\circ\text{C}$ . This temperature is in the melting region of the solder material, and is therefore under no circumstances suited for continuous operations. That can be also confirmed by long time studies carried out with the three given fuse types of different design of melting elements. In Figure 6 is given an example for melting fuse elements at rating current and a temperature of  $130^\circ\text{C}$  of the ambient air.

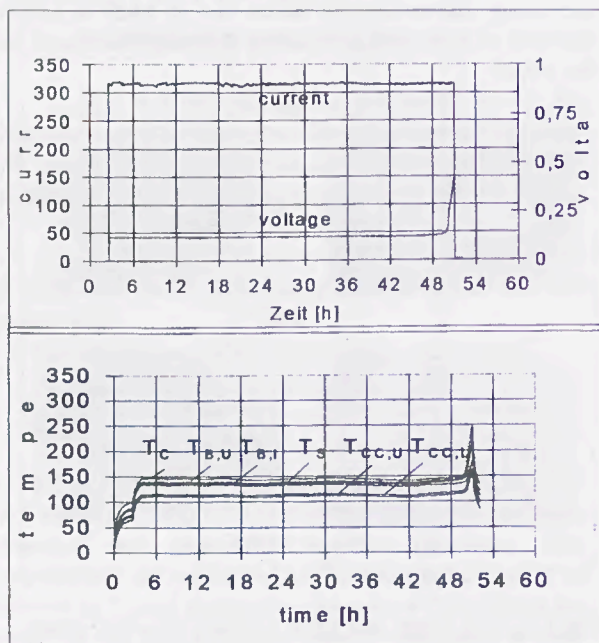


Fig 6: Current, voltage drop and temperatures  $T$  of the fuse link (Type 3) versus the loading time

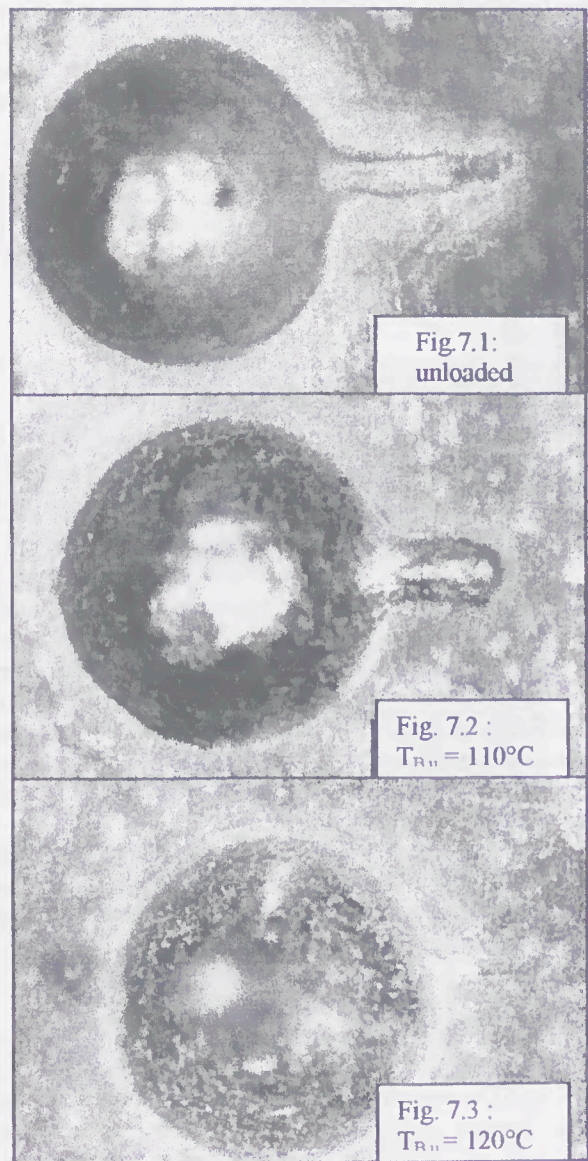
The investigated fuse types (Fig.3) switched off always the rating current, however at different times:

- type 1 :  $t_{\text{melting}} > 35$  h
- type 2 :  $t_{\text{melting}} > 40$  h
- type 3 :  $t_{\text{melting}} > 45$  h

Viewing the transient voltage drop of the example in Figure 6, an interdiffusion process of the solder and the melting element needs at least to about 48 hours. During that time, there is no significant increase in the electric resistance. However, the alloying of fuse element already occurred to such an extend that the temperature of the melting element is about 10% higher than in the beginning.

### V.2 Temperature of the upper blade

As is written before, the solder condition is studied by means of photographs and cross cuttings of solder points after careful dismantling the fuse links. Some results of one series are demonstrated in Figure 7



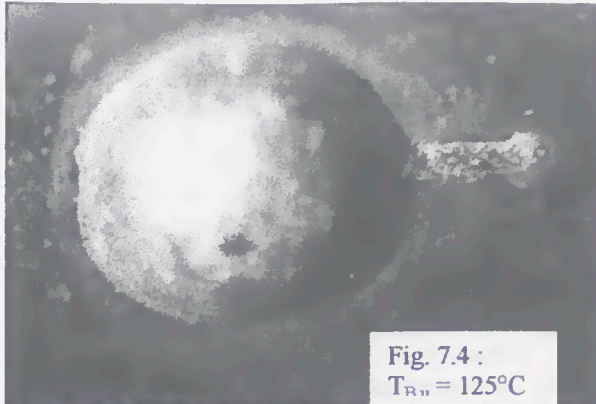


Fig. 7.4 :  
 $T_{R,u} = 125^{\circ}\text{C}$

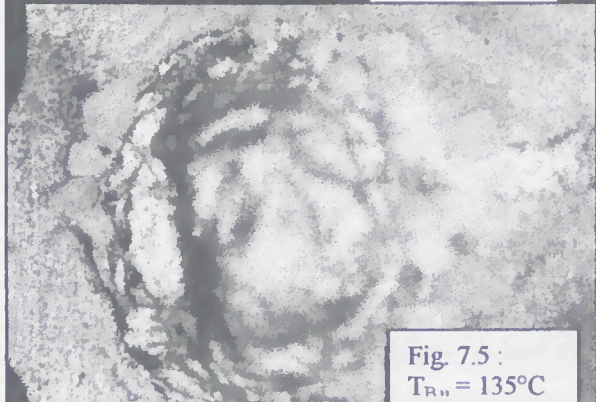


Fig. 7.5 :  
 $T_{R,u} = 135^{\circ}\text{C}$

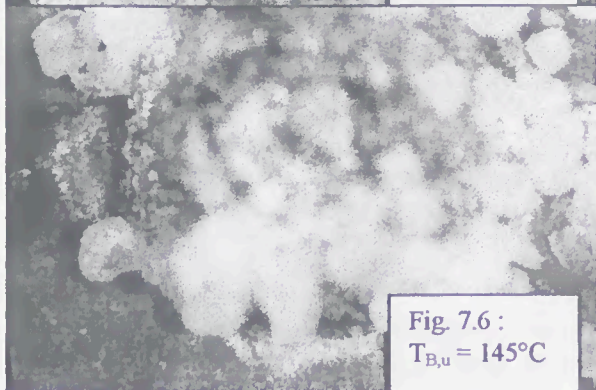


Fig. 7.6 :  
 $T_{B,u} = 145^{\circ}\text{C}$

Fig. 7: Top views of solder points of dismantled fuse elements after loading time, parameter = temperature of the upper blade  $T_{B,u}$

The picture of the top at an upper blade temperature of  $130^{\circ}\text{C}$  is already shown in Figure 5. However, few sand grains are bonded at a temperature of  $125^{\circ}\text{C}$  (Fig. 7) if the fuse-link is carefully dismantled.

From the cross sections (Fig. 8) it is confirmed, that the interdiffusion process starts at a temperature of the upper blade of about  $125^{\circ}\text{C}$ . The ball-like shape of the solder point is already deformed and the composition of the solder material is changed (Fig. 8.4)

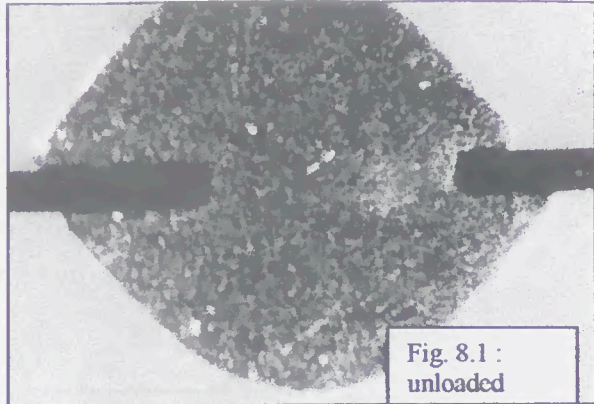


Fig. 8.1 :  
 unloaded

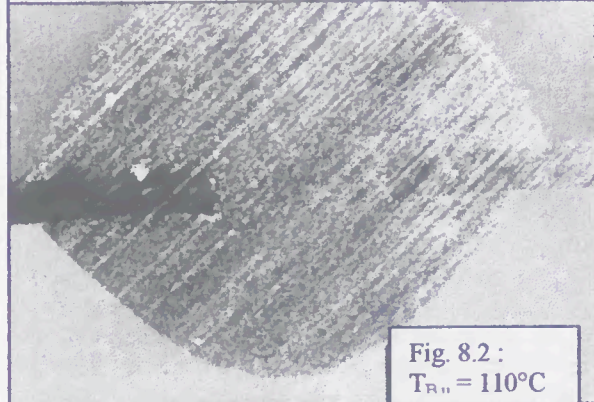


Fig. 8.2 :  
 $T_{R,u} = 110^{\circ}\text{C}$

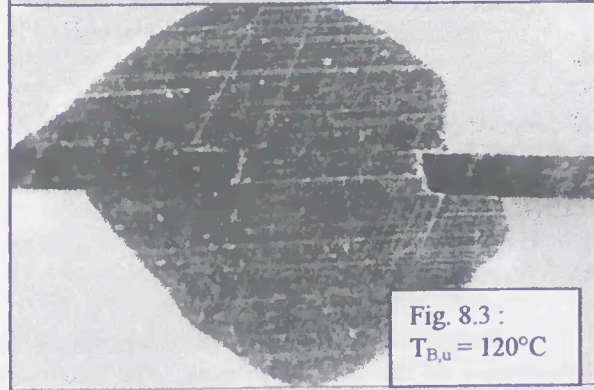


Fig. 8.3 :  
 $T_{B,u} = 120^{\circ}\text{C}$

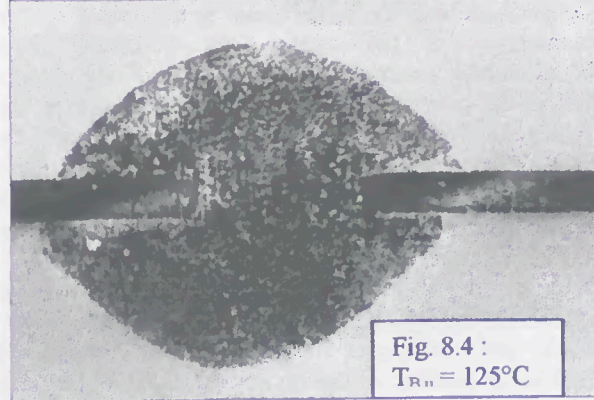


Fig. 8.4 :  
 $T_{R,u} = 125^{\circ}\text{C}$

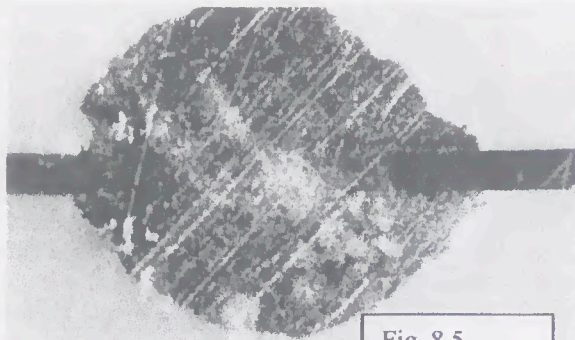


Fig. 8.5  
 $T_{R,u} = 130^{\circ}\text{C}$

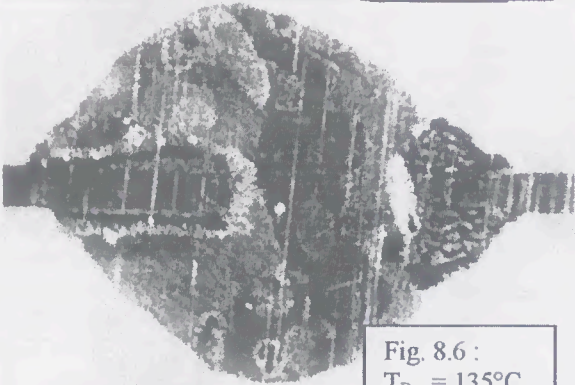


Fig. 8.6 :  
 $T_{R,u} = 135^{\circ}\text{C}$

Fig. 8: Cross sections of solder points after 24h-test  
 Parameter: temperature of the upper blade

At temperatures of about  $130^{\circ}\text{C}$  and higher the interdiffusion makes strong progress and should be avoided.

## VI. CONCLUSIONS

Rating conditions of fuse-links depends on the temperature of the melting element. The maximum temperature near the solder point is influenced by the temperature of the surroundings. Following from experimental results the temperatures of the blades reflect all conditions of the heat conduction to the cables and / or the heat transfer to the ambient air. The upper blade temperature is usually the highest temperature of the fuse-link. Due to this reason the upper blade temperature is a very good criterion of the fuse-link behaviour and the state of solder points.

The limit of the upper blade temperature for continuous operation is obtained by investigation of the solder point state after loading by rating currents and additional heating of the upper and lower blades and after dismantling the fuses.

The usual 8-h-test as a long time test cannot exactly characterise the melting element behaviour. The time consuming diffusion process requires a longer loading time in order to get measurable results. A test time of 24 hours is chosen because of this fact.

The limit of the upper blade temperature of  $130^{\circ}\text{C}$  for continuous operation is obtained from experiments. This limit should never be exceeded for all kinds of operations, independent of which heat transfer conditions apply.

## VII. REFERENCES

- [BEJ] Bejan, A.  
Heat transfer, Wiley, 1993
- [CRC] CRC handbook of chemistry and physics  
75rd edition, 1995
- [FRE] measurements made from  
TU Freiberg, Inst. Wärmetechnik und Thermo-  
Dynamik, 1997
- [MOR] Morgan, V.T.  
Proc. IEE 118 (1971) pp 314
- [WIE] Wieland Buch Kupferwerkstoffe  
Wieland - Werke AG 1986

## VIII Acknowledgements

This work has been supported partly by the Deutsche Forschungsgemeinschaft Nu 59 / 7 - 1,2

# RELIABILITY OF HIGH BREAKING CAPACITY FUSE

Juan C. Gómez, Juan C. Amatti, Claudio A. Reineri, Mauricio Principi.

National University of Rio Cuarto, Engineering Faculty, (IPSEP)  
Ruta 36, Km. 601, (5800), Río Cuarto, Córdoba, ARGENTINA  
Telephone / Fax: 54 358 4676171 or 54 358 4676251  
Email: ipsep@ing.unrc.edu.ar

## Abstract:

The reliability of an electrical system is limited by the reliability of its weakest element. There are several papers on the assessment of the reliability of the electric system components, with some exceptions one of which is on H.B.C. fuses. After an extensive search, only one paper on fuses fault range was found, without any specification about the fuse type or class.

As the fuse is a device with a double performance, passive during most of the time and active when the system is on fault, two different aspects on fuse reliability were presented, because the consequences of a bad-operation under active or passive conditions are very dissimilar from electric system point of view. The determination of the yearly range of faults was done from the information given by the users and by the biggest national fuse manufacturer, related to incidents during the last decade.

Besides, a survey was done between the fuse users in order to assess the relationship between reported and non-reported incidents, doing its evaluation in relation to the fuse type

The information is of fuses following the standards VDE, types HH and NH.

Frequently, the fuses are circulated by transient currents which can start the melting process, without reaching the complete melting due to the current went down to normal conditions, after that the fuse element has been damaged which will be realised in a future operation. This fact and the doubts about the incident reports make that the result of this work be a wide range of values; among them will be the reliability index.

It is deduced the need for a further study of the number of failures and its relation with the complains, in order of getting failure indexes of an accuracy suitable for electric systems reliability analysis, being the present paper a collaboration with this target.

**Keywords:** reliability, HBC fuses, fuse ageing, life span.

## 1- INTRODUCTION

When the word reliability is used, it is refereed to the behaviour of an element or equipment as a whole. The protection devices, as the fuse link, belongs to a special electrical element class with some differences in relation to the normal or general electrical equipment, which are expected to work properly under normal service conditions. The capability of working properly under such conditions is a passive job.

The equipment and components belonging to an electrical system, are protected by other type of devices, between them the fuse; which is in charge of the energy absorption under out of normal conditions and of the switching-off the failed circuit portion before the protected part become damaged. They behave like true sentinels, conducting the current under normal conditions and interrupting when a failure takes part.

In other words, the fuse link should be stronger than the protected element (better capability for conduction of load current) under normal conditions and weaker when the circuit is on fault (start the interruption operation before the protected element become damaged). The reliability, it is understood as the degree of keeping as well the strength as the weakness control, thus, the fuse link should be more reliable than the protected equipment.

The clearest proof about the fuse capability for the fulfilment of both of the tasks, passive and active, is the present widespread fuse applications. Its use is due as well to the apparent simplicity as to its careful design and highly controlled manufacture.

There are several publications on components and equipment's reliability assessment, being of importance on protection devices, but limited to circuit breakers and relays. In the author's knowledge, there is only one present publication where the HBC fuses were mentioned just in a superficial way, being also analysed in another paper which is nearly 30 years old [1] [2].

In reference to expulsion fuses, several papers can be found related to reliability assessment in fuses after several years of field installation [3] [4].

There is an interesting article, in which a model for fuse reliability is proposed, dividing the study in three parts, conduction (resistance), interruption and isolation based upon the different failure types [5].

On the reliability assessment studies, the fuse is always considered as an element suspicious of bad operation. Being highly criticised the fact that after its operation, the replacement (in order to restore the supply) should be done by hand, being necessary the presence of the technician in the installation place. From the author's point of view, such concept is erroneous due to as will be further shown; the fuses reliability index is of the same order that the circuit breakers and relays ones. Besides, anyway the technician should visit the place in case that circuit breaker instead of fuse was used.

The fuse link is an "one time" device, then does not have repairing time but replacement time, which is mainly function of two components, store replacement availability and accessibility of the place of installation. In this work, the replacement time is not analysed, but this time is mentioned in the references being nearly 5.5 hours, very similar to the 5 hours value given for relays in the same reference. [1]

## 2- CAUSES OF FUSE FAILURE

Every component of an electrical system can reach the failure situation, which is more possible to occur as the working time increases towards the end of its life span. That life span can be between 10 and 30 years, depending of the fuse type, being the end of life determined by the ageing, similarly to the cases of transformer oil, chemical attack to a cement pole, fungi effect on a wood pole, etc..

The useful life of an element is determined during the design and manufacture, depending of a series of service conditions considered as normal; but if during its life the conditions are harder than expected, obviously the life consume will be at a higher speed. In general, the equipment have a life span irrespective of the load conditions, in another words the ageing always exist. For example an oil-insulated transformer will be consuming its life in spite of the equipment never suffered overloads or any type of rough service, due to its components suffer normal degradation with the time. The protection device type "no-one time", have a life span mainly function of the level of interrupted currents, suffering of normal ageing yet without any operation due to the ageing of its components parts, requiring maintenance work in order to extend its life.

The fuse link, protective device class "one time" has not life span, mainly (apparently) due that the element does not suffer ageing under normal conditions, and thus does not need any maintenance work. Studies on fuses after periods between 11 and 28 years of field working under service conditions obviously variables and plenty of normal transients have been published. After these time periods, the fuses were thoughtfully tested, without

finding any meaningful moving aside of the tolerance zone comparing with a new condition fuse. Besides, was not detected a higher difference with the older fuses in comparison with the lesser time in the field ones, which is conclusive in relation to the fact that the fuse does not suffer ageing under normal field conditions. [3] [ 6]

Thus, the fuse life in an electrical system can be of just a few seconds or more than several years, depending of the instant in which the fault which cause that its operation will take place. Due to that, it is impossible the forecast of the instant in which the failure will take place, being necessary that the fuse life should be at least higher than the protected element one, which can reach 30 years. [2]

Along its life, the fuse carries currents, which can change from zero to its rated value, suffering cycling with thermal variations, which can lead to mechanical effects. Besides the fuse link is subject to cross-country faults, carried by the fuse until the down stream devices operates. If the overcurrents do not overcome manufacturer-determined limits, the fuse is not going to be altered.

The high load values of any type, steady state, cyclical, transients, etc. can produce fatigue and/or ageing of the fuse. Such ageing lead the fuse to the nuisance premature operation, in other words the fuse operates faster than normal with the same current values. There is not any previous work that identifies any external cause for a delayed operation or with time bigger of the I-t characteristic curve one, except if the fuse is a marginal device, for example with insufficient M-effect material, which is a manufacturing problem. [3]

The paragraph above points out a factor, which can be detrimental for the passive and sometimes for the active (interruption) fuse operation, mainly for the NH classes aR and aM, HH Backup and General Purpose fuses. This situation produces a partial melting of some of the elements leading the whole fuse to operate in the prohibited overload zone. Besides this reason, practically does not exist any other external cause detrimental for the breaking capacity (active function). [7]

The consequences are very dissimilar if the fuse failure is under passive or active conditions. The total failure in passive state is just the energy flow interruption, which is a nuisance and sometimes not very expensive, depending of the involved blackout cost. The passive state partial failure is normally the cause of the fuse weakening, which have serious consequences when the fuse is called to operate, due to its breaking capacity have been seriously affected.

The fuse reliability is closely related with the quality, being critical the manufacture control for two main reasons. Firstly, as the fuse is a protection device its control should be more strict than the protected equipment one and secondly the fuse is a "one time" device for which its behaviour can not be checked without its damage.

When the fuse reliability is under study, results of big importance the discrimination between failure and legitimate operation due to unfortunately and very frequently the fuse is blame of bad-operation when really it has interrupted a current, which can be damaging for the protected equipment. Besides, frequently the circuit designer mistake is charged to the fuse, being the device called to operate in a zone for which has not been designed to.

Following the previous analysis it is considered a fuse failure when the behaviour is not the expected or is out of the manufacture guarantee related with any of its characteristic parameters.

### 3- FAILURE TYPES

Not all of the HBC fuse failures are of the same importance from the circuit point of view, as well in active as passive function, being necessary to specify different failure categories. They are classified in primary, secondary, tertiary and non-functional ones.

The main failure types for each class are:

- a- Primary:
  - interruption failure or inability for the current cut.
  - successful interruption but with excessive overvoltage
  - interruption with let-tru current or energy bigger than the manufacturer data maximum values
- b- Secondary
  - striker does not operate with successful current interruption
  - operation faster than the characteristic curve values
  - fuse body cracked during the interruption
  - partially cut fuse element or bad welded connection, lowering the rated current.
  - indicator failure (active function)
- c- Tertiary
  - indicator does not operate (passive function)
  - temperature higher than the maximum permissible
  - interruption with external effects bigger than the permissible, but without fuse explosion
- d- Non-functional
  - label or characteristic plate lost or illegible
  - rusting on the metallic components
  - small cracking and roughness of the fuse body

For the determination of the failure index, the faults called non-functional were not considered due to they do not prevent the essential fuse job.

### 4- DETERMINATION OF THE FAILURE INDEX

For the failure index determination, there are usually three data sources:

- a- Manufacturer internal quality control tests
- b- Manufacturer homologation or quality control external tests
- c- Customer complains caused for claimed fuse failures (on field)

The information type a is not very reliable because it refers to elements not free or ready for sale. This data is only applicable to the internal quality control.

The source b is not applicable due to it generally corresponds to test under very difficult and unrealistic conditions, done over special samples or prototypes. Also the number of tests is small and the behaviour is usually marginal.

The source c is also objectionable because the client claims are very inexact due to the following reasons:

- The client reports bad-operation when he/she is not able to detect the fault or is not willing to do that. In spite of the inherent security factors, sometimes the client mistake is so big that the element behaves out of design rate.
- Asymmetry of the post-complaint procedure, due to sometimes the problem is very deeply investigated but in other cases the fault is hardly considered.
- Neither all the faults are informed nor all the complaints are strictly true. The number of complains is function of several factors as: fuse price, user knowledge, damage cost, etc. In other words the complaint characteristics is related to the fuse, failure type and the user characteristics.

The first filtering is done after a careful study of the complaint, from which it is concluded if there was a fuse bad-operation or a user mistake. The second data adjusting is done in order to consider the true fuse failures that are not reported, depending mainly of the user and device characteristics.

Based in the experience gained in our country and taking account of a reference more than thirty years old, the values of Table I can be estimated. [2]

For the determination of the Table I values, several factors have been considered, as for example: the cheap fuses are replaced without complains and besides is very popular the custom of replacing the fuse before looking for the fuse operation reason, which normally lead to a new fuse operation.

The special fuses are nearly prototypes, then the quality control is not very well established, expecting high

failure indexes. In the commissioning test a high number of fuses are operated due to calibration and setting problems.

**Table I**  
Relationships between true faults and complaints

Fuse type	Relationship faults / complaints
Distribution, medium voltage ( $\geq 13,2$ kV)	3:1
Industrial, medium voltage ( $<13,2$ kV)	1,5:1
Semiconductors application	2,5:1
Distribution, low voltage	6:1
Industrial, low voltage	4:1
Domestic or small industrial, low voltage	20:1
Traction and d.c. applications	2,5:1
Low power applications	10:1
Special fuses and miscellany	3:1
Average Value	5,8:1

From the main Argentinean fuse manufacturer client complaint reports during the last ten years, the Table II was filled, taking account of the previously mentioned correction factors.

The true complained fault distribution is as follows:

- Primary 30 %
- Secondary 20 %
- Tertiary 50 %

Non-functional nearly 10 % of the total claims amount (not considered in Table II)

Due to the lack of information, was not possible to relate the failure indexes with the fuse time in service.

## 5- CONCLUSION

From this work it is concluded that the general believe that the fuse link is a low reliability device is totally incorrect, due to the yearly and per unit failure range are in the same order of the present circuit breakers.

As general conclusion it is deduced that the yearly and per unit failure index for fuses should be between 0.0002 and 0.002.

The relationship between the complaints and true failures are function of the fuse and user types, being in our country 3:1 in average. The true failures without user complains are function of the same factors, being in average 5.8 times the complained ones.

Depending of its importance, the failure distribution is primary 30 %, secondary 20 % and tertiary 50 %. The non-functional faults are 10 % of the whole. The references shown that the number of faults does not

increase with the installation time, which seems to be confirmed from this work.

It is deduced that further study on fuse failure and user complain is necessary in order to obtain a more precise fuse reliability index, being the present work a collaboration in such direction.

**Table II**  
Analysis of complains and Fault Indexes, Period 1988-1997

Fuse type	Manufactured (thous)	Complains	True complains	Adjusted Faults per unit year
Distribution, medium voltage ( $\geq 13,2$ kV)	25	50	15	0.00018
Industrial medium voltage ( $<13,2$ kV)	15	42	16	0.00016
Semiconductor app.	100	72	34	0.00008
Distribution, low voltage	300	350	105	0.00021
Industrial, low voltage	600	655	210	0.00014
Domestic or small industrial, low voltage	80	44	15	0.00037
Traction and d.c. applications	5	12	8	0.00040
Low power applications	25	45	12	0.00048
Special fuses and miscellany	20	14	5	0.00007
Total or average	1.170	1284	420	0.00023

## References

- 1.- IEEE Std. 493-1990, IEEE Recommended Practice for the Design of Reliable Industrial and Commercial Power Systems, Golden Book, IEEE, 1991.
- 2.- Jacks, E. (1968): Evaluation of reliability: H.R.C. fuselinks. European Nuclear Energy Agency committee on reactor safety technology 27-28 June, 1968, 1-26.
- 3.- Westrom, A.; Law, S. W.; McKenzie, R.; Patterson, R.; Livesay, B. R. (1990): Field service evaluation of distribution fuse links. IEEE trans. on PWRD 5, n - 4, November 1990, 1855-1865.

4.- Costa, S. F.; Rangel, L. P.; Bastos, R.G. (1991): Overload tests for fuses in rolling-mills. 4th. ICEFA 1, 17-22.

5.- Meng, Xianzhong; Wang, Jimei (1990): Estimation of reliability of fuses. Fourth International Symposium on Short-circuit currents in Power Systems 1, 4.5.1-4.5.4.

6.- Jacks, E. (1967): Fuses-some quality and reliability considerations. Electronics & Power January 1967, 1-7.

7.- Gomez, J.C. ,Tourn, D., Campetelli, G., Amatti, J.C., (1998) Debilidad del fusible de alta capacidad de ruptura, to be published in Revista Electrotécnica.



# VARIABLE VOLTAGE RISE BEFORE THE BEGINNING OF THE ARCING PROCESS IN A LV FUSE LINK

Hans-Günter Rex, Consultant Quality Assurance  
D-69207 Sandhausen, Germany

**Abstract:** The constrictions of the melting element are not cut in that moment the voltage rise across the constriction starts. They disrupt only when the voltage drop across the constriction has reached the value  $U_E$ . Breaking tests with LV fuse links and specially designed constrictions show a slow down of the voltage rise up to 0.4 ms for the constrictions to open and ignite the arcing process. This is important to know for a correct model of the arcing voltage. Die Engstellen im Schmelzleiter werden nicht in dem Augenblick unterbrochen, in dem die Spannung über der Engstelle anzusteigen beginnt. Die Engstellen zerfallen erst, wenn die Spannung über der Engstelle auf den Wert  $U_E$  angestiegen ist. Schaltversuche mit NH-Sicherungseinsätzen und speziellen Engstellenformen zeigen eine Verzögerung des Spannungsanstiegs bis zu 0.4 ms, bevor die Engstelle zerfällt und den Lichtbogenvorgang einleitet. Dies muß beachtet werden, um ein genaues Modell für die Lichtbogenspannung anzugeben.

## 1 INTRODUCTION

The strangling of the constrictions in a melting element is a dynamical process that needs power and time. The current delivers the power. The time to strangle the constrictions depends on their shapes and on the melting current. Strangling starts only when the smallest cross section of the constriction has changed to liquid. In this moment the melting integral for adiabatic heating of silver and copper melting elements has grown up to about 85% of its final value. With smaller current densities and growing heat losses the melting moment is shifted to a higher percentage of the melting integral. When a constriction in a melting element is cut by a current and arcing begins, then the arc voltage starts with the value  $1 \cdot U_E$  per arc. The voltage  $U_E$  is made by an electrode effect. The deformation of the electric field next to the electrode needs energy, which is produced by the current in the strangled constriction. When the voltage drop along the strangled constriction exceeds the value  $U_E$ , the voltage drop needs more energy than an arc. The constriction will disrupt and lower the energy. The calculation about the effect of the current forces to the shape of the constriction is difficult. T. Lipski described how to calculate the effect of the pinch forces on a strip fuse element by a short circuit current [1]. We look for a simple connection between the test conditions and the voltage rise.

## 2 FUSE LINKS AND TEST CONDITIONS

Many tests had been performed, in order to know the breaking behaviour of fuses at various working conditions. The voltage rise before the beginning of the arcing process has been analysed many years later. Breaking tests from over a period of ten years were evaluated. The tests were not prepared and not performed to deliver

information for the voltage rise before arcing begins. For the breaking tests we used melting elements with specially formed constrictions in order to have a best heat conduction from the smallest cross section of the constriction to the unharmed area of the melting element (see figure 1). The melting elements were made of silver with three rows of constrictions in line, distance 9 mm. Width and thickness of the melting elements are listed in the table. In most cases an indicator wire has been installed parallel to the melting element. The melting integral of the indicator wire has been 5 A<sup>2</sup>s. The test voltage has been DC between 24 V and 484 V and AC 50 Hz between 245 V and 1117 V. The inner volumes of the fuse links were 18, 31, 56, 100 and 134 cm<sup>3</sup>. In many fuse links only one melting element was installed.

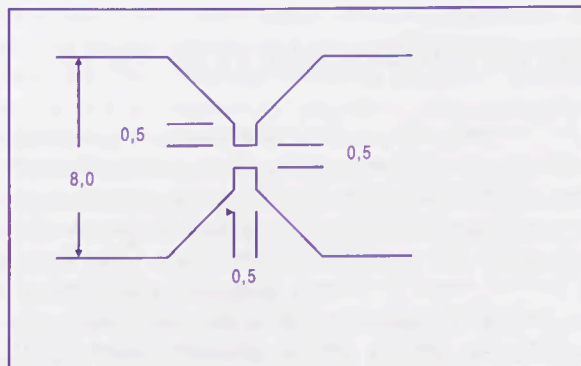


figure 1: Constriction in the melting element of the evaluated tests. Dimensions are in mm

We performed also tests with two melting elements inside the fuse links and tests with copper melting elements, marked by "K" in the file name in the table.

We evaluated some breaking tests, performed with fuse links with copper melting elements and another shape of constrictions, formed by round holes of 3.0 mm dia-

meter and 3.5 mm distance in a row of parallel constrictions. The distance of the rows has been 8.0 mm. There were 6 rows per strip. Test conditions and test results are listed in the table and marked by "C-4".

The tested fuse links mostly were taken out of the production lot. The position of the melting element inside the fuse link and its correctness has not been inspected before the test. The melting elements were embedded in quartz sand.

### 3 THE VOLTAGE RISE TIME

When the constrictions in a melting element are strangled by the current forces, the resistance of the constrictions rises and the voltage drop along the constriction rises too. When the test current density decreases, the voltage drop increases slower up to the value  $U_E = 55V$ . We assume the melting integral and the melting current to have almost the same values before the constriction is strangled and the voltage drop along the constriction rises faster and after the constriction is disrupted. When we determine how the maximum voltage rise time depends on the current density in the melting moment, we get a distribution according to diagram 1. The discrimination is acceptable for current densities above 7000 A/mm<sup>2</sup>. For small current densities below 7000 A/mm<sup>2</sup> the values are closer and closer.

We define the  $i^2t$ -ratio as the value of the actual melting integral divided by the melting integral for adiabatic heating. When we plot the maximum voltage rise time versus the  $i^2t$ -ratio, we get diagram 2. The discrimination is acceptable for an  $i^2t$ -ratio above 3. For a small  $i^2t$ -ratio below 3 the values are closer and closer.

We need both the diagrams 1 and 2. Sometimes only diagram 1 delivers the correct value for the voltage rise time. The value can be calculated before the beginning of the voltage rise and before the arcing process begins.

### 4 THE VOLTAGE RISE TIME AT DC AND AC

An AC current heats up the constrictions in a melting element by current pulses after short pauses. Current values smaller than a limiting value lead to heat losses in the current pause that exceed the heating up effect of the current pulse. The constrictions cool down. Only in the time interval when the current pulse above the limiting value reaches its maximum value, the constrictions are disrupted. For melting current densities below 8000 A/mm<sup>2</sup>, the constrictions according to figure 1 do not disrupt in the first half wave of a 50 Hz current. The melting integral then is more than four times the value for adiabatic heating. For melting current densities above 8000 A/mm<sup>2</sup> the voltage rise time is below 400  $\mu s$ .

A DC short circuit current does not have a current pause before the melting moment. For time constants of 15 ms a melting current density of 8000 A/mm<sup>2</sup> results in about 15 ms melting time. Small differences in the cross section of the constrictions or in the density of the quartz sand can easily lead to a better cooling and to a

remarkable difference in the melting moment and therefore in the voltage rise time. In DC-tests the values for the time to reach  $3 \cdot U_E$  spread about a greater region than in AC tests. The test results for DC-tests therefore are loaded with a bigger error. The evaluation of breaking tests with identical test conditions delivers different values of the voltage rise time. We may use the average value for the diagrams or plot every evaluated value in order to know the error range.

At DC there have been tests performed with melting current densities below 7000 A/mm<sup>2</sup> and  $i^2t$ -ratio up to 9.

### 5 INFLUENCES TO THE RISE TIME

If only the current does the strangling, the  $i^2t$ -ratio and the melting current density define the voltage rise time. There are effects that shorten the time. The constriction is elongated by the heat, but the big rest of the melting element remains nearly at its initial temperature. The sand is only compressed by vibration, not solid. For melting times more than 5 ms the quartz sand next to the hot constriction is heated up some degrees centigrade. For melting times of more than 50 ms the sand is heated up above 300 °C. The temperature rise of the sand can make the sand grains move and can create mechanical forces to the constrictions of the melting element. The liquid constriction can be cut. The rise time then is shorter than in the case of undisturbed strangling.

The more the current density decreases, the more constrictions are cut mechanically. When the number of the constrictions rises, the probability that a liquid constriction is cut mechanically, rises too.

The moving hot sand grains can cut a liquid constriction, but later on it can also put together the ends of the interrupted constriction. This reduces the current density again and enlarges the voltage rise time.

With the current density below 7000 A/mm<sup>2</sup>, the heat losses by conduction along the melting element create different maximum temperatures in the constrictions. Not all constrictions will disrupt simultaneously but only row by row. The voltage cannot rise at once up to  $3 \cdot U_E$ .

If we have current densities below 5000 A/mm<sup>2</sup>, the constrictions next to the ends of the melting element are cooled effectively by the contacts. Their temperature rise slower than that of the middle constriction, which is strangled most and delivers the maximum rise time of the voltage drop value  $1 \cdot U_E$ . When the middle constriction is disrupted and the arc burns, the outer constrictions are heated up faster and strangled faster. The voltage rises faster. This leads to a smaller rise time between  $1 \cdot U_E$  and  $3 \cdot U_E$ . The measured voltage is a mixture of arc voltage and voltage drop along the constrictions.

Parallel constrictions in a row disrupt simultaneously, when there is only the effect of the current. If there is additionally the mechanical effect, then the liquid constrictions can be cut and the voltage rises faster. Is the liquid constriction interrupted before the beginning of the voltage rise, then I assume this to be a mechanically performed disruption.

When all constrictions have the same cross section, then all cross sections have the same current density too. In order to have the rise time to reach the voltage value  $3*U_E$  only influenced by the current heat, we need identical constrictions and a simultaneous voltage rise along the constrictions.

## 6 ONE STRIP MELTING ELEMENTS

We assume to have one strip melting elements with only one constriction per row. The melting element is disrupted, when one constriction is interrupted. It is also possible to have the liquid constriction mechanically cut. When the cross sections of the constrictions differ something, the current density differs too. The strangling does not occur simultaneously. If the cross section differs more than 7.5%, the melting integral differs more than 15%. The smaller cross section is almost strangled, before the greater cross section becomes liquid. The voltage rise up to the value  $3*U_E$  occurs in steps of  $1*U_E$ . One strip melting elements with two and more parallel constrictions in one row mostly deliver the maximum rise time.

## 7 MELTING ELEMENT OF PARALLEL STRIPS

The melting integral is delivered by all parallel strips of the melting element. The rise time becomes maximum, when all constrictions are strangled only by current forces. When the smallest cross section of a strip becomes liquid and is cut mechanically, then this strip does not carry any current any longer. The cross section of the melting element is reduced. The current density in the remaining cross section increases. The voltage along the the remaining strips rises faster and the voltage rise time is reduced. In diagram 1 the rise time is shifted towards a higher current density. The rise time values then harmonize with the values in diagram 1.

When one row of constrictions of the strip is cut mechanically, we cannot read the voltage rise time in diagram 2.

## 8 TEST VOLTAGE BELOW $N*U_E$

Six breaking tests N00R1D until N00R6D were performed at 24 V DC with fuse links with two parallel melting elements inside. In all tests the melting integral is the value of both strips in parallel. The maximum arc voltage values differ very much.

When the test voltage  $u_T$  is small, the inductivity  $L$  of the test circuit must deliver the necessary voltage for the voltage rise. The current must decrease fast, to reach the voltage  $u = -L*di/dt = N*U_E$ . Tests have shown, when sufficient energy is stored in the inductivity, the voltage rises as fast as at high test voltages. When the current density additionally is below  $8000 \text{ A/mm}^2$ , the constrictions are strangled very slowly and the current changes slowly too. A small test current  $i_T$  means a long melting

time. The melting current  $i_M$  is almost equal to the test current. The time constant  $\tau = L/R$  of the test circuit and the test current  $i_T = u_T / R$  deliver  $L = \tau * R = \tau * u_T / i_T$ . When the current changes, the inductivity  $L$  delivers the voltage  $-L*di/dt = \tau * u_T / i_T * (di/dt) = N * U_E$ . The numerical values for the tests were  $N=3$ ,  $\tau = 15 \text{ ms}$  and  $i_T \approx i_M$ . We get for the necessary current change per ms the value  $-di/dt [\text{A/ms}] \approx 3*55*i_M / 15*24 \approx 0.5*i_M$ .

For voltage rise times of  $> 1 \text{ ms}$  and small inductivities, the inductivity cannot deliver the voltage necessary for the voltage drop along the strangled constriction in order to reach the value  $N*U_E$ . In the tests N00R2D and N00R3D the voltage drop reached more than  $1*U_E$  but less than  $3*U_E$ . When we insert the voltage rise time up to  $2*U_E$  in both the diagrams 1 and 2, the values harmonize with the other evaluated voltage rise time values.

When the constrictions disrupt and arcing begins, the arc voltage can rise up to about  $3*U_E$ . The shape of the arc voltage curves (not given here) show, that both strips did the arcing process.

In test N00R1D we found a very short rise time of about  $80 \mu\text{s}$ . One strip has been cut mechanically when the constrictions have changed to liquid. The voltage rise is controlled by only one strip. The increased current density leads to a voltage rise time according to diagram 1. The value  $80 \mu\text{s}$  does not harmonize with the values in diagram 2. In the following arcing process the arc voltage reaches to about 250 V. The arc voltage curve of test N00R1D shows, that only one strip controlled the arcing process.

In the tests N00R5D and N00R6D the voltage rise time of about  $100 \mu\text{s}$  is very short and the melting time of 30 ms is very long. I assume the liquid constriction in one strip to be cut by moving sand grains. Therefore only one strip controlled the voltage rise. The melting current divided by half of the initial cross section delivered the current density  $13400 \text{ A/mm}^2$ . The rise time values  $110 \mu\text{s}$  and  $95 \mu\text{s}$  correspond to the current density for one strip only. The values are plotted in diagram 1. Both test results are not implied in diagram 2. The oscillograms indicate that only one strip led the arc current.

Test N00R4D shows a fast voltage rise along the melting element up to the value  $2*U_E$ . The rise time  $95 \mu\text{s}$  indicates, that only one strip controls the voltage rise. The second strip is cut. The voltage rise time harmonizes with the values in diagram 1.

After  $240 \mu\text{s}$  the voltage drop decreases to 60 V within the next  $300 \mu\text{s}$ . This means that again both strips carry the current. In this moment the current density in both strips is  $5200 \text{ A/mm}^2$ . The voltage drop rises up to  $3*U_E$  within the next  $300 \mu\text{s}$ . We may read the current density  $5200 \text{ A/mm}^2$  and the voltage rise time  $300 \mu\text{s} + 300 \mu\text{s} = 600 \mu\text{s}$ . Both the values harmonize with diagram 1. We may also read the  $i^2t$ -ratio 9.4 and the whole voltage rise time of  $840 \mu\text{s}$ . These values harmonize with the values in diagram 2. Both the evaluations are not quite correct, but they indicate how the diagrams may be completed.

## 9 INFLUENCE OF SHAPE AND MATERIAL

Referred to the  $i^2t$ -ratio the voltage rise time becomes independent on the material and on the shape of the constrictions (see diagram 2). When all strips of the melting element contribute to the voltage rise, diagram 2 delivers the maximum rise time at the selected test conditions.

The shape of the constrictions, the material and the test conditions deliver the actual melting integral value of the melting element, the melting moment and the melting current. There exist methods to calculate the values at the melting moment for different shapes of constrictions, materials and test conditions, e.g. the program STROMex. The melting current and the cross section of the constriction deliver the melting current density. With the maximum voltage rise time of diagram 2 and the melting current density we can draw diagram 1. For each shape of constrictions and each material there exist the diagrams 1 and 2.

Constrictions as defined in figure 1 show an effective heat loss from the constriction to the melting element. The rise time of the voltage drop along the constriction depends on the rise time of the temperature of the constriction. Within the possible accuracy of the evaluation copper melting elements resulted in the same maximum voltage rise time (see diagrams 1 and 2).

The results refer to the investigated constrictions as shown in figure 1. They can be transferred to constrictions with another shape. The voltage rise time normally is smaller for another shape of the constrictions.

Breaking tests with copper melting elements and another shape of constrictions C-4 have been evaluated in the same way. The heatflow from the smallest cross section of the constriction to the unharmed melting element was less. Diagram 2 demonstrates, that the maximum voltage rise time harmonizes with the values for other shape of the constrictions. The rise time of C-4 melting elements did not change much with the melting current density.

We get the minimum rise time for wire melting elements. Even then the rise time is above zero but below 100  $\mu$ s.

## 10 CONCLUSIONS

The rise time has not been found to depend on any inner volume of the fuse link. It is a prearcing effect and not an effect of the arcing process.

The voltage rise time is independent of the test voltage.

For test voltages much less than  $N \cdot U_E$  the voltage drop along  $N$  constrictions does not rise up to  $N \cdot U_E$ .

When there is only the effect of the current, we assume the voltage along the constriction rises linearly up to the value  $N \cdot U_E$ , before the constriction is disrupted. The voltage rise time is controlled by the  $i^2t$ -ratio according to diagram 2. All parallel strips in a fuse link deliver the voltage rise time.

When one row of constrictions of a strip of a multi strip melting element is interrupted mechanically as soon as it has become liquid, the melting current in the remaining strips rises. The current density can be calculated. Diagram 1 delivers the voltage rise time versus the melting current density. Diagram 2 cannot be used.

When one strip fails as soon as the constriction in a row becomes liquid, the rise time must be read in diagram 1. The value can be calculated before the beginning of the voltage rise and before the arcing process begins.

The influence of the test conditions to the rise time can be calculated. Different voltage rise time by a different shape of the constrictions is due to the different heat conduction along the constriction. For  $i^2t$ -ratio  $< 6$  the maximum voltage rise time can be found in diagram 2 or approximately by the formula  $t = 290 \cdot \ln(i^2t\text{-ratio})$ .

At small melting current densities some constrictions very often are interrupted by moving hot sand grains. The current density in the remaining strips rises. The voltage rise time is reduced and can be found in diagram 1. We must therefore calculate all possibilities one by one. Only one possibility will occur in one breaking test. Small test current densities mean currents that leave the range of short circuit currents and enter the range of overcurrents.

When the test voltage is very small, the voltage drop along the melting element cannot reach the value  $N \cdot U_E$ .

The arcing process can be calculated more accurate.

A strip that is cut mechanically before the arcing process starts, maybe takes part in the following arcing process, when the arc voltage exceeds the dielectric strength of the interrupted strip.

## 1 REFERENCES

[1] T.Lipski: Application of the arc-pinch-forces-interaction theory to the calculation of striation modulus of the strip h.b.c fuses ; ICEFA 1984, Trondheim, N



table 1: fuse links, test conditions and test results listed

file-name	melting element	cross sect. mm <sup>2</sup>	test voltage V	test current A	melting current/A	current den-sity A/mm <sup>2</sup>	i <sup>2</sup> t-ratio	rise time µs	remarks
N00R785D	1 x 8 x .150	0,075	484 =	2000	700	9427	3.4	360	
N1R16D	1 x 16 x .20	0,20	400 =	1450	1110	5470	5.78	490	2*U <sub>E</sub>
N1R17D	"	"	"	"	1100	5420	4.80	480	2*U <sub>E</sub>
N1R33D	"	"	"	1000	990	4950	8.6	800	1*U <sub>E</sub>
N1R34D	"	"	"	"	"	"	9.1	700	1*U <sub>E</sub>
K1R35D	"	"	"	"	1000	5000	8.56	620	Cu; 2*U <sub>E</sub>
N00R1D1	2 x 8 x .10	0,1	24 =	1200	810	16000	2.77	80	1B
N00R2D2	"	"	"	"	"	8100	5.08	430	2*U <sub>E</sub>
N00R3D1	"	"	"	"	"	"	5.09	460	2*U <sub>E</sub>
N00R4D1	"	"	"	680	520	5200		600	1B + 1B
N00R5D1	"	"	"	"	670	13400		110	1B
N00R6D1	"	"	"	"	"	"		95	1B
N00R415	2 x 8 x .13	0,13	550 AC	1950	1440	11077	1.48	145	
N0R306	1 x 16 x .150	0,15	"	1830	1870	12467	2.06	140	
N0R308	"	"	"	1000	1600	10667	2.04	160	
N1R885	"	"	"	5700	2900	19333	1.78	40	
N1R886	"	"	"	"	"	"	1.87	60	
N1R889	1 x 16 x .15	"	"	600	1230	8200	3.6	360	
N1R890	"	"	"	"	1250	8333	3.6	430	
N1R013	"	0,21	660 AC	3700	2750	13095	1.47	115	
N0R645	1 x 16 x .10	0,1	550 AC	650	1010	10100	2.29	250	
N2R651	"	"	"	650	960	9600	2.05	260	
N2R652	"	"	"	"	1010	10100	2.20	240	
N3R419	1 x 16 x .20	0,2	380 AC	3000	2610	13050	2.10	100	
N3R425	"	"	"	1300	2200	11000	2.72	160	
K2R27-1	1 x 24 x .217	0,326	660 AC	2400	3590	11012	2.26	190	Cu; 2.HW
K2R30	"	"	"	4400	4130	12700	1.44	90	Cu
K2R25	1 x 24 x .120	0,18	"	2400	2360	13111	1.59	85	Cu
K2R14	"	"	"	1600	2130	11830	1.59	100	Cu
K2R02-25	6 x 8 x .148	0,444	"	2640	4260	9595	1.6	160	Cu
K2R02-26	"	"	"	"	"	19000		60	Cu; 3B/6
K1M14D	1 x 14 x .150	0,30	500 =	1500	1250	4167	2.01	230	C-4
K1M15D	"	"	400 =	1450	1170	3900	2.62	200	C-4; 4*U <sub>E</sub>
K1M39D	"	"	"	1000	990	3310	3.73	320	C-4; 2*U <sub>E</sub>
K1M13D	2 x 10.5 x .15	0,49	550 =	4600	2590	5290	1.69	140	C-4
K2M304	1 x 21 x .15	"	550 AC	1830	3800	7750	1.40	130	C-4
K2M305	"	"	"	"	3790	7740	1.39	115	C-4
K1M410	2 x 10.5 x .143	0,43	1117 AC	25000	7450	17326	1.28	55	C-4

# USING CURRENT-LIMITING FUSES TO REDUCE HAZARDS DUE TO ELECTRICAL ARC-FLASHES

Vincent Saporita  
Cooper Bussmann  
St. Louis, MO  
USA

**Abstract:** Numerous tests were conducted in which arcing faults were initiated in open electrical equipment. Tests were run on circuits protected by both current-limiting fuses and typical industrial circuit breakers. Results showed a dramatic reduction in the amount of damaging energy released upon a worker when current-limiting fuses were utilized. Measurements included voltage, current, temperature, sound, and pressure. High-speed 16mm film, video, and infrared video were also utilized to record the events. Results of the testing were used to develop an award winning IEEE paper[1] and an electrical safety training package now being sold by the Electrical Safety Subcommittee of the Petrochemical Industries Committee (IEEE/PCIC). This paper explains the background for the testing, the tests themselves, and how the fuse industry can use the results of the testing to reduce the hazards associated with electrical arc-flashes.

**INTRODUCTION:** The installation codes in North America require that equipment be installed in accordance with the way it was listed or certified. The installation codes however do not provide guidance for maintenance workers, and the product standards do not require testing for arcing faults that might occur when the equipment door is open and a maintenance worker accidentally creates an arcing short circuit. As a result, numerous workers are injured and killed each year while working on energized electrical equipment. An ad-hoc working group was formed within the IEEE/PCIC safety committee to help address this situation. The intent of the group was to raise the awareness of electrical workers to the dangers associated with electrical arcs and hopefully reduce the incidents of worker injuries and deaths.

The ad-hoc group consisted of 10 members, of which one was a medical doctor with electrical burn expertise, two were consulting engineers, four were engineers for various petrochemical companies, and three were with an electrical manufacturer. The group had no funding outside of the group itself. Everyone participated in the decision process, provided their expertise, and donated actual electrical equipment when possible. Some equipment was brand new. It had never been put into service. Other equipment was taken out of decommissioned plants. Switchboards,

panelboards, busway and motor control centers were donated for these tests. In addition, lab time was donated by a manufacturer in a high-power short-circuit test lab in the Midwest.

**BACKGROUND/RELEVANT PAPERS:** In 1982, Ralph Lee wrote a paper titled, "The Other Electrical Hazard: Electric Arc Blast Burns"[2]. In that paper he developed a formula for the distance required for various degrees of burns as related to the available MVA and time of exposure. These formulae were developed for arcs in open air.

$$\begin{aligned} D_c &= (2.65 \times MVA_{bf} \times t)^{1/2} & (1) \\ D_c &= (53 \times MVA \times t)^{1/2} & (2) \\ D_f &= (1.96 \times MVA_{bf} \times t)^{1/2} & (3) \\ D_f &= (39 \times MVA \times t)^{1/2} & (4) \end{aligned}$$

Where

$D_c$  = distance for a just curable burn, (feet)  
 $D_f$  = distance for a just fatal burn, (feet)  
 $MVA_{bf}$  = bolted fault MVA at point involved  
MVA = transformer rated MVA, 0.75 MVA and over.  
For smaller ratings, multiply by 1.25  
 $t$  = time of exposure, (seconds)

Lee's work showed, for example, that skin temperature above 96 degrees C for .1 second resulted in total destruction of the tissue (incurable burn) and that skin temperature below 80 degrees C for .1 second allowed for skin which could be cured (just curable burn).

NFPA 70E [3], Standard for Electrical Safety Requirements for Employee Workplaces, adopted the Lee Formulae to define the safe working distance from a potential arc. While NFPA 70E is not generally enforced as is the National Electrical Code (NFPA 70)[4], it is a consensus document and can therefore be used in a court of law and is considered "readily available public knowledge".

Ralph Lee followed in 1987 with another paper titled "Pressures Developed by Arcs"[5]. In that paper Ralph Lee explored the affects of the expanding metal and the heating of air because of the arc passing through it. Copper expands by a factor of 67,000

times when vaporized. Compare that to the expansion of water, which is only 1670 times.

In the paper, "Protective Clothing Guidelines for Electric Arc Exposure"[6], the authors used "incident energy" as the basis for choosing the correct protective clothing. The authors state that an incident energy of 1.6 cal/cm<sup>2</sup> is the level at which second degree burns would occur on exposed skin.

In a follow-up paper, "Testing Update on Protective Clothing & Equipment For Electric Arc Exposure"[7], the authors document measured sound pressures of up to 163 dB. For comparison, a 12-gage shotgun produces an intensity level of 130 dB. They state that enclosing a three phase arc in a box has the potential to increase the incident energy approximately three times, depending upon the box dimensions, as compared to an arc in an open air.

The committee was aware of the theoretical papers and wanted to show how the potentially dangerous arc flash events could affect workmen. It realized that it is both equipment failure and human error that contribute to arc flash events. The tests were designed to be different than previous theoretical tests in two ways. First, the tests were to use a mannequin, with measurements taken on or near the mannequin. Second, the tests were carried out with actual electrical equipment, both new and used, with arcs created as they might likely occur in the real world. The purpose of the tests was not to compare equipment manufacturers, but to raise the awareness of arc flash hazards in equipment that was applied according to the manufacturers' recommendations and third-party listing and labeling requirements.

**TESTS:** A preliminary series of 11 tests were run on March 26-28, 1996. The 27 main tests were run from September 10-12, 1996. The mannequins were positioned in front of the arc as though they were working on the equipment. The closest worker was positioned so that his chest was approximately two feet from the source of the arc, with his hand reaching in.

The equipment used in the September tests is listed in Table I. Available fault levels are shown in Table IV. All tests were carried out within the ratings of the equipment, but there were several major differences between the normal certification tests carried out by

the equipment manufacturers and these tests. Normal certification testing is carried out with doors closed, whereas this testing was done with the doors open. Normal testing is done with bolted short circuits, but this testing was accomplished with arcing short circuits. The reasons for these differences are pretty obvious. Certification of the equipment already assures that the equipment will handle relatively high short-circuit currents when the faults are bolted and the doors are closed. But real world troubleshooting techniques often require that maintenance personnel work on hot equipment with equipment doors open. Thus the need for this series of tests.

All equipment was certified by a Nationally Recognized Testing Laboratory except for (1) a field fabricated bus distribution box that was used to distribute power for an outdoor switchrack. (It was removed from service specifically for this testing.), and (2), a shop fabricated three phase, four wire bare copper bus structure with 1/4" x 1" x 6' copper bars spaced 1" apart (arcs were started in the middle of the bars and video-taped as they ran away from the source.).

Whenever possible, arcing faults were created with a screwdriver or a wrench placed from phase to phase or phase to ground. Where it was impractical to use a screwdriver or a wrench, a small piece of #18 copper wire was used to initiate an arc. The tests were staged in such a manner because research had shown that it was as close as possible to actual field conditions.

**TEMPERATURE MEASUREMENTS:** Type "T" thermocouples were placed on the lead mannequin's extended hand(T1), at the front of the neck(T2) and under its shirt at chest level(T3). These thermocouples were connected to an Astromed GE Dash-10 recorder. In addition, temperature measurements were captured by means of an infrared camera and recorded on tape. These measurements were used for the peak temperatures in Table II. The infrared equipment included an Agema Thermovision Scanner 870 (Catalog No. 556192904, Serial No. 4175), monitor, control unit, power supply, dual lenses, and Panasonic VCR. A mirror was used so that the camera could be positioned out of the direct line of the arc-blast.

Table I [1]  
Equipment used in tests and overcurrent device operation

Test No. <sup>a</sup>	Equipment	Overcurrent device	Fault Initiation	Overcurrent device result
1	Size 1 combo starter w/ 30 A fused switch	601A Class L, 30A RK 1	Load side—screw-driver—C to gnd.	30 A RK-1 opened
2	Size 1 combo starter w/ 30 A fused switch	601 A Class L	Load side—screw-driver—C to gnd.	None
3	Size 1 combo starter w/ 30 A fused switch	601 A Class L	Load side—screw-driver—C to gnd.	Class L opened
4	Size 1 combo starter w/ 30 A fused switch	640 A - Pwr CB	Load side—screw-driver—C to gnd.	CB did not open
9	MCC # 2 w/insulated bus	601 A Class L, 30 A MCP	Load side—#18 wire—C to gnd.	30 A MCP tripped
10	MCC # 2 w/ insulated bus	601 A Class L, 70 A MCP	Load side—#18 wire—C to gnd.	70 A MCP tripped
11	MCC # 2 w/insulated bus	601 A Class L, 70 A MCP	Load side—#18 wire—B to C	70 A MCP tripped
12	MCC # 2 w/insulated bus	30 A MCP	Load side—#18 wire—B to C	30 A MCP tripped
13	MCC # 2 w/insulated bus	640 A - Pwr CB	Line side bucket—#18 wire—A, B, C	CB did not open
14	MCC # 2 w/insulated buss	640 A - Pwr CB	Line side bucket—#18 wire—A, B, C	CB did not open
15	600 A distribution duct	640 A - Pwr CB	#18 wire—A, B, C	CB did not open
16	225 A power panel	30 A MCB—3 Phase	Load side—screw-driver—C to gnd.	30 A MCB tripped
17	600 A distribution duct	640 A - Pwr CB	# 8 wire—A, B, C	CB did not open
18	Size 2 combo starter w/ 50 A MCP	601 A, Class L, 50 A MCP—200 A 170 Limiter	Load side—screw-driver—C to gnd.	200 A 170 Limiter and 50 A MCP opened
19	Size 2 combo starter w/ 50 A MCP	601 A Class L, 50 A MCP	Load side—screw-driver—C to gnd.	50 A MCP did not open
20	Size 1 combo starter w/ 35 A MCB	601 Class L, 35 A MCP	Load side MCB—#18 wire—C to gnd	35 A MCP did not open
21	Size 2 combo starter	50 A MCP	Load side MCP—#18 wire—A, B, C	50 A MCP did not open
22	MCC # 4	601 A Class L, 50A MCB	Load side starter A, B, C— #18 wire	50A MCB tripped
23	MCC # 4	601 A Class L	Incoming lugs—wrench	Class L opened
24	MCC # 4	640 A - Pwr CB	Incoming lugs—wrench	CB did not open
25	MCC # 3 Size 2 starter with limiters	601 A Class L, 50 A MCB, M limiter	Load side starter—A, B, C— #18 wire	CB did not open
26	MCC # 3 Size 2 combo starter	601 A Class L, 50A MCB	Load side starter—A, B, C— #18 wire	50A MCB did not open
27	MCC # 3	640 A - Pwr CB	Line side—A, B, C—#18 wire	CB did not open

<sup>a</sup> Tests 5, 6, 7, and 8 were product tests and were not recorded.

Table II [1]  
Measured temperatures

Test No. <sup>a,b</sup>	°C		Time in mS				°C		Time in mS				°C		Time in mS	
	Infra-red Temp.	T1 pk	90% rise	90% fall	90% to 80°C	90% to 70°C	T2 pk	90% rise time	90% fall time	90% to 80°C	90% to 70°C	T3 pk	90% rise time	90% fall time		
3	180	>175					62	220	460							
4		>225	10	2000	>250	>2500	>225	120				50	230	360		
13	150						30									
14	200	105	120	300	70	170	120	200	390	420	450					
16	150															
19		30					30									
20	150											83	190	250		
21	90											45	100	175		
24	200	>100	160	1600	1400	1500	52	1200	2500							
27	150	65	400	500			40	75								

<sup>a</sup> Temperature measurements were not recorded for tests 1,2, 5, 6, 7, 8, 9, 10, 11, 12, 15, 17, 22, 23, 25, and 26.  
<sup>b</sup> The number 18 was not used.

**SOUND MEASUREMENTS:** Sound measurements were recorded in two different ways:

1. Pressure probes were installed on the lead mannequin. These were Omega DPX 101-250 piezo-electric sensors. After amplification, the signals were sent to the Astromed Dash-10. Probes were placed a distances of 2' and 6' from the arc source.
2. Condenser microphones from Bruel and Kjaer were located on tripods at distances of 20'(D<sub>1</sub>) and 25' (D<sub>2</sub>) from the source of the arc. See Table III. It was felt that the reasons for the difference between the ideal and measured

distance effect were due to a nonspherical pressure wave, reflective laboratory, and nonideal source.

For comparison of the advantages of using current-limiting fuses, the measured pressure, in Test 3, when the 22,600 ampere short was cleared by a 601 amp Class L fuse was 504 lbs/ft<sup>2</sup> while, in Test 4, the pressure was measured at greater than 2160 lbs/ft<sup>2</sup> when the circuit was protected by the 640 amp Power Circuit Breaker. Eardrum rupture occurs at a pressure of 720 lbs/ft<sup>2</sup>, while the threshold for lung damage is 1728 lbs/ft<sup>2</sup>.

Table III[1]  
Pressure<sup>a</sup>

Test No. <sup>b</sup>	P1 <sup>c</sup>	P2 <sup>c</sup>	Sound @ 20 ft	Sound @ 25 ft	Sound @ 2 ft <sup>d</sup>	Test No.	P1 <sup>c</sup>	P2 <sup>c</sup>	Sound @ 20 ft	Sound @ 25 ft	Sound @ 2 ft <sup>d</sup>
1						14	5.00	3.75		1.20	8.38
2						15					
3	3.50		0.21	0.15	1.27	16					
4	>15.00	1.80	0.57	0.54	3.38	17	>15.00			6.81	47.10
5						18					
6						19	0.25				
7						20	0.75		4.25	3.49	24.80
8				0.93	6.43	21			2.90	2.31	16.90
9			0.86	0.76	5.06	22			5.81	5.40	31.60
10						23			0.44	0.44	2.59
11			0.52	0.40	3.01	24					
12				0.59	40.50	25			5.05	4.90	29.50
13				6.29	43.50	26			1.02	0.82	5.90
						27			7.74	6.97	45.10

<sup>a</sup> Measured in psi.  
<sup>b</sup> Pressure measurements were not recorded for tests 1, 2, 5, 6, 7, 10, 15, 16, and 24. The number 18 was not used.  
<sup>c</sup> Some of the test data is missing because the pressure-sensing device was destroyed, due to extreme pressure and temperature.  
<sup>d</sup> Calculated by extrapolation.

**VIDEO/FILM:** Tests were filmed(16mm) at 10,000 frames per second using a Photec IV camera no. PSI-164-8-115. This required only 1.5 seconds for 450' of film. Color VHS video was also utilized at ground level and from an observation deck 15' above the test floor.

**ELECTRICAL MEASUREMENTS:** Electrical measurements are shown in Table IV. Note the significant reduction in let-through  $I^2t$  between Tests 3 (22.6kA cleared by a 601 amp Class L fuse) and 4 (22.6kA protected by a 640 amp Power Circuit

Breaker) and between Tests 23 (65kA cleared by a 601 amp Class L fuse) and 24 (65kA protected by a 640 amp Power Circuit Breaker). This is due to the fact that the Class L fuse was current-limiting while the Power Circuit Breaker was set at 12 cycles (to discriminate with downstream overcurrent protective devices). The arc flash energy was greatly reduced, as can be witnessed in the high speed film and VHS video. This reduction in arc flash energy is a tremendous benefit for the fuse industry. It minimizes workmen's exposure, surely saving lives in the long run.

Table IV[1]  
Measured current

Test No.	Avail. Current (kA)	Peak let-through X 1,000				$I^2T$ let-through X 1,000			
		A $\phi$	B $\phi$	C $\phi$	N	A $\phi$	B $\phi$	C $\phi$	N
1	22.60	0	0	29.80	0	0	0	0	0
2	22.60	0	0	0	0	0	0	0	0
3	22.60	17.70	17.40	18.10	19.70	6.54	8.57	7.66	7.72
4	22.60	28.00	27.10	16.00	28.90	>65.85	>24068.00	>1088.00	>3561.00
5	22.60	0	0	1.60	0	0	0	1.04	0
6	18.00	0	0	1.71	0	0	0	11.60	0
7	18.00	0	0	1.21	0	0	0	1.32	0
8	18.00	0	0	2.94	0	0	0	32.40	0
9	40.30	0	0	9.44	0	0	0	222.00	0
10	40.30	0	17.40	17.70	0	0	510.00	511.00	0
11	40.30	0	0	5.47	0	0	0	37.80	0
12	40.30	0	14.80	14.80	0	0	544.00	520.00	0
13	51.10	0	35.10	29.10	12.30	4992.00	4193.00	4278.00	923.00
17	35.00	50.20	39.00	60.00	15.50	85600.00	109351.00	68338.00	12675.00
19	40.30	13.90	6.00	14.20	2.65	436.00	70.60	562.00	9.92
20	40.30	4.58	8.21	17.30	13.10	66.20	235.00	594.00	470.00
22	69.50	13.10	0	13.30	0	290.00	0	312.00	0
23	65.00	24.10	18.90	13.60	2.16	836.00	367.00	279.00	3.85
24	65.00	47.00	63.20	53.60	36.40	130027.00	167438.00	147740.00	30006.00
25	46.10	4.66	0	4.87	0	7.29	0	7.60	0
26	46.10	10.70	0.31	10.90	0.27	201.00	0.13	208.00	0.09
27	46.10	40.00	59.20	36.80	20.80	25634.00	29891.00	20199.00	5920.00

<sup>a</sup> Current measurements were not recorded for tests 14, 15, 16, and 21.

<sup>b</sup> The number 18 was not used.

**ADVANTAGE FOR THE FUSE INDUSTRY:**

Because of the increased requirement for worker safety, consulting engineers and industrial plants are more frequently specifying fuses in their distribution systems. This is due to the tremendous reduction in arc-flash energy that is associated with the use of current limiting fuses. (Workmen still need to wear proper protective clothing while working on or near live equipment because not all faults will be of a high enough value to be within the current-limiting range

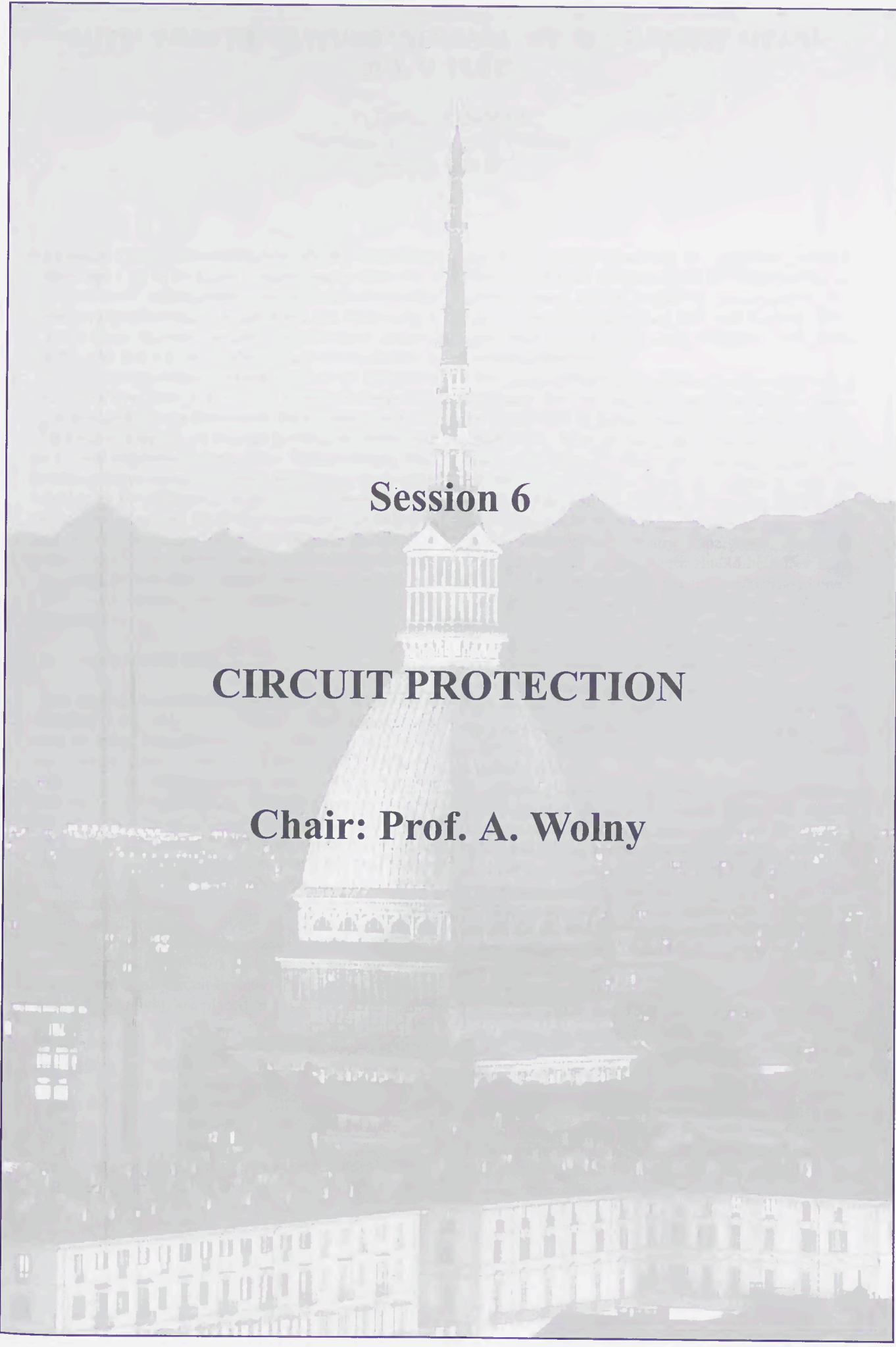
of the fuse.) Fuse manufacturers can take advantage of this opportunity by promoting the IEEE paper and video, or by producing and promoting a similar safety oriented package.

**CONCLUSION:** A volunteer ad-hoc committee was formed to try to increase the awareness of arc-flash hazards in the workplace. After the testing was complete, it became obvious that the current limitation provided by modern current-limiting fuses

provided a real reduction in arc-flash energy, and associated temperatures, pressures, and let-through  $I^2t$ . Various measurements were documented, including very dramatic video and high speed film. Because of the increased level of employee safety, this advantage of current-limiting fuses can be used to help persuade consulting engineers and plant engineers to specify current-limiting fuses as the preferred overcurrent protective devices.

**References:**

- [1] Ray A. Jones, Mary Capelli-Schellpfeffer, Robert E. Downey, Shahid Jamil, Danny P. Liggett, Terry Macalady, L. Bruce McClung, Vincent J. Saporita, Lynn F. Saunders, and Arthur Smith, "Staged Tests Increase Awareness of Arc-Flash Hazards in Electrical Equipment," IEEE Petroleum and Chemical Industry Conference Record, September 1997, pp. 313-322. A copy of the video (VHS), paper, and CD (training presentation) of "Staged Tests Increase Awareness of Arc-Flash Hazards in Electrical Equipment" is available for \$75.00 (US), from: IEEE/PCIC Safety Subcommittee, c/o Kim Eastwood, Thermon Manufacturing Company, 100 Thermon Drive, San Marcos, TX 78666, Phone: (512) 396-5801, Fax: (512)754-2424. Make checks payable to PCIC Electrical Safety Workshop.
- [2] Ralph Lee, "The Other Electrical Hazard: Electrical Arc Blast Burns," IEEE Transactions on Industry Applications, Vol. 1A-18, No. 3, P. 246, May/June 1982.
- [3] NFPA 70E Standard for Electrical Safety Requirements for Employee Workplaces, 1996 Ed. Quincy, Massachusetts: National Fire Protection Association, 1995
- [4] NFPA 70 National Electrical Code, 1999 Ed. Quincy, Massachusetts: National Fire Protection Association, 1998
- [5] Ralph Lee, "Pressures Developed by Arcs," IEEE Transactions on Industry Applications, Vol. 1A-23, No. 4, July/August 1987.
- [6] Dr. T. Neal, A. H. Bingham and R. L. Doughty, "Protective Clothing Guidelines For Electric Arc Exposure," IEEE Petroleum and Chemical Industry Conference Record, September 1996, pp. 281-298
- [7] R. L. Doughty, Dr. T. E. Neal, T. A. Dear and A. H. Bingham, "Testing Update On Protective Clothing & Equipment For Electric Arc Exposure," IEEE PCIC Conference Record, September 1997, pp. 323-336.



**Session 6**

**CIRCUIT PROTECTION**

**Chair: Prof. A. Wolny**

THE HISTORY OF THE

REIGN OF

CHARLES THE FIRST

BY

JOHN BURNET

OF

THE UNIVERSITY OF OXFORD

IN TWO VOLUMES

VOLUME THE SECOND

LONDON

Printed by J. Sturges, in Strand

1734

MDCCXXXIV

Printed by J. Sturges, in Strand

1734

MDCCXXXIV

Printed by J. Sturges, in Strand

1734

# PROTECTION OF DISTURBANCE ARC ON BUS-BARS BY MEANS OF L.V. FUSES

T. Lipski, R. Partyka  
Technical University of Gdańsk,  
Gdańsk, Poland

**Abstract:** Carried out experimental investigations of the disturbance arc in 3-phase l.v. switchboards show that it is possible to interrupt this fault by means of 1-phase interrupting apparatus. A proof of this was made using a flat 3-phase bus-bars system within lumen distance  $d=70$  mm and 90 mm between bars. The prospective metal short-circuit currents were up to ab. 43 kA (RMS) at 3x460 V, p.f.=0.25, 50 Hz. As a protective apparatus a fuse placed only in one central bar has been used. After switching off of the feeding by this fuse of this bar the short-circuit undergoes into 2-phase arcing fault between utmost bars. Then this open arc is interrupted finally by the quenching at its nearest natural current zero. As a result the disturbance arc energy is less than the maximum value 100 kJ permissible for the l.v. switchboards. The conclusion is that 1-phase interrupting apparatus installed in the central bar can prevent such switchboards against destruction due to 3-phase disturbance arc.

## I. INTRODUCTION

The investigations of disturbance arc on switchboards bus-bars have been carried out since several decades and by many authors. The major effort was laid down on medium voltage systems [1] [2] [3] [4] [5]. On the other hand the investigations of disturbance arc in low-voltage (l.v.) switchboards practically were carried out by one, Prof. Stade's, group from TU Ilmenau, Germany, in cooperation with Klöckner Moeller Co [6] [7]. According to Prof. Stade's idea, the protection has an aim to minimize the destructive effects of the disturbance arc by a very quick deenergisation of the whole switchboard, irrespective of the place of that arc appearance. The protective system consists of a number of optoelectronic gauges in a combination with a making-switch and main circuit-breaker. The gauges, tuned to sense the arc light, are placed in several selected spaces of the switchboard. If a disturbance arc will ignite, the gauges, throughout the light-fiber connections, activate the tripping mechanism of the making-switch. As a consequence arise a metal short-circuit on the bus-bars terminals. Thus, the arcing fault will disappear. But still existing metal short-circuit is then finally switched off by the main circuit-breaker.

Described protective system shows several drawbacks:

- The gauges are working with interlinked electronic re-

lays in a system connected by light-fiber network. Hence exists some additional time delay between the arc ignition instant and the instant of making-switch tripping. It should be underlined that each hundred of microseconds of such delay can considerably enlarge the arc destructive effects.

- The gauges should sense relatively narrow light waves bandwidth. On the other hand they should be not sensitive to arc light in the arc-quenching chambers, light of welding arc, light of flash, day light and other light sources. In addition to that, there is a wide range of prospective short-circuit currents in disturbing arcs and places of their ignition in the switchboards. That's why the gauges, tuned on a narrow waves bandwidth, should be selected rather individually to the given switchboard type and number of the gauges should be rather large. Hence the protective system become sophisticated one.

- To get the disturbance arc liquidation there are necessary two special heavy current commutating devices: the making-switch and the main circuit-breaker. Their time of operation should be of order of few ms.

- However, temporary, but appearance, of the metallic short-circuit, between the making-switch contacts closing and final interruption of the fault by the main circuit-breaker. This time should be of order not longer than few ms too.

To note is, that already in 1960 Siemens Co [1] had been suggested an arc disturbance protective system based on a making-switch and a main circuit-breaker, which resembled above sketchy described system of prof. Stade. But at that time the system had no practical implementation. The possible reasons of this were not yet appropriate quality of the optoelectronic gauges at that time and possibility of an unexpected failed making-switch operation which could led to unwanted metallic short-circuit on bus-bars.

Much better solution to the problem under considerations offers a high speed 3-phase hybrid current-limiting and interrupting device (H-CLID) [9].

Using H-CLID, now it means one heavy current device only, one can get similar results, as described above, as concerns the protection of a l.v. switchboard against disturbance arc destruction. Investigations, for example described in [8] [9], show that H-CLID limits the time of disturbance arc duration and its energy to the permissible level suggested by Prof. Stade, which should be not larger than 100 kJ.

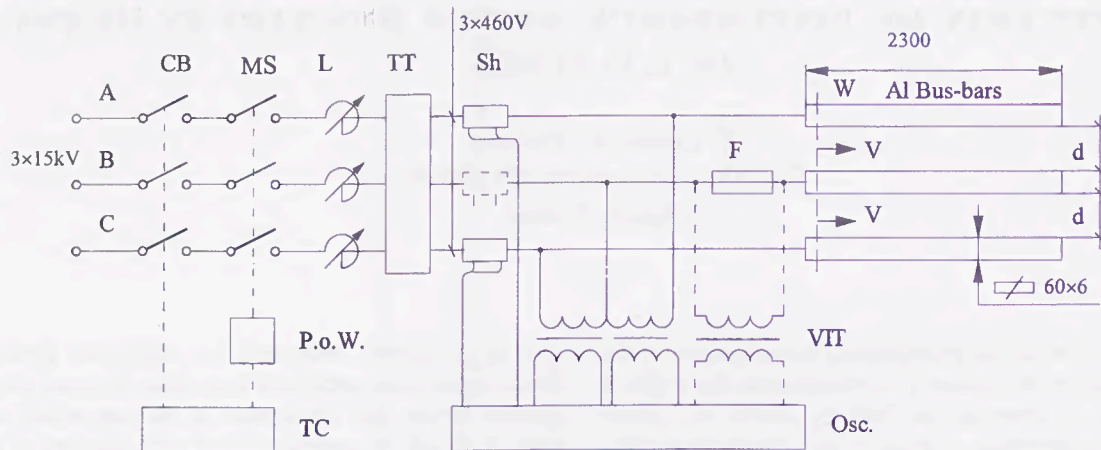


Fig.1 Test's scheme

CB- circuit-breaker, MS- making switch, L- chokes, TT- test transformer, Sh- shunts, VIT- voltage instrument transformers, F- fuse, W- wire for disturbance arc ignition, P.o.W.- point on wave control, TC- time control, Osc.- oscilloscope, d- distance in lumen between individual bus-bars, v- direction of arc-motion

Recently, in doing some experimental research on the disturbance arc in the Chair of Electrical Apparatus of TU Gdańsk, there had been observed a new aspect of that arc behaviour. The aspect pertains to 3-phase l.v. switchboard bus-bars placed in one plane, i.e. flat bus-bars system. It appeared, that if a lumen distance between individual bars is not less than a defined one but still acceptable from practical point of view, a 3-phase arcing fault can be effective switched off by breaking it in one phase only! But the condition is that the switched off phase is the central bus-bar.

To get such a result a l.v. high breaking capacity fuse provided to switch off only central phase was used. In this stage of investigations the use of mentioned fuse instead e.g. of 1-phase H-CLID was dictated by the simplicity of the tests. Such an approach gave an easy control of the interrupting time, by given fault current, by selecting the fuse's rated current.

The paper is going on to describe mentioned protection aspect.

## II. DETAILS OF EXPERIMENT AND RESULTS

In this stage only an experimental approach in real short-circuit conditions was possible.

The investigations were carried out in the 3-phase system (Fig.1) at the prospective short-circuit current ab. 43 kA (RMS), p.f.=0.25 and voltages 3x460 V, 50 Hz. According to preliminary tests for this prospective cur-

rent the arc disturbance current was ab. 27 kA (RMS) (Fig.2). All below described, with some exceptions, tests were carried out in the current conditions corresponding to the point A in Fig.2.

The bus-bars system was placed in horizontal plane within  $d=70$  mm or 90 mm. It was recognised that such distance should be still acceptable by the switchboards designers. Majority of the shots were made using a h.b.c. fuse (F in Fig.1) of the rated current 400 A. This current is large enough to get reasonably good continuous rated power of the bus-bar system, i.e. ab. 320 kVA. Some additional tests using fuses of the rated current 80 A and 125 A were performed to simulate action of a protective device quicker than 400 A fuses. In mind was a possibility of the future application of a 1-phase H-CLID [9], which is a super fast acting apparatus.

To get the disturbance arc-ignition a  $\phi$  0.2 mm Cu-wire had been used, clamped by bolts to each bar in the place W (Fig.1). According to authors experience, selected kind of arc-ignition should have no practical influence on the test results.

Digital oscilloscope in a combination with computer was sufficient to get trustworthy results illustrating the disturbance arc behaviour (Table 1, Fig.3).

In addition to that, to illustrate the influence of an interrupting apparatus switch off time on the time duration of disturbance arc, three different fuse's rated currents were used: 80 A, 125 A and 400 A. All remaining parameters were these same, as mentioned above with one

Table I. Test's results for h.b.c. fuse rated current 400 A

p.o.w. °el	d mm	E <sub>a</sub> kJ	t <sub>a</sub> ms
90	70	77.6	10.2
		79.2	10.9
120		57.2	9.0
		63.3	8.9
150		45.3	11.2
		48.2	11.6
180		45.7	6.3
		46.6	6.3
210		38.0	5.3
		34.9	5.0
240	90	53.1	10.6
		31.8	5.0
270		80.4	10.6
		64.9	10.6
90		63.3	10.0
		52.3	9.4
150		45.4	11.5
		42.8	12.0
210		38.8	5.6
		38.5	5.4
270	39.2	7.6	
	40.1	5.4	

Note:

p.o.w.- point on wave of circuit making, d-distance in lumen between individual bus-bars, E<sub>a</sub>- arc energy, t<sub>a</sub>- arcing time

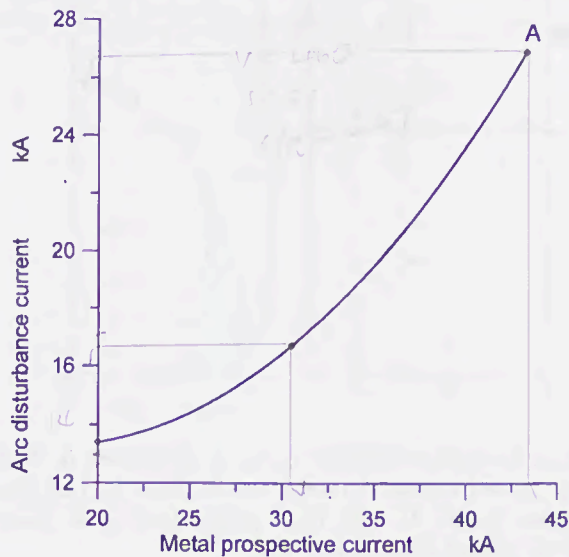


Fig.2 Arc disturbance current versus metal prospective current for d=70 mm (see details in text).

43 27  
31 16.5  
20 13.5

exception. Namely, the distance d=90 for 400 A fuses was chosen. The reason was that at 90 mm easier is to interrupt an open disturbance arc between utmost bars by the natural current zero, after switching off the feeding in the central bar. The results showed that even in such conditions the disturbance arc time for 80 A and 125 A fuses was ab. 15 % shorter than for 400 A fuses. All above results should be considered in a comparison with the arc destruction energy for the case without a quick feeding interrupting of the central bar, by a fuse.

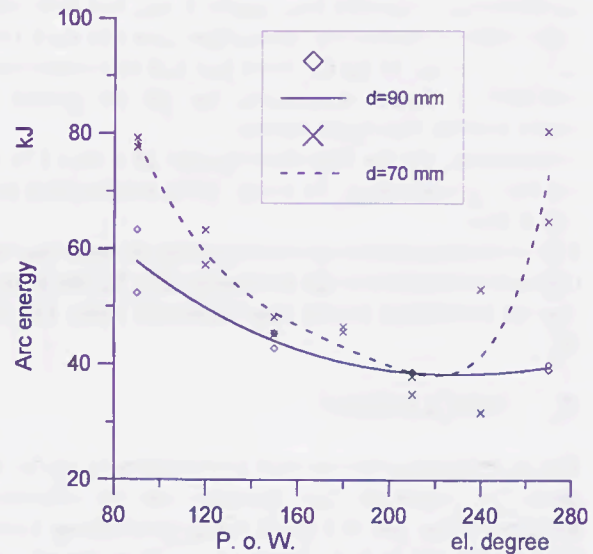


Fig. 3 Disturbance arc energy versus point on wave

That is why also the shots were made without mentioned fuse. In this case for d=70 mm the disturbance arc duration was ab. 19 ms and its energy ab. 190 kJ. Fig.4 shows two typical records.

### III. DISCUSSION

The investigations of Prof. Stade's group [6] at 65...100 kA prospective current led to the statement that, at the time duration of disturbing arc up to 5 ms and liberated arc energy up to 100 kJ, the destruction of a l.v. switchboard is practically negligible. Thus, after small cleaning of the insulating elements and checking of the dielectric withstand the switchboard can be reclosed into service. But the condition is the switchboard compartment should be equipped within a pressure relief reducers.

From records for d=70 mm (Fig.4a), in the instant 1 the feeding of the central bar B become interrupted by the fuse. The 3-phase short-circuit undergoes into 2-phase arcing fault between utmost bars. From this moment the current in both phases is this same, but after several ms also the open arc is finally quenched due to natural current zero.

A different behaviour shows a disturbing arc in the case

of  $d=90$  mm (Fig.4b). Now in the instant 1 the 3-phase arc short-circuit undergoes into 2-phase one, between the phases B and C. The reason is a natural quenching of one arc only, burning between the phase C and outstanding phases. It happens due to large enough distance  $d$ , in this case 90 mm instead 70 mm. So now beyond the instant 1 already a 2-phase (between phases A and B) arcing exists only, which finally has been interrupted by a fuse placed in the central bar B.

The results given in par. II of this paper, in view of Prof. Stade's statement, are very promising. However, the disturbing arc duration was above 5 ms, but their energy, which is crucial for destruction, was less than 100 kJ, i.e. up to ab. 81 kJ for  $d=70$  mm and fuse rated current 400 A. Better results one can get for greater  $d$  and/or smaller fuse rated current.

For example, for the fuse rated current 80 A and 125 A the time of disturbing arc is ab. 15 % smaller than for 400 A fuse.

The investigations also shows that point on wave has an important influence on the arc energy (Fig.3), but in any case its magnitude is less than threshold value 100 kJ [6].

#### IV. CONCLUSIONS

The investigations proves that the disturbance arc in 3-phase l.v. bus-bars flat systems can be effective switched off by use of a quick acting interrupting apparatus placed just in one, central phase. This feature was pointed out by the experiments, for simplicity using h.b.c. fuses as that interrupting device.

Obviously in practical applications the use of one fuse in the central bus-bar is not acceptable. But the results of the investigations show clear that is possible to apply, for example, 1-phase H-CLID instead of a 3-phase one. This conclusion is an important direction how in a cheapest way to protect the bus-bars by a very rapid disturbance arc liquidation without or with a very slight destruction of the l.v. switchboards by means of 1-phase protective apparatus. Of course, the gauges and the whole sensing arc disturbance system will remain as it is in Prof. Stade's solution.

#### ACKNOWLEDGEMENT

Authors have a pleasure to acknowledge that described investigations were carried out in the frames of project nr 8T 10A 03411 sponsored by the Polish Committee of Scientific Research.

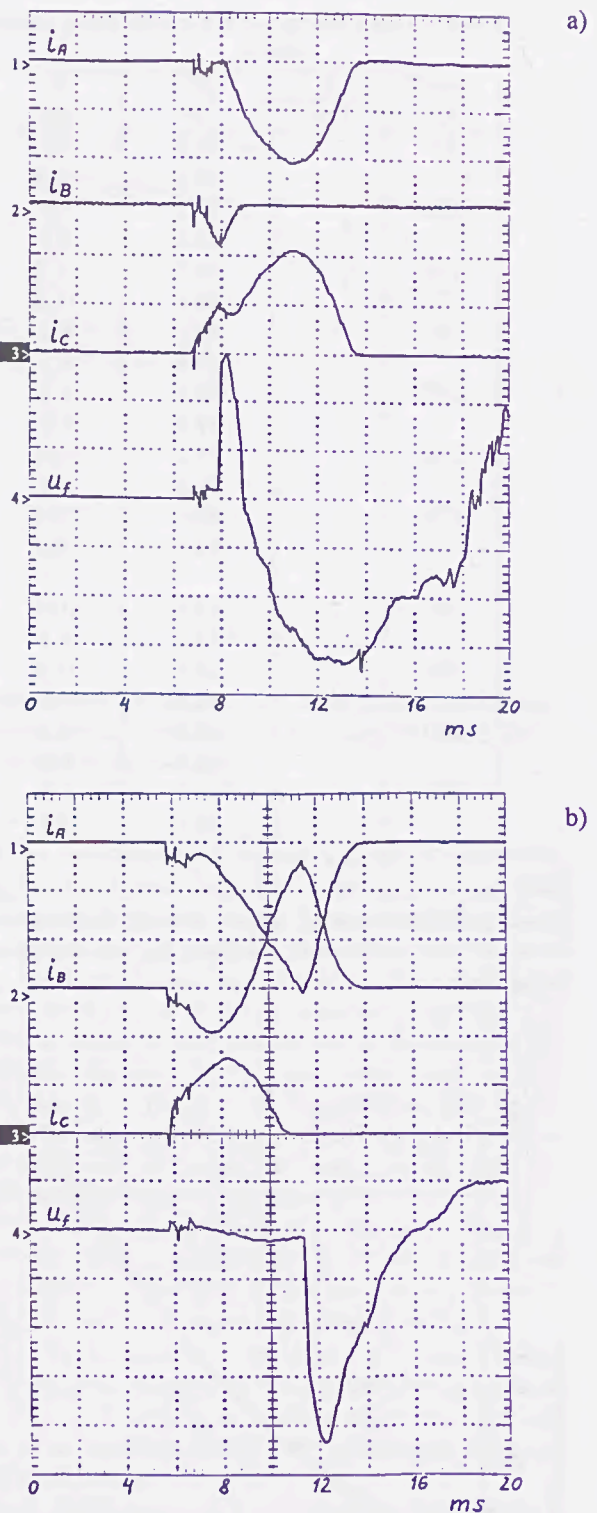


Fig. 4 Records of currents  $i_A$ ,  $i_B$ ,  $i_C$  (in phases A, B, C Fig. 1), and voltage  $u_f$  on the fuse in phase B. Test conditions:  $3 \times 460$  V, 50 Hz, prospective metal short-circuit current ab. 43 kA (RMS);

a- fuse rated current 80 A,  $d=70$  mm  
b- fuse rated current 400 A,  $d=90$  mm  
amplitude factors:

- currents  $k_i=9$  kA/div.
- voltage  $k_u=150$  V/div.

## REFERENCES

- [1] F. Meyer, "Die Beherrschung von Kurzschlußlichtbögen in offenen und gekapselten Mittelspannungsschaltanlagen", Siemens Zeitschrift 34, no. 1, pp. 53-59, 1960.
- [2] A. Hochreiner, "Kurzschlußlichtbögen in Hochspannungsschaltanlagen", ETZ- A 83, no. 7, pp. 202-206, 1962.
- [3] F. Pigler, "Druckentwicklung in Schaltzellen durch Störlichtbogen", Energie und Technik 24, no. 2, pp. 47-50, 1972.
- [4] CIGRE SC23 WG03 "Some aspects for the design of metalclad substations", ELECTRA, no. 34, pp. 63-74, 1974.
- [5] H. Strasser, K. Schmidt, P. Högg, "Effects of arcs in enclosure filled with SF<sub>6</sub> and steps taken to restrict them in SF<sub>6</sub>- switchgear", IEEE- PAS 94, pp. 1051-1060, 1975.
- [6] H. Schau, H. Schäfer, "Lichtbogenenergie- Ein Maß für die Personengefährdung und Zerstörung von Schaltanlagen", Proc. of the 40. Int. Wiss. Kolloquium, pp. 283-288, Ilmenau (Germany), 1995.
- [7] A. Klaus, "Selective optische Erfassung von Störlichtbögen", Proc. of the 40. Int. Wiss. Kolloquium, pp. 289-294, Ilmenau (Germany), 1995.
- [8] J. Czucha, R. Partyka, J. Żyborski, "AC low- voltage arcing fault protection by hybrid current limiting interrupting device", Proc. of the 7th International Symposium on Short- Circuit Currents in Power Systems "SCC '96", Warszawa (Poland), 1996.
- [9] J. Żyborski, T. Lipski, J. Czucha, R. Partyka, M. Pikon, J. Piotrowski, "Arcless current limiting and interrupting device for disturbance arc and other protections", Proc. of the 3rd International Conference on Electrical Contacts, Arcs, Apparatus and their Applications „ECAAA'97", Xi'an (China), 1997.

Faint, illegible text at the top left of the page.

Second block of faint, illegible text in the upper left section.

Third block of faint, illegible text in the upper left section.

Fourth block of faint, illegible text in the upper left section.

Fifth block of faint, illegible text in the upper left section.

Faint, illegible text at the top right of the page.

Second block of faint, illegible text in the upper right section.

Third block of faint, illegible text in the upper right section.

Fourth block of faint, illegible text in the upper right section.

Fifth block of faint, illegible text in the upper right section.

Faint, illegible text at the bottom left of the page.

Faint, illegible text at the bottom right of the page.

# FUSE UNEXPECTED OPERATIONS IN SOFT-STARTERS BY DISSIMILAR CURRENT DISTRIBUTION

Juan C. Gómez, Daniel H. Tourn, German R. Zamanillo, Julio Lepori

National University of Rio Cuarto, Engineering Faculty, (IPSEP)  
Ruta 36, Km. 601, (5800), Río Cuarto, Córdoba, ARGENTINA  
Telephone / Fax: +54 358 4676171 or +54 358 4676251  
Email: ipsep@ing.unrc.edu.ar

## Abstract:

At present time, the application of low and medium voltage soft-starters (permanent or only during the start) and motor drives is wide spread in the industrial systems, being most of these motors short-circuit protected by fuses.

The power electronics introduces harmonics in the current and voltage waves, between them the most important are the 5° and 7°, being measured values of THD as high as 30 %.

Besides, when soft-starters are protected by fuses, the specific energy of the assisted start current is several times the direct start value, being measured ratios between 10 and 20, with starting times of 15 seconds and less than a second respectively.

After the report of several of these fuses bad or unexpected operations, a study was done about the normal load behaviour of commercial fuses under 400 Hz and 1200 Hz supply. The frequency was adopted for the equipment availability, because this is one of the standards for mainframes and aircraft supply, and the second one due to the importance of 20° and 24° harmonic in the driver current waves.

The high-speed fuses normally have several parallel ribbons, regularly distributed inside the fuse body, for which the experimental approach consisted in the determination of the current distribution between the several ribbons and its comparison when connected to 50 Hz, 400 Hz and 1200 Hz. In order to avoid any constructive alteration, the current distribution was obtained for the voltage drop in each fuse element.

The behaviour under 50 Hz conditions is very symmetrical, in magnitude and phase, except by the extremely small constructive differences. Under 400 Hz. and 1200 Hz., the behaviour is dissimilar, being measured amplitude differences of 20 % and phase shifts of 20 ° in average.

Besides, it is necessary carry out a carefully study of the fuse position (inside the starter) in order to take account of the proximity effect, being that matter the objective of further study.

From the preliminary results, the dissimilar current distribution can be the cause of the fuses mal-operation, being necessary the fuse derating in order to avoid the ageing and premature melting.

Keywords: electric fuses, harmonics, current distribution, skin effect

## 1- INTRODUCTION

The advances in the power electronics, microprocessors and magnetic materials of the last 20 years have made possible to get significant advances in the application of induction motor drivers and soft-starters. With these new technologies a notable increment has taken place in the field of application of this type of motors overcoming in many cases, as much in cost as in benefits to the traditional d.c. motor.

With the new second generation electronic switches it has become possible to build commercially attractive electronic inverters which can operate with frequencies bigger than 10 kHz [1]. For these values of commutation frequency inverters are built with pulse wide modulation (PWM) being used in the great majority of the variable frequency converters applied to induction motors.

This type of drive consists of a rectifier with not controlled diodes in the input; a filter formed by a big capacitor so that the rectifier entrance appears like a voltage source with a very small internal impedance; and a inverter having electronic switches (usually IGBT transistors) that allows to control as much the magnitude as the frequency of the exit tension. The input alternating current of

the frequency changer contains a great quantity of harmonic, with a high percentage of fifth one as can be observed in figure 1, situation which is also presented in the start of motors with soft starters, as shown in figures 2.

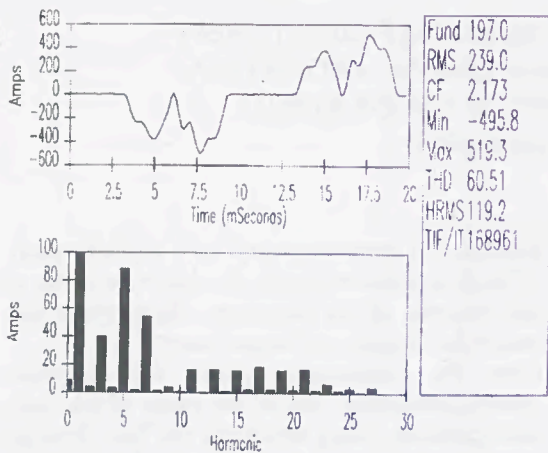


Fig. 1, Steady state current of a 150 HP, 380 V motor drives.

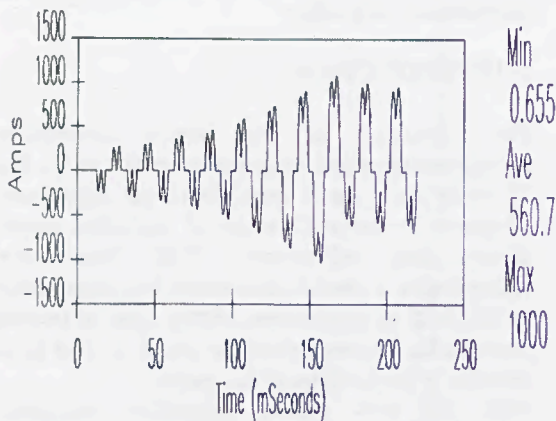


Fig. 2, Start current wave using soft-start in 400 HP, 380V motor.

The protection fuses placed to the entrance of these equipment are usually designed and built to work at the power distribution frequency (50 or 60 Hz) and they are generally of general purpose or motor protection class (gG or aM).

The objective of this work is to establish the influence of the currents with high harmonic content in the behaviour of the industrial type fuse.

## 2- THEORETICAL ANALYSIS

The phenomenon that can affect the behaviour of a fuse with different values of frequencies are the

established ones for the electromagnetic laws. If we consider that a fuse is compound for an or more parallel ribbons, with a current distribution among the different ribbons as well as to the wide of each one of them that depends on its resistance and inductance. It is then concluded that the dependence of this distribution with the frequency is precisely due to the inductance.

If we study what happens in a fusible ribbon when it is travelled by currents of different frequencies, it is clear that the distribution of the current flow in the cross section will depend on the frequency according to that postulated by the well-known phenomenon of skin effect. The skin effect postulates that for high frequencies the current distribution in the conductor cross section is confined to its surface, causing that the effective resistance of the conductor increases as the frequency does. In the references a study is presented that concludes that the influence of the effect skin in thin ribbons as the used as fuse elements, for frequencies smaller than 5 kHz, is worthless in the depth and it can be important in the width. [2]

In the case of having ribbons in parallel, the distribution of the currents would not only depend on its resistances and own inductances but rather the effect caused by the magnetic flux. Which is created by one ribbon on the other ones, inducing stray currents that will also affect the current distribution. This phenomenon that depends on the distance among ribbon conductors denominates proximity effect. In the references a study of the influence of the frequency in the current distribution among three parallel ribbons with frequencies between 0 and 100 kHz was carried out. [2]

## 3- EFFECT OF THE HARMONIC CONTENTS ON INDUSTRIAL FUSES

Although of the theoretical analysis and of that concluded by other authors in the consulted bibliography it comes off that the high frequencies have an important effect in the current distribution among parallel fuse elements. In the authors' knowledge there is not any investigations on the influence of these phenomenon in industrial fuses with frequencies of the order of the harmonics presented in variable speed motor drivers and soft starters. [3].

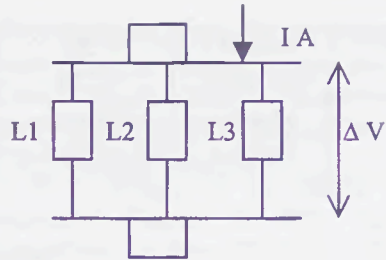
For such a reason was carried out an experimental study using fuses available in the market and also on fuse prototypes to evaluate the influence of some parameters like the ribbons separation and width of the same ones.

#### 4- DESCRIPTION OF THE TEST SERIES.

The way to observe the effect of the frequency on the current distribution consisted on to measure the voltage drops in the similar fuse elements and to quantify the difference among the measurements at different frequencies. The power on 50 Hz was took directly from the main supply, using a variable autotransformer in order to allow the current regulation. The currents in 400 and 1200 Hz were took from two synchronous generator. The voltage measurements were made in direct form, on the other hand the current was measured with an amperometer clip, carrying out the transmission by optic fibres (in order to become independent of the reference earth), having previously tuned the offset aim to avoid phase errors. As the used digital oscilloscope possesses 4 input channels, they registered simultaneously the three voltage signals corresponding to each one of the parallel fuse elements and the indication of the total current.

The selected samples were following VDE 0636 standard, size 3, ceramic body, iron lids and with three copper fuse elements. Part of them were commercial devices, being the remaining ones assembled in the own workshop using commercial fuse element sheets whose separation was of about 5 mm. [4]

The measurements were made after having lapsed a time of the order of the 30 minutes, in order to allow the thermal stabilisation of the under test device. The fuse physical position as also the remaining test conditions (circuit, ambient, etc.), were maintained exactly the same in all the tests. The figure 3, shown the fuse element positions and the corresponding connections.



- Channel 1: fuse element 1 voltage drop signal (L1) in mV.
- Channel 2: fuse element 2 voltage drop signal (L2) in mV.
- Channel 3: fuse element 3 voltage drop signal (L3) in mV.
- Channel 4: signal of the total current (I) in mV.

Fig. 3

It should not be forget that cannot be guarantee an exact geometric distribution of the ribbons inside the fuse body in the commercial fuses, since although it is certain that the devices were dismantled in order to weld on them the signal conductors, the position of the sheets was not altered.

The width of the sheet was modified from test to test, using elements with several bridges, between 2 and 7.

#### 5- RESULTS

The obtained results of voltage drop on the ribbons denominated L1, L2 and L3, jointly with the total current and their absolute and percentile differences, they are indicated in the Tables I and II.

Table I, commercial fuses.

Test N°	Notes	f (Hz)	L1	L2	L3	L1-L2	L2-L3	L1-L3
1	Sample 1	50	12,7	13,36	12,62	-0,66	0,74	0,08
	In= 400 A	400	15,25	13,36	12,62	1,89	0,74	2,63
	6 bridges	difference	2,55	0	0	-2,55	0	-2,55
	I=128 A	% difference	20,08	0,00	0,00			
2	Sample 2	50	22,65	24,8	21	-2,15	3,8	1,65
	In= 400 A	400	20,7	32	23,75	-11,3	8,25	-3,05
	6 bridges	difference	-1,95	7,2	2,75	9,15	-4,45	4,7
	I=226 A	% difference	-8,61	29,03	13,10			

3	Sample 3	50	38,94	40,9	39,36	-1,96	1,54	-0,42
	In= 400 A	1200	39,22	46,34	48,54	-7,12	-2,2	-9,32
	6 bridges	difference	0,28	5,44	9,18	5,16	3,74	8,9
	I=300 A	% difference	<b>0,72</b>	<b>13,30</b>	<b>23,32</b>			

Table II, assembled fuses.

Test N°	Notes	f (Hz)	L1	L2	L3	L1-L2	L2-L3	L1-L3
4	assembled	50	37,32	36,31	37,81	1,01	-1,5	-0,49
	2 bridges	1200	39,6	38,77	37,96	0,83	0,81	1,64
	I=107 A	difference	2,28	2,46	0,15	0,18	-2,31	-2,13
		% difference	<b>6,11</b>	<b>6,77</b>	<b>0,40</b>			
5	assembled	50	80,725	79,23	78,945	1,495	0,285	1,78
	3 bridges	1200	90,58	89,425	83,89	1,155	5,535	6,69
	I=280 A	difference	9,855	10,195	4,945	0,34		
		% difference	<b>12,21</b>	<b>12,87</b>	<b>6,26</b>			
6	assembled	50	43,35	35,64	38,289	7,71	-2,649	5,061
	5 bridges	1200	53,543	41,8	47,95	11,743	-6,15	5,593
	I=288 A	difference	10,193	6,16	9,661	-4,033	3,501	-0,532
		% difference	<b>23,51</b>	<b>17,28</b>	<b>25,23</b>			
7	assembled	50	24,65	21,57	23,972	3,08	-2,402	0,678
	7 bridges	1200	34,2	31,835	29,47	2,365	2,365	4,73
	I=282 A	difference	9,55	10,265	5,498	0,715	-4,767	-4,052
		% difference	<b>38,74</b>	<b>47,59</b>	<b>22,94</b>			

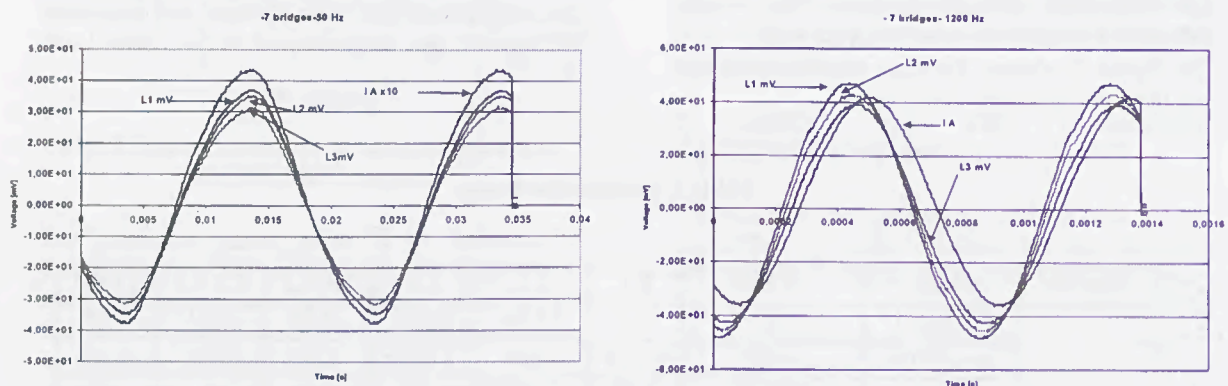


Fig. 4

The figure 4 shows the oscillograms of the voltage drops in the three ribbons and the total current of the test 7; having a number of bridges of 7, with frequencies of 50 Hz. and 1200 Hz., where it is shown the unequal current distribution and the phase shifts.

## 6- CONCLUSIONS

Of the reduced number of determinations, it can be inferred that for the existent frequencies in motor drivers and soft-starters of industrial systems (50 or 60

Hz.), the asymmetry in the voltage drops indicates an unequal current distribution. Such an effect produces bigger losses and operation outside of the fuse range. This problem justifies bigger study, being the present work only a provisional contribution in such a direction.

#### REFERENCES

[1] A. Von Jouanne, P. Enjeti, W. Gray "Application Issues for PWM adjustable speed AC motor drives" IEEE Industry Applications Magazine Vol. 2, N°5, pp 10-18. Sept/Oct. 1996.

[2] S. Duong, C. Schaeffer, R. Desahayes, J. L. Gelet, "Distribution of high-frequency currents through the elements of a fuse", Fifth International Conference on Electric Fuses and their Applications 5<sup>o</sup>ICEFA, pp 229-235. Ilmenau, Germany 1995.

[3] V. E. Wagner et al, Effects of harmonics on equipment" Report of IEEE Task Force, IEEE Transactions on Power Delivery, Vol 8 N° 2 pp. 672-680. April 1993.

[4] VDE 0636 Part 21 and Part 22: "Low-voltage H.R.C. fuses" 1984.



# OVERCURRENT PROTECTION OF CABLES BY FUSES: CONSIDERING LIFE LOSS AND M-EFFECT

Juan C. Gómez, Gabriel N. Campetelli, Marcelo A. Basilico, Marcos Felici.

National University of Rio Cuarto, Engineering Faculty, (IPSEP)  
Ruta 36, Km. 601, (5800), Río Cuarto, Córdoba, ARGENTINA  
Telephone / Fax: 54 358 4676171 or 54 358 4676251  
Email: ipsep@ing.unrc.edu.ar

## Abstract:

A methodology to be used in the studies of low voltage cable protection by fuses has been developed. The procedure includes the cable life loss calculation following Arrhenius law and the estimation of the fuse M-effect diffusion. The method is applicable for steady state loads as well as cyclic or transient calculations, considering load intervals of 5 minutes and taking account of the environment temperature changes, for example in sinusoidal way. The pre-load conditions for both elements can be included in the calculation. The M-effect behaviour was experimentally determined, being the best one the exponential with the coefficient as temperature function and a time proportional exponent. Such law was applied to the calculation of fuse resistance under variable current density; being determined a critical resistance value, which is a reversibility limit. The experiments included oven M-effect diffusion under constant temperature and fuses low current melting for times between a few hundred seconds and several hours. The comparison between the experimental and analytical results is good which confirm the applicability of the proposed law. The calculation needs the knowledge of some fuse constructive characteristics, which can be supplied by the fuse manufacturer or determined by very simple tests. The methodology is of very easy use for most of the practical cases, allowing the study of cable protection for overloads inside the M-effect operation zone.

**Keywords:** Cable, HBC Fuse, protection, overload, short-circuit,

## 1 - INTRODUCTION

The protection of conductors and electric cables is one of the topics less analysed in the specific bibliography, giving the impression that the same one was already out. In spite of it, our experience indicates that the professionals involved with the topic meet with too much frequency in front of damaged conductors, for inadequate performance of the protection, due fundamentally to the ignorance of the requirements to complete for the same one.

The cables are elements classified as of high time constant whose real meaning is that they possess considerable capacity to support overloads, allowing in

such a way to overcome conditions of emergency of the system. Obviously that such a capacity possesses a limit that should be kept in mind by the protection, being a normal practice the exploitation of such an ability not only in emergency but even during the load pick hours.

It should be had in mind that the deterioration of the cable, originated in the electric current takes place exclusively for high temperatures during long times. In other words, a conductor possesses a certain useful life (for example 20 to 40 years according to the type), with a load state generally called rated current. If the conditions of electric load are but high a consumption of useful life takes place to bigger speed and the inverse one its durability extends.

For it the good protection would be that that measures temperature indicating the operating time, but due to economic and technical reasons, in the great majority of the cases the protection acts on the base of the current - time relationship. In this work it will be analysed the characteristics of the protection of cables exclusively using fuses, be already of high rupture capacity like of expulsion.

The protection is studied from two aspects, as it is conductor internal or external fault, if it is external, the protection of the cable acts like back-up to the corresponding to the failed element, should operate before deterioration takes place in the cable for it protected.

The treatment conducive to the selection of the protection should be begun once the characteristics of the cable and the installation conditions are perfectly known.

There are several calculation programs that allow to determine the conductor load capability in function of the installation conditions, indicating in some cases the form of protecting them, procedure that doesn't allow to keep in mind special states of load neither to give consumption of useful life. [1]

## 2 - CABLE STUDY

### 2.1 - Overload and short-circuit capability

The characteristics of the current cables have improved notably in the last years, nevertheless the catastrophe risk continues being important, and neither they are exempts of damage for overheating caused by overcurrent and short circuits.

### 2.1.1 - Steady state or slight overload

The protection is made on the base of the consumption of useful life, using for it the modified expression of the law of Arrhenius. Such a principle considers that the driver can be used to his maximum temperature of work during all his useful life, consuming it in a regular form. Also, the increment of the temperature in 8 °C reduces its life in half and a decrease of temperature in same value duplicates the life of the cable. [2]

The equation of the law is the following one:

$$C_v = \frac{1}{2^{\left(\frac{\theta_a - \theta_n}{8}\right)}} \quad (1)$$

Where:

$C_v$  = consumption of life in p.u.

$\theta_a$  = Temperature reached in °C

$\theta_n$  = Work temperature or continuous regime in °C

The acceptable temperatures for the most important types in cables, vinyl polycloride (PVC), polyethylene thermoplastic (PE), cross linked polyethylene (XLPE) and etilen-propilen rubber (EPR), are shown in Table 1.

Table 1: Acceptable temperatures

Temperature	Steady state	Emergency overload	Short circuit
Type		t < 100 hs./year, t < 500hs./life	Time < 5 s
	°C	°C	°C
PVC ≤ 300mm <sup>2</sup>	70	100	160
PVC > 300 mm <sup>2</sup>	70	100	140
PE	75	90	150
XLPE	90	130	250
EPR	90	130	250

A differentiation should be made in the study, when cables of low and medium voltage are considered. Firstly, in medium voltage the cables usually possess a copper electrostatic screen. The word shield is used when the screen also has as purpose to protect to the cable of the external electric influences. This gives a path to earth for the fault current, with their rising limitation of temperature - time, should keep in mind that most of the faults in cables is or they begin as monophasic. [3]

### 2.1.2 - Short circuit solicitations

The short circuits cause a very intense heating in the cables for effect of the heat generated in the conductor. Due to the short time since the fault settles down until the moment in that this should be interrupted, we can suppose that all the generated heat is used in elevating the temperature, we consider for it an adiabatic phenomenon, valid supposition until times of 5 seconds.

The expression corresponding to the adiabatic process, is the following one:

$$v \cdot C \frac{d\theta}{dt} = r i^2 \quad (2)$$

whose solution is:

$$(I/s)^2 t = C / (\rho \cdot \alpha) \ln ((\theta_2 + 234) / (\theta_1 + 234)) \quad (3)$$

Where:

I = current in A.

s = section in mm<sup>2</sup>.

t = time in s.

C = specific heat in J/°C mm<sup>3</sup>.

$\rho$  = specific resistivity ohm / mm.

$\alpha$  = resistivity variation with the temperature in 1 / °C.

v = volume in mm<sup>3</sup>

$\theta_1$  = initial temperature in °C

$\theta_2$  = maximum temperature allowed in °C

If we consider the cable (screen or armour) working to a temperature  $\theta_1$  and knowing the values of the conductor's constants (copper, aluminium, etc.), we can calculate the time necessary t to elevate the temperature at  $\theta_2$ , when the current has a value I, using the mentioned expression. The equation allows the determination of the times so much for conditions of cold conductor like for any load state, even overload. For example for a conductor isolated in XLPE, considering preload of 100%, the expression given by the maker is:

$$I (A) = k S t^{0.5} \quad (4)$$

With the section in mm<sup>2</sup>, the time in s. and the constant k similar to 143 for copper conductor, 94 for aluminium one and 128 for copper screen.

There is a very precise work, which considers to the mentioned magnitudes, resistivity, thermal conductivity, longitude, density and heat specific variables with the temperature in quadratic form, not being justifiable its complexity for normal cases. [4]

If the corresponding temperatures are placed for nominal work and supported maxim, together with the conductor cross section, the current - time expressions become values of constant specific energy, that is to say,  $I^2 t = \text{constant}$ . Such a value can be traced in the graph current - time of the protection device, being represented by a straight line with slope equals to minus two (-2) whose validity extends only until times of 5 seconds.

According to the short circuit current in the installation place, the times of the current limiting fuse operation will be different, should use in the equations the values corresponding to the sub-transient asymmetric short circuit one when the performance is in the order of less than 100 ms., using the permanent value of the current if the device takes more than the given time.

### 2.1.3 - Rigorous overload solicitations

This problem originates in the excess of conductor connected loads, increase of the consumption, openings of rings, transfer of loads, etc., producing a phenomenon different to the one studied previously. The thermal capacity of the cable is important for what this overload can be allowed during considerable times, for which the supposition of adiabatic regime is not any more valid. The calculation is but complex, being able to make by means of some of the available analytic tools, like finite differences, finite elements, etc. or using the expressions given in the Standards. The standard ANSI/IEEE n° 242, Chap. 8, it specifies an equation that allows to determine the maximum current of the cable in function of the time, for any preload state, applicable from slight overloads until short circuits.

$$\frac{I_E}{I_z} = \frac{[(\theta_E - \theta_0)/(\theta_z - \theta_0)] - \left(\frac{I_0}{I_z}\right)^2 e^{-t/K}}{1 - e^{-t/K}} \cdot \frac{230 + \theta_z}{230 + \theta_E} \quad (5)$$

Where:

$I_E$  = cable emergency load

$I_0$  = cable preload current

$I_z$  = cable rated current

$\theta_E$  = cable load emergency temperature

$\theta_z$  = cable normal load temperature

$\theta_0$  = ambient temperature

$t$  = time after the overload's outburst in hours

$K$  = constant of time of the cable in hours

The value 230 is really an average of 234 corresponding to the copper and 228 of the aluminium.

The time constants can be defined in the following way: [5]

0.5 small cables in air

1.0 cables of medium or small size in air or not directly buried

1.5 big cables in air or directly buried small cables

2.5 direct and not directly buried medium cables

4.5 big buried cables

6.0 big directly buried cables

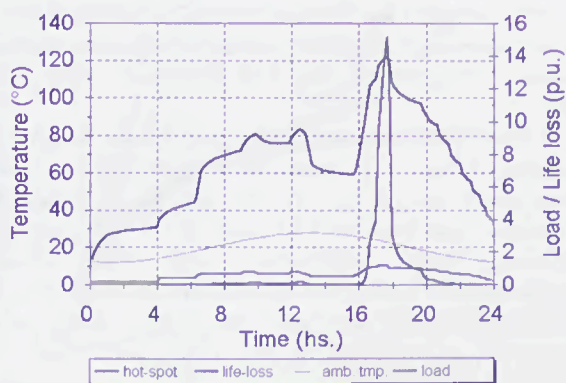


Figure 1, Cable life loss

The given expression allows building the cable time - current characteristic curve, which can be directly compared with the homologous one of the protection device.

### 2.2 - Cable life loss calculation

The elevation of temperature of the cable can be determined by means of the application of the exponential expression whose final value is proportional to the current squared, its time constant takes the previously given suitable values. Knowing the law of variation of the ambient temperature, the load state and the time constant, the cable temperature can be easily calculated along the under analysis period of time. Applying the law of Arrhenius, the consumption of useful life in the under study interval can be predicted. In the Figure 1 the carried out work is shown.

### 3 - FUSE STUDY

The protection of the cable on the part of the fuse in the area of rigorous overloads and short circuit only means the comparison of the characteristic curves, on the other hand when it is a light overload, it is necessary the employment of the concept of loss of useful life. The reaction of the fuse in front of those small overloads is based on the M-effect that will be studied next.

#### 3.1 - M-effect diffusion

In the usual materials of fuse elements, copper and silver, the previous temperature to the arc establishment in the case of overload can reach the 1080 and 960 °C respectively, reducing the thermal differences and thus complicating the energy extraction. The solution to the one mentioned inconvenience was achieved in 1939, with the incorporation of the denominated M-effect, presented by Metcalf. [6]

Such an incorporation consists on the adding of a low melting point material deposit, with what descends the temperature of the filler in the moment of arc initiation, to less than 250 °C. This addition allowed to extend the performance field in front of slight overloads, until values so low as 1,2 times its nominal current, diminishing the heating to steady state regime and simultaneously reducing the power loss.

The complete operation of the fuse at the present time can be calculated by means of the application of analytic models of enough complexity, what allows the investigator and professional of high specialisation to achieve extremely reasonable approaches. Unfortunately the handling of calculation tools and modelling as powerful as they are the finite differences, finite elements, TLM, etc. is not within reach of the normal user.

The modelling of the diffusion process will allow to verify the protection against overload of power equipment in general and of cables in particular, especially in those cases in that the circuit is subjected to recurrent loads.

Independently of the number of section reductions and of the restriction relationship (quotient among shoulder and restriction dimensions), the maximum temperature takes place in the central area of the fuse, because the main one via for the dissipation it is through the extreme contacts. It is in fact in this central area where the material of low melting point is deposited (M-effect), usually tin, lead and cadmium alloys whose melting temperatures are function of the alloy, being between 170 and 200°C. [7].

When the M-effect reaches the melting temperature, it dissolves the bases material (fuse element), either copper or silver, in way of forming an amalgam with more resistivity and with effect initiator, unchaining an accumulative process that eroded the metal bases increasing its resistance and generation of heat until the total melting and consequent electric arc start.

In the case in that the quantity of liberated energy is not enough to liquefy to the M-effect, the breakup process doesn't take place. If there are load picks or high recurrent loads, it can begin the breakup and to advance for stages, until the fuse is melted with even smaller currents than its rated value, process that is denominated ageing. [8].

### 3.1.1 - Behaviour under steady state conditions

The fuse is composed of very varied materials with different thermal constants, however the heating and cooling processes can be assimilated to the heating of a homogeneous body, provided the temperatures of melting of the M-effect is not overcome [9].

For it, the fuse element average temperature responds to an exponential law fixed for:

$$T = T_f (1 - e^{-t/\tau}) \quad (6)$$

Where:

$T_f$  = reached final temperature.

$t$  = time.

$\tau$  = fuse thermal time constant.

The variation of the fuse resistance, experimentally determined in a heating test, based on the measurement of the voltage drop with constant current, follows a similar law to the mentioned equation, therefore one can affirm that the resistance is a trustworthy indication of the temperature average of the fusible element. [10]

Starting from the graph obtained experimentally, the values of "time constant" and "final temperature" can be determined, this last one proportional to the value of the squared current density. Such values allow to predict the temperature changes and thus the average element resistance, when the fuse is subjected to preload cycles, loads, cooling, etc..

The explained method allows studying the behaviour when the fusible element doesn't possess effect M, determining the temperatures, resistances and voltage drop.

Without the M-effect, anything prevents that the temperature in the hottest point in the fuse reaches the melting point of the copper or silver according to the case, that which will damage to other components of the circuit, like they are the fuse holder, connection conductors, protected device, etc.. [9]

### 3.1.2 - Behaviour during the dissolution

The break-up begins when being overcome the M-effect melting temperature. In order to be able to connect the simple model previously explained to the break-up conditions it is required to know the relationship among the external magnitudes: voltage drop and current, with the interior temperature of the hottest fuse element point that is in fact where the deposit of low melting point is placed.

This knowledge will indicate if the break-up process has begun, being to determine like it progresses and that way is affected by overload's conditions.

## 3.2 - Experiments

The study of the diffusion process was made in two ways, firstly by testing on samples fuses operated with overloads of until 200% of the nominal load and later on determining the penetration depth in function of the time and temperature.

### 3.2.1 - Fuse samples

As the objective it is to develop a simple model and of easy application, fusible samples so similar were built those of industrial use as it was possible, type VDE 0636, class gL, size 1, 500 V with rated current of 160 A.. [11]

The fuse in if it consists of a steatite made ceramic body, copper knives, aluminium lids, copper ribbons 99,9% and quartz sand as filler material of grains among sieves 30 and 50 (ASTM standards). The low melting temperature deposits that was applied to 85% of the samples it was carried out using a tin-cadmium alloy 80/20, welded on the bases element by using a butane gas torch.

### 3.2.2 - Fuses low current operation

As first measure the internal resistances of the samples were determined, using the voltmeter - ammeter method whose average value was  $4,45 \text{ E-}04 + / - 0,05 \text{ E-}04$  ohm.

The fuses were installed in the fuse holder, located in vertical form, connected to copper cables, with dimensions responding to the mentioned standards. Constant loads between 130% and 200 % were applied, allowing their stabilisation with the ambient temperature or waiting the operation of the fuse.

During overload's processes the voltage drops were measured in function of the time, with times of sampling inversely proportional to the currents, in order to be able to determine the heating and later diffusion as they processes.

### 3.2.3 - Oven diffusion

Was carried out on samples built with copper ribbons of uniform cross section, purity 99,5%, with the following dimensions: length 60 mm, wide 18 mm and thickness of 0,1 - 0,2 and 0,3 mm. In the central part of the ribbons, the alloy of low melting point (tin-cadmium 80-20) was deposited in cylindrical form of 5 mm of diameter. The process of fixation of the material was carried out using electric solder torch. The samples built in such a way underwent heating in electric oven, with constant temperature (maintained +/- 1 °C), remaining in the oven different samples during growing times that freeze the phenomenon when being extracted. The process was studied for temperatures between 220 and 305 °C, with times being increased of 10 in 10 minutes. The samples treated in this way were injected in resin. The test samples became polished until reaching the mirrored surface, by means of the employment of abrasive with sizes from 200 up to 800 (ASTM), being made a finished with alumina. Later on the diffusion depth was measured by means of a metallographic microscope having a magnification of 200, being studied two hundred samples approximately. In order to check the statement that the penetration is interrupted when the temperature is lower down, remaining without being restarted until the maximum previously reached temperature is overcome, penetration cycles were made with three to five samples in simultaneous form, retiring some, reinserting them later on. The result confirmed the previous enunciated one.

### 3.3- Results

The Figure 2, shows the experimental values of voltage drop during heating - melting tests with 220 V of a gL type fuse of 160 A., using copper fuse element, with ambient temperature of 25 °C. It is experimentally proven that the voltage drop and the average resistance (directly related with the temperature) they follow a law like the one shown in the Figure, which corresponds to a series of fuses without any preload and under overloads of 137, 156, 169, 175, 181 and 187%.

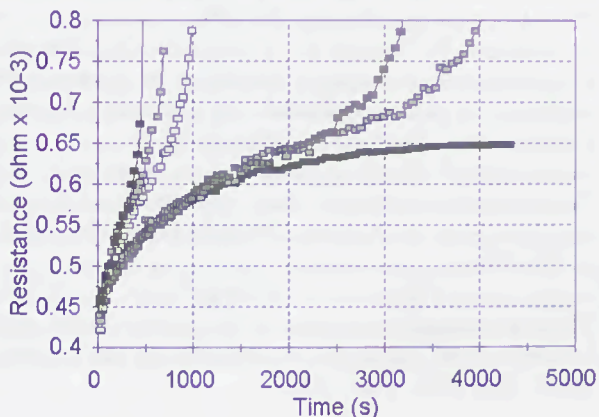


Figure n° 2  
Resistances increase for diffusion

From the graph the value of the resistance limit can be deduced that is in the order of 0,65 mohms that correspond with the maximum temperature before the diffusion initiation, 177 °C.

The penetration depth in function of the time, for variable oven temperatures, is shown in the Figure 3. In the Table II the coefficients and the average quadratic errors of the equations are transcribed that approach the curves of Figure 3, where it can be proven the law of exponential variation of the break-up phenomenon.

$$P = a \cdot e^{bt} \quad (7)$$

Table II  
Coefficients of the exponential equation

Temperature ° C	Coefficients		R <sup>2</sup>
	a	b	
220	10.7	0.0053	0.9886
235	10.1	0.0066	0.9878
265	6.7	0.0063	0.9856
280	12.3	0.0062	0.9348
290	13.6	0.0067	0.9892
305	17.4	0.0074	0.9948
average		0.0064	0.9801

The employment of potential equations to the experimental results gives bigger errors, being the exponents variable between 0,45 and 1, that that partly coincides with other authors' results. [9], [10]

In order to verify the compatibility from the experimental determinations of diffusion to constant temperature and elevation of the resistance in function of the time, it was proceeded to calculate the voltage drop incorporating inside of the exponential heating equation, the variation of current density in function of the penetration expression deduced previously.

In the Figure n° 4, the analytic values are shown jointly with the experimental ones for the case of current of load of 187%.

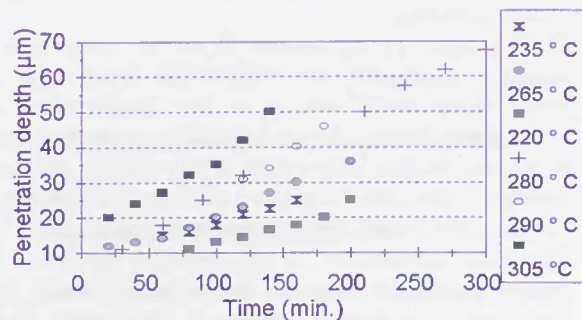


Figure 3, Diffusion as time function

The obtained coincidence is enough for our objective, in case it is wanted to improve it the increase of generation of heat by the variation of the resistance with the temperature could be included. Such an improvement implies a series of analytic complications.

With the shown results, it is possible the building of a model that simulates the behaviour of the fuse, under conditions variables of temperature, preload and overloads.

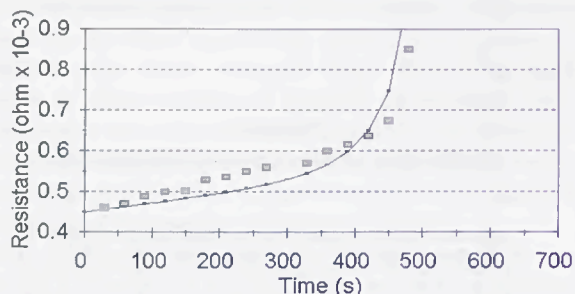


Figure n° 4  
Analytic and experimental comparison

#### 4 - CONCLUSION

By means of the application of the proposed methodology, the loss of useful life of the conductor can be determined as function of the temperature and time of work, being in hands of the operator of the system the determination of the acceptable value of consumption of life. The control of consumption of life can be left to the protection with fusible whose model of long time indicates the allowed duration of the one mentioned overload.

In what concerns to the fuse modelling, it can be affirmed of the existence of a resistance or voltage drop limit values, starting from which begins to be noticed the diffusion, overcome the one which at one time long or short, depending on the intensity of applied current, the fuse will operate. This value represents an irreversibility limit that turned out to be 0,65 mohms in our case example, the one that can be calculated easily by means of the resolution of the typical equation of heating, in function of the time constant, preload and overload values.

The variation of dissolution depth or penetration to constant temperature are exponential function of the time whose coefficient is in turn function of the temperature, being the independent exponent of the same one. As the temperature it is gradually increased the dissolution speed it is also increasing, as function of the temperature and depth (or lapsed time).

The direct introduction of this variation law inside the term of generation of heat of the heating equation, gives for result an enough approach for most of the calculations of protection with fuses.

The law of variation of the dissolution, result of the M-effect allows the development of a model that determines the times of operation of fusible H.B.C. under overloads from the minimum one that causes the melting until the maxim of performance of the M-effect, jointly with the prediction of the ageing caused by recurrent overloads, permanents or not, being able to keep in mind the ambient temperature and the preload state. The method offers the answer about the behaviour of the fuse, in form similar to the way in that the cable overload studies, therefore the times of performance of the fuse can be determined to be compared directly with the ability of supporting such an overload on the part of the conductor in study. For their use it is only required to know the characteristic constants of the process which can be determined starting from simple experiments. Such values, cable and fuse time and heat generation constants, and fuse diffusion constant, can be given by the maker as catalogue data, in such a way that the user can get quickly into such an information.

#### References

- 1.- Pirelli Cabos S.A., Dimensionamento de conductores eléctricos, Makron books, Brasil, 1994.
- 2.- Naot, Y (1984): How far is an insulated conductor protected by a fuse. 2nd ICEFA 1, 87-94.
- 3.- IRAM 2178-1990, Cables de energía aislados con dieléctricos sólidos extruidos para tensiones nominales de 1,1 kV a 33 kV.
- 4.- Morgan, VT (1971): Rating of conductors for short-duration currents. Proc. IEE 118, 555-570.
- 5.- IEEE Std. 242-1986, Recommended Practice for Protection and Coordination of Industrial and Commercial Power Systems, New York, Sixth Printing, 1994.
- 6.- Metcalf, A.W.; A new fuse phenomenon; BEAMA Journal, Vol. 44, 1939, pp. 109-112.
- 7.- Hofmann, M.; Experimentelle und rechnerische Untersuchung von Ansprechkennlinien und Alterungsvorgängen bei Sicherungsschmelzleitern; PhD Tesis; 1987.
- 8.- Daalder, J.E., Kulsetas, J. y Rondeel, W.G.J.; Aging in fuses with M-effect; Fourth Int. Symp. on SAP, Lodz, Poland, September 1981, pp.295-299.
- 9.- Ordoqui, E., Zorzan, C., Campetelli, G. y Gómez, J.C.; Efecto de la precarga estable en la respuesta de fusibles de alta capacidad de ruptura; Revista Electrotécnica, Mayo-Junio 1994; pp. 85-89.
- 10.- Rondeel, W.G., Kulsetas, J. y Bodsberg, K.; Dimensioning criteria for fuses with M-effect; Fourth Int. Symp. on SAP, Lodz, Poland, September 1981, pp.289-294.
- 11.- VDE 0636-DIN 57636, Niederspannungssicherungen NH system, Kabel und Leitungsschutz bis 1250 A und 500 V/440V sowie 660V., Mai 1984. Teil 1, 21/ 22.

# PROTECTION OF A DISTRIBUTION SYSTEM: A WIDE APPLICATION OF ELECTRIC FUSES

C. Ravetta, M. Verdi  
AEM SpA (Milano), Italy

M. Tartaglia

Dipartimento Ingegneria Elettrica Industriale Politecnico di Torino, Italy

**Abstract:** The distribution system of AEM in Milan (Italy) represents a wide application of fuses. The paper will give the main characteristics and structure of distribution system at 23 kV and 400 V, the purposes and constraints of network protection and some criteria to compare fuses and circuit breakers.

## I. INTRODUCTION

In spite of the increasing use of circuit breakers, electric fuses are largely employed mainly in power system distribution by some electric companies. The paper will deal with the protection against over currents in medium (23 kV) and low (400 V) voltage distribution system used by AEM in Milan (Italy) and in 14 smaller towns of the surrounding area. AEM distribution system is mainly constituted by more than 2,300 electrical substations and a cable net 1700 km long, supplying approximately 25.000 buildings and 400.000 electric users. Both medium voltage and low voltage systems have, under rated conditions, a radial structure so that the protection against over currents must be simple and efficient. The distribution system can be split into typical radial structures which include a transformer supplying some main lines with secondary derivations for users. The protection of this kind of structure is performed only by fuses. This protection system must obtain the following results:

- protection against overloads,
- protections against short circuits,
- selectivity.

The analysis of protection system comparing fuses, circuit breakers and their combination was performed some years ago; recently the chosen solution has been submitted to a revision according to the suggestions of the most recent International Standards. The practical experience of many years confirmed the good result obtained using fuses.

The paper deals with the distribution system, the protection criteria, the comparison between circuit breakers and fuses, the final conclusion.

## II. DISTRIBUTION SYSTEM STRUCTURE

Under normal conditions the distribution system can be subdivided in a lot of circuits having a simple structure like in fig. 1 where it is represented a distribution transformer supplying primary branches who supply final users through secondary branches. Transformer sizes and cable sections have been standardised. In Fig. 1 the most frequent distribution transformer is represented; it has a rated power equal to 400 kVA, it is oil immersed and it has a 4% short circuit impedance. Cable normal sections are also indicated.

The protection system must protect the transformer and cables against over currents (overloads and short circuits) with a satisfactory selectivity.

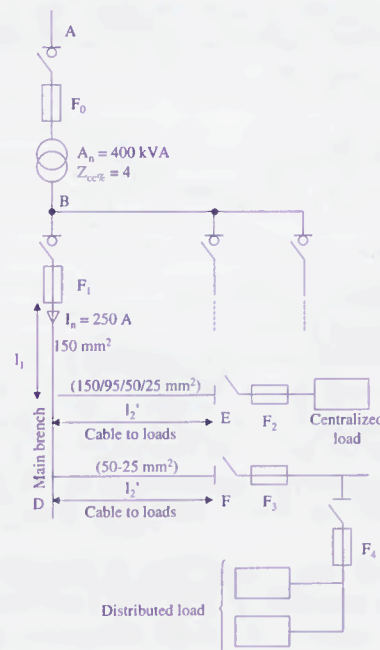


Fig. 1: Typical electrical distribution configuration

### II.1 Transformer protection by fuses

AEM distribution system includes many hundreds of transformers usually oil immersed and, in special cases, dry type ones. Transformer sizes have been

standardized and the most popular value is 400 kVA. IEC International Standards show that it is possible to protect these electrical machines avoiding dangerous over temperatures and guaranteeing a satisfactory life duration in [1] and [2]. In fact, because of the difficulty of monitoring all transformer lives through their loads, AEM protects transformers against overloads by using a simple method which behaves like a thermal image system; it is constituted by temperature sensors which do not allow to overcome hot spot maximum levels and which open substation general switch. According to this limitation no emergency loading capacity is allowed but one doesn't reduce expected transformer life duration and he makes very low fire hazards due to overloads. This simple system works well and transformers have a life duration usually longer than expected values; rare protective interventions occur in few cases due to actual overloads or, more frequently, to poor air cooling conditions during summer hotter months in electrical substation rooms.

Because high voltage cables are protected by main distribution system, high voltage fuses  $F_0$  in Fig.1 protect electrical substations against faults occurring inside the transformer or in the connection systems (cables and bus bars) ahead  $F_1$ . According to [3], high voltage fuses give a satisfactory behavior when they accomplish to some constraints due to the co-ordination with transformer and low voltage fuse-link. The used limits are:

$$I_n \geq 2I_{nt} \quad (1)$$

$$I_{f10} \leq 6 I_n \quad (2)$$

$$I_{f0.1} \geq 7 I_n (I_n/100)^{0.25} \quad (3)$$

Being:

$I_{nt}$ : transformer rated current

$I_n$ : fuse rated current

$I_{f10}$ : pre-arcing current corresponding to 10 s

$I_{f0.1}$ : pre-arcing current corresponding to 0.1 s

An high voltage fuse is also tested near minimum melting current [4] i.e. in the interval 2,7-3,3  $I_n$ ; so, comparing the minimum predicted fault current with the above value, is verified protection against low fault currents.

Usually low voltage loads are supplied by main branches protected by fuses with rated current approximately equal to 1/2 of the transformer rated current so that high voltage and low voltage fuse characteristics do not intersect in low current values and usually an intersection is found only at a current higher than low voltage maximum short circuit current and their satisfactory co-ordination is obtained.

## II.2 Cable protection by fuses

Fig. 1 shows that a transformer supplies up to 3 branches; each branch is constituted by a copper cable having a stated section (150 mm<sup>2</sup>) supplying possible secondary branches having section values from 150 to 25 mm<sup>2</sup>. Also loads can be classified as centralized or distributed ones. System protection against over currents is guaranteed by fuses  $F_1$  and  $F_2$  ensuring :

- primary branch overload and short-circuit protection,
- secondary branch overload and short-circuit protection.

Cables rated currents can be evaluated by means of [6]. and overload protection requires to fulfill the well known relations [7]:

$$I_B \leq I_n \leq I_Z \quad (4)$$

$$I_2 \leq 1,45 I_Z \quad (5)$$

Where:

$I_B$ : operating current for which the circuit is designed

$I_Z$ : continuous current-carrying capacity of the cable

$I_n$ : nominal current of the protective device

$I_2$ : current ensuring effective operation of the protective device.

According to the Italian Standard [8] the current  $I_2$  has been substituted by  $I_f$  i.e. the operating current in conventional time. As a consequence of (4) and (5) one can protect a cable using:

- a circuit breaker having a maximum rated current  $I_n = I_Z$ ;
- gG fuses having a maximum rated current equal to  $1,45/1,6 I_Z = 0,9 I_Z$ .

Unfortunately these rules forget that fuses are submitted to a type test intended to verify their "conventional cable overload protection" which control that fuses operate at  $1,45 I_Z$  [6].

As far as short-circuit protection is concerned, it is obtained by limiting the Joule integral let-through by the protection under cable limit value  $K^2 S^2$ .

It is well known that in the case of a single protection against over currents protection is obtained by a device which satisfies conditions (4) and (5) and which has a breaking capacity suitable to the installation point. In the case of fuses breaking capacity is so high that this condition is always verified in a distribution system. In this way, the values of fuse rated current and cable section of the main branch are coordinated for any cable length.

The above condition is not sufficient when lines are made by cables with a decreasing section. In the scheme of Fig. 1, fuse  $F_1$  ensures short-circuit protection, fuses  $F_2$  and  $F_3$  are chosen for overload protection of secondary branches and for short-circuit protection of the supplied circuits. In this case it is necessary to evaluate maximum protected lengths of  $l_1$  and  $l'_2$ .

The worst conditions to analyze is the minimum current in the case of phase to neutral fault. In the example of Fig. 1 short-circuit currents are computed according to [9]; then one compares these minimum currents with fuse characteristics. In order to ensure fuse operation, one must take into consideration fuse gates stated in IEC 60269 [6]. In order to have satisfactory results for any standardized fuse, the fault current must be  $\geq I_{\max}(5s)$  that is the value which ensures current interruption in any case; in fact  $I_{\max}(5s)$  is defined as the maximum value of current for which the pre-arcing time is not more than 5 s that is the worst case for fuses satisfying IEC characteristics gates. The following Table 1 links cable sections and maximum lengths in the example of Fig. 1; in this example  $I_{\max}(5s)$  is equal to 1.650 A for a fuse rated 250 A.

TABLE 1

$I_1/S_1, m/mm^2$	$F_1, A$	$I_2/S_2, m/mm^2$	$F_2, A$
Any/150	250	-	-
300/150	250	25/95	200
150/150	250	50/50	125
150/25	250	25/25	80

These maximum lengths satisfy all practical situations.

### III COMPARISON BETWEEN FUSES AND CIRCUIT-BREAKERS

The usual considerations in the comparison between circuit-breakers and fuses are:

- i. fuses are cheaper,
- ii. fuses have a very high breaking capacity,
- iii. fuses may cause over voltages,
- iv. overload protection of cables by fuses produces a 10% reduction of cable current carrying capacity [8] with an increased system cost,
- v. fuses produce a single phase interruption,
- vi. circuit-breakers allow to open or close circuits through a remote control.

The first two points (i and ii) represent the main advantages. In fact, it was found a cost reduction of 75% in the case of high voltage protections and a reduction of 20% for low voltage installations. Moreover, high breaking capacity allow to avoid any modification in low voltage network when one increases transformer rated power.

Point iii is a weak consideration because standard fuses must limit arc voltage in order to avoid dangerous over voltages [6]. As stated above, some efforts in a better use of existing Standards may allow to remove the limitation in cable current carrying capacity.

The single phase interruption, mentioned in point v, seems a favourable argument because a lot of users are single phase so that some of them will continue to work also after first fuse operation. Finally, distribution systems usually do not use remote control and the point vi doesn't appear very important.

### IV. CONCLUSIONS

In this paper is described a distribution system using only fuses as a protection against over currents. Approximately AEM has installed 10.000 high voltage fuses and 140.000 low voltage ones. Severe acceptance tests are performed in AEM test laboratories.

In many years no critical situation was individuated and no evidence of fuse aging has been observed.

### ACKNOWLEDGEMENTS

The authors wish to thank prof. G. Cantarella for useful discussion on fuse applications.

### REFERENCES

- [1] IEC 60354 (1991-10) "Loading Guide for Oil-Immersed power Transformers".
- [2] IEC 60905 (1987-12) "Loading Guide for Dry-Type Power Transformers".
- [3] IEC Standard 60787 (1983-01) "Application guide for the selection of fuse-links of high voltage fuses for transformer circuit applications".
- [4] IEC Standard 60282 (1995-09) "High voltage fuses".
- [5] IEC Standard 60287-1-1 (1994-12) (1995). "Electric Cables - Calculation of the Current Rating".
- [6] IEC Standard 60269-1 (1998-12) "Low voltage fuses - Part 1: General requirements".
- [7] IEC Standard 60364-4 (1977-09) "Electrical Installations of Buildings: Protection against overcurrent".
- [8] CEI 64-8 (1998-01) "Norme per impianti elettrici utilizzatori" (in Italian).
- [9] IEC Standard 60909 (1992-09) "Short-circuit current calculations in three-phase ac systems".

Faint, illegible text at the top of the page, possibly a header or introductory paragraph.

Main body of faint, illegible text, appearing to be several paragraphs of a document.

Faint, illegible text at the bottom of the page, possibly a footer or concluding paragraph.

# ELECTROTHERMAL RESPONSE OF FUSES ON INRUSH CURRENT OF DISTRIBUTION TRANSFORMERS

J. Horiszny, K. Jakubiuk, T. Lipski, R. Partyka  
 Technical University of Gdansk  
 Gdansk - Poland

**Abstract:** After presentation of today's approach to the h.v. fuse selection for protection of distribution transformers, the paper shows that more accurate selection can be made using detailed information on the transformer inrush current and the geometry and dimensions of the fuse-element. According to this approach the electrothermal response of the fuse-element on the inrush current should be calculated. As the examples, dry resin transformers of 100 kVA and 1000 kVA, 15/0.4 kV were tested in respect of their inrush current. Then the fuse-links selected according to existing rules were subjected to the inrush current. The existing thumb rule allows to select the same fuse rated current irrespective of the transformer type (e.g. dry resin or oil tank). Meanwhile the measured inrush currents for dry resin types are nearly 2 times lower than for the oil tank ones. Using the measurement results and simulations the paper comes to the conclusion that more realistic approach is when known inrush current has been taken into account in the computational checking procedure of the fuse-element thermal behaviour.

## I. INTRODUCTION

Distribution transformers of the rated power up to ab 2 MVA are often protected by the h.v. fuses as a sole apparatus or as the back-up protection in a combination with the load switches. This technology is a well known practice since nearly of the beginning of the power electric supply. To avoid an undesirable fuse operation due to transformer inrush current the fuses rated current on the supply, i.e. h.v. side, shall be approximate to 2÷3 times of the transformer's rated current. In the last decades this rule was revised. It is now based upon a comparison of the t-I characteristic of the fuse and the transformer inrush current.

Irrespective of the fuse manufacturer the general rules of fuse selection are similar. A transformer imposes three main constraints on the fuse-link:

- It must withstand the current peak that accompanies switching on of the receiver without spurious melting.
- It must withstand the continuous service current and any permissible overloads.
- It must cut off defective currents on the transformer's secondary winding terminals.

Only the first constraint is under discussion in the paper. So the last two will be put aside of the scope.

The switching of the transformer is always accompanied by an inrush current the values of which depend on the moment of application of the voltage and the residual induction of the magnetic circuit (Fig.1).

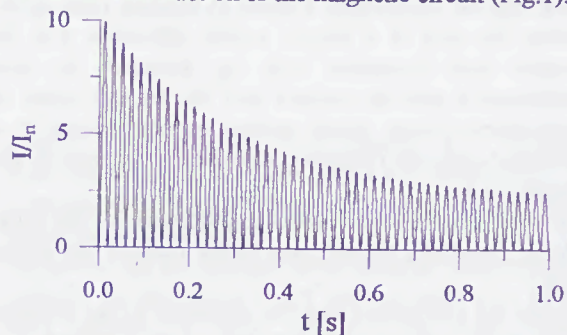


Fig.1. Idealised magnetising current of a power transformer.  $I_n$  – rated current of transformer

The current's asymmetry and value are at their maximum when energization occurs at zero voltage and when residual induction in the same phase is at a maximum.

For selection of the fuse-link the R.M.S. value and time of the inrush current must be known. It is shown that the R.M.S. value of the transient condition current is given by [1]:

$$I_{(RMS)}^2 = 0.125 I_m^2 \frac{\tau}{t} (1 - e^{-\frac{2t}{\tau}}) \quad (1)$$

where:  $I_m$  – maximum peak current,  $\tau$  – time constant of damping of current in seconds,  $t$  – time in seconds taken as  $t=3\tau$  after which it is estimated that the current has reached its final value.

The  $I_m/I_n$  and  $\tau$  depend upon rated power and type of a transformer. Usually larger the rated power lower this ratio and larger the time constant. E.g., France Standards UTE C.52-100, C.52-112 and C.52-113 give  $I_m/I_n$  from 15 to 8 and  $\tau$  from 0.10 up to 0.45 s for the power range 50÷2000 kVA.

A simple and tested practical rule which takes this constraints into consideration and avoids ageing of the fuse-link repetition is to check that the current which melts the fuse in 0.1 s is always equal to or 10 or 12 (sometime even 14) times greater than the  $I_n$  current of the transformer. This rule sometimes is recommended by the fuse manufacturers irrespective of the type of transformer.

The rule has been in general use in many countries, and is, for example specified in the British Electricity Supply Industry (ESI) Specification 12-8. It is sometimes supplemented by the requirement that melting of the fuse-elements should not start in less than 10 ms when carrying 25 times the transformer rated current. The higher multiple (12 times) is used for fuse-links without strikers to provide sufficient margin to ensure that the fuse-links will not melt towards the end of magnetising-current surge.

When fuse-links with strikers which are arranged to trip associated switches being considered, it may than be permissible to accept the risk of a very occasional spurious fuse operation and so the lower multiple of ten times may be acceptable. Clearly if melting does occur toward the end of a surge, switch operation will be initiated and clearance will be effected. In this connection it will be realised that the highest value of magnetising-current inrush seldom occurs because it is associated with energization at particular instants in the voltage cycle.

It is clear that the time/current characteristic of the high-voltage fuse-links should pass to the right of the above points.

Despite the conviction that the approach to the problem given above has been already solved in a proper way since many years, still exist a need to make a closer look into it because:

- The electrothermal instantaneous response of a fuse-element on the inrush current can not be directly evaluated from simple rules mentioned above.
- The inrush current of modern dry resin transformers can be quantitative different than oil tank transformers.

That is why this closer look has been made using analytical simulation, but taking as the base the measured inrush currents of dry resin transformers 100 kVA and 1000 kVA.

## II. ELECTROTHERMAL RESPONSE OF CONSTRICTED FUSE-ELEMENT ON INRUSH CURRENT

To make the simulations rooted in a concrete practice 100 kVA and 1000 kVA, 15/0.4 kV dry resin distribution transformers were tested in respect of their inrush currents using a point on wave (p.o.w.) 3-phase making-switch. Six different p.o.w. switching on were made within distance ab. 30 el. deg. between the consecutive shots. In both cases the maximum recorded  $I_m/I_n$  was ab. 10 times the transformer rated current (Fig.2). Recorded ratio is nearly 2 times smaller than applied now for fuse selection [2].

Also the time constants are smaller than being now in use. They are nearly 2 times smaller.

In the case of 100 kVA a fuse was chosen within notched Ag-strip fuse element, as it is shown in Fig. 3.

For simulations of the electrothermal response of that fuse-element on the inrush current given in Fig. 2 the

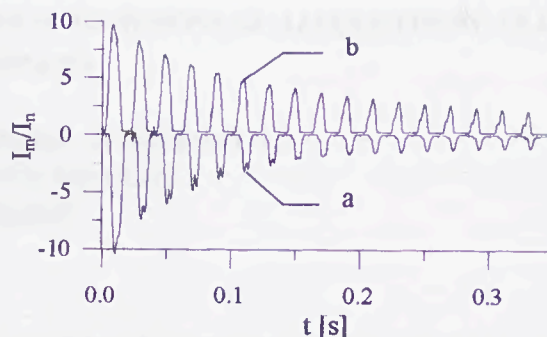


Fig.2. Inrush currents of 100 kVA and 1000 kVA, 15/0.4 kV, dry resin transformer with maximum  $I_m/I_n$   
a - 100 kVA, b - 1000 kVA

following simplifications were assumed:

- The current density in given cross-section is constant.
- The fuse-element number of notches is so large that the simulation can take into account only the section L in Fig.3.
- The heat transferred to the sand is negligible. The thermal conductivity from notches into the fuse-element shoulders in a comparison into the sand is of order  $10^3$  greater. By taking this assumption one can avoid relatively vast computer numerical calculations being in use since the first publication on it [3]. Such a simplification introduces some error in the calculation results. For the pre-arcing times not greater than 0.1 s this error can be practically neglected.
- The heat transfer perpendicular to the fuse-element plane is neglected for the obvious reasons.
- The axial heat transfer to the fuse contacts is also neglected. The fuse-element for h.v. fuses is so long one that only fragments close to the contacts feel their presence.

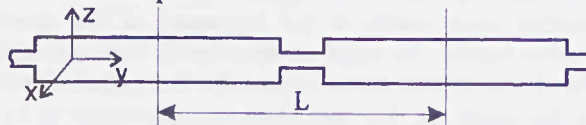


Fig.3. Fragment of fuse-element selected to protect 100 kVA transformer on 15 kV side

For above assumptions the fuse-element heating by the inrush current for 1-D case is described by the relation

$$\rho \cdot c_w \cdot \frac{\partial T}{\partial t} = \lambda \cdot \frac{\partial^2 T}{\partial y^2} + \frac{j^2}{\sigma} \quad (2)$$

in which: T- temperature, t - time, y - space coordinate,  $\rho$  - mass density,  $c_w$  - specific heat,  $\lambda$  - thermal conductivity, j - current density,  $\sigma$  - electrical conductivity.

It has been assumed that the electrical conductivity between the initial temperature and the melting one is described by the relation

$$\sigma(T) = \frac{\sigma_0}{1 + \alpha \cdot (T - T_0)} \quad (3)$$

in which:  $\sigma_0$  – electrical conductivity at the initial temperature,  $\alpha$  – thermal coefficient of electrical conductivity,  $T_0$  – initial temperature.

The current density is defined by

$$j(y) = \frac{i}{S(y)} \quad (4)$$

in which:  $i$  – current,  $S$  – fuse-element cross-section.

The initial and boundary conditions for the fragment  $L$  (Fig.3) re given by

$$T|_{t=0} = T_0 \quad \frac{\partial T}{\partial y}|_{y=L} = 0 \quad \frac{\partial T}{\partial y}|_{y=0} = 0 \quad (5)$$

Using Crank-Nicholson scheme and MathCad package it was calculated temperature/time dependence in the notches up to the melting temperature. Reaching of the melting point means that the fuse-element is destroyed and that its rated t-I characteristic is not already assured. Results of calculations are demonstrated in Fig.4.

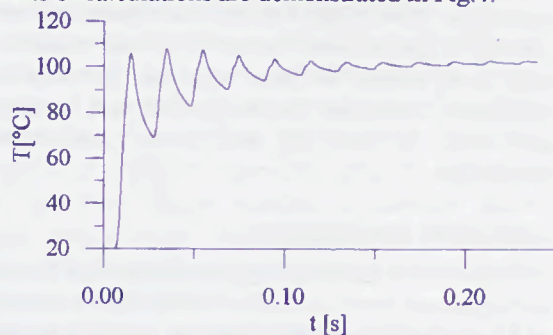


Fig.4. Notch temperature/time dependence for 100 kVA dry resin transformer

It is clear that the inrush current does not create any problem for the fuse-elements in question. The maximum temperature reaches only ab. 110°C. But if one takes into account that for oil tank transformers the  $I_m/I_n$  can reach even 24 (i.e. 2.4 of the tested dry resin transformers), the maximum expected temperature should be much higher. From this reason the temperature notches were recalculated, using the factor  $K$  of a value in the vicinity 2,2 (Fig.5).

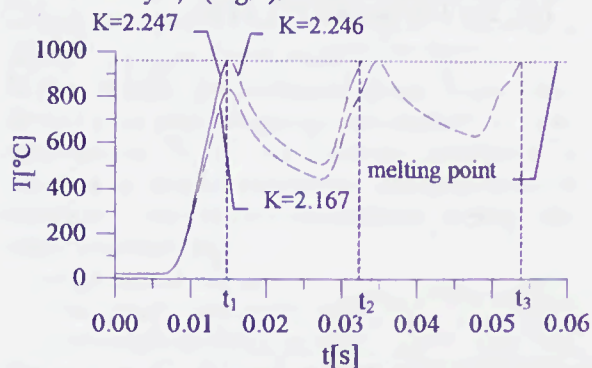


Fig.5. Temperature/time dependence for 100 kVA oil tank transformer recalculated from dependence in Fig.4 using factors  $K$

It can be seen that a slight diminishing of  $K$  from 2.247 to 2.246 the fuse-element will start to melt at the instant  $t_2$  instead  $t_1$ . But a bit greater diminishing of  $K$  down to 2.167 already gives the fuse-element melting in the instant  $t_3$ . So can arise a discontinuity of t-I characteristic similar to that described for semiconductor fuse-links [2]. The notch will reach melting point after 14.88 ms or 32.56 ms or even 53.64 ms by slight inrush current fluctuations.

Similar results one can get if the time constant will be longer than for oil tank transformers ones. To analyse this the time constant  $\tau$  was changed according to the rule

$$K_j = \frac{\frac{t}{\tau} + a}{\frac{t}{\tau_0} + a} \quad (6)$$

where:  $\tau$  – recalculated time-constant,  $\tau_0$  – measured time-constant, for dry resin 100 kVA transformer, a – constant value read out from test record to which tends decaying inrush current.

Results of the calculations with enlarged time-constants indicate the possibility to get melting point after quite a long period of time (Fig.6). The fuse current interrupting ability of such small current can be dangerous, unless the fuse is not full-range one.

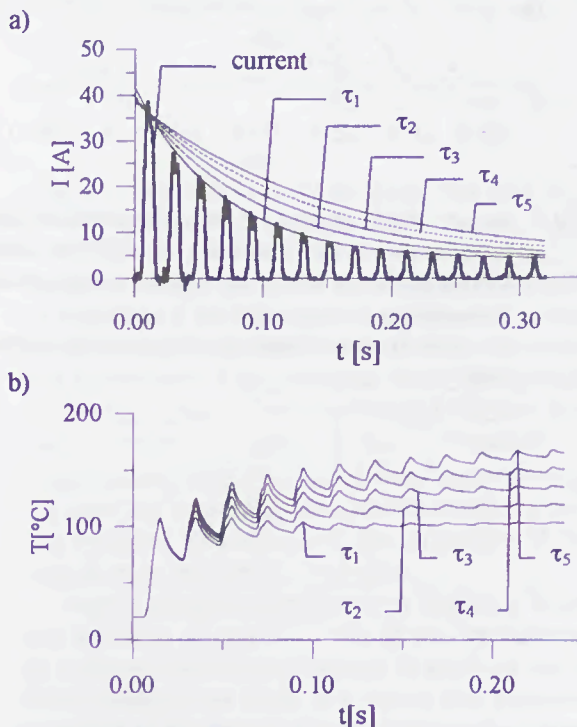


Fig.6. Recalculated inrush currents and notch temperature response in given inrush current  
a - recalculated inrush current maxima envelopes versus time on the base on Fig.2 by use of constant  $K_1$  (6);  
b - recalculated temperature response for different  $K_1$

Evaluation shows that the temperature values given in Figures 4, 5 and 6 up to 0.1 s only a few percents are higher than these but with taking into account the heat transfer into the sand.

It is necessary to underline that similar qualitative simulation results were obtained for 1000 kVA transformer and also for inrush current of a large asynchronous motor of rated power 309 kW, 3×380 V (Fig.7).

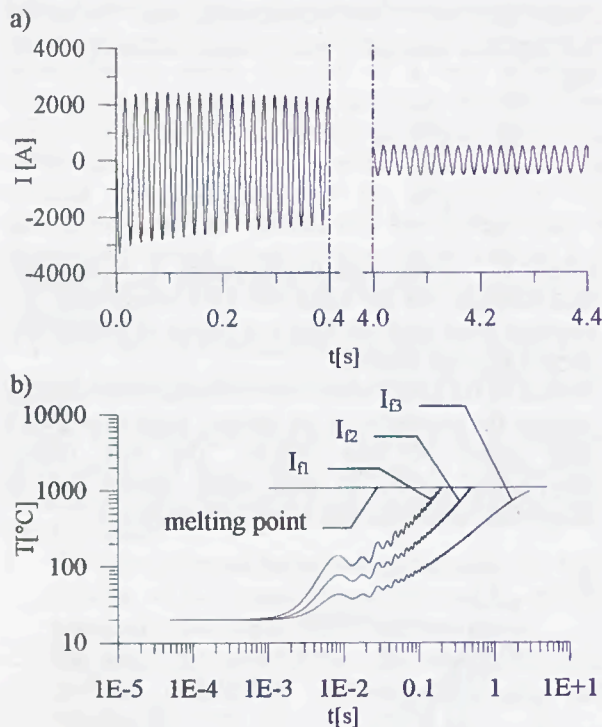


Fig.7. Motor start current and temperature/time dependence of l.v. fuse-links of different rated current  $I_n < I_{l2} < I_{l3}$  selected to protect motor circuit. Asynchronous motor 309 kW, 3 × 380 V.  
a – current versus time, b – temperature versus time

### III. CONCLUSION

The inrush current tests on distribution dry resin transformers of power 100 kVA and 1000 kVA, 15/0.4 kV show that its maximum value within 10 ms is ab. 2 times lower than that usually taken into account in the h.v. fuse-selection procedure. It is because the transformer design details are considerably different for dry resin and oil tank transformers.

Simplified simulations suggest that the fuse-elements subjected to the transformer inrush current during the first ten half cycles show analogous behaviour to the fuse-elements of fuses for semiconductor protection. There can appear discontinuity of the t-I characteristic.

In the case of long time-constants of the inrush current decaying it is possible the fuse arc ignition after some longer time which can lead to the spurious fuse operation.

The general conclusion is that being in use thumb rule, how to select h.v. fuses for the distribution transformers protection is far to be adequate to the electrothermal interaction between the fuse and the transformer inrush current. It seems, more correct h.v. fuse selection in such cases should be based upon the calculations of mentioned interaction. For the time being it is rather an easy task by use of the special computational programme.

### ACKNOWLEDGEMENT

Authors have a pleasure to acknowledge that described investigations were carried out in the frame of project nr 8T 10A 03411 sponsored by the Polish Committee of Scientific Research.

### REFERENCES

- [1] O. Bouilliez, "Design and utilisation of m.v. limiting fuses." Cahier Techniques. Merlin Gerin no 128. P. 1-19.
- [2] A. Wright, P.G. Newbery, "Electric Fuses" (book). IEE 2-nd E. 1995.
- [3] J.G. Leach, P.G. Newbery, A. Wright, "Analysis of high-rupturing capacity fuse-link prearcing phenomena by a finite-difference method." Proc. IEE, vol. 120, pp. 987-993, 1973.

# DUAL-ELEMENT HIGH VOLTAGE BACK-UP FUSES FOR POWER DISTRIBUTION TRANSFORMER PROTECTION

H. Bessei, T. Klemme  
EFEN Elektrotechnische Fabrik GmbH  
Eltville-Germany

**Abstract:** The Authors describe how current-limiting dual-element fuse-links can be advantageously used to protect power distribution transformers against the dramatic effects of internal short-circuits. Originally developed for general purpose or full-range applications, dual-element fuse-links exhibit specific features that make them easily adaptable to the most challenging protection tasks, e. g. the protection of small size power distribution transformers having circuit breakers on the low voltage side.

The favourable time-current characteristics of dual-element fuse-links enable greater tolerances of the transformer impedance and may reduce transformer costs significantly. The combination of different fuse-elements for high and low breaking range enables to design tailor-made time-current characteristics for many applications that cannot easily be covered by single-element fuse-links.

Hermetically sealed dual-element fuse-links have been developed to be installed in transformer tanks under oil. These fuse-links are subjected to new stringent quality control procedures that enable closer tolerance limits and allow to trace each individual product from first manufacturing step until installation in the transformer tank.

## I INTRODUCTION

Dual-element fuse-links have originally been developed to meet the requirements of full-range or general purpose fuses acc. to IEC 60282-1 [1]. Some specific properties of these fuses have shown very advantageous with respect to other applications, e. g. the back-up protection of small size power distribution transformers. In addition to well known advantages of dual element fuse-links like

- high inrush withstand,
- low power dissipation and
- extended breaking range,

the time-current characteristics of dual-element fuse-links offer some features that make them

very adaptable to specific applications and enables to meet the most challenging tasks of transformer protection.

## II PROTECTION OF SMALL SIZE DISTRIBUTION TRANSFORMERS

Power distribution systems in Europe are mainly based on a low-voltage (three-phase 400 V) network which is linked to an overlaying

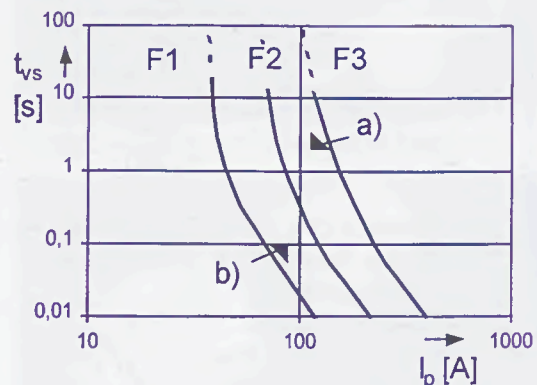


Fig. 1 - Selection of a HV back-up fuse acc. to IEC 60282-1 and IEC 60076-5

medium voltage (e. g. 20 kV) network by means of distribution transformers. L.v. fuses or circuit-breakers are installed on the l.v. side to protect the transformer from potential overloads caused by excess power consumption and to clear high fault currents occurring in the l.v. network. In some cases, when the load is well under control, no overload protection devices but isolators only are installed to enable the disconnection of the transformer from the l.v. network.

High voltage current limiting back-up fuses are installed on the h.v. side of the transformer to prevent catastrophic effects in case of an internal transformer fault. H.v. fuses are therefore selected to be able to safely interrupt the smallest internal transformer fault current, which is three-phase short-circuit current at the l.v. terminals, within two seconds current (see corner a) in fig. 1) and to withstand the maximum transformer inrush current (see corner b) in fig. 1)

[2] [3]. Of the three fuses shown in fig. 1, the time-current characteristic of F2 meets these requirements while F1 and F3 don't.

Depending on the transformer design and protection system, a single-phase earth fault current at the l.v. terminals needs to be considered too. If there are fuses or circuit-breakers installed on the l.v. side, the h.v. fuses shall also be discriminating to these devices, e.g. they must not operate in case of any faults in the low voltage network downstream the l.v. protective device.

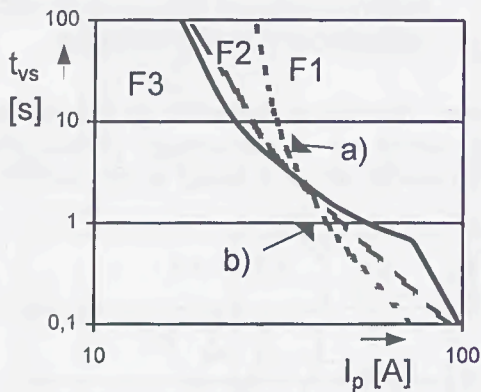


Fig. 2 - Protection of a 100 kVA transformer with h.v. fuse and l.v. circuit-breaker  
 F1 back-up fuse  
 F2 full-range fuse  
 F3 dual element fuse

Small size distribution transformers are especially difficult to protect if they are equipped with circuit-breakers on the l.v. side and a single-phase earth fault at the l.v. terminals shall be cleared by the h.v. fuse. In many cases, the tripping current of the l.v. circuit breaker divided by the transformation ratio is equal or greater than the minimum single-phase terminal fault current of the transformer. Fig. 2 shows an example of a 100 kVA, 20 kV/400 V transformer having a short-circuit impedance of 4 %. The l.v. side is equipped with a circuit-breaker, adjusted to operate at 2.200 A after 1 s (which corresponds to 44 A on the h.v. side, see corner b) of fig. 2). The smallest expected single-phase fault current of 35 A at the l.v. terminals of the transformer shall be cleared by the h.v. fuse within 5 s (see corner a) of fig. 2), while a short-circuit downstream the l.v. network shall be cleared by the circuit-breaker only without operation or whatsoever deterioration of the h.v. fuse.

As can be easily seen from fig. 2, the unusual configuration of the gate, formed by the l.v. current to be tolerated and the h.v. current to be cleared, requires a time-current characteristic

having a gradient as low as possible in the area of the gate. The time-current characteristic of a standard gate back-up fuse-link is hardly able to pass within this gate if reasonable tolerances in the direction of current shall be permitted. General purpose or full-range fuse-links, having single fuse-elements and significantly less gradient in their time-current characteristics than back-up fuses, would possibly fit but still require very tight tolerance limits, i. e. the fuse-links and transformers must be selected during manufacturing process and matched according to their time-current characteristics and their short-circuit impedance respectively. This makes the manufacturing process very complicated and expensive.

The dual-element fuse-link however seems to be best suited to fulfil the requirements of this specific application. It exhibits a very low gradient in the range of 1 s up to 10 s melting time which corresponds to usual transformer short-circuit withstand ratings.

### III FUSE-LINK DESIGN

#### III.1 Selection of fuse-elements

The dual element fuse-link consists of two fuse-elements electrically connected in series and enclosed in one common fuse body (fig. 3). One fuse-element is made of Ag strips having longitudinally arranged restrictions like conventional back-up fuse-links. This fuse-element interrupts high level currents up to the rated breaking capacity of the fuse-link.

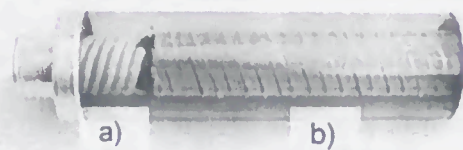


Fig. 3 -Dual-element fuse-link  
 a) Sn fuse-element  
 b) Ag fuse-element

The second fuse-element is composed of one or more partial fuse-elements which consist of Sn wires arranged in an armoured silicone hose. This fuse-element is designed to interrupt lower level currents from its melting current up to the take-over current which is greater than the minimum breaking current of the Ag fuse-element.

Each one of the fuse-elements is able to safely interrupt a fault current in its specific breaking range. Different sizes of both fuse-elements may be combined to a variety of characteristics as needed for individual protection tasks (see fig. 4).

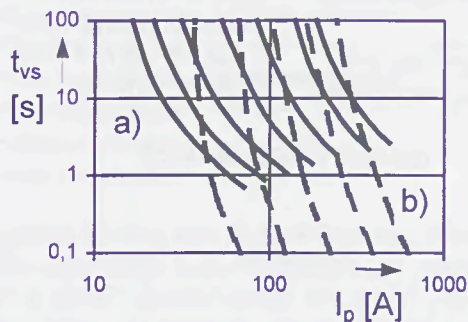


Fig. 4 - Selection of partial fuse-elements  
a) Sn fuse-elements  
b) Ag fuse-elements

The adiabatic temperature rise of the Sn fuse-element extends to a melting time of about one second, its time-current characteristic does therefore exhibit a very low gradient in the range of the gate to be matched. (Note: the minimum gradient in the logarithmic scales acc. to [1] is at a 45° angle.) The Sn fuse-element is chosen to have the time-current characteristic passing

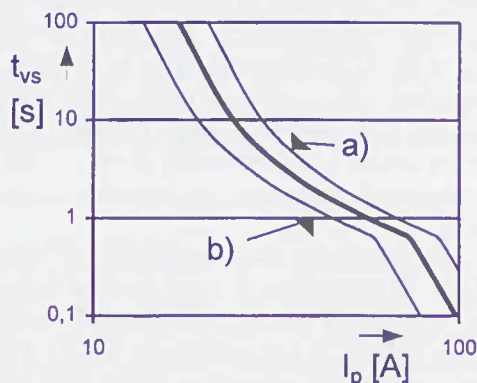


Fig. 5 - Dual-element fuse-link  
Time-current zone  $\pm 20\%$  of mean corners a) and b) as in fig. 2

through the centre of the gate in order to allow for the maximum possible tolerances for both the transformer impedance and circuit-breaker adjustment. Fig. 5 shows that the acceptable tolerance limits of the dual-element fuse are greater than  $\pm 20\%$  in the direction of the current axis. Correspondingly a full range fuse or a back-up fuse would allow for a maximum of  $\pm 10\%$  and  $\pm 5\%$  respectively.

The Ag fuse-element is chosen for high in-rush withstand and low power dissipation. The limitations are given by the take-over current only.

### III.2 Underoil fuse-links

Current-limiting fuse-links that are supposed to operate under oil, have to meet very stringent requirements concerning vacuum and oil tightness as well as reliability in service. The fuse body needs to be hermetically sealed on order to

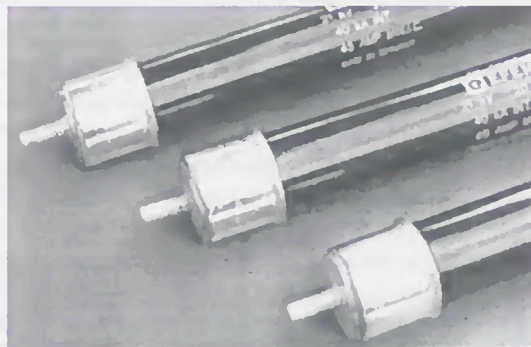


Fig. 6a - Solder sealed underoil fuse-links

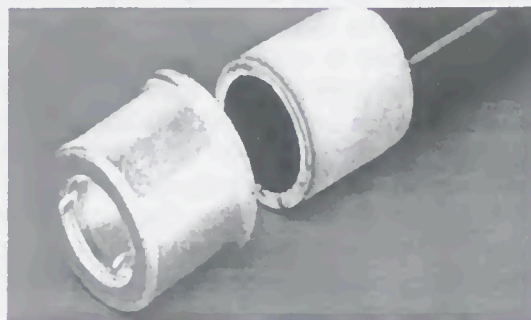


Fig. 6b - Metalized porcelain and contact cap

avoid any leakage of air and/or ingress of oil during the vacuum impregnation process of the transformer or caused by cyclic temperatures and pressure during an extended service life.

The underoil fuse-link shown in fig. 6a has got soldered seals at the endplates as well as at the end caps. The outer surface of the porcelain

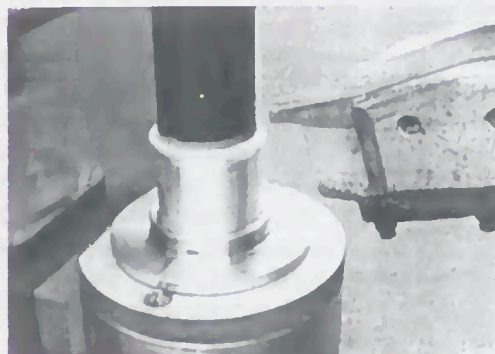


Fig. 6c - Solder casting process

insulator is metalized in the area overlapping to the end caps ( see fig. 6b) and the slot in between is cast with solder (see fig. 6c). This method has proven to provide a very reliable seal for a long service life under even extraordinary service conditions. Several hundred thousands of solder sealed oil-tight fuse-links have been installed since 1970 and accumulate in the meantime a total of about 4 million fuse service years of positive results.

H.v. underoil fuse-links have to be selected and designed as to operate in case of transformer faults only. As they cannot easily be replaced, they must not operate unless an internal transformer fault occurs, i. e. the fuse-links have to be insensitive to transformer inrush and lightning pulses in order to avoid nuisance operation caused by partially damaged fuse-elements.

Mechanical damage of partial fuse-element may also cause nuisance operation of the fuse-links. It is therefore necessary to have adequate physical dimensions of the fuse-elements.

The dual-element fuse-link enables the use of relatively large cross sections of the partial fuse-elements even for the protection of small size transformers. The Sn fuse-element, which is supposed to melt at relatively low currents, because of its low conductivity and melting temperature, requires larger cross sections than a corresponding fuse-element made of higher conductivity and melting temperature material. The Ag fuse-element too may have a larger cross section, as it covers the higher current range only. The dual-element fuse-link does therefore by the nature of its electrical design exhibit superior mechanical strength.

#### IV TYPE TESTS

Extensive type tests have been carried out in order to verify the performance of the dual-element fuses for this specific application. The type tests include all tests applicable to general-purpose under oil fuses acc. to IEC 60282-1 [1]. In addition to the standard tests, mechanical tests as well as thermal tests were carried out. Time-current characteristics were taken at +125 °C and -25 °C. The transformer impregnation process was simulated by means of an autoclave in the laboratory and in real transformer production. Short-circuit tests were carried out on transformers with the fuses installed in order to verify the selectivity as specified. A summary of special tests that were carried out on the fuse-links is given in table I.

Table I - Special tests

Test	Conditions
Oil-tightness test	1000 hPa, thermal cycles 110/25 °C;
Vibration test	70 Hz; 1,2 mm
Mechanical shock test	Free fall over 100 mm
Temperature shock	3 h at +125/-25 °C, transition time 10 s
Impregnation test	140 °C, 48 h, 1 hPa
Time-current curves	-25 °C; 105 °C

#### V QUALITY ASSURANCE

Quality assurance is a very crucial issue on h.v. fuses for installation in transformer tanks under oil. Firstly, the fuses have to match a very narrow gate that does not allow for usual tolerances as defined by [1], i.e., ± 20 %. Secondly the tolerances of the initial material (metal wire or strip) must not be limited too much in order to ensure availability in the market and reasonable prices. Thirdly the transformer manufacturer who installs the fuses in the transformer tank should be able to easily and reliably check the fuses for any potential damage that may have occurred during shipping and handling.

Measurement of the electrical resistance of fuse-elements has proven very useful and convenient to discover many irregularities in the assembly process of single element fuse-links. It is, however, not sufficient to assure consistency of time-current characteristics. The physical dimensions of the fuse-elements need to be carefully controlled, too. Dual-element fuse-links consist of two fuse-elements (each consisting of one or more partial fuse-elements) of very much different electrical resistance, connected in series (see fig. 3).

The total resistance does therefore not vary in proportion to resistance of the individual fuse-elements. In order to detect unacceptable variations of the individual fuse-elements during the assembly process, the tolerances of the total resistance must be set very tight. This is in contradiction to the requirement of reasonable toler-

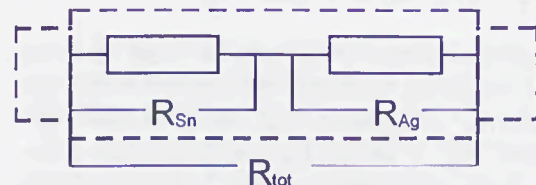


Fig. 7 Resistance measurement

ance limits and acceptable prices for the initial material, i.e. Sn wires and Ag strips. The quality

assurance system during final assembly process has therefore been based on resistance tracing during three consecutive electrical tests as follows (fig. 7):

1. Core winding
  - Resistance of the Sn fuse-element
  - Resistance of the Ag fuse-element
  - Total resistance
2. Core installed inside the fuse-body
  - Total resistance
3. Finished product
  - Total resistance

Resistance tracing means that each resistance value taken after consecutive manufacturing steps is related to the individual product and recorded in a PC. The individual values are then compared step by step during the assembly process. Thus the tolerances of the initial material do not need to be considered and can be excluded from the tolerance limits. The tolerance limits can therefore be set very tight and even minor manufacturing influences, e.g. poor welding or damaged fuse-elements can be detected by means of resistance tracing.

In order to be able to assign the resistance value to the individual product, the first test station (after core winding) is equipped with a barcode printer and the products are marked with a serial number on a barcode label attached to them after the first electrical test. The subsequent test stations are equipped with barcode readers and automatically assign each product the corresponding resistance values which are correlated to the previously obtained values.

Based on the serial number, the products can be traced backwards in case of any irregularities being observed later on. They can also be traced forward and enable the transformer manufacturer to check the product for any potential damage before installation inside the transformer. A second label carrying identical information may be supplied with the fuse-link and attached to the transformer for easy identification of the fuse-links installed which are not accessible any more when put into service.

## VI CONCLUSIONS

Further progress in the development of fuses may be either related to new fuse technologies or new applications showing up in the market. Both directions are needed and helpful to strengthen competitiveness of fuses over other

protective devices. The authors describe a new application demanding non-standard considerations in the selection of h.v. fuses. Dual-element fuses were found to exhibit the most suitable design for back-up protection of small size power distribution transformers. This is especially true, when the fuses are installed under oil inside the transformer tank and not supposed to be replaced during service life of the transformer. Dual-element fuses are extremely adaptable to transformer protection requirements, e.g. Sn and Ag fuse-elements can be selected separately and combined to a wide selection of time-current characteristics. The greater cross-sections of the individual fuse-elements of dual-element fuses compared with single-element fuses make them less sensitive to electrical and mechanical damage. This makes dual-element fuses especially suited for installation under oil in transformers tanks.

Resistance tracing from the beginning of the manufacturing process to the installation in the transformer ensures a high level of reliability in service

## VII REFERENCES

- [1] IEC Publication 60282-1 High-voltage fuses – current-limiting fuses
- [2] IEC Publication. 60787 Application guide for the selection of fuse-links of high-voltage fuses for transformer circuit applications
- [3] IEC Publication. 60076-5 Power transformers – ability to withstand short-circuit

1870

1871

1872

1873

1874

1875

1876

1877

1878

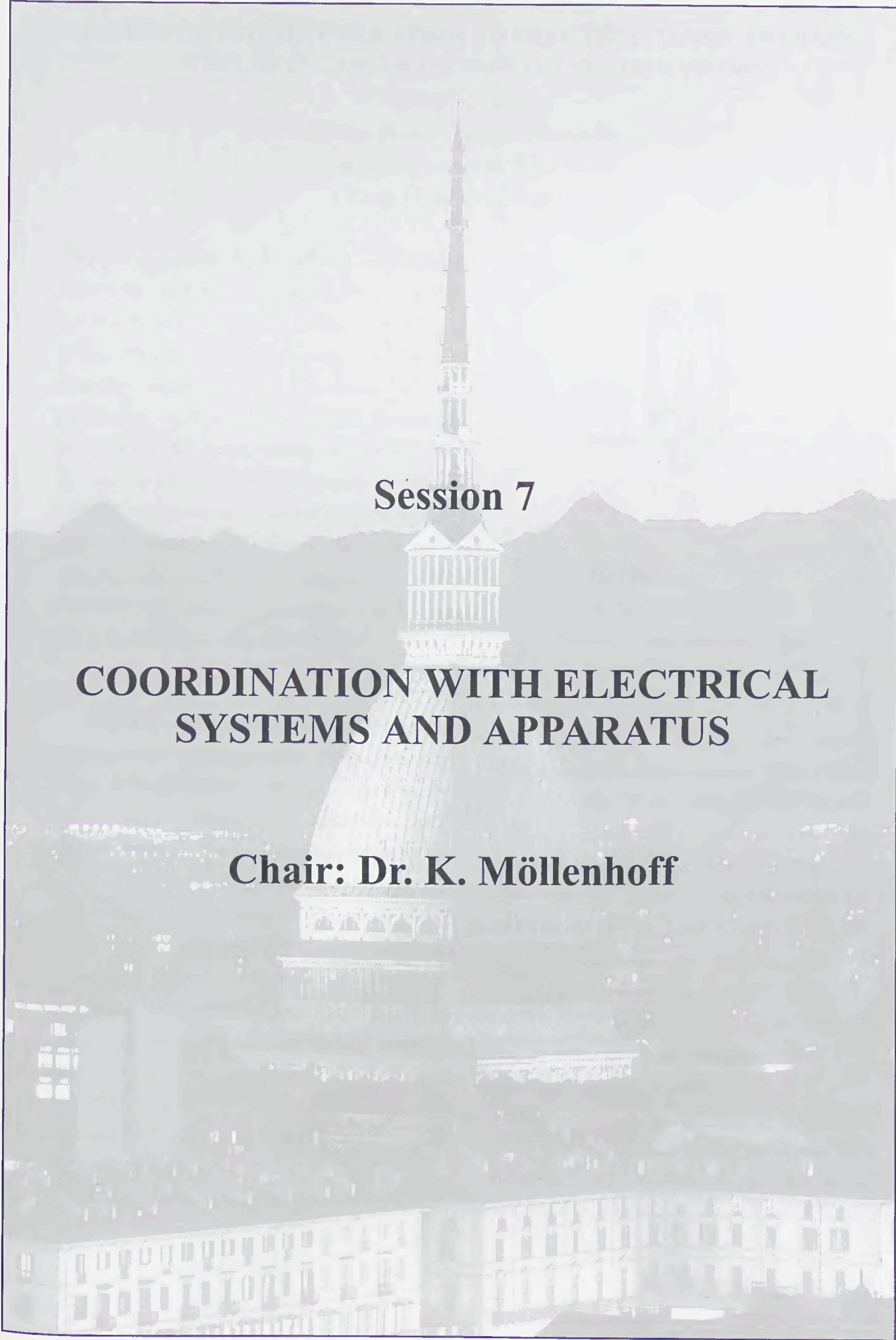
1879

1880

1881

1882

1883



**Session 7**

**COORDINATION WITH ELECTRICAL  
SYSTEMS AND APPARATUS**

**Chair: Dr. K. Möllenhoff**



# RESEARCH ON THE OPERATION CHARACTERISTIC OF THE FUSE STRIKER IN THE SWITCH-FUSES COMBINATIONS

Ma Zhiying Jin Lijun

Division of Electric Apparatus School of Electrical Engineering,

Xi'an Jiaotong University, Xi'an, 710049,

People's Republic of China

**Abstract:** According to the IEC420 international standard [1], the fuse-initiated opening time ( $T_0$ ) of the switch is the key coefficient to determine the transfer current. Through analysis the function on the coordination characteristic of fuse striker in the combination, the  $T_0$  includes the duration of travel of the striker and the inherent opening time of the switch. The result of study is shown that the duration of travel is one of the important factors that determine the transfer current of combination, it is inverse time-delay curve with the current through the striker. For the spring striker, the duration of travel is composed of the melting time of the wire and the striker moving time.

## 1. INTRODUCTION

The fuse-initiated opening time ( $T_0$ ) of switch is one of important coefficient that determines the transfer current. It connects with the fuses and switch. When the transfer current is broken by the combination, under striker operation the breaking duty is transferred from the fuses to the switch. So the striker is the key components for the duty change.

It has close relationship between the operation characteristic of striker and the transfer current of combination for coordination. It is great helpful to analysis the process of breaking the transfer current of the combination by studying the striker operation.

## 2. THE EFFECT OF STRIKER ON COORDINATION CHARACTERISTIC OF COMBINATIONS

The strikers in current-limiting fuses often have

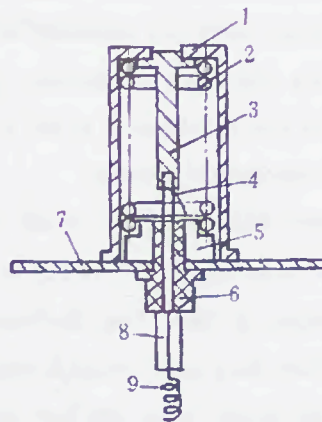


Fig.1 the structure of striker

1top cap; 2spring; 3clasp; 4wire;  
5fixup bush; 6insulation bush; 7plate;  
8impaction bush9series coil

two types. One is actuated by a spring, the other is actuated by an explosive charge. The striker is mounted on the top of the fuse. It is a mechanical device forming part of a fuse-link which, when the fuse operates, releases the energy required to cause operation of other apparatus or indicators or to provide interlock. For explosive type striker, when the main fuse-element has melted, there is enough current passing through the explosive device, kindle the explosive. Explosion pushes the striker moving. The explosive type striker has an advantage of large energy output, but it is difficult to control the process of explosive, to avoid the damp, to keep the safe.

The structure of the spring type striker is shown in fig.1. The top cap is fixed on the metal plate and tightened by a wire. The pressed spring has stored energy. The wire that passes through insulation bushing

series connection with a resistance is parallel connection with the fuse-element.

After the fuse-element has melted, there is enough current passing through the wire by the arcing voltage. The wire is heated by the current, and is fractured by the current and pulling force. The top cap is pushed out by the spring. The spring type striker has many advantages, such as steady movement characteristic, simple structure, production easy, safety and reliability of using etc. In this paper, the movement characteristic is studied and the effect on the coordination in the combination is analyzed for the sprint type striker.

The main function of the striker of fuse in the combination is to trigger the switch to release after initiation arcing of fuse. That the breaking duty is transferred from fuses to the switch is performed by the striker. So the striker is the key part, which connects fuses and switch in the combination.

The circuit of striker is parallel connection with the fuse-element, and there is a large resistance series connection with the striker, for example, the resistance is often several Ohm, but the fuse-element is only several milli-Ohm. So there is only very small current passing through the striker during the pre-arcing time of fuse while the fuse breaks the failure current.

1000A current passes through the fuse, there is only several mA current passing through the striker during pre-arcing time, so the striker isn't triggered. But when an arc is initiated, there is high voltage of arcing on the fuse, and large current passing through the striker that parallel connection with the arcing. So the striker is operated only after the fuse-element melts.

According to the IEC420, the transfer current is defined as the current which gives a melting time equal to  $0.9T_0$  for the minimum time-current characteristic of the fuse.

The ' $T_0$ ' in standard is defined as: the time taken from the instant at which arcing in the fuse commences

to the instant when the arcing contacts have separated in all poles, so the  $T_0$  have relations to the inherent opening time of the switch and the time of the duration of travel of the striker.

### 3. RESEARCH ON THE OPERATION CHARACTERISTIC OF STRIKER

The fuse-initiated opening time ( $T_0$ ) of the switch includes the duration time ( $t_d$ ) of travel of the striker and the inherent opening time ( $t_i$ ) of the switch. The ' $t_i$ ' is assigned by the switch manufacturer, For the  $t_d$ , we should study the movement characteristic of striker further.

#### 3.1 The requirements for the striker

According to the IEC282-1 international standard [2], the striker of fuse should be meet the requirements of table. 12 and fig.12, The type tests includes operation and energy.

The fuse-links used for the striker tests shall be of the highest current rating and/or power dissipation of the range of fuses using a given type of striker system.

##### (1) Operation test:

The fuse-links used for the striker tests shall first be placed in a low-voltage circuit and a current applied to cause the main fuse-elements to melt. The voltage shall be sufficiently low so as to leave the strike circuits of the fuse-links intact. The value of the test current shall be such as to give a pre-arcing time not less than 20 min. The striker operation tests shall be made according to tests a and b. The energy output during the actual travel and withstand force shall be within the limits specified in table. 1.

Test a: Test current:  $\leq 10A$

Test voltage: not specified

Test a: Test voltage:  $\leq 0.075U_r$ ,

Test current: not specified

Where  $U_r$  is the rated voltage of the fuse-links.

##### (2) Test of energy

When the energy is measured from the force-travel

characteristics, this measurement shall be made after the operation tests as follows: forces of the spring  $F_A$  and  $F_B$  at the beginning and at the end, respectively, of the further travel  $AB$  indicated in fig.2 shall be measured for one sample and the energy calculated from the formula:

$$Energy(J) = \frac{(F_A + F_B) \times AB}{2000} \quad (1)$$

Where  $F_A$  and  $F_B$  are expressed in Newtons and  $AB$  in millimetres.

### 3.2 The operation characteristic of the spring type striker

From the structure of spring type striker, the wire of striker is fractured by the current and pulling force. The current that passes through the striker is the main factors that has an effect on the operation characteristic while the condition of the structure of striker established. The duration of travel  $t_d$  is inverse time-delay curve with the current that passes through the striker. It tends to the mechanical movement time that from the striker operation till to the stipulate travel, when the current is large enough.

In this paper, the operating characteristic of the spring type striker (the medium type striker) is studied.

In the experiment [3], the r.m.s. value of current passing through the striker is during 5A ~ 25A, the operation characteristic of striker is measured under different current. The results of the test is shown as fig.2. When the  $I=6A$ , duration of travel  $t_d=300ms$ ; others: $I=10A$ ,  $t_d=90ms$ ;  $I=25A$ ,  $t_d=16ms$ . If the current that passes through the striker increases gradually, the duration of travel of striker shall be decreased.

The sample of the medium type of spring striker had met the IEC282 requirements by the test. The duration of travel of the striker has been measured on the sample fuse that the rated current is 100A, Fig.3 is the oscillogram that test under 1056A and 200V. The curve B is the test current that passes through the fuse. The curve A is the operation signal of striker. The pre-

arcng time of fuse is 117ms, The duration of travel of striker is 11.8ms after the pre-arcng time of fuse. In many other sample fuse tests, the duration of travel of striker is during 9ms ~ 13.1ms .

### 3.3 The duration of travel of striker $t_d$

The  $t_d$  can be divided into two parts, one is melt time  $t_1$  of wire that fix the spring, the other is the mechanism movement time ( $t_2$ ) from the spring moving to the end of the travel.

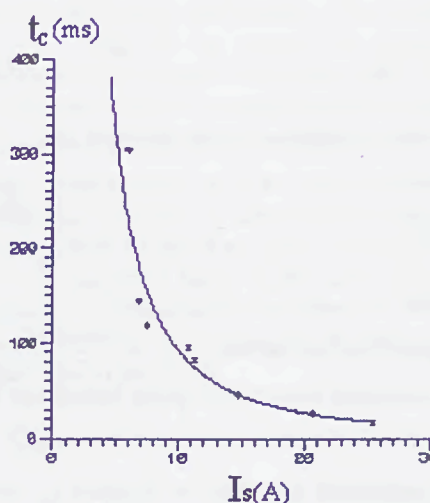


Fig.2 characteristic curve of striker

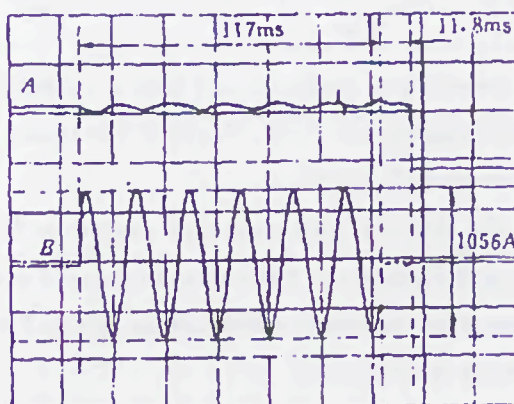


Fig.3 oscillogram of fuse broken

A—the signal of striker motion ;  
B—the curve of test current

The  $t_2$  can be obtained by calculation. The opposite force of spring is :

$$F = - kx \quad (2)$$

Where  $k$  = The elasticity coefficient of spring

$x$  = The coordinate of travel. 'm' is the mass of top cap.

According to the Newton's law, the relation between the spring force  $F$  and the acceleration of the spring is :

$$F = m a = m \frac{d^2 x}{dt^2} \quad (3)$$

The differential equations of the movement of spring is:

$$m \frac{d^2 x}{dt^2} = -kx \quad (4)$$

The solve conditions for the equation are:

$$\begin{cases} v|_{x=A} = 0 \\ x|_{t=0} = 0 \end{cases} \quad (5)$$

Where

$v$  = the velocity of the spring;

$A$  = The compress distance of spring before the striker operation .

The movement rule shall be obtained by solveing the equation (4)

$$X = A \cdot t \cdot \cos \sqrt{\frac{K}{M}} \quad (6)$$

According to equation 1 and table 1 , choose the medium type striker,  $P=1J$  ,  $F_B=20N$ ,  $AB=16mm$ , we shall know the  $F_A=105N$ .

The elasticity coefficient  $k$  of medium is 5.357 kN/mm by equation (2). If the mass of top cap of striker is 15g, After the striker travels 20mm, the  $t_2=5.5ms$ . according to equation (6).

After the initiation of arcing of the fuse, the wire that fixes the spring shall be fractured quickly by the current and the till force,

The process of the wire fracture is very complex, but we can measure the  $t_d$  by test. And  $t_2$  can be obtained by calculation, so the  $t_1$  can be obtained by  $t_d$  minus  $t_2$  . For example, form fig.3 the  $t_d=11.8ms$ , form equation (6), the  $t_2=5.5ms$ ,so the  $t_1=11.8-5.5=6.3ms$ .

#### 4 CONCLUSION

1. The fuse-initiated opening time ( $T_0$ ) of the switch includes the duration of travel of striker  $t_d$  and the inherence open time of the switch  $t_i$ . While the  $t_i$  has fixed, different  $t_d$  has different transfer current.
2. The  $t_d$  has relationship with the current that passes through the striker. The larger the current is, the shorter the time  $t_d$  is. They form the inverse time-delay curve.
3. The  $t_d$  is composed of the wire melting time  $t_1$  and the striker moving time  $t_2$ . The  $t_2$  can be obtained by calculation, the  $t_1$  can be obtained by test.

#### REFERENCE

- [1] International Standard High—Voltage Alternating Current Switch—fuse combinations IEC4201990
  - [2] International Standard High Voltage Fuses Part 1 Current Limiting Fuses IEC2821 1985
  - [3] Jin Lijun. The Research on the Characteristics of Fuse Used on Switch -fuses Combination. M.E.thesis of Xi'an Jiaotong University, 1997
- Ma Zhiying** was born in Zhejiang China in 1937. He graduated from the department of Electric Engineering of Xi'an Jiaotong University in 1958, and he completed his graduate school work In 1963. He is presently a professor in Xi'an Jiaotong University, and he has been engaged in the investigation of arc phenomena and R & D of high voltage switchgears. He is a senior member of CES, of CSEE and of IEEE.
- Jin Lijun** was born in Zhejiang China in 1964. He received B.Sc., M.Sc. degrees in Xi'an Jiaotong University in 1987,1997 respectively. Now he is studying in Xi'an Jiaotong University as a doctor candidate and engaging in the study of "Self-Adapting Intelligent Control Device of High Voltage Circuit Breakers".

# AN ANALYSIS OF COORDINATION OF LOW-VOLTAGE CIRCUIT-BREAKERS AND H.B.C. FUSES

W. Aftyka, K. Jakubiuk, T. Lipski  
 Technical University of Gdansk  
 Gdansk, Poland

**Abstract:** Problem of proper coordination of the downstream h.b.c. fuses with the upstream circuit breakers (CB) classically has been solved by a comparison of  $t$ - $I$  characteristics of both protective devices. More recently also a co-ordination of both apparatus, in the short-circuit region, on the base of a comparison of current impulse characteristics has been suggested. The impulse withstand of CB should be compared with the let-through impulse of the fuse. The paper demonstrates the results of experiments and simulations of the impulse coordination, but taking into account detailed processes in the tripping mechanism of the CB at the short-circuit current. The results show clear that the discrimination can not be always achieved in the short-circuit current region on the base of comparison of CB current impulse withstand and fuse's let-through one. Responsible for that misleading co-ordination is the dynamics of the fuse and the CB operation. Results of the simulations of the dynamics of electromagnetic tripping mechanism and the experiments show a satisfactory agreement.

## I. INTRODUCTION

In respect of overcurrent protection there are under considerations two configurations of the overcurrent apparatus coordination (Fig. 1): "CB-fuses" and "fuses-CB".

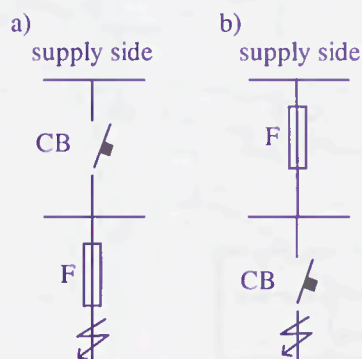


Fig. 1 Configurations of overcurrent coordination of apparatus

a - "CB-fuses (F)", b - "fuses (F)-CB"

Usually shall be achieved a discrimination of apparatus operation in the whole overcurrent region, if both shown in Fig. 1 devices are installed in two different stages of the energy distribution. The configuration "fuses-CB" (Fig. 1b) in respect of discrimination demonstrates less complicated case than "CB-fuses" one. In former case it is enough simply to compare  $t$ - $I$  characteristics in the overload region and  $I^2t$  let-through characteristic of CB with pre-arcing  $I^2t$  characteristic of fuses in short-circuit region. Hence this configuration will not be under considerations.

On the other hand, in the case "CB-fuses", if one makes a coordination according to the existing classical rules (Fig. 2), one can get, in some cases, a not desirable operation of CB.

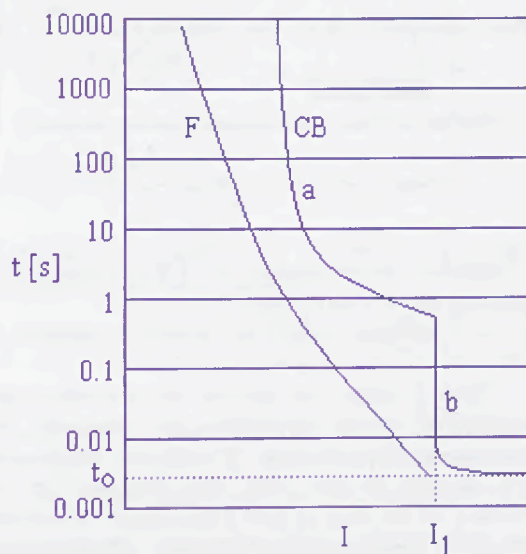


Fig. 2  $t$ - $I$  characteristics approach [1] to ensure a proper discrimination of operation of combinations "CB-fuses" (Fig. 1a)

F - largest times of fuse operation, CB - shortest permissible time to activate CB to get switch off position, a - overload region usually provided by thermal release, b - short-circuit region usually realised by instantaneous tripping device,  $I_1$  - adjustable lowest current setting of instantaneous tripping,  $t_0$  - time of CB operation normally given in catalogue

The  $t$ - $I$  characteristic approach shall take into account the disadvantageous manufacturing tolerances, point on wave of the fault initiation and environmental influences. Also an effect of the ageing of both apparatus shall be considered, by introducing e.g. a safety margin, say 1.5 of the time scale. Aforementioned not desirable operation pertains to the short-circuit region, i.e. above the current  $I_1$ , and will be examined in the paper. Such an operation is manifested by switching off not only of the fuse but also of the CB in a defined short-circuit current region. Below and above this region the discrimination can be maintained. Responsible for such a behaviour is the dynamics of electromagnetic tripping device. That is why the authors of the publications [2, 3] suggest making an *impulse approach*, considering impulse characteristics of CB and fuse (Fig. 3).

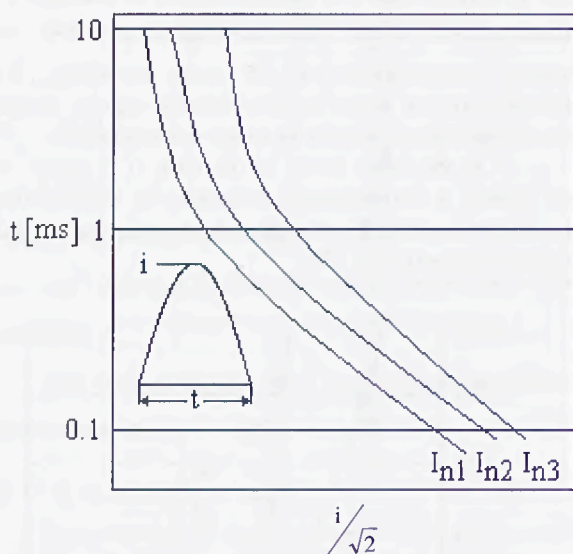


Fig. 3 Impulse characteristics of CB discriminative operation in short-circuit region

$I_{n1}$ ,  $I_{n2}$ ,  $I_{n3}$  - different values of current  $I_1$  marked in Fig. 2

Now to make sure that the discrimination will be achieved it is necessary to compare the characteristics given in Fig. 3 with the let-through current impulse of the fuse. This impulse can be determined on the base of fuse's maximum let-through current for a given prospective current. Moreover the fuse's let-through current shall resemble sine wave impulse because only for such an impulse shape the comparison is rational. Mentioned impulse parameters, i.e. the amplitude and half cycle sine wave can be evaluated on the base of known cut-off fuse's characteristic. It should be, in doing this, assumed that the pre- and arcing-times of the fuse operation are equal.

Mentioned impulse approach, however, much better than  $t$ - $I$  characteristic one, still is a global one and not takes into considerations several details responsible for the discrimination process. This statement is a reason why a closer look into the

problem is desired. The results of experiments and simulations on "CB-fuses" discriminative operation in the short-circuit region is given in this paper.

## II. EXPERIMENTAL INVESTIGATIONS OF DYNAMICS OF CB ELECTROMAGNETIC TRIPPING DEVICE

The dynamics of "CB-fuses" discrimination was investigated at the beginning by an experiment (Fig. 4). Point on wave control 9 assured the switching on the circuit in a defined phase instant. A digital oscilloscope recorded, stored and processed all data on circuit current and anchor move. The current limiting fuse 4 was rechargeable.

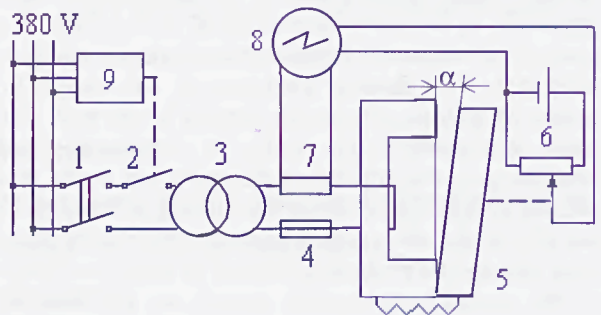


Fig. 4 Scheme used in experimental investigations of "CB-fuses" dynamics

1 - main circuit-breaker, 2 - point on wave controlled making switch, 3 - transformer, 4 - fuse  $F$  in combination shown in Fig. 1a, 5 - CB's electromagnet in combination given in Fig. 1a, 6 - gauge to sense movement of anchor 5, 7 - shunt, 8 - digital oscilloscope, 9 - point on wave control,  $\alpha$  - angle defining anchor position

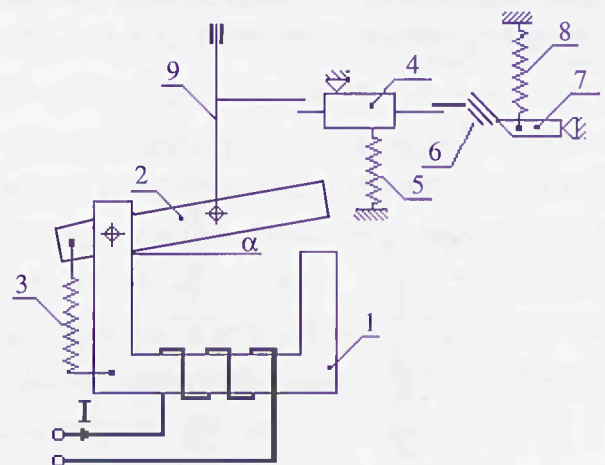


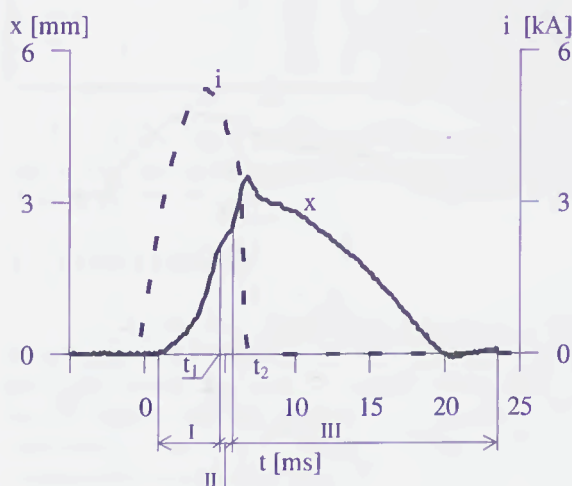
Fig. 5 Scheme of kinematics of investigated electromagnetic tripping

1 - core, 2 - anchor, 3 - anchor spring, 4 - latch lever, 5 - lever spring, 6 - rotating part of latch, 7 - lever, 8 - spring of latch, 9 - pulling member,  $\alpha$  - angle defining anchor position

Its fuse-elements were made from a Cu-wire of different diameters with notches. The diameter, and dimensions and number of notches were selected to control the pre-arcing time and  $I^2t$  and the shape of let-through current decaying to zero, by given prospective current. In turn as CB a moulded case circuit-breaker 200 A rated current, 660 V was chosen. Its thermo-bimetal-electromagnetic release equipped within mechanical latch structure (Fig. 5) was extracted from the circuit-breaker and installed in the circuitry as in Fig. 4.

If a short-circuit appears the anchor 2 is pulled down to the core 1. As a result is transmitted a mechanical impulse throughout interlink lever 4 to the latch parts which finally make free move of the lever 7 causing CB opening.

a)



b)

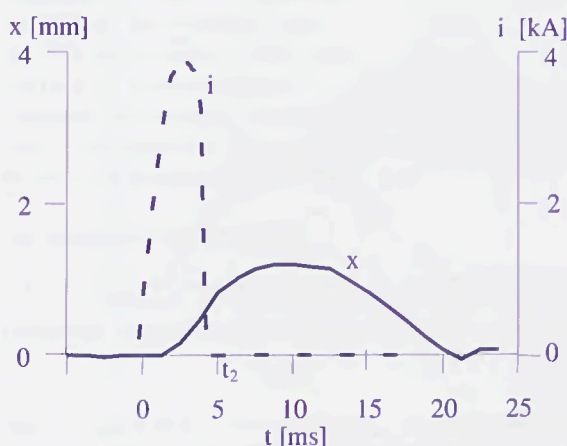


Fig. 6 Typical records of current  $i$  and anchor displacement  $x$

a - fuse interrupts and CB opens, b - fuse interrupts and CB not opens,  $t_1$  - latch first contact instant with lever 4 (Fig. 5),  $t_2$  - forced current zero

Two series of the measurements were made: first at the prospective current 3.75 kA (RMS) at source voltage 17.5 V and 5.5 kA (RMS) at source voltage 35 V. The records show two basic regularities of the CB behaviour (Fig. 6).

In the case Fig. 6a one can recognise three characteristic phases of the anchor movement. Phase I characterizes by movement of anchor alone. In the instant  $t_1$  anchor meets a mechanical resistance of the lever 4 (Fig. 5). Due to this it is recognisable diminishing of the move velocity. Since then the anchor and lever 4 in the phase II are moving together. If the anchor velocity in the instant  $t_1$  is large enough some bounce is possible. During the phase II in a some instant appears the tripping itself, of course, if the rotating latch part 6 reaches a defined position in relation to the latch lever 7. Next phase III means return move of the anchor and associated parts to the initial position because the electric power supply due to fuse operation become zero in the instant  $t_2$ .

In the case Fig. 6b the electromagnet powering stops in the instant  $t_2$ . Beyond this point the anchor still shows free movement ahead due to stored kinetic energy in the instant  $t_2$ . But this energy is too small to get tripping. After reaching a maximal displacement in direction of the core the anchor gets back to the initial position as a result of action of the springs 3 and 5.

### III. SIMULATION OF ELECTROMAGNETIC DYNAMICS

The dynamics of anchor describes the relation

$$J(\alpha) \frac{d^2\alpha}{dt^2} = M_{el}(i, \alpha) - M_{sp}(\alpha) \quad (1)$$

In which:  $J(\alpha)$  - momentum of inertia of the tripping mechanism, defined as follows:

$$J(\alpha) = \begin{cases} J_1 & ; \alpha > \alpha_z \\ J_1 + J_2 & ; \alpha \leq \alpha_z \end{cases} \quad (2)$$

where:

$J_1$  - momentum of inertia of the anchor,  $J_2$  - momentum of inertia of the lever,  $\alpha_z$  - angle of the anchor position in which starts movement of the anchor,  $M_{el}(i, \alpha)$  - electromagnetic momentum of the electromagnet related to the circuit current and the anchor position  $\alpha$  (Fig. 5),  $M_{sp}(\alpha)$  - momentum of the springs 3 and 5 (Fig. 5) is defined as follows

$$M_{sp}(\alpha) = \begin{cases} k_1 r_{11} r_{12} \alpha & ; \alpha > \alpha_z \\ k_1 r_{11} r_{12} \alpha + k_2 r_{21} r_{22} \alpha & ; \alpha \leq \alpha_z \end{cases} \quad (3)$$

where:

$k_1, k_2$  - constants of the springs 3 and 5;  $r_{11}, r_{12}, r_{21}, r_{22}$  - radii of fasten of the springs and joints of the drive

Start of the anchor movement is possible above a certain threshold current value. The angle of the

anchor displacement can vary in the limits  $0 < \alpha < \alpha_0$ , where  $\alpha_0$  - initial angle of the anchor position.

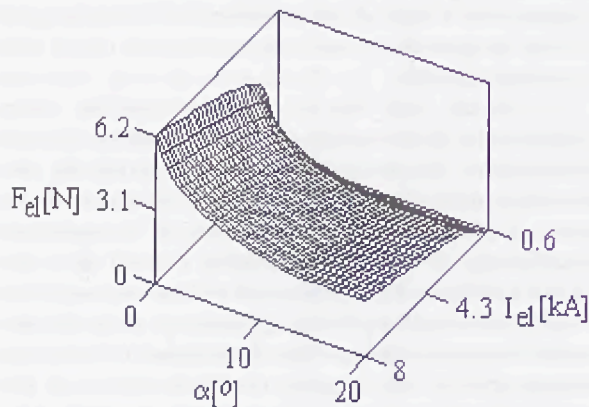


Fig. 7 Exemplary results of simulation by means of FLUX2D programme of pulling force of anchor  $F_{el}$  - pulling force,  $I_{el}$  - maximum let-through current,  $\alpha$  - angle describing position of anchor

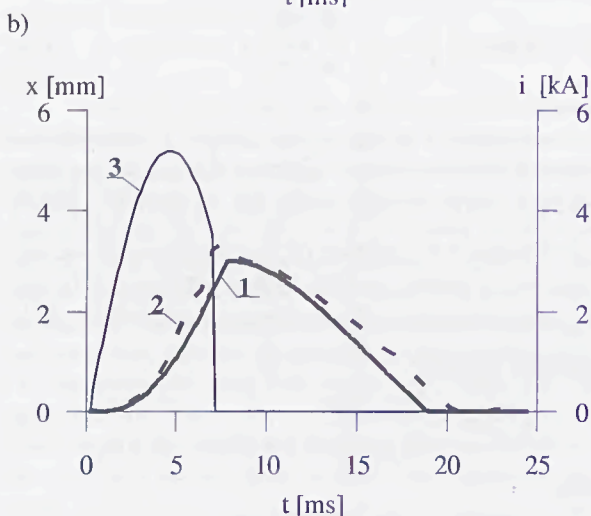
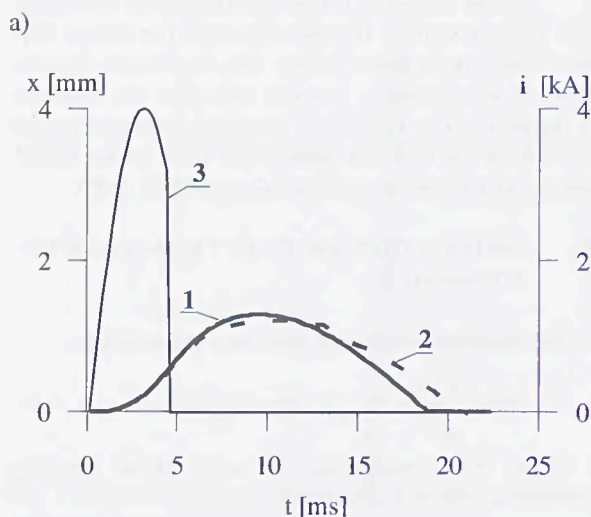


Fig. 8 Experimental (2) and simulation (1) profiles of anchor displacement  $x$  for assumed current impulse  $i$  (3) a - tripping of CB not occurs, b - tripping of CB has take place

The electromagnetic momentum  $M_e(i, \alpha)$  is determined by the magnetic flux distribution. This distribution and hence the pulling forces for a given angle  $\alpha$  and current  $i$  were calculated by means of the 2-D finite-element programme FLUX2D [4] (Fig. 7). In turn, to calculate according the relation (1) the dynamics of anchor displacement, associated members including, was used programme MATHCAD. The results of simulations and from experiments are in a good agreement (Fig. 8). The calculations, among others, reveal that it is possible that the discrimination can have place in a strictly defined short-circuit current region only. At the currents above this region the discrimination is not fulfilled (Fig. 9, Table 1). The reason is an interaction of the anchor inertia and the parameters of the current impulse.

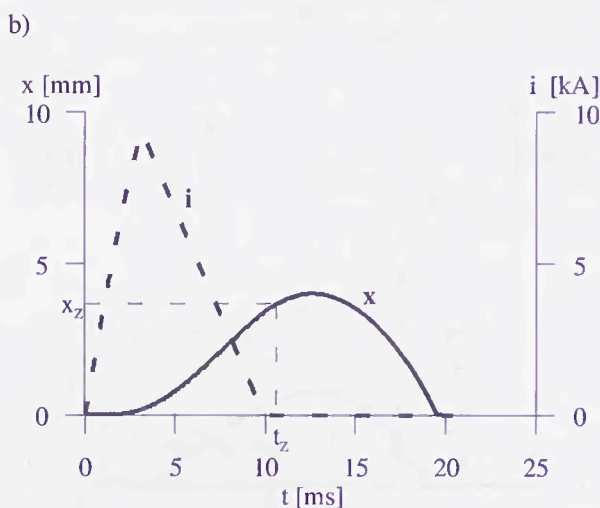
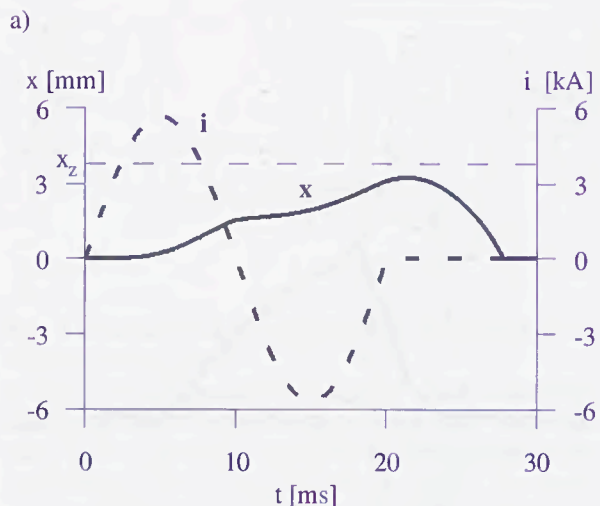


Fig. 9 Results of simulation of "CB-fuses" configuration in respect of discrimination of operation of a moulded - case circuit-breaker 400 A, and a fuse of rated current 200 A

a - prospective current 4 kA (RMS), discrimination is fulfilled; b - prospective current 8 kA (RMS), lack of discrimination;  $x$  - anchor displacement,  $x_z$  - dimension at which static tripping appears

Table 1. Results of simulation of discrimination of a moulded-case circuit-breaker and a fuse

CB rated current	Set of electro-magnet	Fuse's rated current	Test current	Tripping
A	kA	A	kA	yes/no
200	2	100	$I_{sp} < 22$	no
400	4	160	$I_{sp} < 22$	no
	4	200	$I_{sp} < 7.4$	no
	4	200	$7.4 < I_{sp} < 8.5$	yes
	4	200	$I_{sp} > 8.5$	no
630	6.3	250	$I_{sp} < 22$	no
	6.3	315	$I_{sp} < 9.9$	no
	6.3	315	$9.9 < I_{sp} < 22$	yes
	6.3	315	$I_{sp} > 22$	no

At the end it is worth to demonstrate (Fig. 10) that in the case *a* the current lasts much longer than in the case *b*

## I. CONCLUSIONS

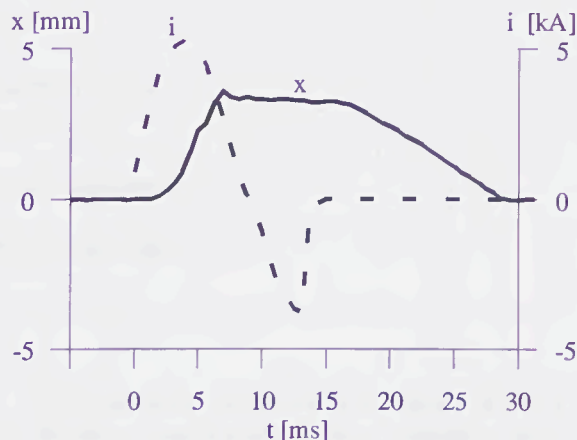
Carried out experiments and simulations concerning discrimination "CB-fuses" combination gave the results that are in a good agreement. The results suggest that the discrimination coordination of "CB-fuses" based on simple comparison of *t*-*I* characteristics can lead to a misleading CB operation in the short-circuit current region. Also the approach based on a comparison of sine half wave impulses can give the misleading results. Simulation, namely, shows that sometimes the discrimination can be ensured within a defined short-circuit region. Above this region there can be lack of discrimination. To avoid in practice such a situation the impulse withstand characteristic of CB shall be established by the experiments in a careful way to discover mentioned region.

## ACKNOWLEDGEMENT

Authors have a pleasure to acknowledge that described investigations were carried out in the frames

of project nr 8T 10A 03411 sponsored by the Polish Committee of Scientific Research.

a)



b)

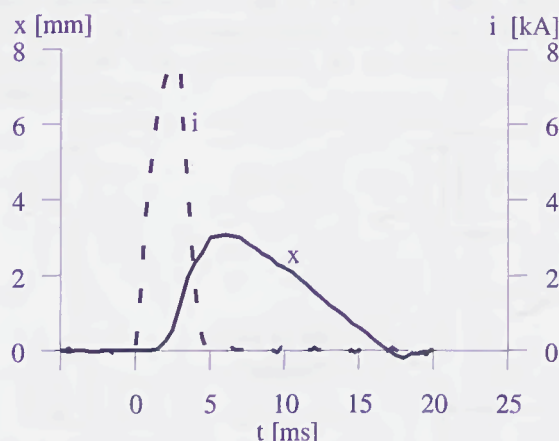


Fig. 10 Tripping behaviour  
a - at smaller current than in case b

## REFERENCES

- [1] IEC Publication, Application guide for low voltage fuses, Project number IEC 61818/Ed 1.0
- [2] Cewe A., Kalisz M.: Characteristics of instantaneous moulded-case circuit-breakers (in Polish). In "Maszy-ny i Wyposazenie"
- [3] Cewe A., Zachariasiewicz W.: *t*-*I* characteristics of screw-in circuit-breakers (in Polish). In "Wiadomosci Elektrotechniczne" 1980, nr 7
- [4] FLUX2D, User's guide, Version 7.30

1870  
1871  
1872  
1873  
1874  
1875  
1876  
1877  
1878  
1879  
1880  
1881  
1882  
1883  
1884  
1885  
1886  
1887  
1888  
1889  
1890  
1891  
1892  
1893  
1894  
1895  
1896  
1897  
1898  
1899  
1900

1870	1871	1872	1873	1874	1875	1876	1877	1878	1879	1880	1881	1882	1883	1884	1885	1886	1887	1888	1889	1890	1891	1892	1893	1894	1895	1896	1897	1898	1899	1900
------	------	------	------	------	------	------	------	------	------	------	------	------	------	------	------	------	------	------	------	------	------	------	------	------	------	------	------	------	------	------

1870  
1871  
1872  
1873  
1874  
1875  
1876  
1877  
1878  
1879  
1880  
1881  
1882  
1883  
1884  
1885  
1886  
1887  
1888  
1889  
1890  
1891  
1892  
1893  
1894  
1895  
1896  
1897  
1898  
1899  
1900

1870  
1871  
1872  
1873  
1874  
1875  
1876  
1877  
1878  
1879  
1880  
1881  
1882  
1883  
1884  
1885  
1886  
1887  
1888  
1889  
1890  
1891  
1892  
1893  
1894  
1895  
1896  
1897  
1898  
1899  
1900

# RESULTS OF SHORT-CIRCUIT TESTS ON CONTACTORS PROTECTED BY FUSES

D. Arato \* , G. Cantarella \* \*

\* Istituto Elettrotecnico Nazionale Galileo Ferraris  
Corso M. d'Azeglio, 42 - 10125 Torino - Italy

\* \* Politecnico di Torino - Dipartimento di Ingegneria  
Elettrica Industriale  
Corso Duca degli Abruzzi, 24 - 10129 Torino - Italy

## I GENERAL

In a previous paper entitled "Advance in short-circuit co-ordination of contactors and motor-starters with fuses" [ 13 ] a survey was presented of the indications that a contactor manufacturer should specify in order to facilitate the pursuing of a given type of co-ordination.

It was emphasized, in particular, by the results of appropriate laboratory tests, that the verification of the overcurrent withstand of a contactor has to be extended to values of prospective currents, if any, which, although lower than current " $I_T$ ", are high enough to cause contact separation of the contactor. In the present paper further considerations are reported, still based on experimental results, about the behaviour of contactors protected by aM fuses under short-circuit conditions.

## II TESTS

The tests were carried out on a complete series of contactors of a European manufacturer, protected by standardized aM fuses.

The following contactor-fuses associations were stated by the manufacturer in order to meet type 2 co-ordination under short-circuit conditions. In relation to the rated values of  $I_c$  (operational current for utilization category AC 3 of the contactor) and of  $I_n$  (fuse rated current) they are :

Contactor $I_c$ ( A )	aM fuse $I_n$ ( A )
700	630
550	500
300	400
300	315
210	250
210	200
120	160
120	100
65	80
40	50
23	20
16	12

The tests were carried out at a voltage of 420 V, 50 Hz, on a single pole of each contactor, with prospective currents up to 50 kA ( r.m.s. value ) and power factor 0.5 up to 10 kA, 0.3 from 10 to 20 kA, 0.25 for currents higher than 20 kA. The contactor pole was connected in the test circuit as shown in fig. 1.

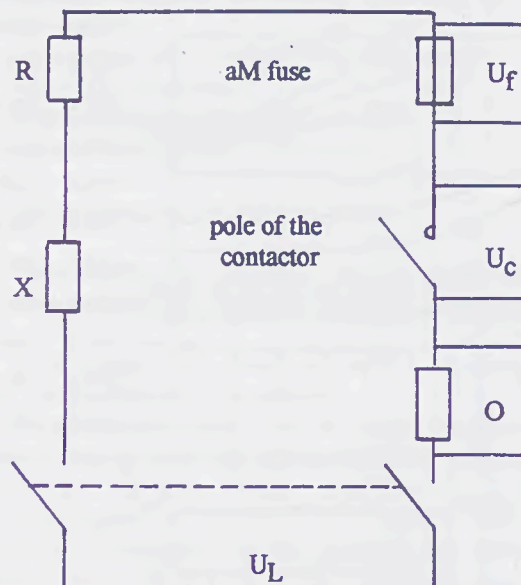


Fig. 1 - Test circuit

R adjustable resistor  
X adjustable reactor  
 $U_f$  recording voltage sensor across the aM fuse  
 $U_c$  recording voltage sensor across the contactor pole  
O recording current sensor  
 $U_L$  supply voltage, 420 V, 50 Hz

The following quantities were recorded in each test, both by an electromagnetic oscillograph and a computer data acquisition apparatus : supply voltage, voltage across the fuse and the contactor pole, test current ( in regards to its duration, peak and total  $I^2t$  ). Each test was carried out on a contactor pole in new conditions and in closed position.

The test current was made by an appropriate switch and broken by the aM fuse in series with the contactor pole.

### III TEST RESULTS AND CONSIDERATIONS

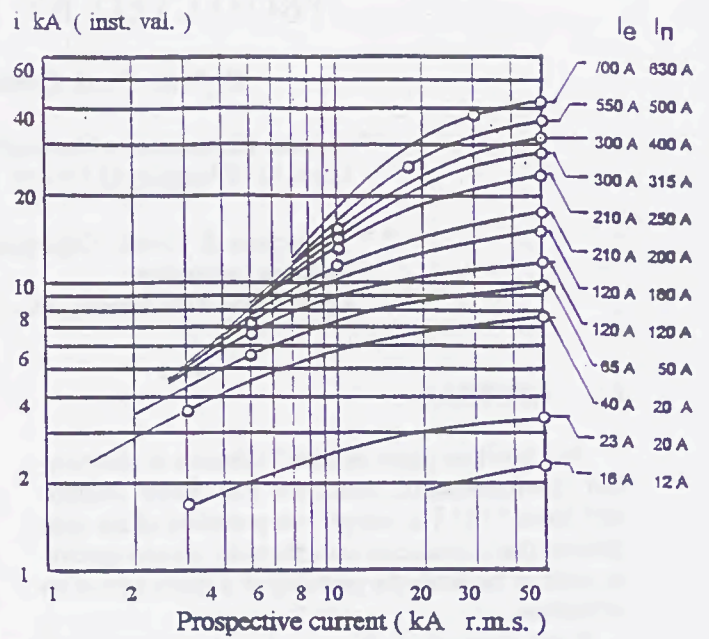
III.1 Behaviour of the contactor poles under test currents between " $I_r$ " and " $I_q$ " as defined by EN Standard 60947-4-1 for test sequence III, performance under short circuit conditions.

The test results are summarized in three diagrams D.2, D.3 and D.4 ( figures 2, 3, 4 ), where, for each of the twelve contactor-aM fuse associations, the let-through  $I^2t$ , peak current and the current duration are reported as function of the prospective test current. On each diagram, the relevant values are shown by appropriate signs (  $\circ$  ) corresponding to the above mentioned  $I_r$  and  $I_q$  test currents.



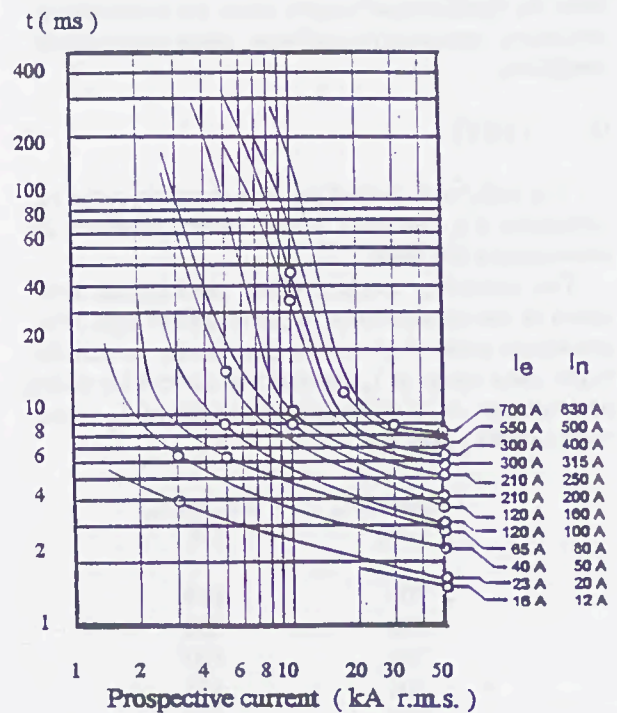
D.2

Fig.2 - Let-through  $I^2t$  of the aM fuse, of rated current  $I_n$ , associated to the contactor of rated current  $I_e$ .



D.3

Fig.3 - Maximum peak value of the current, limited by the aM fuse of rated current  $I_n$ , associated to the contactor of rated current  $I_e$ .



D.4

Fig.4 - Current duration, limited by the aM fuse, of rated current  $I_n$ , associated to the contactor of rated current  $I_e$ .

Diagram D.4, in particular, shows that:

- at prospective test current  $I_q$  (50 kA as above stated) all the contactor-aM fuse associations act like current limiting devices, i. e. they limit the test current duration to times less than 10 ms.
- at prospective current  $I_r$ , which takes up the values 3 - 5 - 10 - 18 - 30 kA in accordance with the ratings of the contactors, only the following seven contactor - aM fuse associations limit the test current duration to times less than 10 ms,

Contactor $I_c$ (A)	aM fuse $I_n$ (A)
700	630
210	200
120	100
65	80
40	50
23	20
16	12

while the five remaining ones show current durations between 10 and 50 ms.

Test current durations higher than 10 ms have to be conveniently discussed, as they may produce repeated separations of the contactor contacts with serious consequences due to the arcing.

It is to be observed, however, that the Standard requirements related to residual conditions of the contactor for type 2 co-ordination were met in eleven out of twelve cases after the tests carried out with the prospective currents  $I_r$  and  $I_q$ .

But, according to the above consideration, further tests with prospective currents lower than  $I_r$  were esteemed to be significant.

### III.2 Behaviour of the contactor-aM fuse associations at prospective currents lower than $I_r$ but capable of producing contact separation of the contactors by electrodynamic effect.

These test current values are not mandatory in the above quoted EN Standards for the verification of the compliance of the contactor - fuse association with the performance requirements under short-circuit conditions. The test results, however, with such prospective currents show that two of five contactor - aM associations had to be derated from type 2 co-ordination to type 1.

These two associations are:

Contactor $I_c$ (A)	aM fuse $I_n$ (A)
300	400
210	250

For them, test currents  $I_r$  and  $I_q$  did not produce the maximum stress likely to be experienced by lower prospective currents. This fact has to be expected on the basis of the behaviour of such associations as represented in diagram D.2, D.3, D.4, where, in particular, higher values of  $I^2t$  and current duration can be noted for lower prospective test currents.

Anyway, the behaviour of each of these associations is deemed to be worthy of more deep considerations.

#### III.2.1 Association of the contactor having $I_c$ 210 A with aM fuse of $I_n$ 250 A.

The oscillograms reported in figures 5 and 6, related to prospective test current of 3.8 kA and 6.3 kA, show current durations of 260 ms and 46 ms and peak current values high enough to produce contact separation of the contactor by electrodynamic effect. The consequences on the test results were:

##### a) with prospective current of 3.8 kA

- contact repulsion and arcing persistent for 260 ms,
- destruction of the contacts and of the contact force springs,
- blackening and burning of arc-chutes,
- general inadequacy of insulation;

##### b) with prospective current of 6.3 kA

- tight welding of contactor contacts, which could not be separated without significant deformation.

It is evident that results a) and b) do not meet type 2 of co-ordination conditions.

A converse conclusion can be drawn from the results of test carried out with prospective currents of 10 kA ( $I_r$ ), 20 kA, 30 kA, and 50 kA ( $I_q$ ).

Oscillograms of figures 7, 8, 9 and 10 refer to such tests. The related current durations are included between 4.5 and 8.5 ms, while the contact separation by electrodynamic effort ceases 5-6 ms after the end of the current, so that the risk of contact welding becomes negligible.

#### III.2.2 Association of the contactor having $I_c$ 300 A with aM fuse of $I_n$ 400 A.

The oscillograms reported in figures 11 and 12, related to prospective currents of 5 and 8.5 kA, show current durations of 340 ms and 78 ms and peak currents still high enough to produce contact separation.

The consequences on the test results are quite similar to those above described under a) and b) of sub-section III.2.1, and also the conclusion, which invalidates type 2 of co-ordination.

As regards the results of the test carried out with prospective current of 10 kA ( $I_T$ ), to which the oscillogram of figure 13 refers, a different performance was found in respect of the above corresponding case, quoted in III.2.1.

In this case the current duration of 57 ms was long enough to determine together with the other necessary conditions a serious contact welding, invalidating by itself type 2 co-ordination.

At last, the tests made with prospective currents of 20 kA, 30 kA, and 50 kA ( $I_Q$ ), corresponding to the oscillograms of figure 14, 15 and 16, produced current durations between 6 and 8 ms with insignificant risk of contact welding and negligible contact erosion.

#### IV. CONCLUSIONS

In accordance with the above test results, it seems reasonable to claim once again that the verification of the overcurrent withstand of a contactor has to be extended to possible values of prospective currents lower than current  $I_T$ , but high enough to cause contact separation of the contactor.

It seems reasonable, as well, to deem that a higher number and worse quality of negative results would be produced by any other contactor association with less current limiting protective devices, such as e.g. gG fuses or circuit - breakers.

#### V. REFERENCES

- [1] Cantarella G., Farina G., Tartaglia M.: "Behaviour of contactors protected by fuses during short-circuit currents". Proceedings IEE, vol. 124, No. 12, 1977.
- [2] Wright A., Newbery P.G.: "Electric Fuses" IEE Power Engineering Series 2. Peter Peregrinus LTD 1982.
- [3] IEC Publication 269 - 1 Second Edition 1986 "Low Voltage Fuse. Part. 1 General Requirements".
- [4] IEC Technical Report - Type 3 First Edition 1996 "Coordination between fuses and contactors-motor starters- Application guide".
- [5] Wilkins R.: "Generalized short-circuit characteristics for h.r.c. fuses". Proceedings IEE, vol. 122, No.1, 1975.
- [6] Turner H.W., Turner C., Williams D.J.A.: "Critical parameters influencing the coordination of fuses and switching devices". Proceedings of the ICEFA 1987.
- [7] Arato D., Cantarella G.: "Contactors protected by fuses : risk of contact welding ". Proceedings of the ICEFA 1991.
- [8] Food A. J.: "Protection of motor controller using North American Time Delay Fuses". Proceedings of the ICEFA 1991.
- [9] Bret M.: "Coordination of fuse-starters : New standards, new needs". Proceedings of the ICEFA 1991.
- [10] Deshayes R.: "aM " fuses and its co-ordination with starters". Proceedings of the ICEFA 1991.
- [11] Schaffer S.: "Dual - Element Time Delay class J fuses for protection of motor circuit utilizing IEC controllers". Proceedings of the ICEFA 1995.
- [12] Bottauscio O., Crotti G., Farina G.: "Numerical analysis of electrical contacts of control devices protected by fuses". Proceedings of the ICEFA 1995.
- [13] Arato D., Cantarella G.: "Advance in short circuit co-ordination of contactors and motor starters with fuses". Proceedings of the ICEFA 1995.

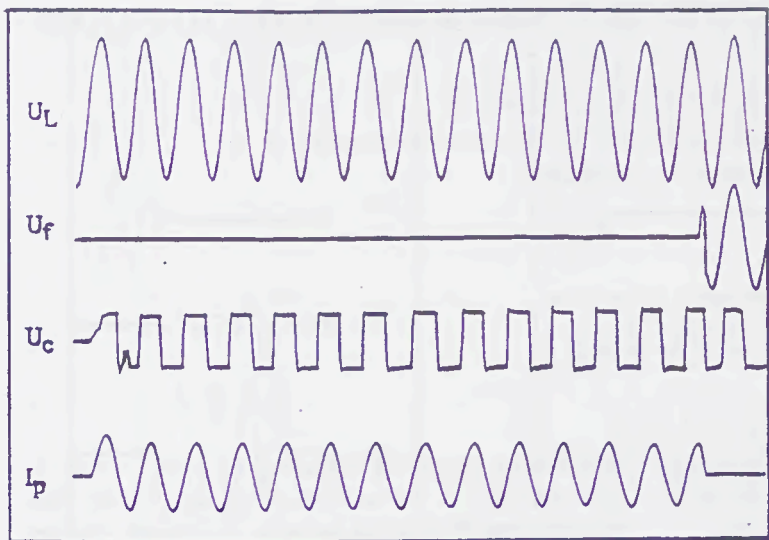


Fig 5 -  $I_p$  3,8 kA (r.m.s.)

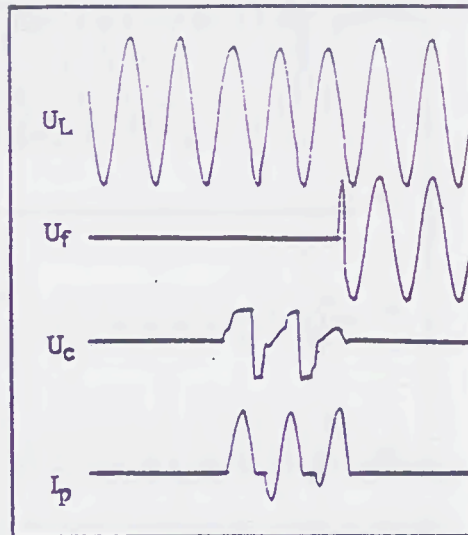


Fig. 6 -  $I_p$  6,3 kA (r.m.s.)

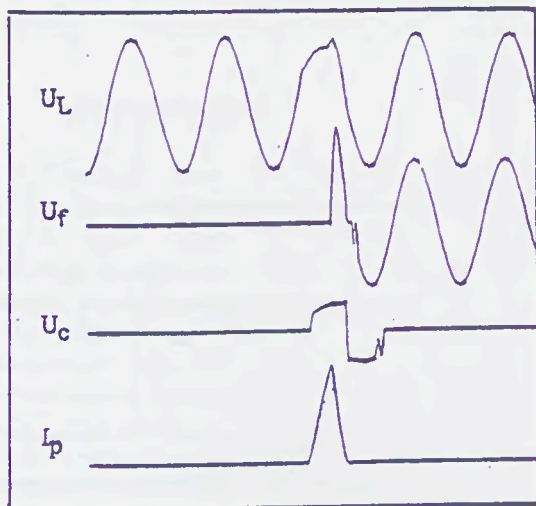


Fig 7 -  $I_p$  10 kA (r.m.s.)

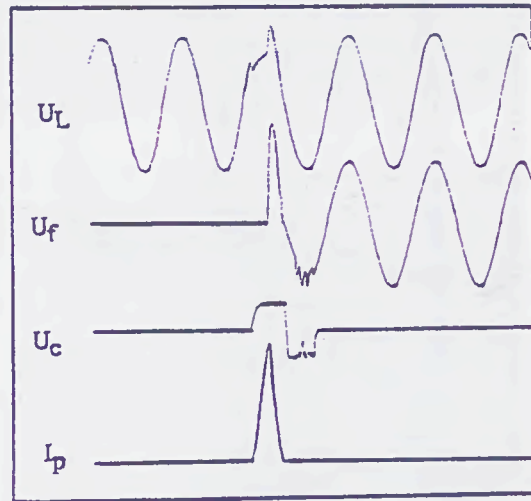


Fig 8 -  $I_p$  20 kA (r.m.s.)

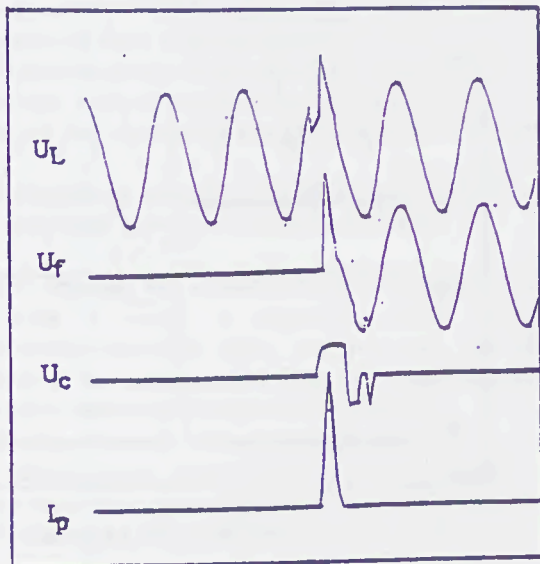


Fig 9 -  $I_p$  30 kA (r.m.s.)

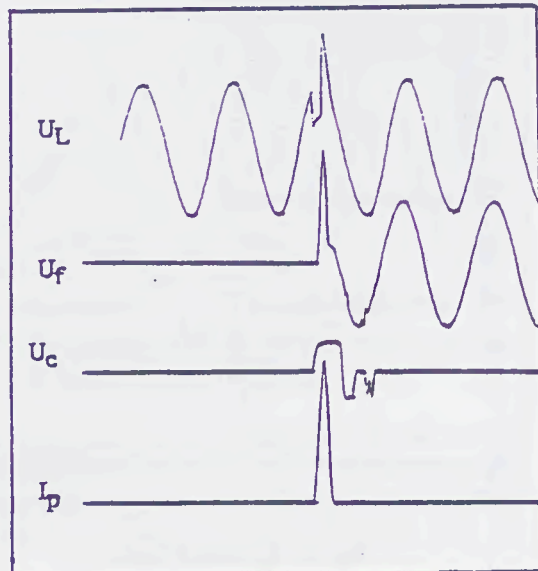


Fig 10 -  $I_p$  50 kA (r.m.s.)

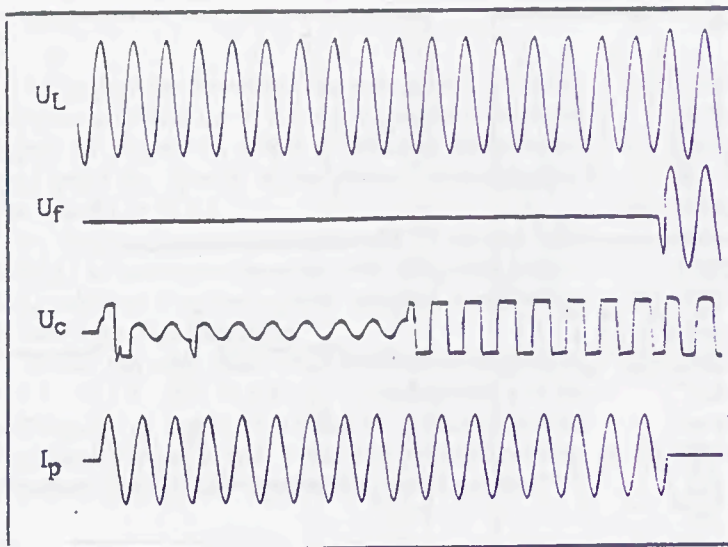


Fig.11 -  $I_p$  5 kA (r.m.s.)

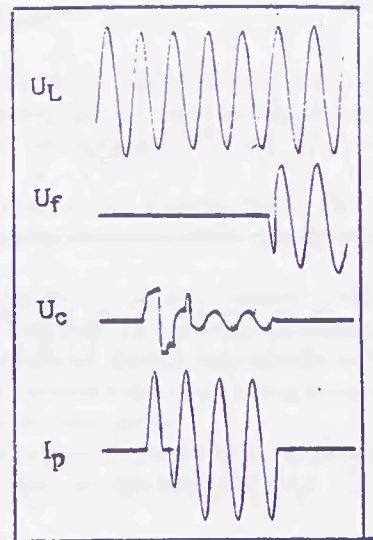


Fig. 12 -  $I_p$  8,5 kA (r.m.s.)

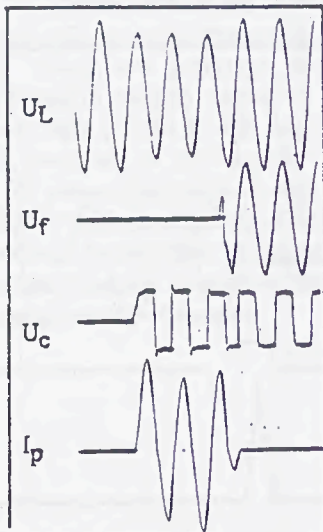


Fig.13  
 $I_p$  10 kA  
(r.m.s.)

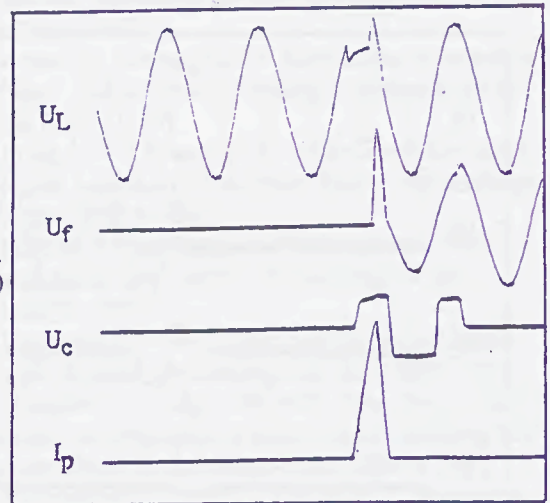


Fig. 14  
 $I_p$  20 kA  
(r.m.s.)

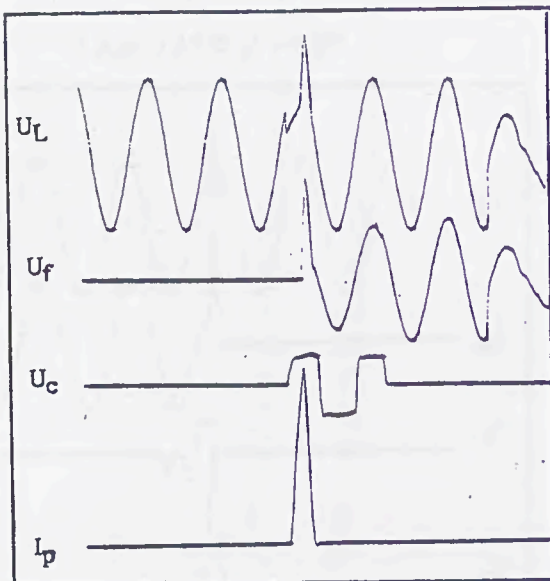


Fig. 15 -  $I_p$  30 kA (r.m.s.)

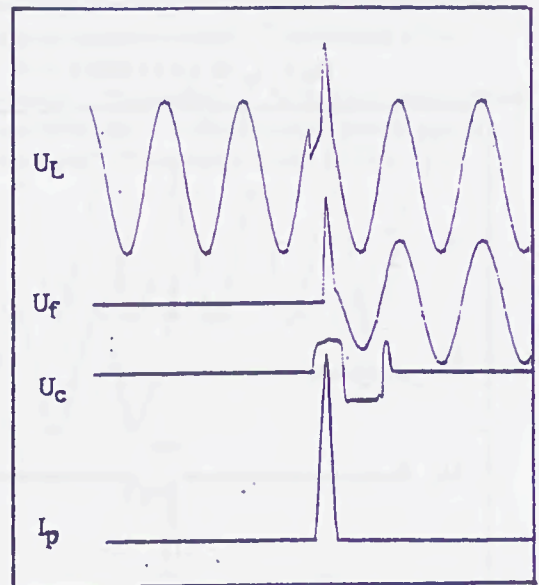


Fig. 16 -  $I_p$  50 kA (r.m.s.)

# HIGH-VOLTAGE FUSE-LINKS FOR MOTOR CIRCUITS PROTECTION

V. Giurgiu, Gh. Oarga, S.Purdel  
Research Institute for Electrical Engineering – ICPE  
Bucharest, Romania

**Abstract:** There are presented pre-arcing time-current and cut-off characteristics obtained in high-rupturing capacity laboratory, principal technical features and the results of specified withstand test to a cyclic starting of the motor, for a new series of fuse-links with improved characteristics and reduced quantity of silver for fuse elements.

## I. INTRODUCTION

High-voltage fuses are basically simple and relatively cheap and because of their features they are used in wide variety of applications, e.g. for distribution transformers, motors and capacitors, as an extremely important mean of protection, [1].

The high-voltage fuse-links for motor circuit protection are used only as short-circuit protection and are connected to the motor in series with an "associated device" which can be a circuit breaker or a contactor, having its own relaying system that protects the motor against overcurrents due to excessive loads.

Fault energy limitation to minimise damage resulting from electrical faults, ability to co-ordinate precisely with protective system of associated device, together with adequate short-circuit capacity of fuse-links are all essential for safety of entire installation.

The development of the new series of fuse-links with improved characteristics and a reduced quantity of silver for fuse elements it was the purpose of this work.

## II. REQUIREMENTS FOR FUSE-LINKS FOR MOTOR CIRCUIT APPLICATIONS

The demands for a typical motor circuit application involving a motor, a protective system against overcurrents based on relays, an associated electrical apparatus, the cable and the fuse-link, regarding their protective characteristics are shown in Fig. 1.

The requirements for such an application are:

- the operation should be as rapid as possible on heavy faults (fast operation), that the cut-off current and the let-through  $I^2t$  should be as low as possible, in the

region below 0.1 s on the pre-arcing time-current characteristics;

- ability to withstand indefinitely under repeated starting condition (slow operation), than have good pulse withstand ability in the region over 10 s on the pre-arcing time-characteristics;

- improved performances under low overcurrent conditions and ability to interrupt satisfactorily all faults beyond the capability of the associated devices up to maximum fault level of the system.

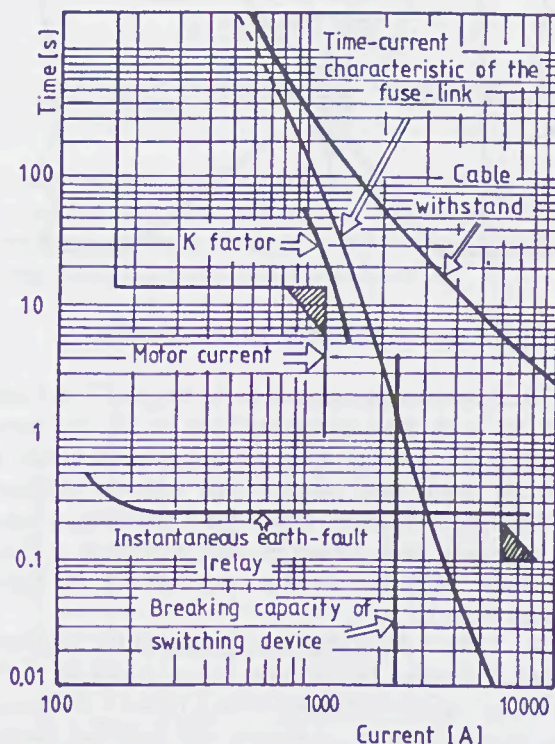


Fig. 1 Co-ordination of characteristics relating to the protection of a motor circuit

The pre-arcing time-characteristics of the motor starting fuse-links, for satisfying these requirements, shall be within the limits indicated in [2]. An overload characteristic to which the motor fuse-link may be

repeatedly subjected under specified motor starting conditions without deterioration is obtained by multiplying the current on the pre-arcing characteristics by the K factor, chosen at 10 s, for a frequency of starts up to six per hour and for not more than two consecutive starts, [2].

### III. THE NEW SERIES OF FUSE-LINKS 7.2 kV 25-400 A FOR MOTOR PROTECTION

The new series of motor protection fuse-links [3], is in according with IEC Publications 281-1 and 644, regarding overall dimensions and the tests. This type of fuse-links, because their time-current characteristics are relatively "slow" in the region above 10 s can have a small number of elements, of relatively large cross-section area and with uniformly spaced restrictions having particular forms. In Fig.2 is shown a type of restriction, with a small cross-section area, which provides a cooling of this region and a withstand to repeated startings of the motor and a fast operation at the short-circuit currents.

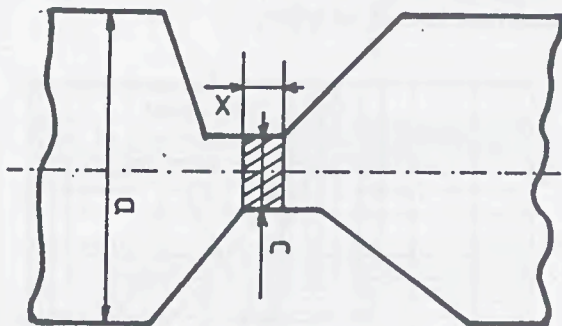


Fig.2 A type of restriction for fuse-element

The number of elements is in the range of 3 to 8 and they are made from silver and can be of the same length as the fuse-link body, with expansion bends at intervals along their length, equal with the distance between the restrictions, to provide a flexibility to take up expansion and contraction due to thermal cycling associated with the starting requirements of high-voltage motors.

In Table 1 and Table 2 are presented the principal technical features for the new series, tested in high-rupturing capacity laboratory from Craiova - Romania, and manufactured in conformity with certified quality assurance system ISO 9001, [4]. The fuse-link bodies are of single resin glass fibre tube for rated currents up to 250 A and of double tubes, mounted in parallel, for rated currents of 315 A (2x160 A) and 400 A (2x200 A). The resin body provides a good withstand to the thermal shock at the test duty 3, the minimum breaking currents being in the range of 3 to 4 times  $I_n$ . All fuse-links have striker (type medium) actuated by a spring,

for operating associated electrical apparatus, to ensure 3-phase tripping on the blowing of a single fuse-link.

The end caps are mounted on the resin body of the fuse-link using a magnetic forming machine, with a very precise control of energy, then an accurate repeatability of the magnetic forming process. That new unconventional technology provides a great productivity and important economy of materials and energy.

Table 1 Fuse-links for rated currents up to 80 A

Type	MOT 7.2 kV/25 ... 80 A					
Overall dimensions	Ø73/508 mm					
Rated current [A]	25	31.5	40	50	63	80
Rated breaking current [kA <sub>cr</sub> ]	45					

Table no.2 Fuse-links for rated currents up to 250 A

Type	MOT 7.2 kV/100 ... 250 A				
Overall dimensions	Ø88/508 mm				
Rated current [A]	100	125	160	200	250
Rated breaking current [kA <sub>cr</sub> ]	31.5				

The fuse-links for the range 25 ... 80 A and for the range 100 ... 250 A are considered as forming homogeneous series because their characteristics comply with the conditions shown in [1]. They may be used in combination with vacuum contactors and another electrical or mechanical switching devices and a precisely co-ordination between their characteristics must be made, to provide a good protection in heavy working conditions (milling, extractive and petroleum industry, etc.).

### IV. TEST RESULTS

According to the IEC 282-1 and IEC 644 standards, were tested more than 240 fuse-links, for determining pre-arcing time-current characteristics, cut-off characteristics and test duty 1, test duty 2 and test duty 3 to demonstrate the capability of operation at extreme conditions, for each rated current of the new series.

Fig.3 represents time-current characteristics for fuse-links type MOT 7.2 kV, 100-400 A, obtained in a low voltage test circuit, with a constant value of the test current through the fuse-link. The limits imposed in [2]:

$$I_{f10} / I_n \geq 3 \text{ for } I_n \leq 100 A$$

$$I_{f10} / I_n \geq \text{for } I_n > 100 A$$

$$I_{f01} / I_n \leq 20(I_n / 100)^{0.25} \text{ for all current ratings}$$

provide slow and fast operation of fuse-links in the 10 s region and 0.1 s region respectively, and characteristics of our new series of fuse-links obtained by a great

number of tests in laboratory, are in accordance with these requirements.

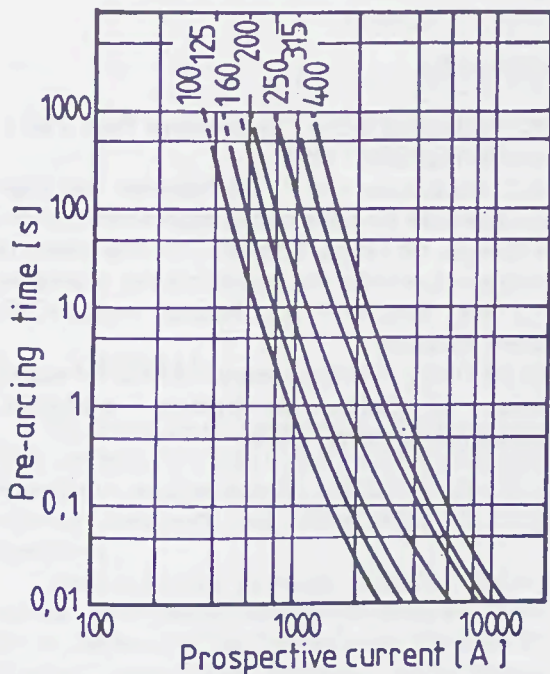


Fig.3 Time-current characteristics for rating currents of 100 - 400 A.

In Fig.4 are represented cut-off characteristics obtained in high-current laboratory, for the same rating currents as above. The new series of fuse-links being a homogeneous series, breaking tests were conducted in accordance with [1], and the results of test duty 1 and test duty 2 are presented in Table 3, for rated currents 100 - 250A. As it was indicated above, the shape of restrictions for fuse-elements, correlated with the number of restrictions, can provide a substantial reduction of the T.R.V. values. The results of tests confirmed that our solution provides reduced values of T.R.V., as can be seen in Table 3.

Table 3 Results of tests for rated currents 100-250 A

Type	MOT 7.2 kV/100 ... 250 A				
Rated current [A]	100	125	160	200	250
Cut-off current [kA <sub>max</sub> ] - duty 1	13.4	17.7	18.1	23.5	26.5
T.R.V.[kV]	11.7	11.2	10.5	9.4	9.6
Cut-off current [kA <sub>max</sub> ] - duty 2	8	12.7	13.6	18.8	25.5
T.R.V.[kV]	10.1	10.7	10.7	10.1	10.1

When fuse-links are used for motor circuit protection together with an associate electrical apparatus, like a

contactor, the main criterion in choice of current rating of the fuse-link is the ability to withstand repeated

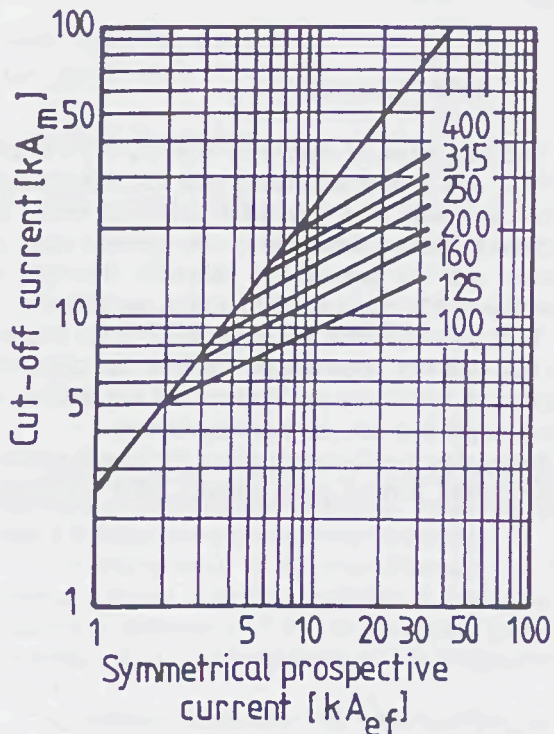


Fig.4 Cut-off characteristics for rating currents of 100-400 A.

starting current surges for the run-up time of the motor, in normal and abnormal service conditions, without deterioration. There are made a gret number of tests for establishing the correct value of K factor, [2].

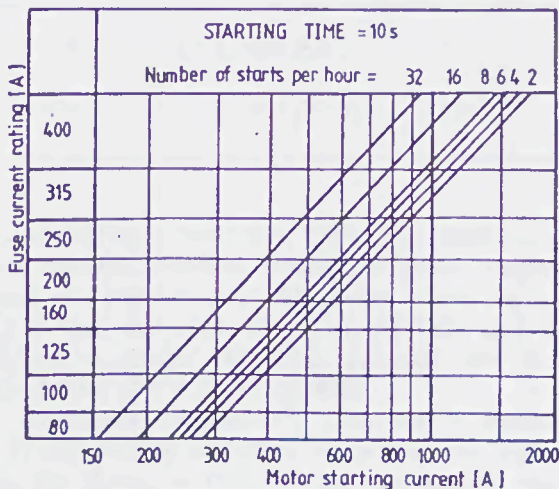


Fig.5 Fuse-link selection chart, for motors with run-up times not exceeding 10 s

The chart presented in Fig.5 is very useful for an user in selection of fuse-link, correlated with the motor power, his number of starts per hour and the starting time.

## V. CONCLUSIONS

The new series of fuse-links with  $U_n=7.2$  kV and  $I_n=25 \dots 400$  A is in accordance with IEC Publications 282-1 and 644. The fuse-links have the ability to withstand, without deterioration, the repeated starts of motors and can provide the character slow-fast of operation in 10s region and 0.1 s region, respectively.

Tests have confirmed the good choice of the solution for fuse-elements, regarding the shape of restriction, the number of restrictions per element and the number of elements per fuse-link, for all rating currents.

A design objective, to remain within the bounds of size and economy, without compromising other essential

parameters, was obtained and the use of magnetic forming in manufacturing process is an example

The charts obtained are very useful for users of such kind of fuse-links, and are instrumental to the choice of a fuse-link for a concrete application.

## REFERENCES

- [1] IEC Publication 282-1, "High-voltage Fuse. Part 1: Current-limiting fuses", 1994.
- [2] IEC Publication 644, "Specification for high-voltage fuse-links for motor circuit applications", 1979.
- [3] V.Giurgiu, Gh.Oarga, S.Purdel, "A new series of high-voltage fuse-links for motor circuits protection,  $U_n=7.2$  kV,  $I_n=25-400$  A", Internal work, ICPE, Bucharest, Romania.
- [4] EN ISO 9001, "Quality systems - Model for quality assurance in design, development, production, installation and servicing", 1994.

# OVERLOAD PROTECTION OF CONTACTORS BY FUSES

D. Arato \* , G. Cantarella \* \*

\* Istituto Elettrotecnico Nazionale Galileo Ferraris  
Corso M. d'Azeglio, 42 - 10125 Torino - Italy

\* \* Politecnico di Torino - Dipartimento di Ingegneria  
Elettrica Industriale  
Corso Duca degli Abruzzi, 24 - 10129 Torino - Italy

## I GENERAL

The protection of contactors against overcurrent by fuses has been the object of many studies particularly as regards the requirements for satisfactory co-ordination between contactors and fuses under short-circuit conditions.

Fuses to be used to protect modern contactors against short-circuit currents can easily be chosen today on the basis of the International Electrotechnical Standard prescriptions. Moreover, comprehensive papers can be found in the technical literature concerning the performance results of the different types of contactor-fuses co-ordination ( \* ).

Additional information can also be found about the fuse ratings which can satisfactorily reduce the risk of contact welding under short-circuit conditions.

Nevertheless further work is still needed, in our opinion, to provide criteria for assisting in the selection of fuses suitable for overload protection of contactors.

## II SCOPE

Scope of the present paper is to contribute to the solution of the above problem by discussing the possibility of utilizing for the contactor overload protection the same fuse previously selected for the contactor short-circuit protection.

( \* ) Some Standard requirements relevant to the present paper are here recalled :

Type 1 co-ordination: damage to the contactors is acceptable. There has been non discharge of parts beyond the enclosure, nor damage to the conductors or terminals.

Type 2 co-ordination: no damage is occurred, except that welding of contactor contacts is permitted, if they are easily separated.

In the following, reference is made to those fuses which proved to be capable to prevent contactors from contact welding under short-circuit conditions.

The background to above considerations is the overload current withstand capability of contactors as specified in sub-clause 7.2.4.4 of European Standard EN 60947 - 4 - 1 ( corresponding to IEC Publication 947 - 4 - 1 ).

Accordingly, contactors with utilization categories AC - 3 or AC - 4 shall withstand the overload current for the duration as specified in the following table :

Table IX

<i>Rated operational current</i>	<i>Test current</i>	<i>Duration of test</i>
$\leq 630$ A	$8 \times I_e$ max AC 3	10 s
$> 630$ A	$6 \times I_e$ max AC 3	10 s

In addition, a Note under Table IX clarifies that these specified overload current withstand requirements of contactors cover also duties where the current is less than that shown in the Table and its duration is longer than 10 s, provided that the related value of  $I^2t$  is not exceeded.

Reasonably, the same  $I^2t$  value can be assumed to be withstood by contactors for overcurrents higher than that shown in Table IX up to the current value at which the contacts of the contactors are just thrown apart by electrodynamic effect [ 7 ].

### III. EXAMPLE OF TEST PROCEDURE

As a consequence, the contactor overload withstand  $I^2t$  characteristic plotted in a time - current diagram (log - log) becomes like that shown in fig.1, i.e. a right line extending from its conventional free - air thermal rated current,  $I_{th}$ , up to current value for which contact repulsion begins,  $I_{rep}$ .

In particular, the example of fig. 1 is referred to a contactor specified as follows :

$I_e = 100$  A ( AC - 3 rated operational current, r.m.s. ).

$I_{th} = 180$  A ( rated conventional free - air thermal current ).

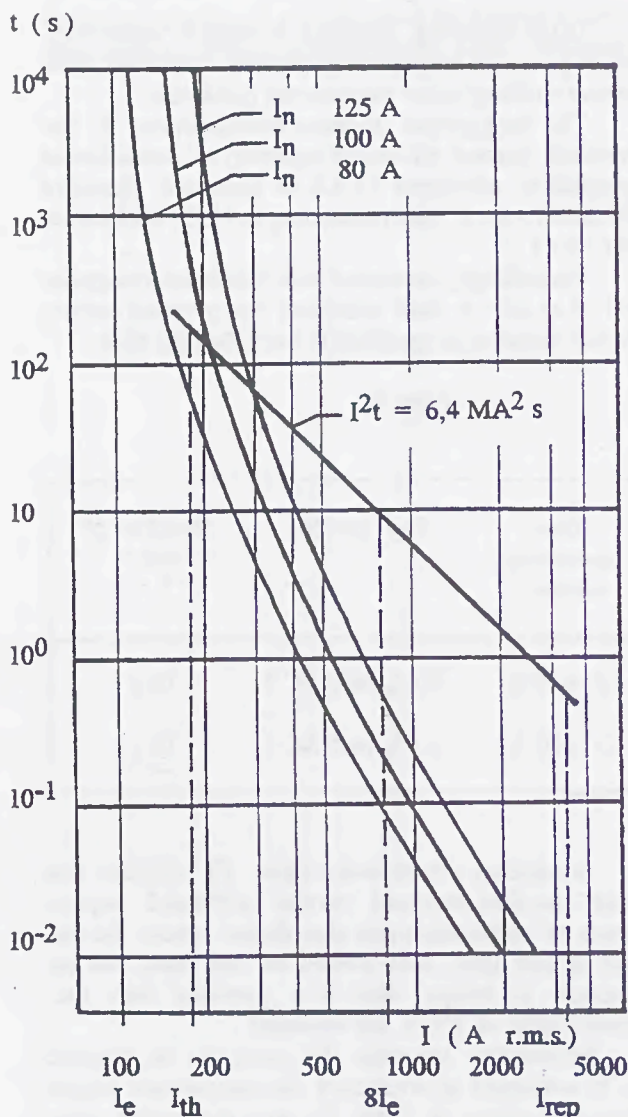


Fig.1

$I_{rep} = 3300$  A ( current value for which the contacts of contactor begin to be thrown apart by electrodynamic effect, r.m.s. ).

$I^2t = 6,4$  MA<sup>2</sup>s ( constant  $I^2t$  value corresponding to  $(8 I_e)^2 \cdot 10$  s, according to which the above right line is reported in figure 1 ).

In the same diagram of fig. 1 the time - current characteristics are also reported of the fuses previously chosen for the protection of the contactor against short - circuit currents .

As above said, these fuses rated 80, 100 and 125 A proved to be capable of preventing the contactor of 100 A from contact welding in an appropriate short-circuit research made in the past [ 7 ].

More generally the fuse parameters identified in that circumstance are recalled in the diagram of figure 2, together with other results of the tests made on 80 types of contactors of different ratings manufactured by different European manufacturers.

Rated current of fuses ( A )

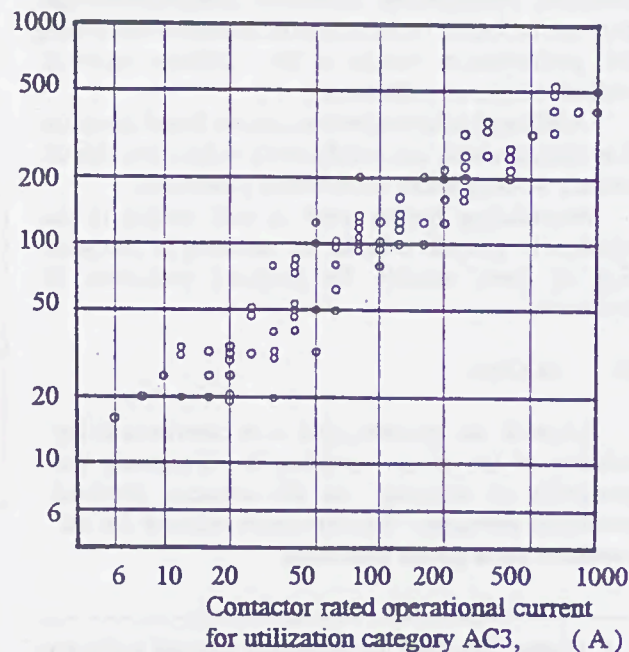


Fig.2

The diagram shows the maximum rating of fuses which prevented the tested contactors from contact welding under short - circuit conditions, as function of the rated operational current for utilization category AC - 3 of the contactors.

Coming back then to the example of fig. 1 let's begin to consider a gG fuse rated 100 A as the overload protective fuse. Its time - current characteristic crosses the contactor withstand time-current characteristic (plotted as  $I^2t$  constant value) in the point 220 A - 120 s. It is obvious that only a region on the left side of this point has to be verified by appropriate tests as regards the temperature - rise overload performance on the contactor. It is included between the current limits 220 ÷ 180 A (as 180 A is the contactor rated thermal current).

That was done under the same test conditions as those specified for type tests and recalled in the following. The test results are summarized in the table below :

Test current (A r.m.s.)	Current duration (s)	Temperature - rise of contacts (K)	Temperature - rise of contacts (K)
220	120	60	39
200	240	79	57
185	800	91	70

According to the values of the table it is proved that the fuse rated 100 A is suitable for the overload protection of the contactor, as in no case the temperature - rise of terminals exceeds the value of 70 K, which is admitted for continuous duty service.

The test results obtained then with a protective fuse rated 125 A, under unaltered remaining conditions, are :

Test current (A r.m.s.)	Current duration (s)	Temperature - rise of contacts (K)	Temperature - rise of contacts (K)
300	70	62	38
230	300	105	83
200	3900	138	115

The data of this table clearly show that the ageing of the contactor insulation and of the cables connected to the contactor terminals, become more important. It appears, as well, that overload currents of longer duration may determine the softening of PVC insulation. As well known, cables manufacturers highly

recommend to avoid that. In favour of safety therefore, the fuse rated 100 A should be preferred for overload protection.

#### IV. OTHER EXPERIMENTAL RESULTS.

By the same experimental procedure, the research was extended to other contactors chosen with rated current uniformly spaced, in a certain degree, in the range of contactors shown in abscissae of figure 2.

They are reported in the following table, together with the corresponding rated currents of the fuses capable to avoid contact welding under short - circuit conditions.

Contactor rated operational current (A r.m.s.)	Protective fuse rated current (gG) (A r.m.s.)
20	20 - 25 - 32
63	50 - 63 - 80 - 100
100	80 - 100 - 125
250	160 - 200 - 250 - 315
630	315 - 400 - 500

The final results of the tests carried out as above said, i.e. under the condition that the temperature-rise of 70 K of contactor terminals is never exceeded under overload conditions, are reported in the following table:

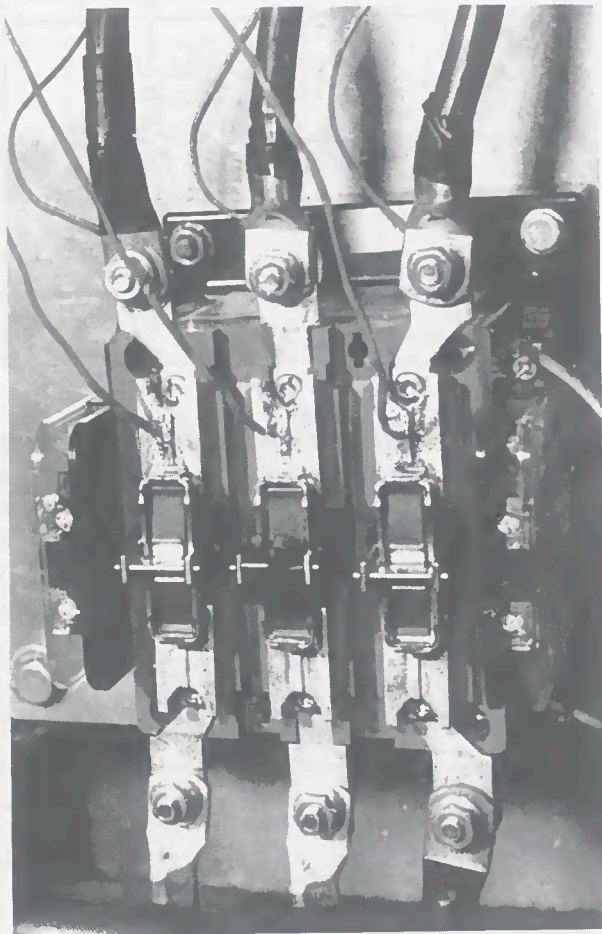
Contactor rated operational current (A r.m.s.)	Protective fuse rated current (gG) (A r.m.s.)
20	20
63	63
100	100
250	200
630	500

The time - current characteristics, corresponding to that of fig.1, on which test considerations were based, are shown in figures 3, 4, 5 and 6.

## V. TEST PROCEDURE SPECIFICATIONS

The tests were carried out in a single phase circuit supplied with alternating current at 50 Hz. The poles of each contactor were connected in series and the terminals were connected to the supply by PVC insulated copper cables having cross sectional areas in accordance with the Standard requirements for the temperature-rise tests.

Temperatures near the contacts and at the terminals of each contactor were measured by suitable thermocouples. Photograph F.1 shows one of the contactor under test, together with its supply connections and thermocouples positions.



F.1

## VI. CONCLUSIONS

A simple way is presented to achieve overload protection of contactors by fuses. As a basis for this protection the utilization is suggested of the fuses previously selected for the protection of the same contactors against short - circuit currents. In particular, reference is made in the present paper to those fuses which afford protection against contacts welding of contactors under short - circuit conditions. The same procedure is obviously applicable to fuses suitable for types 1 and 2 of short - circuit co - ordination.

## VII. REFERENCES

- [1] Cantarella G., Farina G., Tartaglia M.: "Behaviour of contactors protected by fuses during short-circuit currents". Proceedings IEE, vol. 124, No. 12, 1977.
- [2] Wright A., Newbery P.G.: "Electric Fuses". IEE Power Engineering Series 2. Peter Peregrinus LTD 1982.
- [3] IEC Publication 269 - 1 Second Edition 1986: "Low Voltage Fuse. Part.1 General Requirements".
- [4] IEC Technical Report - Type 3 First Edition 1996 "Coordination between fuses and contactors-motor starters- Application guide".
- [5] Wilkins R.: "Generalized short-circuit characteristics for h.r.c. fuses". Proceedings IEE, vol. 122, No.1,1975.
- [6] Turner H.W.,Turner C.,Williams D.J.A.:" Critical parameters influencing the coordination of fuses and switching devices". Proceedings of the ICEFA 1987.
- [7] Arato D., Cantarella G.:"Contactors protected by fuses : risk of contact welding". Proceedings of the ICEFA 1991.
- [8] Food A. J.: " Protection of motor controller using North American Time Delay Fuses". Proceedings of the ICEFA 1991.
- [9] Bret M.: "Coordination of fuse-starters : New standards, new needs". Proceedings of the ICEFA 1991.
- [10] Deshayes R.: " aM " fuses and its co-ordination with starters". Proceedings of the ICEFA 1991.
- [11] Schaffer S.: " Dual - Element Time Delay class J fuses for protection of motor circuit utilizing IEC controllers". Proceedings of the ICEFA 1995.
- [12] Bottauscio O., Crotti G., Farina G.: " Numerical analysis of electrical contacts of control devices protected by fuses". Proceedings of the ICEFA 1995.
- [13] Arato D., Cantarella G.: "Advance in short-circuit co-ordination of contactors and motor starters with fuses". Proceedings of the ICEFA 1995.

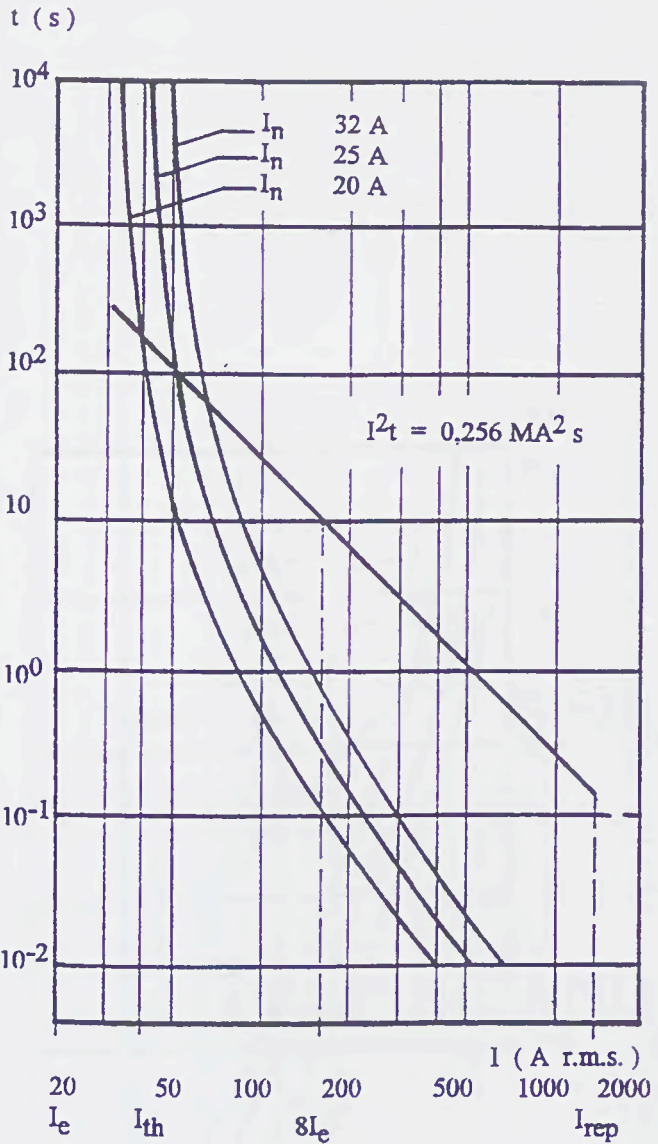


Fig. 3.

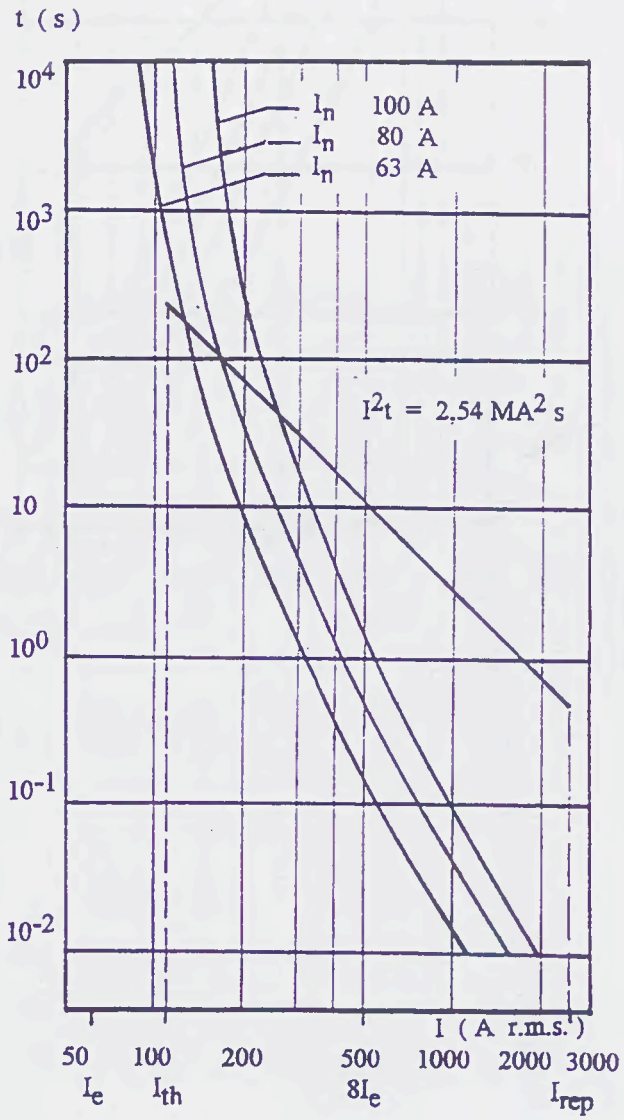


Fig. 4.

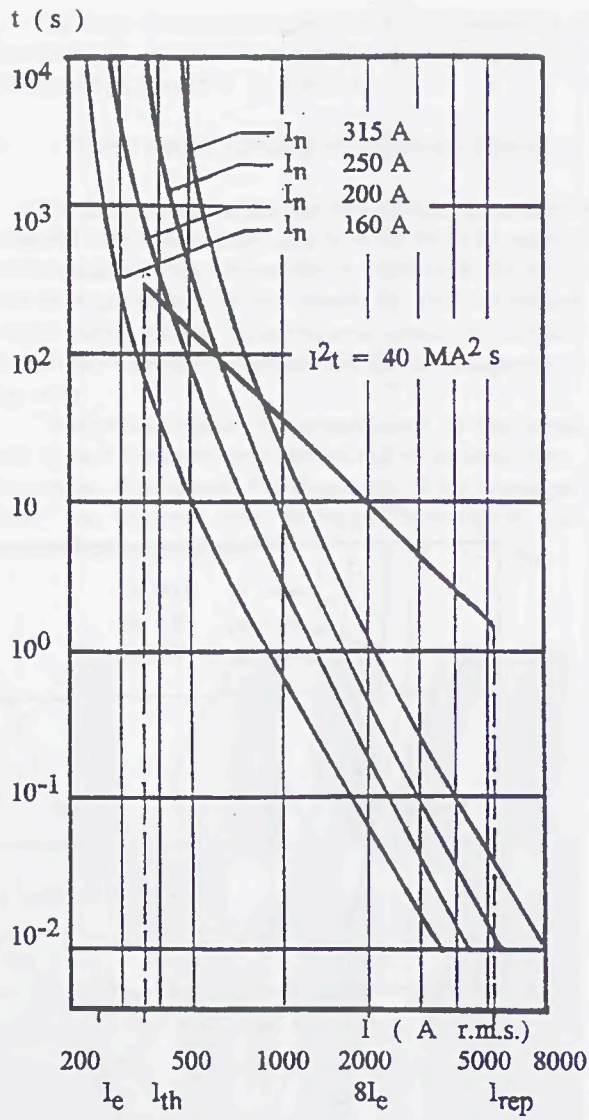


Fig. 5

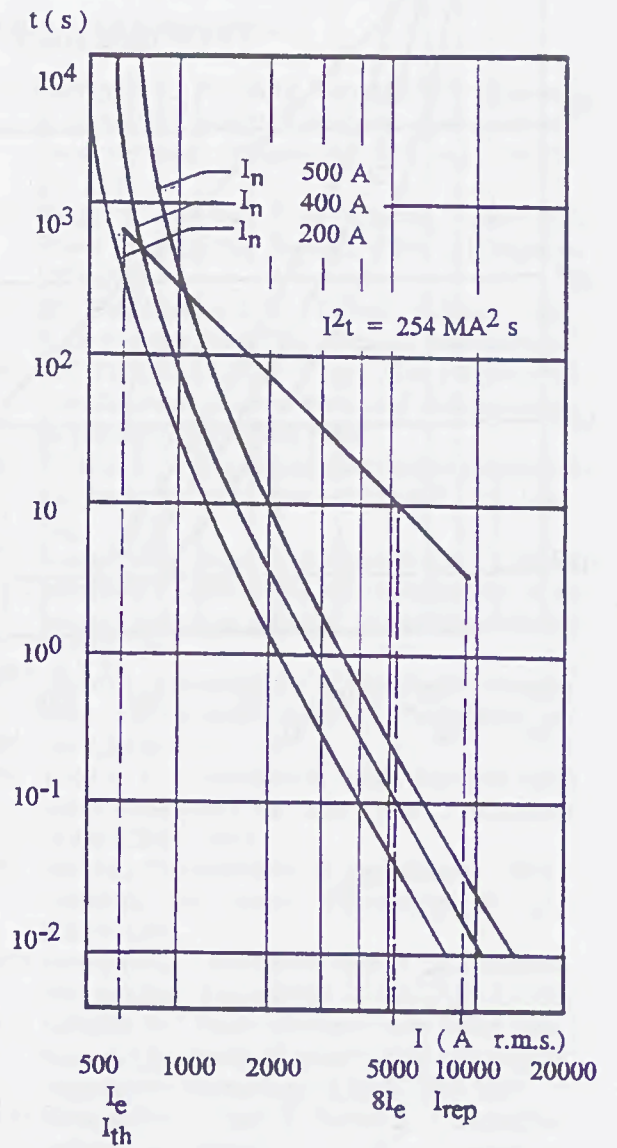
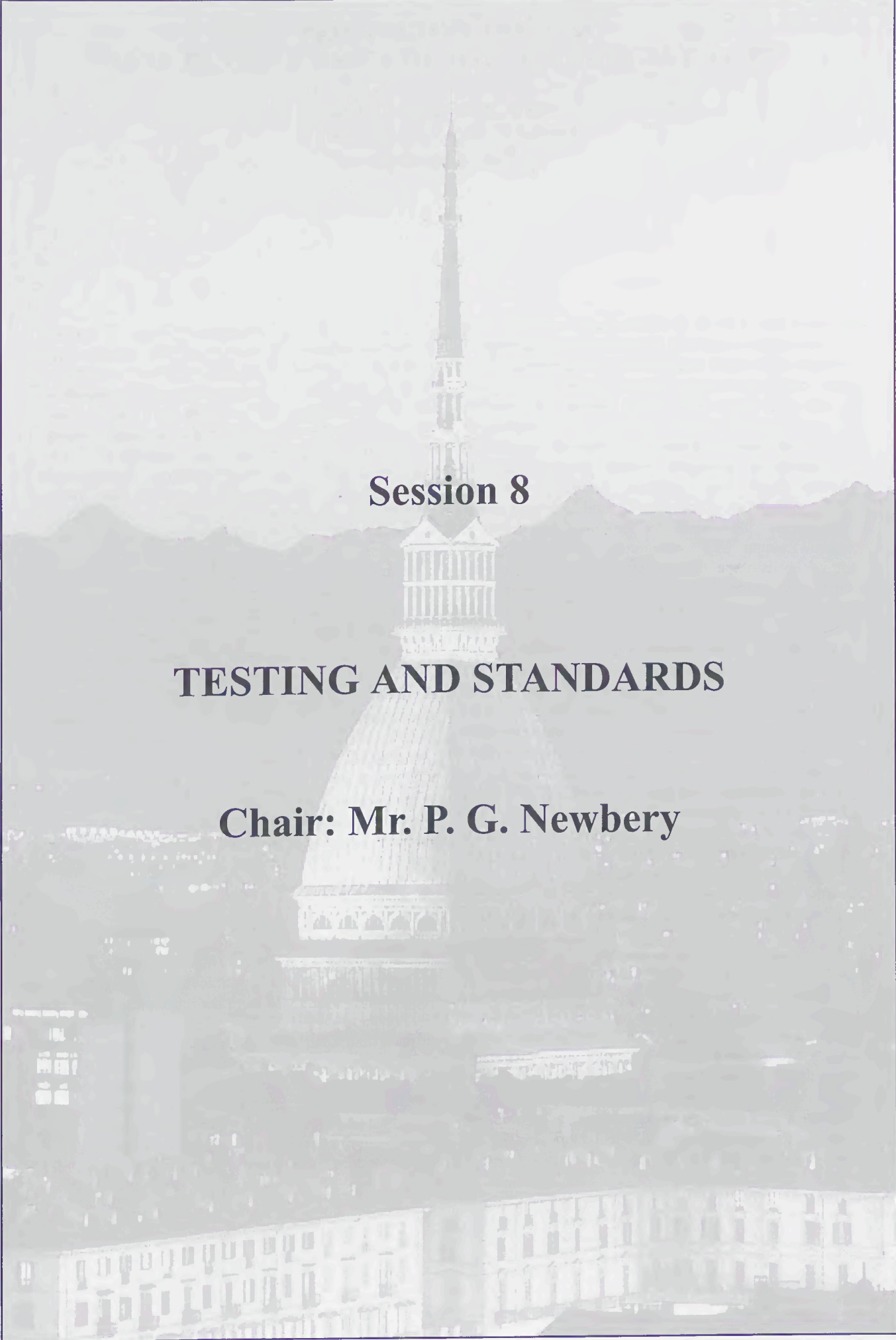


Fig. 6



**Session 8**

**TESTING AND STANDARDS**

**Chair: Mr. P. G. Newbery**

Handwritten text in Arabic script, likely a manuscript page. The text is arranged in several lines, with some lines appearing to be part of a list or table. The script is dense and cursive, characteristic of traditional Arabic calligraphy. The page is framed by a decorative border.

# PROSPECTIVE TRV FOR TEST DUTIES 1 AND 2 OF D.C. TRACTION 3 kV FUSES

Czucha J., Jakubiuk K., Lipski T.  
Technical University of Gdansk  
Gdansk, Poland

**Abstract:** Tests of the breaking capacity of 3 kV D.C. traction fuses shall incorporate the requirements on the prospective transient recovery voltage (P-TRV), analogous to the requirements on high voltage A.C. fuses. Up to now they are not incorporated. In the literature there is lack of data on required P-TRV for 3 kV D.C. traction. The paper summarises preliminary investigations carried out recently in Polish railways system and in one Polish test plant on mentioned P-TRV. The following methods of the P-TRV identification recommended by 56 IEC, 1987, have been used: no-load switching of test circuit, capacitance current injection, calculation from circuit parameters. Moreover small fuse rated current method was also applied. In this method switching of test circuit on short-circuit realised by a fuse of rated current 1 A and 3 A has take place. The major conclusion is that the quantitative data on P-TRV in case of 3 kV D.C. are more severe than for 3.6 kV A.C. The paper suggests streepness of P-TRV ab  $500\div 850$  V/ $\mu$ s for the test duty 1 and ab. 150 V/ $\mu$ s for the test duty 2. Corresponding maximum values are  $1.3\div 1.7 U_n$  and  $2 U_n$  respectively. The paper does not give suggestions about the P-TRV for test duty 3 because lack of such investigations. Finally the paper specifies the problems facing by identification of the P-TRV of 3 kV D.C. traction systems.

## I. INTRODUCTION

In the case of high voltage (h.v.) current limiting A.C. fuses the breaking capacity tests shall be performed at a prescribed prospective transient recovery voltage (P-TRV). IEC 282-1, 1994, Standard [1] strongly requires a defined P-TRV, particularly during the test duties 2 and 3. It seems, for D.C. 3kV traction current-limiting fuses also a P-TRV should be defined. By now there is lack of such requirements on both state and international level. Also the requirements of particular railway managements do not define the P-TRV. It can create a problem how to test these fuses to

fulfil the user requirements on P-TRV and have the comparable results of tests in different laboratories.

Particular railway management requires the breaking capacity tests using several currents too. Often these currents are limited to the test duties 1,2 and 3, understood as for h.v. A.C. current limiting fuses [1]. Decipher of the duties is: 1-rated breaking capacity, 2-breaking capacity within maximum arc-energy, 3-minimum breaking capacity. But some railway managements additionally require the breaking capacity of a short and long line short-circuit tests. In every case prescribed circuit parameters, i.e. source voltage, prospective current, time-constant are realised by the test's plant using different technical means. As a result, by the same parameters, the P-TRV can vary in wide limits.

The P-TRV of a 3 kV D.C. traction system can be absolutely different than that of 3.6 kV A.C. systems. A reason are the capacitances. In D.C. system an essential role play the filter condensers of semiconductor A.C./D.C. inverters, capacitance of which is significant, for example, of order several tenths  $\mu$ F and resonance frequency 300 Hz, 600 Hz, 1200 Hz a.s.o. (Fig. 1). Moreover, the line capacitance of 3 kV D.C. trolley line is ab 14 nF/km whereas of 3.6 kV A.C. systems is ab. 8 nF/km. Additionally to consider is an enhanced equivalent capacitance between the metallic roof of trains and the trolley. Moreover relatively significant are capacitances of the condensers built-in train filters of impulse train drives and lighting protection.

All this indicates that the frequency characteristics of the P-TRV in 3 kV D.C. traction should be complex ones, demonstrating several resonance frequencies.

Finally, it should be noted that, in principle, the test duty 1 of fuses has to be made with the defined values of P-TRV too. However, the current limiting fuses subjected to the test duty 1 usually due to hot fulgurite conductance are not sensitive to P-TRV circuit characteristics. The exception are fuses which generate the highest arc voltage immediately after initiation of the arc. Such behaviour normally show the fuse-links

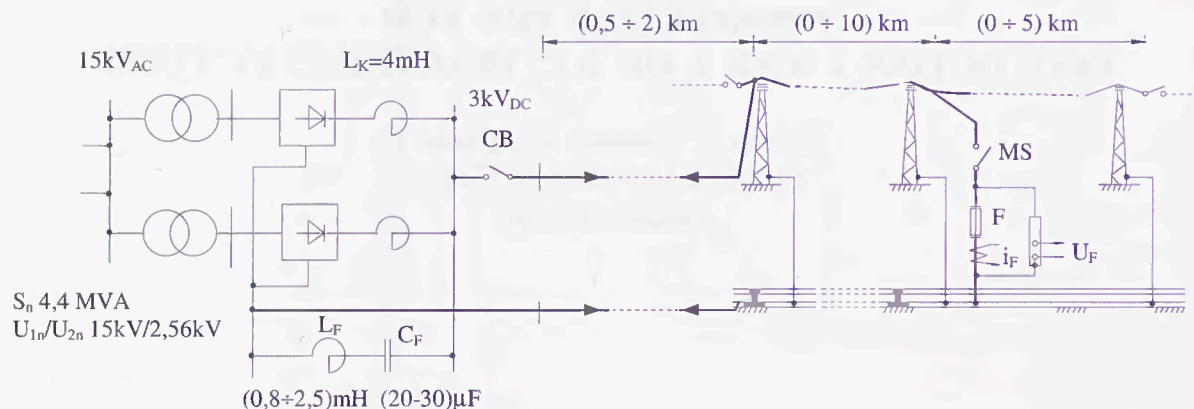


Fig. 1. Typical 3 kV D.C. traction feeding system;  $L_F$  - filter inductance,  $C_F$  - filter capacitance, CB - station circuit breaker, MS - making switch used during tests, F - fuse used during tests,  $i_F$  - current record,  $U_F$  - voltage record

of smaller rated currents, usually up to dozen A. The fuse-links of that rated currents prevail in 3 kV D.C. traction application. On the other hand, by the test duties 2 and 3, as it shows the A.C. test practice, the fuses irrespective of the fuse rated current are susceptible on applied P-TRV characteristic. Same behaviour one can expect in the case of 3 kV D.C. traction.

So bearing in mind all said above, the authors recently carried out several tests and simulations on the P-TRV in 3 kV D.C. traction system in Poland and of one Polish test plant.

## II. METHODS OF P-TRV DETERMINATION

According to 56 IEC 1987, Appendix GG [2] the basic methods for determining the P-TRV waveforms for h.v. circuit-breakers tests are classified as follows:

- Group 1 - Direct short-circuit breaking.
- Group 2 - Power-frequency current injection.
- Group 3 - Capacitance current injection.
- Group 4 - Model networks.
- Group 5 - Calculation from circuit parameters.
- Group 6 - No-load switching of test circuits including transformers.

These same methods are recommended for h.v. A.C. fuses [1]. It seems, there is no obstacle to apply them also in the case of 3 kV D.C. traction systems.

During described investigations only three of above mentioned methods were applied, viz.:

1. - No-load switching of test circuit.
2. - Capacitance current injection.
3. - Calculation from circuit parameters.

Beyond this also a small rated current fuse method [3] was also applied. The fuse-element of such fuses,

after the MS (Fig. 1.) switching on, due to short-circuit current immediately explodes and interrupts the circuit within microseconds time. A cold conductor explosion is not associated with the arcing phenomena. This method, however, resembles no-load switching method, on the other hand, resembles also a direct short-circuit breaking one, mentioned in the Group 1. The use of switching on a fuse will be presented together with no-load switching.

### II.1 No-load switching of test circuit

Using this method the following tests were carried out in:

- a) - a real railway trolley system fed by A.C./D.C. inverter equipped within filter arrangements (Fig. 1),
- b) - a test plant without filter arrangements but with extremely large prospective short-circuit current adjusted by a resistance and inductance.

In the case *a* the circuit-breaker CB (Fig. 1), normally used for outgoing feeder protection, was switching on as a making-switch to get P-TRV across fuse terminals on:

- 1) - an unloaded trolley overhead line directly connected to the steel rail throughout a fuse F, but with removed fuse-link,
- 2) - as above but with installed 1A, 3 kV D.C. standard fuse-link.

Then analogous, as in p. 1 and 2 above, also next two switching on combinations were performed, but keeping the circuit-breaker CB in closed position, whereas the making switch MS was performing the switching on operations.

Records of P-TRV were also obtained in doing similar tests in a test plant according to item *b* above. The only difference was 3 A fuse rated current instead 1 A.

## II.2 Capacitance current injection

A special indicator working on the capacitance current injection base [2], has been used to identify the P-TRV, but only in the case of a 3 kV D.C. test plant mentioned in II.1.b). Indicator capacitance with  $C_0 = 130 \mu\text{F}$  (Fig.2) was pre-charged to the voltage 100 V. It has been evaluated that  $C_0$  value is much greater than the capacitance of the tested circuit. So the last can be neglected by considering the test result. After changing position of the switch P from 1 into 2 the capacitor is discharged through impedance of the test circuit. Thanks to a specially selected diode the current flow ended nearly exactly in first current zero of its natural frequency.

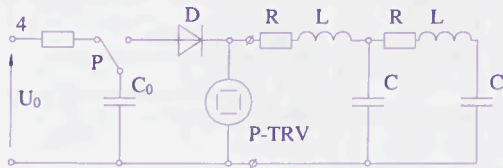


Fig. 2 Scheme of indicator to measure of P-TRV by use of capacitance current injection method;  $U_0$  - D.C. charging voltage; P - turn over switch;  $C_0$  - pre-charged capacity; Sh - shunt; D - nearly „ideal” diode; R, L, C, r - parameters of test plant

## II.3 Calculation from circuit parameters

The calculations pertain to the scheme given in Fig. 3, which is equivalent to the shown in Fig. 1

During numerical modelling arise the problem of identification of the parameters of circuit elements. Basic parameters of the traction 3 kV D.C. network are more or less known. However, the resistance  $R_i$  and conductance  $G_i$  can vary due to skin effect ( $R_i$ ), inductive couplings, contamination ( $G_i$ ), a.s.o. Also a problem is with the identification of  $C_i$  and  $L_i$  in

respect of magnitudes and mutual relation between them of particular circuit components. Superimposed resonance frequencies of the individual system members can have a substantial influence on the P-TRV.

In the case of small fuse rated current method a very troublesome problem is how to model the real making - switch MS (Fig.1) and fuse F. In case of MS, during the contact approaching, the air gap can get break down by 3 kV D.C., before the final contact making. However, the time duration of a possible spark or a glow partial discharge can lasts some tenths or even hundred microsecond only, but this time is essential in respect of the discharge phenomena interference on the P-TRV recorded. The interference is possible due to instabilities in the mentioned discharge.

Moreover, how to model the possible contact bounce of the MS, arising immediately after their first touch. All these troublesome problems were omitted in the calculations, assuming an ideal MS.

Also modelling of the fuse-link operation of rated currents 1A and 3A, particularly the discharge arising in it, is a very hard task. In the simulations, the fuse discharge problem was solved by taking some variable resistance.

## III RESULTS OF INVESTIGATIONS OF P-TRV

Several characteristic results (Table 1, Figs. 4÷12), using all given above four methods of P-TRV identification, indicate a wide range of the measured parameters. In turn the calculation for a small fuse rated current (No 4) shows only a qualitative but acceptable agreement with the test results given under No 3.

Generally, the results do not allow to point out completely convincing conclusion on recommended parameters of P-TRV for the breaking capacity tests of 3 kV D.C. current-limiting fuses. In spite of that several positive statements can be pushed forward.

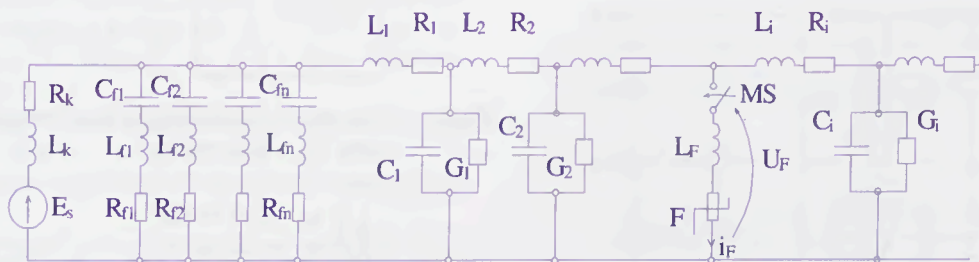


Fig.3 Equivalent scheme of traction system given Fig.1 taken into considerations of P-TRV;  $E_s$  - mean value of rectified voltage;  $L_k, R_k$  - parameters of cathode choke;  $C_{fn}, L_{fn}, R_{fn}$  - parameters of n-branch of filter;  $L_i, R_i, C_i, G_i$  - parameters of feeding cables and traction network;  $L_F$  - inductance of fuse F branch;  $U_F, i_F$  - voltage across and current of fuse

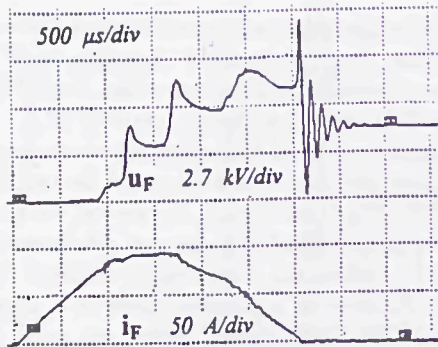


Fig. 4. Test record No.1 using small fuse rated current in test plant.  $U_F$ ,  $i_F$  - fuse voltage and current

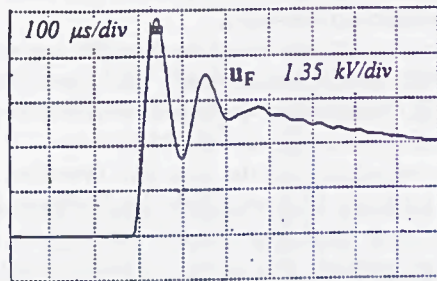


Fig. 5. Test record No.2 using no load switching in test plant.  $U_F$  - fuse voltage

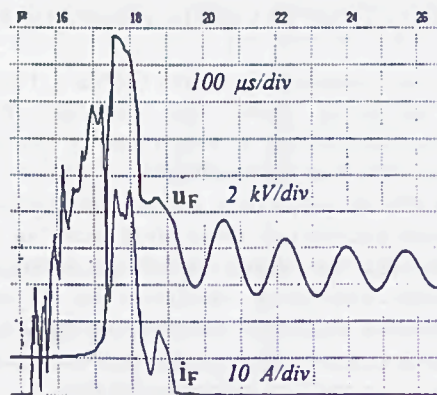


Fig. 6. Test record No.3 using small fuse rated current in traction network.  $U_F$ ,  $i_F$  - fuse voltage and current

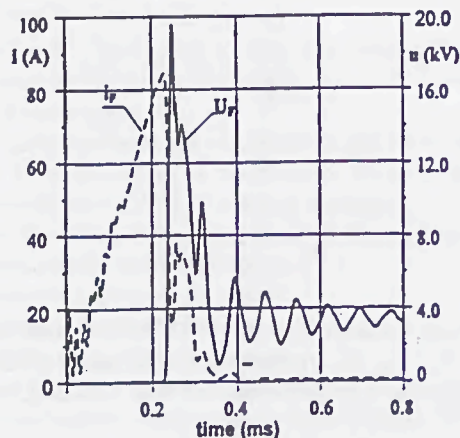


Fig. 7. Profiles of calculation results (No.4) using small fuse rated current ( $i$ ) in traction network.  $U_F$ ,  $i_F$  - fuse voltage and current

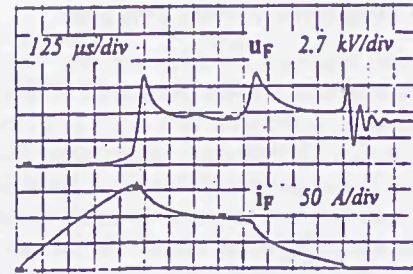


Fig. 8. Test record No.5 using small fuse rated current in test plant.  $U_F$ ,  $i_F$  - fuse voltage and current

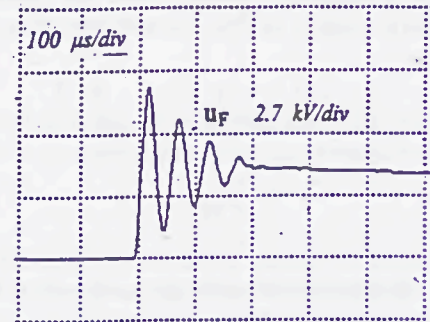


Fig. 9. Test record No.6 using no load switching in test plant.  $U_F$  - fuse voltage

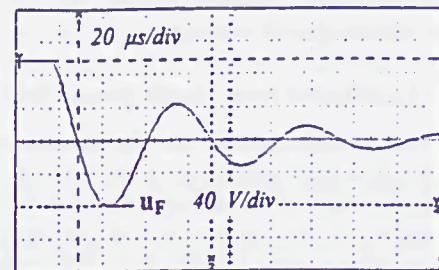


Fig. 10. Test record No.7 using capacitance injection in test plant.  $U_F$  - fuse voltage

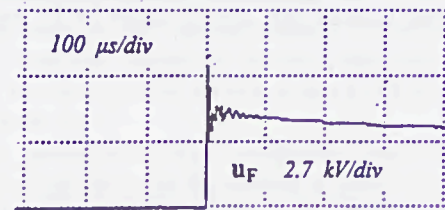


Fig. 11. Test record No.8 using no load switching in test plant.  $U_F$  - fuse voltage

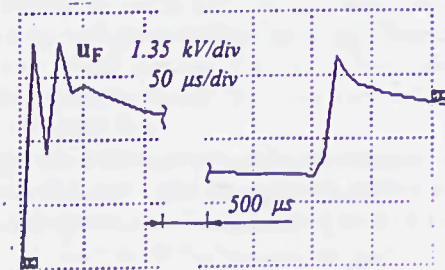


Fig. 12. Test record No.2 using no load switching in test plant.  $U_F$  - fuse voltage

Table 1. Results of P-TRV measurements in 3 kV D.C. test plant, real trolley traction network and exemplary calculations

No.	Measurement method	Place of test	Fig	Circuit parameters					Results of measurement				
				$U_n$ kV	$I_p$ kA	R •	L mH	L/R ms	$U_c$ kV	$t_c$ $\mu$ s	$U_c / t_c$ kV/ $\mu$ s	$U_c/U_n$ -	$f_{P-TRV}$ kHz
1.	small fuse	test plant	4	4.0	1.67	2.4	39	16	10.2	60	0.17	2.5	8.7
2.	no load on	test plant	5	3.6	1.67	2.4	39	16	6.5	50	0.13	1.8	10
3.	small fuse	tr. network	6	3.4	~3.1	~1.1	~16	15	7.6	68	0.11	2.2	7.4
4.	calculations	tr. network	7	3.4	3.1	1.1	16	15	6.8	56	0.12	2.0	8.7
5.	small fuse	test plant	8	4.0	3.3	1.2	13	11	8.1	28	0.29	2.0	18
6.	no load on	test plant	9	3.8	3.3	1.2	13	11	7.6	25	0.30	2.0	~20
7.	capac. inject.	test plant	10	4.0	3.3	1.2	13	11	7.2 <sup>1)</sup>	24	0.25	1.8	16
8.	no load on	test plant	11	3.8	3.0	1.2	3	2.5	5.7	6.5	0.87	1.5	~75
9.	no load on	test plant	12	3.8	45	0.07	1.6	24	4.9	10	0.49	1.3	20
10.	IEC 282 - 1,	3.6 kV A.C. <sup>2)</sup>	3.6	$I_1$	$\cos \phi = 0.07$	45	-	21	6.2	40	0.15	1.2	~12
11.	1994			$I_2$					-0.15	6.6	140	0.05	1.3

Denotations:  $U_c$  - peak value of P-TRV;  $t_3$  - time to peak value of P-TRV;  $U_c/t_3$  - mean value of steepness of P-TRV;  $U_c/U_n$  - overvoltage coefficient;  $f_{P-TRV}$  - equivalent frequency of P-TRV;

Notes: 1) - calculated for equivalent 4 kV network voltage

2) - given for comparison under No.10 and 11 A.C. data are taken from IEC 282-1,1994 for A.C. h.v. current limiting fuses

P-TRV in a 3 kV D.C. trolley traction systems, in a comparison with 3.6 kV A.C. systems, can demonstrate faster increase up to the voltage maximum. As a result one can suggest  $U_c/t_3$  in the limits ab 500+850 V/ $\mu$ s for the interrupting tests of the prospective currents of order few kA. This suggestion, it seems, should be correct for the test duty 1, i.e. for the rated breaking capacity of fuses. Moreover it can be suggested  $U_c$  in the range ab 1.3+1.7 times fuse rated voltage  $U_n$ . In turn, for the test duty 2 can be proposed for further considerations  $U_c/t_3 = ab 200 + 300 V/\mu$ s and  $U_c = ab 2 U_n$ . Unfortunately because of lack a such tests the results do not allow to state some corresponding values of  $U_c/t_3$  nor  $U_c$  for the test duty 3.

The problems arising during endeavours to identify desirable parameters of P-TRV lays in several specific features of 3 kV D.C. traction systems. They are:

- complicated structure resulting in multi-frequency P-TRV (Fig.3),
- substantial influence of the filter capacitances (Fig.1),
- experimental results in the case of small fuse rated current (Figs. 6, 8) additionally can get some very serious interferences of  $U_F$  - trace at least from the commutating processes in making-switch MS (Figs. 1 and 12),
- in the calculations practically it is not possible to model mentioned switching processes,

- from just mentioned reasons a simple comparison of the results of experiments and calculations is not realistic one.

#### IV FINAL STATEMENTS

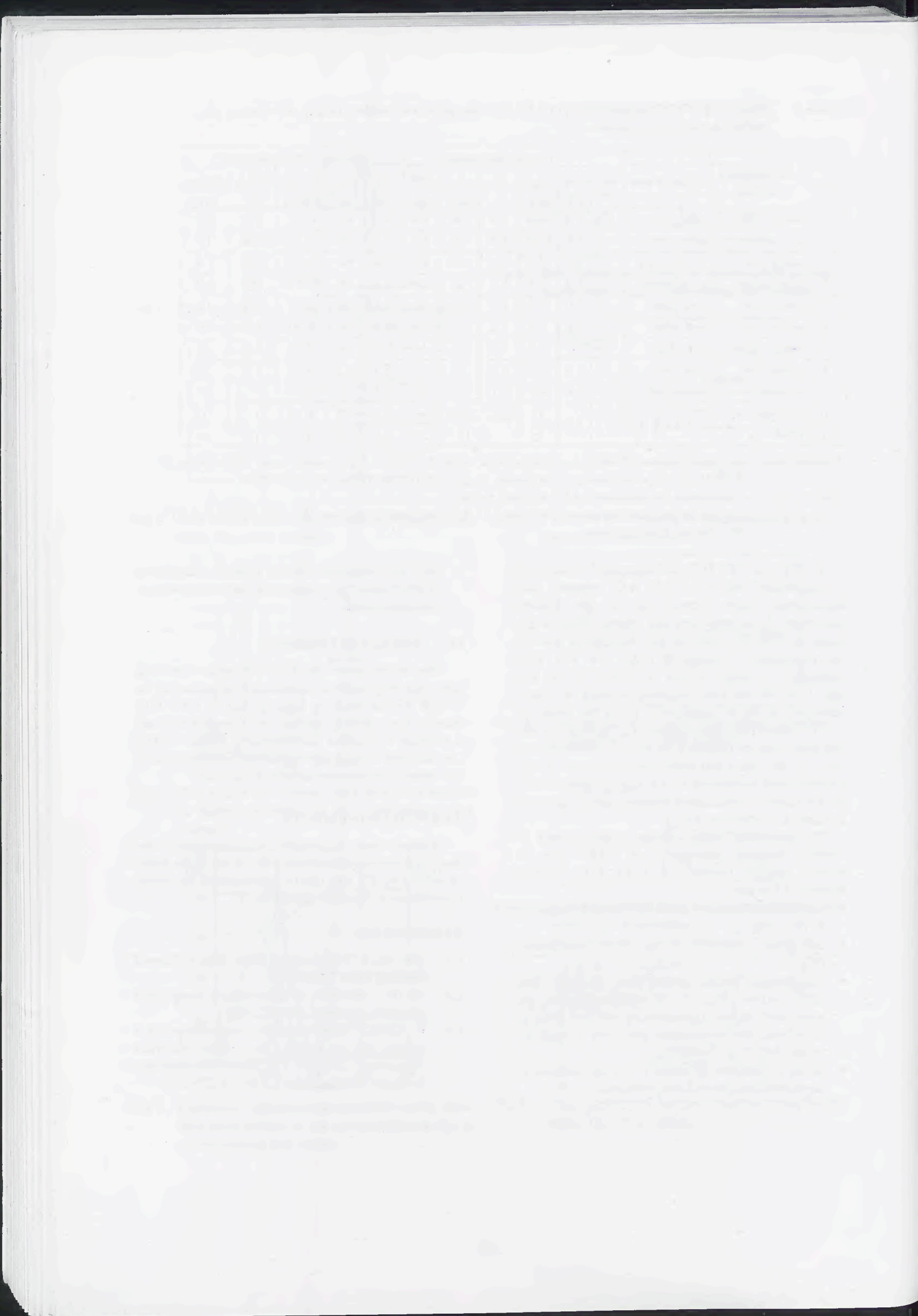
The results given above obviously are not final ones. But they confirm the authors conviction that the P-TRV for the breaking capacity test of 3 kV D.C. traction fuses shall be defined and therefore it is still a problem for further investigations. In this context are desirable similar more extensive investigations in the railway systems not only the Polish one.

#### ACKNOWLEDGEMENTS

Authors have a pleasure to acknowledge that described investigations were carried out in the frame of project No 8T 10A 03411 sponsored by the Polish Committee of Scientific Research

#### REFERENCES

- [1] IEC 282-1 "High voltage fuses, Part 1: Current limiting fuses", 1994.
- [2] 56 IEC "Methods of determining prospective transient recovery voltage", 1987.
- [3] T. Lipski, "Fuse switching overvoltage as a killing shot of an aged h.v. cables electrical insulation". XI Symp. On Electrical Discharges in Gases. Pasm. Poland, 1987, p. 278-292



# AN EXPERIMENTAL REVISION OF TEST DUTIES IEEE C37.41 FOR DISTRIBUTION CUTOUTS AND FUSE LINKS

ALFONSO AVILA R.,  
PROTELEC-MT, S.A. DE C.V.

ENRIQUE BAQUEIRO A., CARLOS CABRERA. R.  
COMISION FEDERAL DE ELECTRICIDAD

## MEXICO

**Abstract.**—Tests for making a comparison of performance of single-voltage-rated distribution cutouts associated with type K (fast) fuse links of different ampere rating were made under rainy and dry environment. The overcurrents applied are comprised within series 4 and 5 of IEEE Std. C37.41-1994.

A sufficient number of test were made to confirm the validity of our hypothesis of different behaviour of such devices under the indicated conditions for taking into consideration these changes proposed in future revisions of the above mentioned Standard.

## INTRODUCTION

Year after year during the summer and fall seasons in the Mexican overhead radial networks are consumed a large quantity of fuse links mainly of the type K (fast) used to protect against overcurrents pole type distribution transformers. In a parallel direction the consumption of the associated cutouts and the number of damaged transformers is also important.

As it has been shown [1] when a cutout used to protect a transformer interrupts relatively small overcurrents, the voltage across its contacts will rise very quickly and can exceed the rated of buildup of dielectric strength in the medium between the contacts due to the particular characteristics of the transient recovery voltage (TRV) associated with that machine.

Practically the great majority of transformers are installed outdoors and therefore the most harmful effects can appear when under raining conditions a cutout interrupts an overcurrent, said this regardless the origin of such fault current

This is the interrupting condition that we have studied with the tests run at the High Power Laboratory of the Comisión Federal de Electricidad of México (CFE).

As an example of the quantity of fuse links operations and therefore of cutouts also, in figure 1 are showed the fuse link ratings more used to protect transformers, its total consumption during 1998 and the percentage of them operated in the rainy season in some overhead radial networks at 13.8 kV in the Central part of México.

Fuse link rating	Consumption 1998	Percentage of fuses operated during raining season
1K	12677	61.9
2K	11642	62.4
3K	12404	61.0
5K	9700	55.9
8K	7553	68.2
10K	9100	61.8

Figure 1. Consumption of type K fuse links used to protect transformers

## TRANSFORMER SECONDARY FAULTS AND THE INFLUENCE OF SYSTEM ON TRV

As a cutout must be capable to interrupt a wide range of fault currents from its rated interrupting current (the less presented in our overhead networks) to the most commonly faced small primary overcurrents due to secondary faults, after current zero it is possible to have a very high rate of rise of recovery voltage (RRRV) and it can happens that the cutout does not interrupt and consequently the arcing current persists for a long period of time with long arcing, the insulation transformer can be damaged and a fault to ground may be established. Under rainfall conditions the possibility that this occurs is greater as we have found with the tests made. The TRV that appears across a circuit breaking device is a compound of the TRV contributions of the source and load sides. Each part of the complete circuit will contribute a voltage component proportional to its impedance with respect to the total fault impedance [2].

We have the following cases:

- For an ungrounded transformer, the system capacitance contributes to reduce the natural frequency.
- In a 3-phase transformer for the case of the first pole to open, the source capacitance is connected to one terminal of the transformer after the interruption of a fault and will contribute to reduce the transformer natural frequency.
- In the case of a grounded connection, after the total clearing time of the fuse-cutout, the system capacitance will be completely isolated and will not have effect on the natural frequency of the transformer.

- A 3-phase ungrounded transformer will produce a lower natural frequency when used on a grounded wye system or on an ungrounded system having substantial amount of line and cable capacitance [3].

TRV components:

Natural frequency (f) and peak factor. Both parameters are directly related to these transformer parameters:

- Impedance and capacitance
- Transformer and system ground connection
- Secondary circuits involved

With transformer impedance can be calculated the fault current magnitude and the inductance using this expression for natural frequency.

$$f = \frac{1}{2\pi\sqrt{LC}}$$

- As it was expected by theoretical predictions [3] the variation of inductance and capacitance of the testing circuit, tends to increase or decrease the severity of RRRV appearing at the cutout contacts.

#### TESTING CRITERIA

- For the purpose of this experimental study the range of magnitudes of primary overcurrents that were applied under dry and rain [4] conditions were comprised between 470 to 36 A. Such values are included within test series 4 and 5 of table 5 respectively of the IEEE std C37.41 applicable when testing single-voltage-rated distribution cutouts.
- Speaking about the secondary faults related to test series 5:
  - We mainly consider the 3- phase short circuit and in few cases the single-phase both at the secondary terminals of transformer.
  - In order to lengthen the useful life of the distribution transformer used, the ampere rating of the fuse links was drastically reduced.
  - Nameplate data of the distribution transformer used: 112.5 kVA, 13.2 kV, 3.5% X and Leakage inductance L= 143.8 mH.

The design tests belonging to the test series 4 and 5 of this Std are:

Parameter ↓	Test 4	Series 5
Power frequency recovery voltage	rated maximum voltage + 5%, -0%	
Transient recovery voltage (TRV)	see table 6	see foot note g
Prospective (available) current rms symmetrical	from 400 to 500 A <sup>c</sup>	from 2.7 to 3.3 times link rating
X/R ratio (power factor)	see table 7	from 1.3 to 0.75 (from 0.6 to 0.8)
Making angle related to voltage zero (degrees)	random timing	
Fuse link rating	min	min
Number of tests on each cutout	2	2
Duration of power Frequency recovery voltage after interruption	not less than 0.5 s dropout fuses	

The foot-notes: a, b, c, d, e and g are indicated in page 36 of the Std under revision.

For the voltage level of 13.8 kV that we have studied, the TRV parameters of table 6 for test series 4 are:

Rated maximum voltage (kV): 15.0 - 15.5

Frequency kHz + 10% - 0% : 24  
Peak factor<sup>a</sup> + 10% - 0%<sup>a</sup>: 1.6

a: this foot-note is at the page 37 of the Std

and the corresponding X<sub>R</sub> values given in table 7 are

Minimum X<sub>R</sub> b : 2.4

rated maximum voltage in kV for single-voltage-rated cutouts: 15.0 - 15.5

the foot-notes b is at the page 37 of the Std .

The testing circuit and TRV parameters are indicated in figures 2 and 3 respectively.

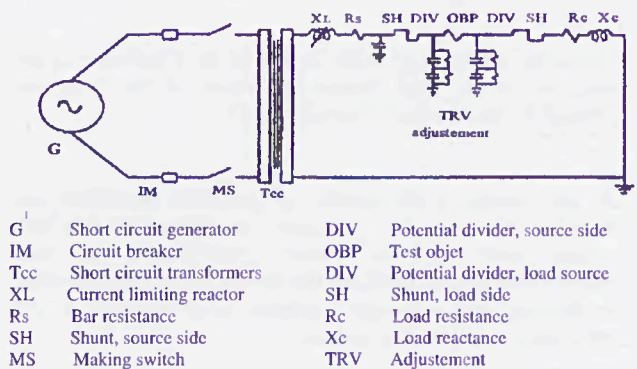


Figure 2. Test circuit for series 4

Measurement Point (fig.2)	Time-to-peak $t_c$ ( $\mu s$ )		Frequency kHz		Peak factor	Figure ↓
	1	2	1	2		
1 source side	18.4		27.17		1.67	3b
2 total	18.4	104	27.17	4.80	1.63	3c

Fig. 3a. Measurement of prospective TRV

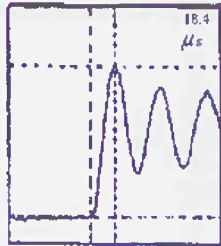


Fig. 3b

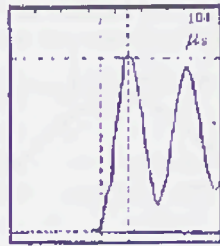
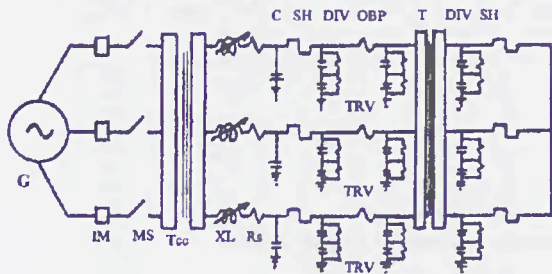


Fig. 3c

Oscillograms correspondent to prospective TRV for series 4 tests.

For the test series 5, the circuit used and the TRV parameters are shown in figures 4 and 5 respectively



- G Short circuit generator
- IM Circuit breaker
- MS Making switch
- Tcc Short circuit transformers
- XL Current limiting reactor
- Rs Bar resistance
- C Added capacitor
- SH Shunt, source side
- DIV Potential divider, source side
- OBP Cutout under test
- T Distribution transformer
- DIV Potential divider, load side
- SH Shunt, load side
- TRV Adjustment

Figure 4. Test circuit for series 5

Measurement Point (fig.4)	Time-to-peak $t_c$ ( $\mu s$ )		Frequency kHz		Peak factor	Figure ↓
	1	2	1	2		
2	60		8.33	1.32	1.28	5b
2	64		7.81	1.28	1.28	5c
1	392		25.71		1.67	5d

Fig. 5a Measurement of prospective TRV

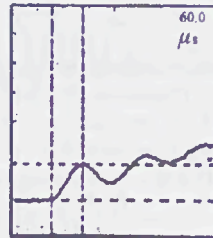


Fig.5b With the short circuit transformer grounded

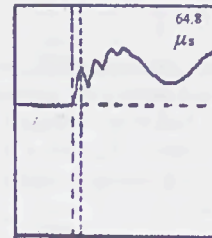


Fig. 5c With the short circuit transformer ungrounded

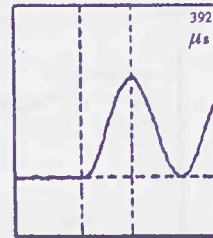


Fig. 5d Including the distribution transformer

Number of test & oscillo.	TRV data				Testing Condition dry or wet	Rated current of fuse link K	Interruption results	
	Freq. kHz	Peak factor	Time-to-peak $\mu s$	RRRV $V/\mu s$			Cutout	
							A	B
001	11	1.62	42.2	864.7	Dry	10	OK	-
002	8.7	1.6	64	223.4	"	"	-	OK
003	-	-	-	-	"	"	-	F
004	11	1.62	-	-	"	"	OK	-
005	11	1.60	55.3	497	"	"	-	OK
006	25	1.7	20	427	"	"	OK	-
007	18	1.6	27.9	214.6	"	"	-	OK
008	19.8	1.68	25.3	213	"	"	OK	-
009	-	-	-	-	"	"	-	F
010	28	1.68	0	0	"	"	OK	-
011	31	1.68	15.6	357	"	"	-	OK
012	27	1.68	18.8	377.8	"	"	OK	-
013	-	-	-	-	"	"	-	F
014	27	1.68	18.8	305.4	"	"	OK	-
015	25.4	1.68	19.7	348	"	"	-	OK
016	30.6	1.68	30.6	308	"	"	OK	-
017	25	1.68	20	375	"	"	-	OK
018	25.7	1.68	19.4	393	"	"	OK	-
019	-	-	-	-	Wet	"	-	F
020	-	-	-	-	"	"	F	-
021	-	-	-	-	"	"	-	F
022	27	1.68	17.6	346	"	"	OK	-
023	25.2	1.68	17.8	317	"	"	-	OK
024	-	-	-	-	"	"	-	F
025	28	1.68	17.4	360.1	"	"	OK	-
026	-	-	-	-	"	"	-	F
027	29	1.68	17.1	417	"	"	OK	-
028	20	1.68	25.3	273	"	"	-	OK
029	-	-	-	-	Wet	"	F	-
030	-	-	-	-	"	"	-	F
031	-	-	-	-	"	"	F	-
032	-	-	-	-	Dry	6	-	F
033	21.7	1.68	23.8	302.4	"	6	OK	-
034	28	1.68	17.2	323.8	"	6	-	OK
035	28	1.68	17.6	389.6	"	6	OK	-
036	25	1.68	19.5	452	"	6	-	OK
037	26	1.68	18.8	400.6	"	6	OK	-
038	26	1.68	18.6	347.6	Wet	6	-	OK
039	27.4	1.68	18.2	435.4	"	6	OK	-
040	-	-	-	-	"	6	-	F
041	29	1.68	16.7	479.3	"	6	OK	-
042	27	1.68	17.3	354.5	"	6	-	OK
043	26.4	1.68	18.9	349	"	6	OK	-

Fig.6 Summary of laboratory interrupting test data corresponding to test series 4

RESULTS

In figures 6 are summarized the results attained for test series 4 for dry and wet testing conditions. From tests 001 to 031 the laboratory data were: voltage= 15.3 kV, test current = 427 A,  $X_L$  surge =  $30 \Omega$   $X/R$  ratio = 2.6 and from tests 032 to 043 these were the changes: voltage = 15.6 Kv, test current = 416 A,  $X/R$  ratio = 2.9

Remarks:

- For test numbers 001 to 040, the fuseholders were changed after four operations

The fuseholders used to test 6K links were previously used for test numbers 41, 42 and 43

- In this figure it is easy to see the effect of the ampere rating of fuse links the number of failures is reduced in both testing environments.

In figures 7 and 8 are shown oscillograms of a successful interruption under dry conditions and in figures 9 is shown an oscillogram of a faulted test made under wet environment. In both tests were used 10K fuse links.

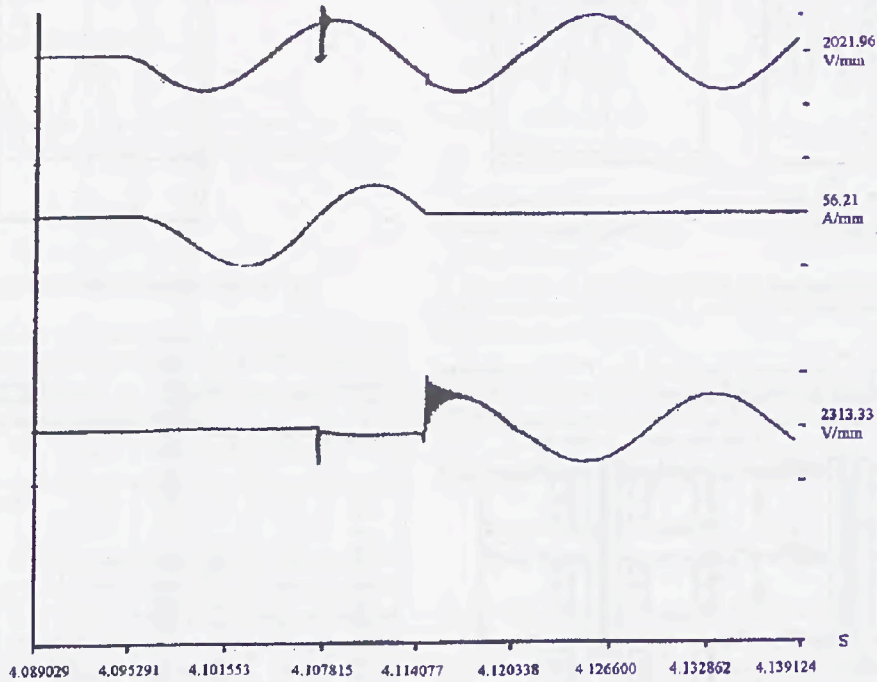


Figure 7. Satisfactory interruption of 427 A. Cutout A with 10K fuse link. Dry test

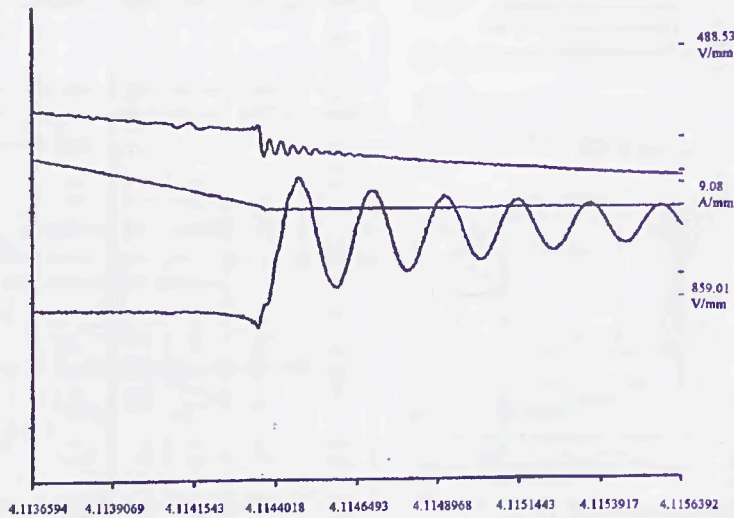


Figure 8. TRV across the cutout contacts after the successful interruption shown in fig. 7

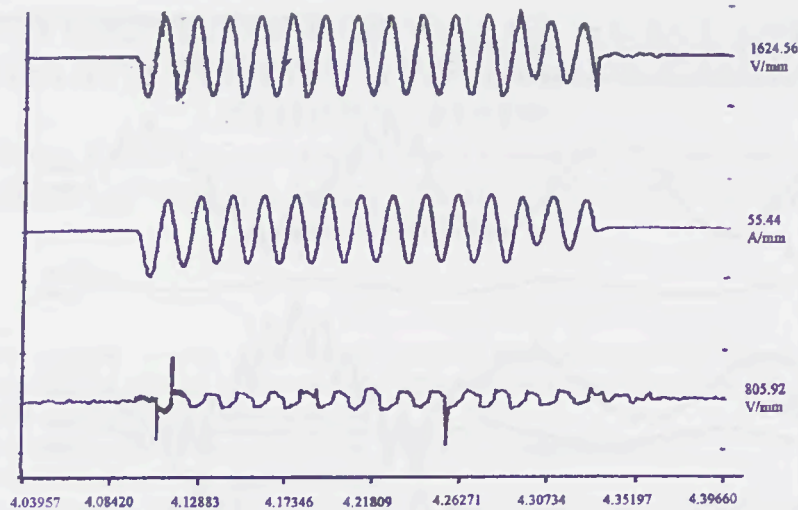


Fig. 9. Failure of the cutout A for interrupting 427, with a 10K fuse link. Wet test.  
External flashover of the fuseholder

In figure 10 are summarized the results obtained for test series 5. In all cases the voltage applied was: 15.3 kV phase-to-phase. 5 made under dry and wet environment.

Number of test & oscillo	Laboratory data				TRV data				Testing condition dry or wet	Rated current of fuse link K	Interruption results		
	Test current A	X <sub>L</sub> source Ω	X <sub>r</sub> /ratio	C add nF	Frequency kHz	Peak factor	Time-to-peak μs	RRRV V/μs			Cutout		
											A	B	B
001	75	49.9	7.4	-	-	-	-	-	Dry	3K	F	F	F
002	"	"	"	-	-	-	-	-	"	3K	F	F	F
003	"	"	"	-	-	-	-	-	"	3K	F	F	F
004	"	"	"	-	-	-	-	-	"	6K	F	F	F
005	"	"	"	-	-	-	-	-	"	6K	F	F	F
006	"	"	"	-	-	-	-	-	"	2K	F	F	F
007	"	"	"	-	-	-	-	-	"	2K	F	F	F
008	"	"	"	500	446	1120	10	"	"	2K	OK	OK	OK
009	"	"	"	500	477	1049	15.4	"	"	2K	OK	OK	OK
010	"	"	"	125	-	-	-	"	"	2K	F	OK	F
011	"	"	"	125	-	-	-	"	"	2K	F	F	F
012	"	"	"	125	-	-	-	"	"	3K	F	F	F
013	"	"	"	125	-	-	-	"	"	3K	F	F	F
014	"	"	"	125	-	-	-	"	"	2K	F	OK	F
015	"	"	"	125	-	-	-	"	"	2K	F	F	F
016	"	"	"	125	-	-	-	"	"	6K	F	F	F
017	40	122.8	5.4	250	563	889	23	"	"	6K	OK	OK	OK
018	40	122.8	"	250	-	-	-	"	"	6K	F	F	F
019	40	122.8	"	250	-	-	-	"	"	6K	F	OK	F
020	40	122.8	"	250	821	609	12.7	"	"	6K	OK	OK	OK
021	36	-	"	250	347	1440	19.9	"	"	6K	OK	OK	OK
022	36	-	"	250	400	1250	9.7	Wet	"	6K	OK	OK	OK
023	"	-	"	250	874	572	21.2	"	"	6K	OK	OK	OK
024	"	-	"	125	-	-	-	"	"	8K	F	F	F
025	"	-	"	125	767	770	19.8	"	"	8K	F	OK	F
026	"	122.8	"	125	-	-	-	Dry	"	8K	F	F	OK
027	"	"	"	125	-	-	-	"	"	8K	F	F	F
028	"	"	"	125	-	-	-	"	"	8K	F	F	F
029	"	"	"	"	645	776	16.2	Wet	"	8K	OK	OK	OK
030	"	"	"	"	483	1036	15.6	"	"	8K	OK	OK	OK
031	"	"	"	"	-	-	-	"	"	8K	F	F	OK
032	"	"	"	"	-	-	-	Dry	"	8K	F	F	F
033	"	"	"	"	-	-	-	"	"	8K	F	F	OK
034	"	"	"	"	-	-	-	"	"	6K	OK	OK	F
035	"	"	"	"	-	-	-	"	"	6K	OK	F	F
036	"	"	"	"	-	-	-	"	"	6K	F	F	10
037	"	"	"	"	-	-	-	"	"	3K	OK	F	10
038	"	"	"	"	-	-	-	"	"	3K	OK	OK	10
039	"	"	"	"	-	-	-	"	"	3K	F	F	10
040	"	"	"	"	-	-	-	Wet	"	6K	OK	OK	10
041	"	"	"	"	542	922	18.1	"	"	6K	OK	OK	10
042	"	"	"	"	327	1529	8.2	"	"	8K	OK	OK	10
043	"	"	"	"	558	896	19.8	"	"	8K	OK	OK	10

Figure 10 Summary of laboratory interrupting test data corresponding to test series 5.

lumped capacitance was of 125 nF por-phase

In figure 11 are shown the TRV characteristics of a successful 3-phase test made under wet environment. In this case the

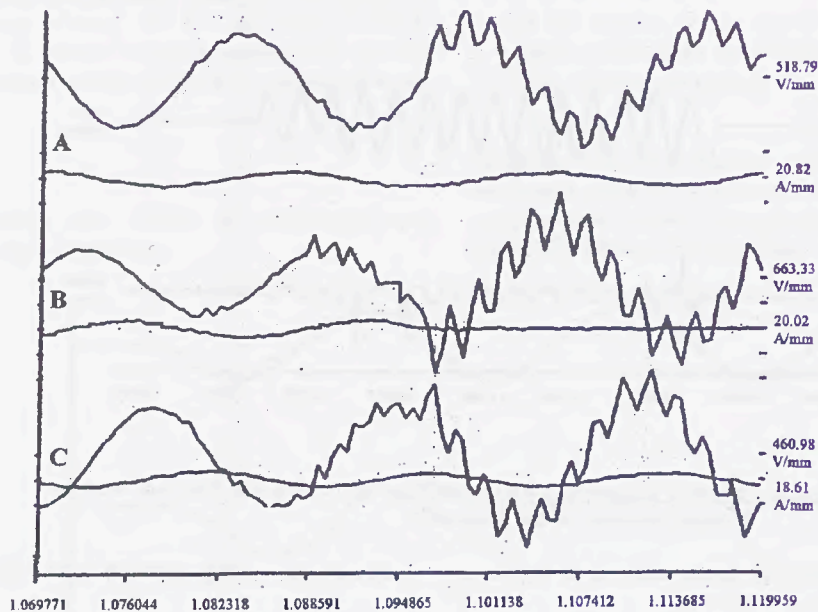


Figure 11. TRV characteristics on phase B, 3-phase test 029, made under wet environment with 8K fuse links

Remarks:

- When was not included a lumped capacitance in all cases we had a spectacular failure.
- With lumped capacitances of 250 nF and greater, the number of failures was drastically reduced.
- For the 3-phase faults when using 8K links and lumped capacitances of 125 nF per phase the results found were aleatory in both testing conditions.
- In the case of single-phase tests the number of satisfactory results of 3K, 6K, and 8K links was improved.

Obviously this conditions may be more critical for low and intermediate ampere rating of fuse links.

- Therefore we recommend to include an intermediate ampere rating besides to the minimum and maximum now indicated.

ACKNOWLEDGMENT

The authors wishes to thank Mr. Julian Adame M. head Manager of LAPEM-CFE, Mr. Carlos Vázquez S. Vice-head Distribution Manager of CFE, Mr. J. Antonio Cerrillo Vice-head Distribution Manager of Division Bajío-CFE and the staff of the High Power Lab. Of CFE-LAPEM for their support and advice.

CONCLUSIONS.

After having revised carefully the results obtained for both series studied with approximately 180 tests, our recommendations are these:

- When a fault current of magnitude considered between the limits given by the test series 4 and 5, is applied under rain, the interruption of the fuse cutout is much more difficult and therefore is necessary to consider this testing condition.
- As it is well known that a more severe interruption can be presented when is applied a symmetrical current because the TRV occurs near or at the maximum of power frequency voltage we propose to test using a making angle between 85 to 105 degrees for test series 4.

REFERENCES

[1] R. Harner, "Distribution System Recovery Voltage Characteristics: 1-Transformer Secondary Fault Recovery Voltage Investigation", Proc. IEEE PAS Vol. PAS-87, february 1968.

[2] K. Ragaller, "Current Interruption in High-Voltage Networks", Plenum Press, New York and London, 1978.

[3] A. Greenwood, "Electrical Transients in Power Systems", Wiley-Interscience, New York, Chichester, Brisbane, Toronto, 1991.

[4] IEEE Std. 4-1978, Standard Techniques for High-Voltage Testing.

# ELECTRICAL FUSES TESTING MODULAR SOURCE USED WITH A NEW METHOD FOR PLOTTED TIME-CURRENT CHARACTERISTIC WITHOUT FUSING

Dr. ing. Emilian Furniça, Dr. ing. Petru Leonte, ing. Traian Plesca  
Technical University "Gh. Asachi", Faculty of Electrical Engineering  
Iasi, ROMANIA

**Abstract:** This paper contains, a short presentation, theoretical analyze and construction, of a new current (and voltage) adjustable modular source with identical ferromagnetic modules, independent primary windings, and a single common secondary. The current (and voltage) of the secondary have a large scale of range. The paper presents then some contribution for plotting time-current characteristic of reconditioned LV high breaking capacity fuses without fusing. The method presented, which can approximated an individually time-current characteristic without fusing is based on the  $\bullet(I)$  plot of the replacement element. The source and the method for plotting time-current characteristic without fusing can offer an independent unit for testing and selection fuses in better protection of electric devices in the overload current area.

## I. INTRODUCTION

The fuses testing are doing in concordance with required conditions of norms and standards [1,2]. Some testings have a particular specificity and they are usefully both in research, production and even exploitation.

Establishing of time-current characteristic means one of the overload testing aims. In this case, it uses different current sources which are usually fixed and especially used within specialized workshops.

It is necessary adjustable and mobile modular current sources in the case of research and exploitation (reconditioning).

On the other hand, the time-current characteristics from catalogues are statistical curves and they are not valid any more in the case of fuses reconditioning.

In this paper, the authors present on the one hand a modular current/voltage source [4,5,6,7] which can be used to fuses testing and on the other hand some contributions about the plotting of time-current characteristic to high breaking capacity fuses (reconditioned fuses) without fusing [8].

## II. MODULAR SOURCE

For the purpose to have currents of kA range, the normal sources are built into a transformer voltage-

current supplied through an adjustable autotransformer. The sources are not normally transportable.

### II.1 Construction

The modular electromagnetic source used in testing, consists of a different number of ferromagnetic modules. Each modules have its own primary winding and a common secondary, Fig.1.

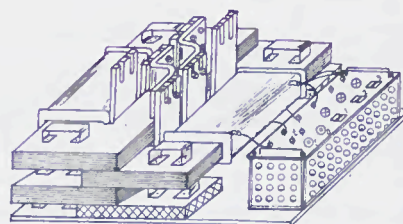


Fig.1 Three modules source

The testings of the fuses were done with the source depict in Fig.2.

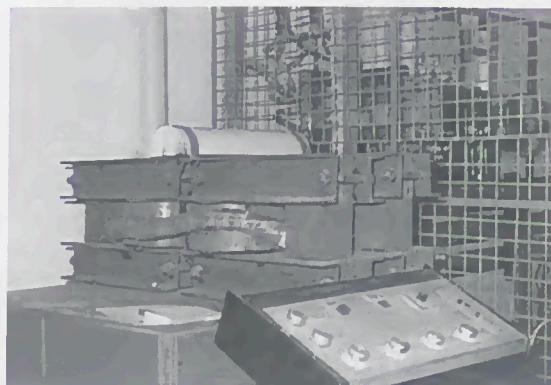


Fig.2 Tesing modular source

There are built some other sources too, with different construction of the ferromagnetic modules with high output and good cooling conditions to windings, Fig.3/A and Fig.3/B

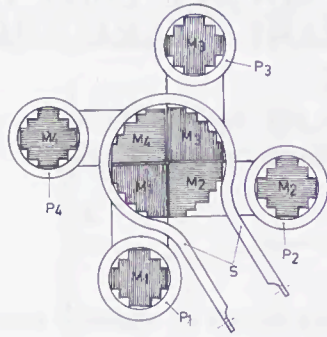


Fig.3/A Four modules source. Crossed section.

## II.2 Basic elements

There follow are some considerations and analyses about operating equations of created current/voltage sources and their equivalent electrical circuits with the following assumptions:

- the losses in the magnetic core iron are considered very small, negligible;
- the cores are unsaturated, the operating takes place on linear section of magnetic core B(H) characteristic;
- it considers that the modules have identical magnetic circuits;
- the equations use the convention from receiver for primary coils and from power plant for secondary (common secondary).

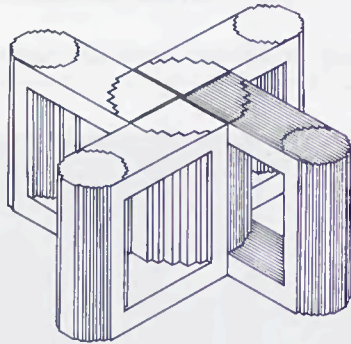


Fig.3/B Four modules source. View without windings

The principle electrical circuit of current source with two ferromagnetic modules is shown in Fig.4.

It can write the next equation systems, using the single-phase transformer model:

$$u_1 = R_1 i_1 + L_{d1} \frac{di_1}{dt} + N_1 \frac{d\Phi_{01}}{dt} \quad (1)$$

$$u_2 = R_2 i_2 + L_{d2} \frac{di_2}{dt} + N_2 \frac{d\Phi_{02}}{dt} \quad (2)$$

$$-e_3 = N_3 \left( \frac{d\Phi_{01}}{dt} \pm \frac{d\Phi_{02}}{dt} \right) \quad (3)$$

When in secondary there is a load (R,L,C) it gets the equation systems:

$$u_1 = R_1 i_1 + L_{d13} \frac{di_1}{dt} + N_1 \frac{d\Phi_{01}}{dt} \quad (4)$$

$$u_2 = R_2 i_2 + L_{d23} \frac{di_2}{dt} + N_2 \frac{d\Phi_{02}}{dt} \quad (5)$$

$$-u_3 = R_3 i_3 + (L_{d31} + L_{d32}) \frac{di_3}{dt} + N_3 \left( \frac{d\Phi_{01}}{dt} \pm \frac{d\Phi_{02}}{dt} \right) \quad (6)$$

where:

$u_1, u_2$  - two primaries voltage supplies;

$R_1, R_2$  - primary coils resistance;

$N_1, N_2, N_3$  - wire numbers of primary and secondary;

$\Phi_{01}, \Phi_{02}$  - core magnetization fluxes;

$i_1, i_2$  - primary coils currents;

$e_3$  - electromotive force to secondary terminals.

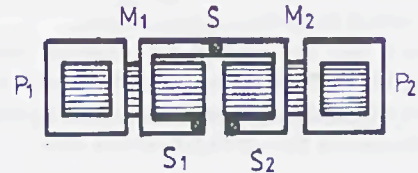


Fig.4 Electrical principle circuit of current source

Principle electrical circuit of modular source with one-turn wire single secondary is shown in Fig.5.

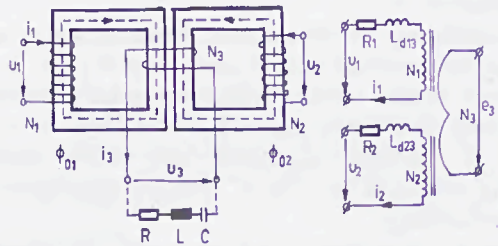


Fig.5 One turn wire common secondary

It considered, for clarity,  $N_3 = 1$  to given build (Fig.5) and it can notice this situation is equivalent with two transformers which  $P_1$  and  $P_2$  primaries are supplied by the same source or different voltage sources and secondaries (single wire) are in series. When  $N_3 \neq 1$  it can notice wire by wire alternating series of primaries. For a three modules assemble, from Fig.6, it can write the equation systems with phase values.

In this case, the equation system becomes (7...15):

$$\underline{U}_{p1} = R_p \underline{I}_{p1} + jX_{dls} \underline{I}_{p1} - \underline{E}_{mpl} \quad (7)$$

$$\underline{U}_{p2} = R_p I_{p2} + jX_{d2s} I_{p2} - \underline{E}_{mp2} \quad (8)$$

$$-\underline{U}_{p3} = R_p I_{p3} + jX_{d3s} I_{p3} - \underline{E}_{mp3} \quad (9)$$

$$-\underline{U}_s = R_s I_s + j(X_{ds1} + X_{ds2} + X_{ds3}) I_s - \underline{E}_{ms}$$

$$N_p I_{p1} + N_s I_s = N_p I_{0p1} ; \quad (11)$$

$$N_p I_{p2} + N_s I_s = N_p I_{0p2} ; \quad (12)$$

$$N_p I_{p3} + N_s I_s = N_s I_{0s} \quad (13)$$

$$\underline{U}_s = \underline{Z}_c I_s ; \quad (14)$$

$$\underline{U}_{p3} = \underline{Z}_R I_{p3} \quad (15)$$

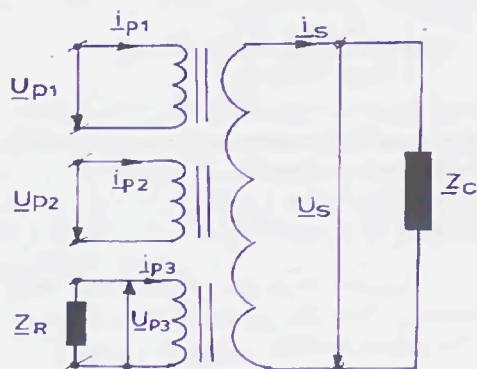


Fig.6 Electrical circuit of three modules source

To get the secondary current expression, for simplification, it considers the following:

- it refers the primary coil data to common secondary (noted "');
- it considers the magnetization currents almost zero:

$$\underline{I}_{pi} + \underline{I}_s \approx 0, \text{ with } i=1...3; \quad (16)$$

- the modules position is symmetrically to get the same dispersions.

After equation systems processing it gets the expression:

$$\underline{I}_s = \frac{\underline{U}_{p1} + \underline{U}_{p2}}{3\underline{Z}_p + \underline{Z}_R + \underline{Z}_c + \underline{Z}_s} \quad (17)$$

where:  $\underline{U}_{p1} = \frac{N_2}{N_1} \underline{U}_{p1}$ ;  $\underline{U}_{p2} = \frac{N_2}{N_1} \underline{U}_{p2}$ ;

$$\underline{Z}_p = R_p + jX_{dp}, \quad X_{dp} - \text{the stray reactance}$$

primary-secondary for one magnetic module;

$$\underline{Z}_R = \underline{Z}_R \left( \frac{N_2}{N_1} \right)^2 - \text{referred adjustment impedance};$$

$\underline{Z}_c = R_c + jX_c$  - load impedance (can be a fuse);

$\underline{Z}_s = R_s + 3jX_{ds}$ ,  $X_{ds}$  - stray reactance secondary-primary for one magnetic module.

From above expression, with done assumptions, it results that secondary current values will depend on following:

- primary voltage supplies;
- adjustment impedance value,  $\underline{Z}_R$ ; with this impedance we can adjust the  $\cos \phi$  factor;
- wires ratio between primary and secondary;
- dispersion inductance values;
- load values;
- magnetic material quality.

When it use these sources it can choose one or a combination of them depending on means.

Generalizing the (17) expression for n modules from among m have connected to primary terminals the adjustment impedance  $\underline{Z}_{Rk} \geq 0$  (where  $k=1...n$ ) and n-m modules are supplied with  $\underline{U}_{pi}$  voltages (with  $i=1...n-m$ ) it gets the expression (18):

$$\underline{I}_s = \frac{\sum_{i=1}^{n-m} \underline{U}_{pi}}{\sum_{j=1}^n \underline{Z}_{pj} + \sum_{k=1}^m \underline{Z}_{Rk} + \underline{Z}_c + \underline{Z}_s} \quad (18)$$

(with  $\underline{Z}_s = R_s + njX_{ds}$ )

### III TIME-CURRENT PLOTTING METHOD

#### III.1 Basic elements

Time-current characteristics shown in catalogues and standards are curves of statistical mean values experimentally established, in the individual cases the deviations could be up to +10% from mean values, an unacceptable error, especially to the protection of installations with power semiconductors.

So, it is necessary to work out a method to establish the individually time-current characteristic of high breaking capacity fuses.

The replacement elements used at tests proceed from those reconditioned to the Distribution Branch within the S.C. "Electrica" S.A. belonging to the National Company of Electricity - "CONEL", Ia• i - Romania.,

for own installations use. The experimental determinations of the temperature values were performed using resistance of the element variation method [8,9].

As a result, it could be measured the temperature values at different currents and it obtained the curve from Fig.7.

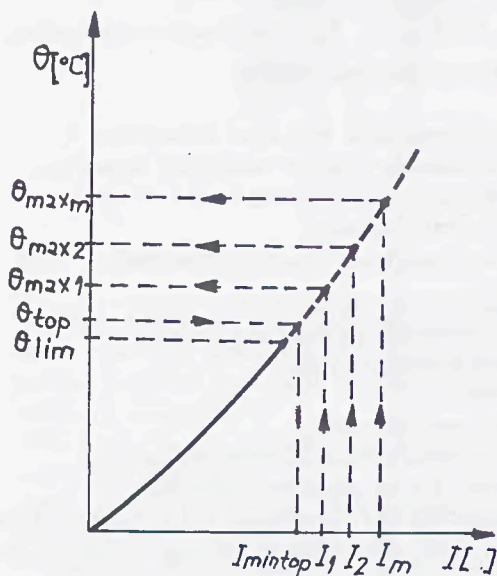


Fig.7 Extrapolated (I) characteristic

The limit temperature what can be attained without fusing, was considered  $\theta_{lim} = 0,9 \theta_{top}$ . The  $\theta(I)$  curve can be approximated with an arc of parabole:

$$\theta(I) = K_{med} I^2 \quad (19)$$

where  $K_{med}$  is a constant (mean value) inferred from experimental data.

A better approximation for  $\theta(I)$  curve is obtained with the expression [10]:

$$\theta(I) = A \operatorname{sh} \left[ a \left( \frac{I}{I_n} \right) \right] \quad (20)$$

where  $A$  and  $a$  are constants what can be calculated from experimental data.

The  $\theta(I)$  curve, from extrapolation, using one of expressions before, can be known over  $\theta_{lim}$ . For value of currents  $I_1, I_2, \dots, I_m$  from area (minimum melting current - breaking capacity) using curve from Fig.7, it can establish the maximum heatings.

Then, it plots the heating curve  $\theta(t)$  for values of currents  $I_1, I_2, \dots, I_m$  Fig.8. In the area  $\theta_{lim} - \theta_{top}$ , the heating curve can be approximated with an exponential curve. The maximum heatings  $\theta_{max1}, \theta_{max2}, \dots, \theta_{maxm}$ , infer from diagram before, Fig.7.

In the crossing points of heating curves  $\theta(t)$  with the line  $\theta = \theta_{lim}$  (points A, B...) it plots the tangents to those curves, getting the time constants  $T_1, T_2, \dots, T_m$ , these

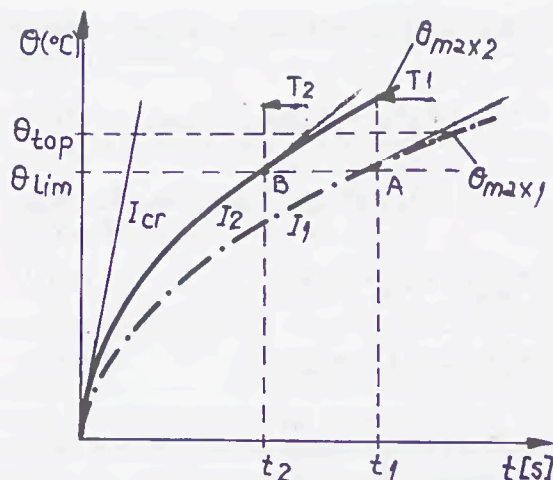


Fig.8 The heating curve  $\theta(t)$

constants can be obtained analytically with the relation:

$$T_i = \frac{t_i}{\ln \left( \frac{\theta_{max i}}{\theta_{top} - \theta_{lim}} \right)}, \quad i = 1, \dots, m \quad (21)$$

There is a critical current value,  $I_{cr}$  [3], which the heating evolution is the line:

$$\theta(t) = c t \quad (22)$$

where  $c$  is a constant what can be calculated using the fuse parameters. Over that current value  $I_{cr}$  the prearcing time has the expression [2]:

$$t_{pa} = \frac{S^2 K}{I^2} \quad (23)$$

where  $K$  is a material constant and  $S$  is the cross section of fuse link.

### III.2 Methodology

Knowing these elements and material constants, it proposes the next methodology to establish the individually time-current characteristic without fusing:

- for some values of currents  $I_1, I_2, \dots, I_m$  from area  $I_{min} - I_{top} - I_r$ , it establishes the maximum heatings  $\theta_{max1}, \theta_{max2}, \dots, \theta_{maxm}$  using a curve like that shown in Fig.7;

- it establishes the times  $t_1, t_2, \dots, t_m$ , resulted from crossing of heating curves  $\theta(t)$  with limit temperature line  $\theta = \theta_{lim}$ , Fig.8;

- plotting the tangents in the crossing points established before, it gets time constants  $T_1, T_2, \dots, T_m$  or using the relation (21);

- it calculates the prearcing time  $t_{p1} = t_1 + T_1, t_{p2} = t_2 + T_2, \dots, t_{pm} = t_m + T_m$ . If currents are over the critical value  $I_{cr}$  the prearcing times calculate with relation (23);

- the time-current characteristic  $t(I)$ , meaning the breaking time variation of one fuse depending on

overcurrent, can express in two alternatives: melting characteristic  $t_{pa}(I)$  and interrupting characteristic  $\tau(I)$ .

Because the arcing time of electric arc is about 5 ms, in the overcurrent area the characteristics  $t_{pa}(I)$  and  $\tau(I)$  actually overlap, Fig.9.

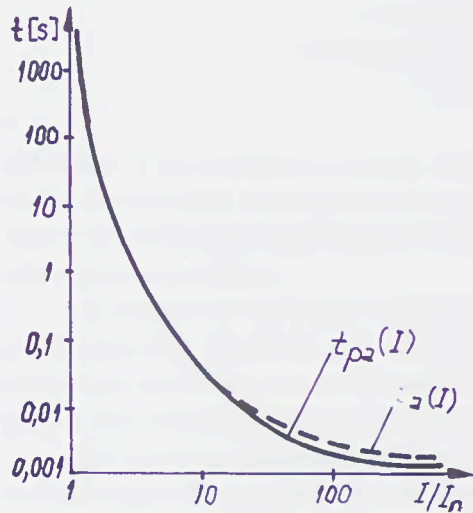


Fig.9 Time-current characteristic

The figure Fig.10 contains a comparison among the time-current characteristics for high breaking capacity fuses of Romanian production (plot1) [1], German production (plot 2) [12] and replacement element with fixed joining in the fuse link with prescribed melting temperature ( plot3).

#### IV CONCLUSIONS

From all experimental data we can notice the following conclusions:

- the time-current characteristic,  $t(I)$  of high breaking capacity fuses is plotted without fusing;
- knowing the time-current characteristic,  $t(I)$  of high breaking capacity fuses, permits a correct ensurance and anticipated checking of electric installations protection;
- the selectivity between fuses in series may be checked and can be settled for certain;
- the quality of installations protection increases;
- it is possibly a better protection for electric devices in the area of overload currents, using replacement elements with fixed joining in the fuse-link with prescribed melting temperature.

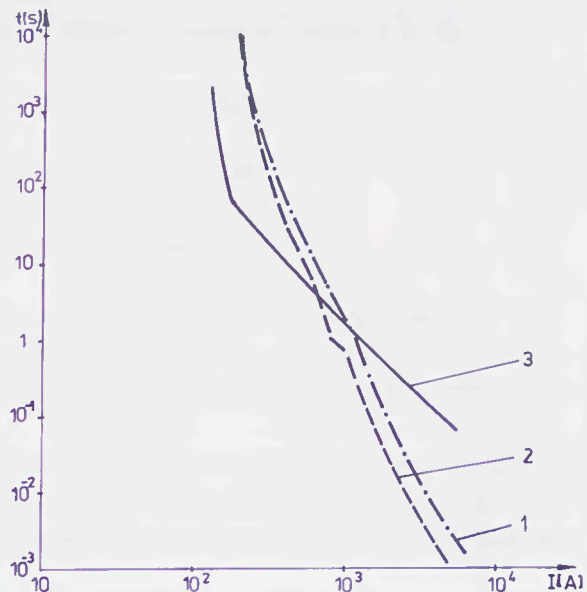


Fig.10 Comparison among the time-current characteristics of different production

#### REFERENCES

- [1] \*\*\* STAS 4173 / 1,2,3-1991.
- [2] \*\*\* IEC Publication 269 "Low voltage fuses".
- [3] A. Wright, P.G. Newbery: "Electric Fuses" Peter Peregrinus Ltd, London - New York 1995, IEE Power Engineering Series 2.
- [4] P. Leonte, a.o.: Current source, patent RO 73416.
- [5] Em. Furnica, P. Leonte: Voltage current transformer for a.c. modular source, patent RO 99994.
- [6] P. Leonte, Em. Furnica: Modular adjustment voltage source, patent RO 108135 / 1993 (Silver medal-EREKA 1995, Bruxelles, Belgium).
- [7] Em. Furnica: Theoretical and experimental contributions about new modular sources using to switching electrical apparatus testing, Doctoral Thesis, Technical University "Gh. Asachi", Iasi 1998.
- [8] T. Plesca, P. Leonte: Some contributions about high breaking capacity fuses working, ICATE'98 Proceedings, pp. 148-153, Craiova 1998, Romania.
- [9] \*\*\* Proceedings of ICEFA'95, Ilmenau, Germany.
- [10] I. Barbu: Low Voltage Fuses, Technical Publishing House, Bucuresti, 1983.
- [11] G. Hortopan: Switchgears, 1st and 2nd vol. 1993/96
- [12] \*\*\* SIBA Sicherungen-Bau GmbH, NH-Sicherungen, 1997



*[The text in this section is extremely faint and illegible. It appears to be organized into two columns, with a header or title at the top of each column. The text is likely bleed-through from the reverse side of the page.]*

# THE REAL-LIFE SEVERITY AND PECULIARITIES OF INTERRUPTING TEST DUTIES OF SEMICONDUCTOR FUSES

N.A. Ilyina\*, G.G. Zhemerov\*\*, E.I. Zaika\*\*, I.G. Shklovsky\*\*\*

\*Kharkov Municipal Academy, Ukraine

\*\*Kharkov State Politechnical University, Ukraine

\*\*\*Kharkov Collegium, Ukraine

**Abstract:** The recommendations and requirements specified by well-known standards IEC and Underwriters Laboratories Inc. in regard to the actual rigorous test conditions are not nearly accurate and unambiguous enough to be in full measure applied in practical designing semiconductor fuses.

The object of the paper is to reveal the truly severe duties under interrupting testing of semiconductor fuses at d.c. and a.c. conditions and to study the peculiarities of fuse behaviour from the view of economic feasibility and completeness of testing as well as proper determination of service conditions.

The basic peculiarities of d.c. and a.c. fault current breaking by semiconductor fuses and the real-life severity of test duties have been investigated as experimental part of an exploration program for development of fuses of 40÷1000A, 380,660V $\cong$  for protection of power semiconductor converters as well as while developing special purpose fuses for large inductance circuit. The results obtained can be represented in the form of three groups.

## 1. ZONES OF LIGHT DUTY TESTING

### 1.1. D.C. testing

The interrupting ability is usually the maximum fault current that can be obtained from the test station. According to the exploration program the semiconductor fuses are developed to qualify under the very strict specifications and codes which were in force for equipment in the former USSR territory. These requirements differ in some respects from the requirements specified by well-known standard IEC and Underwriters laboratories Inc. which does not, in particular, envisage d.c. short-circuit testing for semiconductor fuses. The main problems incorporated the requirements of large time constant, small fuse overall dimensions, coordination with downstream protective apparatus and protected equipment etc. In our maximum breaking capacity tests the ПП40 fuses  $I_{rated} = 400$  A,  $U_{rated} = 660$  V $\sim$  interrupted successfully 134,4 kA at 510 V $\cong$  time constant 20 ms and limited current down to 7

kA in 4,7 ms. These fuses interrupted as well successfully the d.c. short circuit current 93 kA at 510V $\cong$  and time constant 35 ms. Because of the fact that in these tests ПП40 fuses had demonstrated very reliable operation, small let-through integral and very small arc energy which have been estimated both by calculation from oscillogram and by fusing elements burnback value the decision has been taken to upgrade the d.c. short-circuit testing parameters. In the following experiment this fuse interrupted successfully d.c. short-circuit current 100kA at 850 V $\cong$  and time constant 35 ms. The similar results in general have been obtained by ПП38 (1000 A, 380 V) fuses.

The analysis of testing results has led us to conclude that the maximum breaking capacity test stipulated by IEC (publ. 269-4) is in fact the most light duty for semiconductor fuses among three prescribed test types. Moreover, if in general the fuse manufacturers lower the voltage rating of a.c. fuses to be used in d.c. circuit (up to 30-40%) then the semiconductor fuses interrupting the high d.c. short-circuit currents could be even

upgraded in comparison with the a.c. rating. Taking into account as well that high d.c. short-circuit regimes are rather rarely encountered in practice, the question arises as to whether it makes sense to conduct this test at all. If the semiconductor fuse reliably interrupts obviously more severe duty (such as maximum arc energy current) then what is the meaning of this test. If performing this test we are dealing with the verification of maximum let-through current or clearing time then there is no need for the test because at high d.c. short-circuit current when the adiabatic mode of fuse melting is obeyed the calculation is very simple and reasonably precise. In any event there is good reason to consider this kind test as not indispensable.

## 1.2. A.C. testing

The interrupting ability testing (the breaking of maximum fault current) can be considered as the one of the most light duty in actual practice (in our case up to 185 kA (rms), 730 V (rms) even at making angle 57-63 degree when maximum let-through current is achieved.

ППИ40 fuses  $I_{rated} = 400$  A,  $U_{rated} = 660$  V were tested at  $I_{s.c.} = 750$  V; power factor 0.09. At making angle 62 degree  $I_{max} = 19.1$  kA;  $t = 3.4$  ms; at 33 degree  $I_{max} = 14$  kA;  $t_{int} = 4.6$  ms. The criteria with respect to which the evaluation of duty lightness have been made were arc energy and fuse elements burnback values. Both these parameters fully conformed with the determination of this regime as light one.

ППИ60 fuses  $I_{rated} = 630$  A,  $U_{rated} = 660$  V were tested at  $I_{s.c.} = 142$  kA (rms);  $U_{s.c.} = 750$  V; power factor 0.085; making angle =60 degree. Three type specimen of fuses were tested: first one was manufactured by standards production technology with hard filler; second one – without hard filler (with usual filler) and third one – with impregnated but not dried-up filler. Deliberate violation of technology was aimed at verification of lightness of this testing duty. All experiments had confirmed this thesis in full measure. All fuses reliably cleared the short-circuit

however second and third type fuses showed somewhat poor performance ( $I_{max} = 35.6, 40$  and 41 kA respectively).

The testing of ПП38 fuses of  $I_{rated} = 1000$  A,  $U_{rated} = 380$  v at clearing a short-circuit 185 kA (rms), 450 V, power factor 0.09, making angle 58 degree also had confirmed the relatively lightness of the duty ( $I_{melt} = 29.1$  kA,  $t_{int} = 6.3$  ms). Fusing elements of tested fuses had a significant reserve of non-burning out parts.

The interrupting  $I_{s.c.} = 4 I_{rated} = 1600$  A by ПП40 fuses was the very light regime at 730 V, power factor =0.5. the fusing element remained non-burning-out almost at full length. At the same time problems came into existence when interrupting  $I_{test} = 2500$  A at 730V power factor 0.27 by ПП60M with hard filler. Tested fuses were cracked and the end-caps burned up. The fusing element remained non-burning-out almost at full length. The fusing elements asymmetry (series and parallel) of burning-up was arisen due to very intensive heat transfer from elements to fuse body. Owing to doubling the thermal conductivity of the fuse hard fillers the almost all performances had been improved except interrupting  $4I_{rated}$ . Still according to specifications this duty for ПП60M is not specified. This fuse is designed for power converter of variable drivers (railway transport) and it must interrupt mostly more high current and small currents only at low voltage.

At very small currents  $(1.5-2.9)I_{rated}$  a big temperature difference of exterior and internal surface of fuse body arises (40-60 C/mm resulting in cracking of body, but at 3.0-3.3  $I_{rated}$  this phenomenon disappears.

## 2. MAXIMUM ENERGY TEST.

### 2.1 D.C. testing

A fairly extensive exploratory testing program which have been undertaken to investigate the basic peculiarities of d.c. short-circuit breaking by developed semiconductor fuses has enabled making an estimates of the testing severity. As the

results obtained had clearly demonstrated, the most severe duty for semiconductor fuses is the maximum energy testing which is achieved if the current at the arcing starting moment is approximately equal to fault current instead of 0,5÷0,8 of fault current as IEC recommended. In addition, as applied to developed fuses, the fault current of the maximum arc energy (that is to say, the most heavy duty test) proved to be in the range between 5 and 12 of fuse rated current and in fact coincided with the minimum breaking current that is widely encountered in our practice. What this means is a possibility to suggest about combining a standard maximum energy test and a overload test that can be a worthy on numerous occasions.

The severity of this test is mostly attributed to the fact that at such current values the arc energy provided from the circuit inductance increases greatly. In our testing of ПП40 fuse  $I_{rated} = 400$  A,  $U_{rated} = 660$  V~ the transition from d.c. short-circuit current 93 kA, time constant 35 ms to d.c. fault current 4 kA, time constant 35 ms has resulted in more than 20 fold increasing in circuit inductance while the melting current changed from 7 kA to 3,9 kA only. It should be emphasized as well that the tangible intensification of series and parallel asymmetry of burnback of fusing elements at maximum energy currents of this value had in its turns contributed to onerousness of this duty as well.

The field of greatest interest is experimental investigation of a special purpose high-speed fuses. the fuses of this kind have specifically been developed for protection of wagon electrical equipment of metro railway and should satisfy very stringent requirements. Their rating are:  $I_{rated} = 500$  A,  $U_{rated} = 700$  V=; time constant 65 ms. In addition to severe conditions of interrupting duty the fuses must meet a high cyclic withstandability that involved an necessity of using a hard filler. The breaking tests have been conducted at traction substation of experimental railway line. Some results of interruption of d.c. short-circuit currents 5 and 18 kA by special

purpose fuse are by way of example presented in Table.

Table. – Test results.

Characteristics	Short-circuit current (kA)	
	5	18
$U_{test}$ (V)=	950	
$\tau_{test}$ (ms)	65	
$L_{add}$ (mH)	13	3
$t_{melt}$ (ms)	1860	50
$t_{arc}$ (ms)	40	14
$U_{arc}$ (V)	2750	2660
$E_{prearc}$ (kWs)	19	2
$E_{arc}$ (kWs)	201	102

It is amply clear that at 5 kA one of the most severe operation duty is formed not only for fuse and a downstream protected equipment under operating conditions but for test facilities during the fuse testing as well.

The duty of overload current by 200÷300% rated current under full voltage conditions which IEC and Underwriters Laboratories Inc. recommended for overload testing is almost not found in actual practice of equipments in the countries of former USSR, much less the semiconductor fuses are intended for breaking these small currents. Furthermore for high-power semiconductor fuses there are no high power testing station which can offer a comprehensive range of d.c. facilities to cover all voltage, current and circuit conditions that are likely to arise in service (the above-mentioned overload currents at full voltage including).

The difficulties emerge during the d.c. testing even at bigger fault currents. For instance, ПП38 fuse of  $I_{rated} = 1000$  A, 380 V (having hard filler) at d.c. fault current 6 kA, voltage 240 V=, time constant 20 ms did not melt throughout 300 ms after which the circuit-breaker came into action. The test results obtained while studying the other fuse series proved to be analogous to those reported above. In this connection it should be noted that in case when it is in advance known that a fault currents of order 2÷6  $I_{rated}$

are to be interrupted for instance by circuit breaker, it seems it's worthwhile the overload test of semiconductor fuses to combine with a maximum energy testing.

In conclusion it may be said that the situation with the determining a heavy and light duties for semiconductor fuses at d.c. mode is substantially more simple than at the a.c. mode. At any case d.c. current increasing may only lighten the interrupting conditions and conversely, d.c. current decreasing makes the interruption more onerous.

## 2.2 A.C. testing

To reveal the real most severe testing conditions at a.c. short-circuit for semiconductor fuses is very important task from the view of economic feasibility of testing as well as proper determination of service conditions. The most arduous conditions are developing inside of the fuse and they are determined fully by value and rising velocity of arc energy dissipated in fuse which are in its turn governed by many internal and outside factors as well as their combinations.

In this connection it should be noted that a well-known IEC and U.L. recommendations are far from to be unambiguous. Our investigations showed that the arc energy value and the short-circuit-current value at which the arc energy value is maximum are largely dependent on the circuit voltage, fuse rated voltage, arc voltage and making angle. A special role of making angle is dictated by the fact that due to making angle the mean value of circuit voltage during arcing period changes significantly depending on the angle and this voltage can increase or decrease in short-circuit current rising.

In our opinion there is no clear-cut maximum arc energy short-circuit current and the value close to maximum energy could be found in the wide range of a.c. short-circuit currents  $12-100 I_{rated}$  with variation of 10-15% depending on the number factors and in many cases at making angle 0. An absolute current maximum has as

already noted above been discovered at making angle 57-63 degree (not specified by IEC) and naturally at maximum short-circuit current. It might be well to point out that an important role of making angle manifests itself according to the combination of above-mentioned factors. However a dramatic reduction in circuit voltage (or a dramatic increasing of arc voltage) lowers substantially a effect of all short-circuit parameters. At the same time absolute maximum of arc energy appears when circuit voltage is equal to arc voltage.

The transition from range of 12-100  $I_{rated}$  to high currents zone of 150-250  $I_{rated}$  produces an arc energy diminution by 25-35% while in very small current zone of 2.5-5.0  $I_{rated}$  the arc energy is decreased by 2-3 times.

In the light of the results obtained perhaps it is worthwhile to reappraise some of the IEC recommendations. Specifically, the maximum energy fault current which is as recommended by IEC equal  $3-4 I_{10ms}$  needs to be revised with extending the range at least to  $1.75-5.0 I_{10ms}$ . In this case it is worth noting that information of this sort is not very much helpful for testing experts as well as for fuse designers and users not to mention the fact that the IEC does not specify the value of making angle which determines the mean value of circuit voltage during arcing process and is therefore very important factor.

At interrupting ability testing as IEC suggested the short-circuit current has to be chosen in such a way that the beginning of arcing process conforms to making angle 40-65 degree (1 experiment) or 65-90 degree (2 experiments). Yet our investigations revealed that if arc voltage is fairly high and stable that is the case at intelligently designed semiconductor fuses the making angle 40-65 degree establishes a light duty testing due to that in this period circuit voltage is far from maximum. On the other hand, at relatively small arc voltage and its slow rising the making angle 65-90 degree does not form the maximum energy conditions since arcing process captures the area of small circuit

voltage. The U.L. recommendations in the general are close to IEC's.

In the context of the preceding the most onerous conditions of fuse are to be established with due regard for above mentioned investigation results and always after the preliminary tackling a issue about the worthiness of searching a precise value of energy maximum. At the same time it must be emphasized that however much has been learned in the few years, it would be misleading to suggest that testing under worst-case conditions is neatly established. It is interesting to note as well that the key functional performance of semiconductor fuses-let-through integral was kept almost constant throughout the entire current range.

### 3. PECULIARITIES OF FUSE BEHAVIOUR AT A.C. INTERRUPTING TEST DUTES

Perhaps the one of the most peculiar features of fuse behaviour at a.c. interruption testing is the existence of two so called 'singular points'. In spite of the fact that well-known standards give no recommendations on that score nevertheless these points necessitate a special attention in fuse design, testing and service.

First singular point is in the a.c. short-circuit range of 7-11  $I_{rated}$  currents. It is characterized by two-fold scattering of melting time roughly from 7 to 14 ms due to a discontinuity of time-current curve calculated for the first time by J. Leach et al [1]. This phenomenon lies in the fact that the fuse melting in specific combination of value of sin-current, power factor and making angle (mostly 90 degree) does not occur in some time interval, but an increase or decrease of current by 3-8% causes an operation of fuse.

In the course of testing the ПП40 fuses  $I_{rated} = 400$  A,  $U_{rated} = 660$  V interrupted short-circuit 4 kA at 750 V power factor 0.41 at  $t_{melting} = 5.9$  ms. But the diminution of current merely to 3,85 kA produced melting time step up to 15.5 ms. That is to say the

singular point for ПП40 fuses proved to be about 10  $I_{rated}$  current.

The ПП38 fuses  $I_{rated} 1000$  A,  $U_{rated} = 380$  V at  $I_{test} = 8.8$  kA,  $U_{test} = 420$  V, power factor 0.31 making angle 90 degree melted in 6.1 ms, but at 8.5 kA – 15.2 ms.

The current range in which the singular point is discovered constitutes the zone that is very sensitive to small change of current resulting in time jump. This phenomenon is inherent to semiconductor fuses having a high current density in necks (parts of small section) and high ratio between element full section and restrictions. What is more our experiments showed the existence of discontinuity which recurs at regular intervals and the recurrence interval is generally speaking predictable depending of the current value. As part of the experimental study we discovered the discontinuity from 5-7 to 20-23 ms caused by current decreasing by 4-5%.

Second singular point lies in the range of 5-8  $I_{rated}$  current. Its peculiarity consists that at transition from making angle 0 degree to 90 degree causes the great change of fuse melting time from 8-10 ms to 400-600 ms respectively. Such a dramatic alternation of commutation process is attributable to the influence of component of transitional regime. In our experiment in short-circuit of  $I_{s.c.} = 5 I_{rated} = 2000$  A, power factor = 0.2, making angle = 0 the ПП40 fuse had melted in 10 ms at the moment when current reached its maximum 4500 A. However at making angle = 90 degree, i.e. in case when the interrupting process was free from transitional mode, the fuse melting time rised up to 520 ms and the melting occurred a steady state current of amplitude 2800 A. As distinguished from first singular point here the relatively smooth change of melting time had been observed in passing from angle = 0 to 90 degree.

ПП60M fuse had interrupted the short-circuit current  $\sim 8 I_{rated} = 4.9$  kA at power factor 0.27; 730 V, making angle 0 degree melting in 8 ms. That was very light duty for this fuse. But at making angle 75 degree the

fuse did not melt in 300 ms and fault current was cleared by circuit-breaker.

III38 fuse had successfully cleared the current  $6 I_{\text{rated}} = 6 \text{ kA}$  at 420 V power factor 0.27; making angle 0 degree in 9.8 ms, but at 90 degree did not melt in 160 ms.

#### 4. CONCLUSIONS

As a result of experimental investigations of semiconductor fuses the most severe and light test duties are refined,

the correspondent attention to the singular points has been attracted that makes it possible the financial and energy resources to be economized while developing, testing and servicing the semiconductor fuses.

#### REFERENCES

- [1] J.G. Leach, P.G. Newbery and A. Wright, "Analysis of High Rupturing Capacity Fuse Link Preaching Phenomena by a Finite-Difference Method", Proc. IEE, vol.120, • 9, sept. 1973, PP.987-993.

# OVERVOLTAGES PRODUCED BY LOW RATED CURRENT FUSE OPERATION IN L.V. INSTALLATIONS

G. Crotti (\*), G. Farina (\*), R. Tommasini (\*\*)

(\*) Istituto Elettrotecnico Nazionale Galileo Ferraris, Torino - ITALY

(\*\*) Dipartimento di Ingegneria Elettrica Industriale, Politecnico di Torino - ITALY

**Abstract:** The breaking operation of a fault current in an inductive circuit protected by fuses can lead, under particular circuit conditions, to the generation of high overvoltages, which can result dangerous for the plant and its components.

While for fuses with rated current over 16 A the maximum value of arc voltage as a function of the rated voltage of the fuse is stated by the related standard, for fuses with rated current below 16 A the admitted maximum arc voltage is still under consideration.

In the paper the values of arc voltage measured in the breaking operation of low rated current fuses are reported with reference to the test conditions stated by the IEC standard; in addition, a proposal about the values of the test circuit power factor is discussed.

## I. GENERAL

The breaking process of a short-circuit current operated by a fuse is described by the well-known equation:

$$e = v_a + R \cdot i + L \, di/dt \quad (1)$$

where  $e$  is the supply voltage,  $v_a$  is the arc voltage,  $R$  and  $L$  are the circuit resistance and inductance and  $i$  is the current which flows in the circuit.

The arc voltage that appears across the fuse plays a fundamental role in the breaking process. The higher the arc voltage, the shorter will be the arcing time and the let-through energy in the circuit interested by the fault. On the other hand, high values of arc voltage could result harmful for the electrical components to be protected with particular reference to semiconductor devices which are affected by the peak voltage value. For this reason, the manufacturers indicate an upper limit on the arc voltage that the semiconductor can tolerate and semiconductor fuses are designed according to the relevant standards to maintain the arc voltage below such values in all the operating

conditions.

The same considerations can be applied to general purpose fuses which, according to IEC 60269-1 standard [1], must have maximum arc voltage values which are function of the rated voltage of the fuse; compliance with this requirement is verified by the breaking capacity test, which has to be performed according to clause 8.5 of the above indicated standard.

## II. TEST CONDITIONS PRESCRIBED BY IEC STANDARD

The IEC 60269-1 "Low voltage fuses: Part 1 - General requirements" defines the test conditions for fuses. In particular for a.c. breaking capacity test, these prescriptions concern supply and recovery voltage, test current, power factor and making instant where applicable. As regards the power factor the values stated by the standard are reported in Table I as a function of the prospective test current.

Table 1 - Breaking capacity test: circuit power factor as a function of the prospective test current

Test current	$I_1-I_2$ (*)	$I_3-I_4-I_5$ (**)
Power factor	0.2 ± 0.3 for currents up to 20 kA 0.1 ± 0.2 for currents over 20 kA	0.3 ± 0.5

(\*)  $I_1$ : rated breaking capacity;  
 $I_2$ : current corresponding to test conditions giving the maximum arc energy.

(\*\*)  $I_3=3.2I_f$ ,  $I_4=2.0I_f$ ,  $I_5=1.25I_f$  where  $I_f$  is the conventional fusing current.

As regards the maximum values of arc voltage, they are indicated as a function of the rated voltage of the fuse: for fuses with rated voltage of 500 V, as those to which this paper refers, the admitted maximum arc voltage is 2500 V; however, in the case of fuses with rated current up to 16 A the maximum arc voltage is under consideration and is not specified in the standard.

The above limit is quite easily accomplished by the majority of fuses. Generally, the fuse element is realised with one or more restrictions of the cross sectional area in which the arc begins; the arc length then increases up to the total melting of the element. In such a way the arc voltage is gradually increased, the fault current reduces and dangerous overvoltages do not occur in the circuit.

Some problems can arise for fuses with low rated current, usually not exceeding 10 A. For these fuses, the fuse element is constituted by a single wire with constant cross section [2]. In the case of a fault with heavy short-circuit currents, the heating process can be considered adiabatic with a temperature distribution assuming a rectangular form along the element. The melting temperature is reached along the whole length of the fuse element all at once; this fact leads to a uniform disintegration of the fuse element causing the creation of a great number of series arc with a resulting high value of arc voltage.

The overvoltage generation process then occurs in the case of instantaneous evaporation of the whole length of the fuse element, leading to current-free interval [3, 4]. This current-free interval appears in a certain range of temperatures for which the vapours produced by the evaporation of the fuse element are non-conductive. In this case, the current rapidly decreases and consequently the overvoltage, which depends on the derivative of the current and on the circuit inductance, can reach dangerous values for the electrical components of the plant.

### III. EXPERIMENTAL INVESTIGATION

A test campaign aimed at investigating the overvoltages occurring with low voltage fuses has been carried out at IEN on general purpose fuses of different manufacturers with rated current 6 A, 10 A and 16 A and rated voltage 500 V.

The adopted test circuit, shown in Fig. 1, has been accurately designed in order to avoid damages to the components of the circuit and to the measuring instruments. To this end, an air spark-gap calibrated at the discharge voltage of 4500 V has been connected on the supply side of the circuit.

The arc voltage has been measured by means of a suitable voltage divider connected to a transient recorder, while the current has been measured by means of a resistive shunt.

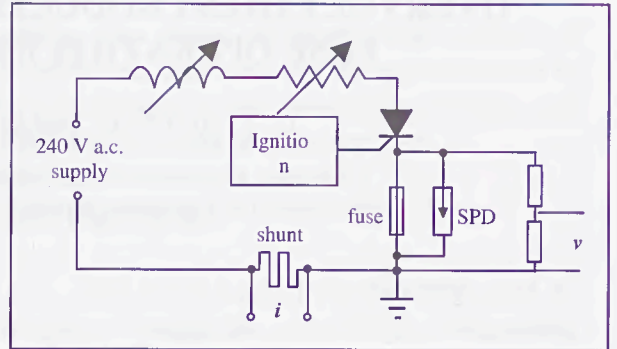


Fig. 1 - Test circuit arrangement.

The test conditions have been stated according to IEC 60269-1. The tests have been carried out with supply voltage of 240 V, 50 Hz, which is a usual voltage for single-phase circuit both for domestic and industrial applications. The test currents ranged from 300 A to 4200 A. For each test current, the making instant  $\psi$  has been varied in order to determine, for each type of fuse, the critical condition as regards the overvoltages.

Fig 2 shows a typical diagram of breaking test of a 10 A fuse (flink type) tested at 1500 A, 240 V, power factor ( $\cos\phi$ ) 0.3. In this case a maximum value of 3500 V was recorded.

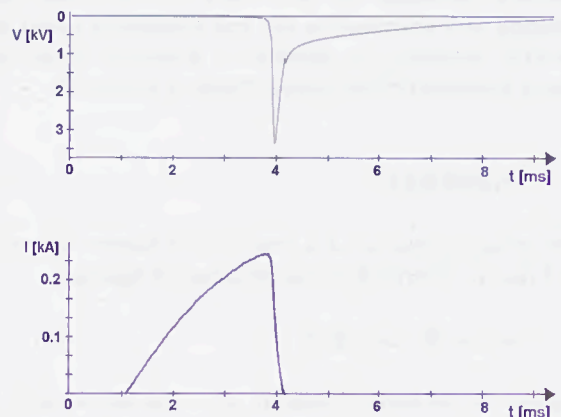


Fig. 2 - Voltage and current behaviour in a breaking test on a 10A fuse at 240 V, 1500 A,  $\cos\phi=0.3$ .

The maximum values of arc voltage measured in the breaking operation of fuses, carried out according to the IEC standard indications, are reported in Figs. 3+5 as a function of the prospective short-circuit current for gL/gI and flink type fuses respectively. Fig. 3 reports the maximum arc voltage values recorded with fuses rated 6 A, while Fig. 4 and Fig. 5 refer to 10 A and 16 A fuses.

From these diagrams, it can be observed that 6 A fuses give, both for gL/gI and flink type fuses, values of arc voltage which are in most cases higher than 2500 V. For 10 A fuses this overvoltage is exceeded only for flink type fuses, while for the 16 A fuses, the measured

values, both for gL/gI and flink types, are always within the voltage limit indicated by the standards.

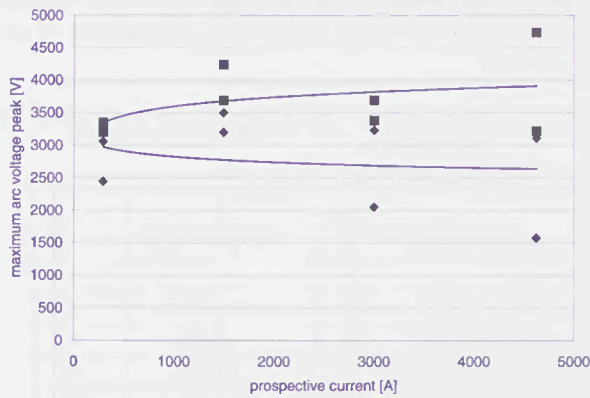


Fig. 3 - Maximum arc voltage values as a function of the prospective current for fuses of two different manufacturers with rated current of 6 A: (♦) flink, (■) gL/gI.

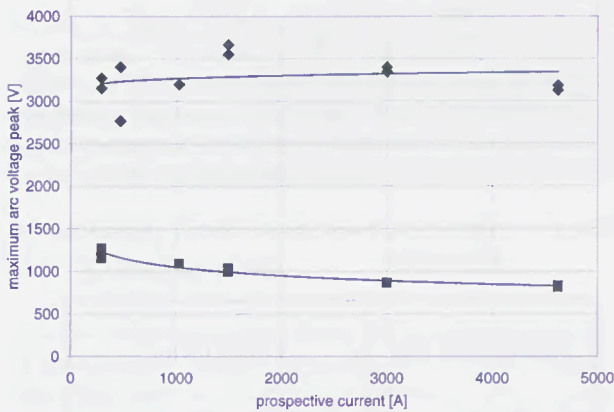


Fig. 4 - Maximum arc voltage values as a function of the prospective current for fuses of two different manufacturers with rated current of 10 A: (♦) flink, (■) gL/gI.

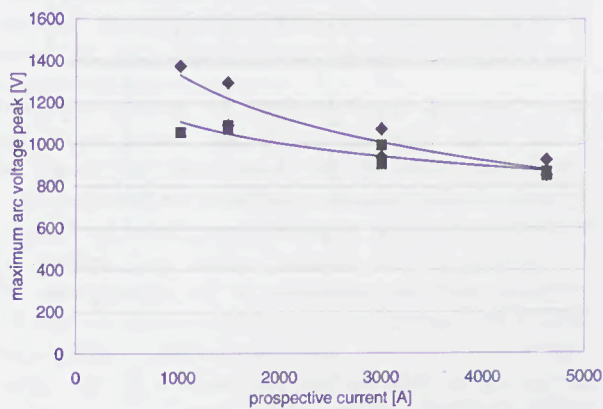


Fig. 5 - Maximum arc voltage values as a function of the prospective current for fuses of two different manufacturers with rated current of 16 A: (♦) flink, (■) gL/gI.

The different behaviour of the tested fuses can be explained taking into account the structure of the fuse element: for the 6 A and 10 A fuses, it is constituted by a single wire of constant cross section area, while for the 16 A fuses the element is a thin blade with a central restriction with a reduced cross section area. This arrangement avoids the contemporary fusion and evaporation of the element and limits the generation of overvoltages in the breaking operations.

The recorded peak voltage values versus the making angle of two fuses rated 6 A, respectively of gL/gI and flink type, are reported in Fig. 6 and Fig. 7 for different values of the test circuit power factor.

In Fig. 8 the peak values of arc voltage versus making angle of three 10 A fuses, two gL/gI and one flink type, are reported in the case of a test performed at 240 V,  $\cos \varphi=0.3$ , with currents of 290 A and 470 A.

As can be observed, for low power factors the maximum arc voltage can reach very high values, which can result undoubtedly dangerous for the circuit and its components.

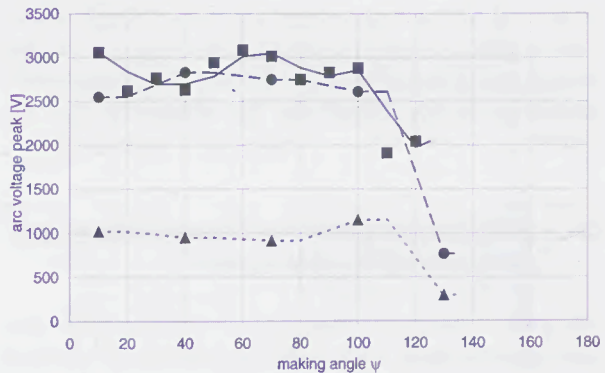


Fig. 6 - Breaking operation of a flink fuse, rated 6 A, tested at 290 A, 240 V: maximum peak values of arc voltage versus making instant for  $\cos \varphi=0.3$  (■),  $\cos \varphi=0.5$  (●) and  $\cos \varphi=0.9$  (▲).

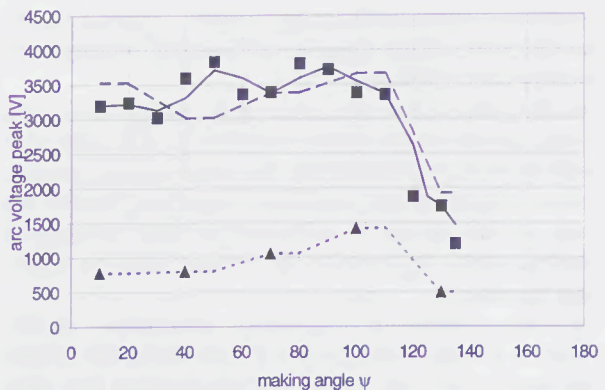


Fig. 7 - Breaking operation of a gL/gI fuse, rated 6 A, tested at 290 A, 240 V: maximum peak values of arc voltage versus making instant for  $\cos \varphi=0.3$  (■),  $\cos \varphi=0.5$  (●) and  $\cos \varphi=0.9$  (▲).

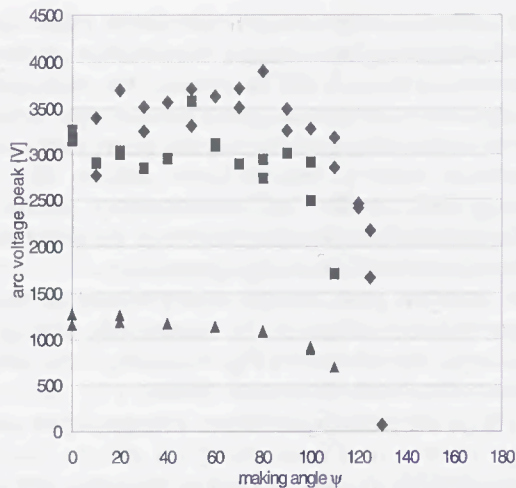


Fig. 8 - Breaking operation of 10 A fuses (gL/gI (▲), flink (■), flink (◆) tested at 290 A (■, ▲) and 470 A (◆), 240 V,  $\cos \varphi = 0.3$ : peak value of arc voltage versus making instant.

In the case of the tests carried out with a circuit power factor equal to 0.9 the maximum peak of the arc voltage has resulted considerably lower than 2500 V and then, according to IEC standards, not dangerous for the circuit.

#### IV. STANDARD PRESCRIPTIONS FOR FUSES AND CIRCUIT-BREAKERS

The tests carried out have put in evidence that low rated current fuses, with a melting element of constant cross section area, can generate dangerous overvoltages in the breaking operation of fault currents with low circuit power factors.

The power factor stated by IEC 60269-1 for the tests at  $I_1$  and  $I_2$  (0.1 ÷ 0.3) is independent of the rated current of the fuses.

For high rated current fuses, the test power factor indicated by the standard undoubtedly corresponds to the one that can be experienced in all installations in short-circuit conditions.

On the other hand, for low rated current fuses, the power factors in the range from 0.2 to 0.3 seem very unlikely to be experienced in the actual circuits; in fact, the resistance of the conductors used to connect the fuses to the circuit is sufficient, at high prospective current values, to increase the power factor to values near the unity.

For this reason, the standards concerning circuit-breakers for industrial [5] and for domestic and similar applications [6] state, for the breaking tests at low value of prospective current (up to 10 kA), values of power

factor much higher than those fixed by the standards for fuses [1], as can be observed by comparing the data of Table 2 and Table 3, which report the power factors indicated respectively by [5] and [6] as a function of the test current.

Table 2 - Short-circuit test power factor prescribed by IEC 60947-1

Test Current (A)	Power factor
< 1500	0.95
1500 ÷ 3000	0.90
3000 ÷ 4500	0.80
4500 ÷ 6000	0.70
6000 ÷ 10000	0.50
10000 ÷ 20000	0.30
20000 ÷ 50000	0.25
> 50000	0.20

As can be seen, the power factor stated for the circuit-breakers becomes very high for low currents, while for fuses a power factor which is practically irrespective of the test current is indicated in IEC 60269-1 (Table 1).

Table 3 - Short-circuit test power factor prescribed by IEC 60898

Test Current (A)	Power factor
< 1500	0.93 ÷ 0.98
1500 ÷ 3000	0.85 ÷ 0.90
3000 ÷ 4500	0.75 ÷ 0.80
4500 ÷ 6000	0.65 ÷ 0.70
6000 ÷ 10000	0.45 ÷ 0.50
10000 ÷ 25000	0.20 ÷ 0.25

Since fuses and circuit-breakers are usually employed in the same type of circuit and being equal the installation conditions, the short-circuit test should be carried out under the same conditions for both devices.

In addition, the value of power factor stated for fuses at low values of test current seems not realistic if compared with the conditions of the actual plants. In Table 4 the current and power factor values in a circuit supplied at 240 V, with prospective short-circuit current up to 100 kA are compared with the actual values resulting in the same circuit when a fuse connection, realised with a cable of 1 m length and cross section area of 1 mm<sup>2</sup>, is considered.

Table 4 – Influence of fuse connections, realised with a cable of 1 m length and 1 mm<sup>2</sup> cross section area, on prospective short-circuit conditions.

Prospective values			Actual values		
<i>I</i> [kA]	<i>Z</i> [mΩ]	cosφ	<i>I'</i> [kA]	<i>Z'</i> [mΩ]	cosφ'
1.5	160	0.3	1.4	170	0.50
3	80		2.4	100	0.64
6	40		3.7	64.8	0.80
10	24		4.6	47.2	0.90
20	12		5.3	43.6	0.96
30	8	0.2	5.7	41.6	0.98
50	4.8		5.8	41	0.99
80	3		5.9	40.6	0.99
100	2.4		5.9	40.5	0.99

It can be easily verified from Table 4 that such a connection, which is suitable for fuses with rated current of 10 A, is sufficient to reduce in the heaviest conditions the current below 6 kA and to increase the power factor value; with longer conductors the power factor will be further on increased.

## V. CONCLUSIONS

The risk of overvoltages during the breaking operation of short-circuit currents operated by low rated current fuses has been investigated by means of short-circuit tests carried out according to the prescriptions of the IEC 60269-1 standard.

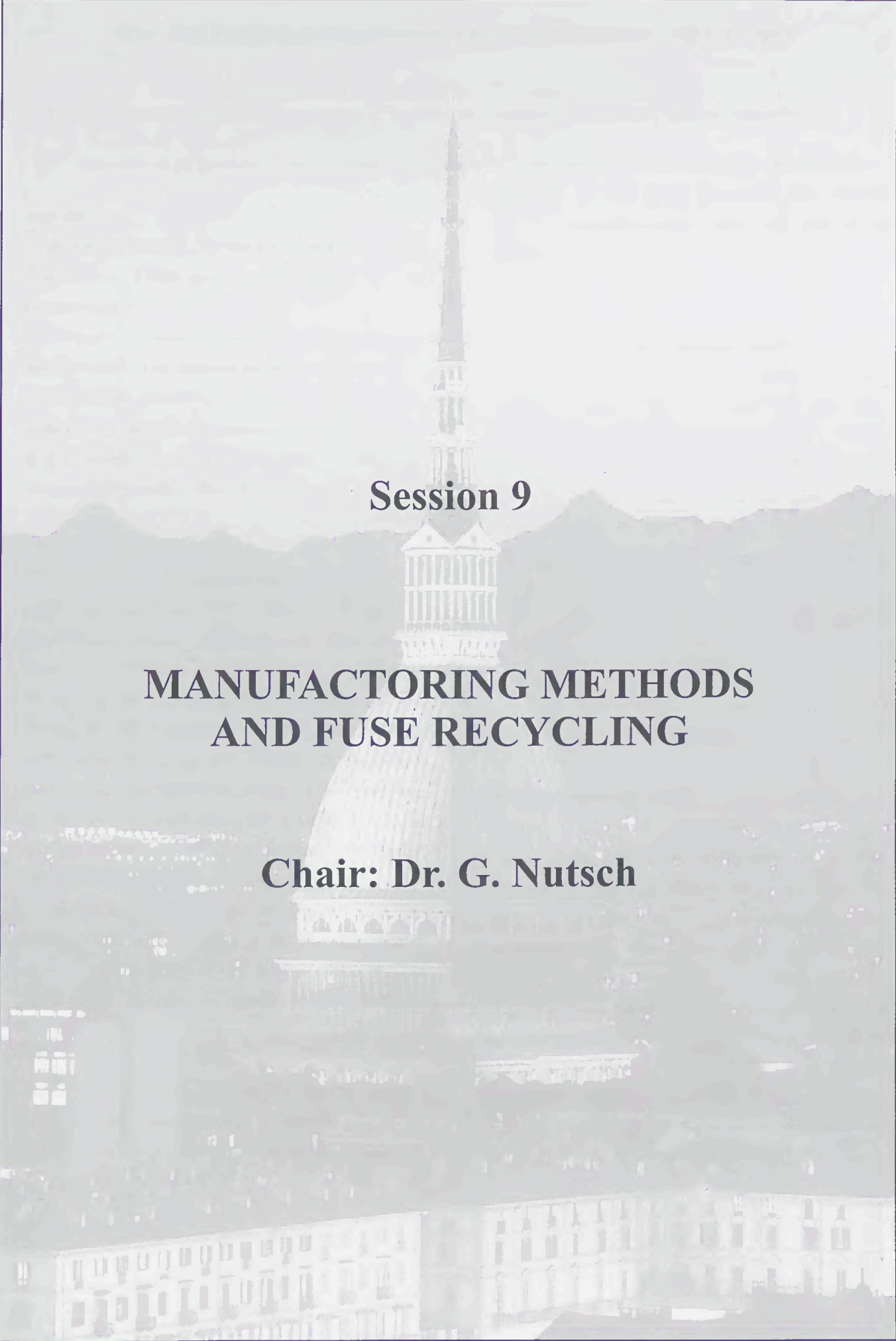
For tests carried out with low values of power factor (cosφ=0.3 for currents up to 20 kA) high overvoltage values, up to 4.5 kV, have been experienced on low rated current fuses characterised by fuse elements of constant cross section. With higher values of power factor the overvoltages in the breaking operation have less probability to occur.

Since in the actual plants low values of power factor are very unlikely to occur for low values of short-circuit current, the test conditions imposed by the IEC 60269-1 do not seem to correspond to the effective situations of the plants. Taking into account that the power factors indicated for fuses are very different from those stated by IEC 60947-1 and IEC 60898, concerning circuit-breakers, it should be advisable to adequate the power factor values of short-circuit tests on fuses to the actual plant conditions by adopting the same values stated for circuit-breakers by the relevant standards.

## REFERENCES

- [1] IEC 60269 Standard: Low-voltage fuses - Part 1: General requirements, 1998.
- [2] R. Wilkins, P.M. Mc Ewan: "A.C. short-circuit performance of uniform section fuse elements", Proceedings IEE, Vol. 122, no. 3, pp. 285-288, March 1975.
- [3] J. Paukert: "Overvoltages produced by fuses", Proceedings of the International Conference on Electric Fuses and their Applications, pp 59-69, Liverpool, U.K., 1976.
- [4] J. Hibner: "The calculation of overvoltage characteristics of H.R.C. fuses", Proceedings of the International Conference on Electric Fuses and their Applications, pp 70-77, Liverpool, U.K., 1976.
- [5] IEC 60947-1 Standard: Low voltage switchgear and controlgear - Part 1: General rules, 1999.
- [6] IEC 60898 Standard: Electrical accessories – Circuit-breakers for overcurrent protection for household and similar installations, 1995.
- [7] A.Wright, P.G. Newbery: "Electric fuses", Peter Peregrinus Ltd, London, U.K. 1984.





**Session 9**

**MANUFACTURING METHODS  
AND FUSE RECYCLING**

**Chair: Dr. G. Nutsch**



# The Test Method to Acquire the Optimal Parameter for CL-Fuse

Sei-hyun Lee\*, In-Sung Kim\*\*, Sang-Ok Han\*\*\*

\* Department of electrical engineering, The Taejon Polytechnic College, Taejon, South Korea

\*\* Korea Electrotechnology Research Institute

\*\*\* Department of electrical engineering, The Chungnam National University, Taejon, South Korea

## Abstract

*In this experiment, the discharge gap and surface roughness for various peak current and pulse on time were evaluated.*

*in this paper we choose 7 parameters with weight value based on study and experimentation and analyzed the characteristics of arcing period. In addition, we proposed the experimental method to extract the optimal design parameters with minimal effort as related the mutual effect from each of the parameters.*

## 1. Introduction

The fuse used in the high voltage distribution line often fails due to the active ionization caused by the strong electric field at fuse terminal. To suppress the ionization at the high voltage and high capacity current limiting fuse, the particle size and compactness of silica sand, the design, length, notch number and material of element, the diameter and the length of fuse body must be considered carefully. However, these are not proper that is treated with the inherent interrupting characteristics from many parameters at present. Because of these reasons, time and effort are needed to develop the new type of fuse by the fuse designers in relation with the inherent characteristics from each of parameters. in this paper we choose 7 parameters with

weight value based on study and experimentation and analyzed the characteristics of arcing period. In addition, we proposed the experimental method to

extract the optimal design parameters with minimal effort as related the mutual effect from each of the parameters.

## 2. Sample and experiment

In the fig.1, the material of the fuse's outer body includes a composite 87% epoxy and 13% glass fiber, the angle of the glass fiber coiled at outer body is  $15 \cdot 20^\circ$ . The core of fuse body is ceramic included 70% alumina. The element is 99.9% pure silver. The silica sand is 99.6%, the size is  $0.45 \cdot 1.05$ [mm]. The test device constructed by charging, interrupting and measuring part is illustrated in the fig. 2.

The experiment is carried out under the condition 1[kV], 50[kA].

## 3. Results

### 3.1 the size of silica sand

In the figure 3, the size of the silica sand to the energy generated during the arcing period is the solid line, and the dotted line illustrates the arcing time. The larger size of silica sand, we see the increased energy during the arcing period in the fig 3, When the size increases from 0.45 to 1.05, the arcing energy increases about three times. And the test oscillogram is illustrated the size 1.05, 0.45 in the fig. 4. The amplitude of current in the arcing period from the fig (b) is more decreased than that of fig (a). The arcing time is about 3.3[ms] in the fig (a), 4.5[ms] in the fig (b), but in case of fig (b), The amplitude of current is very small, and it

is applied to 4.5[ms]. This result is explained as follows. The arc having the generated conductance when the element melting is absorbed into the silica sand. Its size is smaller because the surface area able to collide with silica sand is larger; it is effected to absorb the heat from the silica sand. Consequently, the arc is not easy to arrive at outer body through the small space of silica sand. In case of the size, 1.05 silica sand, When a metal vapor and a silica sand by arc mixed, the fulgurite is not generated. And the metal vapor is mixed with all silica sands in the inner body. Consequently, the arc has the reaction with all silica sands while the high current is applied. So we can guess the arcing time is very short because the coiling is easy. From these results we can see that the size of silica sand has to be considered as the short of arc current and time means the optimal interrupting.

The fulgurite's structure is illustrated in the fig. 5. When silica sand meets the high temperature arc, it melts, structures the mixed fulgurite. The hole is generated in the center that there is the element, there is the empty space in the hole. There is the silica sand, which is not melted and metal vapor at the edge of the fulgurite. The larger size of silica sand, the melted silica sand is the smaller, and the hole's size is the larger.

### 3.2 the compactness

The element's length is 60[mm], the diameter is 0.41[mm] which is twisted, and the notch' number is 24, the silica sand's size is 0.65[mm]. This equation is used to decide the compactness.

$$\Delta Q = \frac{Q - Q_0}{Q_0}$$

$Q_0$  : The weight before the vibration

$Q$  : The weight after the vibration

It illustrates the arc energy, the solid line and the arcing time, the dotted line to the compactness in the fig. 6. The compactness is developed about 40[%] when

using the vibrator, 60[Hz]. It is shown below x axis as per unit. The arcing energy is about 60[kA<sup>2</sup>·sec] when the silica sand is inserted without vibration. The outer body is exploded when the compactness increases above 1.1[p.u]. The arcing energy decreases about 4.87 times. This phenomenon is analyzed as follows. The high temperature is generated when the arcing starts after the element is melted. The arcing which has the generated high pressure by the high temperature is progressing toward the outer body through the silica sand during the very short time. In this time, if the arcing arrived at the outer body easily, the arcing is not eliminated completely by surrounding silica sands. Consequently, because the arc's conducting keeps on, the arc energy becomes larger.

The major parameter in order to arrive at the outer body easily is the small space inside the silica sand. The more space, the easier it is for the arcing to arrive by the high pressure. When the compactness is increased. The small space decreases, but the surface area, which is able to collide with arc increases. The arc can not arrive at the outer body by the results, but collides with the surrounding silica sand. When the collision is generated, the arc having the high temperature lose the heat needed to melt silica sand, so the insulation is recovered quickly.

### 3.3 the thickness of element

The size of silica sand is 0.45[mm], the element's length is 80[mm], the inner diameter of the outer body is 28[mm]. The outer body's length is 40[mm]. And to know the effect of ability of interrupting by the varying the thickness using the press power, we varied the thickness, 0.47, 0.39, 0.32, 0.25, 0.2[mm]. The press extends the notch's width and length. Consequently, the element pressed to equal the resistivity is extended in its length

It illustrates the arc energy and arcing time when the element's thickness is varied in the fig.7. As it gets thinner, the arc energy is decreased to 1 over six and arcing time is decreased to 1 over four So, the thinner,

the more developed the ability of interrupting. Because the notch's region is separated with the certainty, the region without the notch region is not melted, only the part of the notch is vapor, the silica sand extinguishes the arc easily. There is a notch which is extend widely, the metal vapor spreads widely also, the interrupting is carried out easily because the vapor has more chances in order to meet silica sand.

### 3.4 the length of element

The size of silica sand is 0.45[mm], the inner diameter of the outer body is 18[mm]. The outer body's length is 40[mm]. To know the effect of element's length under the notch number is constant, we varied the length 40, 80, 120, 180[mm]. It illustrates arc energy and arcing time to the element length having constant notch number in the fig. 8. From this figure, the arc extinguishing of the element length is optimal at 80[mm]. Although the silica sand absorbs the thermal generated at each notch, under this test condition. The whole region of element is changed to arc because there are close notches very on the element having the shorter length than 80[mm], so because the much melting mass, the interrupting is not easy. And there is a constant distance between notches on the above 80[mm]. But the element's length is extended. Consequently, when it is coiled at core, the distance between the lines are very close, the silica sand didn't control the metal vapor. In this paper, we can get the optimal length of element extinguishing arc under the constant space.

### 3.5 the number of notch

The size of silica sand is 0.45[mm], the inner diameter of the outer body is 18[mm]. The outer body's length is 40[mm]. To know the effect of the notch's number, we varied it from 16 to 44. We can see that the interrupting carries out easy as the number of notch decrease from the fig. 9. When the notch's number is 16, the energy of arc is the smallest. If the notch's number is decreased, the energy of arc is to increase on the contrary after a critical notch.

If an arcing voltage is higher, the arc can be eliminated effectively. In this paper, we can see that the extinguishing of arc is optimal at the element's length having 16 notches

### 3.6 the inner diameter of the outer body

The size of silica sand is 0.45[mm], the outer body's length is 40[mm]. To know the effect of varying inner diameter of the outer body We varied inner diameter 18[mm], 33[mm] When the volume is increased 3.5 times, the arc energy is decreased 1 over 4, and the arcing time is decreased 4 over 5 from this fig. 10. These results can be explained as thinking the physical phenomenon, which the generated high pressure arrives at the outer body when the fulgurite is produced. The pressure, which is generated in the center, spreads toward radial. At this time, The silica sand is relaxed to transfer uniformity of the impact by the high pressure. This relaxation is effected by radial size. Consequently the explosion is not generated by the radial size increased 1.8 times. At the same time, because the silica sand's size is 0.45[mm] the arc's high temperature is transferred easily to silica sand, and the interrupting carries out easily

### 3.7 the length of the outer body

The size of silica sand is 0.45[mm], the inner diameter is 18[mm], the element's length is 80[mm]. To know the effect of the varying outer body's length We varied the outer body's length 40[mm], 60[mm]. There is no difference of the arc energy as the outer body's length increase from fig. 11 but the arcing time is decreased. These results are explained in fig. 12. The generated pressure impact is progress toward  $x$  and  $Z$  when the fulgurite is produced in the center of notch. The direction of the outer body' length is  $Z$ , the length is 20[mm], 30[mm], the perpendicular direction is  $x$ .  $Z$  is longed 2.2[p.u.], 3.3[p.u.] more than  $x$  so the pressure impact generated in the center is progress to the  $Z$

direction as a result, it is the time arrived at the outer body shorter than the time arrived at the end cap. Consequently, the impact arrived at the outer body is higher than that arrived at the  $Z$ . So In the case of the fuse can control the pressure impact properly, although the length is longer toward  $Z$ , The effect of the interrupting is not difference.

#### 4. Results

Among the many parameters affected by the interrupting characteristics. In this paper, we can get the proper design parameter. Through the experiment about the 7 parameters is under the 1[kV], 50[kA] condition. The arc energy is decreased to 1 over four as increased the compactness 15% by the sequence testing method. There is the optimal extinguishing when the size is 0.45[mm], the notch's number is 16 When the inner diameter of the outer body's is increased 1.8 times the ability of arc extinguish is increased 4 times. But the ability of extinguishing is increased by the increase the inner diameter to toward  $Z$ , when the length toward  $Z$  is extend is not different. When the fuse designer develops the new model. There will be the economical benefit about the time and effort as referring to this paper's experiment results.

#### Reference

1. Lee Sei-Hyun, Park Doo-Kee, Koo Kyung-Wan, and Han Sang-Ok, "Element shapes on High-Rupturing-Capacity Fuses", Korean-Japan Joint Symposium on Electrical Discharge and High Voltage Engineering, pp. 49•53, 1996.
2. K. K. Namitokov and Z. M. Frenkel, "Effect of design Features of the Fusible Element of Fuses on the Arc Pocesess in Them", Elektroekhnika [Soviet Electrical Engineering], No. 9, pp. 56•61, 1984.
3. Radhakrishanan Ranjan, " Design, Development And Application Of Smart Fuses Part 1", IEEE Transactions on industry applications, Vol. 30, No.1, 1994.
4. K. Jakubiuk, T. Lipski "Dynamics of Fulgurite Formation During Arcing in hrc Fuses", J. Phys. D: Appl. phys. 26, pp. 424•430, 1993.

5. Lee Sei-Hyun, Han Sang-Ok, "Characteristic Simulation of Equivalent Interrupter and Short-Circuit Generator to Test the Interrupting Performance of CL Fuse", KIEE Vol. 46, No 8. pp. 1279•1284, 1997.
6. V. N. Narancic and G. fecteau., " Arc Energy and Critical Tests for HV Current Limiting Fuses", Int. Conf. on Electric Fuse and Their Applications, pp. 236•251, 1984.
7. Lee Sei-Hyun, Han Sang-Ok, "Interrupting Characteristic Modeling of High Voltage Current-Limiting Fuse", KIEE Vol. 46, No 4. pp. 617•621, 1997.

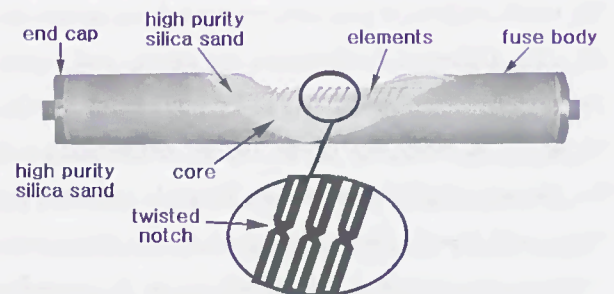


Fig. 1 Cross-sectional view of the tested fuse

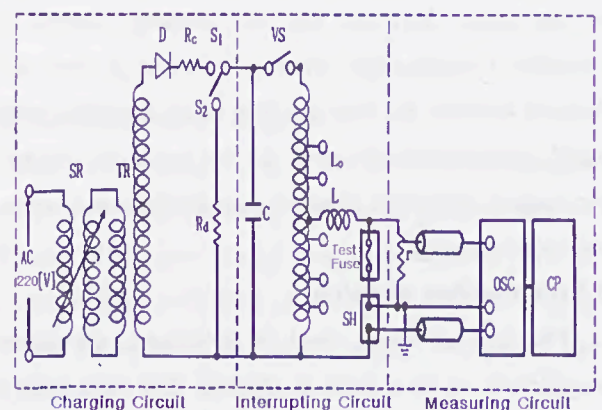


Fig. 2 Schematic diagram of equivalent interrupter

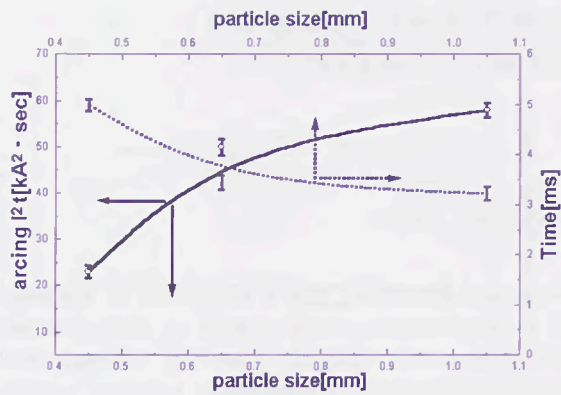


Fig. 3 Particle size effects of silica sand

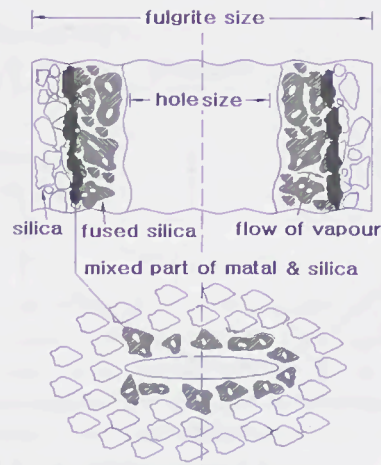
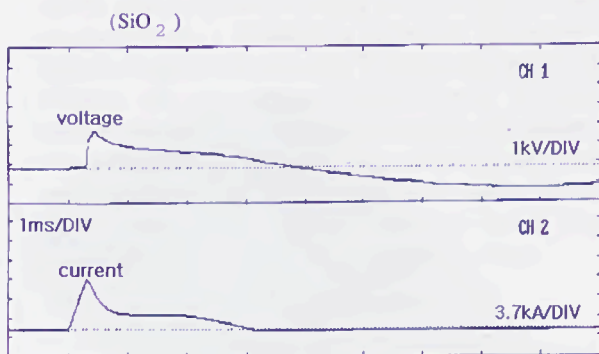
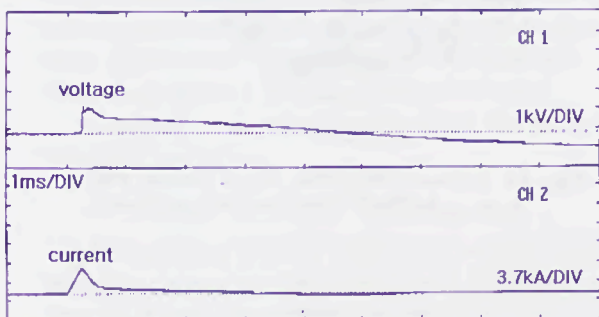


Fig. 5 Structure of fulgurite



(a) Particle size, 1.05[mm]



(b) Particle size, 0.45[mm]

Fig. 4 Interrupting oscillograms of particle size effects

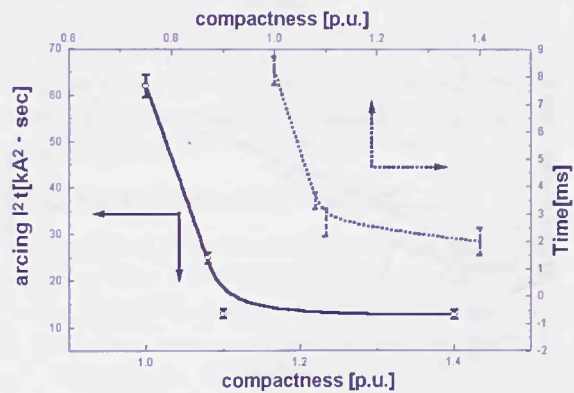


Fig. 6 Compact effects of silica sand ( $\text{SiO}_2$ )

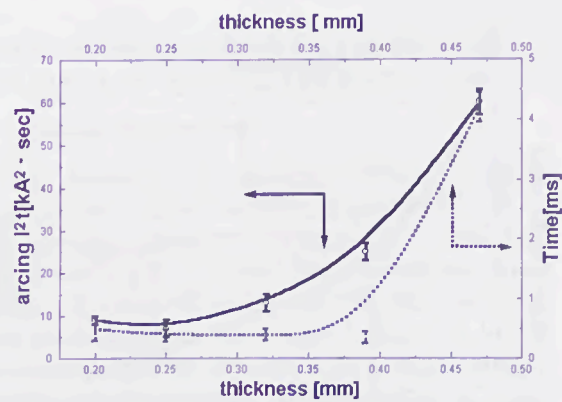


Fig. 7 Thickness effects of element notch

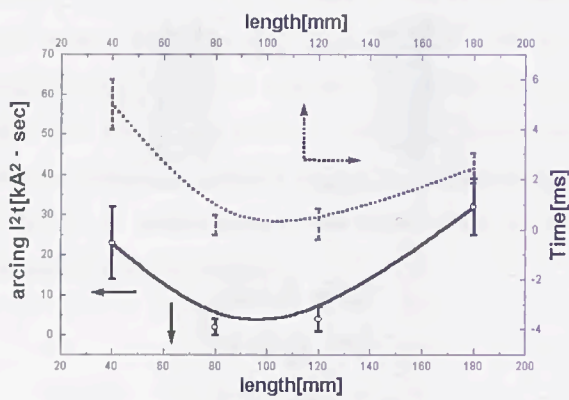


Fig. 8 Length effects of fuse element

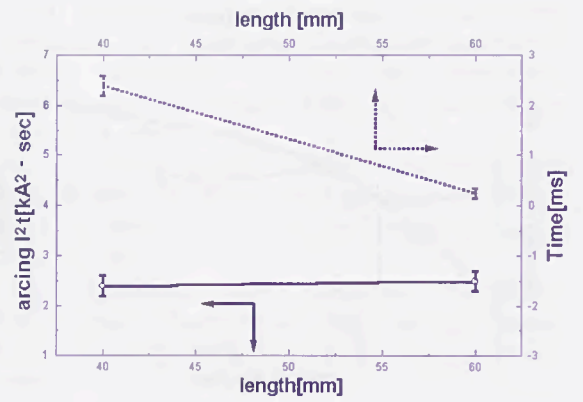


Fig. 11 Length effects of fuse body

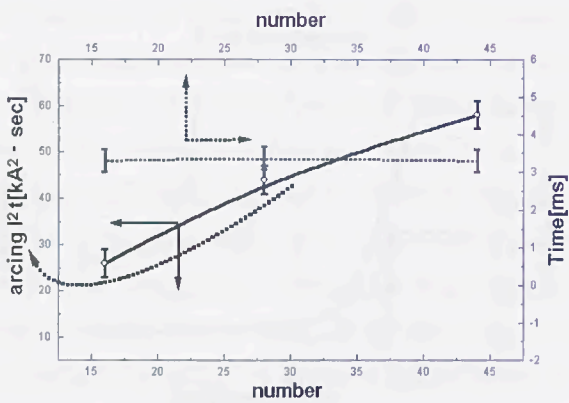


Fig. 9 Notch number effects

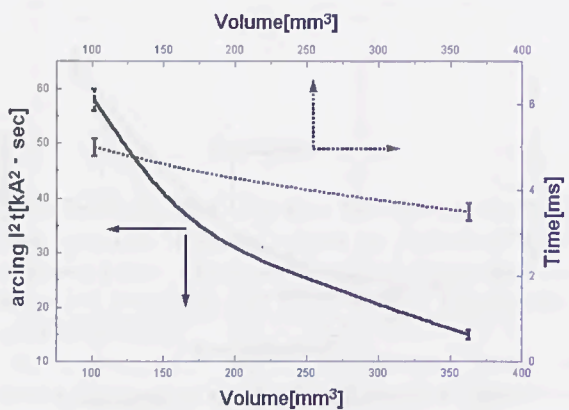


Fig. 10 Volume effects in fuse body

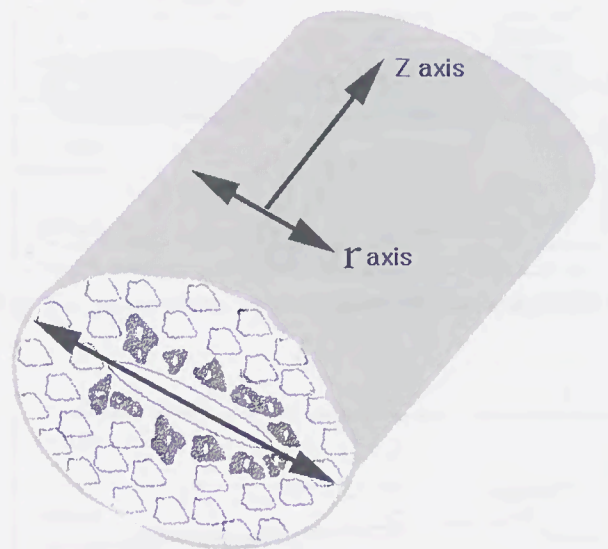


Fig. 12 Forward directions of arc plasma with high pressure

# STUDY ON FLUID-SAND (STONE-SAND) METHOD FOR HIGH-VOLTAGE FUSE

Wang Jimei Kong Fanhong  
Xi'an Jiaotong University

Ma Ziecheng  
Xi'an Fusegear Factory

Xi'an, The people's Republic of China

**Abstract.** In this paper a new fluid-sand (stone-sand) method used in high-voltage current limiting fuse was studied. It may simplify the solidification process of silica sand, reduce the production period and cost raising the efficiency of production. Consequently it deserves to be extended in production. The new process involves three steps. Firstly, mix silica sand with sodium silicate solution of modulus 1 to make sodium silicate crystals filmed on the whole surface of silica sand, and then a certain amount of pure alcohol is added to dehydrate the mixture which will become fluid similar to dry sand. Finally, dry the mixture in an oven at constant temperature till to get enough strength. Moreover, the mechanism of adhesion in the mixture was studied and the breaking capacity of fuse with solidified silica sand was tested showing much better performance than that of ordinary silica sand.

## INTRODUCTION

So far, silica sand is quite widely used as arc extinction medium in electric fuse. Furthermore, the breaking capacity of fuse can be much improved by using the technology of stone-sand. That is why so many manufacturers in the world produce their fuses with stone-sand as arc extinction medium to meet their consumers' requirement. Consequently, the stone-sand method is in need of further study.

Generally, the stone-sand method can be briefly described as follows:

### Blending Stone-Sand Method

Mix sodium silicate solution of certain modulus with silica sand, stir the mixture well to clayish state, then fill it into a fuse cartridge compactly and tightly. Finally, keep the fuse with the mixture in an oven at constant temperature till dry, then cool down. The shortcomings of this process involve: to fill the mixture in a fuse cartridge needs great effort; the compactness of silica sand can not be what is expected; and to make the mixture dry enough requires much electrical energy consumed, thus lengthen the production period.

### Stone-sand Vacuum Method

Fill silica sand in a cartridge of fuse, then place the assembled fuse in a vacuum-tight vessel.

Vacuumize the vessel to a certain degree of vacuum, then inject sodium silicate solution. Finally, dry silica sand infiltrated with sodium silicate in an oven at constant temperature. The method is characterized by high efficiency, but too much electrical energy is needed due to the lengthy time of drying.

### Stone-sand Sodden Method

Place the assembled fuse with silica sand in a proportionally prepared sodium silicate solution which will infiltrate into silica sand through the hole where silica sand was poured, till silica sand is wholly sodden. It will take a long time to make silica sand sodden with sodium silicate solution and dry the infiltrated sand. The method has similar shortcomings as mentioned above.

### Fluid-Sand (Stone-sand) Method

Make sodium silicate crystallize on the surface of silica sand to form a film which will have the quality of flowing as easily as dry silica sand with no film. When the filmed sand is filled in a fuse cartridge to enough compactness, only vibrating operation of fuse cartridge is required with no tamping necessary. It takes less time for drying sand, so high in efficiency. This is supposed to be an advanced than stone-sand method.

## ADHESION MECHANISM OF FLUID-SAND METHOD AND MIXING TECHNOLOGY

### Adhesion Mechanism.

The modulus of sodium silicate solution commonly used in the foundry ranges from 2.0~3.3 with specific gravity between 1.3 and 1.5 approximately. Fig. 1 shows the trielemental phase diagram of  $\text{Na}_2\text{O}-\text{SiO}_2-\text{H}_2\text{O}$  (Isothermal section), where the material in the region 1 enclosed by the dashed lines (Shadow Portion) is of a table colloidal solution, but the material in the region is under unstable state where sodium silicate crystallizes out and the saturated solution of sodium silicate is formed. In region 3, there are sodium silicate crystals set out from the solution.

When some amount of sodium hydroxide is added to adjust the modulus of sodium silicate to 0.7~1.2 and make the solids( $\text{SiO}_2+\text{Na}_2\text{O}$ ) content to 40~50% by weight, mix this solution of low modulus

with silica sand. At this time there will be sodium silicate depositing on silica sand and forming a thin film on the surface during mixing. Naturally, the sand filmed like this will have the similar quality of flowing like that unfilmed. So it is called "fluid sand".

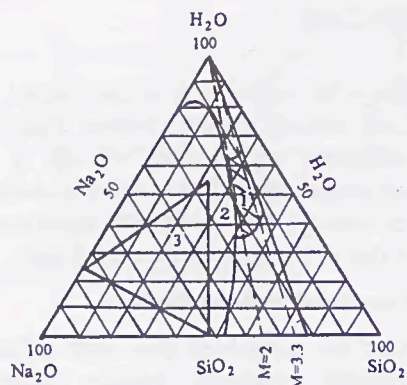


Fig. 1 Ternary phase diagram of  $\text{Na}_2\text{O}-\text{SiO}_2-\text{H}_2\text{O}$

In order to speed up the deposition of sodium silicate solution with low modulus, some hydration agents like alcohol are often applied to improve the quality of flowing of sodium silicate. Meanwhile, the evaporation of alcohol will take some heat away by which the undesired drying effect of wet sand is avoided and that will be convenient for the subsequent technical process.

#### Mixing Technology

Silica sand is mixed with the proportionally prepared sodium silicate solution by a specialized mixer of 500 mm in diameter at 36 rpm for this purpose. Meantime pure alcohol is properly poured in the mixer. Let the mixture be agitated for about 10 minutes.

#### EFFECT OF SODIUM SILICATE ON FLUID SAND

##### Modulus of Sodium Silicate Solution

In the preparation of fluid sand, the proper modulus of sodium silicate solution is the key technique for the sand solidification. Effect of the modulus on the fluidity and strength of fluid sand is shown in Fig.2. It can be seen that the modulus too high or too low will significantly affect the fluidity and strength of silica sand as shown in Fig.2. The optimal modulus prepared is between 0.9 and 1.0, in which the collapsing diameter is 360 mm, the compactness greater than  $1.22\text{g/cm}^3$  and the dry shearing bigger than  $10.5\text{kg/cm}^2$ .

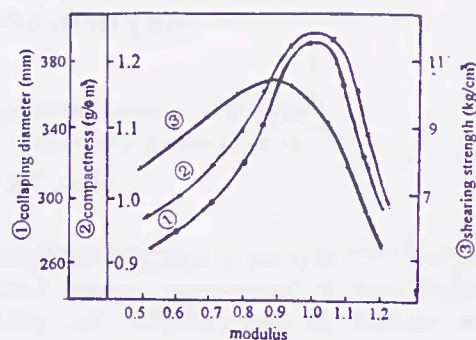


Fig.2 Effect of the modulus on the fluidity and strength of fluid sand

##### Influence of Weight Percentage of Solids in Sodium Silicate Solution

Fig.3 shows the effect of solids content in sodium silicate on the fluidity and strength of fluid sand. In general, the best choice for the solids content in sodium silicate is 40~50% by weight. If it is lower than 40% by weight, the indexes of collapsing diameter, compactness and dry shearing strength will be depreciated.

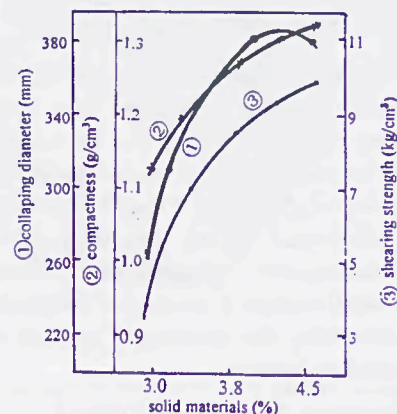


Fig.3 The effect of solids content in sodium silicate on the fluidity and strength of fluid sand

##### Ratio of Sodium Silicate Solution to Silica Sand

Fig.4 shows the effect of ratio of sodium silicate solution to silica sand on the fluidity and strength of fluid sand. The ratio nearly makes no influence on the fluidity of fluid sand, but exhibits an obvious and great effect on the strength of fluid sand. The more sodium silicate solution is mixed, the higher the strength of fluid sand will be. The ratio of 1.5% is the optimal percentage to be chosen in consideration of the dielectric strength of silica sand.

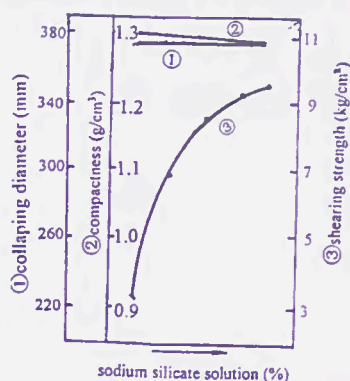


Fig.4 The effect of ratio of sodium silicate solution to silica sand on the fluidity and strength of fluid sand

#### Effect of Standing Time of Fluid Sand in Fluidity

As soon as the fluid sand is prepared, it should be used up for filling the fuse cartridge within 1hr. Otherwise, the fluidity of it will be lessened. It becomes solidified and adhered together, forming small solid blocks and can no longer be used.

#### Effect of Various Solidification Methods on Fluidity

Base on the adhesion mechanism of fluid sand, sodium silicate crystals will be dehydrated when exposed in air and become effloresced and solidified finally. The sample fuse was experience by heating in an oven in addition to natural drying for solidification. The experimental results show that when the fluid sand mixture is prepared and immediately kept in an oven at 100°C for 20~30 minutes, the dry shearing strength is read higher than 10kg/cm².

#### Effect of Sand Mixing Process

The mixing process for fluid sand should strictly follow that the surface of sand must be evenly covered by sodium silicate solution, the crystals of which will be deposited on to ensure the good fluidity of sand. The time is critically important in this process. In the very beginning of the mixing process, fluid sand is viscous. With the time elapsed the sand becomes fluid. When small amount of alcohol is added, the sand viscosity becomes obviously less. Therefore, the time of sand mixing should be well controlled. Otherwise, the fluidity of sand will increase while the strength of it will decrease. Normally, the time of sand mixing needs 3~5 minutes, then small alcohol is poured in. Stirred for 2~3 minutes, the mixture can be filled into the fuse cartridge.

## EXPERIMENTAL RESULTS

The electric fuse with silica sand prepared following the above process was conducted for the short-circuit current breaking capacity and antioxidant ability tests

### Short-circuit Current Breaking Capacity Test

Three fuse samples with fluid sand solidification were tested to interrupt the short-circuit current as high as 35.2 kA. The experimental results show that the samples fuses exhibited good current limiting characteristics. The peak value of current is 5.2 kA. The fuse elements was deserved uniform burst when the samples detached apart.

### Antioxidant Ability Test

The copper fuse element was assembled with solidified sand by fluid-sand method. The fuse was continuously tested with a rated current of 50A for one year, and then the resistance of fuse-element was measured. The experimental result showed that there was little change in resistance and no obvious oxidation was observed on the surface of copper element.

## CONCLUSION

The fuse with copper fuse element and silica sand prepared by the fluid sand method shows the breaking capacity as same as ordinary current limiting high voltage fuse.

No obvious oxidization on the surface of copper element. The new stone-sand method deserves to be widely extended in the field of high-voltage fuse.

## REFERENCES

- [1] Hu Aiguo, "Steady on the arc quenching ability of fuses with silica sand and solidification sand, High-voltage Apparatus, No, 4, 1991.
- [2] Wang Jimei, "High-voltage Current Limiting Fuse", Xi'an Jiaotong University Publishing House, 1992
- [3] Kong Fanhong, "Research on Drop-out Type Fuse with Replaceable Solidified Sand Fuse-Link", Master Thesis, Xi'an Jiaotong University, 1996
- [4] Institute of Kun-Ming, "Foundry Moulding Material". People's Publishing House. Yun-Nan Province, 1978

THE HISTORY OF THE  
CITY OF BOSTON  
FROM 1630 TO 1800

IN TWO VOLUMES  
BY  
NATHANIEL PHIPPS

VOLUME I  
FROM 1630 TO 1700

NEW-YORK:  
PUBLISHED BY  
J. B. ALLEN, 10 NASSAU ST.

1850



THE HISTORY OF THE  
CITY OF BOSTON  
FROM 1630 TO 1800

IN TWO VOLUMES  
BY  
NATHANIEL PHIPPS

VOLUME II  
FROM 1700 TO 1800

# CHARACTERISTICS OF FUSE ARCING IN DIFFERENT FILLERS

M.A. Saqib and A.D. Stokes  
School of Electrical and Information Engineering  
The University of Sydney  
NSW 2006 Australia

## Abstract:

Aluminum hydro-oxide, boric acid, zinc oxide, titanium oxide and boron trioxide have been investigated here for their prospects as filling media in high-voltage, high breaking capacity fuses. The results of these tests are compared with those on silica sand at high currents. This study demonstrates that silica sand is far superior filler in HBC fuses for heavy current interruption than the compounds tested.

## I. INTRODUCTION

The primary purpose of a high breaking capacity (HBC) fuse is to interrupt heavy fault currents effectively in a very short time, even less than quarter of an AC cycle. Silica sand, which is known to possess excellent interrupting capabilities at heavy currents, has been used as filler in HBC fuses for many years. We have investigated the potential of aluminum hydroxide, boric acid, zinc oxide, titanium oxide and boron trioxide as replacement fillers in HBC fuses. Some of these inorganic compounds are considered to be suitable lining materials in expulsion fuses. The purpose of this study was to search for an inorganic compound that may have better interrupting characteristics in HBC fuses than those of sand.

## II. EXPERIMENTAL SETUP

We have constructed an experimental version of a high-voltage, high breaking capacity fuse, cylindrical in shape with a length of 240 mm and diameter of 43.7 mm, and with a uniform silver wire of 0.55 mm diameter as fuse element. Different fillers of comparable grain size (10  $\mu\text{m}$  to 100  $\mu\text{m}$  diameter) were poured in the fuse holder under vibration to keep the packing density similar in each case. All materials were tested under the same conditions of supply voltage and prospective currents. The diagram of the circuit used to energise the fuse is shown in Figure 1. The fuse fillers were tested at 6 kV, 50 Hz, 4 kA prospective current [1].

## III. EXPERIMENTAL RESULTS

The voltage across the fuse was measured as a function of time by a resistive voltage divider: a Tektronix P6015, 1000:1, 20 kV, 100 M $\Omega$  voltage probe (rise time of 5 ns). Current was measured using a 190.8 A/V coaxial current shunt (rise time approximately 60 ns). A Nicolet Pro 42C digital oscilloscope was used to monitor voltage across and the current through the test fuse. From the curves of voltage and current, the energy in the arc was calculated as well as the let-through energy  $\int i^2 dt$  in each case. Insulation resistance of the fuse fulgurite was measured one minute after each test. The internal and external diameters of the fulgurite were also measured. In some cases, the fulgurite cross section was highly irregular and an average diameter was taken. Care was taken to extract the full length of the fulgurite to measure its mass. The maximum arc voltage developed across the fuse was also noted. The results of these measurements for a range of fillers are shown in the Table 1.

## IV. DISCUSSION

The current was successfully interrupted only with the sand and boric acid fillers. It starts to decrease immediately after the arc ignites for the case of sand, but continues to increase for a few milliseconds for boric acid. There is a clear distinction between the fulgurite of sand with those of the other fillers. In case of sand, the fulgurite is very strong and robust and the internal diameter is the smallest noted so that the arc diameter is the minimum in this case. The fulgurite shape is also regular in case of sand where in almost all other cases the fulgurite was irregular indicating arc instabilities. In many cases simple visual inspection of the fulgurite can enable one to predict whether the fuse has been successful in interruption or not.

Post-arc resistance of the fulgurite for these materials shows interesting results. In case of sand and boron trioxide, the insulation resistance exceeded 100 M $\Omega$  in about 20 seconds after the tests indicating their high dielectric strength. The smallest arc  $\int i^2 dt$  value was measured for sand, indicating that it is the most suitable HBC fuse filler material. Furthermore, the arc energy is the highest in the case of sand, which shows it can conduct the heat very effectively to its surroundings.

The high arc energy is a result of the high arc voltage developed due to the constriction of arc channel for sand. We believe that the much of the arc energy is not used to fuse the sand and form fulgurite, but that a large fraction of this energy escapes through the interstices present in the sand to the surroundings. The energy expended to form one gram of the fulgurite here is 2.20 kJ which, compares well with our earlier experimental results discussed in reference [2]. Although grain sizes in other fillers were comparable to those of sand, the heat energy appeared to be contained within the fulgurite that consequently formed larger arc channels. The heat conducting capability of the sand enables it to absorb heat from the arc and conduct it to the surroundings [3]. This feature along with the rapid dielectric recovery makes sand the best filler for current limitation and interruption at heavy currents in high breaking capacity fuses. The results shown in Table 1 also contradict the assumption adopted in reference [4] about the linearity of arc energy with the arc  $\int i^2 dt$ . Figures 2-7 show plots of current and voltage for the fillers investigated as a function of time along with the calculated values of  $\int i^2 dt$  and arc energy.

The behaviour for current interruption is different in expulsion and high breaking capacity fuses. In expulsion fuses, plasma is forced to exit the fuse barrel whereas in case of HBC fuses plasma energy is to be conducted by the fillers to the surroundings. The plasma should remain wholly within the filler of an HBC fuse so that a good liner in an expulsion fuse is not

necessarily a good filler in an HBC fuse. The results show that silica sand is superior filler for HBC fuses than the other fillers tested.

#### Acknowledgements

The authors wish to thank Mr. Gregory J. Toland for his assistance during experimentation.

#### REFERENCES

- [1] M.A. Saqib, A.D. Stokes, B.W. James and I.S. Falconer, "Measurements of electron density in a high-voltage fuse arc", Proceedings of the sixth ICEFA, Turin, Italy, September 20-22, 1999.
- [2] M.A. Saqib, A.D. Stokes and P.J. Seebacher, "An insight into the fulgurite of a high-voltage fuse" Proceedings of the third annual international conference on Industrial Engineering Theories, Applications and Practice, Hong Kong, December 28-31, 1998.
- [3] D. Konig, J. Trott, H.J. Muller and B. Muller, "Switching performance of high-voltage fuse-elements in different solids and gaseous filling media", Proceedings of the third ICEFA, Eindhoven, Netherlands, May 11-13, 1987.
- [4] J. Paukert, "Search for new extinguishing media for LV fuses", Proceedings of the third ICEFA, Eindhoven, Netherlands, May 11-13, 1987.

Table 1: Results of measurements of arc and fulgurite properties for a range of fillers.

	Sand (SiO <sub>2</sub> )	Al (OH) <sub>3</sub>	TiO <sub>2</sub>	B <sub>2</sub> O <sub>3</sub>	ZnO	Boric acid
Arc energy (kJ)	46.72	42.50	30.13	42.58	28.74	30.18
Arc $\int i^2 dt$ (*10 <sup>3</sup> amp. <sup>2</sup> -sec)	34.17	70.06	132.22	75.05	135.40	72.01
Weight of the fulgurite (gms)	21.22	12.60	25.00	69.61	20.00	130.00
Internal dia. of fulgurite (mm)	3.70	13.92	23.60	10.00	28.50	18.00
R (after 1 min.)	> 100 MΩ	0.075 MΩ	0.8 MΩ	> 100 MΩ	0.4 MΩ	0.8Ω
Current interruption?	Yes	No	No	No	No	Yes
Max. arc voltage (kV)	9.888	7.752	7.200	7.992	6.136	7.968

0.5 mm  
approx  
grain size

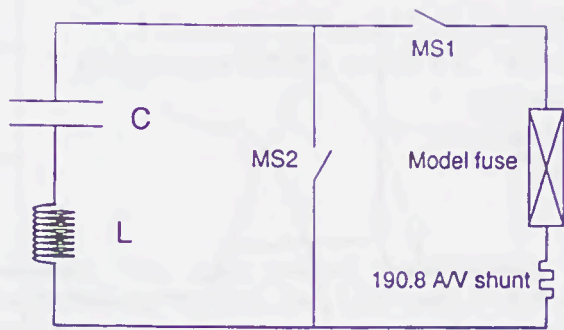


Figure 1: Electrical circuit to energise the test fuse.

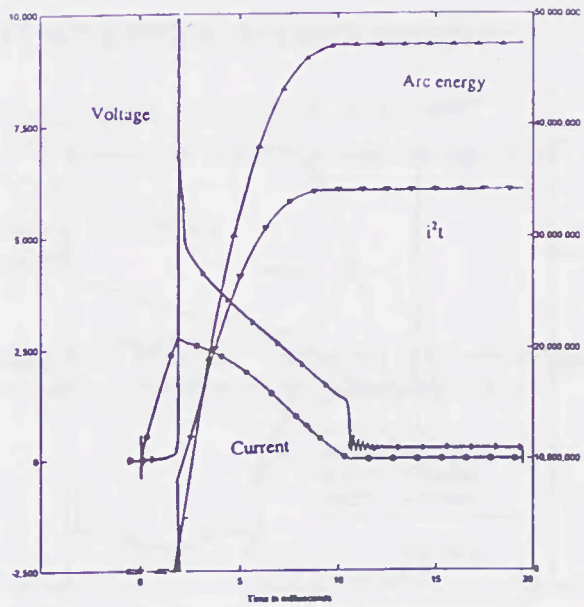


Figure 2: Plots for current and voltage (on left side) and arc energy and arc  $i^2t$  (on right side) for silica sand.

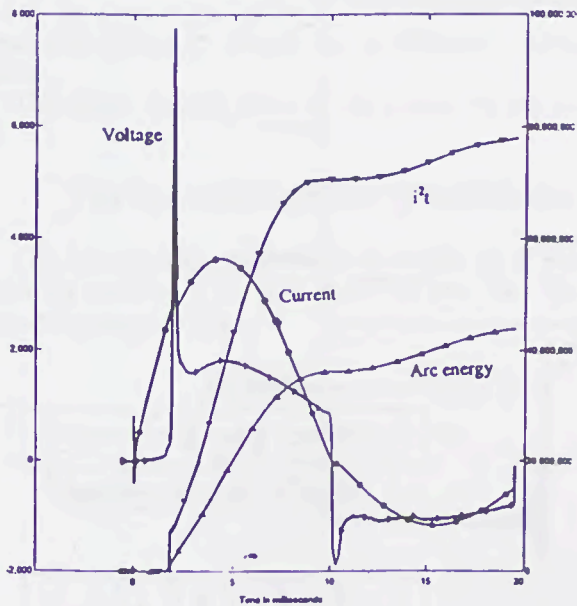


Figure 3: Plots for current and voltage (on left side) and arc energy and arc  $i^2t$  (on right side) for  $Al(OH)_3$ .

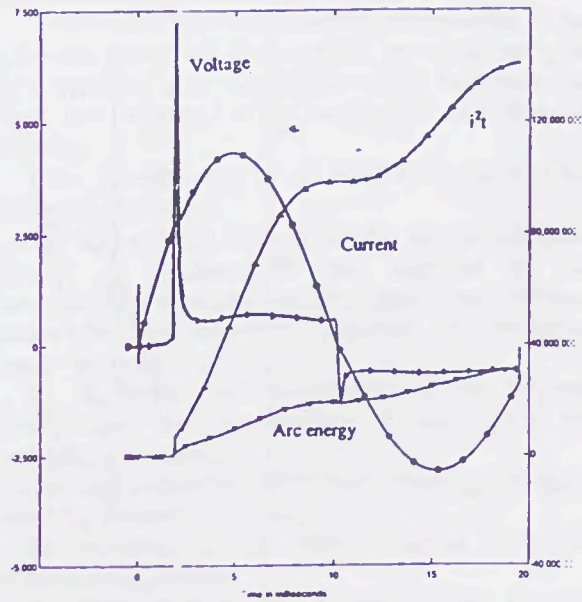


Figure 4: Plots for current and voltage (on left side) and arc energy and arc  $i^2t$  (on right side) for  $TiO_2$ .

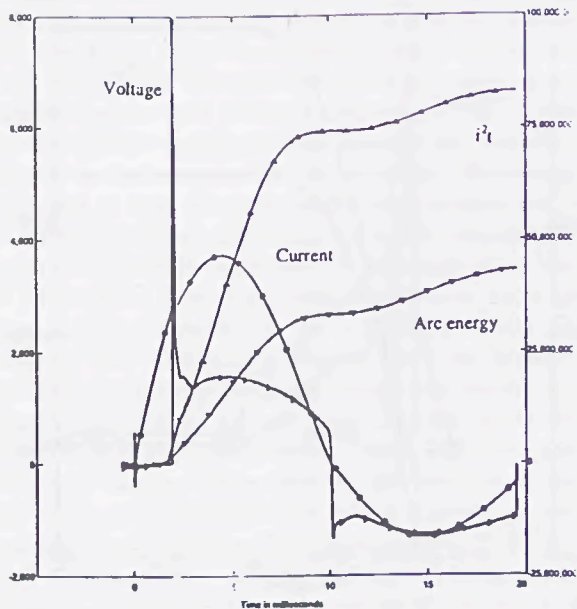


Figure 5: Plots for current and voltage (on left side) and arc energy and arc  $i^2t$  (on right side) for  $B_2O_3$ .

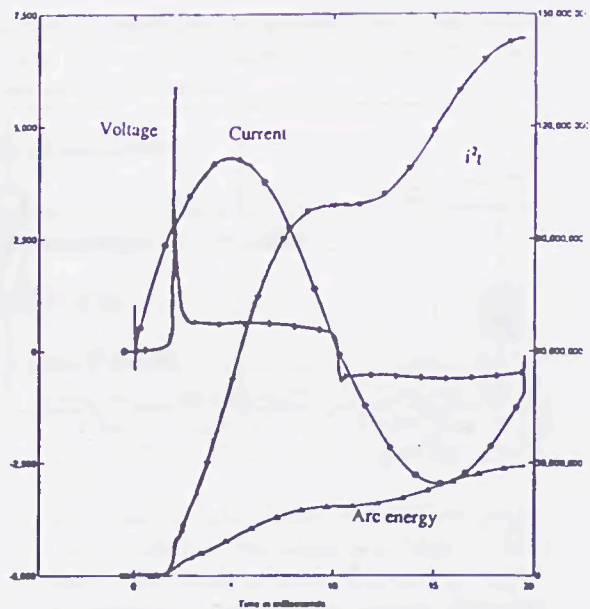


Figure 6: Plots for current and voltage (on left side) and arc energy and arc  $i^2t$  (on right side) for  $ZnO$ .

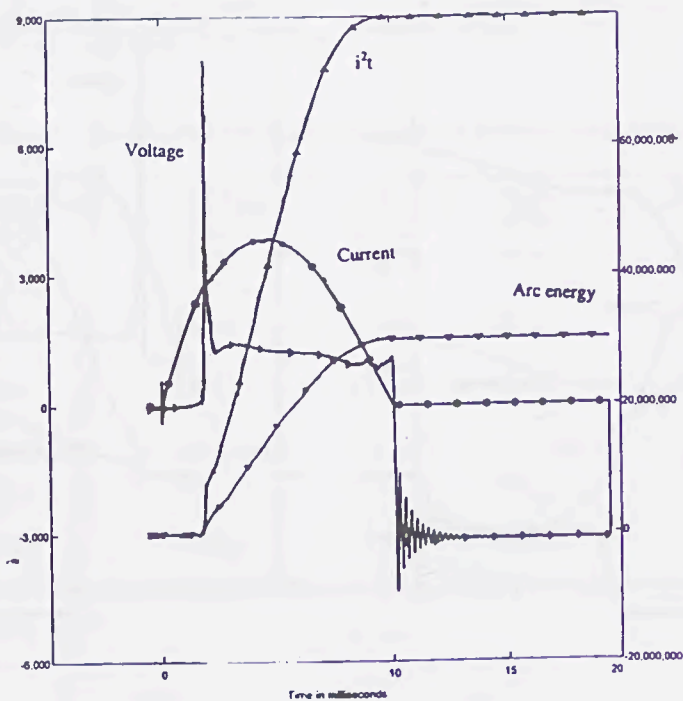


Figure 7: Plots for current and voltage (on left side) and arc energy and arc  $i^2t$  (on right side) for boric acid.

# RECONDITIONING THE HRC FUSE LINKS. A TEST PLANT

I.Ciutea\*, T.Pleşca\*\*, P.Leonte\*\*, O.Dumbravă\*, N.Sufleţel\*, C.Iacob\*

\* Distribution Branch within S.C. "Electrica" S.A. belonging to the National Company of Electricity - "CONEL"

\*\* "Gh.Asachi" Technical University  
Iaşi - Romania

**Abstract:** This paper presents a methodology for reconditioning the HRC fuse links made in Romania and a plant for testing and assigning the protection characteristics related to the reconditioned fuse cartridges.

## I. GENERAL CONSIDERATIONS

The Distribution Branch within the S.C. "Electrica" S.A. belonging to the National Company of Electricity - "CONEL", in co-operation with the "Gh.Asachi" Technical University, both of them residing in the city of Iaşi - Romania, have organised the reconditioning of the replacing elements of the HRC fuse links, the rated current series 63...300 A according to [1], used in the low voltage distribution networks of the country with short-circuit currents under 20 kA ever since 1986.

The reconditioning and exploitation activities led to certain improvements of the replacing elements [2,3] and to the conceiving, designing and achieving of an installation meant to control the reconditioned fuses quality.

This paper presents some of the results we got so far.

## II. THE RECONDITIONING TECHNOLOGY

The fuse links are punched out of copper tin of the following calibres: 0.10; 0.15 and 0.20 mm with the geometric shapes in Fig 1

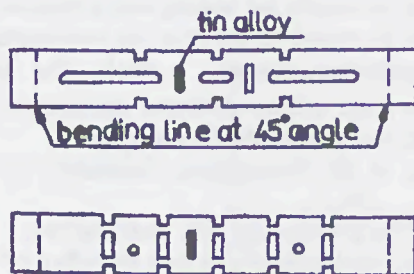


Fig.1 Punched fuse links used in reconditioning the replacing elements

The extinguishing medium of the electric arc is the quartz sand retrieved by drying and sifting from the wasted fuse cartridges, sometimes supplemented with

sand from Miorcani - Romania. The reconditioning technology comprises the operations listed in Fig.2.

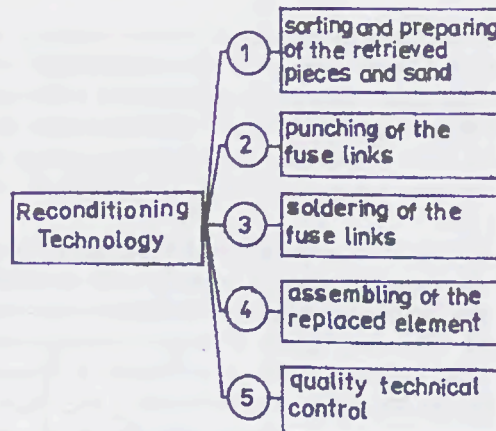


Fig.2 The reconditioning technology

The wasted replacing elements corresponding to the retrieving criteria are disassembled, sorted according to their types and sizes (metallic pieces, the fuse body, the sand) then subjected to the mechanical and chemical cleaning.

The reconditioning of the HRC fuses presents the following advantages:

- prime cost reduced down to half for the reconditioned element as compared to that supplied by the manufacturing enterprise resulting from: the retrieved pieces, the transport-storing expenses, the enterprise employees manual labour;
- the improving and modernizing of the existent constructions and the finding of new better for exploitation solutions;
- the prompt and without difficulties ensuring with spare replacing elements;
- the recycling of the wastes resulted from the reconditioning process;
- the diminishing of the expenses made for the exploitation of the power distribution installations.

## III. THE TESTING INSTALLATION

The basic component of the installation is an electromagnetic device, Fig.3, permitting the variation of the electric current through tests within very large limits, in steps and continuously.

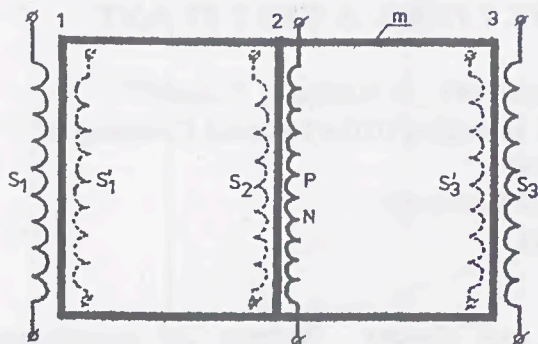


Fig.3 Adjusting electromagnetic device

The device has a ferromagnetic core  $m$ , similar to the three-phase transformers, with three columns, 1-2-3, identical or to the monophaser transformers with cased core which has a primary  $P$  with a number of turns  $N$ , a secondary  $S_2$  or several ones on the central column, the lateral columns having one or more secondaries ( $S_1, S_1', \dots; S_3, S_3'$ ).

The primary  $P$  is assembled between the phase and the null of the network (source), in series with the tested object, and the device behaves as an inductive reactance adjustable within large limits, in steps and continuously through: the variation of the turns number  $N$  between two limits, the secondaries short-circuiting, the variation of secondaries short-circuited turns number by coupling an adjustable autotransformer to the clamp of one of the secondaries.

The measuring of the testing current can limitedly use current transformers with ferromagnetic core, coaxial shunts also permitting the oscillography (of the current derivative with a derivative electronic block included), air-core transformer (TMA) requiring integrating circuit for currents (RC), or, more adequately, the transformer orthogonal magnetization (TMO), Fig.4, [4,5].

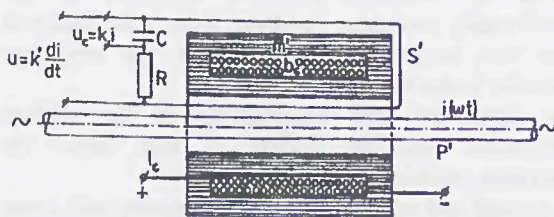


Fig.4 Measuring transformer with orthogonal magnetization

It has a ferromagnetic core  $m$ , spiral toroidal coil with rectangular section and a window for the command coil,  $b_c$ , crossed by the direct current  $I_c$ , the primary  $P$  being a bar or a cable (with one or more passes) crossed by the testing current  $i(\omega t)$ , and the secondary  $S'$  (more simply represented by one single turn) has an adequate circuit RC. The TMO functioning is similar to that of the TMA [5]. To get this thing it is necessary that the hysteresis cycle, the  $B(H)$  or the  $u_c(I_m)$  characteristics became a

straight line, Fig.5, whose slope  $\alpha$  depends on the  $I_c$  current, a transformer with a variable transformer ratio, easily adaptable to the apparatus of measuring and recording current and its derivative resulting.

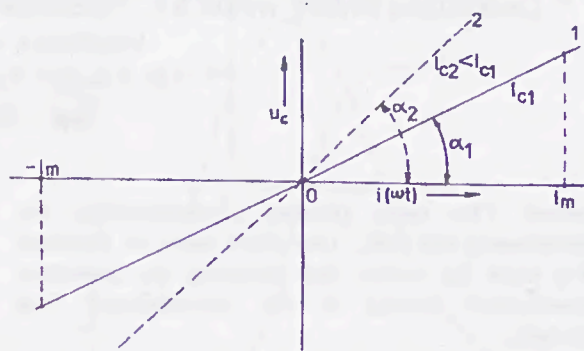


Fig.5 The  $u_c(I_m)$  characteristic of transformer orthogonal magnetization

The installation possesses the principle force circuits according to Fig.6, comprising between the phase (R) and the null (O) an automatic circuitbreaker  $I_a$  for remote or manual switching on/off; a short-circuiting device  $S_c$  associated with a command block  $B_c$  meant to connect the circuit to a prescribed phase  $\varphi = \omega t$  of voltage; the adjusting electromagnetic device DE to adjust the current in steps by means of the relay switches  $c_1-c_1', c_2-c_3'$ , and continuously by means of the autotransformer ATR as well as with the turns number  $N$  of the primary  $P$ .

To measure the currents two possibilities are provided: the current transformer TI associated with the ammeter  $A$  in the case of the long-lasting currents and TMO for the measuring and the oscillography the currents and their derivatives through the circuit RC. An oscillograph with memory can record and visualize the phenomena that may be taken over by a computer.

The testing fuses are set in an enclosure  $K$  in order to simulate the exploitation conditions, having in parallel a voltmeter  $V$  for the control of the voltage in stationary state after the fuses burnt, a thermometer with thermocouple  $t^0$  to control the heating and a resistive  $R_u$  voltage divisor  $D_u$  meant to perform the oscillography of the reestablishing voltage,  $u_r(\omega t)$ . The time measurement is made with an electronic chronometer.

The installation permits the following tests:

- the checking of the characteristic parameters of the HRC fuses;
- the tracing of the time-current,  $t(I)$ , characteristic;
- the measuring, oscillography and recording of the testing currents and of their derivatives;
- the oscillography of the reestablishing voltage;
- the measuring and recording of the components of the fuses in stationary and transient state heatings.

The installation can also be used for the testing of any product as regarding its behaviour at the variation of the currents within the limits prescribed for it.

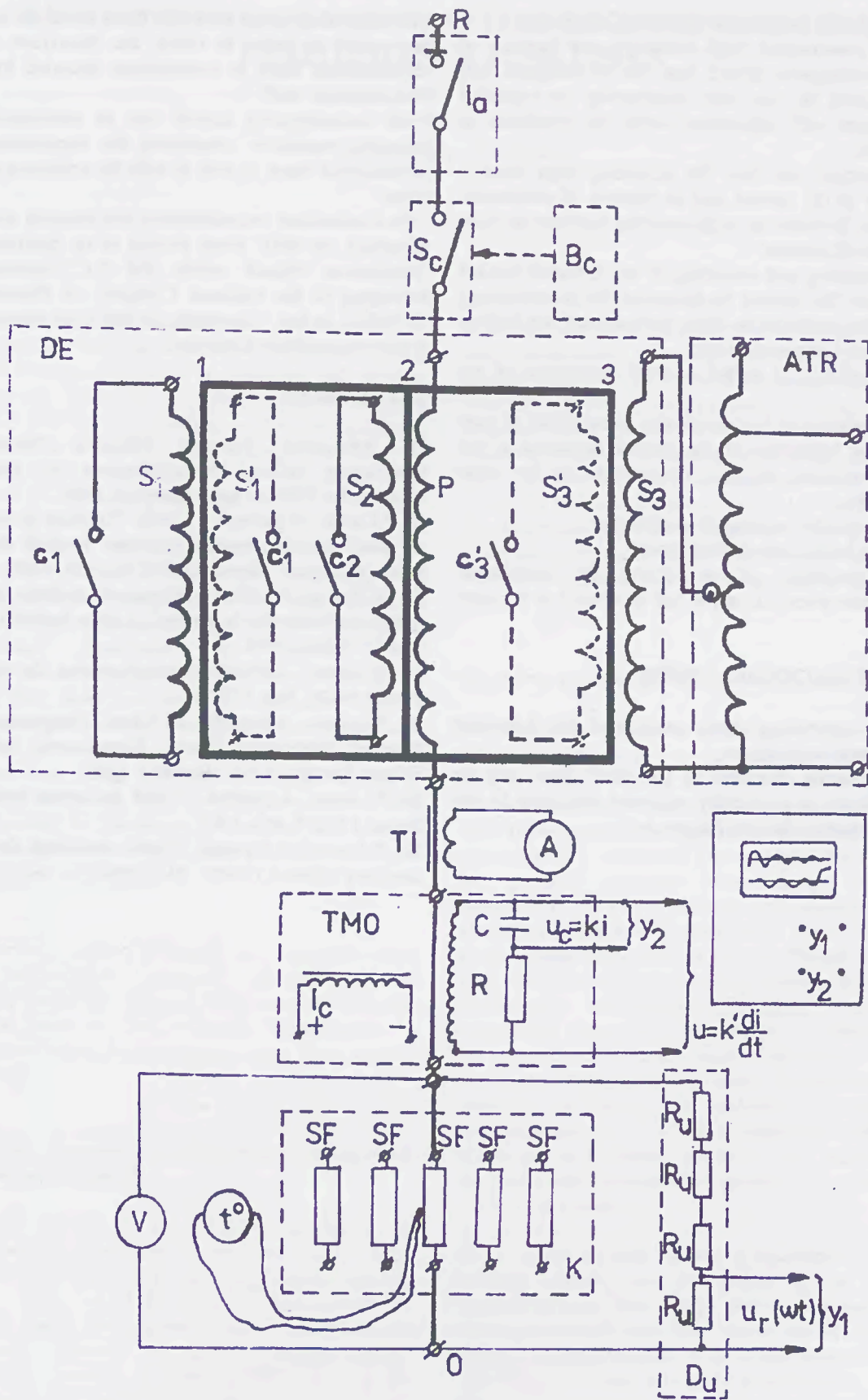


Fig 6 The testing installation circuit

The installation presents the following advantages:

- simple construction, high reliability and duration of the electromagnetic device that can be designed and manufactured by any unit constructing or repairing transformers with adjustment under the condition of voltage on;
- the structure can have the adjusting steps number necessary to the current and an interval of continuous adjustment between the steps covering together the field of presumed currents;
- the measuring and recording of the elements needed by the tests (the current, its derivative, the reestablishing voltage, the temperature of the environment, the heating of the fuses component parts);
- the possibility of partial or total automation of the tests;
- the adaptation of the installation to any kind of tests concerning behaviour of the electric apparatus at the current variation, of their components or for other equipments;
- great flexibility in using the installation;
- it can be built at any desired power;
- the possibility of re-utilizing the installation components when it is not in use or when it is no more used.

#### IV. FINAL CONCLUSIONS

From everything above mentioned the following conclusions can be drawn:

- the replacing elements of the HRC fuses can be reconditioned in a specially equipped workshop by the great companies that use this product;

- the enterprises using the HRC fuses could set up their own stand in order to check the behaviour of the reconditioned fuses at overcurrents attended by their own technical staff;
- the reconditioning activity can be associated with scientific researches concerning the exploitation and perfecting of fuses, as well as with the achieving of new types;
- the concomitant reconditioning and research activities regarding the HRC fuses proved to be profitable for Distribution Branch within the S.C."Electrica"S.A. belonging to the National Company of Electricity – "CONEL" in Iași – Romania, so that their continuation is sure to constitute a real aim.

#### REFERENCES

- [1] Ministerul Energiei Electrice "Instrucțiuni tehnologice privind recondiționarea în atelier a siguranțelor MPR de joasă tensiune", 1986.
- [2] P.Leonte, N.Suflețel, I.Ciutea, "Element de înlocuire de joasă tensiune pentru siguranțe fuzibile de mare putere de rupere", Brevet 114052 B1, RO, 1998.
- [3] T.Pleşca, P.Leonte, "Siguranță fuzibilă specială pentru redresoarele de putere", Cerere brevet invenție 98-01739, RO, 1998.
- [4] P.Leonte, "Bobină și transformator de măsură", Brevet 56426, RO, 1972.
- [5] P.Leonte, A.Baraboi, M.Adam, "Magnetizarea în câmpuri ortogonale. Teorie. Experiment. Aplicații", Editura Spectrum, Iași, România, 1998.
- [6] P.Leonte, A.Baraboi, "Trusă de curent modulară", Brevet 112829, RO, 1983.
- [7] P.Leonte, E.Furnică, "Sursă modulară de curent continuu", Brevet 109491, RO, 1995.

# ENVIRONMENTALLY COMPATIBLE RECYCLING OF HIGH PERFORMANCE FUSE LINKS

Gerd Fink  
Siemens AG  
Regensburg - Germany

Everyone knows how important the environment is to us all and how we must all do whatever we can to help protect it. Industry too has an important role to play, not only by employing manufacturing processes that cause as little harm as possible to the environment in the first place but also by ensuring that when its products come to the end of their lives they can be disposed of safely and efficiently.

*The task of the Verein zur Förderung des umweltgerechten Recycling von abgeschalteten NH/HH-Sicherungseinsätzen e.V., a non-profit association established by German fuse manufacturers, is to process the various materials of which fuse links are made so that they can be returned to the cycle of manufacture for further use. In 1998, for example, the association collected and recycled more than 140 tonnes of materials. It is currently estimated that, in Germany alone, this figure could be increased to around 600 tonnes. Other manufacturers and users are being encouraged to participate in the project.*

The practice of simply disposing of old products at the refuse tip without a moment's thought for their recycling potential is not only frowned upon these days from the point of view of social responsibility for future generations but, in many cases, it is actually illegal too.

## **The law demands environmentally-compatible recycling and disposal**

Article 1 § 22 of the German legislation on environmentally-compatible recycling and waste disposal states that products must be designed in a way which, at the end of their service life, allows the materials which they are made of to be recycled and any waste disposed of in an environmentally-compatible manner. Another requirement of the legislation is that products must be returnable and any recyclable waste must be used again.

Since most products are made of a very wide variety of different materials it is no easy task to take them apart and recycle each raw material separately. Plastics, for example, are often joined by thermowelding processes whereas other parts are either screwed, bolted, soldered, welded or bonded. This means, of course, that disassembly is very labor-intensive and therefore costly. In addition, the process of disassembly also has its dangerous side, such as when asbestos gaskets, glass-fiber-reinforced plastic parts, solders containing harmful substances, etc. have been used in the original items.

## **Recycling symbols clarify matters for users**

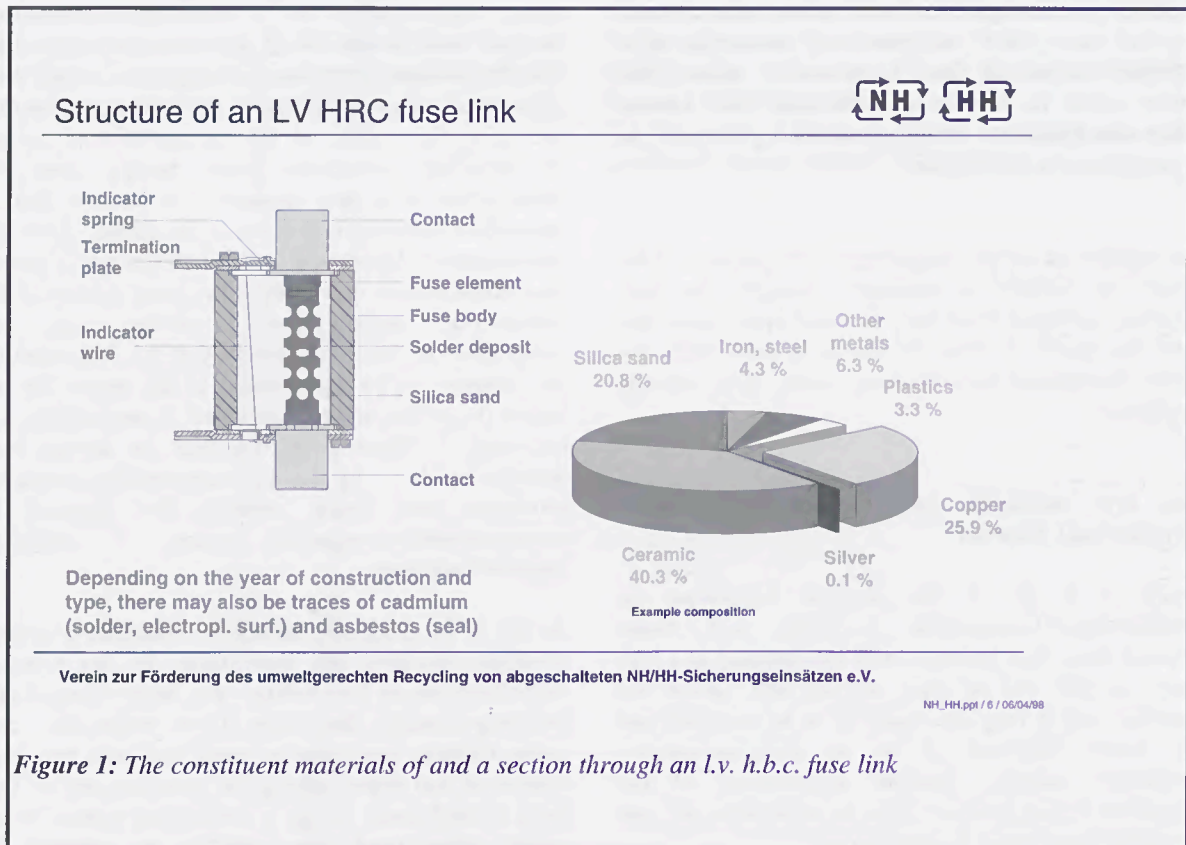
Environmental protection and waste disposal do not come free-of-charge so a thorough fundamental analysis must be carried out first in order to determine whether recycling, disposal or separation is the most appropriate course of action as far as the environment and safety are concerned. For example, if the process of recycling consumes more energy than the manufacture of a new product it is obvious that an alternative solution will have to be found. Also, the environmental legislation in Western Europe is stricter than elsewhere so inevitably it becomes a factor in the commercial market-place involving, say, our competitors in Asia. This means that it is important for the customer to be made aware of the reason for any higher price that might be involved. Consequently, it is necessary to identify the products as having been manufactured by environmentally-compatible processes and being suitable for disposal by environmentally-compatible means - "recycling symbols" are used.

As far as the electrical industry is concerned, a ground-breaking initiative has been taken by the German manufacturers of low-voltage and high-voltage high-breaking-capacity fuse links. Even before the most recent German legislation on recycling came into force customers had begun asking the manufacturers of fuse links if they could set up a methodical system which would allow used fuse links to be returned for environmentally-compatible disposal. As a result, several fuse manufacturers began offering and charging

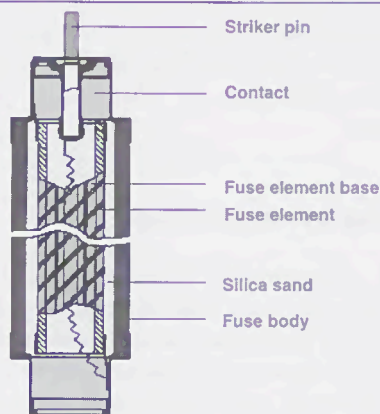
for a disposal service for used fuse links. Then, in 1995, with the aim of putting the subject of environmentally-compatible disposal on a regular footing, a number of the manufacturers involved (Fritz Driescher KG, Efen GmbH, M. Schneider-Annaberg GmbH, Jean Müller GmbH, Siba GmbH and Siemens AG) joined forces with the ZVEI (Zentralverband Elektrotechnik- und Elektronikindustrie) and, through an initial working party, established the non-profit-making "Verein zur Förderung des umweltgerechten Recycling von abgeschalteten NH/HH-Sicherungseinsätzen", otherwise known as "NH/HH-Recycling", registered in Regensburg and with its Head Office in Frankfurt.

### Recycling the products and materials of 20 years ago

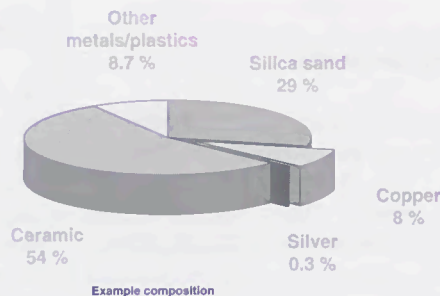
For many applications, fuse links represent a relatively cheap and safe way of providing protection for electrical systems and equipment. L.v. h.b.c. (NH) fuse links (low-voltage high-breaking-capacity) are used in low-voltage installations and h.v. h.b.c. (HH) (high-voltage high-breaking-capacity) fuse links in medium-voltage installations. The volume of the l.v. h.b.c. fuses varies between 45 and 900 cm<sup>3</sup> (5 to 15 cm long and 3 to 10 cm wide). The h.v. h.b.c. fuses, on the other hand, are substantially larger: 20 to 65 cm long and 5 to 8.5 cm in diameter. The service life of these fuses, provided they are not called upon to blow, is approximately 20 years, which is well above the average life of most other types of electrical equipment. This means that, with these long-life products, recyclers are having to deal with materials that were in common use 20 years ago. In "old" fuse links, for example, asbestos was still being used as a jointing material. Fig. 1 shows a cross section through an l.v. h.b.c. fuse link and lists the other materials used in its construction; similarly Fig. 2 illustrates an h.v. h.b.c. fuse link.



## Structure of an HV HRC fuse link



Depending on the year of construction and type, there may be slight amounts of asbestos (seal)



Verein zur Förderung des umweltgerechten Recycling von abgeschalteten NH/HH-Sicherungseinsätzen e.V.

NH\_NH.ppt / 5 / 06/04/98

Figure 2: The constituent materials of and a section through an h.v. h.b.c. fuse link

### The result: copper, silver and materials for the building trade and the chemical industry

The percentages of different materials also listed in Fig. 1 show that the recycling and re-use of copper and silver is thoroughly worthwhile and, as "valuables", do not deserve to be included amongst the residual waste or dumped on the refuse tip. The classic alternatives of disassembly or shredding offer the possible means by which the materials can be recovered.

Although disassembling these fuse links is a labor-intensive process, some successful projects have been set up, e.g. with power utilities and disabled people's organizations working together, in which the fuses are disassembled and the valuable materials they contain recovered so that they can be returned to the manufacturing cycle. The actual cost of disassembly is not covered by the profit obtained from the raw materials so the disabled people's organizations have to make a small charge for each fuse. The asbestos joint gaskets mentioned previously also cause some problems with disassembly.

The strict rules that apply when working with asbestos make disassembly a complex and costly process - as also is shredding or processing by pan grinder (a crushing process producing coarser results than a

shredder) with subsequent melting down in the blast furnace. This situation has led to further tests being carried out in conjunction with a copper smeltery which have demonstrated that fuse links can be processed directly in a converter without any pre-processing at all. Under normal circumstances it is necessary to add quartz sand during the process in order to produce slag and promote the precipitation of iron. Since the fuse links that are being melted down already contain around 30% quartz sand, however, this "waste product" actually helps in the process.

Following an inquiry among various copper smelters and recycling companies throughout the country, the Norddeutsche Affinerie in Hamburg was eventually chosen because of its capacity and environmental capabilities.

For direct processing in copper converters the fuse links must normally satisfy the following specification:

- Plastics content less than 3.5%
- Asbestos content less than 0.05%
- Cadmium content less than 0.005%

The plastics are utilized to produce heat with continuous monitoring of the flue gas. During the melting, any zinc that originates from, say, brass

contact blades is converted into zinc dust and collects in the plant filters. However, this is not a problem provided the total amount of zinc remains below 50 tonnes per annum - as it will given the total amount of recycling anticipated. The ceramic body of the fuses and the quartz sand are converted to slag that can be used again for road building and in the concrete industry. Another end-product, sulfuric acid, can be re-utilized by the chemical industry. The asbestos is rendered harmless by being incorporated into the slag.

### Research benefits from the profits

Most of the l.v. and h.v. h.b.c. fuse links come from the country's power utilities and general industry. They are usually collected in "egg box" pallets placed at specified collecting points. The various sales organizations, which also function as collecting points, provide information for smaller users, such as electrical contractors and installers, on the recycling facilities that are available. Nedlloyd Unitrans, with branches all over Germany, has been awarded the contract for collecting the egg-box pallets when they are full and transporting them to the company's own buffer store. When a collecting point has full pallets to be collected it notifies the transport company by fax and the pallets are then collected within three days and replaced with new empty pallets.

When a sufficient quantity of fuse links has accumulated in the buffer store, the haulier delivers them to the copper smeltery and invoices "NH/HH-Recycling" for its work. There are no charges to users for any aspect of the logistics involved or the recycling process.

The costs incurred by "NH/HH-Recycling", e.g. for transporting the egg-box pallets, for processing and

refining the copper and silver and for the production of information brochures and advertising, are offset by the income obtained from selling the copper and silver. At current price levels, "NH/HH-Recycling" is able to achieve a modest surplus, which, in conformance with its memorandum and articles, is spent on further research into the recycling of fuse links - the Technical University of Ilmenau is one of the recipients.

### Spreading throughout Europe

In 1997, approximately 125 tonnes of used l.v. and h.v. h.b.c. fuse links were collected and recycled; in 1998, by the end of December, the collected total had already reached 145 tonnes. For Germany alone the estimated annual figure of used fuse links is approximately 600 tonnes so it can be seen that the potential of recycling is very considerable indeed. Over the next few years "NH/HH-Recycling" expects the collected total figure to increase to around 300 tonnes per annum, which it regards as perfectly feasible in view of the rate of increase that has been achieved so far (Fig. 3).

"NH/HH-Recycling" intends to also enable foreign customers of the member companies to have their old fuse links disposed of by environmentally-compatible means. The organization's trade-marks have already been registered in more than 28 countries and inquiries about the concept of the recycling process have been received from Austria and Sweden.

*Dipl.-Ing. Gerd Fink (49)  
President of NH/HH Recycling and Senior Engineer of  
the materials research department at Siemens AG,  
Regensburg (Germany).*

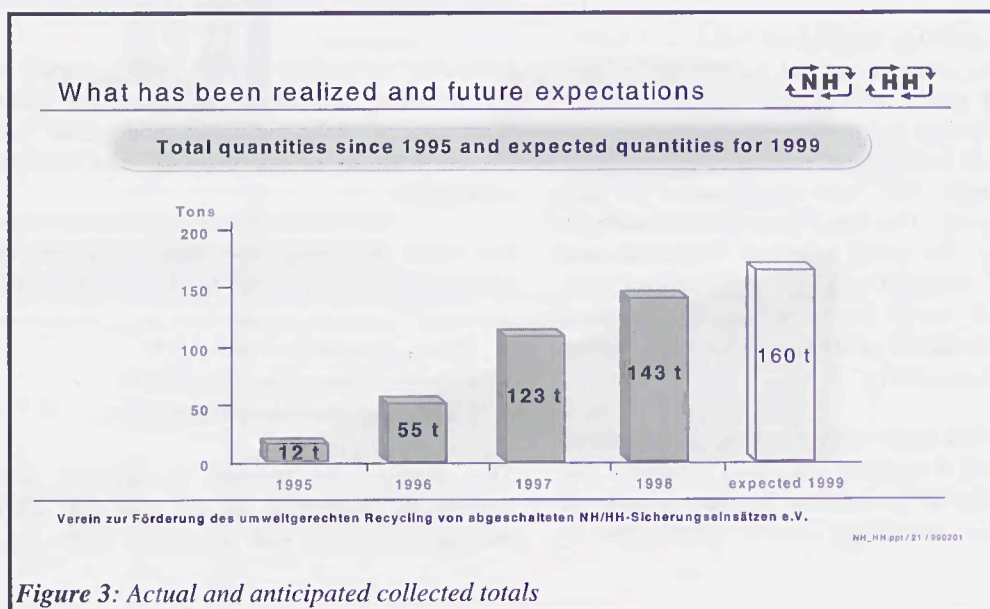
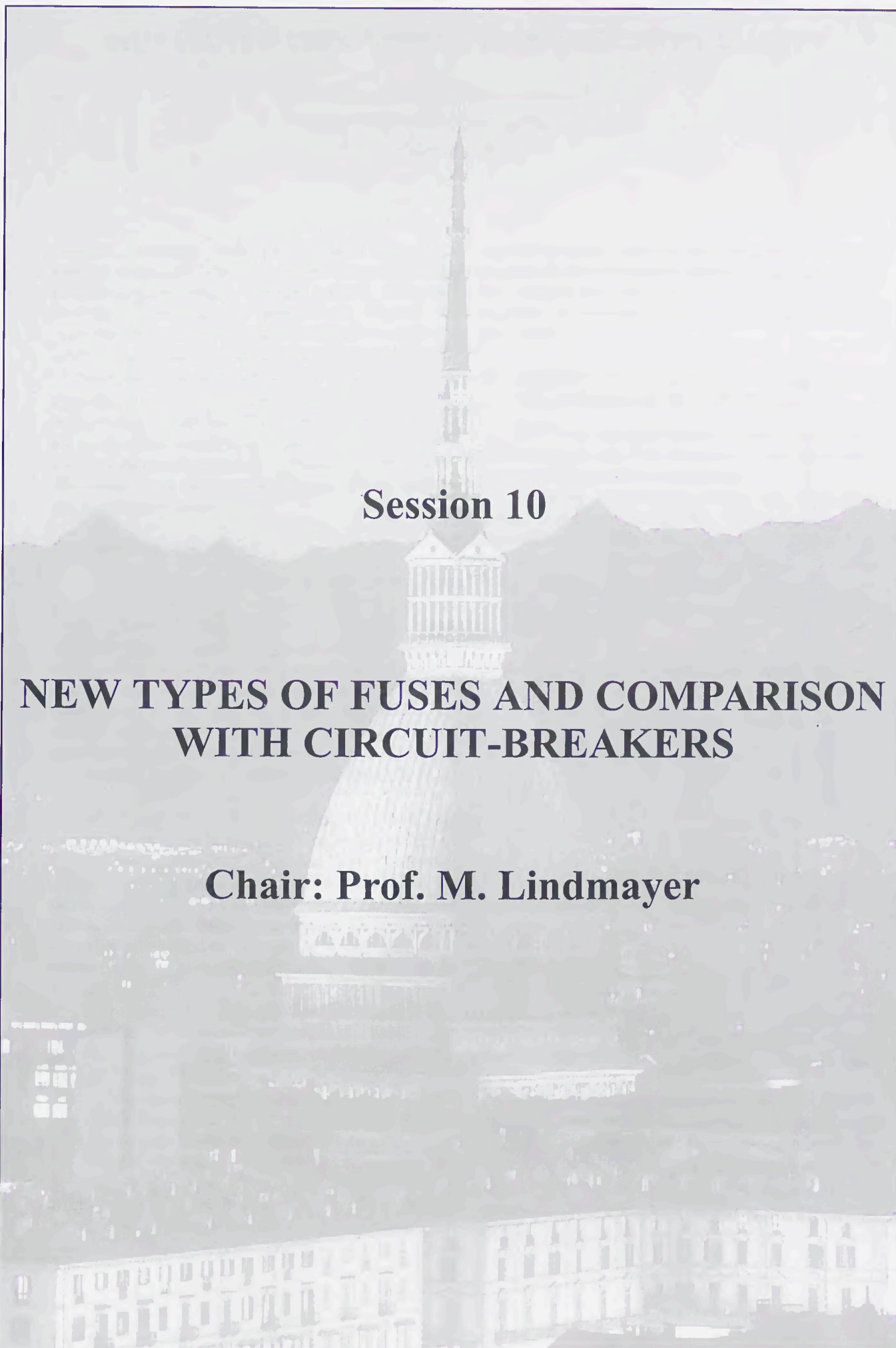


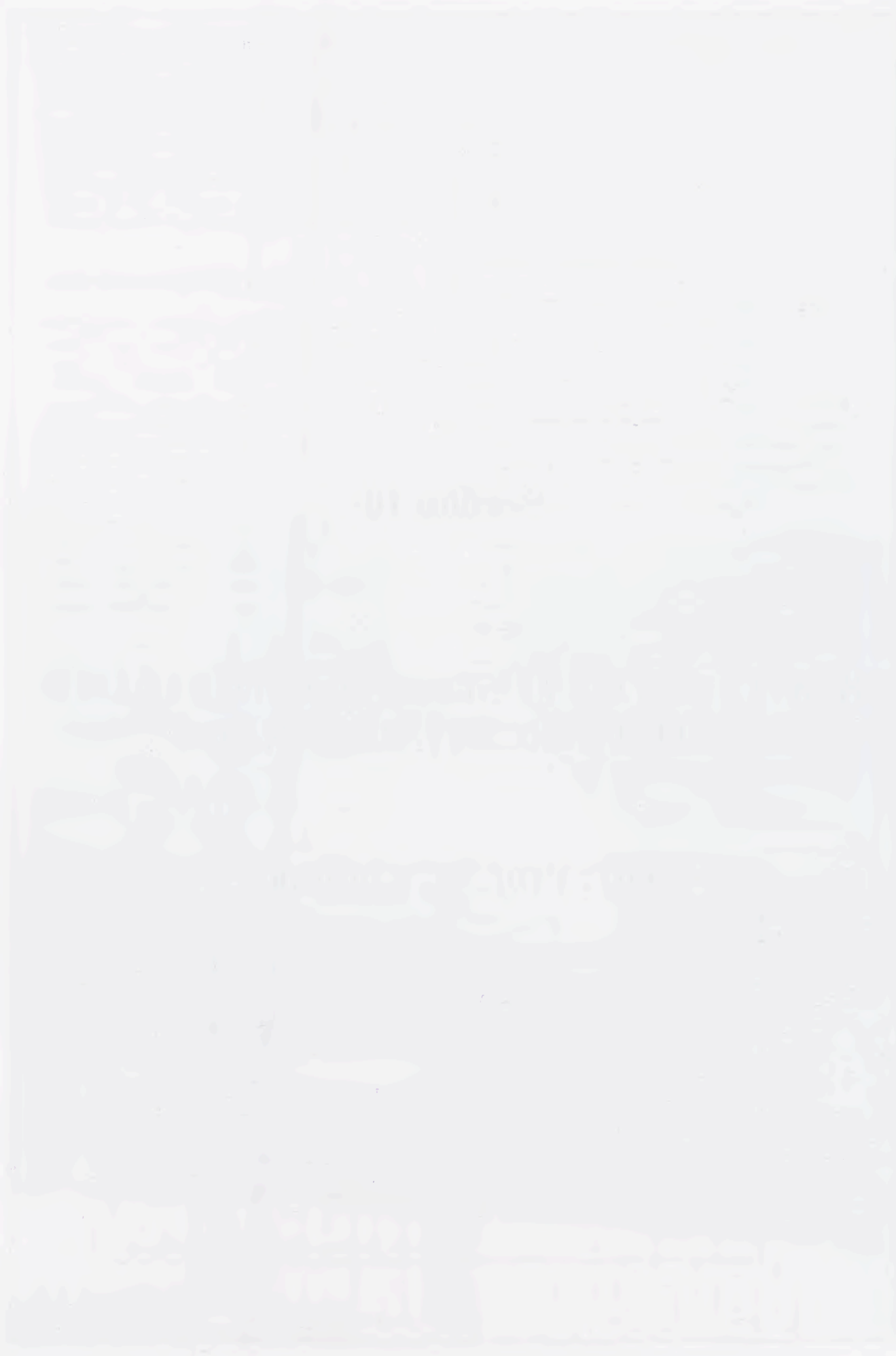
Figure 3: Actual and anticipated collected totals



**Session 10**

**NEW TYPES OF FUSES AND COMPARISON  
WITH CIRCUIT-BREAKERS**

**Chair: Prof. M. Lindmayer**



# MINIATURE LAYER FUSES OF HIGH BREAKING CAPACITY

Sulikowski J., Ćwidak K., Ossowicki J.  
Electrotechnical Institute, Gdańsk Branch  
Gdańsk - Poland

**Abstract:** Miniature layer fuses possess thin fuse-element (e.g. silver) placed between two insulating plates (e.g. glass-crystal). They are destined, before all, to protect semiconductor systems and devices. To overcome the problem of critical overload currents is a key factor in widening of the application of such fuses.

The authors, by application of the glaze layer doped by metal oxides or carbonates obtained a considerable improvement of the breaking capacity, particularly of the critical overload currents. During interrupting of the overload currents lower than 12 times of the fuse rated current the arcing time became distinctly shorter and the arc quenching very effective.

## I. INTRODUCTION

Modern semiconductor elements and systems need the fuses with increasing technical requirements. The fuses, before all, shall indicate a distinctly lower operating  $I^2t$ , high speed  $t$ - $I$  characteristic and a small susceptibility on the mechanical and thermomechanical ageing. Such features shall be achieved by manufacturing cheap and of small dimensions fuses [1]. In the case of semiconductor elements and systems of low rated power the only fuses which can fulfil above requirements are the miniature layer fuses (MLF) [2, 3, 4, 5].

MLF possess a thin fuse-element (often Ag) usually placed between two insulating plates made, e.g. from alumina, quartz or pyroceram. The Ag-element commonly is deposited on an insulating substrate not direct but using one or two intermediate metallic thin layers. These additional layers provide an appropriate fuse-element adhesion to the substrate despite a considerable temperature fluctuations of the fuse in service.

Experiments [4, 5, 6] show that the known MLFs demonstrate a considerable difficulty during the overload current interruption, specifically in DC circuits. Above difficult critical current range is 3 to 12 times of the fuse rated current. Similar behaviour shows also MLF, despite the arc is quenched in the narrow slots between the insulating plates.

Gdańsk Branch of Electrotechnical Institute for several years has been carried out investigations of the MLFs within arc quenching in a pyroceram slot. In spite of achieved a considerable short-circuit breaking capa-

city, the problem was with the interruption of already mentioned critical overload currents. Only introducing the essential processing and designing modifications, described in the paper, gave fully positive solution to the problem.

## II. REASONS FOR EXISTING OF THE CRITICAL OVERLOAD CURRENTS RANGE

MLFs can correct interrupt a current if the energy delivered to the arc from the circuit will be lower than one absorbed by that arc surrounding.

At large short-circuit currents the interrupting process is a very quick one (Fig. 1) due to high-speed fuse-element explosion. The speed is so high that the fuse-element volume remains practically constant during this explosion. A supercritical state of the matter has been achieved, what means metal-insulator sudden transformation [7].

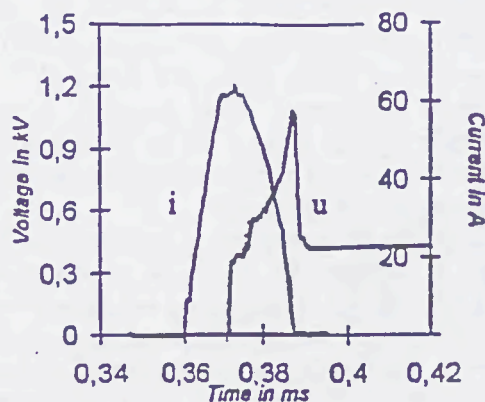


Fig. 1 Records of interrupting of the prospective current ab. 48 kA, 440 V DC,  $R = 9.2 \text{ m}\Omega$ ,  $L = 37.5 \text{ }\mu\text{H}$  by a MLF of rated current 1.6 A, within fuse-element of length 4 mm, thickness  $1 \text{ }\mu\text{m}$ . Supply source a capacitor bank 16.5 mF.

On the contrary, during interrupting of an overload current the speed of fuse-element disintegration is much smaller. The slot walls at the arc beginning are now pre-heated due to relatively long pre-arcing time. As a result the arc-voltage is relatively small causing the arc-time elongation and even noninterrupting of the circuit (Fig.2).

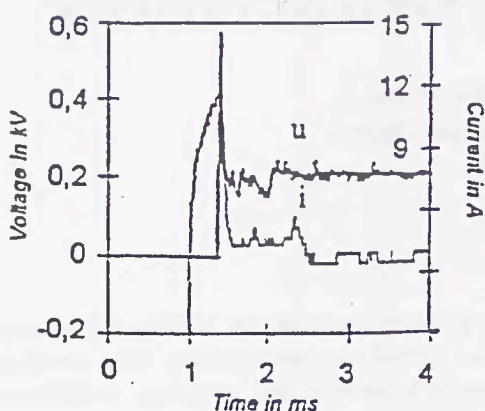


Fig.2 Records of noninterrupting of the prospective current 16 A, 300 V DC,  $R = 18.7 \Omega$ ,  $L = 1.2 \text{ mH}$  by MLF of rated current 1,6 A.

So any improvement of the arc cooling in the critical current region is desirable.

### III. NEW MLFs

Well known are the composite contact materials in which the oxides of some metals ( $\text{CdO}$ ,  $\text{ZnO}$ ,  $\text{SnO}_2$ ) are used as one of the components [8]. In the electric arc a thermal dissociation process of these oxides has taken place. Liberated metal in arc immediately sublimates. Since all these transformations are endothermic, they are extremely advantageous for arc quenching.

Bearing in mind above observations, the authors decided to proof a hypothesis that implementation of the afore-mentioned oxides, particularly during the critical overcurrent interruption, should drastically lower the arc temperature and enhance the arc column pressure. Both processes should extremely positively improve the critical overcurrents interruption.

To confirm the correctness of the hypothesis it was decided to evaluate, for  $\text{CaCO}_3$  as an example, the energy liberated due to dissociation and phase transition of this substance, in the case of a direct action of the arc heat on it. The  $\text{CaCO}_3$  was selected first of all because the reactions of decomposition of the substance are particularly very endothermic ones. The results of calculations are given in Table 1.

Table 1. Energy of thermal decomposition of  $\text{CaCO}_3$  [9]

Energy	kJ/mol	J	Total in J
1	2	3	4
Dissociation $\text{CaCO}_3 \rightarrow \text{CaO} + \text{CO}_2$	200	0,008	0,021
Dissociation $\text{CaO} \rightarrow \text{Ca} + \frac{1}{2} \text{O}_2$	600	0,010	
Phase transition Ca	A 8,7 B 172	0,000 0,003	

A - melting, B - evaporation

To calculate in Joule's the dissociation and phase transition energy in a defined fuse (see heading 3 in Table 1), has been assumed that doped glaze layer is of  $1 \mu\text{m}$  thick and contains 15 % in weight of  $\text{CaCO}_3$ , and that the full reaction embraces ab.  $0.001 \text{ mm}^3$  of this layer. These data evaluated by a microscopic observations.

From earlier authors' measurements it is seen that in the case of overload critical currents the total arc energy usually is from 0.06 up to 0.5 J. From a comparison these values with the given in Table 1 one can conclude that the endothermic reactions during the dissociation of  $\text{CaCO}_3$  in the temperature close to the arc temperature may have a significant influence on the arc temperature diminishing causing the improved arc quenching.

Fig. 3 shows a simplified drawing of the MLF according to the new suggestion. The substrate 1 and plate 2 are made from glaze crystal material. The surface of the plane facing to the fuse-element is covered by a glaze layer of 1 to  $20 \mu\text{m}$  thick, doped uniformly by  $\text{CaCO}_3$  or  $\text{ZnO}$ . The chemical and phase components properties of the basic component of layer are agreed with corresponding properties of the substrate whereas the chemical and phase components properties of the doping material are selected to create an endothermic physical-chemical reaction in the arc, i.e. to generate the dissociation and phase transition.

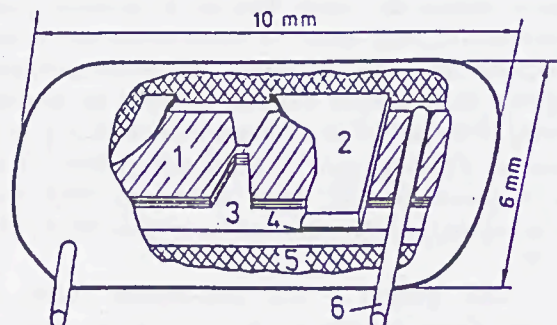


Fig. 3 New MLF of limited critical overload current interrupting ability

1 - fuse-element ( $\text{Ag} + \text{Cu} + \text{V}$ ), 2 - cover plate; 3 - insulating substrate; 4 - doped glaze layer; 5 - hermetic envelope from epoxy resin; 6 - termination

### IV. RESULTS OF TESTS ON MLFs MODEL

Tests of the new MLFs with and without above described doped glaze layer exactly in the same test circuit were carried out. At the beginning the tests were limited to the critical overcurrents which were unsatisfactory interrupted by the fuses without mentioned layer. Two samples of the new MLFs were used for any test current value. The total number of shots was several tenths pieces. In every case all the

new MLFs with glaze layer doped by ZnO or CaCO<sub>3</sub> passed satisfactory the tests.

Fig. 4 illustrates typical test records for new MLF (Fig. A) and MLF without mentioned layer (Fig. B).

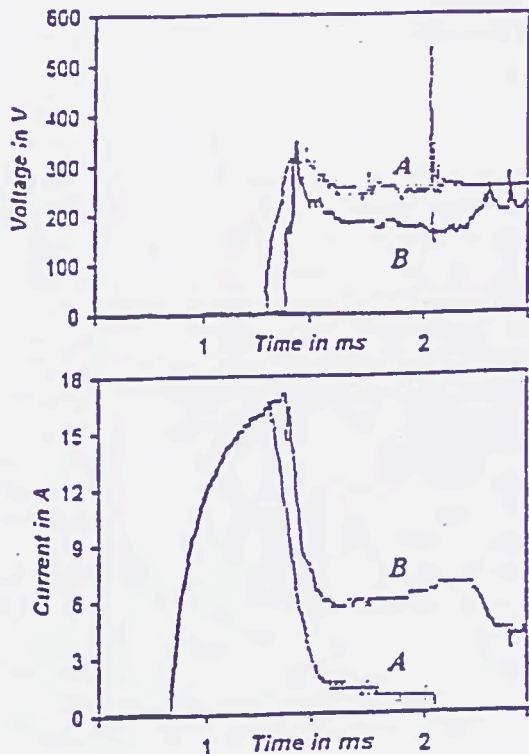


Fig. 4 Records taken from the interrupting tests by MLFs of two kinds. Prospective current 20 A, 250 V DC,  $R = 12.5 \Omega$ ,  $L = 1.7 \text{ mH}$   
A - MLF with doped glaze layer, B - MLF without doped glaze layer.

## V. CONCLUSIONS

The investigations carried out on several tenths MLF with a glaze layer doped by the metal oxides (ZnO) and carbonates (CaCO<sub>3</sub>) made a considerable improvement of the breaking capacity, particularly of the critical overload currents.

The physical-chemical processes taking part in that doped glaze layer make possible to get MLFs: of low-power losses, of small dimensions, of desirable quick acting t-I characteristic, demonstrating very good interrupting ability of the critical overload currents. Moreover they possess a large impulse ageing withstand and a very good current-limiting ability.

By interrupting of the currents greater than 12 times of the MLF rated current up to 50 kA, the arc

voltage trace over the whole arcing period is higher than the source voltage. However, the arc voltage is not higher than 2.5 times of the source test voltage. Due to doped glaze layer by interrupting of the overload currents lower than 12 times of the rated currents the arcing time became distinctly shorter and the arc quenching is a very effective one.

Carried out for the time being investigations are aimed to the experimental justification of the layer thickness and the proportion between its basic and dopic components.

## ACKNOWLEDGEMENTS

The work has been carried out in frames of the research project 8T10A01310 financed by the Committee of Scientific Research in Poland.

## REFERENCES

- [1] IEC Publication 60127-4 "Miniature fuses - Part 4: Universal Modular Fuse-links (UMF)", 1996.
- [2] D. Cogan, M. Henini, "TLM Modelling of Thin Film Fuses on Silica and Alumina", Proc. of the Third ICEFA Conference, pp. 12 - 17, Eindhoven, 1987.
- [3] R.D. Harrison, I. Harrison, A.F. Howe, "Thin film fuse link" Proc. of the Fifth ICEFA Conference, pp. 169 - 175, Ilmenau, 1995.
- [4] J. Ossowicki, J. Sulikowski: "Bezpieczniki warstwowe na podłożu szklano-krystalicznym", Zeszyty Naukowe Wydziału Elektrycznego Politechniki Gdańskiej, No 9, pp. 95-99, Gdańsk, 1966.
- [5] J. Ossowicki, J. Sulikowski: "Postępy w rozwoju bezpieczników topikowych o charakterystyce ultraszybkiej", Zeszyty Naukowe Politechniki Poznańskiej, No 44, pp. 201-208, Poznań, 1997.
- [6] M. Luther, "Flinke Hochleistungs-Metallschichtsi-cherungen, Experimente und Simulation", VDI Reiche 21, No 134, 1993, VDI Verlag, Düsseldorf.
- [7] K. Jakubiuk, "Mechanizmy rozpadu prążkowego eksplodujących przewodów", Zeszyty Naukowe Politechniki Gdańskiej, Elektryka, No 75, Gdańsk, 1994.
- [8] U. Harmsen, "Pulvermetallurgisch hergestellte Kontaktwerkstoffe auf Basis Ag/CdO, Ag/ZnO und Ag/SnO<sub>2</sub>", Information der Firma Dr E. Dürrwächter-Doduco K.G. Pforzheim, No 1/11.
- [9] Praca zbiorowa, "Poradnik fizyko-chemiczny" WNT, Warszawa, 1962.
- [10] M. Lindmayer, M. Luther: "Fusing and short-circuit interruption behaviour of metal film fuses", Proc. of the Fourth ICEFA Conference, pp. 107-113, Nottingham, 1991.



# NEW CURRENT- LIMITING AND INTERRUPTING DEVICE CONTRA CURRENT- LIMITING FUSES

J. Czucha, T. Lipski J. • yborski  
Technical University of Gdansk  
Gdansk - Poland

**Abstract:** Advent of new era in the overcurrent protection of both l. v. and h. v. power electric system which is going to offer a new current interrupting possibility, is a good opportunity to compare the classical current limiting fuses (CLF) and the new hybrid current- limiting and interrupting devices (H-CLID). The last, also developed in the Technical University of Gdansk (TU Gdansk), in a comparison given in the paper, show their advantages and disadvantages and their preferential fields of applications. Despite their costs the H-CLIDs are promising devices to apply in those systems, where, generally speaking, the capitalised costs (installation and maintenance costs) are lower or comparable with CLFs. It denotes that H-CLIDs shall be used in the systems from which one requires a high degree of reliability, super very quick operation resulting in practically negligible let- through integral and peak let-through current and generally the CLFs elimination.

## I. INTRODUCTION

Most recent developments to overcurrent protection in both l. v. and h. v. electric systems are so-called intelligent circuit breakers (CB). This tendency has been pushed forward as the preferential subjects of CIGRÉ and CIRED Conferences. Among intelligent CBs the current - limiting (CL) l. v. and h. v. CBs are one of the promising apparatus which are able not only to a considerable limitation of the current but also to its final interruption. Beside these devices there are also such ones which limit the current only, whereas an additional apparatus serves to final current interruption. This reason makes possible, for the purpose of the paper, to distinct:

- current- limiting and interrupting devices (CLID) and
- current- limiting devices (CLD).

The advantages of mechanical (contact) CBs and semiconductor CBs (usually based on thyristors and GTOs) led to so-called hybrid circuit breakers (HCB)s and to hybrid current limiting interrupting devices (H-CLID)s. On the contrary to HCBs, as concerns their operation, their counterpart, which is H-CLID, usually possesses more or less developed electric schemes those obviously shall not resemble a mechanical CB

operation. Hybrid solution makes possible to exploit the advantages of both, semiconductor and mechanical CB principles of operation.

Recently, the Chair of Electrical Apparatus of the TU Gdansk made several new developments to achieve an effective and reliable H-CLID for AC and DC purposes, which demonstrate a number of benefits. On these background a question arose how far the new H-CLID can be a challenge to the classical current limiting fuses (CLFs). The paper is going to make a comparison between mentioned H-CLID and CLFs and to point out the preferential fields of their applications.

## II. PRINCIPLES OF H-CLID OPERATION

Obviously, there is no need to describe here the principles of CLFs operation. But the basis of H-CLID operation is worth to a summary to get a better acquaintance with this modern device.

Hybrid circuit breaker (HCB) being discussed in this paper, comprises a mechanical contact in the main current path, counter current injection circuit for forced commutation in the main contact and ultra rapid electrodynamic drive, Fig. 1. The DC HCB, type DHR, was worked out by Collart and Pellichero [1].

The HCB enables current limitation and interruption as fast as a contactless circuit breaker, e.g., thyristor circuit breaker (TCB) but without TCB's drawbacks as big dimensions, power losses in the ON state, etc. There is no upper limit on the prospective current that the DHR circuit breaker is capable to break. A limiting factor for DHR operation is the initial value of  $di/dt$  but it may be greater than  $15 \text{ A}/\mu\text{s}$ . On the other hand, a sophisticated mechanical system is a drawback of that HCB. It is due to the requirements on the very short pre-arcing time that needs very high contact opening speed. An initial acceleration of order of  $(20,000 \div 40,000) \text{ g}$  must be applied to give the moving contact a speed of  $10 \div 50 \text{ m/s}$  on the way  $1 \div 5 \text{ mm}$  and to obtain the pre-arcing time of order  $100 \mu\text{s}$  [1]. The kinetic energy of the fast moving system must be absorbed by a breaking system that complicates the design of HCB and makes it very expensive.

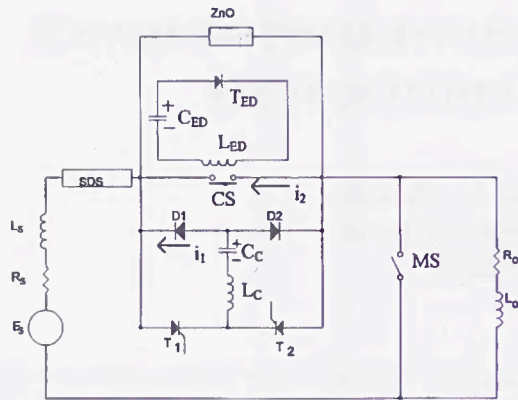


Fig.1 Schematic circuit diagram of AC-HCLID

$E_s, R_s, L_s$  - source parameters;  $R_o, L_o$  - load parameters; CS - contact switch; MS - short-circuit making switch;  $L_c, C_c, T_1, T_2, D_1, D_2$  - elements of commutation circuit; SDS - short-circuit detection system; ZnO - varistor suppressor;  $L_{ED}, C_{ED}, T_{ED}$  - elements of electrodynamic drive circuit;  $i_2$  - counter current;  $i_1$  - diode  $D_1$  current

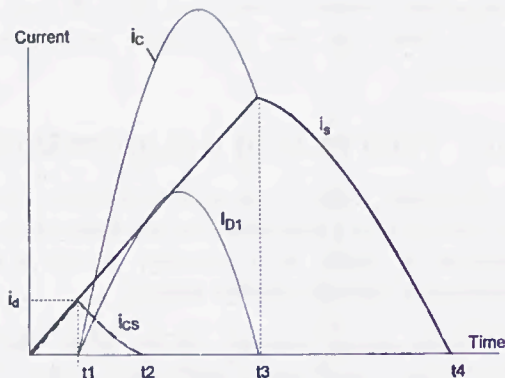


Fig.2 Current wave forms of AC-HCLID

$i_{CB}$  - contact switch current;  $i_{D1}, i_{D2}$  - diode currents;  $i_C$  - commutation capacitor current;  $I_d$  - discrimination current;  $t_1$  - commutation starts;  $t_2$  - contact CS separation starts;  $t_3$  - final current interruption in CS;  $t_4$  - recovery voltage starts;  $t_4$  - final fault current interruption

That is why a simplified, inexpensive device named H-CLID (hybrid current limiting and interrupting device) was worked out and tested by the authors [2 ÷ 5]. A "one shot" contact is used in the H-CLID. Normally, the contact is kept in closed position by a clamping arrangement so the device is in the ON state. The contact can be opened by tear down due to the repulsion force developed by the electrodynamic drive circuit. The contact itself (or a damping element in the contact assembly) must be replaced after each operation. Please notice an analogy to fuse element that is also a "one shot" device.

The operation of H-CLID is shown in Fig. 2, at the assumption that the forced current commutation is ideal, it means the contact S is open exactly at zero current. The H-CLID operates very fast so in AC circuit the line voltage can be considered as almost constant during current breaking. Thus the basic waveforms of current and voltage at H-CLID operation are essentially the same in DC and AC circuit.

The research carried by the authors on the H-CLID has shown that the following fields of application can be taken into account:

- short-circuit protection for diode and thyristor converters, then the semiconductor fuses can be entirely eliminated [3, 5];
- disturbance arc protection in l. v. systems [4].

Further discussions have shown that the H-CLID could also be used as a protection against:

- explosion of high power transistors;
- earth faults in converter circuits (ability to interrupt fault currents with DC component).

### III. FEATURES OF CLF AND H-CLID

Amongst the features of CLF and HCLID there are recognised in the paper 3 groups of them, juxtaposed in the Tables 1, 2 and 3.

The information given in Table 1 need more extensive comments, whereas given in Tables 2 and 3 do not.

### IV. COMMENTS TO TABLE 1

No. 1. From the obvious reasons there is a practically unlimited bottom boundary as concerns the fuses' rated voltages. To get very small rated voltages it is enough to limit the fuse-element length. But the voltage upper limit is limited because of the service reasons. The electricity utility company as a protection means for the line voltage, say 36 kV, usually has not accepted the use of CLF. Namely, the power outage costs due to the time required to fuse-links replacement become so significant that the circuit breakers be used instead. Moreover, DC CLF are needed up to 3 kV only, usually to railway purposes.

No. 2. For the time being even sub-miniature (micro and pico) fuses for few mA are available. The only limitation is to manufacture a very small, in cross-sectional area, fuse-element within an acceptable reproducibility level. On the other hand, fuses of several kA, for protection of heavy power semiconductor inverters (e.g. American „Amp-trap" fuses) can be relatively easy designed and manufactured.

Table 1. Electric features of CLF and H-CLID

No.	Feature	CLF	H-CLID
1.	Rated voltages $U_n$	Few volts up to 36 kV	Up to 3 kV DC
2.	Rated currents $I_n$	Few mA up to several kA	Few A up to several kA
3.	Rated breaking capacity	Unlimited	Almost unlimited, e.g., 150 kA DC, 100 kA <sub>RMS</sub> AC
4.	Minimum breaking current $I_m$	Depends on fuse type: back-up - several rated currents general purpose- 1 h current full range- rated current	Unlimited small current
5.	Total Joule integral $I^2t$	Depends on rated current $I_n$ (for given short circuit conditions )	Depends on discriminated current level $I_d$ but the $I^2t$ parameter is always lower than for fuse of equivalent $I_n$
6.	Peak let-through (cut-off ) current $i_0$	Depends on rated current $I_n$ (for given short circuit conditions )	Depends on discriminated current level $I_d$ but the peak let-through current is always much lower than for fuse of equivalent $I_n$
7.	Total operating time at rated breaking capacity	Depends on rated current $I_n$ (for given short circuit conditions )	Depends on discriminated current level $I_d$ but the total operating time is always shorter than for fuse of equivalent $I_n$
8.	t-I characteristics	Common, time-lag, transformer, high-speed, back-up and any other needed for special purposes, e.g., for coal mine	Depends on t-I characteristics of electronic short circuit current detection system (SDS ) those can be designed to meet customer's requirements; however, for fast rising fault currents the operation of SDS must be instantaneous
9.	Permissible di/dt	No limits	Depends on HCB's design; di/dt > 50 A/ $\mu$ s seems to be an available limit
10.	Overvoltages $U_0$	Not higher than permissible for given rated voltage of installation	Level of overvoltages is dependent upon commutation capacitance and/or $Z_nO$ voltage clamping varistor
11.	Discrimination	Between neighboring fuses of nearest network distribution nodes not less than 1.6 of ratio of their rated currents	Depends on SDS design. For simple electronic overcurrent trip there is possible discrimination overload currents only; for fast rising fault currents the operation of SDS must be instantaneous. However, for advanced SDS a precise discrimination is possible
12.	Ability of operation at DC	Special fuses for DC purposes	No problem with breaking DC currents, however, for highly inductive DC loads a free-wheel diode (thyristor ) may be required
13.	Rated power losses $P_n$	Depend on rated voltage, rated current and fuse type	Negligible as in conventional mechanical circuit breaker of similar rated current

Table 2 Service features of CLF and H-CLID

No.	Feature	CLF	H-CLID
1.	High breaking capacity	No need for complex short-circuit calculations. No concerns about costly future upgrades due to system expansion with increased fault currents	Need complex verification (computer simulation) of breaking capability for increased fault currents
2.	Reset-ability	Fuses can not be reset thus forcing the user to identify and correct the over-current condition before energizing the circuit	H-CLID with expandable contact can be easily reset
3.	Reliability	No moving parts to wear out or become contaminated by dust, oil or corrosion. Fuse replacement ensures protection is restored to its original state of integrity	No problems with contact erosion or wear of arc chambers. Line test and device revision after breaking heavy faults is not required before next making. H-CLID with expandable contact needs very low maintenance.
4.	Safety	No emission of gas, flames, arcs and other materials when clearing currents. The speed of operation limits the flash hazard at fault condition. Quiet operation.	Similar features as fuses and in addition no acoustic effects at current interruption, however, noise is caused by the electrodynamic drive
5.	Power supply dips	Minimum voltage dips in power system at clearing high fault currents	Duration of voltage dip is almost negligible, e.g., 1 ms
6.	Tamperproof	Fuses can not be modified or adjusted to change their level performance once installed, thus avoiding improper adjustment and malfunctions	Setting of short circuit current detection system (SDS) can be adjusted according to customer requirements, in limits of device breaking capability
7.	Life security	Limited to large overcurrents. At overload, particularly low, due to fault to earth too long time existence, no security for human being	Can be easily incorporated phase-to-earth fault protection at any fault current
8.	Possibility of 1- or 2-phase failure in system supply	Exists but can be eliminated by use of fuse-switch combination	Can be eliminated by simultaneous activation current breaking in three phases
9.	Impulse ageing	Due to fuse-element oxidation, its pulsed ageing in constrictions and M-effect, -ageing exists. It leads to unexpected operation, hence supply system expensive outage	Unexpected operation at impulse loads does not exist, contacts ageing is possible as in conventional CB
10.	Influence of environment	Relatively high influence of the ambient temperature	The influence of environment on electronic control system can be eliminated by proper design of electronic circuits
11.	Electromagnetic compatibility	During arcing in CLF modest electromagnetic field radiates. But it is a very seldom case	Emission of high electromagnetic field at operation of electrodynamic drive. Both electrodynamic drive and electronic control system must comply EMC standards
12.	User qualifications	Simplest among possible	Qualified technician electrician

Table 3. Economical features of CLF and H-CLID

No.	Feature	CLF	H-CLID
1.	Cost of system supply outages	Considerable due to time needed for fuse-link replacement	H-CLID - similar cost as for fuses
2.	Investment costs	Very small. Fuses are so-called installment overcurrent protection	Relatively high in comparison to fuses
3.	Dimensions	Very small	Medium
4.	Weight	Very small	Medium

No. 3. Due to the current-limiting ability, which is based upon the pre-arcing Joule integral and then due to the effective and quick forced current diminishing to the artificial zero, the CLF's rated breaking capacity normally is unlimited. But a problem may arise with the current interruption of so-called critical (test duty 2) which usually is in the range of three to four times of one-half cycle current taken from a CLF t-I characteristic.

No. 4. A serious problem within CLFs is the minimum breaking current. With exception of the special fuses, i.e. so-called the full range fuses, all other types possess this breaking current boundary. The majority of the CLFs show this current as equal to several times of their rated current. It seriously limits their application as a sole overcurrent protective device. Thus in many applications it is necessary to apply an additional apparatus, very often a load switch

No. 5. Pre-arcing and in a consequence also arcing and hence also operating  $I^2t$  of CLFs strongly depend on their rated current because the fuse-element cross-sectional area is related to this current. Larger rated current, larger that area; hence larger is pre-arcing  $I^2t$ . In turn, larger pre-arcing  $I^2t$ , larger is the cut-off current and greater are both arcing and operating  $I^2t$ , because the energy to dissipate in a CLF strongly relate to  $Li_0^2/2$  (where: L- the circuit inductance,  $i_0$ - the cut-off current).

To illustrate the differences between  $I^2t$  of CLF and H-CLID let us compare these values for a typical 660 V h.r.c. fuse of 100 A & 1000 A rated current and of H-CLID for 100 kA(RMS) prospective current, Table 4.

No. 6. The cut-off current  $i_0$  for conditions as above, Table 5 and Fig. 3.

No. 7. Supremacy of the H-CLID is also very distinct as concerns the time  $t_0$ .

No. 8. In respect of t-I characteristics both compared apparatus can meet the users specific requirements. In the case of CLF an appropriate shaping of the fuse-element that can not be modified past manufacturing, can do it. On the contrary, in the case H-CLID its t-I characteristics can be adjusted and controlled in service.

Table 4. Operating  $I^2t$  for typical CLF and H-CLID

CLFs				H-CLID	
common h.r.c.		for semiconductors			
$I_n$	$I^2t$	$I_n$	$I^2t$	$I_n$	$I^2t$
[A]	[A <sup>2</sup> s]	[A]	[A <sup>2</sup> s]	[A]	[A <sup>2</sup> s]
100	80,000	100	9,000	100	6,000
1,000	$25 \times 10^6$	1,000	650,000	1,000	15,000

Table 5. The cut-off current  $i_0$  for typical CLFs and H-CLID

CLFs				H-CLID	
common h.r.c.		for semiconductors			
$I_n$	$i_0$	$I_n$	$i_0$	$I_n$	$i_0$
[A]	[kA]	[A]	[kA]	[A]	[kA]
100	20	100	7	100	6
1,000	80	1,000	25	1,000	7

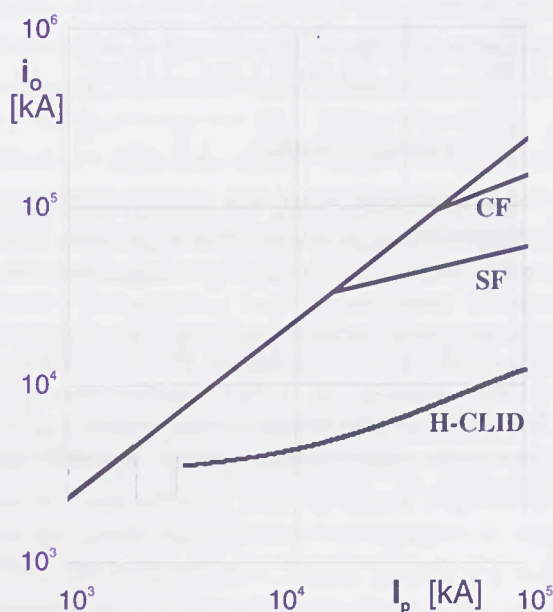


Fig.3. Cut-off current  $i_0$  for typical: CF - common fuse, SF - semiconductor fuse, and H-CLID of  $I_n=3,000A$

No. 9. Fuses prevail H-CLID in respect of the permissible  $di/dt$ . They are not susceptible on this parameter, whereas H-CLID is.

No. 10. For both apparatuses in question there is no hard obstacles to keep the overvoltages on a required level, however, absolutely different designing means are used to achieve this. It should be remembered that for CLFs the overvoltages could be practically the same at lower rated voltages. That is why this problem should be a subject of careful considerations before their use in the systems of rated voltages lower than the rated voltage.

No. 11. In respect of discrimination the CLFs are devices which relatively easy can be selected along a feeding grid to ensure their proper co-ordination. Similarly, the H-CLIDs can do that, if an advanced electronic SDS is applied.

No. 12. For DC applications often entirely different fuses' design is needed. On the contrary, there is no problem with breaking DC currents by the H-CLID. Its design becomes simpler and less expensive than at AC applications.

No. 13. Unfortunately the power losses  $P_n$  of CLFs are very large as compared with H-CLID. For example, in conditions gives in No. 5 above approximate values of  $P_n$  are given in Table 6.

Table 6. Power losses  $P_n$  for typical CLFs and H-CLID

CLFs				H-CLID	
Common h.r.c.		for semiconductors		$I_n$	$P_n$
$I_n$	$P_n$	$I_n$	$P_n$		
[A]	[W]	[A]	[W]	[A]	[W]
100	10	100	35	100	1
1,000	100	1,000	180	1,000	10

## V. CONCLUSIONS

Current limiting fuses will probably ever dominate the field of overcurrent protection as a simplest amongst possible means of overcurrent protection. However, the physical principles of fuse performance decide on available parameters characterising fuse operation at clearing faults, as the operational  $I^2t$  and cut-off current  $i_0$ . The research on hybrid current limiting and interrupting circuit breakers and devices has shown a new way towards improvement of short circuit protection.

The available parameters of H-CLID as operational  $I^2t$  and cut-off current  $i_0$  are now a technical challenge to current limiting fuses. Therefore it may be expected that the H-CLID at least will soon:

- replace fuses in power converter protection,
- enable effective arcing fault protection for l. v. switchgear.

## ACKNOWLEDGEMENT

The work on hybrid current limiting interrupting circuit breaker has been carried out in frames of the research project 8 T 10 A 029 08 financed in the years 1995- 1997 by the Committee of Scientific Research in Poland.

## REFERENCES

- [1] P. Collard, S. Pellichero, "A new high speed DC circuit breaker: the DHR", Proc. of the IEE Colloquium on Electronic-aided Current-limiting Circuit Breaker Developments and Applications, IEE Digest No. 1989/137, London, (UK), 1989.
- [2] S. Hasan, J. • yborski, T. Lipski, M. Piko• , J. Wittstock, „A hybrid current limiting interrupting device for DC circuit protection”, Proc. of the West-East Technology Bridge International Conference on Power Electronics, Motion Control, pp. 824-829, Warsaw (Poland), 1994.
- [3] J. • yborski, T. Lipski, S. Hasan, J. Wittstock, "A new hybrid AC current limiting interrupting device for semiconductor converter protection", Proc. of the 6th European Conference on Power Electronics and Applications "EPE'95", Vol. 3, pp. 3.117-3.120, Seville (Spain), 1995.
- [4] J. Czucha, R. Partyka, J. • yborski, "AC low-voltage arcing fault protection by hybrid current limiting interrupting device", Proc. of the 7th International Symposium on Short-Circuit Currents in Power Systems "SCC '96", Vol. 2, pp. 3.8.1-3.8.4, Warsaw (Poland), 1996.
- [5] J. Czucha, T. Lipski, J. • yborski, „Hybrid current limiting interrupting device for 3-phase 400 V AC applications”, 5<sup>th</sup> International Conference on Trends in Distribution Switchgear: 400 V- 145 kV for Utilities and Private Networks „DS'98”, pp.161-166, London, (U.K.), 1998.

# A NEW REPLACEABLE FUSE-ELEMENT WITH CURRENT LIMITING CHARACTERISTICS USED ON DROP-OUT FUSE

Kong Fanhong    Wang Jimei

Ma Zhicheng

Xi'an Jiaotong University

Xi'an Fusegear Factory

Xi'an, The People's Republic of China

*Abstract.* The structure of new replaceable fuse-element which is made of pure copper surrounded by stone sand with current limiting characteristics was studied and the manufacture process of this element was described briefly also. The fuse-element of this type is applied to out-door drop-out fuse of 7.2-12kV. According to IEC282 this out-door drop-out fuse tested on 12kV under a short-circuit breaking capacity of 31.5kA. The results of which were analyzed in the paper.

## I. INTRODUCTION

High-voltage current limiting fuse is an old-fashioned apparatus for electrical protection. However, it is still widely applied in power systems for the features of quick-acting, high breaking capacity, remarkable characteristics in current limiting, compactness in structure and so on.

At present, there are two types of high-voltage fuse under mass production and broad application in China, i.e. expulsion type and current limiting type. The drop-out fuse for out door purpose is categorized in the expulsion type of non-current limiting. The principle of arc extinguishing in drop-out fuse is dependent on that once the fuse element is self-melted, it will produce an electric arc of very high temperature to vaporize the filled material in extinguishing arc tube, thus generate abundant gases with high pressure which expels off arc itself. If the current reaches zero, the arc will be extinguished. After the arc extinguished, the fuse body will be automatically unlocked and rotationally falls down in drop-out position, forming a visible breaking space. The fuse of this type is quite simple in structure, convenient in operation, lower in production costs, visible breaking space formed after acting, etc. Therefore, it is broadly used in 10-63 kV power systems and power transformers as for over-load and short circuit protection.

The main problems of this kind of fuse are: (a) Low performance in arc extinguishing, (b) Less stability

in time-current characteristics, (c) Low breaking capacity.

Based on the rapid development of power industry in China, it is estimated that the annual increment in power system capacity will be about 10 million kW. That means to say with the growing of power system capacity, the breaking capacity of expulsion type drop-out fuse will no longer meet the requirements of power system developed. The results have shown that the high-voltage fuse of current limiting type in power distribution transformers for protection exhibits its superior performance to any of the kind, e.g. remarkable current limiting to reduce greatly the requirements of thermal stability and dynamic stability of protected apparatus, thus showing the distinct increase in economical value. In order to keep pace with the development of present market situation, a drop-out high-voltage fuse of current limiting type was jointly designed and developed by Xi'an Jiaotong University and Xi'an Fusegear Factory with rated voltage 12 kV, rated current 100A and breaking capacity 31.5 kA, in which solidified silica-sand and pure copper are used as fuse element instead of the expulsion type drop-out non-current limiting fuse. Moreover, the newly designed drop-out fuse during interrupting is soundless, no light flash, safe and reliable. It has much higher breaking capacity than that of the expulsion type. Hence it opens up a new way for the development of drop-out type fuse.

## II. STRUCTURE OF NEWLY DESIGNED DROP-OUT FUSE

Fig.1 shows the principal structure of the newly designed current limiting drop-out fuse where two Insulators 7 are vertically fixed on Base 8 respectively, Upper and Lower Bracket 4 and 5 are installed on each insulator, the hook of lower bracket catches the bolt positioned near the lower end of Fuse-Body 1, the upper end of Fuse-Body 1 tightly secured on Spring Plate 3 and

hooked by Release-Lock Rod 2. Electric current flows in at Terminal 6 on the insulator and out at Terminal 9 through metallic Upper Bracket 4 and Fuse-Body 1, then Lower Bracket 5.

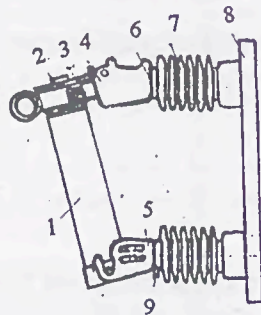


Figure 1. Principal structure of the newly designed current limiting drop-out fuse

If over-load current or short circuit current runs through the fuse, the striker will act while the fuse element is melted to push the firing pin opening Release-Lock Rod 2. Fuse-body 1 is released and drops down automatically along the bolt on the lower end of Fuse-body 1. Eventually, the fuse is freely hung down on Lower Bracket 5 in drop-out position.

### III. SOLIDIFYING PROCESS OF FUSE ELEMENT

Place a mixture of solidification agent and silica sand in proper proportion into a mixer, mix up them evenly for 15-20 min., then pour out the mixture into an assembled fuse body. To impact silica sand in the fuse body tightly, it is placed on a vibrator for mechanical vibration. Keep the impacted fuse body in an oven for 2 hrs at 120°C, then remove it out to cool down at room temperature. Seal the fuse body before assembling.

### IV. TESTING RESULTS AND DISCUSSION

Main parameters of the sample is rated voltage 12 kV, rated current 100A and breaking capacity 31.5 kA. The dimension of the fuse-element is shown in Fig. 2. The element material used is of pure copper (electrical grade) with  $\delta = 0.13\text{mm}$  in thickness and resistance per meter 68 milli-ohm. The fuse body is made of glass fibre in 4mm thickness which is sustained to high temperature, moisture-proof, fire-proof, high strength, and prevention from ageing of ultraviolet rays.

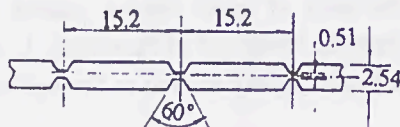


Figure 2. The dimension of the Fuse-element

### IV.1 Testing Results

Breaking capacity test of Test duty 1 and Test duty 2, temperature-rise test and time-current characteristics test were completed on the sample fuse.

#### 1. Breaking capacity test of Test duty 1

Fig.3 shows the prospective current oscillograph under metal short circuit for breaking capacity of Test duty 1, where  $U$ , the voltage of power source and  $I_k$ , the prospective short circuit current.

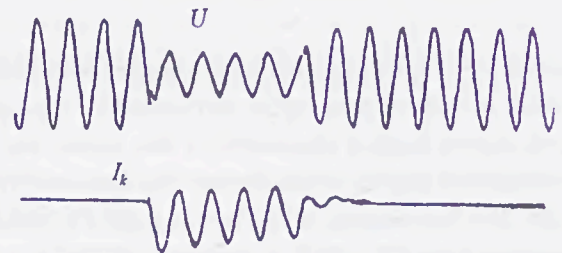


Fig.3 The prospective short circuit current

Fig.4 shows the typical oscillograph of breaking capacity of Test duty 1 for solidified fuse element. The striker acted normally after the fuse melted, then dropped out to normal position.

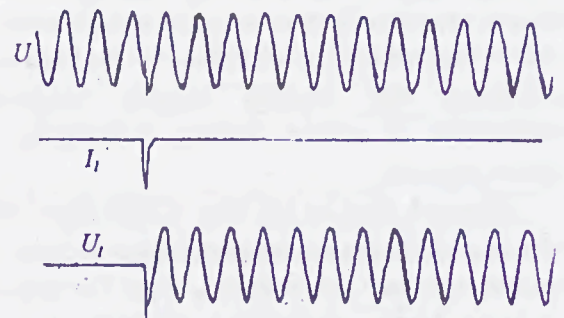


Fig.4 Typical oscillogram of Test-duty 1

#### 2. Breaking capacity test of Test duty 2

The prospective current oscillograph under metal short circuit for Test duty 2 is shown in Fig.5, in which  $U$ , the voltage of power source and  $I_k$ , the prospective short circuit current.

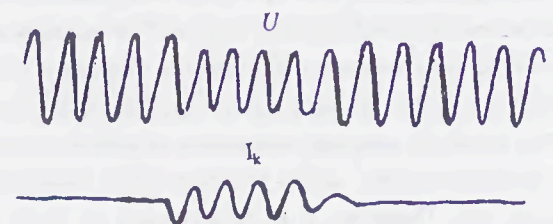


Fig.5 Prospective short circuit current

Fig.6 shows the typical oscillogram of Test duty 2 for solidified fuse element. After the fuse melted, the striker acted normally and the fuse dropped out to normal

position.

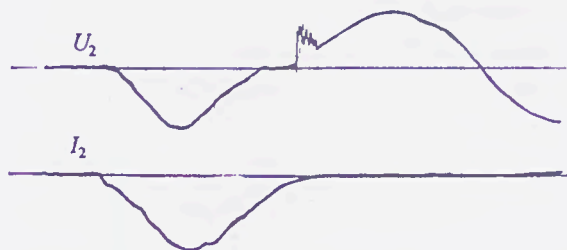


Fig.6 The typical oscillogram of Test duty 2

### 3. Temperature rise test

The points of temperature measurement for temperature rise test is shown in Fig.7. The temperatures measured are listed in Table 1.

Table 1 Results of temperature rise test

Measured points	Temperature rise °C
$\Delta T_1$	23
$\Delta T_2$	38
$\Delta T_3$	80

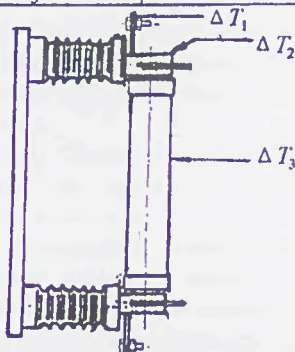


Fig.7 Measured points for temperature rise test

### 4. Time-current Characteristics test

When the rated currents of fuse were set at 6.3 to 100 A, the time-current characteristic tests on the fuses under low voltages are shown in Fig.8.

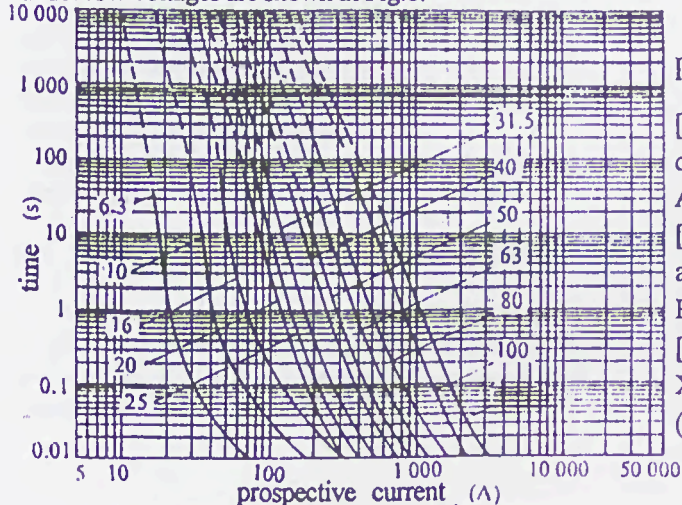


Fig.8 Time-current characteristic curves

## IV.2 Discussion (Analysis of results)

A number of fuse samples were used to complete Test duty 1 and Test duty 2, some of them were dissected for observation. As shown in Fig.9, it can be seen that the element was melted much evenly just as prospected in our design requirements.

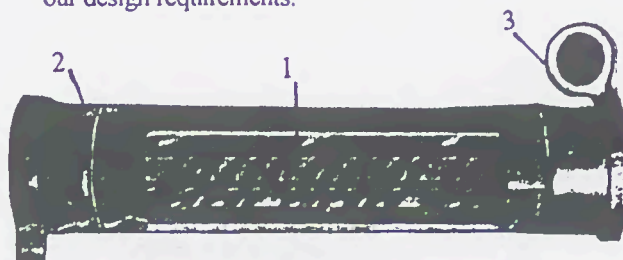


Fig.9 Photo of interrupted fuse element

1-interrupted fuse element; 2-lower terminal;  
3-upper terminal

The data of temperature rise as listed in Table 1 are below the specified standard temperature. Moreover, little variation in resistance was measured pure copper element after solidification for one year's. No trace of metallic oxides on the surface of fuse element was detected. Also, the time-current characteristic curve of fuse element showed less difference in comparison with that made of pure silver.

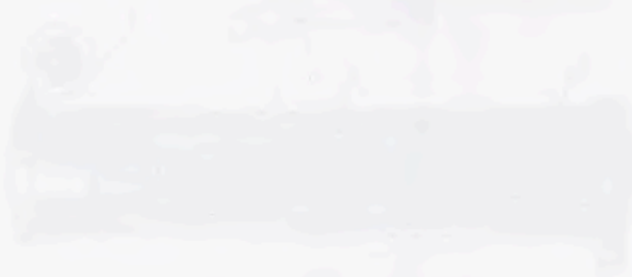
## V. CONCLUSION

The current limiting drop-out fuse made of pure copper element as fuse element is possible to be used in power systems range from 7.2 to 12 kV for over-load current and short circuit current protections. The breaking capacity of which is much higher than that of the expulsion type one. The element shows no obvious metallic oxides on the surface and ageing phenomenon after action.

## REFERENCES

- [1] Jiao Qiuzhong, "Summarize in out door high-voltage drop-out fuse", China High-voltage Switch-gear Industry Association, 1995, No.2. (Chinese)
- [2] Wang Pu, "Brief introduction of high-voltage fuse. application and development in domestic and abroad." High-voltage Apparatus, 1994, No.6, P46 (Chinese)
- [3] Wang Jimei, "High-voltage current limiting fuse". Xi'an Jiaotong University Publishing House, 1994 (Chinese)

THE HISTORY OF THE  
CITY OF BOSTON



FROM THE  
PUBLISHED RECORDS

AND  
OTHER AUTHENTIC SOURCES

BY  
JOHN H. COOK

AND  
OTHERS

IN  
CONJUNCTION WITH  
THE  
CITY OF BOSTON

AND  
THE  
CITY OF NEW YORK

THE HISTORY OF THE  
CITY OF BOSTON

FROM THE  
PUBLISHED RECORDS

AND  
OTHER AUTHENTIC SOURCES

BY  
JOHN H. COOK

AND  
OTHERS

IN  
CONJUNCTION WITH  
THE  
CITY OF BOSTON

AND  
THE  
CITY OF NEW YORK

AND  
OTHERS

# NEW HIGH BREAKING CAPACITY FUSES

P.Leonte, T.Pleca, E.Furnic  
 "Gh. Asachi" Technical University  
 Iași - Romania

**Abstract:** A few new types of high breaking capacity fuses able to carry out the protection functions of universal automatic circuitbreakers to overload and short-circuit fault conditions are shown in this paper.

## I. GENERAL CONSIDERATIONS

The nowadays universal automatic circuitbreakers with dynamic switching have thermal releasers (bimetallic release, easy fusing alloy release) to overload protection and electromagnetic releasers to short-circuit protection, and modern circuitbreakers have current protection transformer with electronic devices and microprocessor.

The protection function to overcurrents for some operating conditions could be take over by high breaking capacity fuses if these kind of fuses had a time-current characteristic,  $t(I)$ , similar to automatic circuitbreaker protection characteristics which fulfils beneficiary requests.

There are already requests from some users which catch a glimpse of economic and operating advantages to new fuse type.

The universal automatic circuitbreakers could have only galvanic isolation function of electric circuits, with manual or automatic handling.

To meet halfway of new requests, the authors had investigated the using possibilities and this paper presents some solutions from obtained results [1].

## II. NEW TYPES OF HIGH BREAKING CAPACITY FUSES

For new types of high breaking capacity fuses it had in view to ensure a partial adjustable or full range currents of time-current characteristic,  $t(I)$ , and the shape of this characteristic adapts to thermal characteristic of protected object.

So, fuses take over the thermal release functions to overload protections. It presents some examples:

### II.1 Replacing element with easy fusing alloy

The high breaking capacity (HRC) fuses structure is meant to short-circuit protection [2,4]. For an overload protection it is necessary a component part designed to this purpose.

The simplest solution means to section the fuse links, Fig.1, in the middle area then those two pieces are joined using easy fusing alloy which fulfils overload thermal release function.

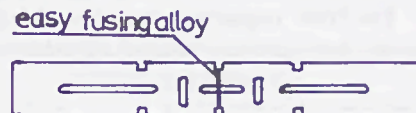


Fig.1 HRC fuse link with rated current  $I_n=100$  A

The time-current characteristic is not adjustable and its shape is shown in Fig.2, curve 1, comparatively with conventional fuse, curve 2 (rated current,  $I_n = 200$  A). It can observe that it gets a non-adjustable time-current characteristic but it ensures overload protection.

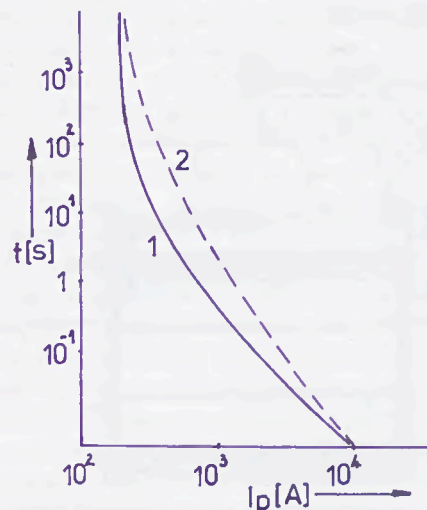


Fig.2 The time-current characteristics

A few experimental data are shown in the next table:

$I_p$ [A]	500	800	1000
$t_1$ [s]	2.50	1.10	0.66
$t_2$ [s]	50	6.23	2.20

where:

$I_p$  means the RMS prospective current;  
 $t_1$  - breaking time of new fuse;  
 $t_2$  - breaking time of conventional fuse.

In the given case the replacing element was with two fuse links, one of them was sectioned. As a result, those two fuse links work successively: first, the sectioned fuse link breaks off without arc and the second works with a period of time corresponding to breaking time. In the case of necessity it can section all fuse links, getting a shorter breaking time at overloads.

It established, experimentally, these new kind of fuses have a better behaviour at testing and operating conditions also because of small overvoltage levels when it recorded reestablishing voltage on a memory oscilloscope. Also, it observed a fuse working without noises and shining effects.

## II.2 The HRC replacing elements with time-current characteristic limited adjustable

The replacing element, Fig.3, has in parallel with fuse links F, outside of fuse body A, an elastic link Le soldered at one of end and stucked at the other end with an easy fusing alloy Af. The elastic link Le is jointly with a spring blade Sb. At overcurrents, the alloy is melting under thermal action of branched current and the elastic link Le sets free which is suddenly removed by spring blade Sb, without arc, the electric current being wholly directed through both fuse links F which finally will break off the electric current [1].

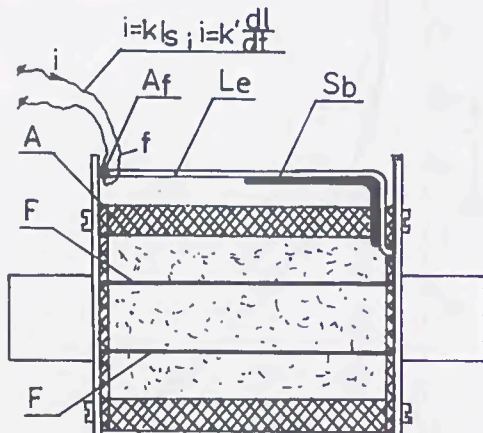


Fig.3 Low tension replacing element for HRC fuses

It can get a limited adjustable time-current characteristic. For instance, if resistance wire f melted the alloy Af in a negligible period of time and the electric currents on both branches were equally, then working time would reduce corresponding to double current and initial thermal state of fuse links and, so, the time-current characteristic to "cold state" will be the curve 2, Fig.4, comparatively with conventional fuse, curve 1.

Changing the currents ratio and heating current through resistance wire f, the time-current characteristic becomes limited adjustable.

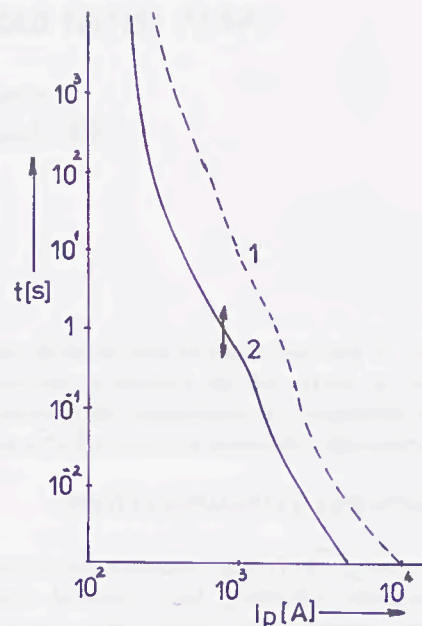


Fig.4 Semi-adjustable time-current characteristic

The outside parallel branch can be introduced into a compartment of fuse body or it can use two compartmented fuse bodies. Fixed joint through alloy can be replaced by a switch which belongs to a momentary primary current relay or a delay current relay adapted to given device.

Fig.5 presents the time-current characteristics of an universal automatic circuitbreaker with dynamic switching fitted out with thermal DT and electromagnetic DE releasers which points out the following aspects:

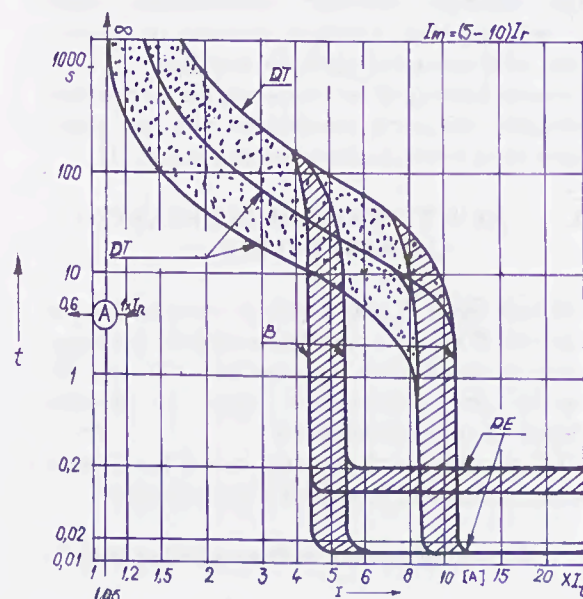


Fig.5 Time-current characteristic of an universal automatic circuitbreaker with thermal and electromagnetic releasers

- the time-current characteristic,  $t(I)$  is adjustable;
- the cut-off current is variable in the range  $(5...10)I_r$  or other prescribed range;
- it can provide for at least two variants of universal automatic circuitbreakers which allow selectivity in the range of electromagnetic releasers.

The achievement of alike time-current characteristic with HRC fuses it can make only using commanded fusing both overload and short-circuit ranges. An example is shown in Fig.6.

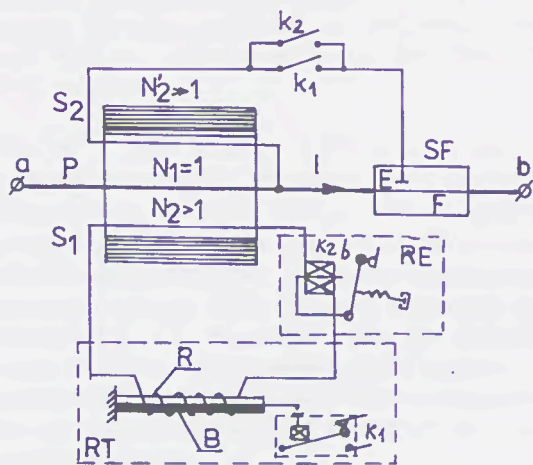


Fig.6 Fuse with self-commanded fusing

In this case the arc ignition into fuse SF is doing through electrode E about fuse link(s) F. At overloads it uses an adjustable thermal relay RT with bimetal B (direct, indirect or mixed heating by resistance R) and it is fitted out with a suddenly switching device.

This thermal relay RT is supplied from a current protection transformer TI through secondary  $S_1$  with primary P in series with fuse SF. The switch  $k_1$  turns on the second secondary  $S_2$  which establishes commanded fusing through local fuse link(s) cut-off with an auxiliary arc. In these conditions the fuse breaking time has a negligible value in comparison with delay time of bimetallic thermal relay, actually overload protection is made in accordance with time-current characteristic of this relay.

Any electromagnetic or electronic current relay can fulfil this function with required time-current characteristics.

At short-circuits, it can be in series with thermal relay RT an electromagnetic or electronic relay RE with adjustable turn-on current to achieve the cut-off current at prescribed value and momentary or adjustable delay operating for a good selectivity. The relay RE achieves the commanded fusing through switch  $k_2$  in the same way.

The three-phase variant results from three monophasic units.

The command block remains after every operating stages being necessary only replacing elements changing with a new one or reconditioned element.

In this way it gets a primary adjustable commanded protection with fuses of electric circuits and consumers.

The improving of presented model can offer a competitive solution to universal automatic circuitbreakers in certain operating conditions.

The advantages which results from presented solutions are:

- removing of operating drawbacks because of universal automatic circuitbreakers with dynamic switching;
- benefitting by advantages to use HRC fuses;
- diminished global expenses;
- large limit adjustable possibilities through transformer ratio of current transformer TI and used relays.

### III. CONCLUSIONS

From new type fuses presentation results the following conclusions:

- it can be made new type of fuses with non-adjustable time-current characteristic adapted to overload protection with a better behaviour at overvoltages;
- the protection characteristic of universal automatic circuitbreakers with dynamic switching can be reproduced using fuses with commanded fusing; it preserves the adjustable possibilities of protection characteristic but in the larger limits;
- the ensemble of HRC fuse and commanded fusing block offers the advantage of current limiting effect which can be anticipated when it is necessary;
- the quality to reproduce the protection characteristic of universal automatic circuitbreakers with overcurrent protection remains to any kind of used fuse, including resettable fuses;
- the commanded fusing can be initiated in momentary or delayed time;
- the fuses operating selectivity can be solved much better through commanded system which can be coordinated using microelectronic systems;
- it can command the working of any fuse from a given protection system when it is necessary;
- the commanded fusing can be achieved also with an independent auxiliary power source, in this case it can be started by any supervised parameter which could compromise the installation operating; in this way it achieves a generalized protection to a given installation;
- the commanded fusing can be started by any means what can ignition the local arc;
- the reconditioning is necessary only for replacing elements;
- in different operating conditions the command block can be the same only current protection transformer TI have to change (in some cases, only its primary);

- the circuitbreakers used for galvanic isolation of electric circuits and consumers can have a simplified design because they don't have to provide for short-circuit breaking capacity (fuses take over this function).

#### REFERENCES

[1] P.Leonte, N.Sufle• el, I.Ciutea, "Element de înlocuire de joas• tensiune pentru siguran• e fuzibile

de mare putere de rupere", Brevet 114052 B1, RO, 1998.

[2] A.Wright, P.G.Newbery, "Electric Fuses", Published by The Institution of Electrical Engineers, London, United Kingdom, 2nd Edition, 1995.

[3] Fifth International Conference on Electric Fuses and their Applications, Technical University of Ilmenau, Germany, 1995.

[4] I.Barbu, "Siguran• e electrice de joas• tensiune", Editura Tehnic• , Bucure• ti, 1983.

# CURRENT LIMITATION BY CIRCUIT-BREAKER AND POLYMER COMBINATION

Claudio Brazzola  
ABB Elettrocondutture  
Vittuone - Italy

**Abstract:** A new technology using current limitation offered by semiconducting polymers in combination with breaking capacity, provided by traditional miniature circuit-breakers, allows to merge the best characteristics of both solutions.

PROLIM™ (PROtection LIMitation), the ABB commercial name of his "permanent fuse", consisting in a semiconducting polymer device, with a temperature-dependent transition from very low ( $3\text{m}\Omega$ ) to very high ( $300\text{m}\Omega$ ) internal resistivity, is current limiting device of short-circuit current level ( $I_k$ ) and associated specific thermal energy ( $I^2t$ ), in similar, better way as traditional devices: fuses and current limiting circuit breakers. An associated-coordinated circuit-breaker is necessary to clear the residual current and to permit the requested necessary selectivity.

This solution improves the short-circuit protection for motor starters and distribution applications.

PROLIM™, together with miniature circuit-breaker, is the ideal solution when there are:

- High short-circuit levels
- Medium current levels ( $I_n < 63\text{ A}$ )
- Voltages between 400 - 500 V (depending of the circuit-breaker).

The most likely applications are:

- Off shore
- Mining
- Power Generation
- Wind mills

This work shows how PROLIM™ operates, why and when gives real advantages.

Many short-circuit tests up to 50kA are included; these tests also compare PROLIM™ performances vs traditional components; the main results out of this comparison are:

- Cost saving
- Space saving
- Smaller cable area
- Personell safety
- Reliability of service
- Selective back-up

## I PRODUCT PRESENTATION

Short-circuits are the cause of high or even very high fault currents flowing in distribution systems.

If effective protection is not provided, these currents can cause serious damage to plants and equipment connected to the systems.

Short-circuit protection therefore has to interrupt fault currents as quickly as possible.

In practice, this means it has to prevent the first high "spike" of the fault current from forming.

The time it takes to form depends on the actual circuit and the moment switching takes place, but is in the range of just a few milliseconds.

The development of PROLIM™ should be regarded as a logical step in meeting the steadily increasing requirements made of apparatus in the low-voltage range-apparatus for high performance.

Designing fast, reliable electromechanical circuit-breaker to fulfil present and future requirements is becoming more and more difficult.

The break-time of conventional circuit-breakers is several milliseconds.

In most breakers, arc extinction takes place when the current passes through zero - ie, if the moment of switching is not ideal, after about 10 to 15 ms (50Hz).

Even high speed circuit-breakers take 3 to 5 ms to open. Circuit-breakers designed for short-circuit duty therefore have to be dimensioned for very high current values.

Because of mechanical constraints, traditional circuit-breaker technology offers hardly any potential for a further reduction in breaker operating time.

Many R&D efforts were spent on finding a new solution, in which short-circuit currents are limited safely and effectively before the current is interrupted using a conventional miniature circuit-breaker.

The current limiting device represents innovative technical thinking in the electrical business, where mechanical breaking contacts have always been found in some form or other to interrupt or limit short-circuit currents.

The new material technology involved will probably make a breakthrough in many other areas too.

The polymer material of the PROLIM™ contains electrically conducting particles.

In normal operation no change takes place and the entire polymer body remains in a state of low resistance.

PROLIM™ is a short-circuit limiting device available both as a product alone and as a combination unit together with a miniature circuit-breaker.

In any case it operates only together with a circuit-breaker: PROLIM™ limits the short-circuit current level ( $I_k$ ,  $I^2t$ ), then the circuit-breaker interrupts the current.

As a result, a significant improvement in the break time has been achieved and, even more dramatic, the let-through energy and the current peak are very limited.

PROLIM™ improves the short-circuit protection especially where a strong limitation of energy is required and it's important to save space.

## II HOW IT WORKS

PROLIM™ is made like a sandwich: the polymer material is inserted between two copper electrode plates, a strong pressure is mechanically applied by springs on both sides; all this assembly is encapsulated.

Polymers are usually non-conductive.

Some, however, can be transformed by doping into a state in which they conduct electricity.

The polyethylene current limiter is connected in parallel with an ohmic protective resistor.

Its purpose is to carry the current during the transitional phase during which the resistance increases.

This also reduces the voltage drop across the limiter.

During normal circuit operation (see figure 1) the current will flow through the current limiter.

Only when a short-circuit occurs, and the conductivity of the doped polymer decreases drastically, does some of the fault current flow through the resistor.

The distinctive feature of the current limiter is that when a short-circuit occurs the temperature, and therefore the resistance, rises only in the thin surface layer adjacent to the copper electrodes.

A rise in temperature of this layer to about 120°C, which is the crystalline melting point of polyethylene, causes the resistance to increase within only 0.1 to 0.5 ms to some hundred times its original value.

It is also this ohmic resistor that decides the value of the current passing to the circuit-breaker in series with the current limiter.

The reason behind such a phenomenon is that when after a short-circuit, the dramatic temperature rise inside PROLIM™ makes the polymer to melt and to lose its conductivity and also to create a high pressure gas that pushes the two electrodes away from the polymer producing a high resistive gap.

After the fast response time the resistance increases by some 100 times and the current peak is limited.

The let-through energy ( $I^2t$ ) becomes independent of the short-circuit current, and obviously advantage of this is that the calculation work on short-circuit currents is then unnecessary.

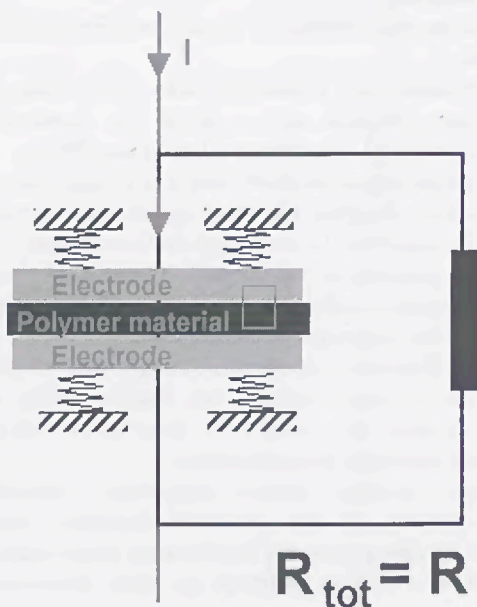


Figure 1 – Situation up to the nominal current

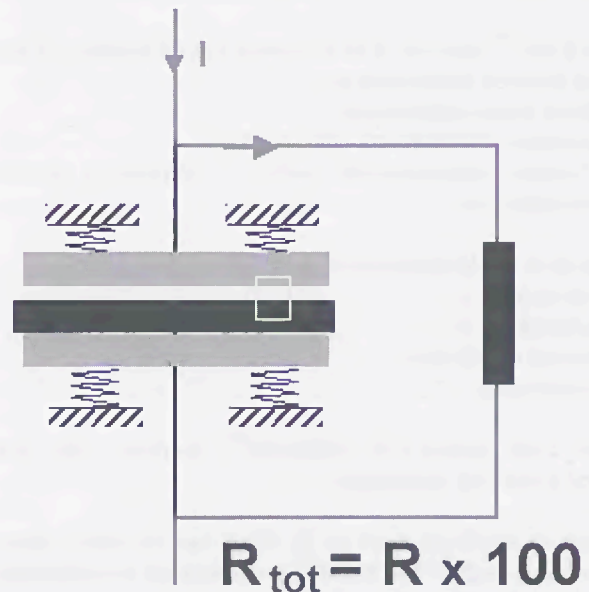


Figure 2 – Situation during the short-circuit

Laboratory tests shows that PROLIM™ is very quick and able to dramatically limit the current and therefore the energy.

The following diagrams show current and voltage during the first 30ms after the short-circuit; the prospective short-circuit current is 50kA r.m.s.

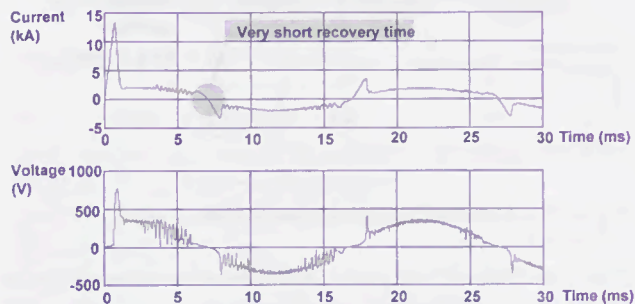


Figure 3 – PROLIM™ alone

Looking into these diagrams it's quite clear that the actual current is always very far from the prospective value, and therefore this current can be easily interrupted by a circuit-breaker.

These diagrams also show that when the current pass through the zero value the PROLIM™ is so quick to recover that it's possible to appreciate a current attempt to increase again suddenly limited by the PROLIM™ increasing again its resistivity.

### Function

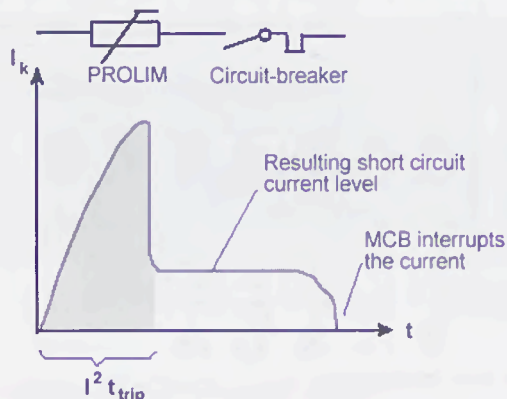


Figure 4 – Coordination with a circuit-breaker

PROLIM™ always have to be coordinated with a specified circuit-breaker.

The diagram in figure 4 shows the cooperation between PROLIM™ and a miniature circuit-breaker.

The short-circuit current is drastically reduced as a result, for some circuits to as much as one fifth of the original value.

The lower fault current has to interrupted by the circuit-breaker and its breaking time must still be fast so as not to endanger the thermal strength of the current limiter.

As mentioned, only thin surface layer is heated by the current: otherwise, the polymer material remains completely intact.

The surface layer automatically “resets”; the copper electrodes cool the surface, close the gas gap while the polyethylene plate absorbs some of the heat.

Overload currents are a normal situation in distribution networks in which there are motors, and short-circuit protection are not supposed to respond for them.

For example the current can rise to 7 to 10 times the continuous rating for a period of several seconds as a result of direct starting of a cage-induction motor.

During this time interruption is not desired.

The current limiter therefore has to be dimensioned so that the critical surface temperature will not be reached in such cases.

This is the reason for the two solid copper electrodes, which absorb the heat energy produced during the first 10s.

During the short-circuit, however, the current rises so fast that the heat cannot be transferred to the electrodes in this time.

### III Advantages

The main advantages given by the PROLIM™ solution are:

- Cost saving
- Space saving
- Smaller cable area
- Personell safety
- Reliability of service
- Selective back-up

### Comparison – Conventional solution versus PROLIM

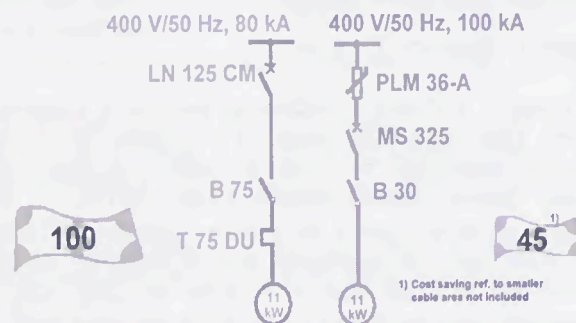


Figure 5 – Cost comparison

In figure 5, there are two different solutions to feed the same 11kW motor: on the left we use a current limiting MCCB type ABB SACE Limator LN125 with 80kA as breaking capacity a strong contactor ABB B75 and a thermal relay ABB T75DU; on the right a PROLIM™ PLM36-A in combination with a small manual motor starter ABB MS325 and a small contactor ABB B30 gives the same service with an higher breaking capacity. Even not considering the saving in the smaller cross sectional area the PROLIM™ solution cost only 45% than the traditional one. (Price list comparison)

Also the space saving can be easily shown by an example:

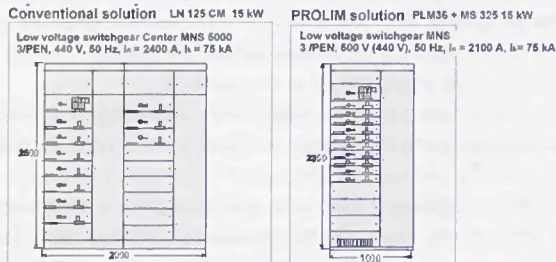


Figure 6 – Space comparison

These two ABB low voltage switchgear center have the same performances but the volume of the one on the right (MNS) is only 50% of the one on the left (MNS 5000).

Another important advantage is the very interesting possibility to have selectivity and back-up at the same time.

#### Motor start application

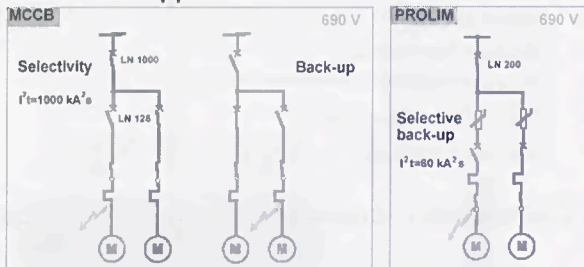


Figure 7 – Selective Back-up

In Figure 7 is shown a comparison between a traditional motor start application where it's possible to choose between selectivity by using as many expensive and strong current limiting breaker (ABB LN125) as the number of motors and a big breaker upperstream (ABB LN1000) that can withstand the short-circuit current during the breaking time or back-up by using only a limiting breaker but facing a total black-out when there is single fault in one motor.

On the right of the figure, vice-versa, thanks to PROLIM™ it's possible to have total discrimination

without expensive current limiting devices and because of the let-through energy limitation of the PROLIM™, without a big breaker upperstream.

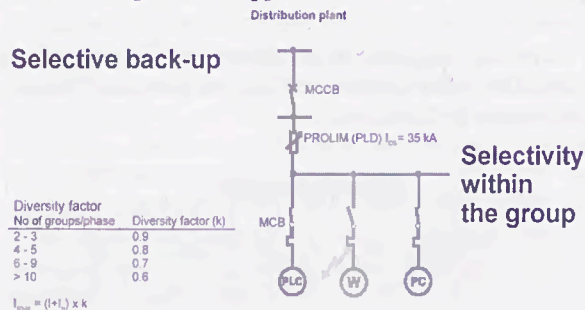


Figure 8 – Distribution plant selective back-up

Also in distribution plant application it's possible to obtain this special selective back-up.

In figure 8 there is a typical example of a distribution plant where considering also the diversity factor it's possible to save a lot when dimensioning the line and the size of the main breaker without losing total discrimination.

Please note that, in this case, only one PROLIM™ is sufficient, and also if the prospective short-circuit current is pretty high (35kA r.m.s.) it's possible to use standard 6kA miniature circuit-breaker.

Since also PROLIM™ it's available in modular compact shape suitable to be fit onto a standard din rail, the practical solution above described it's very small (see figure 9).

#### Total selectivity within the distribution group

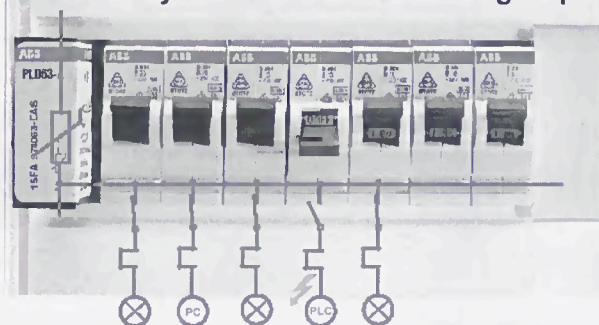


Figure 9 – Real dimension

#### IV Constructive solution

Actually PROLIM™ is available in two different sizes:

- 32A
- 63A

The lower size is available in single pole version and in three poles one, while the 63A is only available in the single pole configuration.

## "The PROLIM family"

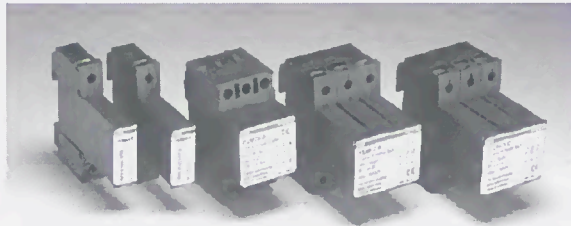


Figure 10 – PROLIM™ family

### V Technical Data

Here below the most significant technical data of PROLIM™ available on the market:

Specifications:	IEC 60947-2, IEC 60947-4-1
Rated operational voltage:	$U_c=400V$ and $500V$
Rated operational current:	$I_c=25$ and $36A$
Max short circuit current:	$I_k=50kA$
Max ambient temperature:	$55^\circ C$
Power losses per phase:	Approx. $3-4W$
Current limiting	$6kA$ peak (at $50kA$ )
Response time	$0.5ms$ (at $50kA$ )
Total break time	$2.5ms$ with MCB

## Diagram 1b Let-through energy

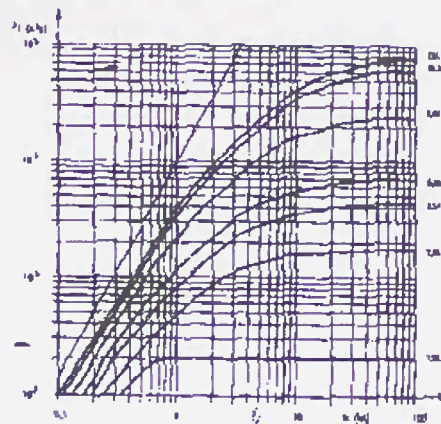


Figure 12 – Let-through energy diagram

### VI Likely future

ABB R&D efforts are actually concentrated on the integration of the PROLIM™ inside the miniature circuit-breaker.

## Diagram 1a Current limiting

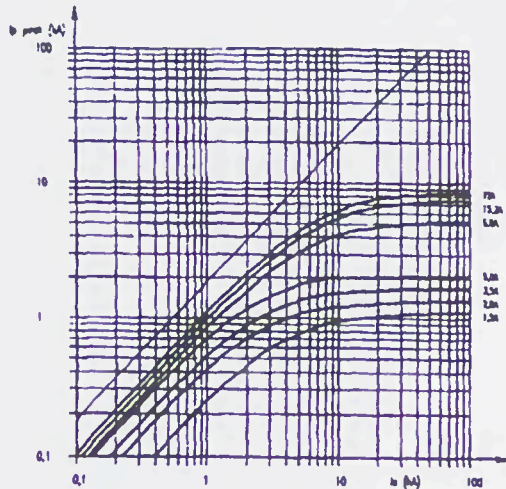


Figure 11 – Current limiting diagram

Response energy (PROLIM™)	$I^2t = 15 \cdot 10^3 A^2s$
Total let-through energy	$I^2t = 40 \cdot 10^3 A^2s$
Resistance, cold:	$3m\Omega/phase$
Resistance, tripped	$300m\Omega/phase$

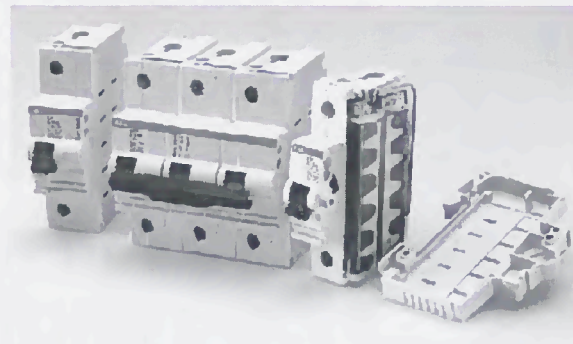


Figure 13 – New integrated version S620

It consists of the combination in one device of a standard miniature circuit-breaker designed for motor protection and a PROLIM™.

It can be assembled to have multipole version, typically 3p.

The tripping curve is the "K" typically tailored for motor protection: it carries 1.05 times the nominal current for one hour and it trips within one hour when the current is 1.2 times.

The breaking capacity of this new device is  $50kA$  while the performance of the mcb from which it derives it's only  $6kA$ .

THE HISTORY OF THE

ROYAL SOCIETY OF LONDON

FROM THE YEAR 1660 TO 1700

BY JOHN VAUGHAN

IN TWO VOLUMES

VOLUME THE SECOND

LONDON

Printed by R. and J. DODD, Strand

1825

THE HISTORY OF THE

ROYAL SOCIETY OF LONDON

FROM THE YEAR 1660 TO 1700

BY JOHN VAUGHAN

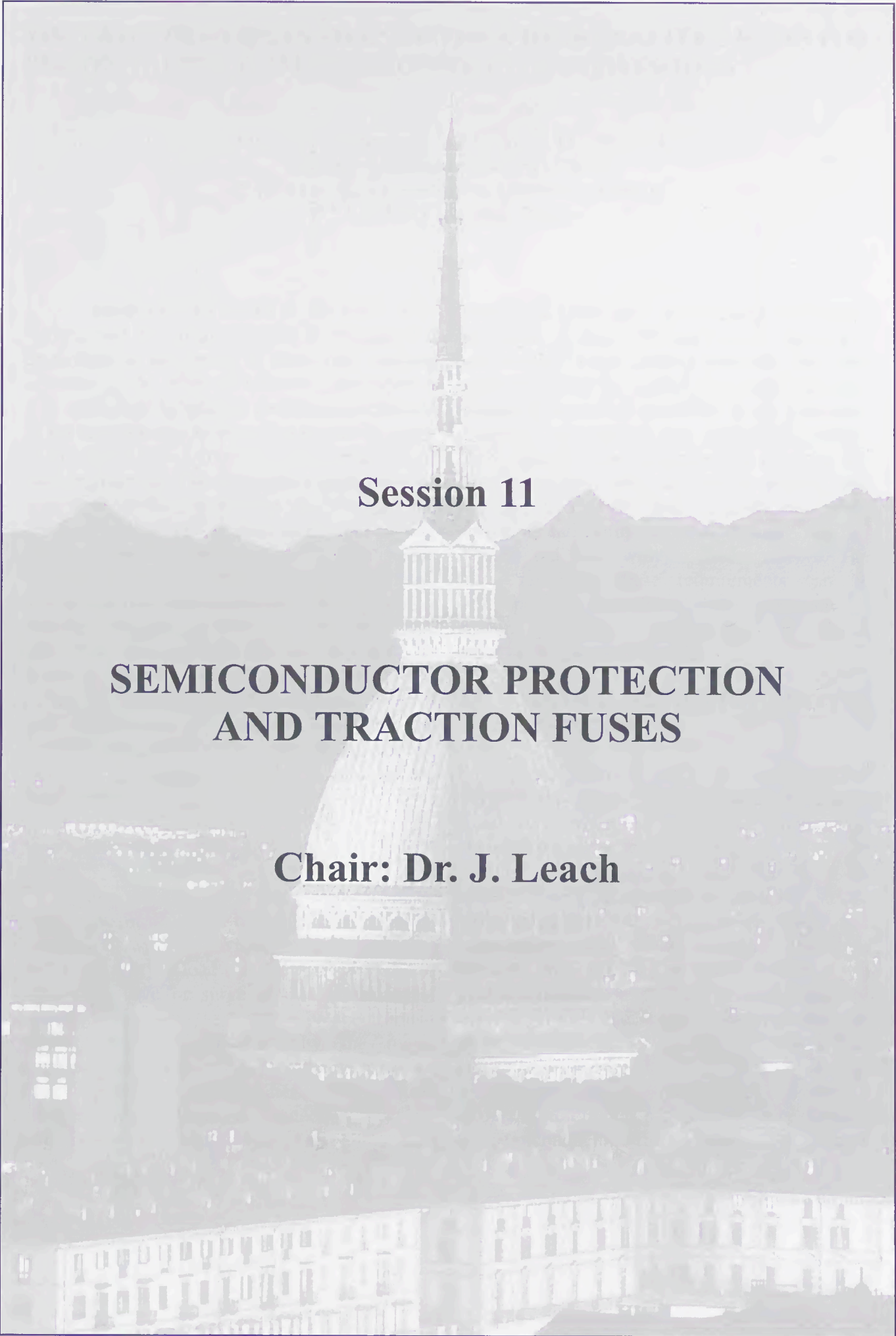
IN TWO VOLUMES

VOLUME THE SECOND

LONDON

Printed by R. and J. DODD, Strand

1825



**Session 11**

**SEMICONDUCTOR PROTECTION  
AND TRACTION FUSES**

**Chair: Dr. J. Leach**



# THE BASIC PRINCIPLES TO ENGINEER A HIGH QUALITY'S FUSES FOR PROTECTION OF POWER SEMICONDUCTOR CONVERTORS

N.A.Ilyina\*, G.G.Zhemerov\*\*, E.I.Zaika\*\*, I.G.Shklovsky\*\*\*

\* Kharkov Municipal Akademy, Ukraine

\*\* Kharkov State Politechnical University, Ukraine

\*\*\* Kharkov Collegium, Ukraine

**Abstract:** The object of the paper is to analyze and cristallize experience accumulated by authors in the course of their long standing activities in the field of research, development and testing (under service conditions including) of the semiconductor fuses and as one outcome of this work – to formulate a key principles of fuse engineering. The imaginative application of suggested generic guidelines can provide the designer with much – needed assistance, helping him to accept the challenge and to manage the complex problem of developing a high quality semiconductor fuses shortening an engineering date and economizing money and resources. The theoretical and practical concepts embodied in author's approach can be also applied to the problem of developing a semiconductor fuses of new generations. These principles are the following as applied to fuse current and voltage rating 25÷3600A, and 380÷1000V~ respectively.

## 1. INTRODUCTION

In the high power semiconductor equipments in which the high speed fuses can be put in series with the devices, in the lines of feed transformer, at the load side they are subjected to either repetitive or surge working currents of arbitrary waveforms and very wide spectrum of default conditions. That's why the major requirements on these fuses are the high working life, coordination with other fuses, circuit breakers and "electronic protection system" (algorithms of recognizing, revealing and

analysis of faults, their location and interruption by means of turn –off and turn-on thyristors), and reability when clearing precisely that fault operation which are needed to with the minimum aftermath regarding converter to be protected, actuating mechanism and processing duties. Quite naturally, the requirement of economy are close associated with the above remains and implies watt loss and overall dimension reduction and optimization of loading rate for devices and fuses with no excess reserve. The fuses satisfying these requirements can be developed by combining three suggested by authors principles, establishment of which presents the goal of the work.

## 2. OPTIMAL GEOMETRY OF FUSE ELEMENTS

Fuse element zone of small section incorporates three main parameters: shape, length and section of neck. The criterion for choosing the shape we consider the minimum non--uniformity of current density distribution at basically steady state conditions. The theoretical study and calculations, using FEM; physical simulation through the conductive paper models in association with the real fuse elements made of Ag, Cu, Al foils and, lastly, analysis of heat and clearing duties performed for the purpose of investigation of pattern of current density distribution in zone of small section had enabled to determine circular perforations as best suited to semiconductor fuses. The neck length

(perforation diameter) is compromise between heat duty which asks the minimal length and interrupting process which may reliably be realized only at neck length of no less than 1,3÷1,9mm. The minimal neck width (at standard metal Ag, Cu, Al – strip thickness of 0,05÷0,25mm) is determined by a feasibility of a technological facility available which in actual practice is about 0,05mm. The maximal neck section governed by Meyer equation  $\int i^2 dt = K_m S^2$  in such a way that a permissible let-through integral and peak let-through current would be within a specified limits that results in current density of order 700÷900A/mm<sup>2</sup>.

Of special importance is designing full-section part of fuse elements. Here we have three main parameters too: fuse element width, length (step between series necks) and space form. The investigations and many-years experience make it possible to consider the fuse element width of 10÷40mm as optimal for current rating of 25÷3600A. The fuse element width depends mostly upon the current rating. The fuse element length is determined primarily by the voltage rating (and d.c. circuit inductance) and for 380÷1000V is adopted within 10÷16mm.

Yet even at the same element width and length the space form of full section part plays key role in fuse performance. At the heart of the matter is the fact postulated by authors that the fuse cyclic withstandability is controlled [all other factors being the same] by the rigidity of fuse element. On general physical grounds we might expect the different values of rigidity of flat and bent fuse elements but how great are the distinction?

By application of the special approach using in particular the integral evolved by Moore on the basis of Castigliano theorem the relationship was derived for calculation of rigidity of an arbitrary bent full section part of fuse element as compared with the flat full section part. This relationship represents the rigidity as a force-to-displacement ratio [1]:

$$G = EJ \int y^2(x) \sqrt{1 + [y'(x)]^2} dx \quad (1)$$

where:

G – rigidity, E – Young's modulus, J – moment of inertia of the element cross-section, y(x) – arbitrary curve which determines the bending shape of fuse element. For important particular case, namely when full section part is bended in the shape of circle, semicircle, triangle and rectangle the relationships are as follows:

$$G_{\text{circle}} = EJ/3 \pi R^3 \quad (2)$$

$$G_{\text{semicircle}} = 2 EJ/3 \pi R^3 \quad (3)$$

$$G_{\text{rectangle}} = 3 EJ/a^2 (2a + 6b) \quad (4)$$

$$G_{\text{triangle}} = 3EJ/A^2 \sqrt{l^2 + 4A^2} \quad (5)$$

where respectively:

R – circle radius (1,5÷2,5mm)

a – height of rectangle (2÷4mm)

b – one half of rectangle foundation (2,5÷5,0mm)

A – height of triangle (2÷3mm)

l – one half of triangle foundation (2÷4mm)

In theory accordingly to calculations the rigidity of element bent in the form of circle, semicircle, rectangle and triangle is lower than the rigidity of flat element by 45000, 20000, 15000 and 9000 times respectively (the case of one series bend). In real practice cyclic withstandability of semiconductor fuses having bent elements is higher by 20÷200 times compared with flat elements. The theoretical and experimental investigations of effects of bend shape and amplitude, number of series bends in coupling with packing density of filler and other factors as well as operating experience had shown that all the fuse element full-section parts must be bent the necks being placed at the borders of bends. The bends themselves are to face the inner surface of the fuse body which among others improves heat transfer and excludes damage of necks while inserting quartz filler.

### 3. MAXIMAL FILLING COMPACTNESS WITH OPTIMAL SET OF GRAIN SIZES. HARD FILLER.

To ensure the reliable fuse performance it is vitally important that the maximal degree of compaction which is of order  $1,78 \div 1,84 \text{g/cm}^3$  would be achieved under optimal collection of quartz sand grain sizes instead of grains of one size. In practice it will suffice to have ternary – quinary mixture. Within the boundaries of the mean grain sizes of  $0,1 \div 1,1 \text{mm}$  which is optimal the absolute value of grain size has little or no effect on packing density (compactness), taking into consideration large diameter of fuse body which is  $20 \div 100$  times as bigger as grain size. The only thing that matters is the ratio of grain sizes in the sand mixture. If use the sand grain of one size be it  $0,1 \text{mm}$  or  $1,0 \text{mm}$  the packing density would be the same low of order  $60 \div 70\%$  in both cases. The utilizing the ternary mixture permits to obtain packing density up to  $85\%$ , a multicomponent mixture – theoretically up to  $100\%$ . Optimal grain mean sizes ratios for quinary mixture are:  $1$ ;  $1,2 \div 1,6$ ;  $1,6 \div 2,0$ ;  $2 \div 3$ ;  $3 \div 5$  at their % contents  $7 \div 13$ ;  $30 \div 50$ ;  $20 \div 30$ ;  $15 \div 25$ ;  $2 \div 8$  respectively. The filling in the fuse cartridge with quartz sand is carried out by means of special vibration facility.

Application of hard filler in semiconductor fuses is advantageous under almost every operation condition except, perhaps, of interrupting small overload current. The authors had developed the original up-to-date technologies for forming hard filler structure. It incorporates the filling a fuse with quartz sand, composition and method of injection of binding agent, subsequent blowing of air at different pressure  $0,25 \div 2,0 \text{atm}$  and temperature  $20 \div 150^\circ\text{C}$  if necessary and lastly process of filler hardening by passing current through fuse. The attempt was made to present an theoretical picture of physical processes during filler hardening by method suggested by authors as well as experimental investigation

aimed at elucidation of qualitative and quantitative effects of process factors. Some results of this work were published [2]. The results yielded which portray the influence of hard filler on the fuse functional characteristics can be summarized briefly as follows with respect to mechanical and electrical properties of hard filler. Filler leakage very dangerous by its consequences is fully prevented which is of high priority, for instance, for transport converters operating under constant strong vibrations. Intactness of fuse elements in fuses operating in rotary rectifiers of brushless excitation systems in nuclear power station is totally assured. The fuse have ability to withstand  $6000$  “g” continuously in addition to the acceleration and deceleration stresses and operate satisfactorily under maximum fault conditions. Increasing of heat condition twice as high as at conventional filler permits up rating of current about  $10 \div 20\%$  or decreasing of power losses in the same degree. Coupled with bent elements the hard filler increases additionally up to several times cyclic service life. The employing of bent elements and hard filler makes it possible to use Al and Cu as an element material through the neutralizing the drawbacks of this material as fuse elements. The main functional characteristics of semiconductor fuses – let-through integral and arcing energy under short-circuit fault – are essentially diminished up to  $1,5 \div 2,0$  and  $2 \div 4$  times correspondingly. The ratio of fusing integral to let-through integral is substantially improved as well as withstandability to the repetitive small operating overload is increased.

### 4. TWO-SIDED WATER COOLING

Almost all high power semiconductor converters operate with water cooling of devices which up-rates current rating up to  $5 \div 8$  times. The semiconductor device water cooling system can be utilized for cooling fuses as well. As experimental studies and operation experience have shown the water cooling is especially

effective for fuses having bent element and hard filler at rated current over 1000A and voltage 220÷660V. The two-sided water-cooling has increased current rating for example from 1600A to 2500A. In this case when water flow rate was varied from 0,2 to 0,033 l/s the temperature changes of water were within a limits 5÷30°C. The heating of water under nominal power take-off of order 200÷300Wt was found to be no more than 1÷2°C. The alterations of water flow rate by 5÷6 times caused nearly no change in power loss. When employing water cooling the thermal constant of fuse is 10÷20 times smaller than at natural air cooling. That is under two-sided water cooling the fuse of 1600A attains the steady state regime within 15min as compared to 3÷4 hours at natural air cooling. Two-sided water cooling complicates the problem of assigning fuse current rating. The conventional procedure based on measuring the fuse terminal temperature doesn't work in this case because both fuse terminal are at water temperature which is practically constant. In such a situation two approach has proven to be sufficiently reliable. The first employs as criteria the fuse body temperature the idea being that its temperature must not exceed the value permissible for fuse terminal (130÷170°C). The second is based on the assumption that at steady state condition the fuse voltage drop is within the limits of 1,3÷1,5 times regarding to initial value. Two-sided water-cooling provides additional (to the above mentioned) resistance against small operating overloads and increases slightly the cyclic ability. However, on the other hand, in the short-circuit duties at interrupting 50÷200 rated current when energy dissipated in the fuse before melting is 1000÷5000 times as

much as in steady state and this process is 1÷6ms long, the water cooling doesn't retard fuse melting. The oscillograms of interrupting short-circuit current from 50 rated current with water-cooling and without it are almost identical. Yet because fuse which due to the water cooling is for example of rated current 2500A has in effect a neck cross-section pertinent to 1600A then as a result the let-through integral has proved to be smaller more than twice, arcing energy-by three times and peak let-through current up to 40%.

## 5. CONCLUSIONS.

Integrated utilization of: optimal geometry of both neck and full section part of fuse element; maximal filling compactness with optimal set of grain sizes and hard filler; two-sided water cooling allows to constitute the principles than can be thought of as a conceptual and in the same time methodological approach to tackling a problem of engineering up-to-date sophisticated fuses for protection of high power semiconductor equipment.

## 6. REFERENCES

- [1] N.A. Ilyina, K.K. Namitokov, I.G. Shklovsky. "Pulse withstandability of the semiconductor protection fuses", Sixth Int. Conf. On Switching Arc Phenomena, 12-15 Sept.1989, Lodz, Poland.
- [2] N.A. Ilyina, G.G. Gemerov, K.K. Namitokov, I.G. Shklovsky. "Principal Manufacture Technologies for Semiconductor Fuses", Fourth Int. Conf. On Electric Fuses and their Appl., 1991, 74-80, Nottingham, UK.

# THERMAL STRESSES OF FUSES AND PROTECTED SEMICONDUCTOR DEVICES

M. Adam, A. Baraboi, C. Pancu, T. Plesca

"Gh. Asachi" Technical University, Faculty of Electrical Engineering,  
Iasi, Romania

**Abstract:** The paper presents thermal stresses of fuses and semiconductor devices (particularly for a type of ultra-rapid fuse and protected semiconductor devices such as thyristor) for different current waveforms through ones.

The research of thermal stresses is doing through tantamount to RC circuits of thermal models of considered devices. Transient conditions' analysing to electrical circuits is doing with EMTP software.

## I. INTRODUCTION

The rectifier semiconductor devices (diodes, thyristors) are very sensitive to overcurrents. The losses due to those overcurrents bring about overheating of junctions that can destroy the semiconductor device. The semiconductor devices can support overcurrents only a limited short time, that time depending on the overcurrent values. The thyristor limiting thermal characteristic is shown, in principle, in Fig. 1, curve no. 1. It indicates the time how long can be supported the overcurrent, depending on the ratio value between overcurrent ( $I_{oc}$ ) and rated current ( $I_n$ ). So, it is necessary a protection to interrupt the current before to reach the limit value.

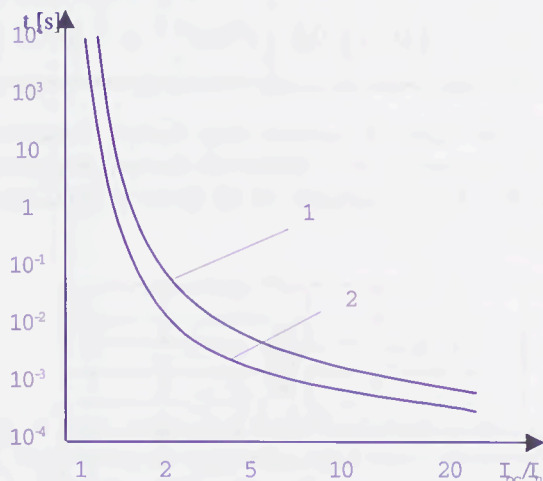


Fig. 1: The thyristor limiting thermal characteristic (curve no. 1) and time-current characteristic of fuse (curve no. 2).

One of the protection achievement means is by using ultra-rapid fuses. In this case it must be a full coordination between time-current characteristic (Fig. 1, curve no. 2) of fuse and limiting thermal characteristic of protected semiconductor device.

## II. MODELING WITH RC CIRCUITS OF ELECTRIC FUSES AND SEMICONDUCTOR DEVICES

### II.1. Analogy between thermal and electrical field

The thermal resistance between medium 1 and medium 2 could be written:

$$R_{t12} = \frac{\Delta\theta}{P}, \quad (1)$$

where:  $\Delta\theta = \theta_1 - \theta_2$ , over temperature between medium 1 and medium 2;  $P$ , the thermal flux.

The thermal resistance of conduction is determinate by similar relation with electrical resistance:

$$R_{t12} = \frac{d}{\lambda \cdot S}, \quad R_e = \frac{\rho \cdot l}{S}, \quad (2)$$

where:  $\lambda$ , thermal conductivity;  $\rho$ , electrical resistivity;  $d$ ,  $l$ , length;  $S$ , section. For heat exchange with convection the thermal resistance is calculated with following relation:

$$R_c = \frac{\Delta\theta}{\alpha_c \cdot S_c}, \quad (3)$$

where:  $\alpha_c$ , the thermal transfer coefficient for convection;  $S_c$ , the exchange surface for convection.

The thermal capacity, respectively electrical is give by following expressions:

$$C_t = \frac{\int_0^t P \cdot dt}{\Delta\theta}, \quad C_e = \frac{\int_0^t i \cdot dt}{u}. \quad (4)$$

The analogy between thermal and electrical parameters is shown in Tab. 1, [1], [3].

Tab. 1

Thermal parameters	Electrical parameters
Flux - P [W]	Electrical current - I [A]
Density of thermal flux - q - linear [W/m] - surface [W/m <sup>2</sup> ]	Density of current - j - linear [A/m] - surface [A/m <sup>2</sup> ]
Temperature - $\theta$ [°C] Over-temperature - $\Delta\theta$ [°C]	Potential - V [V] Voltage - U [V]
Thermal resistance - R [°C/W]	Electrical resistance - R [ohm]
Thermal capacity - C [J/°C]	Electrical capacity - C [As/V]
Ohm law - $P = \Delta\theta/R$	Ohm law - $I = U/R$

## II.2. RC models for electric fuses and semiconductor devices

For modeling, it was considered the ultra-rapid fuses type UR by 40 A and thyristor T63N by 63 A, these devices being component parts of commanded rectifier type RUT.

The fuse constructive structure was divided in 3D cells like one from Fig. 2 [2], [4], [6].

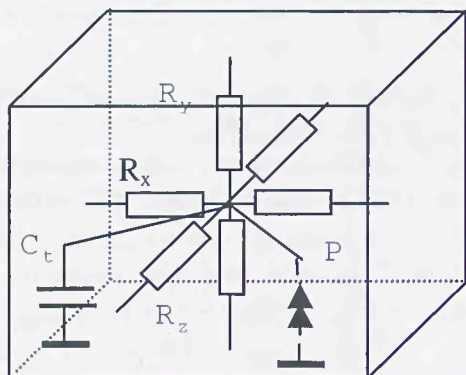


Fig. 2: Elementary cell of RC models for electric fuses.

The equivalent thermal resistances  $R_x$ ,  $R_y$  and  $R_z$  which characterize each direction was divided (fifty-fifty) and are connected between central knot and each face. There are connected in the central knot of each cell the equivalent thermal capacity  $C_t$  together with current source P which means the thermal flux because of Joule losses. The current source P will be present only to the cells that contain component parts from conducting wire flowing by the electrical current (for instance, the fuse links).

In the case of semiconductor device assuming cylinder symmetry, the equivalent thermal circuit of semiconductor device contains concentrated thermal resistances and capacities Fig. 3. The meaning of notation are the following:  $R_{J-C}$ ,  $R_{C-R}$ ,  $R_{R-A}$  the junction-case, case-heatsink, heatsink-environment thermal

resistances;  $C_J$ ,  $C_C$ ,  $C_R$ , - the junction, case and heatsink thermal capacities;  $P_J$  thermal flux because of loss power into semiconductor.

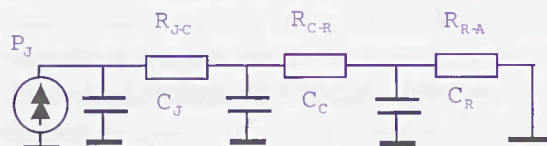


Fig. 3: The equivalent thermal circuit of semiconductor device with concentrated thermal resistances and capacities.

The forward mean power loss in a period of time can be calculate with the relation:

$$P_J = \frac{1}{T} \int_0^T u_F i_F dt = \frac{1}{T} \int_0^T (U_{T0} + r_T i_F) i_F dt = U_{T0} I_{Tmed} + r_T I_{Tef}^2, \quad (5)$$

where:  $U_{T0}$  - threshold on-state voltage;  $r_T$  - equivalent resistance;  $I_{Tmed}$  - root mean square (r.m.s.) on-state current;  $T$  - period of time.

Referring to internal constructive structure of thyristor type T63N (the layers of silicium, molybdenum, copper), its case (B27) and considering an aluminium heat type TNF, it was calculated the values of thermal resistances and capacities, Tab. 2 [5].

Tab. 2

Thermal resistance [°C/W]			Thermal Capacities [J/°C]		
$R_{J-C}$	$R_{C-R}$	$R_{R-A}$	$C_J$	$C_C$	$C_R$
0,417 (a.c. 180 °el)	0,08	0,6	$4,5 \cdot 10^{-3}$	25	577,39
0,4 (d.c.)					

The value of junction-case thermal resistance  $R_{J-C}$  is increasing with additional thermal resistance  $\Delta r(\alpha)$ , Fig. 4, [5], depending on the thyristor conduction angle  $\alpha$ .

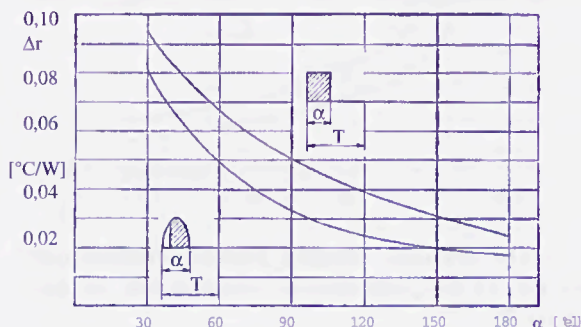


Fig. 4: The additional thermal resistance  $\Delta r(\alpha)$  vs. thyristor conduction angle  $\alpha$ .

### III. NUMERICAL RESULTS

The study of thermal stresses is doing through equalization of thermal models of considered devices with RC electrical circuits, using the analogies from Tab. 1. The analysis of transient conditions from electrical circuits is doing with EMTP software.

For a mean on-state current by 63 A, the over temperature on junction  $\Delta\theta$  is about 105.7 °C and on case is about 64.4 °C, Fig. 5.

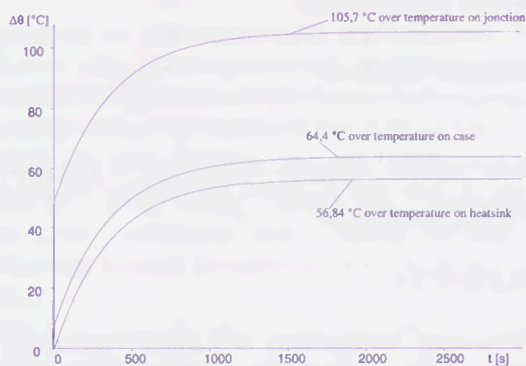


Fig. 5: The over temperatures in various points for a mean on-state current by 63 A.

To an environment temperature by 20 °C, these values are checking by sheet data: 125 °C – operating junction temperature; 85 °C – case temperature.

In Fig. 6 are shown the evolution of over temperature  $\Delta\theta$  in the case of thyristor and fuse in the next condition: sinusoidal r.m.s. current by 40 A, conduction angle by 180 °el. and 120 °el.

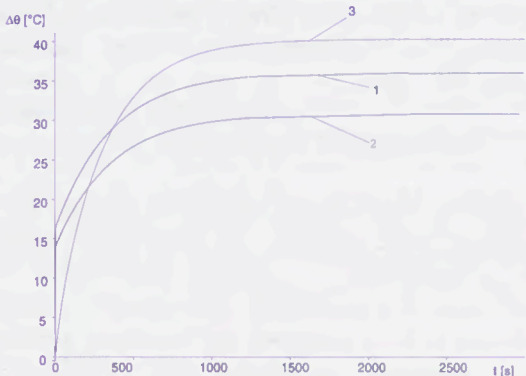


Fig. 6: The evolution of over temperature in the case of thyristor and fuse for a sinusoidal r.m.s. current by 40 A, conduction angle by 180 °el. and 120 °el.

It notes that over temperature on thyristor junction is about 35.91 °C (curve no. 1) for 180 °el conduction angle, respectively 30.8 °C (curve no. 2) for  $\alpha=120$  °el and 40.18 °C (curve no. 3) on fuse link.

The operating condition over temperature is the same in the case of fuse link because the loss power depends on r.m.s. current value, but in the case of junction, the loss power depends also on mean current value which is different in these two cases.

The evolutions of over temperature  $\Delta\theta$  on fuse link and thyristor junction in the next conditions: square pulses r.m.s. current by 40 A, conduction angle by 180 °el and 120 °el, respectively direct current (d.c) are shown in Fig. 7.

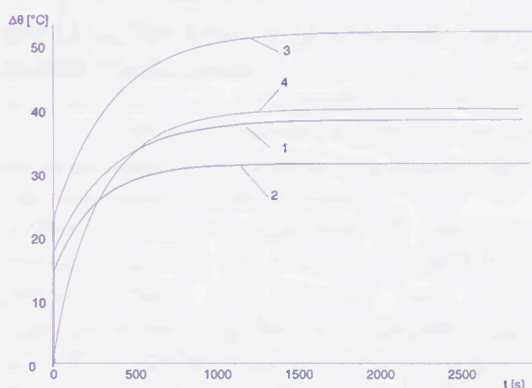


Fig. 7: The evolutions of over temperature on fuse link and thyristor junction for square pulses r.m.s. current by 40 A, conduction angle by 180 °el and 120 °el, respectively direct current (d.c).

The operating conditions over temperatures on junction are 39.4 °C ( $\alpha=180$  °el, curve no. 1) 31.9 °C ( $\alpha=120$  °el, curve no. 1), respectively 52.01 °C to d.c. (curve no. 3). The over temperature value on fuse link has the same value like in the previous case 40.18 °C (curve no. 4).

The evolution from Fig. 8 and Fig. 9 is getting for a sinusoidal overcurrent, respectively square pulse overcurrent with a period by 10 ms and r.m.s. current value by 282 A where is noted: 1 – junction over temperature; 2 – fuse link over temperature; 3 – thyristor junction loss power.

It notices that while on junction the maximum over temperature are approximately equal (223.8 °C – sinusoidal current, 219.3 °C – square pulse current), the over temperature on fuse link, in the same moment has higher values in the case of square pulse current. The over temperature in the case of square pulse current, because of small time thermal constant of junction (about 2 ms), is getting fast an approximately constant value. Further on, its rising is very little observable because the case time thermal constant is about seconds.

On these characteristics, the melting temperature of silver fuse link is reached in 6.3 ms to sinusoidal pulse current, respectively in 48 ms to square pulse current. So, it can affirm that in the case of square fault currents the fuse will work faster.

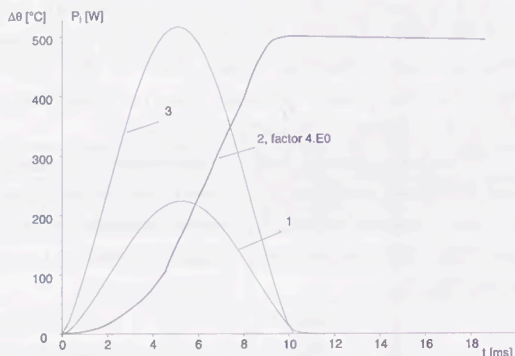


Fig. 8: The evolutions for a sinusoidal overcurrent with a period by 10 ms and r.m.s. current value by 282 A. 1 – junction over temperature; 2 – fuse link over temperature; 3 – thyristor junction loss power.

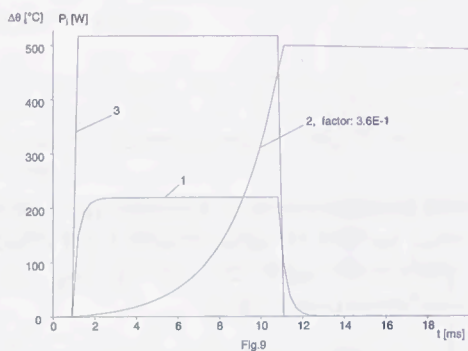


Fig. 9: The evolutions for a square pulse overcurrent with a period by 10 ms and r.m.s. current value by 282 A. 1 – junction over temperature; 2 – fuse link over temperature; 3 – thyristor junction loss power.

It comes out, experimentally, that at a sinusoidal pulse current with a period of 10 ms and r.m.s. current value by 1400 A, the thyristor destroyed after 273 ms from the moment when the electrical current was in the circuit. On the thermal model of thyristor, at this moment is reached the melting temperature of silicium (1412 °C). In the case of fuses, at this current is reached the melting temperature of silver (960 °C) after 0.54 ms. This fact shows that the fuse can protect the thyristor if

the period of time between fuse melting time and electric arc extinguish doesn't exceed 2.19 ms.

#### IV. CONCLUSIONS

The EMTP software allows thermal stresses simulation of fuses and semiconductor devices using the analogy between electrical and thermal parameters.

The operating conditions over temperature for ordinary currents, the case of thyristor, are bigger for square pulses current then sinusoidal current, at the same r.m.s. current value.

The numerical results show that, in the case of short-circuit currents, the fuses prearcing time is smaller for square pulses current then sinusoidal pulses current.

The analyses and simulation of thermal processes using this method allow to establish easily the thermal stresses of fuses and thyristors at different evolution of current and overcurrents.

#### REFERENCES

- [1] M. Adam, A. Baraboi, P. Leonte, "Modeling of thermal stress and the monitoring of circuit breakers", 5<sup>th</sup> International Conference on Optimization of Electric and Electronic Equipment OPTIM'96, Brasov, Romania, 1996, 641-646.
- [2] A. Baraboi, M. Adam, P. Leonte, T. A. Baraboi, "Simulation des contraintes thermiques de l'appareillage électrique", ICATE '96, Craiova, Romania, 1996.
- [3] Suci I., "Bazele calcului solictarilor termice ale aparatelor electrice", Editura Tehnica, Bucuresti, 1985.
- [4] Beaujean D. A., Newbery P. G., Jayne M. G., "Modeling fuse elements using a CAD software package", Fifth International Conference on Electric Fuses and their Applications, Ilmenau, Germany, 133, 1995.
- [5] M. Bodea, A. Silard, s.a., "Diode si tiristoare de putere", Editura Tehnica, Bucuresti, 1989.
- [6] A. Baraboi, I. Ciutea, M. Adam, C. Pancu, T.A. Baraboi, "Modeling and simulation of the thermal stress at the electric fuses contacts", Sixth International Conference on Electric Fuses and their Applications, Torino, Italy, 1999.

# SHORT CIRCUITS IN 3 kV DC TRACTION SYSTEM AND FUSES - SIMULATION AND TESTING

Author: Ing. Gabriele Alessandro ANTONACCI

F.S. S.p.A. – Unità Tecnologie Materiale Rotabile  
Direzione Tecnica - Sperimentazione  
V.le Spartaco Lavagnini, 58 - 50129 Firenze, Italy  
Tel. ++39 0 55 2353199; ++ 39 0 55 484111 ; Fax ++39 0 55 2353522  
E-mail: Antonacci@asamrt.interbusiness.it

**Abstract.** This paper consider several aspects related to 3 kVdc fuses, taking into consideration short circuit simulation and testing methods. A presentation of some activities made by FS in this field is made.

The first part of this paper describes quickly standard developments and some short circuit measurements on line. Then a preliminary simulation code able to make a simulation of 3 kVdc electric feeding system during short circuits is drawn.

In the end the new FS High Voltage Test Facility at the FS Electric Substation of Empoli is described.

## I CONTEST

The separation between management of the power supply system and the traction system, the interconnection between the European railway networks, and technical developments of on-board equipment, all require a series of operations for which simulation and experimentation is essential, particularly in the case of verifying the aspects governing safety and reliability.

Several factors representing a focal point today:

a) All products for railway use should be subjected to a course standardized at European level, regarding their qualification and/or homologation; the procedure “**Conformity assessment and acceptance of railway products**”, at its highest level of definition in UIC-UNIFE-UITP, foresees the instituting of test laboratories which must supply all data pertaining to test results to the Organization in charge of qualification.

b) The definition of technical specifications of railway “interoperability” foresees, in particular for the electrical part, the definition of the regulations and test specifications which rolling stock and components

have to be subjected to in order to guarantee their use on all the various railway networks.

c) The evolution in the field of electrical and electronic equipment has brought to light a series of questions related to electrical and electronic interaction between the various apparatuses, and for which there is the need for systems designed to simulate as closely as possible their real conditions.

## II STANDARDS

At the level of the IEC (International Electrotechnical Commission) the revision of the IEC77 “Regulations for electrical traction equipment” is currently being completed by the WG 23 of the CT9 (Traction). The updating of this document foresees the issuing of a new family of standards, illustrated in table 1, which will pertain to the general operating conditions of electrical equipment for traction, electromechanical equipment, power switches, and fuses. They will be included in European Standards.

*Table 1: Several IEC Publications, of recent or future issuing.*

IEC60077-1	: Railway applications – Electric equipment for rolling stock – Part 1: General service conditions and general rules
IEC60077-2	: Railway applications – Electric equipment for rolling stock – Part 2: Electrotechnical components – General requirements
IEC60077-3	: Railway applications – Electric equipment for rolling stock – Part 3: d.c. circuit breakers
IEC60077-4	: Railway applications – Electric equipment for rolling stock – Part 4: a.c. circuit breakers
IEC60077-5	: Railway applications – Electric equipment for rolling stock – Part 5: High Voltage fuses

- Within the frame of the UIC (Union International des Chemin de Fer) standards several "Fiches" to be considered are the 550 OR, "Installations pour l'alimentation en énergie électrique du matériel à voyageurs" and the 550-2 OR, "Installations pour l'alimentation en énergie électrique du matériel à voyageurs - Essais de types". Amongst other things, the tests involving high voltage fuses, the measurements of harmonic currents and the inlet impedance of the vehicles are described in these.

- Following FS specification define the tests pertaining to the supply of high voltages fuses the Ferrovie dello Stato S.p.A:

Spec. FS N° 309532: "General specification for the supply of HT fuses for DC circuits.;

### III SHORT CIRCUIT IN DC TRACTION SYSTEM

#### III.1 General

Due to the severity of the extreme conditions involving short circuits, these are a critical point when it comes to dealing with railway safety and interoperability, for the aspects related to defining energetic and electrodynamic stress, and those concerning electromagnetic compatibility.

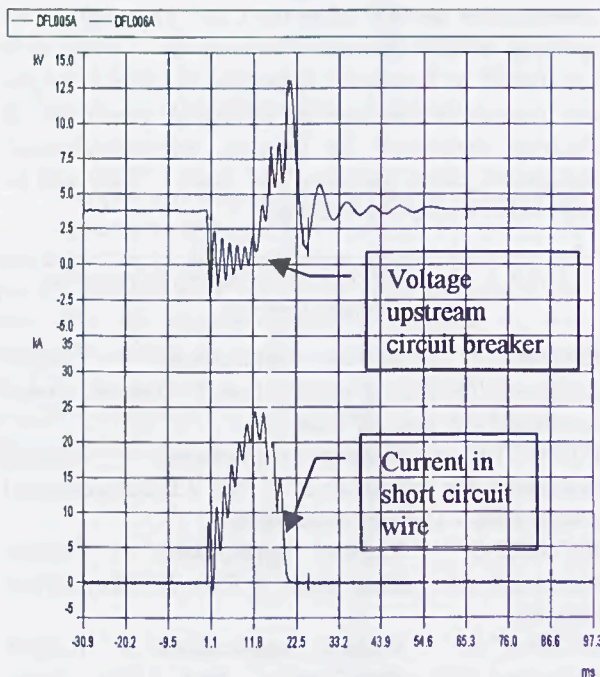


Fig. 1: voltage and current measurements during a short circuit near a substation opened by a circuit breaker

In the field of electrical experimentation of rolling stock, the following developments have evolved

regarding the definition of stress deriving from short circuits:

- monitoring of test vehicles and testing of safety equipment; conducting short circuit tests on the line and on rolling stock [fig. 1 and 2];
- the developing of calculation models designed to simulate the 3 kV dc electrical system during a short circuit ;
- classification of the main stress agents caused by such transitory phenomena.

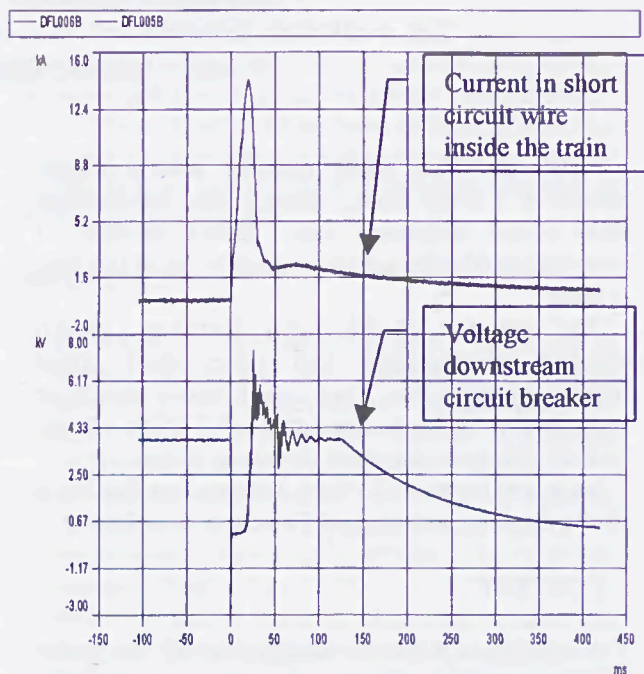


Fig. 2: measurements during a short circuit between substations opened by a circuit breaker

This paper considers 3000 Vdc systems, seeing that present day experimental and theoretical research is focalized on this type of system typology. It must be pointed out however, that these results may also have an effect on 25 kVac systems for the following reasons:

- a short circuit in this system may have dynamic elements which are in part similar to those associated with the 3000 Vdc system;
- the need to have poly-voltage rolling stock calls in any case, for compatibility between the on-board systems and the existing power supply systems.

#### III.2 Classification

In order to make a classification of the short circuits and to make their simulation on board rolling stock there are various points which must be taken into account.

- The position of the rolling stock in relation to the substations, in the following situations:
  - short circuit in proximity of the substation terminals;

- short circuit on the line;
- short circuit in interconnection.

Circuit-wise the elements to be defined at this point are: the substation circuits (transformers, rectifiers, inductive and capacitive filters, protections); the contact lines and the return circuits, (inductance, resistance and capacity transversal and mutual coupling between lines next to each other); the earthing system (ground, piling, strands, tracks).

b) The position of the short circuit inside the rolling stock:

- upstream from the DC circuit breaker;
- downstream from the DC circuit breaker, upstream from the filters;
- downstream from the filters;
- on the train line;
- on rolling stock in composition.

The main elements to be considered related to rolling stock are the characteristics of the DC circuit breaker, the fuses, the specifications of the overvoltage arresters, the body of the vehicle, the inductive-capacitive filters, the cable laying, the traction motors, the converters .

c) The presence of other vehicles:

- in the train composition;
- not in composition, on the same track;
- not in composition, on the next track.

The rolling stock in composition interacts by means of the DC circuit breaker, the overvoltage arresters, the inductive-capacitive filters, the motors and converters; in particular, in the case of two interconnected locomotives, as happens with the ETR500, or with interconnected machines in double traction, added oscillations of a considerable entity may be created, with the filters of the two locomotives at each end of the train and connected via the contact line and the track, also entering into oscillation with them as well.

#### IV SIMULATION

One of the first stress evaluation methods to use is that obtained via by simulation of the system.

For this purpose a calculation program has been developed for simulating the electrical power supply system. As inlet variables to choose from, this considers the configuration of the system, the circuital parameters of the substation (number of units, short circuit voltage, transformers, filter characteristics), the geometric characteristic of the lines, the operating curves of the overvoltage arrester, and the characteristics of the DC circuit breaker of the locomotive, with the impedance of the fault point.

As an outlet it supplies the wires of the voltages and the currents in the nodes and branches of the system,

together with the energetic parameters correlated to the phenomenon. This calculation model, even if not complete, has given good match-ups, especially in assessing the current, with respect to the measurements obtained via experimentation.

In Fig. 3, as an example, a simulation of a short circuit in an interconnection point is showed: the two curves are related to an opening by a circuit breaker and by an "ideal" fuse.

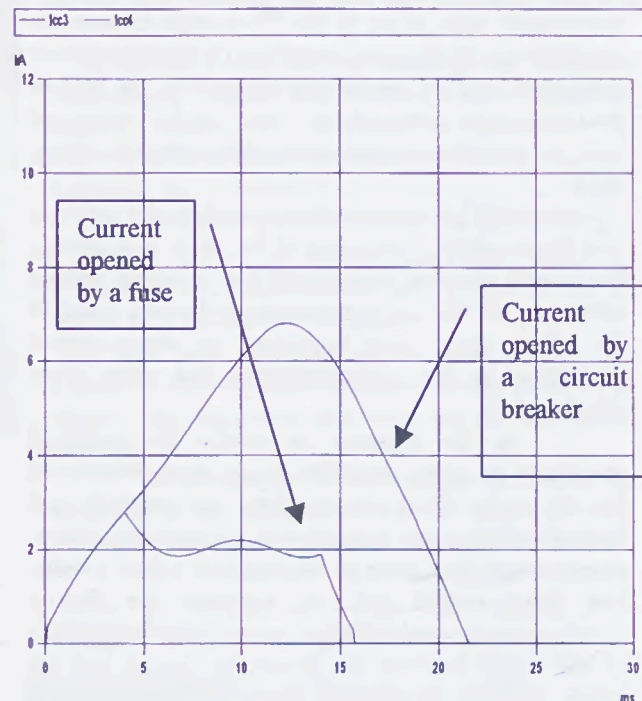


Fig. 3: simulation of short circuit currents in an interconnection point

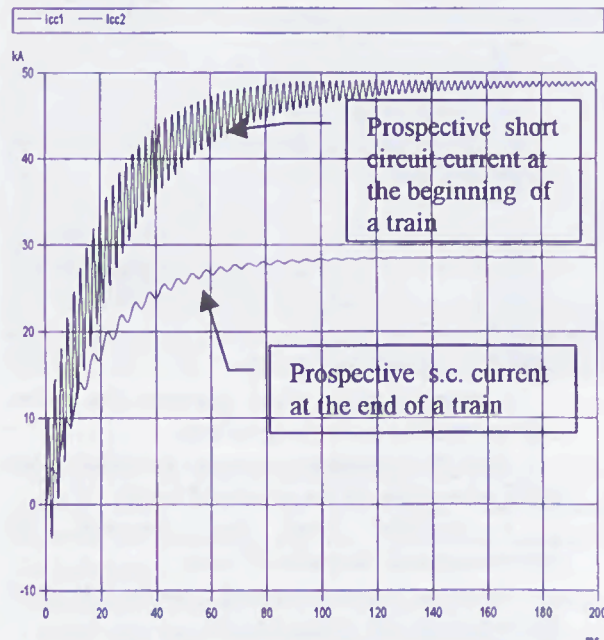


Fig. 4: prospective short circuit currents near a substation

In Fig. 4 is showed short circuit prospective current waveforms in a position of the train near a substation, with the waveform related to a short circuit at the beginning and at the end of a train.

## V THE NEW TEST ROOM

### V.1 General

The new High Voltage Electrical Test Room at Empoli has recently been set up by the FS in order to meet the demands related to experimentation of electrical power equipment, and for conducting research in the field of electromagnetic compatibility. Tests can be carried out both on individual apparatuses and complete rolling stock.

This system has been created to replace the previous Test Room which, at the end of the '80's after having for several decades represented the principal testing laboratory for the electrotechnical equipment used in FS rolling stock, was beginning to show evident limitations as far as performance and space were concerned.

At the moment in which the technical specifications of the new Test Room were determined (in the early 90's), apart from the renewal and intensification of the capacities of the existing system, consideration was given to the fact that a high voltage test room should also be equipped for testing electromagnetic compatibility, seeing that the problem of interaction between the signalling devices and the power systems represented one of the most critical questions for the future, and also in view of the know-how acquired in the old test room in perfecting digital instrumentation for carrying out operational surveys.

### V.2 Description of the system

The test room is equipped with the following installations and systems:

- a 3000 Vdc high voltage testing system, powered by Unit C of the Electric Substation, and consisting of line and load simulators (rheostat and inductance), an electromechanical configuration system, and protection devices;
- a control system, which manages the system and controls the performing of tests ;
- 380/220 V auxiliary systems, including a no-break generating set for privileged loads;
- a shielded room and pre-room for electromagnetic compatibility tests;
- operating tracks energized from the test room, and equipped with inspection pit.

### V.3 The 3 kV dc system

Fig 5 illustrates the block diagram. This system consists of the following:

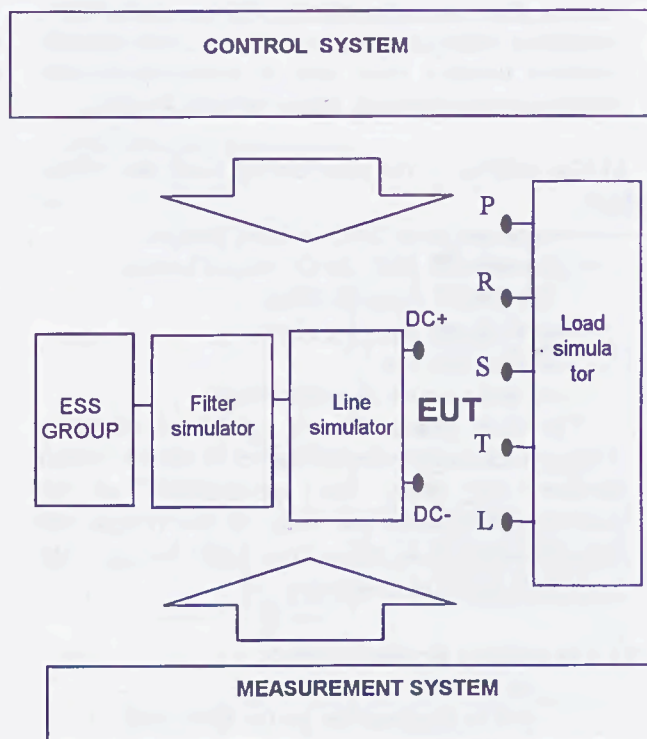


Fig. 5 HV circuit block-diagram

- a) Power outlet: UNIT C of the ELECTRIC SUBSTATION, inlet power supply 130 kV ac, power rating 5.4 MW, outlet voltage 3600 Vdc, adjustable.
- b) Filter simulator: inductance of network filter  $L=6$  mH with a 2 mH terminal also available, filter condensers, bench with 1100  $\mu$ F .
- c) Line simulators:
  - c.1) RX rheostat line simulator -  
The resistance values are variable from 0.1 to 6.3  $\Omega$ , in steps of 0.1  $\Omega$ . This rheostat is sized to support ON/OFF cycles with current values exceeding 10 kA. Packets are also available designed specifically for short circuit testing. The line resistance is controllable via the PLC by means of the contactors.
  - c.2) LXA1, LXA2, LXB1, LXB2, LXB3 inductance line simulators (Fig. 6) :  
Type LXA inductor : N° 2 inductors, each of 6.5 mH. The constructive features are such that the parasitic currents are minimized to approx. 1 MHz.

Type LXB inductor: N° 3 inductors, each with 13 mH.

All the inductors are located inside the building on special stainless steel frames for minimizing the dynamic actions deriving from the coils during the tests. The line resistance is controllable via the PLC by means of the contactors.

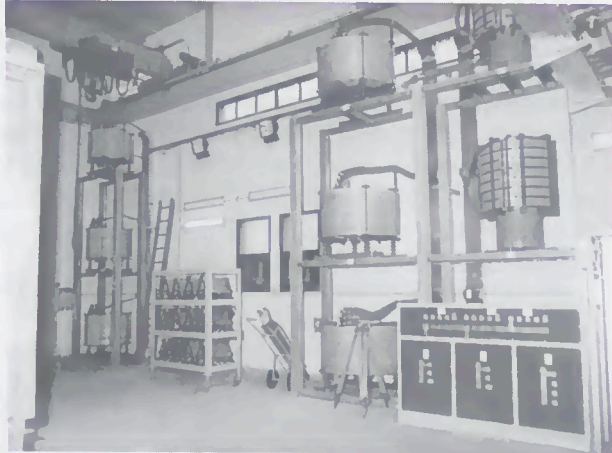


Fig. 6 : inductance simulators

d) Load-resistance Simulator:- The resistive load in configuration series, powered at 3600 V, which can absorb, on a continuous basis, a current varying from 1 up to more than 750 A, with steps adjustable up to 1 A.

- in parallel configuration, currents over 1000 A can be absorbed on a non-continuous basis.

- The load can be set in three-phase configuration, with three R S & T terminals available

The resistances are electrically divided into four benches; to each bench resistances are attributed which can instead be controlled individually via the PLC by means of the contactors

The line and load resistances have been installed in stainless steel cabinets located on the roof of the building.

This load is split up into sections with natural air ventilation and sections with forced air ventilation in order to reach higher dissipating capacities throughout the overall dimensions: a careful layout of these sections has been necessary in order to reduce to a minimum acoustic emission towards the outside, decisions which have proved correct at the end of operation.

e) Load - inductance simulator: The inductive load is composed of 3 inductors, LC1, LC2 and LC3 each with  $L = 13$  mH.

The following intermediary terminals are also provided : 3 mH; 6.5 mH; 9 mH.

#### V.4 The control system

Management of the test room, the choice of network/load characteristics, and the setting of automated test sequences are all handled by means of a PC, with specifically designed software (in Fig. 7 a comprehensive image of the control room). From the very first page of the menu it is possible to set a new test, recall an already programmed and filed test, file a current test, perform the test and visualize past and present alarms.

For setting a new test the operator has numerous menu pages on hand which allow him to choose the network voltage, the insertion of the filter, the selection of inductance values and those of the network resistance, the prearrangement of the star load in case of tests with three-phase lines, or in series for tests with DC or in any case, single-phase power supply, the setting of the threshold alarms on the current and the voltage with the relative delays etc.

The four load benches can be entered from the program in various ways, totally, partially, in series, in parallel, and in parallel and star series for three-phase loads.

The prearrangement of the load is made at the beginning of the program in the configuration phase by means of motorized isolating switches.

The contactors and motorized isolating switches are installed on an open frame located on an elevated platform on the top floor of the building.



Fig. 7 - control room

Apart from the test controlling devices various other control lines and logics have been implemented between the substation and the Test Room, related to the following:

- emergency opening of the circuit breakers (130 kVac, 3 kVdc, 380 Vac), both during the tests and while the Test Room is unattended;
- adjusting of the voltage via the variations in the transformation ratio.

## V.5 Experimental possibilities

The characteristics of this system allow for performing tests on electrical traction equipment in a wide variety of configurations. As an example several test typologies are listed below.

### V.5.1 Tests of 3 kV dc equipment

Typologies of tests performable (both on equipment and stationary vehicles):

- performance and functional tests of new components and electronic converters;
- tests of DC circuit breakers, contactors, isolating switches, fuses, overvoltage arresters.

These tests, for example, include the following:

- performing of continuous load and overload cycles;
- switchover tests, overvoltage checks
- short circuit tests.

### V.5.2 Electromagnetic compatibility

The following typologies of tests are possible:

- measuring of electromagnetic emissions of equipment and rolling stock at radio frequency and low frequency ;
- study of interaction phenomena between power devices and signal devices;
- studies of harmonic currents generated by towed rolling stock and by converters.

## V.6 Aspects regarding the quality

### V.6.1 Management procedures

During the phase of operative activation of the system a special management procedure has been established - "procedure for conducting tests and experimental activities in the FS High Voltage Test Room at Empoli", in order to guarantee a correct Client/Supplier rapport and to ensure conditions of impartiality and discretion in carrying out tests.

This procedure, which is put into force in the transitory phase before the final certification and accrediting, has been perfected by using as references, the standards UNI EN ISO 9001 "Model for assuring the quality during the design, development, construction, installation, and assistance" and UNI CEI EN 45001 "General criteria for the functioning of test laboratories".

### V.6.2 Operating procedures

Specific procedures have been determined for each type of test, each of which, on the basis of the requirements of the relative standards and technical

specifications, provide an exact definition of the test modalities and equipment. In this context the test procedures regarding contactors and fuses for example, have been developed.

### V.6.3 Certification and accrediting of the Laboratory

The activities necessary for obtaining the certification based on the UNI EN ISO 9001 standard and the accrediting according to the UNI CEI EN 45001 standard are currently in the phase of being developed by the Experimentation Structure which supervises the laboratory. Following these procedures, the Test Room will operate in an ISO 9001 Structure, and it will request the accrediting for performing tests required by the regulations for the homologation of the equipment and vehicles under its own competence.

## V.7 Future developments

This Test Room, with its capacity to recreate the electrical conditions of the railway system without having to use the systems actually in operation, is proposed as an advanced test laboratory for studying the electrical systems for traction, and is available for use by the Technical Structures of Railways, Industries, and Universities.

The development of the Test Room is foreseen contextually with the certification and accrediting process, and its objective is that of being able to offer a testing and electrical experimentation service with a laboratory which is the most complete possible and compliant to standard requirements.

It will also be possible to implement power supply systems with 25 kVac and 1.5 kVac, climatic and vibration test equipment and systems for controlling electromagnetic immunity on complete rolling stock in the future, in the aim of supplying a wide coverage of the experimentation necessary both for research, and for the homologation of the electric railway products.

## VI CONCLUSIONS

The separation between line and rolling stock management, European interoperability specifications and technological development need in general an improving in simulation capability and testing procedures. In particular short circuit is a typical system phenomena, in which various elements has to be taken into consideration: for example vehicle position and configuration, feeding system parameters, components specifications. These aspects have to be taken into consideration in fuses standard, design and testing.

# SPECIAL ULTRARAPID FUSES TO POWER SEMICONDUCTOR CONVERTERS PROTECTION

T.Pleşca, P.Leonte, E.Furnică  
 "Gh. Asachi" Technical University  
 Iaşi – Romania

**Abstract:** The paper refers to ultra-rapid fuse cartridges meant to protect both power semiconductor converters and its power semiconductor devices against overloads and short-circuit fault conditions.

## I. GENERAL CONSIDERATIONS

The nowadays ultra-rapid fuses to power semiconductor devices have the next drawbacks [1,5]:

- an inadequate overload protection;
- the time-current characteristic,  $t(I)$ , is not adjustable;
- it doesn't exist the possibility to adapt the protection characteristic to thermal characteristic of protected device;
- the short-circuit current limiting effect is uncontrollable;
- in direct current they can't work to reverse current;
- they are not sensitive to power line sense;
- the changing of wasted fuse cartridges is exclusively only manual;
- they can't be a part of a flexible protection system with microprocessor or microcontroller.

This paper proposes a solution to remove the above drawbacks and this solution is in the middle of our researches, a laboratory stage for the time being.

## II. SPECIAL ULTRARAPID FUSE TO POWER SEMICONDUCTORS AND POWER SEMICONDUCTOR CONVERTERS

To eliminate the mentioned above drawbacks it set up the commanded fusing principle of fuse cartridges, accompanying by an example what can be materialized from different means.

Further on, it presents a special ultra-rapid fuse what contains a current transformer with its toroidal core  $m$  with rectangular section, Fig.1, the primary being concomitantly a part of secondary. The branched out current  $I_1$  from total current  $I$ , flows through one single turn,  $N_1 = 1$ , of primary P.

The short-circuited secondary S, with  $N_2 = 1$ , has the a-b section in common with primary P. The secondary S' is galvanic isolated by primary P and secondary S and it has the turns  $N' > 1$ .

If it supposes initially the situation without core  $m$ , the currents will distribute depending on branch impedances, resulting equal currents,  $I_1 = I_2$ , if the

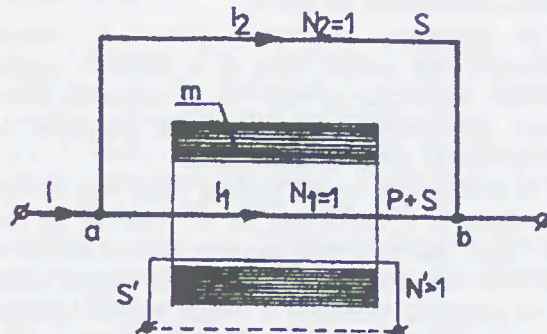


Fig.1 Special current transformer

branch impedances are theoretically equal, actually near values.

Using the core  $m$ , it complies with the magnetomotive force law:  $N_1 I_1' = N_1 I_0 + N_2 I_2'$ , with  $N_1 = N_2$  and  $I_0 \cong 0$  (magnetization current), leads to  $I_1' = I_2'$ . In accordance with effects superposition principle, referring to current senses, it results that total current  $I$  will flow through branch S and the current will be theoretically zero, actually only magnetization current,  $I_0$ , through branch a-b.

If the second secondary S' is short-circuited, the currents become equal on both branches or near values. This current transformer feature is used to special ultra-rapid fuses.

Let consider that ultra-rapid fuse SF meant to protect power semiconductors and their devices, Fig.2, will be made up of two identical fuse cartridges,  $F_1$  and  $F_2$ , placed on two parallel branches 1 and 2, with their impedances actually equal in normal operating conditions, so that currents  $I_1$  and  $I_2$  will be also equally.

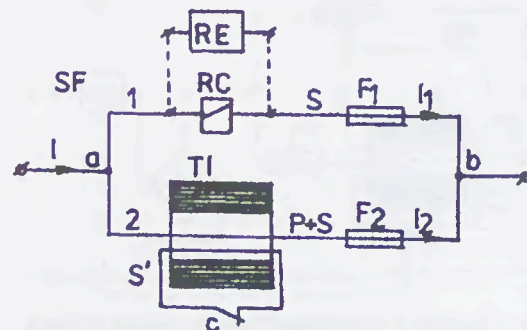


Fig.2 Special ultra-rapid fuse with adjustable time-current characteristic

One of branch, 2, has a current protection transformer with itself primary as conducting wire 2 and secondary  $S'$  (traced with one single turn, by simplicity) is short-circuited. The secondary  $S'$  can be short-circuited using a current relay RC or an electronic relay RE which turns off its normally closed contact  $c$ .

The opening of contact  $c$  introduces an inductance because of current transformer TI on branch 2, changing the current repartions. So, the main current which flows through branch 1, provides for working of fuse  $F_1$  followed successively by fuse  $F_2$ .

The adjustment possibilities offered by current transformer and current relay or a sensitive current electronic device can provide for an adjustable time-current characteristic and it can be adaptable to protected object thermal characteristic.

The short-circuit current limiting effect will become controllable if it anticipates the arc ignition. In this case, Fig.3, moreover that previous electric circuit, it introduces a sensitive element to derived current,  $di/dt$  and an additional secondary  $S''$  which supplies through switch  $k$  an arc ignition device such: a local miniexplosion; an auxiliary arc etc.

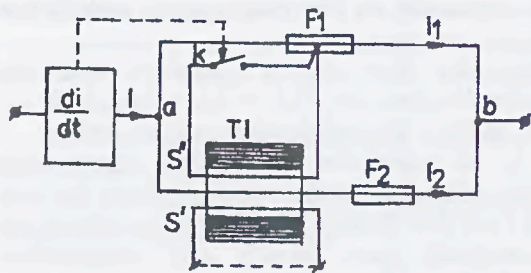


Fig.3 Special ultra-rapid fuse with controlled current limiting effect

So, it starts the anticipated working of fuse and the manifestation of short-circuit current limiting effect when its coming out is clearly.

In the case of power rectifier, Fig.4, when the fuse is on alternative current side, then it introduces a sensitive element to current sense, ES, which commands the

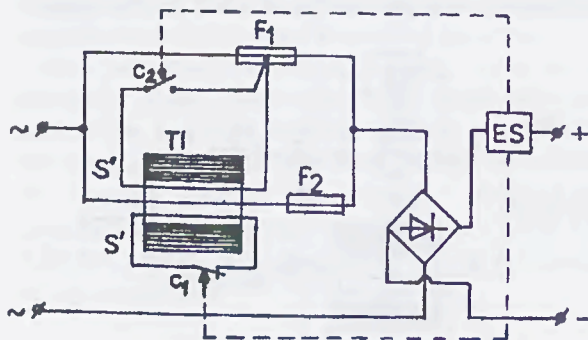


Fig.4 Sensitive ultra-rapid fuse to reverse current (monophase rectifier bridge variant)

fusing through: turn-off normally closed contact  $C_1$  from secondary  $S'$  of current transformer TI; turn-on normally open contact  $C_2$  from secondary  $S''$  which leads to arc ignition or combined methods.

At three-phase rectifier bridges the sensitive element ES will simultaneously command three fuses.

The working to power line sense changing, in alternative current, can be done using a power line directional element for fusing command.

It traced, experimentally, the time-current characteristic for the new type ultra-rapid fuse with rated current,  $I_n = 200$  A, Fig.5. It used the electric circuit from Fig.2 with the next elements:

- $F_1, F_2$  - two fuse cartridges with rated current by 100 A;
- RC - current relay with its own tripping time,  $t_t = 16$  ms;
- TI - protection current transformer with its transformer ratio by 150/5.

It can notice, Fig.5, that new time-current characteristic consists of two characteristic parts: curve 1 to overload ranges and curve 2 to short-circuit ranges. Also, there is a better protection in the range of overloads, curve 1, Fig.5.

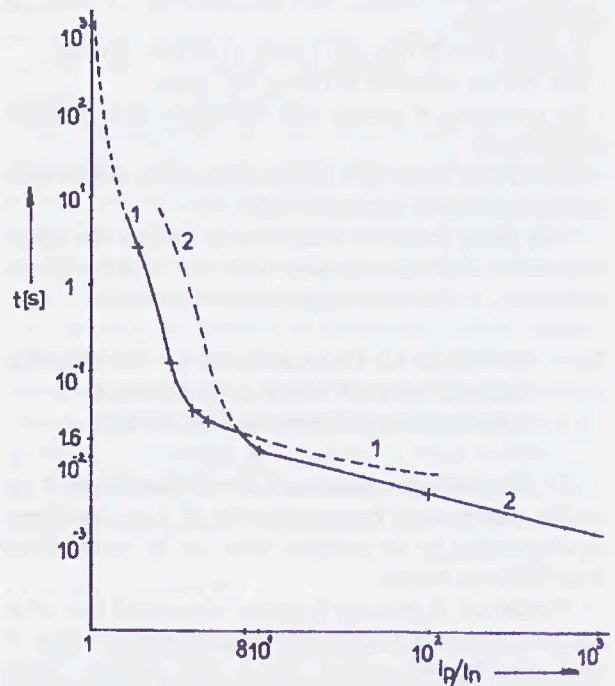


Fig.5 Time-current characteristics

If the commanded fusing spreads to resettable fuses (metal-liquid fuses) then it can implement the above principles to these kind of fuses. The fuses with commanded fusing from an overcurrent protection systems could benefit by microelectronic world services like microprocessor, microcontroller etc.

So, it comes true the modelling of protection characteristic fuses which can have the shape of any overcurrent protection electrical apparatus. Using the

commanded fusing, the fuses can work depending on any established parameter into a system when it is necessary. Also, there is a better selectivity.

The new type fuses offer more safety conditions about power semiconductor and converter protections when it is known the admissible maximum limit of stresses.

This paper showed only an application variant of commanded fusing in the case of ultra-rapid fuses. In the research stage there is other set up variants to offer an optimal solution for established conditions [2,3,4].

### III. CONCLUSIONS

It results the following conclusions from examination of proposed solutions to achieve special ultra-rapid fuses for power semiconductor protection:

- ultra-rapid fuses for power semiconductor protection can be set up with commanded fusing;
- the commanded fusing increases the adapting capability of ultra-rapid fuses to modern protection requests;
- the commanded fusing spreads the protection possibilities from overload currents to short-circuit currents;

- at the new type fuses, the protection can be sensitive to direct current sense or power line sense in alternative current, at derived currents and any supervised parameter if that device is compatible with command block to use;

- electricity supply systems allow to use ultra-rapid fuses with commanded fusing because of its adjustable time-current characteristic, commanded current limiting effect, time-current characteristic modelling possibility.

### REFERENCES

- [1] A.Wright, P.G. Newbery, "Electric Fuses", Published by The Institution of Electrical Engineers, London, United Kingdom, 2nd Edition, 1995.
- [2] T.Pleşca, P.Leonte, "Siguranță fuzibilă specială pentru redresoarele de putere", Cerere brevet invenție, Dosar OSIM nr. 98-01739, 1998.
- [3] T.Pleşca, P.Leonte, "Element de înlocuire specializat pentru siguranțe ultrarapide", Cerere brevet invenție, Dosar OSIM nr. 98-01740, 1998.
- [4] P.Leonte, T.Pleşca, "Siguranță ultrarapidă pentru protecția semiconductoarelor de putere", Cerere brevet invenție, Dosar OSIM nr. 98-01131, 1998.
- [5] SIBA – FuseLinks for power semiconductor protection, URA-06/98.

Faint, illegible text in the upper left column, possibly bleed-through from the reverse side of the page.

Faint, illegible text in the upper right column, possibly bleed-through from the reverse side of the page.

Faint, illegible text in the middle left column, possibly bleed-through from the reverse side of the page.

Faint, illegible text in the middle right column, possibly bleed-through from the reverse side of the page.

Faint, illegible text in the lower left column, possibly bleed-through from the reverse side of the page.

Faint, illegible text in the lower right column, possibly bleed-through from the reverse side of the page.

# BEHAVIOUR OF ELECTRIC FUSES IN AUTOMOTIVE SYSTEMS UNDER INTERMITTENT FAULT

B. Dilecce, F. Muzio  
Centro Ricerche FIAT, Orbassano (Torino), Italy

A. Canova, M. Tartaglia  
Dipartimento Ingegneria Elettrica Industriale Politecnico di Torino, Italy

**Abstract:** This paper deals with the behaviour of electric fuses in automotive systems when intermittent faults occur. In this case the fuse intervention time cannot be predicted by means of manufacture fuse characteristic only but a more general dynamic model of fuse behaviour is needed. Here, a simple dynamic thermal model able to take into account this kind of fault is proposed and numerical and experimental tests are presented.

## I. INTRODUCTION

Fuses for automotive systems are mainly used in order to protect electric power distribution network against short-circuiting and overloading. The most critical situations occur when fault current is comparable with the rating of the fuse; furthermore, the presence of an intermittent fault can also influence fuse intervention time; such a fault can be produced by an intermittent contact. The waveform of operating time versus fault current frequency of a stated fault current value is expected to increase monotonically in spite of some results found in literature [1] which predicted the existence of a range of critical fault frequencies avoiding fuse current interruption. These last results, based on experimental tests, require an accurate and a satisfactory validation.

The paper deals with the behaviour of fuses for automotive applications under the above critical conditions, which cannot be directly predicted by means of technical data given by manufacturers. Therefore, experimental verification were conducted, in order to identify a fuse model, both under step and intermittent input current condition. The model includes the circuit equations and the fuse thermal equations deducing model parameters from the above-mentioned experimental results. The thermal model is implemented by means of equivalence of thermal and electrical systems solved through a SPICE solver for electric circuits.

Finally, a parametric analysis, for different amplitude and frequency of the input current, has been performed and compared with experimental results.

## II. TIME-CURRENT CHARACTERISTIC

### II.1 Experimental Measurements

In order to perform the experimental measurements, the equipment sketched in Fig.1 is used. The main components of the circuit are:

- DC supply: 12V
- Electronic power switch
- Current amplitude and frequency controller
- Shunt and Oscilloscope
- Automotive 10A Fuse

In particular, the current controller imposes a certain constant amplitude with changes of series circuit impedance; moreover, through the electronic power switch it sets the intermittent condition at the requested frequency and duty-cycle, controlling the rise and fall times of the current waveform.

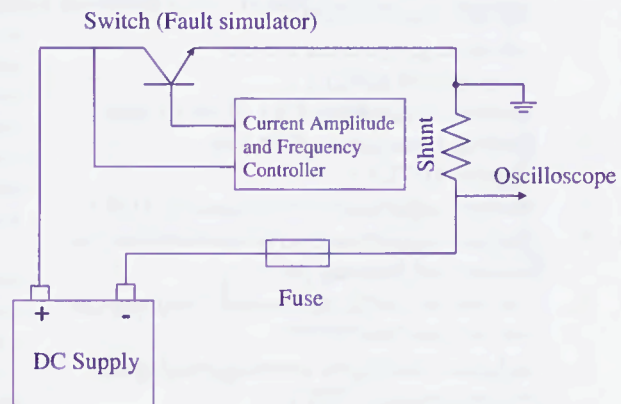


Fig. 1. Measurement equipment

### II.2 Fuse Model Identification

In order to perform the simulation of the fuse behaviour in presence of an intermittent fault, an identification process of the fuse model based on time-current characteristics has to be conducted.

The fuse model presented in this paper is electro-thermal, and it is implemented by means of equivalence of thermal and electrical systems through a SPICE solver for electric circuits.

The component is represented by a bipole in which the relationship between voltage and current is dependent on fuse element and housing's temperatures with respect to the external ambient. These temperatures are function of electric power dissipated on the fuse element. The model is then based on the following equations:

a) electrical equation:

$$V = R_0 I [1 + (T_1 - T_0) \alpha] \quad (1)$$

b) thermal equations:

$$R_0 I^2 [1 + (T_1 - T_0) \alpha] = C_1 \frac{dT_1}{dt} + K_{ci} (T_1 - T_2) \quad (2)$$

$$K_{ci} (T_1 - T_2) = C_2 \frac{dT_2}{dt} + K_{ie} (T_2 - T_a)^{esp} + K_{irr} (T_2^4 - T_{ak}^4) \quad (3)$$

where:

- $V$  voltage at fuse element nodes [V]
- $I$  current through the fuse [A]
- $R_0$  fuse element resistance [ $\Omega$ ]
- $T_1$  fuse element temperature [ $^{\circ}\text{C}$ ]
- $T_2$  housing temperature [ $^{\circ}\text{C}$ ]
- $T_a$  ambient temperature [ $^{\circ}\text{C}$ ]
- $T_0$  reference temperature for the measurement of  $R_0$  [ $^{\circ}\text{C}$ ]
- $T_{ik}$  absolute temperature [ $^{\circ}\text{K}$ ] of an element
- $C_1$  thermal capacitance of the fuse element [ $\text{J}/^{\circ}\text{C}$ ]
- $C_2$  thermal capacitance of the housing [ $\text{J}/^{\circ}\text{C}$ ]
- $K_{ci}$  thermal conduction coefficient between fuse element and housing [ $\text{W}/^{\circ}\text{C}$ ]
- $K_{ie}$  convection coefficient between housing and external ambient [ $\text{W}/^{\circ}\text{C}$ ]
- $K_{irr}$  radiation coefficient between housing and external ambient [ $\text{W}/\text{K}^4$ ]
- $\alpha$  resistivity thermal coefficient for copper ( $\alpha = 3.757\text{e-}3 \text{ } 1/^{\circ}\text{C}$ )
- $esp$  convection exponent

The electrical equation represents the electrical behaviour of the fuse element, in terms of a resistance linearly dependent on the difference between  $T_1$  and  $T_0$ . The thermal equations can be interpreted as follows:

1. the thermal flux generated on the fuse element is distributed as power increasing fuse element

temperature and power transmitted to the housing by conduction.

2. the power transmitted to the housing is transferred to the external ambient by convection and radiation.

This model does not take into account the thermal exchange with the contacts, supposing to consider a very large value for their thermal capacitance. Besides, in the computation of thermal flux, only the fuse element resistance is considered, in order to be closer to the manufacturer's experimental data, conducted in almost ideal and contact-free conditions. The circuit representation of the model equations is depicted in Fig.2.

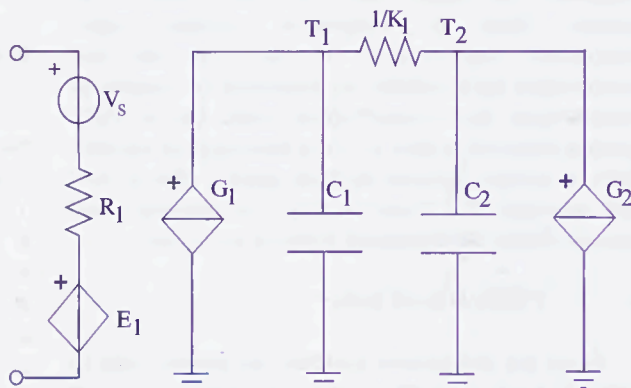


Fig. 2. The circuit model of the fuse

A bipole including the series of a resistance  $R_1$  and a controlled voltage source  $E_1$  implement the electrical equation. The independent source with null value  $V_s$  is a current sensor. The controlled current source  $G_1$  is the equivalent representation of the thermal flux, whose value is the dissipated power on the electric bipole. The resistance  $1/K_1$  represents the thermal conductance between the fuse element and the housing, whose thermal capacitances are respectively indicated by  $C_1$  and  $C_2$ . The controlled current source  $G_2$  is the representation of convection and radiation phenomena of thermal exchange between housing and external ambient.

The identification of model parameters consists in a fitting procedure whose the target is to minimize the root mean square error between the time-current characteristic calculated and the one provided by data manufacturers, for a certain set of currents. This procedure is implemented in the solver MATLAB, and is based on a specialized routine, that accepts a scalar valued function  $F(X)$  and an initial guess  $X_0$  for the vector variable  $X$ . It returns a vector  $X_1$  that is a local minimizer of  $F(X)$  near the starting vector  $X_0$ . In this case  $X$  is the vector of the model parameters, and  $F(X)$  is a suitable norm of the vector difference between the calculated curve and the manufacturer's one.

As can be seen in Fig.3, there is a good link between the experimental characteristics, defined by a maximum and a minimum curve, and the calculated ones, provided at two different temperatures in order to take into account

the external temperature excursion during the measurements.

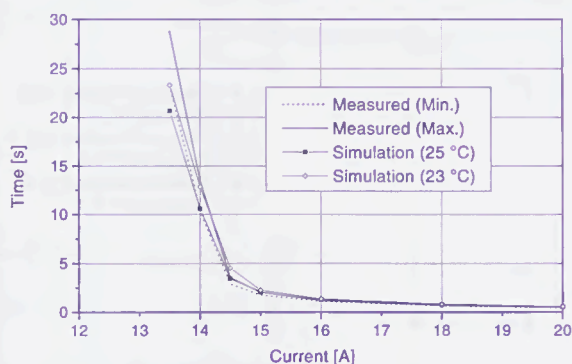


Fig. 3. Fuse time-current characteristic under step constant current

### III. INTERMITTENT FAULT BEHAVIOUR

#### III.1 Experimental Measurements

The measurements were conducted on a 10A ATO Blade Fuse designed by LITTELFUSE. The ATO Blade Fuse is a family currently used on almost all car, trucks, buses and off the road vehicles world-wide.

The single wire used in the experiment is a 1mm<sup>2</sup> cross section of automotive low-voltage cable.

The simulation of the intermittent short circuit requires a stepwise current with different values of amplitude and frequency. The controller depicted in Fig.1 sets these current parameters. In particular, the values chosen for the peak of the stepwise current were 20, 22.5 and 25A. The frequency values were fixed to 10, 50, 100 and 200 Hz, and in each test the duty-cycle was assumed to be 0.5. In Fig.4 an experimental survey of the circuit current, is represented.

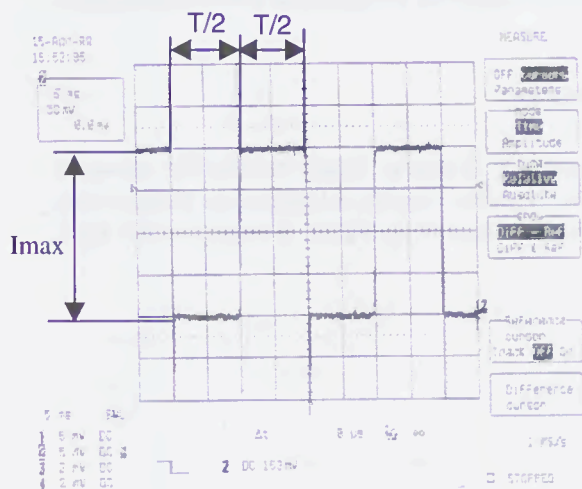


Fig. 4. Supply current during intermittent fault analysis.

At a fixed frequency and for a certain peak current value, a number up to 11 measurements was carried on, in order to take into account the statistic variance in the fuse behaviour.

#### III.2 System Model Identification

In order to simulate the whole electrical system, the circuit represented in Fig.5 has been implemented in the SPICE solver.

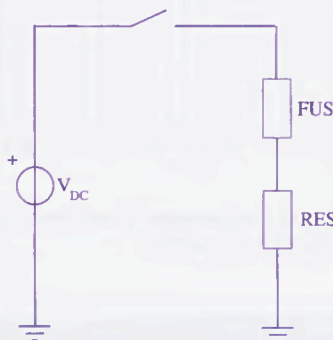


Fig. 5. The equivalent circuit of the whole electrical system

This is an equivalent circuit, that involves a constant DC source, an ideal switch to produce the intermittent current, the fuse model identified basing on the time-current characteristics, and an electro-thermal macro-model of the remaining part of the circuit.

In Fig.6 the electro-thermal macro-model of the part of the circuit including wires and terminations, is presented.

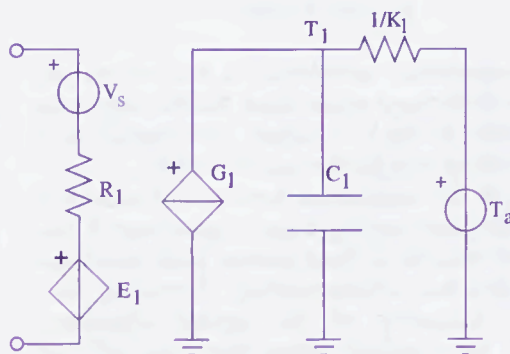


Fig. 6. The circuit model of the remaining part of the circuit

The series including the resistance  $R_1$  and the controlled voltage source  $E_1$ , in which a certain amount of power is generated, represent the electrical part of the model. The thermal flux, represented by the controlled current source  $G_1$ , is flowing to the external ambient through the thermal conductance  $K_1$ ; the capacitor  $C_1$

represents the thermal capacitance of the electrical part considered.

In Fig.7 and Fig.8, simulated waveforms of intermittent current ( $I_{max}=22.5A$ ) and fuse element temperature are represented for  $f=10$  Hz and  $f=50$  Hz.

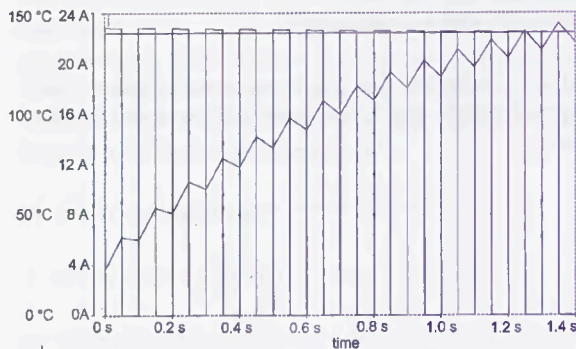


Fig. 7. Current and temperature waveforms for  $I=22.5A$ ,  $f=10Hz$

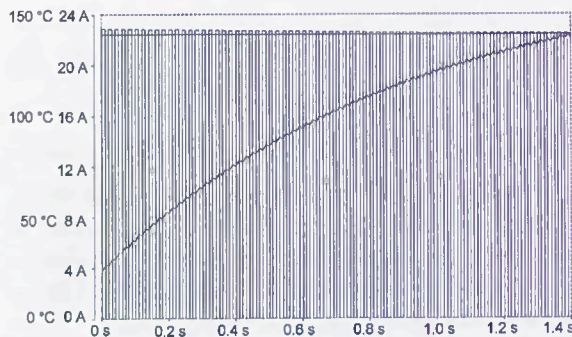


Fig. 8. Current and temperature waveforms for  $I=22.5A$ ,  $f=50Hz$

The temperature waveforms in the two curves have almost the same mean value, but the amplitude of the curve in Fig.7 is higher, contributing to a smaller melting time for the case of  $f=10$  Hz.

In Fig.9, the comparison between the measured and the computed melting times, is presented. It can be noticed that, for a fixed current peak value, the melting time has a monotonically increasing flow with the frequency of the applied waveform. Moreover, the calculated values share quite well the measured data, since for each couple current-frequency considered, the melting time computed is included in the range of the experimental data.

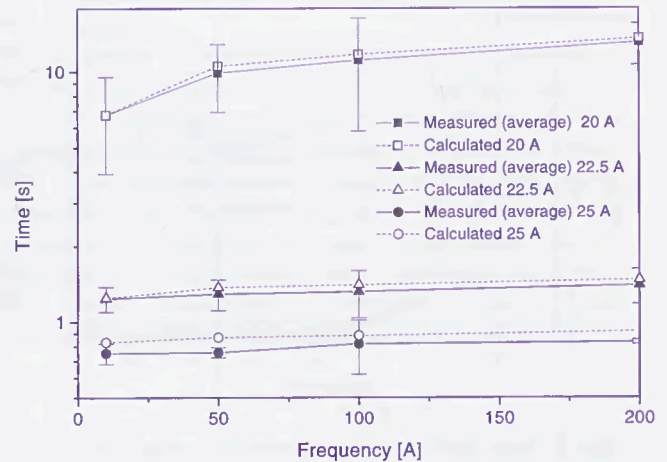


Fig. 9. Computed and measured melting times vs. current frequency

#### IV. CONCLUSIONS

In this paper, the behaviour of electric fuses in automotive systems under intermittent fault is examined. The condition of an intermittent short-circuit has been reproduced by supplying a pulse-wise current to a 10A ATO Blade Fuse.

A parametric analysis has been conducted; the range of current amplitude has extended from 20 to 25A, and the supplied frequency from 10 to 200Hz. Unlike the results of a typical case-study in literature [1], the present analysis has revealed a monotonically increasing behaviour of melting time with frequency of the input current.

#### ACKNOWLEDGEMENT

The authors wish to thank Mr. F. Quarona (Politecnico di Torino) for his support in experimental parts of this paper.

#### REFERENCES

- [1] J. Suzuki, Y. Tamura, Japan Automobile Research Institute, "Ignition Process of Intermittent Short-Circuit on Modeled Automobile Wires", Copyright 1996 SAE, Inc.



卷之三

一

二

三

四

五

六

七

八

九

十

十一



